AN INVESTIGATION INTO THE PERFORMANCE AND DESIGN OF PRESSURE-EXCHANGERS

by

ABDUL AZIM, M.Sc.

A thesis submitted for the degree of

Doctor of Philosophy

in the Faculty of Engineering,

University of London

CITY AND GUILDS COLLEGE,
IMPERIAL COLLEGE OF SCIENCE AND TECHNOLOGY,
UNIVERSITY OF LONDON

March 1974

TO MY PARENTS

1. ABSTRACT

A brief description of the pressure exchanger, its fundamental processes and various operational cycles is followed by a summary of the historical background of the pressure exchanger and a brief survey of previous work. The objectives of the present work are then stated and the criteria of the performance of four-port pressure exchangers are deduced.

An approximate method has been extended and computerised to cater for four-port pressure exchanger cycles with and without transfer passages. This method is then used to determine roughly the influence of including a transfer passage on the performance and geometry of four-port pressure exchangers.

A new method, given the name Pressure Differential Method, is developed for rapid calculations of the performance and geometry of pressure exchangers with any number of transfer passages. This method makes use of the performance and geometric characteristics of the fundamental processes of pressure exchangers obtained by application of the method of characteristics. It also provides boundary conditions at the transfer ports.

A numerical procedure for the solution of the governing partial-differential equations in unsteady compressible flow has been previously developed at Imperial College. This procedure is based on a "hybrid method". In order to further develop this numerical procedure, a study of various pressure exchanger performance losses has been carried out. Friction, heat-transfer and mass leakage are introduced into the existing procedure. Two further methods to account for leakage have been developed. Effects arising from the unstreamlined cell exit and entry and the transfer passage losses are calculated from steady flow loss data. The loss calculations are introduced into the original procedure. Criteria of the port geometry have been

deduced and relationships have been derived to calculate the assumed steady state conditions in the pressure exchanger ports. A computer program has been developed incorporating the basic numerical procedure, the performance loss calculations, the port geometry criteria, the steady-state condition relationships and the calculation of the overall performance of pressure exchanger cycles.

The computer predictions are compared with experimental data on pressure-equaliser performance obtained by Kentfield, and also by the Author on four and six port pressure exchanger cycles. Good agreement between the theoretical and experimental results has been found.

The computerised procedure is then used to investigate the performance and geometry of four-port-pressure exchangers without transfer passages. The effects of pressure ratio, temperature ratio, scavenge ratios, finite cell width, blank spaces and performance losses are examined. Similar studies have been carried out for four-port-pressure exchangers with one transfer passage and the effects of a transfer passage on the performance and geometry have been deduced.

These investigations have also led to the establishment of pressure exchanger design charts.

An analysis of the results is followed by suggestions and recommendations for future work.

It has been concluded that the computerised procedure gives good results and it has been successfully used to analyse pressure exchanger cycles. Transfer passages improve the performance of four-port-pressure exchangers in terms of bulk input but result in low mass flows and port velocities, and an increase in the losses and size of pressure exchangers to achieve some scavenge ratios.

CONTENTS LIST

Section		Page No.
TITLE		1
1.	ABSTRACT	3
	CONTENTS LIST	5
	ACKNOWLEDGEMENTS	10
2.	INTRODUCTION	11
	2.1 Definition and Description of Pressure Exchanger.	11
	2.2 Pressure Exchanger Basic Processes.	12
	2.2.1 Cell Filling.	12
	2.2.2 Cell Emptying.	13
	2.2.3 High-Pressure Scavenging.	13
	2.2.4 Low-Pressure scavenging.	15
	2.3 Pressure-Exchanger Cycles.	15
	2.3.1 Pressure Equaliser and Divider	15
	2.3.2 Four Port Pressure-Exchanger.	16
	2.3.3 Four Port Pressure-Exchanger with transfer passages.	17
	2.4 Historical Background and Previous Work.	18
	2.5 Objectives of the present work.	20
3.	PRESENTATION OF THE PERFORMANCE OF PRESSURE-EXCHANGERS	22
	3.1 Non-Dimensional Bulk Input.	22
	3.2 Scavenge Ratios.	23
	3.2.1 High-Pressure Scavenge Ratio.	23
	3.2.2 Low-Pressure Scavenge Ratio.	23
	3.3 Steady Flow Mach Numbers at Ports.	23
	3.4 Steady Flow Stagnation Temperatures at Outlet Ports.	24
4.	THE THEORY OF PRESSURE EXCHANGERS	25
	4.1 Outline of Theoretical Approach.	25
	4.2 The Approximate Method.	26
	4.3 The Pressure Differential Method.	27

Page No.

4.4 Application of The Method of Characteristics to the Studies of Pressure-Exchangers. 29

4.4.1 Numerical Solution Procedures. 29

(a) The Method of Characteristics. 29

(b) The Finite Difference Method. 30

(c) The Hybrid Method. 30

4.4.2 The Mathematical Model. 31

(a) The Basic Equations. 31

(b) The Initial Conditions. 33

(c) The Boundary Conditions. 34

4.4.3 Numerical Procedure for Hybrid Method. 44

(a) The Grid and Outline of Procedure. 44

(b) Stability Criterion. 45

(c) Calculation Procedures. 46

5. PERFORMANCE LOSSES IN PRESSURE-EXCHANGERS 50

5.1 Entropy Losses Due to Shock Waves. 50

5.2 Finite Cell Width Losses. 50

5.3 Frictional Losses. 50

5.3.1 Cell Wall Friction. 51

5.3.2 Cell Entry and Exit Losses. 51

5.4 Leakage Losses. 52

5.4.1 Calculation of Leakage Flows. 52a

5.4.2 The Energy and Mass Flow Correction Method. 53

5.4.3 The Porous-Cell Wall Method. 53

5.4.4 The Partly-Open End Method. 54

5.5 Heat Transfer Losses. 55

5.6 Transfer Passage Losses. 56

5.7 Mixing & Diffusion Losses. 56

6. STEADY STATE CONDITIONS IN PRESSURE-EXCHANGER PORTS 57

7. THE COMPUTER PROGRAM 58

		Page No.
7.1	General Comments.	58
7.2	A Description of the Program.	60
	7.2.1 Main	60
	7.2.2 GAMMA	65
	7.2.3 INIT	65
	7.2.4 AUX	65
	7.2.5 STEP	65
	7.2.6 SLOPE	66
	7.2.7 LININT	67
	7.2.8 PORTX	67
	7.2.9 CYCLE	69
	7.2.10 PORTS	69
	7.2.11 FINI	73
	7.2.12 OPTIM	73
	7.2.13 CEMF	76
	7.2.14 PHASE	78
	7.2.15 CSCR	79
	7.2.16 INITIA	82
	7.2.17 RESID	82
	7.2.18 IRESID	82
	7.2.19 CFST	82
	7.2.20 LEK1	82
	7.2.21 LEK	83
	7.2.22 INTEG	83
	7.2.23 CEXEN	84
	7.2.24 BLEAK	84
	7.2.25 DUCT1	85
	7.2.26 DUCT2	85
	7.2.27 RESULT	85
	7.2.28 EQUAL	86

7.2.29 DIVIDE 86

7.2.30 DESIGN 86

7.2.31 KING 86

8. APPARATUS 88

8.1 Specification for a Suitable Test Rig. 88

8.2 Description of Pressure Exchanger. 89

8.3 Instrumentation. 91

8.4 Outline of the Experimental Procedure. 92

8.4.1 Transfer Passage Tests. 92

8.4.2 Four Port Pressure Exchanger Tests. 92

8.4.3 Limitations of Experiments. 92

9. ANALYSIS OF THE THEORETICAL AND EXPERIMENTAL RESULTS 94

9.1 Use of Normalised Quantities. 95

9.2 Optimisation Studies of Pressure Exchangers. 96

9.2.1 Optimisation Studies of Basic Processes. 96

(a) Cell Filling Process. 97

(b) Cell Emptying Process. 99

(c) High-Pressure Scavenging Process. 100

(d) Low-Pressure Scavenging Process. 101

9.2.2 Optimisation Studies of Four Port Pressure Exchangers without Transfer Passages. 102

(a) The Approximate Methods. 102

(b) The Hybrid Method. 104

9.2.3 Optimisation Studies of Four Port Pressure Exchangers with One Transfer Passage. 112

(a) The Approximate Methods. 113

(b) The Hybrid Method. 115

9.3 A Study of Performance Losses in Pressure Exchangers. 123

9.3.1 Performance Losses in Four Port Pressure Exchangers. 124

9.3.2 Performance Losses in Four Port Pressure 126

Page No.

Exchangers with one Transfer Passage.

9.4 Comparison of the Theoretical and Experimental Results. 128

9.4.1 Equaliser Cycles. 129

9.4.2 Four Port Pressure Exchanger Cycles. 131

9.4.3 Four Port Pressure Exchanger with One Transfer Passage Cycles. 133

10. DISCUSSION AND RECOMMENDATIONS 136

10.1 Approximate Methods. 136

10.2 Hybrid Method. 136

10.3 Optimisation Studies. 139

10.4 Transfer Passages. 141

10.5 Performance Losses. 143

10.6 The Computer Program. 144

10.7 Comparison of Theoretical and Experimental Results. 148

11. CONCLUSIONS 149

12. GRAPHICAL REPRESENTATION OF RESULTS 150

13. DIAGRAM AND ILLUSTRATIONS 249

14. REFERENCES 268

15. APPENDICES 273

15.1 Appendix I; Notation. 273

15.2 Appendix II; The Approximate Method. 276

15.3 Appendix III; The Pressure Differential Method. 286

15.4 Appendix IV; The Hybrid Method. 293

15.5 Appendix V; Evaluation of Losses. 299

15.6 Appendix VI; Steady State Conditions. 313

15.7 Appendix VII; Listing of Variables. 317

15.8 Appendix VIII; Flow Charts. 329

15.9 Appendix IX; Computer Program.

ACKNOWLEDGEMENTS

The Author wishes to express his sincere appreciation to Mr. J. A. Barnes who suggested the subject of the research, gave useful criticism during the course of this work and extended help in all possible ways. Sincere appreciation is expressed to Professor D. B. Spalding, Professor of Heat Transfer at Imperial College, who initiated the work on the computer program for pressure exchangers.

Thanks are also due to the members of the staff of the Imperial College computer centre, who despite heavy demands on their computers managed to provide the Author with much-needed computer time and all possible assistance and to the members of the staff of the Mechanical Engineering department who assisted the Author on numerous occasions.

Generous financial assistance received from Volkart Education Foundation is also gratefully acknowledged.

Thanks are also due to Mrs. G. M. McEwen for the typing of this Thesis and Mrs. Roe for assistance with the tracing of the graphs.

2. INTRODUCTION

2.1 Definition and description of the Pressure Exchanger

The term pressure exchanger stands for a device which aims at providing means for direct exchange of energy between flows which are initially at different pressure levels. One fluid expands exerting its pressure forces to compress another fluid. The fluids are in direct contact and no intermediatory mechanical means are required to accomplish the energy transfer.

The pressure exchanger has a simple construction. In its simplest form it consists of a rotor having plane, axially extending blades mounted radially on a shaft. The spaces between the blades are called cells and they are straight passages of constant and uniform cross-sectional area. The rotor is surrounded by a cylindrical end casing which holds two end plates one at each end of the rotor in such a way that there is a small clearance between the rotor and its end plates. The end plates contain ports through which the cells can communicate with the connecting ducts. The rotor shaft is supported by bearings located in the end plates. The number of ports and their relative positions on the plates determine the type and conditions of the pressure exchanger cycle. Fig. (13.1) shows a typical pressure exchanger rotor and end plates.

The Pressure exchangers may be classified in two classes:-

(i) Semi-static Pressure Exchangers.

(ii) Dynamic Pressure Exchangers.

The Semi-static Pressure Exchanger is a low-speed device associated with the name of Lebre (1).. In this type of pressure exchanger the cell and duct pressures do not depend upon wave effects.

The Dynamic Pressure Exchanger takes advantage of pressure wave effects and to do so the rotor has to move at a substantial speed. A similar example is the case of wave effects being utilised in the exhaust and intake

ducts of reciprocating engines. In order to make correct utilisation of the wave effects proper rotor dimensions, speed and tuning of the ports are essential.

The use of wave effects results in higher pressure ratios and efficiency for a given energy input.

2.2 Pressure Exchanger basic processes

Most pressure exchanger cycles comprise the following basic processes

2.2.1 Cell filling

A cell-filling process, as utilized in a pressure exchanger, is initiated when a cell containing a fluid at a lower pressure is exposed to a port which contains a fluid at a higher pressure. The fluid in the port passes into the cell compressing the cell contents. After an initial phase the flow in the port becomes steady due to a succession of cells communicating with the port, whereas the flow in the cell is unsteady and a compression wave advances into the cell. The compression wave, when it reaches the closed end, is reflected back as another compression wave travelling in the opposite direction in order to bring the cell contents to rest. When the reflected wave reaches the open end, three different possibilities exist:-

(i) If the cell is still exposed to the port, the incoming compression wave is reflected as an expansion wave and causes a flow reversal.

(ii) If the cell has already been closed, the compression wave interacts with an expansion wave generated at the point of cell closure.

(iii) If the cell closes at the instant the compression wave arrives at the open end, then all wave interactions are

eliminated and the cell contents, now at a higher pressure than that of the fluid in the port, come to rest. Fig. (13.2) shows a simplified case of cell filling. In this case the cell opening/closing time is infinitely small so that the compression wave, shown by a full line, is established instantly as a shock wave. Any entropy discontinuity between the fluids separated by the contact surface shown by the dash-dot line has also been neglected.

2.2.2 Cell emptying

A cell-emptying process is initiated when a cell containing a fluid at a higher pressure is exposed to a port which contains a fluid at a lower pressure. The fluid in the cell passes out to the port by means of an expansion wave which advances into the cell. The expansion wave on reaching the closed end of the cell is reflected back as another expansion wave which travels towards the open end bringing the fluid in its wake, to rest. When the second expansion wave reaches the open end three different possibilities, similar to those of the cell-filling process, exist. In the cell-emptying process the fluid motion is set up by expansion waves which have the property of fanning out, a phenomenon which makes it difficult to arrange the closure of port such that all waves are eliminated in the cell receding from the port. Fig. (13.3) shows a simplified case of cell emptying. In this case the cell opening/closing time is again infinitely small and the fanning out of the expansion waves has been neglected. The expansion waves are represented by dashed lines, a convention which will be followed throughout this report.

2.2.3 The high-pressure scavenging process

In a high-pressure scavenging process in pressure exchangers, the

fluid contents of a cell are compressed and scavenged out of the rotor through an outlet port and replaced by a fresh fluid which is then ideally expanded to a pressure equal to the initial pressure of the fluid originally in the cell.

The high-pressure scavenging process begins with a cell-filling process. A cell containing fluid at a lower pressure is exposed to a port containing a fluid at a high pressure. A compression wave advances into the cell, compressing the fluid content in the cell followed by the fluid in the port and the interface also travels along the cell in the same direction.

When the initial compression wave of the cell-filling process reaches the opposite end the cell may now be exposed to an outlet port at that end to commence the discharge of the compressed fluid even while the fresh fluid is still entering the cell at the opposite end. The opening of an outlet port produces an expansion wave which moves along the cell towards the inlet ports. If the pressures in the inlet port and the outlet port are equal and outlet port opening is correctly tuned then the two waves at the outlet port will cancel each other out. This is what happens in the first part of the high-pressure scavenging process. At this point in the process the fluid in the cell as well as in the two ports is in a state of steady flow.

The next event in the scavenging process is the closure of the inlet and outlet ports. For full scavenge the closure of the outlet port is so chosen as to allow the interface between the fresh fluid which has entered the cell and fluid originally contained in the cell to reach the outlet port just at the point of closure. The inlet port is closed at such an instant that the expansion wave, generated by the closure of the inlet port, overtakes the interface just at closure of the outlet ports. This expansion wave reduces the fluid to a lower

pressure, ideally equal to the initial pressure, and also brings to rest the fluid in its wake. The high-pressure scavenging process has now been successfully completed. Thus the process may be regarded as the combination of a cell-filling and a cell-emptying process taken in that order. Fig. (13.5) shows a simplified case of a high-pressure scavenging process.

2.2.4 The low-pressure scavenging process

The low-pressure scavenging process can be regarded as a combination of a cell-emptying process followed by a filling process, taken in that order, the reverse of that for a high-pressure scavenge process.

In a low-pressure scavenging process the fluid contents of a cell are expanded and scavenged out of the rotor through an outlet port and are replaced by a fresh fluid which is then ideally compressed to the initial cell pressure. The tuning and closure of the ports follow the similar considerations as in the case of the high-pressure scavenging process. Fig. (13.4) shows a simplified case of a low-pressure scavenge process.

2.3 Pressure Exchange Cycles

2.3.1 Pressure Equalisers and Dividers

A pressure divider is defined as a machine taking in a single stream of gas or vapour and discharging two separate streams, one at a higher and other at a lower stagnation pressure than that of the ingoing stream. The work needed to compress the fluid emerging from the high-pressure outlet is obtained from the expansion of the remainder of the fluid. Fig. (13.6) shows a simple case of a single-ended divider.

A pressure equaliser is defined as a machine taking in two streams of (not necessarily identical) compressible fluid, one stream having

a higher stagnation pressure than the other. The fluids are discharged from a common outlet with a common stagnation pressure between those of the ingoing streams. The work required to compress the low-pressure fluid is obtained from the expansion of the high-pressure fluid. Fig. (13.7) shows a simplified case of a single-ended equaliser. Pressure divider and pressure equaliser cycles were investigated by Kentfield (2) who describes them in detail.

2.3.2 Four-port pressure exchangers without transfer passages

Pressure equalisers and dividers are those pressure exchanger cycles which do not need an external supply of energy to achieve compression of fluids. In both cases the compression of one fluid is achieved through the expansion of either another stream of fluid or the remainder of the same fluid. Four-port machines consist of those pressure exchanger cycles which needs an external source of energy to sustain them. These machines are characterised by the inclusion of scavenging processes in them. The high-pressure scavenge process is employed to compress and scavenge out the fluid initially in the cell and replace the driven fluid with the driver fluid. The low-pressure scavenging process is used to expel the driver fluid which has filled the cell after the completion of the high-pressure scavenging process and fill the cell with the fresh driven fluid to start the next cycle. In order to achieve this at least four ports are required hence the name four port machine. In the four-port machines the high-pressure scavenging ports are generally connected to each other by ducts forming a loop. The energy source is placed in this loop between the high-pressure ports. The energy source may be one of the following:

(i) Compressed gas supply.

(ii) Combustion chamber.

The former source, in conjunction with a heat exchanger, is employed in

the cooling cycle, while the latter is used in a gas-generator cycle to produce thermodynamically useful gases. When the combustion chamber in a gas-generator cycle is replaced by either the cylinder of an internal combustion engine or the air circuit of a boiler, the pressure exchanger acts as a supercharger.

Fig. (13.8) shows a four-port machine with a heat source placed in the high-pressure scavenge loop.

2.3.3 Four-port machines with transfer passages

A transfer passage, as utilised in a pressure exchanger, connects a high-pressure region to a low-pressure region of the same rotor. The fundamental processes at the two ends of a transfer passage consist of a cell-filling process at the entrance and a cell-emptying process at the exit. They are both at substantially the same pressure. The inclusion of one or more transfer passages results in a superior cycle performance. This happens because a portion of the compression work is done by the expansion of the fluid residing in the cells after the completion of the high-pressure scavenge process. The inclusion of a transfer passage also results in a considerable weakening of the pressure waves, accompanied with a reduction in entropy losses and a significant increase in the range of attainable pressure ratios. Fig. (13.9) shows a simplified case of a transfer passage in a pressure exchanger which shall sometimes be referred to as a six-port pressure exchanger in this thesis.

Although inclusion of one or more transfer passages in a pressure exchanger cycle results in a superior performance in terms of the energy requirement, their effect on the mass flows and the velocities through the ports, on the geometry of the machine and on the performance losses may not all be beneficial.

A transfer passage may also be included in a pressure exchanger cycle in such a way that the transfer ports are at opposite ends as opposed to the arrangement shown in the Fig. (13.9) in which both the ports are situated at the same end.

2.4 The historical background and previous work

The pressure exchanger has been known to engineers since the beginning of this century and it has appeared in the technical literature for many decades. Lebre (1) in 1928 proposed a practical SSPE cycle for a refrigerator. The first commercial use of the SSPE was disclosed in 1943 by the Swiss Company Brown-Boveri , the application being that of a heat pump based on the patents of Lebre (1) . Wave effects in a pressure exchanger were not given attention until 1940 when a successful pressure exchanger mechanism based on the utilization of the wave processes was embodied in the Brown-Boveri model based on proposals by Seippel (3) . Investigations on the machine, called the Comprex, were carried out by Berchtold (4,5) and Burri (6) at the Federal Institute of Technology, Zurich.

In the United Kingdom, Jendarasik pioneered interest in pressure exchangers and in collaboration with him Power Jets (Research and Development) Ltd. agreed to build and test a pressure exchanger. Power Jets were then responsible for carrying out intensive theoretical and experimental investigations to examine pressure exchanger cycles and their potential applications. Spalding, Barnes and Azouri are a few among many names which appear in the technical literature of Power Jets. Their investigations led to a better understanding of the pressure exchanger process, cycles and potential applications. The best application proved to be an air cycle refrigerator which was designed and tested for use as a spot cooler in deep gold mines. Kentfield (2) investigated pressure equalisers and dividers. NGTE, CEGB and Rolls-Royce all showed interest in pressure exchangers.

In most cases, investigations consisted of experimental studies. Theoretical investigations were limited and insufficient. The methods available for the theoretical studies of the pressure exchangers were too complex, laborious and time-consuming. The theory of the pressure exchangers is based on that of unsteady compressible flow. It predicts the relations between the pressures, mass flows, velocities and temperatures likely to be obtained in the pressure exchanger rotor and the ports. A method of calculation which is sufficiently accurate to deal with pressure exchanger processes and developed by Schultz Grunow (7), Jenny (8) and de-Haller (9) is known as the Method of Characteristics. The application of this method to solve various unsteady flow problems has been explained by Rudinger (10) The application of the method of characteristics to pressure exchanger cycles has been explained by Spalding (11). Kentfield (2) has used this method to study pressure equalisers and dividers. In spite of the availability of such a powerful method, its application to many pressure exchanger cycles was inhibited by the excessive time and labour consumed by the graphical solution procedure. With the introduction of high-speed and large-capacity computers it became possible to study the complex nature of unsteady flows by application of the method of characteristics. Benson (12) studied wave effects in the intake and exhaust of combustion engines. Spalding (13) O'Shea (14) and Mathews (15) were responsible for the development of a computerised numerical procedure at Imperial College and this has been further developed by the Author in the present work to provide for the first time a comprehensive theory and algorithm for performance and design calculations of pressure exchanger cycles. The geometry of pressure exchangers which can have a great influence on their performance has not been sufficiently investigated. Azouri (16) has given a simple expression for the optimum number of cells in the pressure exchanger rotor. Kentfield (2) calculated the optimum geometries for pressure equaliser and divider cycles. Azouri (17) carried out limited investigations into the geometry of

cell filling, cell emptying and scavenging processes.

Very little published literature is available on the evaluation of performance losses in pressure exchangers. Kentfield (2) evolved a simple procedure to include friction, leakage and the cell exit and entry losses in performance estimates of pressure dividers and equalisers. Kentfield's method was based on certain correction procedures, for various performance losses, to be applied to the otherwise complete characteristics calculations carried out independently of the performance losses. Spalding (18) proposed a linear leakage theory for pressure exchangers having large blank regions between set of ports. Cotter (19) evaluated the effect of friction losses on cell-filling and cell-emptying performance.

To the Author's knowledge no published work is available in the literature on the effects of including transfer passages in pressure exchanger cycles except for some very preliminary results due to Azouri (20)

Temperature discontinuities can also play significant role in the performance and design of the pressure exchangers. Azouri (21) has done some work on this topic.

Azim (22) gives a comprehensive document which deals with pressure exchangers, their historical background and development and their potential applications. It also gives a full survey of literature available on pressure exchangers.

2.5 Objectives of the present work

The objectives of the present work include:

(i) To extend and computerise the approximate method to cater for four-port pressure exchangers and investigate the approximate performance geometry of four-port pressure exchangers with and without transfer passages.

(ii) To develop a method for the rapid calculation of the performance and geometry of four-port pressure exchangers with any numbe:

of transfer passages and to predict the approximate boundary conditions at the transfer ports.

(iii) To develop a numerical procedure based on a hybrid method for performance and design calculations of pressure exchanger cycles including the performance losses due to friction, heat transfer, leakage, unstreamlined cell exit and entry and energy degradation in transfer passages.

(iv) To use the computerised numerical procedure for the theoretical investigation of performance and geometry calculations for four-port pressure exchangers with and without transfer passages in order to establish the effects of various parameters and also to establish the design charts.

(v) To compare theoretically-predicted equaliser performance with available experimental results.

(vi) To carry out experimental investigations into the performance of four-port and six-port pressure exchangers and to compare these with computer predictions.

3. Presentation of the Performance of Pressure Exchangers

A knowledge of the performance of pressure exchangers implies a knowledge of the pressures, temperatures, mass flows and the physical properties of the fluids passing through the ports of a pressure exchanger for a given geometry and rotor speed. In order to present the performance this information should be supplied preferably in a non-dimensional form and in such a way as to be able to be compared with that of an idealised pressure exchanger cycle.

Performance criteria and the method of their presentation for pressure equalisers and dividers were deduced by Kentfield (23) In the following sections performance criteria, their significance and the methods of their presentation for four-port-pressure exchangers have been described

3.1 The Non-dimensional Bulk Input

$$\mu = (m_{HPin}\, T_{HPin} - m_{HPout}\, T_{HPout})/m_{sw}\, T_{LPin} \qquad (3.1.1)$$

The non-dimensional bulk inputs representing the difference of the energy flows through the high pressure scavenge ports in a non-dimensionalised form, is directly related to the pressure difference across the rotor by the relationship

$$\gamma\mu = \Delta p/p_{LPin} \qquad (3.1.2)$$

The non-dimensional bulk input is zero for the reversible pressure exchangers. This means that in a reversible or ideal four-port-pressure exchanger cycle no energy input would be required to maintain a certain pressure ratio. Due to irreversibilities a certain energy input will always be needed to maintain a given pressure ratio. This means that the non-dimensional bulk input is a good measure of the irreversibilities in pressure exchangers. The relationship (3.1.2) has been derived in Appendix III.

3.2 Scavenge Ratios

3.2.1 High-pressure Scavenge Ratio

The high-pressure scavenge ratio is defined as the ratio of the mass flow rate through the high pressure outlet-port to the mass flow swept across the rotor referred to the conditions in the cell at a position just before the commencement of the process. The high-pressure scavenge ratio is a measure of the degree of scavenging achieved in the high pressure scavenge section and it has a marked influence on the temperatures of the fluid streams in the outlet ports. It also determines the size of the ports at the high-pressure scavenge section.

3.2.2 Low-pressure Scavenge Ratio

The low-pressure scavenge ratio is defined as the ratio of the mass flow through the low-pressure inlet port to the mass flow swept across the rotor just after the completion of the low-pressure scavenging process. The low-pressure scavenge ratio is a measure of the degree of scavenging achieved in the low-pressure scavenging section and again it has a marked influence on the temperatures of fluid streams through the outlet ports and it also determines the size of the low-pressure ports.

Measurement of the flow conditions in the cell at any position during rotation is a difficult task. It is therefore more convenient to quote the values of the mass flows at the high-pressure outlet port and the low-pressure inlet-port-respectively in place of the two scavenge ratios when presenting experimental results.

3.3 Steady-flow Mach numbers at the ports

The values of the steady-flow Mach numbers at the high-pressure outlet port and at the low-pressure inlet port have been chosen to indicate the flow velocities in the pressure-exchanger ports. Relationships for cal-

culating the values of the steady-flow Mach numbers at various ports, involving the integrated port mass and energy flows, the port area and the boundary conditions have been derived in Appendix (VI).

3.4 Steady-flow stagnation temperatures at the outlet ports

The stagnation temperatures at the inlet ports of a pressure exchanger usually have fixed values. In most cases, when air is the working fluid, the temperature of the fluid entering the low-pressure inlet port can be taken to be equal to the atmospheric temperature. The temperature of the fluid entering the high-pressure inlet port is fixed by the manner in which the external energy is supplied.

The temperatures of the fluids at the outlet ports are determined by the events which take place inside the pressure-exchanger rotor. The temperature profiles at the outlet ports are usually non-uniform and their shapes depend upon the temperature discontinuities in the cycle and also upon the scavenge ratios. The outlet temperatures play a significant part in determining the performance of pressure exchangers, in the various applications of the latter. In a cooling cycle it is the low-pressure outlet temperature which is the main consideration. In a supercharger cycle it is desirable that the fluid temperature at the high-pressure outlet port be as low as possible in order to supply a dense charge to the engine. For a machine, with unity scavenge ratios, the outlet temperatures also indicate the isentropic efficiencies for the compression (and expansion).

4. The Theory of Pressure Exchangers

4.1 The following steps largely outline the theoretical approach.

(i) A pressure-differential method, based on the use of the performance and geometric characteristics of component processes, obtained by application of the method of characteristics, was developed for the rapid calculation of the performance and geometry of four-port pressure exchangers with any number of transfer passages. It was also used to predict the transfer port boundary conditions.

(ii) An approximate method was extended and computerised to cater for four-port pressure exchanger cycles. It was then used to make a preliminary study of four-port pressure exchangers with one transfer passage.

(iii) A "skeleton" computer program incorporating a numerical solution procedure based on the hybrid method for homentropic flows was developed to obtain the approximate performance of pressure exchanger cycles and to test the validity of the numerical procedure.

(iv) Various sources of performance losses in pressure exchangers were examined. Different methods were devised to account for the effects of friction, heat transfer, leakage, unstreamlined cell entry and exit and energy degradation in the transfer passages. These methods were introduced into the existing numerical solution procedure.

(v) The design criteria for the pressure exchanger ports taking part in the fundamental processes of the cell filling, cell emptying, high-pressure scavenging and low-pressure scavenging were selected from the considerations of the tuning of the ports, correct directions of flow, the optimum performances and the mass flow and scavenging requirements of the pressure

exchangers.

(vi) Relationships were derived to relate the steady state conditions in the ducts of a pressure exchanger to the ports mass and energy flows, the boundary conditions and the respective port area.

(vii) Criteria of the performance of four port pressure exchangers were deduced.

(viii) A general-purpose research computer program incorporating steps (iii) to (vii), for performance and design calculations of pressure exchangers was developed with special consideration given to providing means for efficient programing, maximum possible flexibility, simplicity and to make it easily understandable to the potential user in future.

(ix) In order to check and verify the validity of the proposed method of solution, the computer program was applied to a study of the performance of pressure equalisers, of fixed geometry and running at constant speed. The predicted performance was compared with the experimental data of Kentfield (23).

(x) The computerised procedure was extensively used to study various aspects of the performance and geometry of four-port pressure exchangers without transfer passages.

(xi) A theoretical investigation into the effects of including a transfer passage in four-port pressure exchangers was carried out with the help of the pressure differential method, the approximate method and finally the computerised numerical procedure and comparisons were made with the experimental data on transfer passages.

4.2 The Approximate Method

The approximate method is a graphical procedure, originally developed by Kentfield (23) for rapid and approximate calculation of pressure

exchanger cycles. It does not provide such detailed knowledge of pressure exchanger processes as the method of characteristics but it is suitable for exploratory surveys of pressure exchanger cycles. This method is based on the generalised presentation of experimentally obtained cell-filling and cell-emptying data.

The basic aspects of this theory and its application to the study of pressure equalisers and dividers are given by Kentfield (2) This method has been extended to make it applicable to the computerised calculation of four-port pressure exchanger cycles in the following way:

(i) Algebraic expressions have been derived for the Mach number versus static pressure ratio relations and the static temperature ratio versus static pressure ratio relations for the single wave processes (given in graphical form by Kentfield (2)) by fitting curves using the least squares method to the graphical sets of data. These expressions are given in Appendix II.

(ii) Methods have been evolved to take account of temperature discontinuities and pressure drop in the heating circuit. These methods are described in Appendix II.

(iii) A general computer program has been developed to calculate the performance and geometry of pressure exchanger cycles using the approximate method. The computer program is also described in Appendix II.

4.3 The Pressure Differential Method

The pressure differential method is a graphical procedure (it may easily be computerised) for rapid and approximate calculation of the performance and geometry of pressure exchangers. It makes use of the performance and geometric characteristics of the pressure-exchanger component characteristics. These component characteristics are obtained by

application of the method of characteristics in the present version. The pressure differential method is based on the following procedure involving six steps. The first five steps establish the graphical set of data and only the final step is required to be repeated for subsequent cycle calculations.

(i) Establishment of the performance and design characteristics of the cell-filling process which consists of the $\Delta^P_{CF/p_{OCF}}$ versus R_{CF}, $\Delta^P_{CF/p_{1CF}}$ versus R_{CF} and τ_{CF} versus R_{CF} relations.

(ii) Establishment of the performance and design characteristics of the cell-emptying process consisting of the $\Delta^P_{CE/p_{XCE}}$ versus R_{CE}, $\Delta^P_{CE/p_{1CE}}$ versus R_{CE} and τ_{CE} versus R_{CE} relations.

(iii) Establishment of the performance and design characteristics for a given scavenge ratio of the high-pressure scavenge process consisting of $\Delta^P_{HP/p_{1HP}}$ versus R_{HP}, τ_{HPout} versus R_{HP}, ϕ_{HP} versus R_{HP} and A_{HP} versus R_{HP} relations.

(iv) Establishment of the performance and design characteristic for a given scavenge ratio of the low-pressure scavenge process consisting of $\Delta^P_{LP/p_{XLP}}$ versus R_{LP}, τ_{LPin} versus R_{LP}, ϕ_{lp} versus A_{LP} and A_{LP} versus R_{LP} relations. A_{LP} has been assumed to remain unity in the present calculations.

(v) Establishment of the transfer characteristics from the cell filling and cell emptying characteristics consisting of $\Delta^P_{TP/p_{2CF}}$ versus $\Delta^P_{TP/p_{1CF}}$ relations.

(vi) Calculation of pressure exchanger cycle performances with the help of the component characteristics which have been established in the steps (i) to (v) and presented in Figs. (12.1 to 12.12 & 12.100) for unity scavenge ratios and no temperature discontinuities.

The method may be extended to include various scavenge ratios and temperature discontinuities in the pressure exchanger cycles.

The pressure differential method is described in Appendix III.

4.4 Application of the Method of Characteristics to the studies of pressure exchangers

The physical laws of mass, momentum and energy conservation governing unsteady compressible fluid flow pressure exchanger in a cell, with friction, heat transfer and leakage, in combination with the thermodynamic properties of the fluid result in a set of three hyperbolic partial differential equations. With a knowledge of the initial conditions in the cell, the boundary conditions at the cell ends and the estimated frictional forces, heat flows and the mass injection, or removal, at the cell walls, a solution of these equations predicts the transient motion of the fluid in the pressure exchanger cell.

The method of characteristics is in fact one of the three numerical solution procedures to solve the set of these differential equations. Although the procedure adapted in this work is not the pure method of characteristics, we shall still sometimes refer to it as the method of characteristics to differentiate it from the Approximate and the Pressure Differential Method.

4.4.1 Numerical solution procedures

The following three solution procedures have been used to solve the governing set of equations for the unsteady compressible fluid flow.

(a) The Method of Characteristics

This method is based on the general properties of the partial differential equations of hyperbolic type. The basic principle involved in this method is the transformation of the basic equations, with the help of the thermodynamic relations to the characteristic forms containing the well-known Riemann variables. The Riemann variables are the disturbances moving along lines of definite slopes in the x-t plane. These curves, displaying the disturbances in the flow field, form a network of lines which cover the domain of

integration and consist in general of three sets of curves such that the lines of one particular set do not intersect each other, whereas the lines of two different sets do. The method is considerably simplified for an isentropic flow in which case one set of curves is completely eliminated.

For non-isentropic flow this method poses certain problems. Firstly, the intersections of the characteristics do not always coincide with the points along which the boundary conditions are specified thus requiring an interpolation procedure, secondly the three characteristics do not necessarily coincide all at one point.

(b) The Finite-Difference Method

Finite difference methods usually employ a fixed grid system in which the grid points lie at the intersections of constant x and constant t lines. The application of a finite difference method often gives unrealistic results. The reason for this is the fact that the network formed by the characteristics perhaps the only natural grid for these types of flow and the employment of the fixed grid system results in physically unrealistic interpolation. Patankar (24) describes a finite-difference fixed-grid procedure for the calculations of unsteady compressible flows based on a newly developed technique for three-dimensional parabolic flows.

(c) The Hybrid Method

The hybrid method originally developed by Hartree (25) is regarded as a combination of the better aspects of the method of characteristics and the finite difference method. It uses a fixed grid system but the values of the dependent variables at the grid points are calculated utilising the special features of the characteristic equations. Thus this method provides a fixed grid

which can be arranged for convenience of the analysis, without losing the valuable information supplied by the characteristic curves. In the following section the hybrid method is described.

4.4.2 The mathematical model

The basic equations

The equations of conservation of mass, momentum and energy for the flow process in a pressure exchanger cell of constant and uniform area, with friction, heat transfer, and mass leakage are as follows:

$$\frac{\partial \rho}{\partial t} + \frac{\partial}{\partial x}(\rho u) = -\psi/A \qquad (4.4.1)$$

$$\frac{\partial}{\partial t}(\rho u) + \frac{\partial}{\partial x}(\rho u^2 + p) = -f \qquad (4.4.2)$$

$$\frac{\partial}{\partial t}\{\rho(h - p/\rho + u^2/2)\} + \frac{\partial}{\partial x}\{\rho u(h + u^2/2)\} = q - \psi/A\, h_{o\ell} \qquad (4.4.3)$$

where ρ = density of fluid

u = velocity of fluid

p = pressure of fluid

h = specific enthalpy of fluid

f = friction force (in negative x-direction) per unit volume of fluid

q = heat transfer rate to fluid per unit volume

ψ = mass leakage rate per unit length of the cell (perpendicular to the main flow and positive outflow)

A = cell cross-sectional area

These three equations, in conjunction with the thermodynamic relations for the perfect-gas (an assumption which need not be applied unless desired) and with the introduction of new variables P, U and σ can be manipulated to give the final form of equations in a non-dimensionalised form.

$$\frac{\partial}{\partial t}(P\sigma + U) + (u + a)\frac{\partial}{\partial x}(P\sigma + U) = D + \frac{E\partial s}{\partial x} - G - B1$$

$$- B2 + B3 - B4 + B5 \qquad (4.4.4)$$

$$\frac{\partial}{\partial t}(P\sigma - U) + (u - a)\frac{\partial}{\partial x}(P\sigma - U) = D - \frac{E\partial s}{\partial x} + G - B1$$

$$- B2 + B3 - B4 - B5 \qquad (4.4.5)$$

$$\frac{\partial \sigma}{\partial t} + u\frac{\partial \sigma}{\partial x} = \sigma(F - B2 + B3 - B6) \qquad (4.4.6)$$

New terms have been introduced into the equations for simplification. These are given by ($\psi' = \beta\psi$)

$$P = p^{\frac{\gamma-1}{2\gamma}} \qquad (4.4.7)$$

$$U = \frac{\gamma-1}{2}u \qquad (4.4.8)$$

$$\sigma = \exp\left(\frac{\gamma-1}{2\gamma}s\right) \qquad (4.4.9)$$

$$D = \frac{\gamma-1}{2}\frac{a}{p}(q + uf) \qquad (4.4.10)$$

$$E = \frac{\gamma-1}{2\gamma}a^2 \qquad (4.4.11)$$

$$F = \frac{\gamma-1}{2\gamma} \left(\frac{q+uf}{p}\right) \tag{4.4.12}$$

$$G = \frac{\gamma-1}{2\gamma} \frac{a^2 f}{p} \tag{4.4.13}$$

$$B1 = \frac{\gamma-1}{2} \frac{a}{\rho} \psi'_A \tag{4.4.14}$$

$$B2 = \frac{\gamma-1}{2} \frac{a^2}{p} (h_\ell + u^2_{\ell}/2) \psi'_A \tag{4.4.15}$$

$$B3 = \frac{\gamma-1}{2} \frac{a^2}{p} (h + U^2/2) \psi'_A \tag{4.4.16}$$

$$B4 = \gamma \frac{\gamma-1}{2} a/p \ (u^2 \psi'_A) \tag{4.4.17}$$

$$B5 = \frac{\gamma-1}{2} \frac{a^2}{p} u\psi'_A \tag{4.4.18}$$

$$B6 = u^2/p \ \psi'_A \times \frac{\gamma-1}{2} \tag{4.4.19}$$

These equations are derived in Appendix IV..

(b) The initial conditions

To commence to obtain a solution of the differential equations it is first necessary to specify the initial conditions in the pressure exchanger cell, which means the specification of the distribution of the three variables P, U and σ each as a function of the spatial coordinate x' for $\tau = \tau_{initial}$. In all cases $\tau_{initial} = 0$.

In many unsteady flow problems the initial conditions are known from the physical description of the problem, for example, the fluid may be at rest and will be of a uniform entropy. But in pressure exchanger problems the unsteady flow is cyclic and the fluid will neither be at rest nor be of a uniform entropy at the start of a cycle and without knowing the solution in advance it is impossible to specify

correctly the required information. In such cases it is usual to make a simplified, physically reasonable, guess at the initial conditions and to perform successive calculations until equilibrium conditions have been established. The equilibrium conditions are established when the final cell conditions are found to be the same as the initial cell conditions for the last cycle.

The cycle calculations can be started with the pressure exchanger cell in any position relative to ports during its rotation. It is most appropriate to start the cycle calculations for four port pressure exchangers with and without transfer passages when the cell is just receding from the low pressure scavenge section. The conditions in the cell in this position are very nearly atmospheric due to a long exposure to the low pressure ports. Therefore, a reasonable guess at the initial conditions in the cell in such a position would be to assume the pressure and temperature to be atmospheric and the fluid velocity to be zero. Successive cycle calculations are then carried out until equilibrium conditions are achieved.

When large temperature discontinuities are involved and scavenge ratios are not equal to unity, the initial temperature in the cell at the start of a cycle will not be nearly atmospheric. In such cases the value of the initial temperature is assumed to be equal to the weighted mean of the peak and the atmospheric temperatures.

(c) The boundary conditions

The following list gives the different boundary conditions which may exist at the cell ends.

(i) Cell closed.

(ii) Cell fully open, subsonic outflow.

(iii) Cell fully open, sonic outflow.

(iv) Cell partly open, subsonic outflow.

(v) Cell partly open, sonic outflow.

(vi) Cell fully open, subsonic inflow.

(vii) Cell fully open, sonic inflow.

(viii) Cell partly open, subsonic inflow.

(ix) Cell partly open, sonic inflow.

Relationships have to be derived for each case to supplement the available equations for solving the flow conditions at the cell ends. These relationships are usually derived based on an approach by Jenny (8). The derivation of these equations are fully described by Spalding (13).

The new parameters which are involved in the calculation procedures for the cell ends are as follows.

(i) The area ratio of the cell opening denoted by ϕ defined as the proportion of the cell area which can be regarded as free for inflow or outflow. In the present procedure the opening fraction ϕ is assumed to vary linearly with time from 0 to 1 being unity when the cell is fully open.

(ii) The pressure and temperature in the inlet ports are usually specified as the stagnation values, P_o and T_o respectively denote these values.

(iii) For outflow the pressure recovery is usually neglected and the static pressure in the port is described which is denoted by p_x.

The following notation is used for the pressure ratios in inflow and outflow respectively.

$$\xi = \frac{P_o}{P} \qquad \text{Inflow} \qquad (4.4.20)$$

$$\zeta = \frac{P_{\sim}}{P} \qquad \text{Outflow} \qquad (4.4.21)$$

where P, unsubscripted, represents the static pressure at the cell

boundary. Obviously $\xi > 1$ and $\zeta < 1$ are the valid regions for inflow and outflow respectively. P_o and P_x are related to p_o and p_x by a relationship similar to (4.4.7). The terms inflow and outflow are used with respect to the cell.

Outlets

Assumptions implicit in the setting up of boundary conditions for outlets are as follows:

(i) Wall friction and heat transfer are absent in the outlet region.

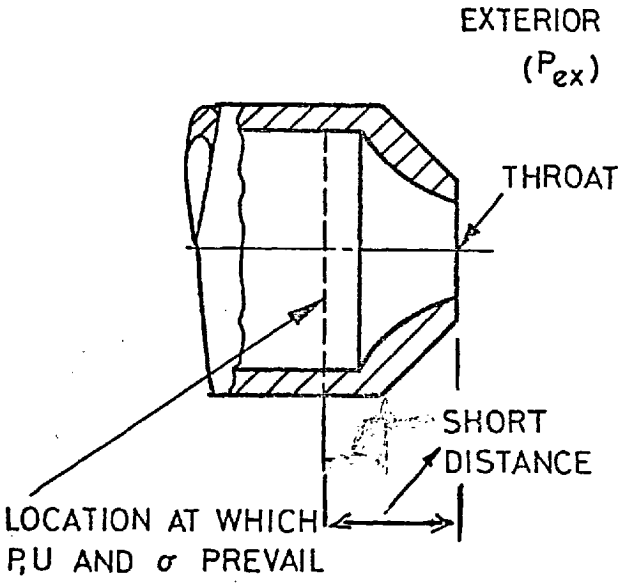
(ii) Flow out of a fully or partly open outlet is assumed to be isentropic (up to the throat of the exit).

(iii) Vena contracta effects are absent.

(iv) The axial distance occupied by the outlet and its associated flow field is small compared with the length of the cell.

(v) Flow is one-dimensional in the vicinity of the outlet.

The assumed geometry of an outlet is shown in the following sketch.



a) OUTFLOW

Fig. 4.4.1

Critical pressure ratio

The condition for sub-critical flow, i.e. $u < a$ is

$$p_x \geq a^{\frac{2\gamma}{\gamma-1}} e^{-s} \left[\left(\frac{2}{\gamma+1}\right) + \left(\frac{\gamma-1}{\gamma+1}\right)\left(\frac{u}{a}\right)^2\right]^{\frac{\gamma}{\gamma-1}} \qquad (4.4.22)$$

or in terms of new dependent variables is

$$\zeta \geq \sqrt{\left(\frac{2}{\gamma+1}\right)\left[1 + \left(\frac{2}{\gamma-1}\right)\left(\frac{U}{P\sigma}\right)^2\right]} \qquad (4.4.23)$$

Subsonic Flow

(i) Fully open port

If the port is fully open $P_x = P$ and so the boundary condition in this case is

$$P = P_x \qquad (4.4.24)$$

(ii) Partly open port

For a partly open port the following relationship is used to supplement the available equations.

$$\left(\frac{u}{a}\right)^2 = \left(\frac{2}{\gamma-1}\right)\left[1 - \left(\frac{p}{p_x}\right)^{\frac{1-\gamma}{\gamma}}\right] / 1/\phi_2 \left(\frac{p}{p_x}\right)^{2/\gamma} - 1 \qquad (4.4.25)$$

or in terms of new dependent variables

$$\left(\frac{U}{P\sigma}\right)^2 = \frac{\gamma-1}{2}(1 - \zeta^2) / 1/\phi_2 \; \zeta^{\frac{-4}{\gamma-1}} - 1 \qquad (4.4.26)$$

Sonic Flow

If condition (4.4.23) is not satisfied, the flow is sonic.

(i) Fully open outlet

Sonic flow through a cell of constant cross-section implies

$$u = a \qquad (4.4.27)$$

Hence, if the port is fully open

$$\left(\frac{U}{P\sigma}\right) = \frac{\gamma-1}{2} \qquad (4.4.28)$$

(ii) Partly-open outlet

Applying continuity to choked isentropic flow through a a constriction gives the relationship

$$\frac{u}{a} = \phi\left[\frac{2}{\gamma+1} + \left(\frac{\gamma-1}{\gamma+1}\right)\left(\frac{u}{a}\right)^2\right]^{\frac{\gamma+1}{2(\gamma-1)}} \qquad (4.4.29)$$

In terms of new variables

$$\frac{U}{P\sigma} = \phi\left(\frac{\gamma-1}{2}\right)\left[\left(\frac{2}{\gamma+1}\right)\left\{1 + \left(\frac{2}{\gamma-1}\right)\left(\frac{U}{P\sigma}\right)^2\right\}\right]^{\frac{1}{2}\left(\frac{\gamma+1}{\gamma-1}\right)} \qquad (4.4.30)$$

In all these relationships the entropy variables σ is calculated from the entropy equation (4.4.6)

Inflow

The assumptions relating to the inlet boundary conditions are as follows.

(i) Wall friction and heat transfer as absent in the inlet region.

(ii) Flow into a fully open inlet is assumed to be isentropic.

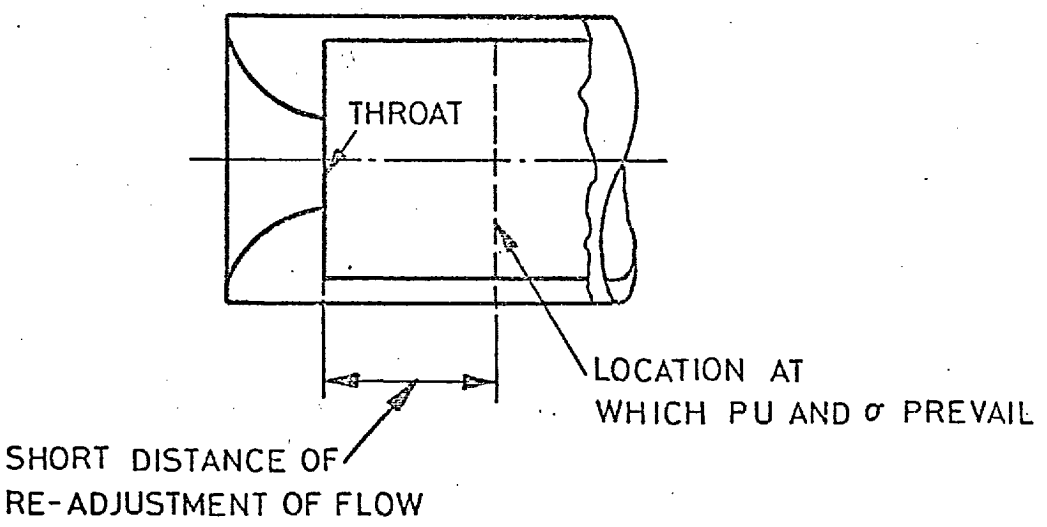
(iii) Flow from the port upto the throat of the inlet restriction is assumed to be isentropic.

(iv) Vena-contracta effects are ignored.

(v) The axial distance occupied by the inlet and its associated flow field is small compared with the length of the cell.

(vi) Flow is one-dimensional in the vicinity of the inlet.

The following sketch represents an inlet pictorially.



b) INFLOW

Fig. 4.4.2

In the following relationships the static pressure recovery downstream of the throat is neglected.

Critical Pressure Ratio

The condition for subcritical inflow is:

$$p_o < \left(\frac{\gamma-1}{2}\right)^{\frac{\gamma}{\gamma-1}} a^{\frac{2\gamma}{\gamma-1}} e^{-s} \qquad (4.4.31)$$

which in terms of P reduces to

$$\xi = \sqrt{\frac{\gamma+1}{2}} \qquad (4.4.32)$$

Subsonic Inflow

(i) Fully open inlet

Flow through a constant cross-section is isentropic, hence for fully open ports:

$$S = S_o \qquad (4.4.33)$$

or $$\sigma = \sigma_o \qquad (4.4.34)$$

and

$$p_o = \frac{a^{\frac{2\gamma}{\gamma-1}} e^{-s}}{\left[1-\left(\frac{\gamma-1}{2}\right)\left(\frac{u}{a_o}\right)^2\right]^{\gamma/\gamma-1}} \qquad (4.4.35)$$

which reduces to

$$\left(\frac{U}{a_o}\right)^2 = \left(\frac{\gamma-1}{2}\right)(1 - \xi^2) \qquad (4.4.36)$$

where

$$a_o = P_o \sigma_o. \qquad (4.4.37)$$

(ii) Partly-open inlet

The relationship between velocity and pressure is

$$\frac{\left(\frac{u}{a_o}\right)}{1-\left(\frac{\gamma-1}{2}\right)\left(\frac{u}{a_o}\right)^2} = \phi\left(\frac{P_o}{p}\right)^{\frac{\gamma-1}{2\gamma}} \sqrt{\left(\frac{2}{\gamma-1}\right)\left[\left(\frac{p_o}{p}\right)^{\frac{\gamma-1}{\gamma}} - 1\right]} \qquad (4.4.38)$$

which in terms of new dependent variables is

$$\frac{\left(\frac{U}{a_o}\right)}{\left(\frac{\gamma-1}{2}\right) - \left(\frac{U}{a_o}\right)^2} = \phi\, \xi \sqrt{\left(\frac{2}{\gamma-1}\right)\left[\xi^2 - 1\right]} \qquad (4.4.39)$$

The entropy is given by:

$$S = \ln\left\{\left(\frac{p_o}{p}\right)\left[1 - \left(\frac{\gamma-1}{2}\right)\left(\frac{u}{a_o}\right)^2\right]^{\left(\frac{\gamma}{\gamma-1}\right)}\right\} + S_o \qquad (4.4.40)$$

or

$$\sigma = \sigma_o\, \xi \sqrt{1 - \left(\frac{2}{\gamma-1}\right)\left(\frac{U}{a_o}\right)^2} \qquad (4.4.41)$$

Sonic Inflow

If condition (4.4.32) is not satisfied, the following relations apply

(i) Fully-open inlets

$$\sigma = \sigma_o \tag{4.4.42}$$

and u/a is unity hence,

$$p_o = a^{\frac{2\gamma}{\gamma-1}} e^{-s} \left(\frac{\gamma+1}{2}\right)^{\gamma/\gamma-1} \tag{4.4.43}$$

which reduces to

$$\xi = \sqrt{\frac{\gamma+1}{2}} \tag{4.4.44}$$

(ii) Partly-open inlets

For choked flow the relation is

$$\frac{\frac{u}{a_o}}{1-\left(\frac{\gamma-1}{2}\right)\left(\frac{u}{a_o}\right)^2} = \phi\left(\frac{2}{\gamma+1}\right)^{\frac{1}{2}\left(\frac{\gamma+1}{\gamma-1}\right)} \frac{p_o}{a\left(\frac{2\gamma}{\gamma-1}\right) e^{-s}} \tag{4.4.45}$$

and this in terms of dependent variable is

$$\frac{\left(\frac{U}{a_o}\right)}{\left(\frac{\gamma-1}{2}\right) - \left(\frac{U}{a_o}\right)^2} = \phi\left(\frac{2}{\gamma+1}\right)^{\frac{1}{2}\left(\frac{\gamma+1}{\gamma-1}\right)} \xi^{\left(\frac{2\gamma}{\gamma-1}\right)} \tag{4.4.46}$$

The entropy is given by

$$S = \ln\left\{\frac{1}{\phi}\left(\frac{\gamma+1}{2}\right)^{\frac{1}{2}\left(\frac{\gamma+1}{\gamma-1}\right)} \frac{u}{a_o}\left[1 - \left(\frac{\gamma-1}{2}\right)\left(\frac{u}{a_o}\right)^2\right]^{\frac{1}{\gamma-1}} + S_o \right. \tag{4.4.47}$$

or

$$\sigma = \sigma_o \left[\frac{1}{\phi}\left(\frac{\gamma+1}{2}\right)^{\frac{1}{2}\left(\frac{\gamma+1}{\gamma-1}\right)} \left(\frac{2}{\gamma-1}\right)\left(\frac{u}{a_o}\right)\right]^{\frac{\gamma-1}{2\gamma}} \left[1 - \frac{2}{\gamma-1}\left(\frac{U}{a_o}\right)^2\right]^{1/2\gamma} \tag{4.4.48}$$

Inflow with Pressure Recovery

The assumption that the static pressure in the unsteady duct flow adjacent to an inlet is equal to the static pressure in the inlet throat for subsonic flow can be relaxed by introducing the

conservation of momentum consideration. It is assumed that the throat static pressure acts over the entire back face of the throat thus enabling the static pressure recovery downstream to be calculated from conservation equations. These relationships were first proposed and derived by Cotter (19), for pressure exchanger applications.

Critical Pressure Ratio

The condition for sub-sonic flow takes the form

$$p_o < \left(\frac{\gamma+1}{2}\right)^{\frac{\gamma}{\gamma-1}} \left[1 + \frac{\gamma+1}{2}\left(\frac{u}{a_o}\right)^2\right] a^{\frac{2\gamma}{\gamma-1}} e^{-s} \qquad (4.4.49)$$

$$/1+\phi\gamma\left[1-\tfrac{\gamma-1}{2}\left(\tfrac{u}{a_0}\right)^2\right]$$

or in terms of new dependent variables

$$\xi^{\frac{2\gamma}{\gamma-1}} < \frac{\left(\frac{\gamma+1}{2}\right)^{\frac{\gamma}{\gamma-1}} \left[1 - \frac{2(\gamma+1)}{(\gamma-1)^2}\left(\frac{U}{a_o}\right)^2\right]}{(1+\phi\gamma)\left[1 - \left(\frac{2}{\gamma-1}\right)\left(\frac{U}{a_o}\right)^2\right]} \qquad (4.4.50)$$

Subsonic Inflow

The flow relationship is expressed in the form of two simultaneous equations

$$\frac{1 + \phi\gamma\left(\frac{u_i}{a_i}\right)^2}{1 + \frac{\gamma-1}{2}\left(\frac{u_i}{a_i}\right)} \frac{\gamma}{\gamma-1} = \frac{p}{p_o}\left[\frac{1 + \frac{\gamma+1}{2}\left(\frac{u}{a_o}\right)^2}{1 - \frac{\gamma-1}{2}\left(\frac{u}{a_o}\right)^2}\right] \qquad (4.4.51)$$

and

$$\frac{\left(\frac{u}{a_o}\right)}{1 + \frac{\gamma+1}{2}\left(\frac{u}{a_o}\right)^2} = \frac{\phi\left(\frac{u_i}{a_i}\right)\sqrt{1 + \left(\frac{\gamma-1}{2}\right)\left(\frac{u_i}{a_i}\right)^2}}{1 + \phi\gamma\left(\frac{u_i}{a_i}\right)^2} \qquad (4.4.52)$$

where subscript i refers to conditions in the throat. The term $\left(\frac{u_i}{a_i}\right)$ can be eliminated from the pair of equations.

In terms of the new dependent variables

$$\frac{1 + (\frac{2}{\gamma-1})^2 \phi\gamma(\frac{U_i}{a_i})^2}{1 + (\frac{2}{\gamma-1})(\frac{u_i}{a_i})^2} = (\frac{1}{\xi})^{\frac{2\gamma}{\gamma-1}} \left[\frac{1 + \frac{2(\gamma+1)}{(\gamma-1)^2}(\frac{U}{a_o})^2}{1 - (\frac{2}{\gamma-1})(\frac{U}{a_o})^2}\right] \qquad (4.4.53)$$

and

$$\frac{(\frac{U}{a_o})}{1 + \frac{2(\gamma+1)}{(\gamma-1)^2}(\frac{U}{a_o})^2} = \frac{\phi(\frac{U_i}{a_i})\sqrt{1 + (\frac{2}{\gamma-1})(\frac{U_i}{a_i})^2}}{1 + (\frac{2}{\gamma-1})^2 \phi\gamma(\frac{U_i}{a_i})^2} \qquad (4.4.54)$$

The entropy relation is given by (4.4.41). The boundary conditions for fully open port and also for sonic flows remain same as those derived for inlet without pressure recovery.

Closed Ports

This boundary condition obviously implies

$$U = 0. \qquad (4.4.55)$$

Entropy variable is calculated from equation

Boundary conditions in Transfer Ports

Whereas the boundary conditions at the high and low pressure scavenging ports of a four port pressure exchanger are determined from the values of overall pressure ratio, temperature ratio, the pressure drop in the high pressure loop, the degree of diffusion in low pressure outlet port and atmospheric conditions, the boundary conditions in the transfer ports cannot be specified as such. These conditions include:

(i) The values of p_o and T_o at the filling port.

(ii) The value of p_x at the emptying port.

These values can only be determined by a trial and error procedure until the mass continuity in the transfer passage is satisfied. The values of pressure and temperature in the filling and emptying ports of a transfer passage are also related to each other and this

relationship depends upon the energy degradation in the transfer passage. The transfer passage calculations are based on the assumption that the flow in the passage is steady.

The calculation procedure is simplified if friction, heat transfer and minor losses in the transfer passage are neglected. In such an ideal transfer passage the stagnation values of pressure p_o and temperature T_o in the filling and emptying ports are equal. Starting with this assumption, the boundary conditions are obtained by successive cycle calculations until the mass conservation in the transfer passage is satisfied. These boundary conditions are then modified to accommodate the losses in the transfer passage calculated on the basis of the ideal transfer passage values. Pressure differential method is used to give the first approximation of the stagnation pressures in transfer ports.

The stepwise procedure to obtain the boundary conditions in transfer ports is described in Appendix V.

4.4.3 The numerical procedure for the hybrid method

In this section the numerical procedure which has been adopted to solve the differential equations in conjunction with the boundary conditions is described.

An explanation of the grid and the geometric relation between the points which have to be considered during a forward step in time is followed by a derivation of the integral equations along the respective characteristics. The finite difference formulae are then derived and the calculations at the boundary points are explained.

(a) The grid and an outline of the procedure

Fig. (13.10) shows the grid and an outline of the calculation procedure at the central points in the grid and also at the boundary points.

For all central points the following procedure applies.

As shown in Fig. (13.10) our task is to calculate the values of P, U and σ at the point P given in the values of these variables at the adjacent points T, U, and W located at the previous time step. Firstly, characteristics QP, RP and SP are drawn. Their slopes are $1/(u+a)$, $1/(u-a)$, and $1/u$ respectively. The slopes are calculated from the average of the values of the variables u and a at the two points selected from T, U and W such that the feet of the respective characteristics lie between them. The values P, U and σ at points Q, R and S are calculated by interpolating between the two surrounding points. Increments in $P\sigma + U$, $P\sigma - U$ and σ are now obtained from the relevant integral equation. The calculation of the values of P, U and σ at P is then a simple matter.

At the boundary points some of the information is missing. Fig. (13.11) shows an outflow from a left-hand boundary. In this case the "n" characteristics is missing and therefore additional information in the form of the boundary condition is needed to make up for the insufficient information. Fig. (13.12) shows an inflow from a left-hand boundary. In this case the "n" characteristics and the path characteristic both are missing and hence again the given information has to be supplemented by the boundary conditions. Similar considerations apply to inflow and outflow from the right-hand boundary.

(b) The stability Criterion

The stability criterion for the numerical solution procedure under consideration is given by the following relationship:

$$\frac{\Delta T}{\Delta X} = \frac{1}{A + |U|} \qquad (4.4.56)$$

This stability criterion makes the solution procedure unconditionally stable. It was developed by Courant et al. (37) . The physical

reasoning for this stability condition is very simple. The values of P, σ and U at P are calculated from the values of these variables at points T, U and W. It would be physically unreasonable to have point P outside the zone of dependence of points T and W which is defined by the zone enclosed between TW and the characteristics drawn from T and W respectively. The condition that P must lie within the zone of dependence is only fulfilled when the stability criterion is satisfied. The stability criterion for numerical solution methods of the hybrid type for unsteady flows was also discussed by Benson et al. (12).

(c) The calculation procedure

The calculation procedure involves the following three steps:

(i) The locations of the feet of characteristics (points Q, R and S in Fig. (13.10)) along the x-direction and hence their x-coordinates are determined by drawing characteristics PQ, PR and PS with slopes $2/(u_T + a_T + u_U + a_U)$, $2/(u_T + u_U)$ if R lies to the left of U and $2/(u_W + u_U)$ if R lies to the right of U, and $2/(u_W + a_W + u_U + a_U)$ respectively.

The x-coordinate of points $\mathcal{Q}$, $\mathcal{R}$ and $\mathcal{S}$ are given by the following relations

$$x_Q = x_U - (\bar{u} + \bar{a})\delta t \qquad (4.4.57)$$

$$x_R = x_U - \bar{u}.\delta t \qquad (4.4.58)$$

$$x_S = x_U - (\bar{u} - \bar{a})\delta t \qquad (4.4.59)$$

(ii) The locations of the feet of characteristics having been determined, the next task is to determine the values of $P\sigma + U$, $P\sigma - U$ and σ at points Q, R and S (the values of

P, σ and U need not be known at these points). This is done by simple linear interpolation. More complex numerical interpolation procedures may be employed if so desired.

(iii) The final task is to calculate the values of P, U and σ at point P given the values of $P\sigma + U$, $P\sigma - U$ and σ at points Q, R and S respectively. The increments $\delta(P\sigma + U)$, $\delta(P\sigma - U)$ and $\delta(\sigma)$ are obtained by integrating equations (4.4.4, 4.4.5 & 4.4.6) along the characteristics PQ, PR and PS respectively to obtain the values of $P\sigma + U$, $P\sigma - U$ and σ at point P. The calculation of P, σ and U at P is now a simple problem. The integration of equations along their respective characteristic gives

$$P_P\sigma_P + U_P = PQ\sigma Q + U_Q + \int_Q^P E\frac{\partial\delta}{\partial x}\,dt + \int_Q^P (D-G-B1-B2+B3-B4+B5)dt \qquad (4.4.60)$$

$$P_P\sigma_P - U_P = PS\sigma S - US - \int_S^P E\frac{\partial\delta}{\partial x}\,dt + \int_S^P (D+G-B1-B2+B3-B4-B5)dt \qquad (4.4.61)$$

$$\sigma_P = \sigma R + \int_R^P \sigma(F-B2+B3-B6)dt \qquad (4.4.62)$$

These equations contain integrals on the right-hand side which have to be evaluated before they can be solved for point P. The integrals containing D, G, F and B_S are known as the loss terms. They can be converted into simple averages and their evaluations are described in section Considering the term involving the entropy term $\frac{E\partial\delta}{\partial x}$, it can

be evaluated from the relationship given by Issa (26)

$$\int_Q^P E\frac{\partial \delta}{\partial x}\,dt = \tfrac{1}{2}(P_P + P_Q)(\sigma_P - \sigma_Q) - \frac{1}{\gamma}\int_Q^P D\,dt + \frac{1}{\gamma}\int_Q^P B4\,dl \qquad (4.4.63)$$

$$-\int_S^P E\frac{\partial \delta}{\partial x}\,dt = \tfrac{1}{2}(P_P + P_S)(\sigma_P - \sigma_S) - \frac{1}{\gamma}\int_S^P D\,dt + \frac{1}{\gamma}\int_S^P B4\,dl \qquad (4.4.64)$$

These equations when substituted in equations (4.4.60) and (4.4.61) gives: $(B4' = \frac{\gamma-1}{\gamma} B4)$

$$P_P\sigma_P + U_P = P_Q\sigma_Q + U_Q + \tfrac{1}{2}(P_P + P_Q)(\sigma_P - \sigma_Q) + \int_Q^P (\frac{\gamma-1}{\gamma} D - G - B1-B2+B3-B4'+B5)\,dt \qquad (4.4.65)$$

$$P_P\sigma_P - U_P = P_S\sigma_S - U_S + \tfrac{1}{2}(P_P + P_S)(\sigma_P - \sigma_S) + \int_S^P (\frac{\gamma-1}{\gamma} D - G - B1-B2+B3-B4'-B5)\,dt \qquad (4.4.66)$$

and changing from the integral form to an average form:

$$P_P\sigma_P + U_P = P_Q\sigma_Q + U_Q + \tfrac{1}{2}(P_P + P_Q)(\sigma_P - \sigma_Q) + (\frac{\gamma-1}{\gamma} D - G - B1-B2+B3-B4'+B5)_{QP}\delta t \qquad (4.4.67)$$

$$P_P\sigma_P - U_P = P_S\sigma_S - U_S + \tfrac{1}{2}(P_P + P_S)(\sigma_P - \sigma_S) + (\frac{\gamma-1}{\gamma} D + G - B1-B2+B3-B4'-B5)_{SP}\delta t \qquad (4.4.68)$$

and a proper manipulation of these equations leads to the

final form:

$$P_P = \{\tfrac{1}{2}(\sigma_P + \sigma_Q) + \tfrac{1}{2} P_S(\sigma_P + \sigma_S) + U_S + (\tfrac{\gamma-1}{\gamma} D - G - B1-B2 +B3-B4+B5)_{QP}\delta t + (\tfrac{\gamma-1}{\gamma} D + G - B1-B2+B3-B4-B5)_{SP}\delta t\} /\{\sigma_P + \tfrac{1}{2}(\sigma_Q + \sigma_S)\} \quad (4.4.69)$$

$$U_P = \left[\tfrac{1}{2}P_Q - \tfrac{1}{2}P_S + U_Q/(\sigma_P + \sigma_Q) + U_S/(\sigma_P + \sigma_S) + \{(\tfrac{\gamma-1}{\gamma} D - G - B1-B2+B3-B4+B5)_{QP}\delta t/(\sigma_P + \sigma_Q)\} + \{(\tfrac{\gamma-1}{\gamma} D + G - B1-B2 +B3-B4-B5)_{SP}\delta t/(\sigma_P + \sigma_S)\}\right] /\left[(1/\sigma_P + \sigma_S) + (1/\sigma_P + \sigma_Q)\right] \quad (4.4.70)$$

$$\sigma_P = \sigma_R \times \{2 + (F-B2+B3-B6)_{RP}\delta t\}/\{2 \mp (F-B2+B3-B6)_{RP} \times \delta t\} \quad (4.4.71)$$

Equation (4.4.71) is used to calculate σ_P. This value in conjunction with equations (4.4.70) and (4.4.69) is then used to calculate P_P and U_P.

At the grid points at the boundaries, all of the finite-difference formulae are not applicable. For a left-hand boundary equation (4.4.68) in conjunction with the appropriate boundary conditions is used to calculate the flow variables at that point. For a right-hand boundary equation (4.4.67) in conjunction with appropriate boundary conditions is used to calculate the flow variable at that point.

5. Performance losses in pressure exchangers

In the following sections various performance losses in pressure exchangers are examined and different methods of taking these losses into account are described.

5.1 Entropy losses due to shock waves

Shock waves are non-isentropic. The differential equations derived for flow processes in unsteady flow do not allow for shock waves. Issa (26) has shown that isentropic losses due to shock waves are significant only at pressure ratios much higher than the pressure ratios at which pressure exchangers are normally operated. Therefore, entropy losses in pressure exchangers due to shock waves can be neglected.

5.2 Finite cell width

Due to a finite width, the pressure exchanger cell takes a finite time to open or close. The main effect of finite cell width is to spread out the pressure waves. Finite cell width effects are generally handled by using Jenny's (8) method. The boundary conditions take account of these effects.

5.3 Frictional losses

Viscous effects in pressure exchangers are due to:

(i) Cell wall friction

(ii) Cell entry and exit losses

The mechanism of frictional effects in unsteady flow are extremely complex even for a single shock wave. Emrich & Wheeler (27) give a review of shock attenuation theories. Trimpi & Cohen (28) and Mirels (29) presented different approaches to this problem. Cotter (19) combined the better aspects of both the theories to predict the frictional effects on cell-filling and cell-emptying performance.

In the present work frictional effects have been estimated in the following way:

5.3.1 Cell Wall Friction

Referring back to the governing equations in section the factor f represents the friction force per unit volume of the fluid. It is necessary to provide a reasonable estimate of its value. In Appendix V , it has been shown that this parameter is given by the following relation

$$f = {}^{4}/_{d_h}\, \gamma\, C_f\, P\, u|u| \qquad (5.3.1)$$

where

d_h = hydraulic diameter of the cell

C_f = co-efficient of friction.

Bakhtar (30) has shown that a reasonable estimate of the local value of C_f is given by the following relationnship for the turbulent pipe flow

$$C_f = \text{constant}/R_e^{0.214} \qquad (5.3.2)$$

The best value of the constant term in equation (5.3.2) has been found by Issa (26) based on comparison with experimental results by Glass (31) to be equal to 0.035. Hence;

$$C_f = 0.035/R_e^{0.214} \qquad (5.3.3)$$

The calculation of Reynolds number is based on the hydraulic diameter of the cell and the local flow variables. The value of f can now be estimated.

5.3.2 Cell entry and exit losses

Steady flow loss data is used to estimate the head loss due to the sudden enlargement of area for an outflow and sudden contraction of area for an inflow in the pressure exchanger cells due to the

unstreamlined entry and exit shapes. The contraction and enlargement ratios are based on the cell area and the cell annulus area. The total head loss at any instant of time during the solution procedure is calculated on the basis of conditions prevailing at the cell ends at that moment.

An apparent co-efficient of friction based on the total head loss is calculated using the well known equation

$$C_f = S\not{x}(\ell/d_h) \qquad (5.3.4)$$

The apparent co-efficient of friction is added to the co-efficient of friction given by (5.3.3) and the resultant co-efficient is then used to calculate the value of f from equation (5.3.1).

5.4 Leakage losses

Leakage in pressure exchangers occurs through the gap between the rotor and its end plates. It is a complex phenomenon as it induces a three-dimensional flow in the vicinity of the gap. It can be classified as follows:-

(i) Circumferential Leakage

This type of leakage includes leakage between adjacent cells, from cell to a port and vice versa.

(ii) Radial Leakage

This type of leakage includes leakage in the radial direction through the inner and outer rims of the rotor to the leakage sink and vice versa.

Fig. (13.13) shows various possible combinations of leakage flows at a cell end.

The performance of pressure exchangers is effected by leakage in the following ways:-

(a) There is a net loss of energy due to leakage.

(b) The pressure waves in the rotor are weakened.

(c) The mass and energy flows through the ports are altered.

Three different methods have been tried to study leakage in pressure exchangers in the present work. These methods are discussed in the following sections.

5.4.1 Calculation of the Leakage Flows

The fundamental assumptions for leakage flow calculations are as follows:-

(i) Leakage flow through the gap between the rotor and its end plates is assumed to be a quasi-steady one-dimensional flow through an orifice whose area is equal to the clearance area. Vena-contracta effects are taken into account by assigning a discharge co-efficient whose value is a function of the orifice pressure ratio and the clearance geometry.

(ii) For radial leakage, the conditions in the leakage sink are assumed to be those of the surrounding atmosphere.

(iii) The conditions at the cell end to be used in the leakage flow calculations are taken to be those which exist there before leakage is taken into account.

(iv) The various leakage flows are independent of each other.

The leakage flows are calculated according to the following expression due to Kearton & Keh (32).

$$m_\ell = A_\ell C_d \sqrt{\frac{2g\gamma}{\gamma-1}\frac{P_e^2}{RT_\ell}\left\{\left(\frac{P_x}{P_\ell}\right)^{2/\gamma} - \left(\frac{P_x}{P_\ell}\right)^{\frac{\gamma+1}{\gamma}}\right\}} \qquad (5.4.1)$$

where

P_x = Static pressure at the discharge of the leak.

P_ℓ = Effective stagnation pressure at entry to the leak.

A_ℓ = Cross-sectional area of the leakage path.

C_d = The discharge co-efficient of the leakage path.

The computerised procedure provides means for the calculation of the radial and circumferential leakage flows at the cell ends for each time step.

5.4.2 The Energy and Mass Flow Correction Method

In order to apply this method, the leakage flow calculations are carried out in such a way that at the end of the cycle, the individual values of the leakage mass and energy flow through each port and also through the blank ends are known. The total energy loss is also calculated.

The mass flows through the ports are corrected for leakage according to the following convention:-

(i) If the main and the leakage flows through a port have the same direction, the corrected flow is the difference of the two flows.

(ii) If the main and leakage flows through a port have different directions, the corrected flow is the sum of the two flows.

The energy requirements to sustain the given pressure exchanger cycle are corrected by adding the net energy lost due to leakage to the energy requirement calculated for the leakage-free operation.

This method does not consider the effects of leakage on the strength of the pressure waves. It can be considered as an extention of the leakage model method due to Kentfield (2).

The Porous Cell Wall Method

In this method, the leakage flow through the cell ends is simulated by mass flowing in or out in a direction normal to the main flow through porous cell walls at the cell ends. The porous portion is assumed to cover a cell length equal to ΔX at each end and a perforation co-efficient is supplied to take into account the ratio of the gap width to the length ΔX. Szumowski (33) and Wu &

Ostrowski (34) have used this approach to predict the attenuation of pressure waves in a perforated shock tube.

The term ψ in the governing equations supplies the leakage flow rate at the cell ends for the porous cell wall method. The terms B1, B2, B3, B4, B5 and B6 are to be calculated only when the porous cell wall method is being used to account for the leakage losses. The calculation of these terms is explained in Appendix V.

5.4.4 The Partly-Open End Method

In a leakage-free operation of a pressure exchanger it may be recalled that the fluid velocity at a closed end becomes zero according to the boundary conditions in Chapter 4. This situation does not exist when leakage through the clearance gap is considered. In this situation some fluid is still in motion through the clearance area. In order to satisfy the mass continuity at the cell ends, the boundary conditions must be altered in such a way that a small residual velocity exists at the cell end.

The same analysis when applied to the situation when the cell is open to a port and fluid is already in motion through the port leads to the conclusion that in such situation the fluid velocity has to be corrected to account for the leakage flow.

The main task is now to calculate the fluid velocity due to leakage in order to apply a correction to the main velocity. In order to carry out these calculations, the calculation procedures for the boundary conditions at the partly-open end (already provided in the numerical procedure) are used. Therefore calculations of the residual velocities due to leakage follow the same assumptions and procedure as those for the calculations at the partly-open end. Fig. (13.14) shows the assumed geometry at the cell ends for leakage calculations.

The corrected velocity is then used to calculate corrected values

of the other variables. Leakage calculations by the partly-open end method are now complete.

Further details of the partly-open end method are described in Appendix V.

5.5 Heat-transfer Losses

Heat transfer in pressure exchangers takes place between the cell walls and the fluid in the cell and also at the interface of the fluids at different temperatures. Heat transfer losses increase with the peak cycle temperature. It is due to heat transfer that the rotor assumes a temperature much lower than the peak temperature. In the present work only heat transfer between the cell walls and the fluid in the cell is accounted for.

Referring to the governing equations in section 4.4.1 factor q simulates the heat transfer rate to per unit volume of fluid. The task is to provide a reasonable estimate of its value. In Appendix V , it is shown that this parameter is given by the following relationship.

$$q = {}^{4}/_{d_h}\, St\, \rho\, C_p |u| (T_w - T_o) \qquad (5.5.1)$$

where

d_h = hydraulic diameter of the cell

S_t = Stanton number

T_w = cell wall temperature

T_o = local value of the stagnation temperature of the fluid.

According to Bakhtar (30) a good estimate of the local value of Stanton number is given by the turbulent pipe flow formula:-

$$S_t\, P_r^{0.6}\, R_e^{0.2} = \text{constant} \qquad (5.5.2)$$

For a constant Pr

Issa (26) proposed the value of ~~the~~ a constant to be 0.02 such that

$$S_t\, R_e^{0.2} = 0.02 \qquad (5.5.3)$$

The value of q can now be estimated.

5.6 Transfer passage losses

Steady flow is assumed in a transfer passage. The losses associated with transfer passages are therefore steady-flow losses due to friction, heat transfer and flow disturbances at bends. These losses are estimated from steady-flow loss data and accommodated in the transfer ports boundary conditions. The procedure is described in Appendix V.

5.7 Mixing & diffusion losses

Mixing and diffusion losses in pressure exchangers occurs at the interface between different fluids or fluids having different thermodynamic properties and due to leakage inflows and finite cell width. In the present work mixing and diffusion losses have not been considered.

6. The steady state conditions in Pressure Exchanger Ports

The following relationships have been derived to calculate the steady state conditions in pressure exchanger ports from considerations of the predicted port-mass and energy flows and the prescribed boundary conditions after the cycle calculations are complete. Cell wall thickness has been taken into account.

(i) Inlet port, stagnation pressure and temperature prescribed at the port.

$$\bar{M} = \frac{\sqrt{T_o}}{P_o} \times \frac{K}{\tau_p} \times \left(\int_{\tau_1}^{\tau_2} m d\tau\right)\left(1 + \frac{\gamma-1}{2}\bar{M}^2\right)^{\frac{\gamma+1}{2(\gamma-1)}} \qquad (6.1)$$

(ii) Outlet port, static pressure prescribed at the port.

$$\bar{M} = \frac{K}{\tau_p}\left[\left(\int_{\tau_1}^{\tau_2} E d\tau\right)\left(\int_{\tau_1}^{\tau_2} m d\tau\right)\right]^{\frac{1}{2}} \times \frac{1}{P_x} \quad \left(1 + \frac{\gamma-1}{2}\bar{M}^2\right)^{-\frac{1}{2}} \qquad (6.2)$$

(iii) Outlet port, stagnation pressure prescribed at the port.

$$\bar{M} = \frac{K}{\tau_p} \times \left[\left(\int_{\tau_1}^{\tau_2} E d\tau\right)\left(\int_{\tau_1}^{\tau_2} m d\tau\right)\right]^{\frac{1}{2}} \left(1 + \frac{\gamma-1}{2}\bar{M}^2\right)^{\frac{\gamma+1}{2(\gamma-1)}} \times \frac{1}{P_o} \qquad (6.3)$$

The derivation of these equations and an explanation of various terms is given in Appendix VI.

7. THE COMPUTER PROGRAM

7.1 General comments

In previous sections a pressure exchanger theory has been developed. This theory includes a numerical procedure to solve the governing equations, different procedures to calculate the performance losses, the design criteria of the port geometry, and the performance criteria of different pressure exchanger cycles.

A computer program, based on this pressure exchanger theory, for the performance and design calculations of pressure exchangers has been developed. It is a very general program and covers almost all pressure exchanger cycles including pressure equalisers, dividers and four port pressure exchangers with or without transfer passages. The present version, as presented in this report, is capable of dealing with two transfer passages. A higher number of transfer passages can be dealt with without much difficulty.

The program can be used to predict the fixed-geometry operation of any pressure-exchanger cycle and the performance predictions may be either only for a homentropic process or it may include one or more performance losses as the need may be.

The program may also design the ports of the given pressure-exchanger cycle during the performance calculations. The number and arrangement of the ports is completely arbitrary without any restriction and is solely left to the choice of the designer.

The computer program also provides for a Calcomp or Kingmatic plot and a microfilm of the pressure exchanger, designed by the program or otherwise. The computer plot, shows in the conventional manner, the rotor development, the port opening and closing times, the velocity profiles at the ports and the paths of the contact surfaces inside the rotor. With this facility provided in the program along with the interactive graphics facilities

available at Imperial College, computer aided design techniques for pressure exchangers can now be used without much difficulty.

The name of the program is "GENPX". It is written in Fortran IV language. It has been successfully run on the CDC 6400 and 6600 computers and can also be run on other computers having appropriate storage. Its storage capacity requirements are less than 35K and can be further reduced by use of special methods such as overlays. The time taken by the program for the performance and design calculations varies from cycle to cycle and also from computer to computer.

Following good programming practice, the computer program "GENPX" has been divided into a number of subroutines. Each subroutine carries out a certain specific operation whenever it is called from any part of the program. The main program starts and controls the whole operation. In order to reduce the burden on the main program and also for the sake of simplicity certain subroutines are used as "sub-main" routines and their job is to start and control the execution of certain parts of the calculations.

The computer program can be broadly divided into following sections:-

(i) The first section incorporates the numerical solution procedure to solve the governing differential equations.

(ii) In the second section, the calculation procedures for the performance losses are programed.

(iii) The third section deals with the design calculations of pressure exchanger cycles.

(iv) The fourth section calculates the steady-state conditions at the pressure exchanger ports.

(v) The fifth section calculates the overall performance of pressure exchanger cycles from the information provided by the previous sections.

(vi) The sixth section plots the pressure exchanger rotor, the port widths and their opening/closing times, the velocity profiles at the ports and the paths of the contact surfaces in the rotor.

In addition to the main sections, means have also been provided to read and print out the input data, to control the sequence of calls to various subroutines and to recycle the calculations until equilibrium conditions are attained.

7.2 A description of the program

In the following sections, the computer program GENPX and its various subroutines are described. The relevant-flow charts are given in Appendix VII.

7.2.1 Main

The main routine initiates and controls the sequence of operations. It's first task is to read the input data which includes the following information:-

(i) Indexing System

In order to provide maximum possible flexibility in the program, the indexing system has been extensively used. The indexing system consists of a number of indicators which help the computer to assess the number of operations it has to perform during the cycle calculations and their sequence. The following indicators have been used:-

ILEAK

ILEAK controls the leakage calculations. It should be set equal to one if leakage effects are to be ignored. The partly-open end method, the mass-flow method and the porous-cell-wall methods are called for values of ILEAK equal to 2, 3 and 4 respectively.

IFRIC

IFRIC controls the calculation of the viscous and heat transfer effects which are completely ignored if it is set equal to unity. Only wall-friction and heat transfer effects are considered if IFRIC is set equal to 2 and cell-entry and -exit losses are also included for IFRIC equal to 3.

ITP

Transfer-passage losses are ignored if ITP is set equal to 1, whereas they are included if ITP is given a value equal to 2.

IRES

Residual wave effects are included in design calculations when IRES is set equal to 2.

IDESIN

If IDESIN is set equal to unity, this indicates that the pressure-exchange cycle under consideration has a known geometry and no design calculations are required, whereas a value of 2 triggers the design section in the program into action.

IPR

A value of IPR equal to 1 ignores the pressure recovery downstream of a partly open inlet whereas a value of 2 takes this phenomenon into account.

The indexing system is instrumental in providing flexibility and generality to the program.

(ii) The geometry of the pressure exchanger

The geometry of the pressure exchanger is specified by the following information:-

(a) 1-D array TIMO represents the port opening times.

(b) 1-D array TIMC represents the port closing times.

(c) 1-D array BSPAC represents the blank spaces between the ports.

(d) FACTH and FACTL represent the high-pressure and the low-pressure port area ratios respectively.

(e) PHIMIR and PHIMIC represent the radial and circumferential clearance gap geometry respectively.

(f) PHIEFF represents the cell-wall blockage factor.

(g) D represents the cell hydraulic diameter.

(h) XL represents the cell length.

(i) TMAX represents the maximum cycle time.

When the pressure exchanger geometry is not known and it has to be designed, arrays TIMO and TIMC and variable TMAX are given dummy values and FACTH and FACTL are given a guessed value.

(iii) The boundary conditions

The boundary conditions consist of the following information:-

(a) The stagnation pressures at the inlet ports and also at outlet ports where applicable.

(b) The static pressures at outlet ports where stagnation pressure has not been prescribed.

(c) The stagnation temperatures at inlet ports.

(d) 1-D array IDATA which is unity for those ports where static pressure is prescribed and is equal to 2 for the remaining ports.

(iv) The initial conditions

The initial conditions in a pressure-exchanger cell at the beginning of a cycle calculation are specified as follows:-

(a) XI and XII are distance variables which indicate the pressure and temperature distribution in the cell. If both are set

equal to unity a uniform distribution is indicated.

(b) PI and TI specify the pressure and temperature prevailing in the cell at the beginning of the cycle.

(v) Miscellaneous Data

(a) RATIOH and RATIOL specify the required high-pressure and the low-pressure scavenge ratio respectively.

(b) CP & CV are the two specific heats of the working fluid.

(c) AK specifies the fraction of the time step and N specifies the number of spatial steps.

(d) TPS is the estimated head loss in the transfer passages.

(e) KMAX specifies the number of cycles the performance and design calculations have to be repeated in order to attain equilibrium conditions.

As soon as the specified information is read in, the program main prints out the read data to check their values.

Program Main then calls the following subroutines in the given order:-

(i) Subroutine GAMMA is called to calculate different functions of γ which are to be frequently used in subsequent calculations.

(ii) Subroutine INIT processes the initial conditions.

(iii) Subroutine INITIA is called to set various factors equal to their initial values.

(iv) Subroutine AUX and RESID are called to store the values of P, σ and U at $\tau = 0$.

(v) A DO loop is started with a call to the subroutine OPTIM which handles the design calculations.

(vi) Subroutine AUX is then called to calculate the values of pressure, temperature, etc., from the values of P, U and σ computed previously elsewhere in the program.

(vii) Subroutine LEK1 is then called twice to carry out leakage calculations for the two cell ends.

(viii) Subroutine INTEG then performs the integration of various quantities such as the mass flow through the ports.

(ix) Subroutine FINI is then called to give the mass and mean pressure in the cell at $\tau = 0$.

(x) Subroutine CEXEN is then called to calculate the apparent co-efficient of friction for the cell-exit and entry losses.

(xi) Subroutine STEP and PORTX are then called to calculate the values of P, σ and U for a forward time step at the central grid points and boundaries respectively. The DO-loop is complete if $\tau = \tau max$, and the final conditions in the cell at the completion of one cycle are now calculated by calling FINI.

(xii) The whole procedure is repeated until either the final conditions match the initial conditions, the mass conservation at the scavenging ports and at the transfer ports are satisfied or the maximum allowable number of cycles have been run.

(xiii) The steady state conditions in the ports are now calculated by calling subroutines DUCT1 and DUCT 2.

(xiv) Subroutine TPLOSS is then called to calculate the transfer passage losses and the cycle is re-run with the modified boundary conditions.

(xv) Subroutines RESULT, EQUAL or DIVIDE may then be called to calculate the overall performance of four-port pressure exchangers with or without transfer passages, pressure equalisers and pressure dividers respectively.

(xvi) The plotting and microfilm package controlled by subroutine KING is called at the end, to provide the pressure exchanger plot and its microfilm and for this subroutine DESIGN has to be called between steps (v) and (vi).

The main calling system is organised in such a way that certain calls can be ignored by supplying appropriate values to the indicators.

7.2.2 GAMMA$

Subroutine GAMMA$ calculates different functions of γ. It also supplies the values of the critical pressure ratio and the kinematic viscosity of the fluid. The spatial coordinates and the steps are also calculated in this routine. It is called only once in the program.

7.2.3 INIT

This subroutine processes the initial conditions in the cell. The velocity everywhere is assumed to be zero. The cell wall temperature is assumed to be uniform and its value is the mean of the peak and lowest temperature of the cycle.

7.2.4 AUX

Subroutine AUX calculates the local values of the velocity and sonic speed at all grid points because these values are needed to calculate the slopes of the characteristics. The values of the static pressure and temperature, stagnation pressure and temperature, Mach numbers, density and entropy are claculated only at boundaries. These values are calculated from arrays AM($P\sigma$ + U), AN($P\sigma$ - U) and SIG(σ) supplied by other routines to AUX.

7.2.5 STEP

Subroutine STEP performs and controls the calculations of the new

values of the arrays AM, AN and SIG at all central grid points at time T + DT from the values of these arrays at a time T. in the following steps:-

(i) Arrays BEM, BEN and BES representing the slopes of the m, n and s characteristics respectively are calculated for the central grid points.

(ii) The time step DT is calculated according to the stability criterion.

(iii) Subroutine SLOPE is then called to calculate an array X1 representing the x-coordinates of the feet of the m characteristics at the previous instant of time.

(iv) Subroutine LININT is then called thrice to calculate arrays AM1, AN1 and SIG1 respectively by simple linear interpolation. These are the values of $P\sigma + U$, $P\sigma - U$ and σ at X1.

(v) Steps (iii) and (iv) are repeated for the n and s characteristics.

(vi) Subroutine CFST is then called to calculate the values of the local values of friction factors, Stanton Numbers and D, G and F at the central grid points. B1, B2, B3, B4, B5 and B6 are not calculated for central grid points for leakage flows is zero at the central grid points.

(vii) Finite difference formulae are now used to calculate the values AM, AN and SIG at all central grid points for time T + DT. The variable SIG is calculated first followed by the calculations of AM and AN.

7.2.6 SLOPE

Subroutine SLOPE finds the intersection between the characteristics passing through the grid points at time T + DT and the T- abcissa. The characteristic slopes at time T + DT are approximated by taking the

mean of the slopes of the two bounding characteristics at time T. The subroutine operates on all internal grid points. It also operates on the left-most grid point if the local characteristics slope is negative and on the right-most grid point of the local characteristic slope is positive.

7.2.7 LININT

Subroutine LININT uses backward linear interpolation to calculate the values of the dependent variables at the intersection points calculated by SLOPE.

7.2.8 PORTX

Subroutine PORTX operates on grid points at the boundaries in the following steps:-

(i) The values of the static pressure or the stagnation pressure at the ports are calculated according to the values of IDATA.

(ii) Subroutine CYCLE is then called to check if the cell is closed, partly-open or fully-open to a port on either side and if it is partly-open then to calculate the fraction of cell area open to the port. Calls to subroutine CYCLE are arranged in such a way that if the cell is open to a port, the port in question is also immediately recognised. This arrangement requires the numbering of the ports, in the present version, in such a way that the first two ports are on the left hand side and the remaining ports are on the right hand side of the rotor. The whole procedure can now be explained.

Index NPORT is set equal to 1. CYCLE is called to check on the first port. If the port is open, the fraction of the cell area open to port PHIL is determined and index IOPEN

is set equal to 2. No more scanning of ports on the left hand side is necessary and the subroutine can begin to commence scanning on the right hand side. If the port is closed, IOPEN is set equal to 1 and scanning on the left hand side is continued until either an open port is found or the last port has been scanned. A similar procedure procedure is applied to the right hand side.

The following information has been gathered at the end of step (ii):

(a) Whether the cell ends are closed, partly open or fully open to a port.

(b) If the cell is open, which port it is in contact with.

(c) If the cell is partly open what is the fraction of the cell opening.

(d) The boundary conditions to be applied at the cell ends.

(iii) The necessary information having been supplied at the end of step (ii) subroutine PORTS is then called twice, once for each end to calculate the values of the dependent variables at the boundary points.

(iv) Finally steps are taken to incorporate the partly-open end method in order to calculate the dependent variables corrected for leakage effects.

The partly open end method, as described earlier in Chapter (5) is essentially based on the calculation of a residual velocity for each type of leakage flow. This residual velocity is calculated by assuming that the cell is partly open to leakage sink. The fraction of cell opening is based on the clearance geometry. The leakage sink

conditions depends upon the type of leakage The partly-open end method calculations are performed by utilising the velocity calculation procedures already existing in subroutine PORTS. In order to perform the radial leakage calculation, PORTS is called at each time step, once for each end. The clearance geometry and the leakage sink conditions are supplied through its dummy arguments. Similar procedure is adapted for the circumferential leakage claculations which are performed only when the cell is adjacent to a port.

7.2.9 CYCLE

Subroutine CYCLE, at each forward step, determines the position of the cell ends, which are either closed, partly open or fully open to a port. It calculates the fraction of cell opening PH1 and sets up boundary conditions for subroutine PORTS.

7.2.10 PORTS

Subroutine PORTS solves for the values of dependent variables at the cell boundaries. The value of the fraction of cell opening PH1, the stagnation pressure PO, the stagnation temperature TO and static pressure PX at the ports are supplied to PORTS through its argument list. The partly-open end method calculations are also incorporated in this subroutine.

The boundary conditions and the partly-open end calculations are complicated and involved and therefore one may find the subroutine PORTS to have complicated logical procedures particularly because a great deal of effort has been made to utilise the common features and the similarities existing between different equations as much as possible so that maximum possible efficiency in terms of programming space and time is achieved.

In the following sections, various chapters of the subroutine PORTS are therefore described in some detail.

(i) Commence 0

The implied sign convention is that an inflow to the cell is positive. The implication of this is that while outflow at a right hand port has a positive sign for velocity, outflow at a left hand port has a negative sign; and vice-versa for an inflow. The sign convention therefore makes it necessary for the subroutine to recognise a left-hand port from a right-hand port. The grid points are numbered from left to right so that the grid point 1 is the left-most one. The grid point number I is transferred to the subroutine as an argument and it enables the subroutine to recognise whether a left hand or right hand port is under consideration and it sets IHAND equal to an appropriate value.

(ii) CHAPTER 1

In chapter 1 new parameters are defined in terms of the subscripted variables used elsewhere in the subroutine. These parameters are set differently for the left-hand port and the right-hand port. Subroutine CFST and BLEAK are called to calculate loss factors D, G, F and B's to be used later in the subroutine. If the partly-open end method calculations are to be performed arrangements are made to store the value of the velocity-variable AM in a temporary location, to be called later for leakage correction.

(iii) CHAPTER 2

Chapter 2 operates on a closed cell. The velocity variable AM is set equal to zero. The entropy variable SIG is calculated from the entropy equation and the pressure variable is calculated from the relevant cell equation.

(iv) CHAPTER 3

Chapter 2 is ignored if the cell is open to a port. Chapter

3 now determines the direction of flow through the port, based on the direction of velocity at the previous step. If the velocity at the previous step had been zero, the flow direction is determined by comparing the static pressure of the cell at the previous step with the static pressure at the port.

The flow direction having been determined, the next task is to determine whether the flow is sub-critical or super-critical by comparing the pressure ratio with the critical pressure ratio. An indicator IND is then set to identify the local type and direction of flow. The indicator IND is extensively used to direct the computational procedure to the appropriate equations through the computed GOTO statements. For an outflow entropy variable is now calculated from the entropy equation.

(v) CHAPTER 4

Chapter 4 contains the port equations to be solved simultaneously. The equations for super-critical inflow and for sub-critical outflow through fully open ports, because of their simplicity, are excluded from this section and are coded elsewhere in the program.

The port equations are written in terms of appropriate pressure ratios and the port opening fraction and are solved in terms U/a_o for an inflow and U/a for an outflow. The entropy variable SIG is obtained from the entropy equation before the port equations are solved. Arrangements are also made in this section to utilise the appropriate port equations to solve for the residual velocity due to leakage. The residual velocity is converted to the velocity variable

form and added algebraically to the velocity variable calculated for the leakage free operation.

(vi) CHAPTER 5

In this chapter are coded the cell equations for the left hand and the right hand port. The cell equation is solved simultaneously with the appropriate port equation. A modified Newton-Raphson procedure due to Mathews (15) has been used.

(vii) CHAPTER 6

In chapter 6 the port equations, for the super-critical inflow and the sub-critical outflow through the full-open port, are coded.

(viii) CHAPTER 7

The cell and port equations having been solved simultaneously for P, the value of P is now substituted into the cell equations to calculate

(ix) CHAPTER 8

The assumed sub-critical or super-critical flows were based on the values of the dependent variables at the previous time step. The validity of these assumptions is now checked with the calculated values of the dependent variables and if the assumption is not valid then the whole procedure is repeated for the new conditions.

(x) CHAPTER 9

The entropy variable for the inflow cases is now again calculated using the new values of P and U

(xi) CHAPTER 10

If convergence is not obtained for one assumed flow direction then the whole procedure is repeated for a different flow direction. The necessary coding has been provided in this chapter.

7.2.11 FINI

In this subroutine, Simpson's Rule is used to calculate the mean static pressure and the mass flow in the cell.

7.2.12 OPTIM

Subroutine OPTIM handles the design calculations of pressure exchangers. It is ignored when the geometry of the pressure exchanger cycle being processed is fixed and known. It calls subroutine CEMF to design a cell-filling or a cell-emptying port, subroutine PHASE to calculate the phasing of the scavenging ports and subroutine CSCR to determine the widths of the scavenging ports. The blank spaces between ports are supplied through the 1-D array BSPAC. The sequence and the number of calls to these subroutines depend upon the required arrangement of the ports selected arbitrarily by the designer. An indicator INDEX1 is used to control the sequence of calls to subroutine CEMF, PHASE and CSCR as an index to the computed GO TO statements. In the following the structure of this routine for the design calculations of a four port machine with two transfer passages with the porting geometry and numbering as shown in Fig. (13.15). The cycle calculations are initiated at the start of the cell-filling process in transfer passage number one.

(i) The indicator INDEX1 is set equal to 3. NPORT is set equal to INDEX1.

Subroutine CEMF is called to examine the conditions at the cell end. If these conditions satisfy the design criterion set for the cell filling port, the value of TIMC for the port number 3 is set equal to TIM and the value of TIMO for the next port, i.e. the port number 4 is set equal to a value TIM + BSPAC the design of port number 1 is now complete. If the conditions at the cell ends do not satisfy the cell filling design criterion, subroutine CEMF immediately transfers

control back to OPTIM which continues to call CEMF at each time step until TIMC for port number 3 has been determined.

The width of the cell filling port, designed by the above procedure, may now be further refined to take account of finite cell width effects. Experience has shown that the effects due to finite cell width on the cell filling and cell emptying ports may be neglected. However, the performance calculations for the designed ports must be repeated to account for the finite cell width on the cell filling performance. The necessary coding to repeat the performance calculations for the designed ports has been arranged in CEMF.

The indicator INDEX1 is now increased by 1 to direct the computed GO TO statement to the next appropriate call.

(ii) The next port is again a cell filling port in transfer passage number two. NPORT is increased by 1 and CEMF is again called until the width of port number 4 has been determined. The procedure is similar to that in step number 1.

(iii) The next section to be dealt with, is the high pressure scavenging section. The port opening time TIMO for port number 5 which is the high pressure inlet port has already been fixed in the previous step. The following information completely specifies the high pressure scavenging section geometry.

(1) The phase difference between the two ports ϕ_{HP}.

(2) The width of the high pressure outlet port τ_{HPout}.

(3) The ratio of the width of the high pressure outlet port to that of the high pressure inlet port. A_{HP}.

The initial steps taken to determine these three factors

include the allocation of the appropriate values to indicators INPORT and JNPORT. INPORT specifies the number of the high pressure outlet port which is 2 in this case. JNPORT specifies the number of the high pressure inlet port which is 5 in this specific case. Subroutine PHASE is then called to examine the end conditions in the cell. If the end conditions satisfy the design criterion for phasing the value of port opening time TIMO for the high pressure outlet port is set equal to TIM. If the design criterion for the phasing is not satisfied, subroutine PHASE immediately returns the control to OPTIM which continues to call PHASE until the phasing has been determined. The value of indicator INDEX1 is increased by 1.

The phasing having been determined the values of INPORT and JNPORT are readjusted and subroutine CSCR is called to carry out its operation in two distinct steps with an indicator NSCR controlling the sequence of its operation.

(a) While both the ports remain open, OPTIM calls subroutine CSCR to test the design criterion of the high pressure scavenge section. If the design criterion is satisfied, the value of TIMC for the outlet port is set equal to TIM + DTP/2 and the value of TIMC for the inlet port is set equal to a value based on a guessed estimate of the area ratio.

(b) In the second step, the value of TIMC for the inlet port is adjusted by trial and error such that the design criterion for the high pressure scavenge section is again satisfied while effects due to the finite cell width and the expansion waves fanning out from the trailing edge of the inlet port are also accounted for.

The design of the high pressure scavenge section is now complete. INDEX1 is increased by 1.

(iv) The next port is the cell-emptying port in transfer passage number 2. The design procedure for the emptying port is similar to that for a filling port.

(v) The next port is the cell emptying port in transfer passage number 1.

(vi) Finally, the low pressure scavenging section is reached. The design procedure in this case is similar to that for the high-pressure scavenge section.

The design of a four-port pressure exchanger with two transfer passages is now complete.

It can easily be noted that a pressure exchanger cycle with any arbitrary arrangement of ports can be designed with a proper calling sequence for the subroutines CEMF, PHASE and CSCR.

7.2.13 CEMF

The function of subroutine CEMF is to design a cell-filling or a cell-emptying port. The design criterion for a cell-filling or a cell-emptying port is thus that the width of the port in both cases should be such that flow reversal in the port is just prevented. The avoidance of flow reversal is consistent with the condition of maximum mass flow into the cell in case of filling and out of cell in case of emptying which according to Cotter (19) ensures optimum performance in both cases.

In order to enable the subroutine to differentiate a lef-hand port from a right-hand port, the grid point number I is transferred to the subroutine through the argument list. In addition to I, variables TIM, UEX (the velocity at the previous step) are some of the arguments of the subroutine.

As an initial step, the subroutine CEMF stores the values of the dependent variables, TIM and NSTEP first before the commencement of

the filling or emptying process by calling subroutine RESID. This is to ensure that these values are available when required at a later stage.

The procedure for testing the design criteria is to examine the product of the present and previous values of the velocity at the cell end. If the product is positive, the flow still has the same direction and therefore the present value of the velocity is set equal to the previous value and control is transferred to OPTIM which continues to call CEMF until the product suddenly becomes zero or negative which indicates the beginning of flow reversal. The design criterion is thus satisfied. The value of TIMC for the port under consideration is set equal to TIM.

The situation for a filling port at this stage is as shown in fig. (7.2.1).

It can be seen from the figure that the effects of finite cell width on the design and performance of the filling or emptying have not been taken into account.

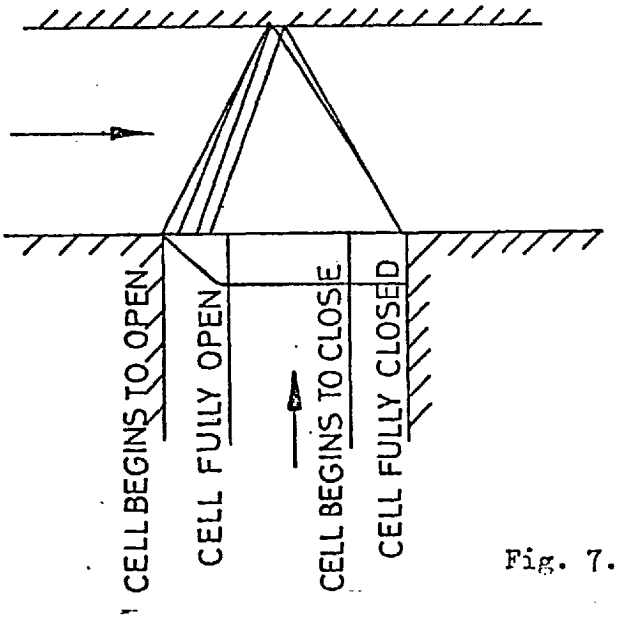


Fig. 7.2.1

Experience has shown that the design of the cell filling or cell emptying port is not much affected by finite cell width but the performance in terms of mass flow and pressure difference, must take

into account these effects and therefore the performance calculations have to be repeated one more time.

In order to repeat the performance calculations subroutine INITIA is called. INITIA is a general-purpose initialising subroutine. In this case INITIA resets the integratal values of mass, energy and leakage flows through the designed port. CEMF then calls subroutine IRESID to rewind the calculation procedure and position it at the beginning of the designed port. IRESID recalls the values of the dependent variables, TIM and NSTEP at the beginning of the process which had earlier been stored by RESID.

The task now remains to carry out the performance calculations for the designed port. At the completion of this step the finite cell width effects have been taken into account.

7.2.14 PHASE

The function of subroutine PHASE is to determine the phase difference between the opening times of pair of ports in a scavenging section.

In the case of high-pressure scavenging ports the opening time of the high pressure inlet port, in most cases, is determined from considerations of the blank space between the high-pressure inlet port and the preceding port. The opening time of the outlet port and hence the phase difference is ideally determined by locating the time when the compression wave initiated at the inlet port just reaches the opposite end. This is the time when the outlet port should be opened. The location of such a point is difficult particularly in the case of the low pressure scavenge process because of the fanning out of the expansion waves.

The criterion chosen for the high pressure scavenging section phase difference is to examine the cell-end conditions at each step and to compare the static pressure at the cell end with that at the

port. As soon as the former becomes greater than the latter and an outflow is possible, the outlet port is opened.

Similar considerations apply to the low-pressure scavenging section. In this case the opening time of the inlet port is determined for an inflow.

In order to enable the subroutine to differentiate a left hand end from a right hand end, the grid number I is again used as an argument. NFLOW is an index which indicates whether a high-pressure scavenging process is under consideration or a low-pressure scagenging process.

As an initial step, subroutine RESID is called to store the values of the dependent variables, TIM and NSTEP at the beginning of the process.

The subroutine then examines the index NFLOW and goes to the appropriate section in the routine. In each case it compares the static pressures at the cell end and the port respectively. If the desired flow direction can be attained the opening time of the relevant port (outlet port in the case of the high pressure scavenging section and inlet port in the case of the low pressure scavenging section) is set equal to TIM. The value of INDEX1 is increased by 1 and the control is returned to OPTIM.

7.2.15 CSCR

The function of the subroutine CSCR is to determine the port widths in the scavenging sections.

For a high-pressure scavenging section, it determines the width of the outlet ports in order to achieve the given high-pressure scavenge ratio. The position of the trailing edge of the inlet port is then adjusted by trial and error such that the expansion wave fanning out from the edge reaches the opposite end when the outlet port has been just closed.

A similar procedure applies to the low pressure scavenge process. In this case the width of the inlet port is first determined such that the required scavenge ratio is attained and then the position of the trailing edge of the outlet port is so arranged by trial and error that the compression wave generated at the edge reaches the opposite end when the inlet port has just closed.

In order to enable the subroutine CSCR to differentiate a high pressure scavenge section from a low pressure scavenge section, an indicator ISCR is used. If ISCR is equal to 1 it indicates that a high-pressure scavenge section is under consideration. If ISCR is equal to 2 a low pressure scavenge section is under consideration.

NSCR is an index which indicates to the routine which one of the two stages in the design calculations is in process. If it is equal to zero the design calculations are in the first stage and if it is equal to 1 the design calculations are in the second stage.

Initially, NSCR is set equal to zero. The design procedure is in the first stage. The calculated scavenge ratio is compared with the desired value at each step while both ports remain open. If the calculated value is less than the required value, the control is transferred to OPTIM which continues to call CSCR until the calculated scavenge ratio is either equal to or just greater than the required ratio. The value of TIMC for the relevant port is set equal to TIM + $DTP/_2$. The situation at this moment is shown in fig. (7.2.2).

Fig. (7.2.2) shows that the design of the scavenging ports is far from being complete. The width of the inlet port has not been determined and the finite cell width effects during the closing stages have not been accounted for.

In order to complete the design the following steps are taken.

(i) The inlet port width is guessed. NSCR is set equal to 1.

(ii) Subroutine IRESID is called to rewind the calculation

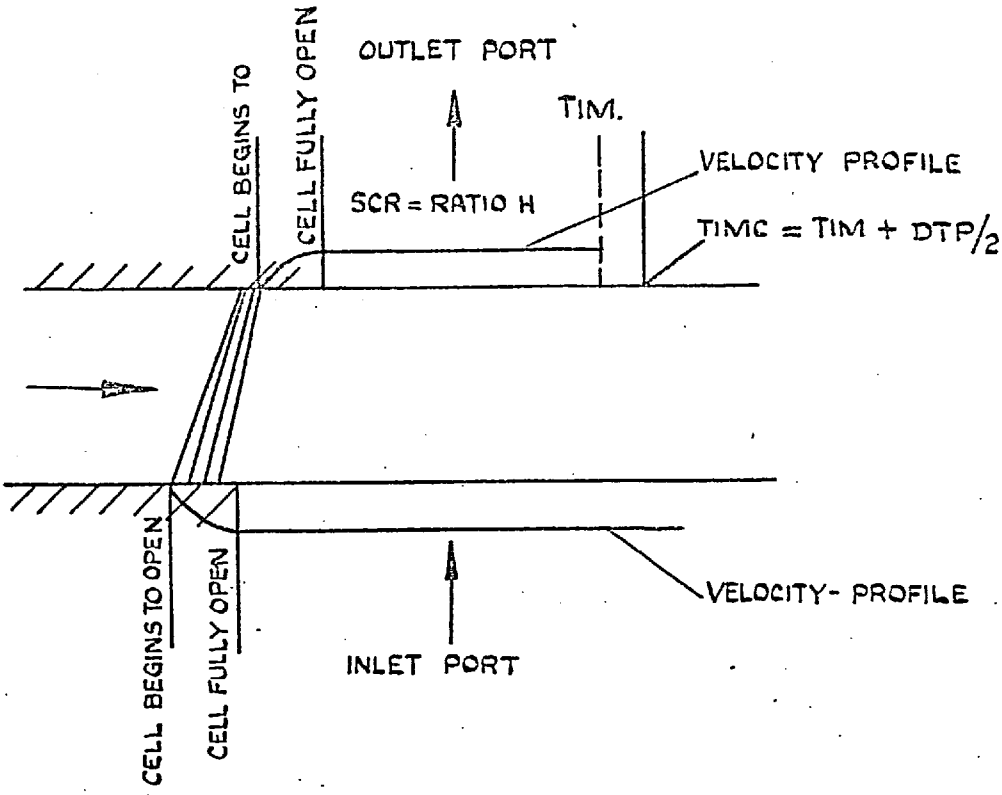


Fig. 7.2.2

procedure and position it at the beginning of the process. This time the widths of the port approximately are known.

(iii) Subroutine INITIA is then called to initialise the values of the mass, energy and leakage flows through the scavenging ports and sets them equal to zero.

The calculation procedure is then resumed until the scavenge section is completely processed. The calculated scavenge ratio is then examined. If the calculated value is not satisfactory, the trailing edge of the inlet port is adjusted until the desired scavenge ratio is achieved. The design calculations of the scavenging port are now complete.

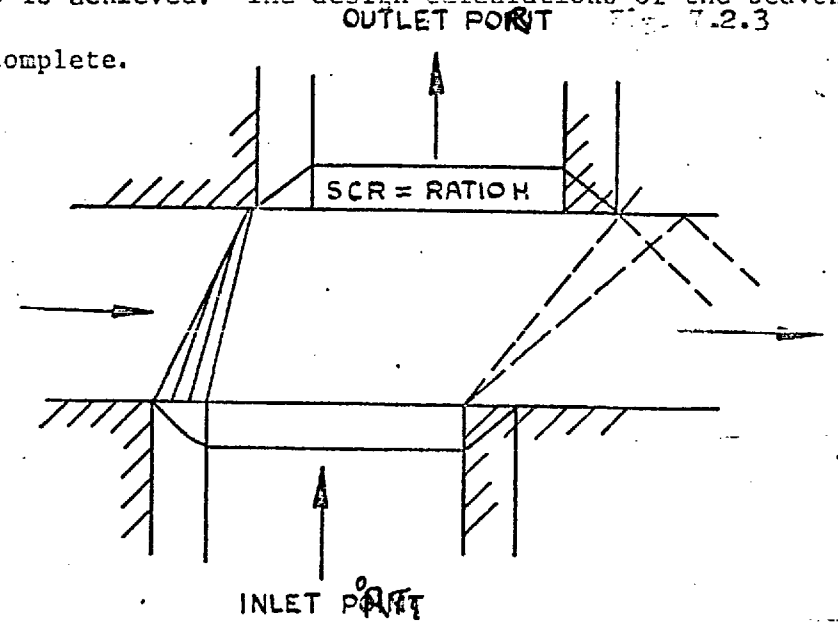


Fig. 7.2.3

7.2.16 INITIA

Subroutine INITIA is a general-purpose initialising subroutine. During the calculation procedure (as one may note) several initialisations are required. In each initialisation different variables and different number of ports are involved.

Subroutine INITIA has been so coded as to be able to handle all types of initialisations. This is done by the proper manipulation of arguments I, J and K. The logic of the subroutine is self-explanatory.

7.2.17 RESID

Subroutine RESID stores the values of the dependent variables AM, AN and SIG, at any time step or their mean values in two-dimensional arrays A4, B4 and C4. Variables TIM and NSTEP are also stored in one-dimensional arrays D4 and 1E4.

7.2.18 IRESID

The function of this subroutine is to recall the values stored by RESID, when needed, and convert them into arrays AM, AN and SIG and variables TIM and NSTEP respectively.

7.2.19 CFST

The function of subroutine CFST is to calculate the values of the local values of Reynolds number, friction factor, stanton number, D, G and F at all the grid points which are then transferred to other routines through the argument list. This subroutine is called from STEP and PORTS.

7.2.20 LEK1

This subroutine handles the leakage flow calculations which include the radial leakage through the outer and inner rim of the rotor and the circumferential leakage from port to cell and vice versa. It is called twice from the main, once for each end. The grid point subscript is again utilised to enable the subroutine to differentiate a left-hand end from a right-hand end.

Initially the subroutine sets the leakage flows equal to zero and allocates values to IHAND, NINIT and NMAX according to whether a left hand end or a right hand end is under consideration. It then calls subroutine LEK to calculate the radial leakage flow rate BLEK1. The cell position is then examined and if it is adjacent to a port then circumferential leakage rate from port to cell (and vice versa) BLEK3 or BLEK4 are also calculated. An average of all leakage flow rates, BLEK is then transferred to other subroutines.

7.2.21 LEK

The function of subroutine LEK is to calculate the leakage flow rates. The clearance geometry and the leakage sink conditions are supplied to it through the argument list.

Subroutine LEK compares the pressures in the leakage sink PSINK and the pressure at the cell end to determine the flow direction. It then checks for the critical pressure ratio and sets various parameters to be used in leakage flow calculations.

The co-efficient of discharge is calculated from an expression which has been fitted to the graphical data by Snow (35) . Leakage flow is now calculated for a simple leak according to a formula given by Kearton & Keh (32). The implied sign convention is that an inflow is positive.

The next task is to find the distribution of the leakage flows to calculate the integrated leakage flows for each port in order to make the required corrections in the mass flow through the ports. The necessary coding for this procedure has been provided in the subroutine which is self-explanatory.

7.2.22 INTEG

This subroutine carries out the integration of the mass and energy flow rates along the pressure exchanger ports. A trapezoidal rule has been used for integration. The integration formula for a

left hand port is different from that for a right hand port to comply with the sign convention.

7.2.23 CEXEN

The function of the subroutine CEXEN is to determine the cell entry and exit losses in the following manner.

(i) The value of PHIL is examined to check if the cell is open to a port at the left hand side. If it is closed, cell exit and entry losses at the left hand end are not needed. If the cell is open the velocity at the previous step is used to determine the flow direction.

(ii) If it is an inflow the head loss at entry is calculated from the formula

$$S = (1 - \phi_{eff})/2 \qquad (7.2.1)$$

where ϕ_{eff} is the effective area of the cell.

(iii) If it is an outflow, the head loss is given by the formula

$$S = (1 - \phi_{eff})^2 \qquad (7.2.2)$$

(iv) A similar procedure is applied to a right hand port.

(v) The total head loss is the sum of the head losses at the cell ends.

(vi) The apparant co-efficient of friction for the cell entry and exit losses can now be calculated.

7.2.24 BLEAK

Subroutine BLEAK calculates the values of leakage functions B1, B2, B3, B4 and B5 for grid points at the boundaries. These functions are then transferred to subroutine PORTS if the porous cell wall method is used for leakage calculations.

7.2.25 DUCT1

Subroutine DUCT1 operates upon the outlet ports with a uniform static pressure, to determine the steady state conditions in them.

The relevant equation is solved by the Newton-Raphson method for the steady flow Mach number in the port which is then used to calculate other steady state conditions in that port.

This, subroutine also contains the necessary coding to correct the mass and energy flows through the relevant ports according to mass and energy correction method for leakage.

7.2.26 DUCT2

Subroutine DUCT2 operates upon the inlet ports, and those outlet ports where a uniform stagnation port is specified, to determine the steady state conditions in them.

The relevant equations for the two types of port are solved by the Newton-Raphson method for the steady flow Mach number. The similarities between the two equations have been exploited to the effect that the same section is used to solve both types of equations.

The steady flow Mach number is then used to calculate the other steady state conditions in the duct.

This subroutine, like DUCT1, also contains the necessary coding to correct the mass and energy flows through the relevant ports according to the mass and energy correction method for leakage.

7.2.27 RESULT

The information and knowledge obtained from the previous subroutines is not in an appropriate form for presentation. The function of subroutine RESULT is to process this information, for four port pressure exchanger cycles and printout the performance and geometry in an appropriate form.

The performance parameters include the pressure ratio R, the temperature ratio Z, the bulk input XMEW, the mass and energy flow

through the ports, the leakage flow through the ports and closed ends, the pressure drop in the high pressure loop and the steady state conditions in the ports.

The pressure exchanger geometry is specified by the filling and emptying widths of the transfer ports, the port phasings at the scavenging section, the widths of the high pressure outlet and low pressure inlet ports and the area ratios of the high pressure and low pressure scavenging sections.

7.2.28 EQUAL

Subroutine EQUAL processes the information and prints out the performance and geometry of the pressure equaliser cycles.

7.2.29 DIVIDE

Subroutine DIVIDE processes the information and prints out the performance and geometry of the pressure divider cycles.

7.2.30 DESIGN

Subroutine DESIGN performs two tasks.

(i) It calculates the distances XP travelled by the contact surfaces at each nth step according to the value of NPRINT. The distances XP are stored in a two-dimensional array DIST against corresponding values of TIM in another two-dimensional array TIMX.

The necessary coding to perform this task is different for left hand and right hand ports.

(ii) The fluid velocity u at the cell ends is stored in a two-dimensional array UK against the corresponding values of TIM which are also stored in another two-dimensional array TIMU for each port.

7.2.31 KING

Subroutine KING processes the information supplied by the main program GENPX and arranges for a display of the development of the

pressure exchanger rotor, the port geometry of the pressure exchanger, the paths of the contact surfaces inside the rotor and the velocity profiles at the ports in the form of either a Kingmatic plot or a microfilm.

Subroutine KING calls many other subroutines to accomplish its task. These subroutines are especially written to perform different jobs. Only a brief description of the whole package is given here.

(i) The data for subroutine KING is in two forms. The first includes the information obtained from GENPX and is transferred to KING through COMMON statements. The second is supplied by the plotter himself in a block form which consists mainly of the information regarding the size and scale of the plot, the information to be printed on the plot and relative coordinates of various known locations in the plot.

(ii) All parameters are then scaled according to the size of the plot and the coordinates of various parameters are calculated to fix their relative sizes and positions. Subroutine SYMBOL is then called to print various Alphanumeric characters.

(iii) Subroutine TIME is then called to plot the time axis.

(iv) Subroutine BOX and INFORM are called to print the information box.

(v) Subroutine ROTOR is called to print the rotor development.

(vi) Subroutines PORTP, SYPOT, FDIREC and PORTX are called to plot the ports of the pressure exchanger, print information about port opening and closure and the flow directions.

(vii) The next task is to plot the paths of the contact surfaces in the rotor development.

(viii) The velocity profiles at the ports are now plotted.

The plotting routine KING is a fairly general program and can be used for any pressure exchanger cycle.

8. Apparatus

8.1 Specification of a Suitable Rig

A brief experimental investigation was carried out into the performance of four-port pressure exchangers with and without transfer passages. The aims of the experimental investigations were:

(i) To make a preliminary study of the effects of including a transfer passage in a four-port pressure exchanger on its performance.

(ii) To compare the experimentally obtained results of these cycles with the theoretically predicted performance.

The main performance parameter to be investigated was the non-dimensional bulk input. Additional measurements were also made of the pressures, temperatures and the mass flows at the high pressure ports. The conditions at the low pressure ports were assumed to be atmospheric.

No provision was made for heating or cooling the fluid in the high-pressure loop. The primary fluid was augmented by make up compressed air supply to overcome the irreversibilities in the cycle.

The facilities required for a suitable experimental rig were therefore as follows.

(1) Provision of a pressure exchanger with suitably arranged ports in which the rotor speed and the relative phasing between the ports could be varied easily.

(2) Provision of a compressed air supply and means to inject it into the high pressure loop and also to control it and to measure its pressure, temperature and mass flow rate.

(3) Provision of instrumentation for allowing measurements to be made of the mass flows, mean pressures and temperatures of the fluids passing through the high pressure ports.

(4) Provision of a facility to allow the function of the rig to be readily changed from a four port pressure exchanger without

transfer passage to a four port pressure with a transfer passage.

8.2 Description of the pressure exchanger

The pressure exchanger itself was based upon a design by Power Jets (R & D) Ltd. commissioned by Messrs. John Taylor and Sons Ltd. for a Mine Spot Cooler for use by the Kolar Gold Fields Undertaking of India.

The dimensions relevant to the pressure exchanger rotor are as follows:

Rotor cell outer diameter	5.30 inches.
Rotor cell inner diameter	3.20 inches.
Rotor cell length	6.75 inches.
Rotor cell wall thickness	0.04 inches.
Number of complete cycles/rev.	1
Number of cells in the rotor	36
End clearance	0.004" - 0.003"

The relative phasing between the two end plates can be varied by intervals of 1.5 degrees. This was possible due to the Vernier arrangement of the studs connecting the two end plates with cylindrical end casing.

A 2-hp 3-phase induction motor drove the rotor through first a variable ratio V-belt system with pulleys giving up to a $3\frac{1}{2}$ to 1 step-up speed ratio and finally a 48 in. long flexible drive. The rotor speed could be controlled anywhere in the range 4000 to 7000 rev/min.

The high-pressure air was supplied to the loop injector by the City and Guilds College compressor plant. Control of the make-up air supply pressure and mass flow was effected by a simple throttle valve. It was injected into the loop by means of a variable area centre body nozzle. (Spear valve.)

In order to allow the function of the test rig to be readily changed from a four port pressure exchanger without a transfer passage to a four

port pressure with one transfer passage, two different sets of end plates were provided. Figs. (13.16) show the pressure exchanger test rig.

The end plates used for the four port pressure exchanger without transfer passage are shown in fig. (13.17). These are the end plates originally designed for the pressure exchanger rotor.

The end plates used for the four port pressure exchanger with one transfer passage were designed according to the following considerations:

(i) The diameter of the end plates and the radial height of the ports have to be the same as for the previous end plates, the angular width of the low pressure ports were reduced to accommodate the cell-filling and the cell-emptying ports. The high pressure ports were not reduced because they were already small and also a reduction in their widths would have meant new duct work to connect the high pressure ports.

(ii) The transfer ports were arranged to be situated on the same end plate. The end plate containing the transfer ports was selected to be the one which contained the high pressure inlet port. The first decision was made to avoid a stiff transfer passage making an undesirable effect on the otherwise uniform clearance area between the end plates and end casing. The second decision was taken to avoid the transfer passage being on the same side as the flexible drive.

The width of the transfer ports were designed using the numerical procedure to give optimum performance for a design pressure ratio of 1.8. The theoretical investigations into the transfer port widths have shown that optimum widths of these ports do not show significant variation with the variation in pressure ratio. The nozzle angles were also calculated on the basis of the steady flow velocities in the ports at an overall pressure ratio of 3 (they become very large for low pressure ratios) and a speed equal to 6500 r.p.m. (very close to the optimum speed).

The blank spaces between the ports were equally distributed. The material used was Duralumin. These end plates are shown in the fig. (13.18). The duct connecting the transfer ports was made of mild steel and provisions were made in it to check the flow direction in the transfer passage and to measure the static pressures at the two ports and the temperature in the duct.

8.3 Instrumentation

The instrumentation comprised of the following:-

(i) A D-$D/_2$ orifice meter for recording the compressed air mass flow entering the rig.

(ii) A nozzle flow meter to measure the mass flow rate in the high pressure loop.

(iii) Temperature measurement in the upstream and downstream sections of the nozzle flow meter and the upstream section of the orifice meter. All temperatures were measured by copper-constantan thermocouples. The temperature upstream of the compressed air orifice meter was measured by a mercury in glass thermometer.

(iv) Static pressure measurements in the high pressure inlet port, upstream section of the nozzle flow meter and the orifice flow meters and at the transfer ports. The transfer port pressures were measured by mercury manometers. The remaining pressures were measured by Bourdon pressure gauges.

(v) The pressure differential at the orifice meter was measured by a mercury manometer and at the nozzle flow meter by a water manometer.

(vi) The rotor speed was measured by Hasler Tachometer.

(vii) Measurements were also made of atmospheric pressure and temperature at each run.

8.4 Outline of the Experimental procedure

8.4.1 Transfer Passage Tests

The transfer passage experiments were aimed at a preliminary study of the effects of the inclusion of a transfer passage on the performance of a four port pressure exchanger.

The following procedure was adopted for the transfer passage tests:-

(i) For a fixed speed and phasing, the overall pressure ratio was varied at regular intervals from 1 to 3. The changes in pressure ratio were brought about by variations in the compressed air supply using the throttle valve.

(ii) The same procedure was repeated for the pressure exchanger running at different speeds. The rotor speeds were varied from 5000 r.p.m. to 6500 r.p.m. at intervals of 500 r.p.m.

(iii) The same procedure as in step (i) was repeated for different phasings between the pressure exchanger ports.

8.4.2 Four Port Pressure Exchanger Tests

A limited number of tests on a four port pressure exchanger without a transfer passage were also carried out for two different speeds and the designed phasing.

8.4.3 Limitations of the Experiments

In this section an explanation is given for the major factors limiting the performance of the rig and the scope of the experimental investigations.

1. The shortage of time a[illegible] was the major factor in limiting the experiments to a preliminary study of the four port pressure exchangers with and without transfer passages.

2. The pressure exchanger rotor used in the experimental investigations has been designed to run at a pressure ratio up to 1.8.

Under off design conditions it could be run up to an overall pressure equal to 2.5 atmospheres. The inclusion of transfer passages considerably weakens the strength of the pressure waves in the rotor and hence it was considered safe to run the pressure exchanger rotor up to an overall pressure ratio equal to 3.

3. The speed of the rotor could be varied only from 4000 to 7000 r.p.m. The tests were carried within a range of 5000 to 6500 r.p.m.. This does not impose a serious limitation for the optimum speed very close to 6500 r.p.m.

4. Among the geometrical variables only the relative phasing between the ports on the opposite end plates could be changed. Any variations in the port widths and the blank spaces required new end plates.

9. Analysis of the Theoretical & Experimental Results

The development of a numerical procedure for the design and performance calculations of pressure exchanger cycles and of a general purpose computer program completed the first phase of the research work.

The next phase was to apply the computerised procedure to the optimisation studies of four-port pressure exchangers with and without a transfer passage. The optimisation studies were carried out in three stages, those for:

(i) the basic pressure exchanger processes

(ii) a four-port pressure exchanger without a transfer passage

(iii) a four-port pressure exchanger with one transfer passage.

The optimisation studies were then followed by a study of the performance losses in pressure exchangers. The performance losses were mainly studied with reference to the energy requirements to overcome these losses. The main object of these investigations were;

(i) to make quantitative estimate of the energy requirements of the performance losses

(ii) to make estimate of the relative significance of these losses in pressure exchanger cycles

(iii) to determine how the performance losses are affected by the inclusion of a transfer passage in four-port pressure exchangers.

In order to justify the application of the computerised procedure to these studies and to check the validity and accuracy of computer predictions, the following steps were taken:

(i) a pressure equaliser cycle of a fixed geometry and constant speed, for which Kentfield (2) experimentally obtained optimum pressure boosting performance, was selected and its experimentally-obtained performance was compared with computer predictions.

(ii) tests were carried out on a four-port pressure exchanger without a transfer passage and the experimentally obtained performance

was compared with the theoretical predictions.

(iii) tests were carried out on a four port pressure exchanger with one transfer passage and the experimentally obtained performance was compared with the theoretical predictions.

9.1 Use of normalised quantities

All quantities presented in the theoretical and experimental results are in normalised form. The normalising factors were so chosen that they are both convenient and consistent, denoting the normalised quantities by a prime;

$u' = u/a_{ref}$ $\qquad A' = A/Aref$

$a' = a/aref$ $\qquad \phi_r$ = radial clearance $Area/Aref$

$\tau' = t\ aref/\ell$ $\qquad \phi_c$ = circumferential clearance $Area/Aref$

$x' = x/\ell$ $\qquad \phi_{eff}$ = actual cell area$/Aref$

$S' = S/R$

$f' = f\dfrac{\ell}{Pref}$

$q' = \dfrac{q\ell}{aref\ Pref}$

The widths of the port are given in the form of normalised time τ such that $\tau_{port} = \dfrac{(30 \times \theta_{port} \times aref)}{(\pi \times N \times \ell)}$ where θ_{port} is the angular width of the ports and N is the rotor speed. Similarly, the phasing between ports is given in the form of normalised time τ such that

$\phi = \tau_{phase} = \dfrac{30 \times \theta_{phase} \times aref}{\pi \times N \times \ell}$.

Cell width has been normalised such that

$$\delta = \frac{aref\ d}{\ell\ U}$$

The mass flows through the ports are usually presented in the form of integrated mass flow rate per cycle through each port. Thus $G' = \int_{\tau_2}^{\tau_1} \rho' u' A' d\tau$.

where τ_1 and τ_2 are the normalised times when the port begins to open and is fully closed respectively. In order to convert these mass flows through the port into mass flow rates, G has to be multiplied by the number of cells $\dot{N}$ which pass through a fixed point in unit time. $\dot{N} = {}^{1}/_{\delta}$.

Therefore, the mass flow rate $\dot{m}' = {}^{G'}/_{\delta}$ in normalised form.

The reference quantities aref, Pref are calculated from the atmospheric conditions. & and Aref refer to the cell dimensions.

9.2 Optimisation studies of Pressure Exchangers

In the following sections the results of optimisation studies of pressure exchangers are described and discussed. The performance of pressure exchangers is extremely sensitive to their geometry. This is a direct consequence of the unsteady nature of the flow in pressure exchanger cells. The port geometry of pressure exchangers generally includes the angular width of the ports and the angular phase difference between the ports and the blank spaces. The design of the ports and their relative positions depend primarily on the pressure ratio, temperature ratio, non-dimensional cell width, high pressure scavenge ratio, low pressure scavenge ratio and the mass flow requirements. Secondary influences are derived from cell hydraulic diameter, clearance geometry, cell wall thickness and the geometry and shape of transfer passages.

The optimisation studies of pressure exchangers were carried out in three steps.

9.2.1 Optimisation studies of basic pressure exchanger processes

Optimisation studies of the individual cases of basic pressure exchanger processes of cell filling, cell emptying, high & low pressure scavenging were carried out in order to gather a preliminary knowledge about the design and performance of these processes, and also to obtain the performance and geometrical characteristics of these processes for the pressure differential method. These studies were carried out with the help of the computerised procedure. Friction,

heat transfer, cell entry and exit and leakage losses were excluded. The temperature ratio in each case was assumed to be unity. High and low pressure scavenging calculations were carried out for complete scavenging. The performance of each process was based on the values of the mean pressures in cells.

(a) CELL FILLING

Figs. (12.1 to 12.3) show the results of such studies for a cell-filling process. In fig.(12.3) the optimum port width τ_{CF} is plotted against the cell-filling pressure ratio R_{CF} for various values of non-dimensional cell width δ. For a constant δ, τ_{CF} first decreases and then increases with the pressure ratio R_{CF}.

The strength of the waves during the first part of cell filling increases with pressure ratio and hence they move faster at higher values of R_{CF}. The waves during the second part slow down at higher values of R_{CF} because they move against the flow. These two effects cancel each other out. But the second wave moves in a hotter fluid due to compression by the first waves and therefore the net effect is a tendency to reduce the port width. We have so far neglected the effect of the temperature discontinuity which exists in the process. An interface always travels behind the first waves. The fluid ahead of this interface is at a higher temperature due to its compression by the first wave whereas the fluid behind it has a fixed temperature which was in present case a lower value. The interface does not effect the first part of cell filling substantially but the waves during the second part encounter this interface at some distance inside the cell and they slow down as they enter the cold region behind the interface. This delays their arrival at the open end and hence increases the port width. The interface penetrates deeper in the

cell at higher pressure ratios and the deeper it penetrates the greater is its delaying effect. Therefore, at higher pressures the port width tends to increase.

The delaying effect due to the interface is only because the temperature of the in-going fluid has been given as being lower than the temperature of the compressed fluid. If it is equal there will be no delaying effect. If the in-going fluid has a higher temperature the delaying effect is substituted by an accelerating effect and the port width tends to decrease. In Appendix III it is shown that the pressure rise during a filling process depends upon the bulk (product of mass flow rate and temperature) pushed into the cell during the process. Since a greater bulk is pushed in through wider ports, it can be concluded that the filling process improves with the lower temperatures of the in-going fluid.

The finite cell width tends to decrease the port widths very slightly this is because although the waves are spread out but the cell can be closed earlier to take advantage of the cell closing time (the port widths shown in figure include the cell closing time).

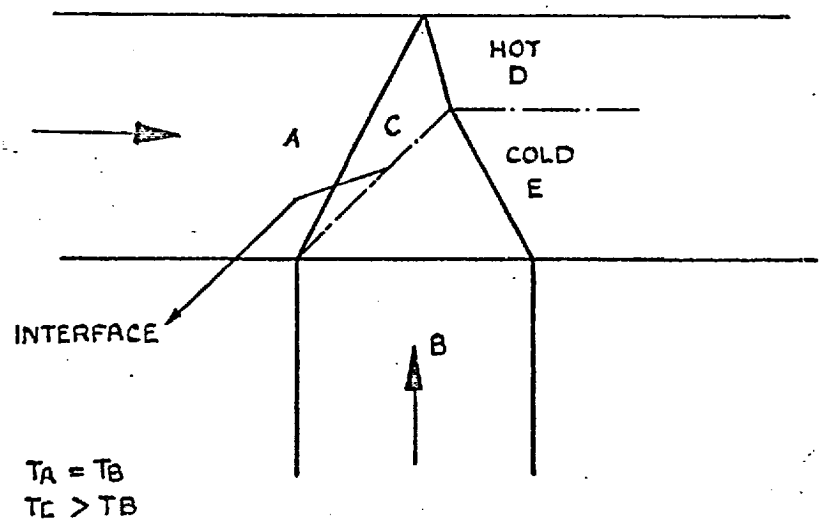


Fig. 9.2.1

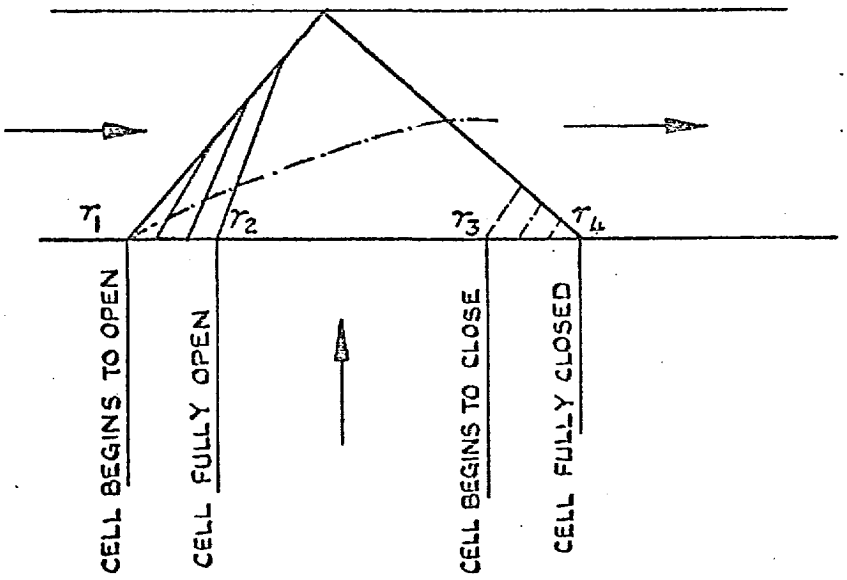


Fig. 9.2.2

$\tau_{CF} = \tau_4 - \tau_1$

Actual port width $= \tau_3 - \tau_1$

The corresponding performance characteristics of cell filling process are shown in fig. (12.2) as non-dimensional pressure rise $\Delta p_{CF}/p_{1CF}$ plotted against R_{CF} for various values of δ.

(b) CELL EMPTYING

Figs.(12.4, 12.5) show the results of such studies for a cell-emptying process. In Fig. (12.4) the optimum port width τ_{CE} is plotted against the cell-emptying pressure ratio R_{CE} for various values of δ. The cell-emptying port width τ_{CE} tends to increase with increasing values of R_{CE}. In the case of cell emptying, as in the previous case the effects of the increasing R_{CE} on the strength of the incident and reflected waves cancel each other out but the second wave moves in a colder fluid due to its expansion by the first wave and hence the port width tends to increase. The expansion waves tend to fan out, a phenomenon which increases with the pressure ratio

In the present case a temperature discontinuity does not come into consideration because the cell is initially filled with a

fluid of uniform temperature. In many cases this may not be so. A non-uniform temperature distribution in the cell would result in effects similar to those in the case of cell filling and it can be shown that the existence of some hotter fluid in the cell results in a requirement for narrower ports which means worse performance. Hence it can be concluded that the cell-emptying port width increases and its performance improves with lower temperatures of the fluid initially in the cells.

The finite cell width has very small effect on the cell-emptying port widths, this is again because even though the expansion waves are more spread out, the cell can be closed earlier to take advantage of the cell closing time.

Fig. (12.5) shows the corresponding performance characteristics of the cell-emptying process showing non-dimensional pressure drop $\Delta p_{CE}/p_{ICE}$ plotted against R_{CE} for various values of δ.

(c) HIGH-PRESSURE SCAVENGING

Figs. (12.6 to 12.10) show the results of the optimisation studies of the high-pressure scavenging process. The optimum high-pressure port phasing ϕ_{HP} is shown in fig. (12.8)

The phasing ϕ_{HP} decreases with increasing pressure ratios R_{HP} due to the increasing strength of the waves.

The finite cell width tends to increase ϕ_{HP} and flatten the curves. The increment is due to the spreading out of the waves and the flattening of curves is due to the reflection of wavelets from the closed end at low pressure ratios

In fig. (12.7) the values of high pressure outlet port τ_{HP} are displayed. For a given value of δ, τ_{HP} is very large at lower values of R_{HP}. It decreases with increasing values of R_{HP} and tends to become constant as some threshold is approached. τ_{HP} seems to be insensitive to the finite cell width again because the

reduction in mass flow during the cell-opening time is compensated by the mass flow which occurs during the closing period. (The port widths shown in fig.(12.7) include the cell closing time.)

The port area ratio $A_{HP}\ (\frac{\tau_{HPout}}{\tau_{HPin}})$ is shown in fig. (12.10) The area ratio is less than unity in all cases. The family of curves converge to unity at unity pressure ratio. This means that the high pressure inlet port width is always greater than the outlet port width in a properly designed pressure exchanger. This is so because the shock waves during the first part of the process moves slower, relative to the cell, than the head of the expansion wave during the second part of the process.

This result means that for equal static pressures at the two ports, a greater bulk of fluid flows in the cells than flows out.

The area ratio decreases with increasing pressure ratios.

The area ratio also decreases with increasing cell widths. The outlet port remains unaffected by increased cell width. If the inlet port width is not increased, the head of expansion wave which is generated earlier due to finite cell width reaches the outlet port before it has closed. Therefore, the inlet port has to be made wider.

The corresponding performance characteristics of the high pressure scavenge process is shown in fig. (12.6) as values of $\Delta p_{HP}/p_{IHP}$ plotted against pressure ratio R_{HP} for various values of δ.

(d) LOW-PRESSURE SCAVENGE

Figs. (12.9 to 12.12)show the results of optimisation studies of low-pressure scavenge process.

The low-pressure port phasing ψ_{LP} is shown in fig. (12.9) which increases with pressure ratio and finite cell widths.

The low-pressure inlet port width τ_{LP} is shown in fig. (12.11) The port widths were calculated for unity mass ratio $(\frac{m_{LPin}}{m_{2LP}})$ instead of unity scavenge ratio $(\frac{m_{LPin}}{m_{1LP}})$ and hence they curl over to show a minimum.

The corresponding performance characteristics of the low-pressure scavenge performance are shown in fig. (12.12).

In the following sections the results of the optimisation studies of four port pressure exchangers are described and discussed. The cycle investigated is shown in fig. (13.19). Other variations in port arrangements are possible. The cycle calculations were started at the beginning of the high-pressure scavenge section because the conditions in the cells after a long exposure to the low pressure ports are nearly uniform and can be readily approximated. However, the calculations were recycled until initial conditions in the cells match the final conditions.

9.2.2 Optimisation studies of four port pressure exchangers without transfer passages

The optimisation studies of the basic pressure exchanger processes were followed by similar studies of four-port pressure exchangers without transfer passages. The component processes involved in these cycles are a high-pressure scavenge process followed by a low-pressure scavenge process. These cycles can be designed and analysed by using the pressure-differential method and the approximate method.

(a) The Approximate Methods

Fig. (12.13) shows such a design chart by the pressure-differential method. The different design parameters show similar trends as shown during the component process optimisation studies. Fig. (12.14) shows similar design chart using the approximate method and this chart also shows similar trends. These design charts supply valuable preliminary information about four port pressure exchanger

cycles, particularly the port area ratios which when supplied as an initial guess to the computerised procedure saved much computer time.

These preliminary investigations were followed by wide-ranging optimisation studies of these cycles by application of the computerised numerical procedure. The pressure differential and the approximade methods are limited in their application for two main reasons:

(i) they fail to take into account the effects of the residual waves which remain in the cells between two processes. These waves influence the pressure exchanger performance in two ways:

(a) the blank spaces between ports involved in two different processes and adjacent to each other have to be optimised because existence of residual waves between the two processes means that location, in terms of time, has to be found when the most favourable conditions for the opening of the port which begins the next process are attained.

(b) the residual waves decay with time. The time-dependent nature of their decay implies that the longer they stay the less is the available energy in cells.

These two factors imply that although some blank spaces may have to be supplied to optimise the geometry, it could result in increased performance losses.

(ii) The pressure differential and the approximate methods both fail to take into account the effect of the temperature discontinuities in pressure exchangers. (Although the approximate method has been modified to take temperature discontinuity into account, it is limited and simple-minded.) The computerised numerical procedure is capable of taking both these effects into account. In the present work no

attempt has been made to optimise the blank spaces.

In the following sections, the results of the optimisation studies of a four port pressure exchanger without a transfer passage by the hybrid method are described and discussed. A value of non-dimensional cell width equal to 0.5 was used in all studies unless otherwise stated. Friction, heat transfer, leakage and cell entry and exit losses were also generally ignored.

(b) Optimisation studies of four port Pressure Exchangers without transfer passage by the Hybrid Method

(i) Performance and design for unity scavenge ratios and unity temperature ratio

The performance and geometry of a four-port pressure exchanger for unity scavenge ratios and unity temperature ratio are shown in figs. (12.15 to 12.17).

This performance and geometry is used as a standard with which to compare the performance and geometry for other values of temperature and scavenge ratios.

A comparison of these predictions with those by pressure differential and approximate method shows that the two methods give reasonably good results.

(ii) Effect of a temperature discontinuity on the performance and design of four-port pressure exchangers without transfer passages

Temperature discontinuities exist in a pressure exchanger even for a temperature ratio equal to unity but they are too weak to exert any significant influence. In order to investigate their effects it was decided to employ temperature ratios equal to 3 and 0.7 representing hot and cold pressure exchangers respectively.

Figs. (12.15 to 12.17)show the performance and geometry of these cycles for the three temperature ratios 3, 1 and 0.7. The high and low pressure scavenge ratios are both unity. Compared with the corresponding values of temperature ratio equal to 1, for the temperature ratio equal to 3 fig. (12.15) shows that the high pressure outlet port width τ_{HPout} is not much affected. The most interesting result is that for the high pressure port area ratio A_{HP} which decreases for higher temperature ratios which implies a wider inlet port in the high pressure scavenge section. This can be explained by the behaviour of the head of the expansion wave during the second part of the high pressure scavenge section. At the higher temperature ratio, the cell is almost completely filled with hotter fluid, the expansion waves at that juncture moves faster. The closing edge of the outlet port having been fixed the closing edge of the inlet port has to be brought forward to delay its closing in order to enable the head of the expansion wave to reach the opposite end just at the closing of the outlet port.

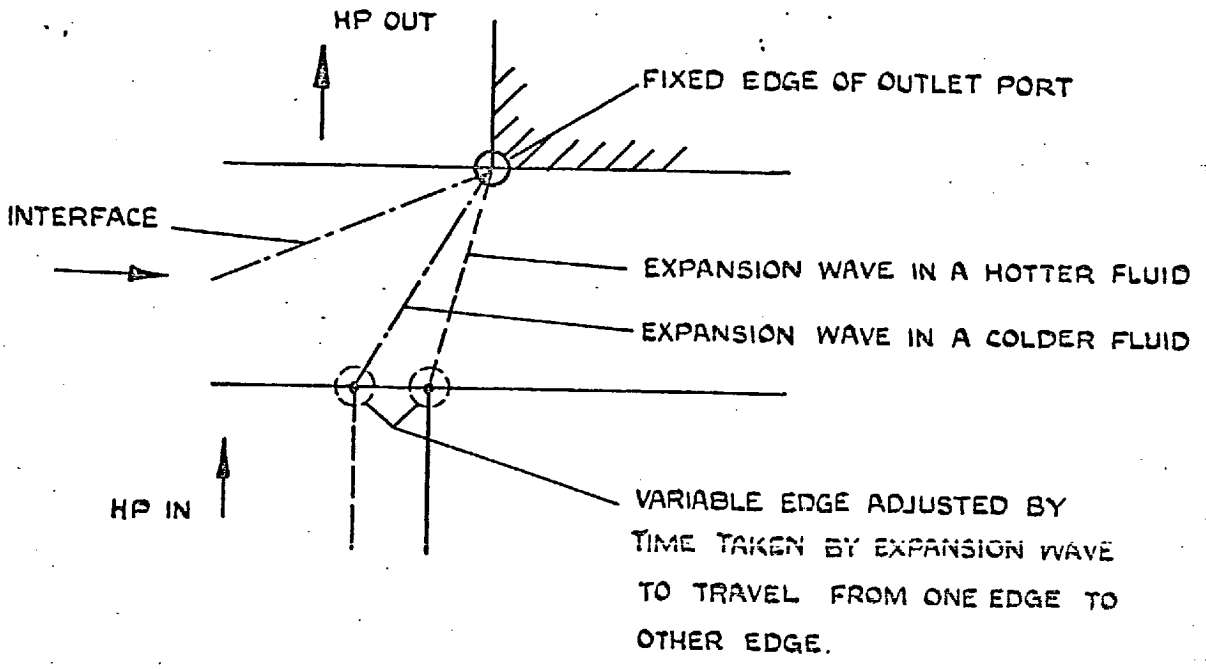


Fig. 9.2.3

This result implies that in addition to increased mixing and heat transfer losses, a hot pressure exchanger would need additional bulk input due to a wider high pressure inlet port as well. This deduction has been substantiated in fig. (12.16) which shows that a hot pressure exchanger needs a higher bulk input than a cold one. The mixing effects are demonstrated by higher high pressure outlet temperatures and lower high pressure outlet Mach numbers.

A greater value of μ at a higher temperature ratio means higher pressures in the cells receding from the high pressure scavenge section according to equation (3.1.2). This means a narrower low pressure inlet port and a higher low pressure inlet Mach number as shown in figs.(12.16). The low pressure outlet temperature is obviously very high.

The low pressure port phasing ϕ_{LP} decreases in spite of higher low pressure scavenge pressure ratio because the expansion waves which determine ϕ_{LP} move in a hotter fluid. Ideally, the high pressure port-phasing ϕ_{HP} should remain unaffected for unity scavenge ratios but due to the mixing of hot and cold fluid at the end of the low pressure scavenge process, the compression waves which determine ϕ_{HP} move in a fluid that is hotter than expected and hence ϕ_{HP} is also reduced.

Reverse trends are obtained for lower temperature ratio of 0.7.

Thus, one can conclude that in order to achieve given degrees of scavenging a hot pressure exchanger is more compact than the cold pressure exchanger but its performance in terms of non-dimensional bulk input μ is worse. A more compact pressure exchanger means that for the same geometry it has to

run at higher speeds to attain the same degrees of scavenging.

(iii) Effect of degree of scavenge

If temperature discontinuities in pressure exchangers are ignored, the scavenge ratios would not have any effect on the port phasing and port area ratios. The port widths will decrease to accommodate lower scavenge ratios (and increase for higher scavenge ratios). This would result in a reduction in maximum cycle time and a subsequent reduction in the time-dependent performance losses. This means that, ignoring the temperature discontinuity-scavenge ratio interactions, the performance of pressure exchanger will improve for lower values of scavenge ratios.

In the following studies it is sought to investigate how temperature discontinuities and scavenge ratios interact with each other to effect the geometry and performance of four-port pressure exchangers without transfer passages. Figs. (12.18,20) show the performance and geometry of these pressure exchanger cycles for the three temperature ratios 3, 1 and 0.7 respectively. The high pressure scavenge ratio is equal to 0.5 and the low pressure scavenge ratio is equal to 1.

For all temperature ratios, (comparing again with the corresponding values for unity scavenge ratios) the high pressure ports are reduced in size. This is a direct consequence of the lower value of the high pressure scavenge ratio. In order to analyse the effects on other parameters we shall again discuss these values for a temperature ratio equal to 3 and compare them with the corresponding values for unity scavenge ratios.

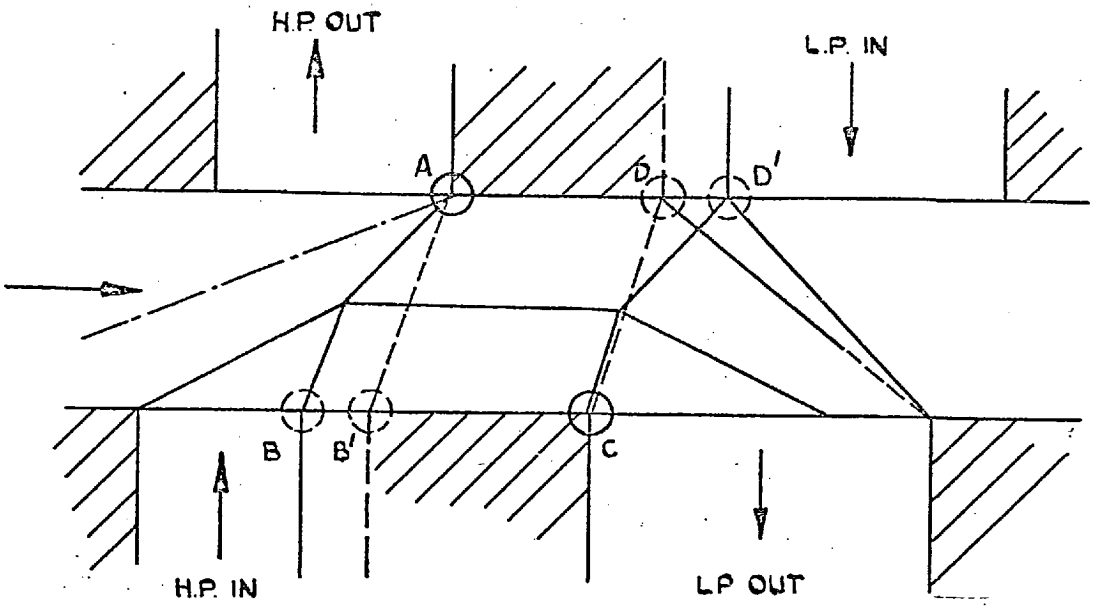


Fig. 9.2.4

The sketch shown above is a simple diagram of a four port pressure exchanger. The full lines show the situation when the high pressure scavenge ratio is equal to 0.5. The dashed lines show the situation when the high pressure scavenge ratio is equal to unity. The regions affected by the scavenge ratio-temperature discontinuity interaction are the second part of high pressure scavenge section and the first part of low pressure scavenge section. The points shown by full circles are fixed points and those shown by dashed circles are variable points determined by the behaviour of waves in that region.

It is now clear from the sketch that for a lower value of high-pressure scavenge ratio (less than unity) the waves at both regions take more time to reach the opposite end because they have to move in colder fluid for some time. This results in (relatively) smaller high pressure inlet ports and higher low pressure port phasings. These tendencies are confirmed in fig. (12.18). Smaller difference between high pressure inlet and outlet port width means an improvement in

performance. Thus, low values of high pressure scavenge ratio result in an improvement in performance of hot pressure exchanger and worsening of performance of cold pressure exchanger due to scavenge ratio-temperature discontinuity interaction. This is confirmed by fig. (12.19) which shows lower values of μ for temperature ratio equal to 3 and slightly higher values for temperature ratio equal to 0.7. Mach numbers at high pressure outlet and the width if low pressure inlet ports are increased as a result of lower temperatures due to low scavenge ratio for temperature ratio equal to 3.

Figs. (12.21,23) show the performance and geometry of four-port pressure exchangers without transfer passage for three different temperature ratio equal to 3., 1. and 0.7 respectively. The high pressure scavenge ratio is equal to 1. and the low pressure scavenge ratio equal to 0.5.

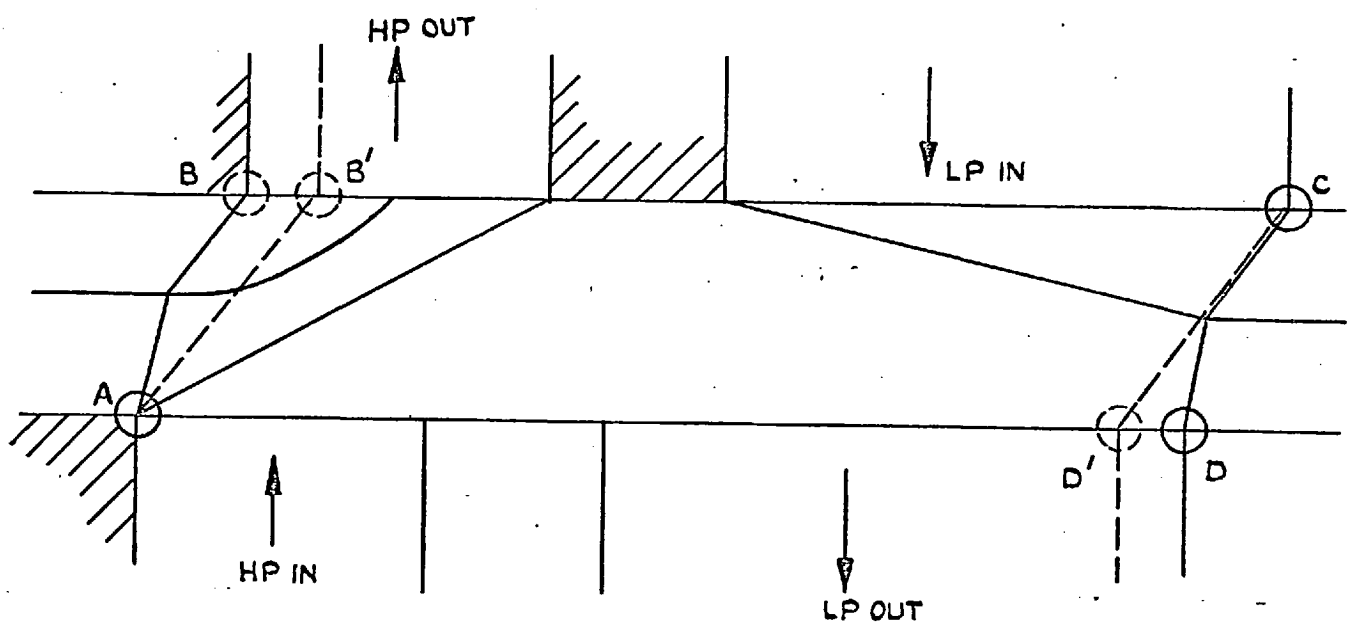


Fig. 9.2.5

The sketch shown above is a simple diagram of a four port pressure exchanger. The full lines represent the situation

when low pressure scavenge ratio is equal to 0.5. The dashed lines represent the situation when it is equal to 1. The regions affected by the scavenge ratio-temperature discontinuity interaction are the second part of low pressure scavenging and the first part of high pressure scavenging processes. The points in full circles are fixed points and those shown in dashed circles are variable points depending upon the behaviour of waves in that region, as before. Discussing these effects again for a temperature ratio equal to 3 and comparing with the corresponding values for unity scavenge ratios (as shown in the sketch) it is shown that the waves in both regions take less time to reach the opposite ends because they move in a hotter fluid for some time. The high pressure port phasing decreases and the difference between the width of low pressure inlet and outlet ports increases. This results in a higher pressure after the low pressure scavenge section. This decreases the pressure ratio across the high pressure scavenge section resulting in wider ports but less bulk input. These trends are confirmed in figs. (12.21 to 12.23) which also show lower Mach numbers and higher temperatures at high pressure outlet ports. Reverse trends (as expected) are shown for lower temperature ratio equal to 0.7.

Figs.(12.24,34) show the performances and geometry of four port pressure exchangers for various combinations of scavenge ratios and now most of them are self-explanatory.

(iv) Effect of finite cell width

Figs.(12.35,36)show the performance and geometry of four port pressure exchangers without transfer passages for non-dimensional cell width equal to 0, while figs.(12.37,38) show that for non-dimensional cell width equal to 1. In all cases

the high and low pressure scavenge ratios and the temperature ratio are equal to 1.

A comparison of these two figures gives the effect of finite cell width on the performance and geometry of these cycles. The two figures confirm the results of the component process optimisation studies. The high pressure outlet and low pressure inlet ports remain uneffected. The high pressure inlet and low pressure outlet port increase and both these effect result in worse performance confirmed by fig. (12.35,38)

(v) Effects of performance losses

Figs(12.39,40) show performance and geometry of four port pressure exchangers for unity values of scavenge ratios and temperature ratio. The non-dimensional cell width equal to 0 with friction, heat transfer, cell entry and exit and leakage losses taken into account for representive values of cell hydraulic diameter, clearance geometry and cell wall thickness.

The design characteristics show that these losses do not have a significant effect on the geometry of these pressure exchanger cycles. At low pressure ratios when the ports are wider the performance losses lead to some significant increase in port widths. This demonstrates the time-dependent nature of these losses. The inclusion of performance losses in design calculations takes a great deal of computer time. Since it has been shown that performance losses do not have a significant effect on the geometry of pressure exchangers it would be advisable to carry out design calculations without taking these losses into account under normal circumstances. The effect of performance losses on the performance of these cycles is to increase the bulk input, slightly lower the high

pressure outlet Mach number and increase the low-pressure inlet Mach numbers. The temperatures and mass flows are also only slightly affected. The performance losses are discussed in detail in section

9.2.3 Optimisation studies of four-port Pressure Exchangers with one transfer passage

In the following sections the results of the optimisation studies of four port pressure exchanger with one transfer passage are described and discussed. The cycle investigated is shown in fig.(13.20). Other variations in port arrangements are possible. The cycle calculations were started at the beginning of the cell filling process because the conditions in the cell after a long exposure to the low pressure ports are nearly atmospheric and can be approximately guessed. The calculations have to be recycled until initial conditions in cells match the final conditions. In the case of transfer passages the boundary conditions in transfer ports are also unknown. These boundary conditions include:

(a) Stagnation pressure and temperature of the fluid in the filling port.

(b) Stagnation or static pressure of the fluid in the emptying port.

The boundary conditions in transfer ports depend upon a number of factors. The number of unknowns are reduced if the losses in transfer passages are ignored. In an ideal transfer passage the stagnation pressures and temperatures at the two ports are equal. The following procedure was applied.

1. An initial guess of the stagnation pressure at the transfer ports was obtained from the pressure differential method. An initial guess of the stagnation temperature at the filling process was taken to be the temperature obtained by isentropic expansion of the fluid entering the high pressure inlet port to the pressure

in the emptying port.

2. Initial conditions in the cell just before the cell filling process were guessed. The velocity everywhere was assumed to be zero and pressure and temperature were assumed to be uniformly distributed.

The calculations were then performed until one cycle was completed. The calculations were then repeated for the next cycle with,

(a) Initial conditions for the new cycle were set equal to the final conditions for the previous cycle.

(b) The stagnation temperature in the filling port was set equal to the calculated steady flow stagnation temperature in the emptying port.

(c) The stagnation pressure in the transfer ports was adjusted to satisfy mass conservation in the transfer passage.

The whole procedure was repeated for a number of cycles until the three conditions were satisfied to an acceptable degree. It took a number of cycles to reach such a stage. Although transfer passage losses were not taken into account during the optimisation studies, the procedure to take these losses into account (for an investigation into these losses, see section 9.3.2) was to calculate the pressure drop in the transfer passages based on the conditions in them obtained from calculations for ideal transfer passage and the geometry and shape of the duct, and repeat the cycle calculations to accommodate this pressure drop and also satisfy the three conditions discussed earlier.

(a) <u>The Approximate Methods</u>

Figs.(12.41,43) show the performance of four port pressure exchangers with one, two, three and four transfer passages respectively, in terms of the non-dimensional bulk input μ required to achieve a certain

pressure ratio R. The performances for unity values of high pressure scavenging, low pressure mass ratio and temperature ratio were worked out for various values of δ using the pressure-differential method and are of a very preliminary nature. They show that the pressure exchanger performance should improve with increasing number of transfer passages in the absence of friction, heat transfer, leakage, cell exit and entry, transfer passage losses. Ultimately, no energy input would be required to achieve a pressure ratio. These performance estimates also show how the performance deteriorates with increasing widths of cells and that this effect is more significant as the number of transfer passages increased.

Fig. (12.44) shows a design chart for a four port pressure exchanger with one transfer passage. The pressure differential method was used. The high pressure scavenge ratio, the low pressure mass ratio and the temperature ratio all unity. The non-dimensional cell width is equal to 0.4. A comparison of this design chart with that for a four port pressure exchanger design chart also by the pressure differential method reveals that for given pressure and scavenge ratios the main effect of the inclusion of a transfer passage on the geometry is to increase the widths of the high and low pressure ports. The inclusion of two more ports for the transfer passage itself means the maximum cycle time is greatly increased. Figs.(12.45,46)show the transfer port boundary conditions predicted by the pressure differential method for an ideal transfer passage and properly designed ports.

Fig. (12.47) shows performance of a four port pressure exchanger with one transfer passage predicted by the approximate method. The high pressure scavenge, low pressure scavenge and temperature ratios are again all unity. The non-dimensional cell width δ is equal to 0.54. A comparison of this performance with that of four port pressure exchanger without a transfer passage show for one transfer passage lower values of bulk input, but the Mach numbers and hence velocities

at high pressure outlet and low pressure inlet ports are much smaller. The high pressure outlet temperatures are also slightly smaller because of the recirculation of colder fluid via transfer passage. The geometry of a four port pressure exchanger with one transfer passage predicted by the approximate method in fig. (12.48) shows trends similar to those predicted by the pressure differential method. The approximate method predicts narrower ports than the pressure differential method. This is so because in the approximate method no account is taken of the effect of the waves travelling back and forth along the cell to influence the mass flow rates in the ports.

(b) Optimisation studies of four port pressure exchangers with one transfer passage by the Hybrid Method

In the following sections, the results of optimisation studies of a four port pressure exchanger with one transfer passage by the hybrid method are described and discussed. A value of non-dimensional cell width equal to 0.4 was used in all studies unless otherwise stated. In order to save computer time, the area ratios of the high and low pressure ports were assumed to be unity, an assumption justified by the fact that at low pressure ratios, as often involved with a transfer passage, the area ratio tends to be equal to unity anyway. Friction, heat transfer, cell entry and exit, leakage and transfer passage losses were generally ignored unless otherwise stated.

(i) Performance and geometry of a four port pressure exchanger with one transfer passage for unity scavenge ratios and unity temperature ratio

Figs.(12.49,51)show the performance and geometry of these cycles for the given conditions. A comparison with the performance and geometry of four port pressure exchangers without a transfer passage for similar conditions by the hybrid method again shows that for a given pressure ratio the non-

dimensional bulk input decreases but the flow velocities are much smaller resulting in larger port widths for high and low pressure scavenge sections.

At this point is is appropriate to discuss how wider ports can be incorporated in a pressure exchanger. The port widths are calculated in terms of non-dimensional time τ which is equal to

$$\frac{60 \times \theta_{port} \times a_{ref}}{2\pi N \times \ell}$$

This means for a given a_{ref}

$$\tau \propto \frac{\theta_{port}}{N \times \ell}$$

In order to increase τ following alternatives can be tried

1) Reduce the length of cells ℓ. This would reduce the volumetric capacity of cells unless cell height or width is increased proportionately and increase the value of δ. An increment in cell width is not desirable. In order to increase cell height the outer diameter of the rotor has to be increased. This would result in a shorter rotor with a bigger diameter. The mean width of cells would also increase and to prevent this the number of cells will have to be increased.

2) Reduce the rotor speed N. In order to maintain the same value of δ, either the cell length or the number of cells would have to be increased.

3) Increase the angular width of the ports θ_{port}. The angular widths of the ports is restricted by the total available angle which is equal to 2π radians.

Here an examination of the pressure exchanger plots is useful. Figs. (12.52, 53) show the computer plots for a four port pressure exchanger without and with one transfer passage respectively for unity values of scavenge and temperature ratios. A comparison of the two plots gives the following results.

(a) The non-dimensional maximum cycle time τ_{max} for a four port pressure exchanger without a transfer passage is approximately equal to 13, whereas for a four port pressure exchanger with one transfer passage it is equal to 56. These two figures show that the changes in rotor dimensions to accommodate the given scavenge ratios in a four port pressure exchanger with one transfer passage are quite appreciable.

(b) The number of interfaces separating the fluids of different temperatures inside the rotor increases in a four port pressure exchanger with one transfer passage. This results not only in increased mixing losses but also in fluid streams of different temperatures flowing out of the high pressure outlet port and this phenomenon is undesirable in many pressure exchanger applications. Thus, the recirculation of the high pressure inlet port fluid via transfer passage and its escape from the outlet port means that even for a unity scavenge ratio in the high pressure region the temperature of the out-going fluid is not independent of the temperature of the in-going fluid. This independence can only be ensured by following the interface in the cell filling process and closing the high pressure outlet port when the interface reaches the opposite end. In case of more than one

transfer passages it will be the interface at the first filling process which has to be followed resulting in a further reduction in high pressure port and lesser mass flows.

(c) An examination of the velocity-profiles of the two diagrams reveals that the velocities in the scavenging ports of a four port pressure exchanger with one transfer passage are very low. This means very large fairing angles at this port will have to be incorporated to provide the required whirl component to the velocities. An increasing number of transfer passages would result in extremely low velocities and either a fan would have to be provided to help the scavenging or transfer passages should only be employed to attain higher pressure ratios rather than lower bulk inputs for same pressure ratios. The velocities in the transfer ports are quite appreciably greater than those in the scavenging ports. The pressure losses associated with transfer passages are proportional to the square of velocity and hence this means that transfer passage losses are quite significant and may have an appreciable effect on the performance of four port pressure exchangers with transfer passages. The wavy pattern of the velocity profiles in the scavenging sections demonstrates the increasing effects of residual waves and the need to optimise the blank spaces as transfer passages are included in pressure exchanger cycles.

(ii) Effect of temperature discontinuity

Figs.(12.49, 51) show the performance and geometry of four port pressure exchanger with one transfer passage for three temperature ratios equal to 3, 1 and 0.7 respectively. The

high and low pressure scavenge ratios are both equal to unity. The effect of temperature discontinuity may now be assessed by comparing the geometry and performances of these cycles for temperature ratios of 3 and 1. A reverse trend would be expected for 0.7.

The comparison shows that again a hot pressure exchanger is more compact than a cold pressure exchanger. The filling port is smaller because of the hot fluid being recirculated via transfer passage. This results in a lower pressure before the high pressure scavenge section which leads to smaller high pressure ports, increased bulk input and high pressure outlet Mach number. The temperature at the high pressure outlet port also increases because of the hot recirculated fluid excaping through the high pressure outlet port, and hence the Mach number does not vary much. The high pressure port phasing ϕ_{HP} also decreases for the relevant compression wave moves in a hotter fluid for some time.

The emptying port is smaller because the expansion waves move in a hotter fluid. This results in a higher pressure before the low pressure scavenge section and this implies narrower low pressure ports and higher low pressure inlet Mach number. The low pressure port phasing ϕ_{LP} also decreases.

These trends are shown in figs. (12.49,51) and the opposite trends (as expected) are shown for lower temperature ratio equal to 0.7.

The effect of a temperature discontinuity on a four port pressure exchanger with one transfer passage is greater than that on the pressure exchanger without a transfer passage. (It may be added here that for given conditions the transfer passage pressure slightly decreases with higher temperature ratios.)

(iii) Effect of scavenge ratios

In this section the effects of scavenge ratio-temperature discontinuity interaction for a four port pressure exchanger with one transfer passage has been studied. These effects are assessed by comparing the performance and geometry of these cycles for a given combination of scavenge ratio with the performance of the same cycle for the same temperature ratio and unity scavenge ratios. The temperature ratios selected for this purpose are again 3 and 0.7. Figs. (12.54,56) show the performance and geometry of four port pressure exchangers with one transfer passage for three different temperature ratios 3., 1. and 0.7 respectively. The high and low pressure scavenge ratios are 0.5 and 1 respectively.

For a temperature ratio equal to 3, the comparison with the performance and geometry for unity high pressure scavenge ratio shows;

1. The cell-filling port width τ_{CF} and high pressure port phasing ϕ_{HP} remain unaffected. A lower scavenge ratio still results in some hot fluid being recirculated.
2. The high pressure ports are smaller because of lower port widths. The difference between the outlet and inlet port (not shown in diagram) would decreae resulting in lower bulk input.
3. The high pressure outlet Mach number remains unaffected. (It increases slightly to show less mixing.) The temperature at the outlet port is also decreased.
4. The cell emptying ports are wider because the relevant expansion waves move in colder fluid for some time.

5. A wider emptying port means a lower pressure in the cells before the low pressure scavenge section resulting in wider ports and lower low pressure inlet Mach numbers. The temperature at the low pressure outlet ports are also lower.

These trends are shown in figs. (12.54,56) andthe opposite trends (as expected) are shown for the lower temperature ratio 0.7.

Figs. (12.57 to 59) show the performance and geometry of four port pressure exchangers with one transfer passage for three different temperature ratios 3, 1 and 0.7 respectively. The high and low pressure scavenge ratio are 1 and 0.5 respectively, i.e. the reverse of the previous case.

For a temperature ratio equal to 3, the comparison with the performance and geometry for unity scavenge ratios show;

1. The cell emptying port width τ_{CE} and the low pressure port phasing ϕ_{LP} remain unaffected because they do not come into the zone of dependence of the low-pressure scavenge ratio.
2. The cell filling port is smaller because additional hot fluid is recirculated by the cells receding from the low pressure scavenge section and entering the filling process. This further worsens the filling performance and results in a lower pressure before the high pressure scavenge section.
3. The high pressure port widths are therefore increased and so are the bulk input and high pressure outlet Mach number.
4. The temperature at the high pressure outlet port is increased. The temperature at the low pressure outlet port is also increased because of the reduced mixing.

5. The high pressure port phasing ϕ_{HP} is also reduced for same reasons as given in (2).

to 69)
Fig.(12.60/show performance and geometry of four port pressure exchanger with one transfer passage for various combinations of scavenge ratios and most of these are now self-explanatory.

(iv) Effect of finite cell width

Figs. (12.70,71) show the performance and geometry of a four port pressure exchanger with one transfer passage. The high and low pressure scavenge ratios and the temperature ratio are all equal to unity. The non-dimensional cell width is equal to 0. The performance and geometry of the same cycle for the same conditions but for non-dimensional cell width equal to 0.8 is shown in figs. (12.72,73).

The cell width seems to have greater influence on the geometry and performance of a four port pressure exchanger with transfer passage than on a pressure exchanger without transfer passages. The high and low pressure port widths are both reduced and the bulk input is increased. The increased effect is due to worse filling and emptying performances with finite cell width.

(v) Effect of performance losses

Figs. (12.70,71)show the performance and geometry of a four port pressure exchanger with one transfer passage. The high and low pressure scavenge ratios and the temperature ratio are all equal to unity. The non-dimensional cell width is equal to 0. Figs (12.74,75) show the performance and geometry of the same cycle for the same conditions but with friction, heat transfer, cell entry and exit and leakage losses taken into account for representative values of cell hydraulic diameter, clearance geometry and cell wall thickness.

The effect of these losses are to increase the widths of the scavenging ports. The time-dependent nature of these losses is demonstrated by the fact that they have more significant effect on the ports of the four port pressure exchanger with one transfer passage (because they are wider) than on the ports of four port pressure exchanger without transfer passage, and also because their effects are more pronounced at low pressure ratios (wider ports).

The performance, as expected, worsens due to these losses and they are discussed in section .

9.3 A study of the performance losses in pressure exchangers

In the following sections an analysis of the results of a study of the performance losses in four port pressure exchangers with and without transfer passages is presented. The results of the study would in general also apply to other pressure exchanger cycles.

In a reversible pressure exchanger the non-dimensional bulk input is always equal to zero. The compression of the driven fluid is completely carried out by the expansion of the driving fluid and no external energy has to be supplied to the pressure exchanger. But there are always some irreversibilities to be encountered and in order to overcome these external energy in some form has to be supplied to the pressure exchanger. Friction, heat transfer, leakage, unstreamlined cell exit and entry and energy degradation in transfer passages are all different sources of irreversibilities in pressure exchanger. A certain amount of energy is required to overcome these losses. Thus the non-dimensional bulk input required to overcome any loss is a measure of its effect on the performance of that pressure exchanger cycle. Therefore, the non-dimensional bulk input μ has been used as the main criterion to study the various sources of performance losses and their relative significance.

9.3.1 Performance losses in four port pressure exchangers without transfer passages

Fig.(12.76)shows the non-dimensional bulk input required to overcome different sources of performance losses. These non-dimensional bulk inputs were obtained for a four port pressure exchanger without transfer passage having a fixed geometry and constant speed shown in fig. (13.21).

The friction and heat transfer losses increase with pressure ratio. Higher velocities are associated with higher pressure ratios. Although the co-efficient of friction and Stanton number both decrease slightly with increasing Reynolds number, factors f and q both increase as the cube and square of the velocity respectively hence friction and heat transfer both increase with pressure ratio.

The cell entry and exit losses also increase with the pressure ratio. These losses are also proportional to the square of velocity.

The leakage losses, calculated by the mass and energy correction method increase very slowly with pressure ratio.

The total losses, therefore, also increase with pressure ratio.

These losses in decreasing order of their relative significance are as follows.

1. Wall friction & heat transfer.
2. Cell entry and exit losses.
3. Leakage losses.

If the following phenomena are included (which are also the causes of the departure of the actual performance from the isentropic ideals) in the performance losses

(i) The basic wave effects taken into account when performance is predicted by the hybrid method for infinitely narrow cells.

(ii) The effects of finite-cell widths on wave events.

then the performance losses in order of decreasing significance are:

1. The basic wave effects.
2. The finite cell width.
3. Wall friction & heat transfer.
4. Cell entry and exit losses
5. Leakage losses.

This analysis is valid for a fixed geometry and constant speed operation of a four port pressure exchanger without a transfer passage. It has been shown that the total losses increase with pressure ratio. In fact, this pressure exchanger is designed for one pressure ratio at which unity scavenge ratios in the high and low pressure sections are achieved. The performance at other pressure ratios are "off design performances'.

In order to evaluate the performance losses for each pressure ratio at its design point, total losses were obtained for a fixed scavenge ratio operation of a four port pressure exchanger without transfer possages in which the high and low pressure scavenge ratios were fixed at unity.

Fig. (12.77) show these losses plotted as non-dimensional bulk input μ_{Loss} against pressure ratio R. A comparison of these losses with the corresponding losses for a fixed geometry operation show that the total losses have increased at low pressure ratios and decreased at higher pressure ratios. This happens because of the time-dependent nature of friction, heat transfer cell entry and exit and leakage losses. At low pressure ratios, although the velocities are the same for a fixed scavenge ratio operation the port widths are much bigger than those for fixed geometry operation. Thus τ_{max}, i.e. the maximum cycle time is much greater for fixed scavenge ratio operation resulting in increased losses. Similar considerations apply to fixed scavenge ratio operation at higher pressure ratios when τ_{max} is less and hence the losses decrease.

Since τ_{max} can be decreased by increasing the rotation speed N it follows that the friction heat transfer, cell entry and exit and leakage losses reduce at higher speeds.

(A note about heat transfer)
In present investigations friction & heat transfer affects have been calculated as one loss. Since the temperatures are low the dominant part is obviously friction only. Hence, the friction & heat transfer may be taken as only friction loss. Heat transfer loss is likely to be dominating at higher temperature ratios and this case has not been investigated.

9.3.2 Performance losses in a four port pressure exchanger with one transfer passage

Fig. (12.78) shows the non-dimensional bulk input required to overcome different sources of performance losses. These performance losses were obtained for a four port pressure exchanger with one transfer passage having a fixed geometry and constant speed. This cycle is shown in fig. (13.22).

The friction and heat transfer losses again increase with increasing pressure ratios. Comparing these losses with the losses for the four port pressure exchanger without transfer passage (which had the same τ_{max} and are described in previous section) it is found that the friction and heat transfer losses are less in the case of the four port pressure exchanger with one transfer passage. This is due to the lower velocities in these cycles predicted in section

The cell entry and exit losses also decrease as compared with the

case of no transfer passage again due to lower fluid velocities.

The leakage losses again increase with pressure ratio but they are much greater for a four port pressure exchanger with one transfer passage. This is due to an increase in the pressure level in the cycle due to insertion of transfer ports and reduced low pressure port widths.

The transfer passage losses are small at low pressure ratios but increase rapidly at higher pressure ratios and are the most significant losses in the range of pressure ratios at which transfer passages are more useful.

The transfer passage losses are of such significant magnitude because fig. (12.78) shows that even though the fluid velocities in the scavenging sections are quite low, velocities in the transfer ports are appreciable and transfer passage losses, being proportional to the square of the velocities in transfer port, therefore assume significant magnitude.

Thus, the performance losses in order of their decreasing importance in a four port pressure exchanger with one transfer passage are as follows.

1. The basic wave effect.
2. The finite cell width.
3. Transfer passage energy losses.
4. Friction & heat transfer.
5. Leakage losses.
6. Cell entry and exit losses.

As in the case of the four port pressure exchanger without transfer passage, in order to evaluate the performance losses for each pressure ratio at its design point the total losses were evaluated for operation at fixed unity scavenge ratios. Transfer passage losses are not time-dependent hence they were not calculated.

A comparison of the total losses (excluding transfer passage losses) for fixed scavenge ratio operation shown in fig. (12.79) and for fixed geometry operation, again show similar trends to those shown for the four port pressure exchanger without a transfer passage. A Comparison of the total losses for fixed scavenge ratio operation of the four port pressure exchanger with and without transfer passage respectively show that for this type of operation the total losses (inclusive of transfer passage losses) in a four port pressure exchanger with one transfer passage are greater.

9.4 Comparison of Theoretical & Experimental Results

The application of the hybrid method to the unsteady flow in shock tubes with friction, heat transfer and variable entropy by Issa (26) and to the inlet and exhaust systems of internal combustion engines with friction, heat transfer, area change and variable entropy by Benson et al (12) has given satisfactory results. Matthews (15) showed that for homentropic flows in pressure exchangers, the predictions by the hybrid method are in good agreement with predictions by a graphical procedure.

The comparison of the theoretical and experimental predictions in the case of shock tubes and the inlet and exhaust systems of an engine does not present any significant problem because the measurements of the flow conditions in these unsteady but stationary systems is relatively simple.

The pressure exchanger differs from these two systems in two distinct ways.

(i) The relative motion of the cells makes it very difficult to measure the conditions inside the cells. The conditions in the cell ends can be measured through holes in the stationary end plates but even then the measurements would be misleading because of the leakage through the clearance gap. In this respect a stationary rotor with rotating end plates seems to be a better proposition. Azouri (16) and Cotter (19) employed this idea by

providing a sliding vane across the open end of a duct to simulate cell filling and emptying processes.

(ii) Our main task is to be able to predict the performance of pressure exchanger cycles which, although dependent upon the unsteady flow in the cells, is usually related to the conditions in pressure exchanger ducts. The conditions in these ducts naturally depends upon the flow conditions in cells which are predicted by the computerised procedure. In order to predict the conditions in the ducts some co-relation has to be found between the unsteady flow in cells and the flow in ducts which may or may not be steady.

In the present work these relations have been derived by assuming steady flow in the ducts such that the mass and energy flows through the ports, as predicted by the unsteady flow in cells, are conserved in an area equal to the port area allowance being taken of the cell wall thickness.

The losses in pressure exchanger ducts are external losses and they have to be calculated separately in performance estimates. In the present work the losses in the high pressure loop are taken equal to one dynamic head. The low pressure exhaust kinetic energy is assumed to be unavailable and the transfer passage losses are calculated from the steady flow loss data depending upon the geometry and shape of transfer passages and the conditions in them.

The conditions in the ducts are simpler to measure for no relative motion is involved in this case.

These additional considerations for pressure exchanger cycles are liable to render the theoretical predictions less accurate than those for shock tubes and the inlet and exhaust systems of an engine.

9.4.1 Comparison of the Theoretical and Experimental predictions for an Equaliser cycle

The most reliable experimental data, in the Author's opinion, from the published works on pressure exchanger cycles are those related to

the pressure equaliser and divider cycles by Kentfield (2).

The pressure equaliser cycle having a fixed geometry and a constant speed for which Kentfield obtained the best pressure boosting equaliser performance was selected for the comparison. The geometry of the cycle is shown in fig. (13.23).The experimentally obtained performance of this cycle is shown in fig. (12.80) from reference (2). The performance chart shows the values of ξ and M_H in a P_{Ho}/P_{Mo} plane. The significance of these performance criteria is explained by Kentfield (2).

Theoretical predictions of the performance of this equaliser cycle were made not only to check the validity and accuracy of the computerised procedure as a whole but also to be able to compare the three different methods proposed for taking into account the leakage effects.

The performance calculations were started with the cell in a position when the high pressure ports begins to open. The initial conditions of a uniform pressure and temperature in the cell were guessed. The velocity everywhere was assumed to be zero. The calculations were repeated for several cycles until the initial and final conditions in the cell matched and mass conservation at the equaliser ports was satisfied.

Normally, the equilibrium conditions were attained in six cycles. Friction, heat transfer, cell entry and exit and leakage losses were taken into account.

Fig. (12.81) shows the equaliser performance chart. Leakage losses were taken into account by the mass and energy correction method.

Fig.(12.82) shows a similar chart in which leakage losses were taken into account by the porous cell end method.

Finally, Fig. (12.83) shows the performance chart in which leakage losses were taken into account by the partly open end method.

These figures show that the computer predictions are, generally, in good agreement with the experimental results. The constant ξ curves are predicted quite accurately. The values of M_H are predicted more accurately at lower values than at higher values.

There is little to choose between the three leakage methods. So a better criterion would be to consider the computing time taken by each method. The three methods in order of increasing computing time required are as follows.

(i) The mass & energy correction method.

(ii) The partly open end method.

(iii) The porous cell wall method.

9.4.2 Comparison of the Theoretical and Experimental predictions for a four port pressure exchanger without a transfer passage

The general features of the experimental rig on which tests for a four port pressure exchanger without a transfer passage were carried out are described in section 8.4.1. The experimental rig could not be designed for great accuracy due to the shortage of time and funds. An additional feature which made measurements more difficult was the way in which the make-up mass flow was introduced by a nozzle injector very close to the high pressure inlet port. The pressure of the make up air was usually kept much higher so that the air which was recirculated from the high pressure outlet port towards the inlet port could be pumped up by the injector effect. This arrangement made the flow condition in the high pressure inlet port very uncertain due to the mixing of the two different streams in that region. It was decided to measure the mass flow rates at the high pressure outlet port and of the make up air supply at a safe distance upstream of the loop injector. The mass flow rate in the high pressure inlet port was then calculated from the sum of two flows. Similarly, the temperatures of the make up air supply and of the air escaping through the high

pressure outlet port were measured and the temperature of the air entering the high pressure inlet port was calculated by application of the energy equation. The static pressure at the high pressure inlet port was measured assuming that even in a mixing flow the static pressure at any cross-section is uniform. The stagnation pressure in each port was established from a knowledge of the mass flow and static pressure by substitution in the well-known isentropic relation

$$P_o = P\{1 + \frac{\gamma-1}{2} M^2\}^{\frac{\gamma}{\gamma-1}} \qquad (9.4.1)$$

Thus,

$$P_o = P^{-\frac{1}{\gamma-1}} \{P + \frac{\gamma-1}{2\gamma} \frac{m^2}{\rho(A_{port})^2}\}^{\frac{\gamma}{\gamma-1}} \qquad (9.4.2)$$

In order to generalise the experimental results and assist their comparison with theoretical results port widths, phasing angle, cell widths etc. have again been expressed in dimensionless units. Atmospheric conditions were used as reference conditions. The normalisation has been explained in section

Pressure drop in the high pressure loop was neglected and conditions in the low pressure inlet port were assumed to be atmospheric.

The mass flows through the high pressure outlet port are again presented in the form of the normalised mass flow through the port per cycle. To convert them to normalised mass flow rate through the port, they must be divided by δ.

Figs.(12.84,85) show the performance chart of a four port pressure exchanger without transfer passage at rotor speeds of 5000 and 6000 rev/min. respectively. The performance chart shows the values of the bulk input μ, mass flow through the high pressure outlet port, steady flow Mach number M_{HPout} and the stagnation temperature T_{HP} at the

high pressure outlet port, against in normalised form overall pressure ratio R. The theoretical predictions are shown in full lines.

The experimentally obtained values of non-dimensional bulk inputs are slightly higher than the theoretical values, the temperatures at the outlet ports are accurately predicted. The experimental high pressure outlet values at the steady flow Mach number and mass flows are slightly smaller than the theoretical values. In general, good agreement between the experimental and theoretical predictions is found.

9.4.3 Comparison of the Theoretical & Experimental Results for a four port pressure exchanger with one transfer passage

The general features of the experimental rig on which tests for a four port pressure exchanger with one transfer passage were carried out are described in section 8.4.1. The limitations and shortcomings of the test rig were similar to those for the four port pressure exchanger without a transfer passage. The mixing at the high pressure inlet port in the case of a transfer passage resulted in greater discrepancies due to lower fluid velocities there. The additional measurements made were of the static pressures and the temperature in the transfer ports. Arrangements were also made to check the flow direction in the transfer passage.

Figs.(12.86,89)shows the performance chart of a four port pressure exchanger with one transfer passage for various rotor speeds.

These show, the values of the bulk input μ, mass flow through the high pressure outlet port, steady flow Mach number M_H and the stagnation temperature at the high pressure outlet port in normalised form against overall pressure ratio R. The theoretical predictions are again shown in full lines.

The experimental values of non-dimensional bulk input are higher than those predicted by some. The temperature at the high pressure

outlet port is quite accurately predicted. The experimental values of Mach numbers and the mass flows through the high pressure outlet port are lower than predicted by some. Taking into account the limitations of the experimental work one can say that the theoretical predictions are in reasonable agreement with the experimental results.

A comparison of the experimentally obtained performances of the four port pressure exchangers with and without a transfer passage respectively confirm the trends obtained by the theoretical studies. Experimental results, like the theoretical predictions, show that the effect of the inclusion of a transfer passage in a four port pressure exchanger results in lower values of non-dimensional bulk input for a given pressure ratio. But it also results in lower fluid velocities and mass flows (for the same geometry) for the same pressure ratio. The experimentally predicted temperatures (as well as the theoretical predictions) show no effects of the inclusion of a transfer passage. This was predicted during the optimisation studies that for a lower temperature of the fluid entering the high pressure inlet port, the inclusion of a transfer passage would result in colder fluid being recirculated through the transfer passage and escaping through the high pressure outlet port. This means that the temperature of the stream at the outlet port should be lower. In the present case this does not happen because for the given port widths the scavenge ratios are so small that no recirculated fluid manages to escape through the high pressure outlet port. This view is confirmed in figs. (12.90,91) which show computer plots of the pressure exchanger cycle for pressure ratios of 2 and 3 respectively and in both cases the interface at the filling port travels through to escape from the low pressure outlet port.

The experimentally obtained performance of a four port pressure exchanger with one transfer passage at various rotor speeds and at

various phasing angles between the scagenging ports are shown in figs. (12.92 to 99).

An examination of these charts show that the performance of the four port pressure exchanger with one transfer passage, in terms of the non-dimensional bulk input μ, is worst at lower speeds and improves with increasing speeds. Although the performance at 6500 r.p.m. for all phasings is generally better than the performance at 6000 r.p.m., the difference is small which means that the optimum speed is very close to 6500 r.p.m.

The performance does not vary with the hp port phasing over the limited range used, i.e. 13.5 to 19.5 degrees.

10. DISCUSSIONS AND RECOMMENDATIONS

10.1 Approximate Methods

Two approximate methods have been used for rapid calculations of the performance and design of four port pressure exchangers with any number of transfer passages. The pressure differential method has proved to be a very useful method to compare the geometry and performances of pressure exchanger cycles. It can be further extended to predict the port mass flows, steady state Mach numbers and temperatures and also to include the effects of the temperature discontinuity and friction. The approximate method is less accurate than the pressure differential method. This is because the scavenging processes are assumed to be waveless in the steady flow region. The velocity profiles at the ports have shown that the scavenging sections are by no means waveless. In any case no great accuracy is to be expected from either of the two methods and they shall only be used to compare pressure exchanger cycles, for feasibility surveys and to form a preliminary idea about the behaviour of the pressure exchanger cycles.

10.2 The Hybrid Method

The hybrid method has been successfully developed to cater for pressure exchanger cycles. Calculation procedures for friction, heat transfer, unstreamlined cell entry and exit, leakage and transfer passage losses have been introduced into the numerical procedure. The assumed steady flow in the ports has been related to the unsteady flow in cells. The design criterion for various ports have been incorporated in the calculation procedure such as the pressure exchanger can be designed simultaneously with the performance calculations. The whole procedure has been computerised to develop a general purpose research computer program "GENPX".

The hybrid method fails to take into account:

(i) The formation of a shock wave due to the convergence of compression waves and associated entropy rise due to shocks.

(ii) The mixing and diffusion losses.

Pressure exchangers are normally operated at low pressure ratios and the shock waves involved are generally very weak. Inclusion of a transfer passage has been shown to result in weaker waves for a given overall pressure ratio. The shock tube calculations by Issa (26) have shown that entropy rise due to a shock wave can be ignored at lower pressure ratios at which pressure exchangers are normally operated. — but exp!

Mixing and diffusion also do not seem to have a significant effect on the performances of pressure exchangers at low pressure ratios and small temperature discontinuities as good agreement between the theoretical and experimental predictions of pressure exchanger cycles operating under these conditions, has been found. These effects are expected to have a greater influence at higher pressure ratios and stronger temperature discontinuities. Inclusion of a transfer passage results in recirculation of fluid streams at different temperatures which increases the mixing losses. Therefore, calculations of pressure exchanger cycles at higher pressure ratios, strong temperature discontinuities and greater number of transfer passages may have to take into account these effects. Smearing of the discontinuities due to the interpolation procedures in the numerical method has no physical justification but since in actual processes some smearing is bound to occur due to mixing, diffusion and viscous effects, this phenomena does not have a serious effect on the results and its effects may be reduced by increasing the mesh size.

Factors f and q simulate the friction and heat transfer in the mathematical model. Calculations of f and q involve a co-efficient of friction C_f and Stanton number S_t. The co-efficient of friction C_f amd the Stanton number S_t are calculated from the turbulent pipe flow formulae. The constants in these formulae are based on the work of Issa (26) on shock tubes. In future works these constants may be varied to achieve greater accuracy and this may perhaps lead to a better understanding of friction and heat transfer in unsteady flows.

The cell entry and exit losses have been converted into equivalent friction losses and an "apparent" co-efficient of friction is calculated to simulate these losses. An alternative method would be to calculate a discharge co-efficient based on the steady flow loss data available on the unstreamlined cell entry and exit shapes. This method is not expected to reduce the computational time to a considerable extent. A co-efficient of discharge based on cell dimensions and the respective loss of heads due to sudden contraction, sudden enlargement and wall friction in the cell can also be calculated, and this method, like a proposal by Mathews in which the cell is never allowed to be fully open, is expected to result in considerable reduction in computer time.

The three different methods to take leakage effects into account have worked successfully. Each method has given reasonable estimates of leakage flows. Due to small leakage effects there is not much to choose between them. Under normal conditions the mass and energy correction method is recommended to be used because it takes the least time. At higher pressure ratios and with wider clearance gaps when leakage can have a considerable effect on the strength of the pressure waves inside the rotor the partly-open-end method is recommended because it is quicker than the porous-cell-ends method.

The last two methods can be extended to take into account the inter-cell circumferential leakage but the small leakage effects do not justify the complicated and iterative procedures which would be involved to cater for inter-cell leakage.

The pressure exchanger port geometries have been successfully predicted and checked by the computer plots. These diagrams, particularly in case of one transfer passage, show that optimisation of blank spaces may result in smaller ports. Four port pressure exchangers are normally operated at unity scavenge ratios. This is to ensure that maximum mass flow rate is

achieved without allowing the driving fluid to escape through the respective outlet port. Mixing necessitates slight adjustments in unity scavenge ratios. These adjustments depend upon the application of the pressure exchanger. In a pressure exchanger engine supercharger, for example, it is advisable to slightly under-scavenge the high pressure section in order to ensure that fluid at a low and uniform temperature flows out of the high pressure outlet port. This would mean that a denser charge is supplied to the engine and no exhaust gas is re-circulated.

The transfer passage diagrams show that the recirculation of fluid through the transfer passage ducts change this situation. A unity scavenge ratio in the high pressure scavenge section does not mean that the exhaust gas is not recirculated and supplied to the engine with the fresh charge. This object can only be achieved by following the path of the interface at the first filling port and closing the high pressure outlet port at the instant it reaches that end. Mixing would again necessitate the closing of the high pressure outlet port a little bit earlier.

The relationships between the unsteady flow in cells and assumed steady state flow in pressure exchanger ducts has given satisfactory results. The steady state conditions in the connecting ducts may not exist in many situations. In a pressure exchanger engine supercharger, the pressure waves in the inlet and exhaust pipes of the engine will influence the flow in pressure exchanger ducts.

10.3 The Optimisation Studies

These studies have shown that:

(i) The widths of the filling and emptying ports and the high and low pressure phasings vary slightly with pressure ratio and finite cell width. Temperature ratio has a greater influence on them.

(ii) At lower pressure ratios, the scavenging port widths are much sensitive to the pressure ratio. Greater care is needed to closing these

ports. The performance of pressure exchangers designed for one pressure ratio can be appreciably different under off-design conditions. In a fixed geometry pressure exchanger the scavenge ratios can always be varied by proper adjustments in the rotor speed. The effects of temperature discontinuities, scavenge ratio-temperature discontinuity interactions, residual waves and performance losses on the geometry and performance of pressure exchangers have been predicted using the continuous design procedure. The procedure is capable of designing a pressure exchanger with any number of ports in whatever arrangements. In transfer passage calculations the boundary conditions at the transfer ports have to be very accurate because these conditions determine the pressure ratios across the scavenging sections. Since extremely low pressure ratios may be involved, a small variation in transfer ports conditions can have a large influence on the port geometry of the pressure exchanger.

The performance of a "hot" pressure exchanger in terms of bulk input is worse than that of a "cold" pressure exchanger. This means that the application of pressure exchangers in cooling cycles is a more attractive proposition but a hot pressure exchanger requires smaller port widths and therefore these pressure exchangers can be run at higher speeds and the performance losses are reduced.

The temperature discontinuity-scavenge ratio interaction has been shown to have some effect on the performance of pressure exchangers. In a hot pressure exchanger the performance generally improves with decreasing scavenge ratios the cold pressure exchangers have shown opposite trends. Lower scavenge ratios result in reduced performance losses but at the same time the capacity of the pressure exchanger is reduced.

10.4 Transfer Passage Results

Inclusion of one transfer passage results in improved performances in terms of bulk input. It also results in lower fluid velocities and bigger ports for given conditions of the pressure ratio and scavenge ratios.

Lower fluid velocities means the pressure waves are weaker and therefore the entropy losses are much reduced. The low values of the fluid velocities also improve the erosion resistance of these machines. Therefore four port pressure exchangers with transfer passages are more suitable for use with dirty gases or wet vapour.

The wider ports in case of a transfer passage means that these pressure exchangers have to be run at lower rotor speeds. In order to reduce finite cell width losses the rotor would be required to have greater number of cells and this would increase frictional losses. The performance losses on the whole increase at low rotor speeds.

Transfer passages are included in pressure exchangers either to:-

(i) Attain a given pressure ratio for lower values of energy inputs.

(ii) Attain higher pressure ratio for a given amount of energy input.

The object of the first exercise is to make the low pressure applications of pressure exchangers more efficient. The computer predictions have shown that although for a given pressure ratio, lower energy inputs are required, but frictional losses increase due to wider scavenging ports, leakage losses increase due to higher pressures at transfer ports and wider scavenging ports, mixing losses increase due to recirculation of fluid streams at different temperatures and the energy degradation in the transfer passages are the additional losses which are found to be increasingly significant as the pressure ratio is increased. Therefore

the improvement in pressure exchanger performance by including one transfer passage is not as good in actual case as it has been predicted for homentropic flows.

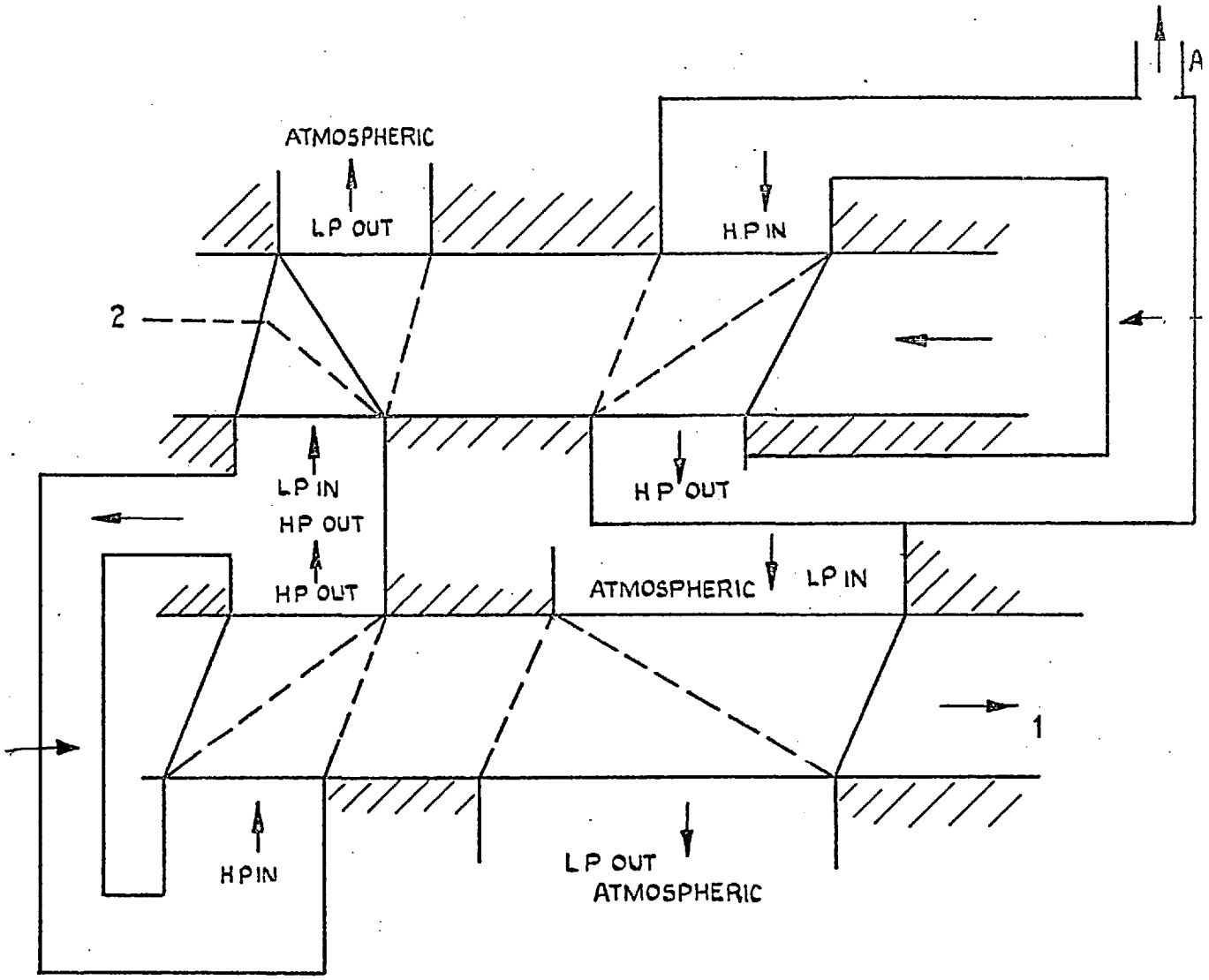
When the object is to attain a higher pressure ratio for the same energy input, the machine remains roughly the same size, the leakage losses increase and the transfer passage losses also increase to assume a far greater significance and again the advantage of attaining a higher pressure is again not as good as it is predicted for homentropic flows. The recirculation of fluid through the transfer passage ducts, as it was pointed out earlier in this section, necessitates the closing of high pressure outlet port when the interface at the first filling port reaches that end. This reduces the capacity of the machine.

These trends show that there is an optimum number of transfer passages which can be incorporated in a pressure exchanger after which, in addition to engineering complexity, the performance losses and port width become so great that no improvement in the performance is possible. The optimum number may not be far from two or three.

An alternative arrangement in which pressure exchangers are compounded to attain higher pressure ratios will not possess some of the disadvantages associated with the transfer passages. Such an arrangement is shown in the following sketch.

This sketch shows a two stage pressure exchanger which supplies compressed air through the bleeding point A.

Pressure exchanger No.1 takes in air at atmospheric pressure and temperature and compresses it to a pressure equal to R1 atmospheres. Part of this compressed air is bled out, depending upon the heat input in the high pressure loop, and the rest is recirculated. The bled air is then fed to pressure exchanger No.2 where it is further compressed to a higher pressure equal to R2 atmosphere, and a part of it is again recirculated



while the remainder of the compressed air is bled at point A which can be used to do some thermodynamically useful work.

10.5 Performance Losses in Pressure Exchangers

A study of the performance losses has shown that the finite cell width and the frictional losses are the most significant losses in pressure exchangers in addition to the transfer passage losses. The cell width has opposite effects on the friction and finite cell width losses. The frictional losses increase with narrower cells whereas the finite cell width losses increase with wider cells. Azouri's (16) δ-rule is based on

the two considerations and the existing numerical procedure can be used to verify this rule.

The significance of transfer passage losses means that the transfer ducts have to be designed carefully. They should be provided with smooth surface. Sharp bends should be avoided.

Leakage losses are not significant in four port pressure exchangers without transfer passages, but inclusion of transfer passages increase the leakage losses.

10.6 The Computer Program

The computer program "GENPX" is in a well developed stage. It can handle the performance and design calculations of all pressure exchanger cycles with no internal combustion in cells. The program can be applied to perform the following tasks:

(i) To determine the performance of a pressure exchanger having a fixed geometry for homentropic flow.

(ii) To determine the performance of a pressure exchanger having a fixed geometry with variable entropy taken into account.

(iii) To determine the performance of a pressure exchanger having a fixed geometry with one or more of the following performance losses taken into account.

  (a) Finite cell width.

  (b) Friction and heat transfer.

  (c) Leakage.

  (d) Cell entry and exit.

  (e) Transfer passage.

(iv) To determine the performance and optimum geometry of a pressure exchanger for homentropic flow.

(v) To determine the performance and optimum geometry of a pressure exchanger with variable entropy taken into account.

(vi) To determine the performance and optimum geometry of a pressure exchanger with one or more of the following performance losses taken into account:-

(a) Finite cell width.

(b) Friction and heat transfer.

(c) Leakage.

(d) Cell entry and exit.

(e) Transfer passage.

The provision of the pressure exchanger conventional diagram to be plotted by the computer would enable the future user to use the interactive graphics and computer aided design techniques for the optimisation studies of the pressure exchanger cycles. The program can be extended to take into account variable specific heat, cell area changes and internal combustion in cells.

The program does not require large storage and therefore its running on computers of smaller core is not expected to pose any problem. Computational time is a matter of more concern. Since the program is a general program it is very difficult to formulate a general expression in order to calculate the approximate computational time for a given operation. The maximum cycle time depends upon the rotor speed and also upon the angular width of the ports. The computational time also depends upon the number of different operations to be performed during the cycle calculations. The computer program contains a large number of iterative procedures. The number of cycles required to achieve equilibrium conditions also varies from cycle to cycle and it increases with the number of transfer passages in a pressure exchanger cycle. Since the boundary conditions at transfer ports can influence each other the computational time increases drastically with transfer passages. A large number of tests would have to be carried out to establish the influence of various parameters that control the computing time.

The time controlling parameters for a given pressure exchanger cycle calculations are:

(1) The number of spatial grid points N.

(2) The time step. $\Delta\tau$

(3) The accuracy discriminators in the sub-routines using numerical techniques for convergence of solutions.

The computing time varies inversely with the number of spatial grid points N and the time step $\Delta\tau$ but a greater value of N and the time step $\Delta\tau$ result in reduced accuracy. Similarly, any adjustment in the accuracy discriminators to reduce the computing time would obviously result in reduced accuracy. In the present version a compromise value of N equal to 30 has been chosen. The time step Δt is calculated on the basis of the stability criteria. The accuracy discriminators for numerical solutions and for various other purposes have also been set equal to the compromised values.

The program has been run by the Author mainly on the CDC 6600 computers at Imperial College computer center. The performance calculations for a hometropic, fixed geometry operation of a four port pressure exchanger without a transfer passage with rotor speed equal to 6000 RPM and one cycle per revolution, took about 20 seconds. The equilibrium conditions were attained in three cycles. The performance calculations of the same cycle with all irreversibilities taken into account increased the computing time by a factor of three. The optimisation of geometry increases the computing time again approximately by a factor of 3 and the inclusion of irreversibilities further increased the computing time. The transfer passage calculations takes even greater computing time because of the unknown boundary conditions at the transfer ports.

The following considerations would help to keep the computing time for a given pressure exchanger cycle to a minimum.

(i) A good initial guess of the conditions in the cell at the start of the cycle calculations. This would reduce the number of times the cycle calculations have to be repeated to attain the equilibrium conditions.

(ii) A good initial guess of the boundary conditions in the transfer ports. The pressure differential may be used to find the approximate values of these boundary conditions.

(iii) Since the performance losses do not play a significant role in determining the port geometry of pressure exchangers it is advisable to exclude these effects from the design calculations of pressure exchanger cycles.

(iv) A good initial guess of the port area ratios for the given conditions during the design calculations also results in considerable reduction in computing time. The pressure differential or the approximate method may be used to obtain an approximate value of the port area ratios.

The computer program as it stands is a general purpose research computer program. It has been written to cope with different pressure exchanger cycles and various aspects of pressure exchangers in isolation. This generality in its application has been provided by incorporating a number of "IF" and computed "GO TO" statements in the text of the program. Inclusion of these statements results in considerable increase in computing time. Any user who may be wishing to use this program for a specific purpose is advised to eleminate the subroutines which he does not need in his calculations and also get rid of the resulting redundant fortran statements. This will result in a considerable saving in computing time.

The total execution time will depend upon the computer operating system, the compiler and the computer type.

10.7 Comparison with experimental results

The computer predictions have shown good agreement with the experimentally obtained performances of pressure equalisers and four port pressure exchangers without and with one transfer passage. The computer predictions may be further tested for stronger temperature discontinuities when mixing and heat transfer effects are bound to be considerable and also the values of specific heats would vary considerably. An experimental program covering wide ranges of rotor speed, port geometries, temperature discontinuities and transfer passages would result in further improvements in the present procedure. The computer program can then be applied to investigate the application of pressure exchangers in various fields as a cooler, engine supercharger, boiler supercharger, thrust augmenter, pressure booster, gas generator and compressor.

11. Conclusions

The pressure differential and the approximate methods can be used to compare pressure exchanger cycles, for feasibility surveys and to form a preliminary idea about the behaviour of pressure exchanger cycles. These two methods may also be used to provide the main computer program "GENPX" with good estimates of the initial values of the conditions in the cells before the start of a cycle, the boundary conditions at the transfer ports and the port area ratios.

A numerical procedure to solve for the unsteady flow in pressure exchanger cells with friction, heat transfer, leakage, unstreamlined cell entry and exit and the energy degradation in transfer passages taken into account, based on hybrid method has been developed. Calculations for the optimisation of the pressure exchanger ports and the relationships between the steady flow in pressure exchanger ducts and the unsteady flow in the cells have also been incorporated in the procedure.

A general purpose research computer program "GENPX" has been developed to cater for pressure exchanger cycles. This program has been written in Fortran IV language and tested on CDC 6600, CDC 6400 and IBM 7094 computers.

Good agreement between the computer predictions and the experimentally obtained performances of pressure equaliser, four port pressure exchanger without and with one transfer passage has been found.

The program "GENPX" has been used to make an optimisation study of pressure exchanger cycles. The behaviour of performance losses has been investigated and the effects of including a transfer passage in four port pressure exchanger cycles have also been studied.

CHAPTER 12

GRAPHICAL REPRESENTATION OF RESULTS

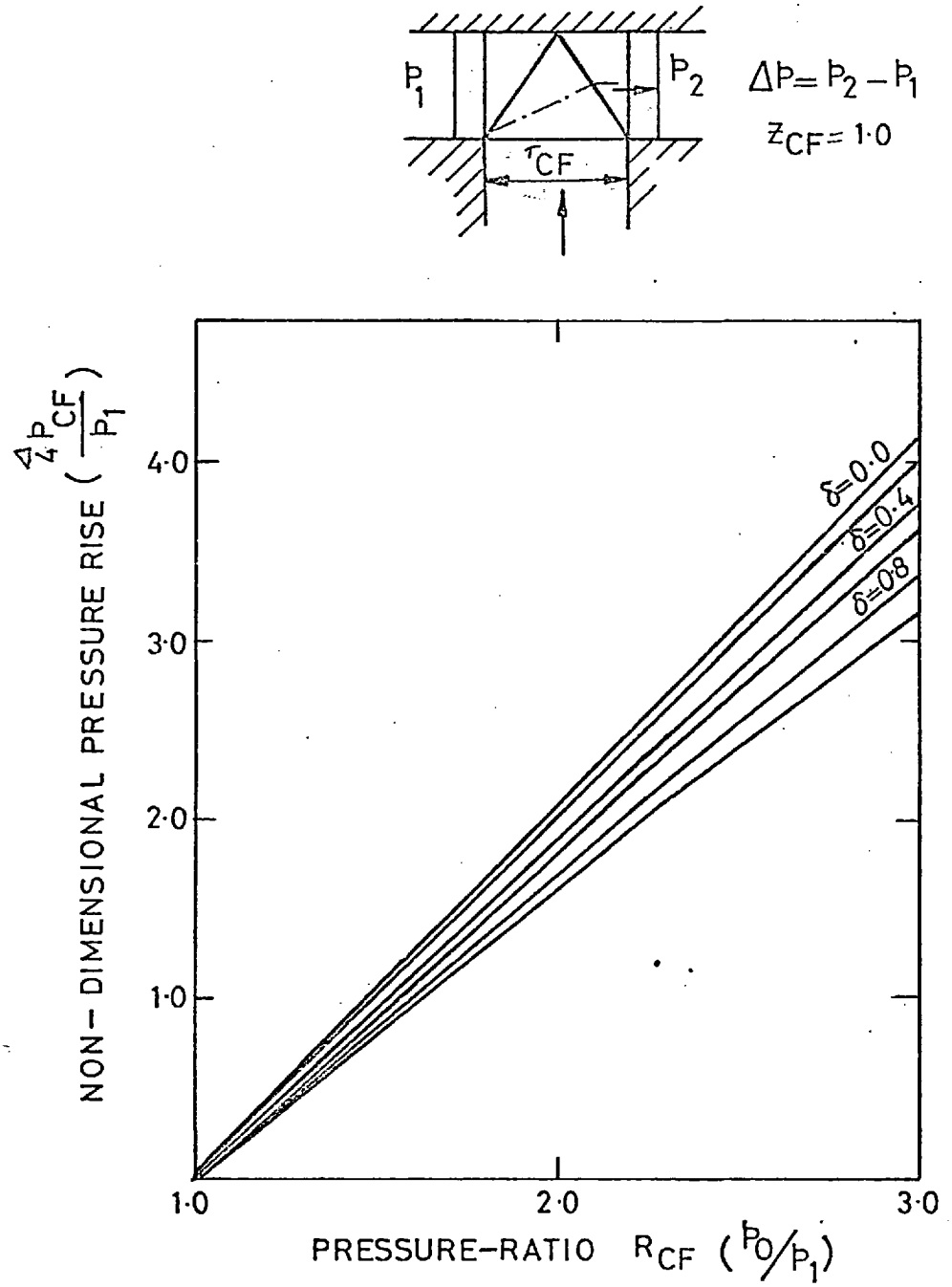
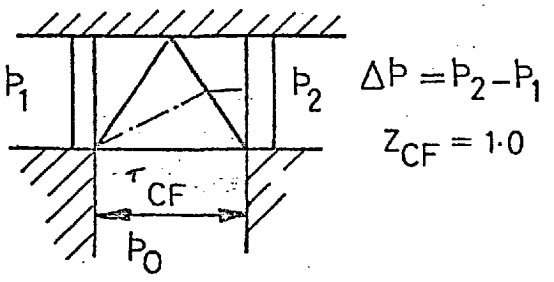
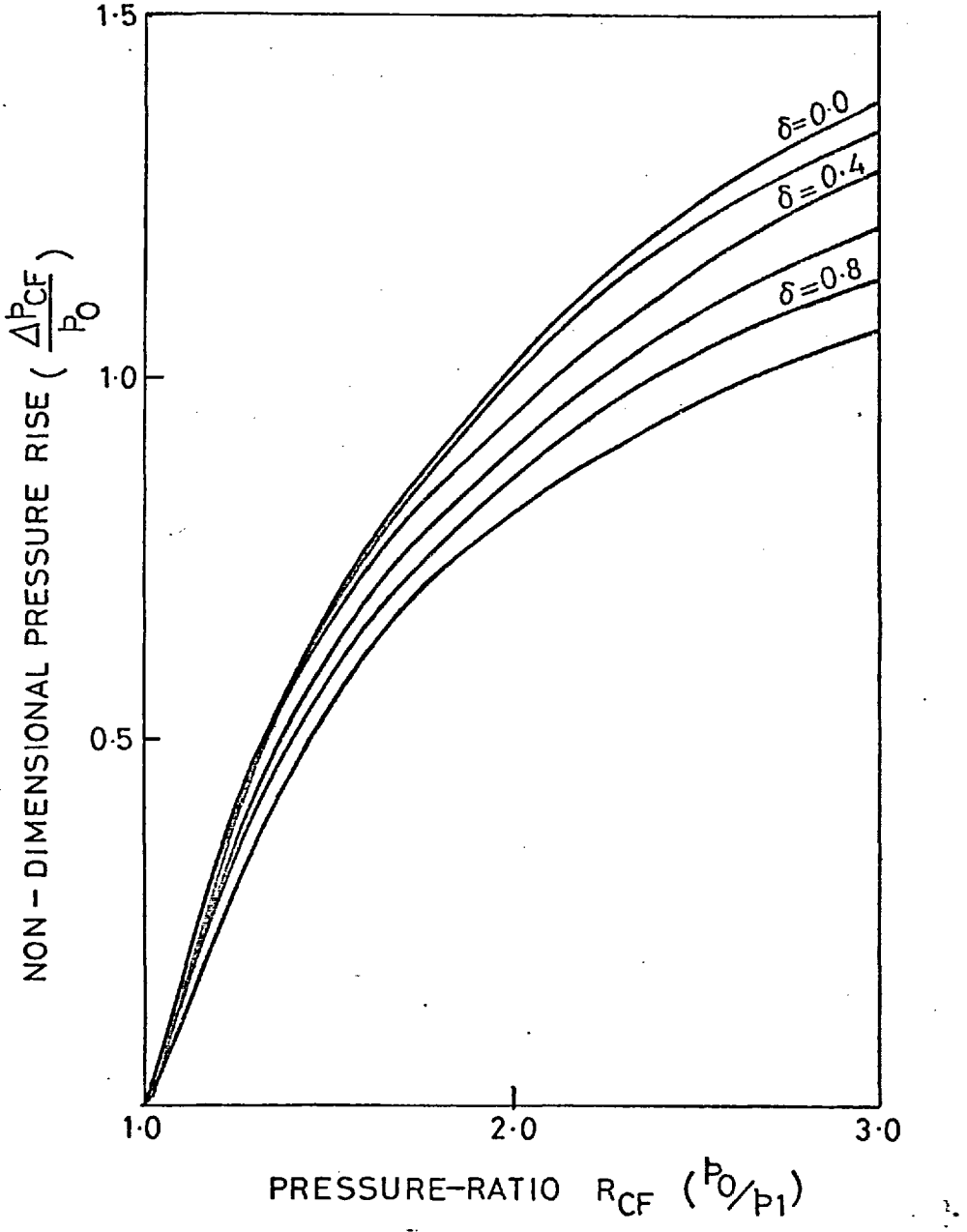


FIG. 12.1 CELL FILLING PERFORMANCE





CELL FILLING PERFORMANCE

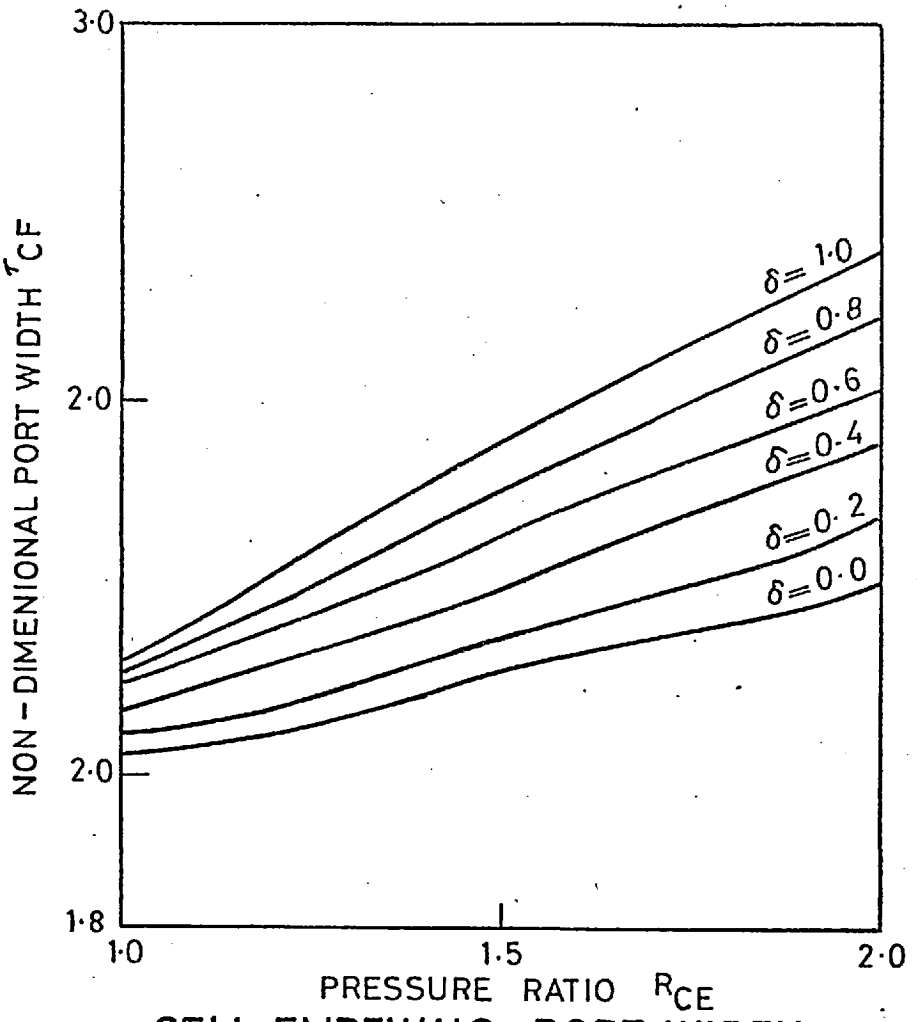


FIG. 12.4 CELL EMPTYING PORT WIDTH

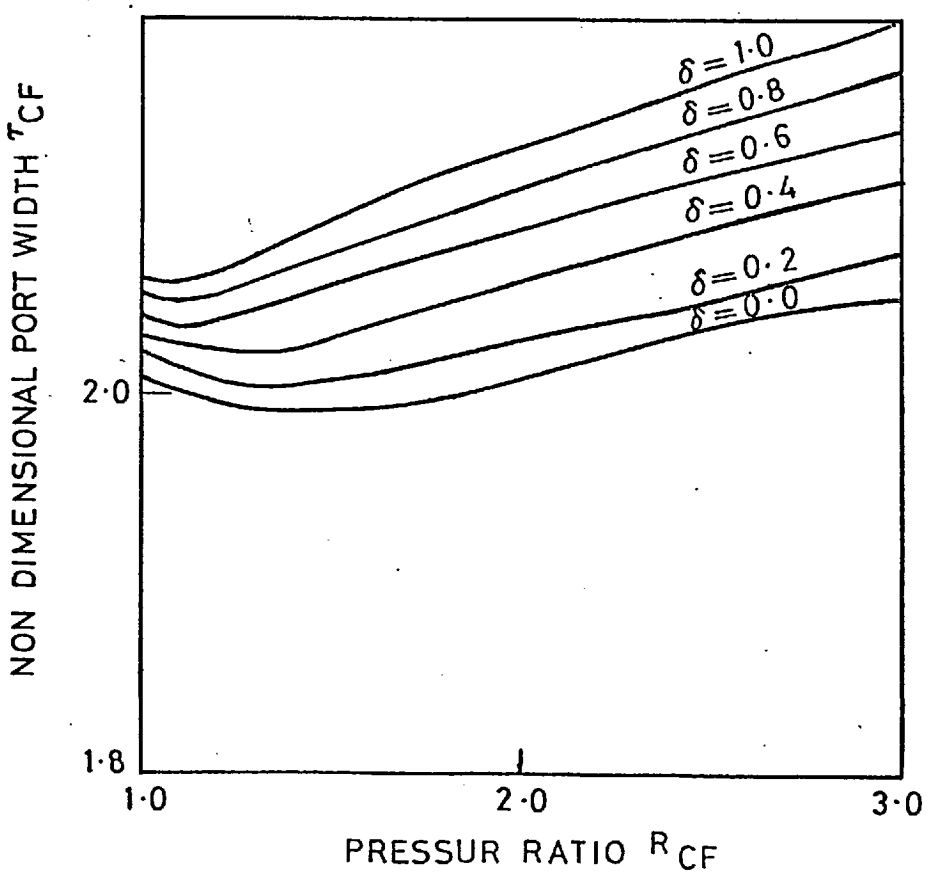
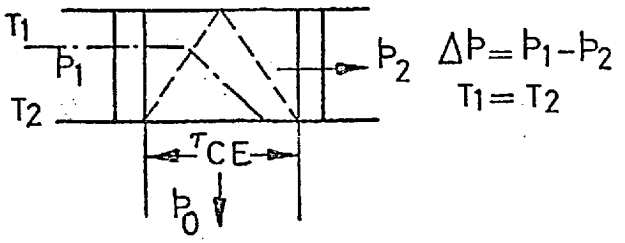


FIG. 12.3 CELL FILLING PORT WIDTH



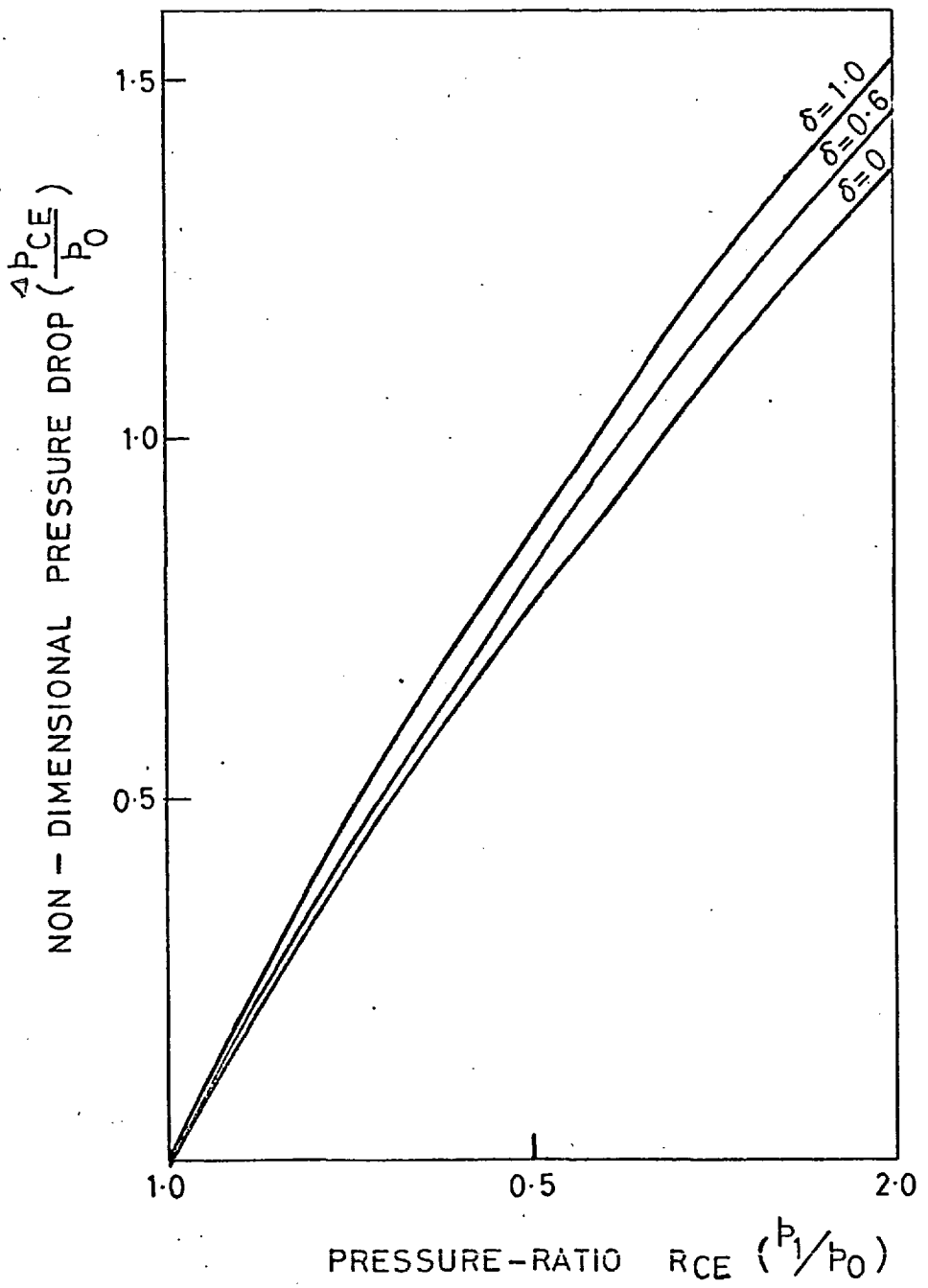
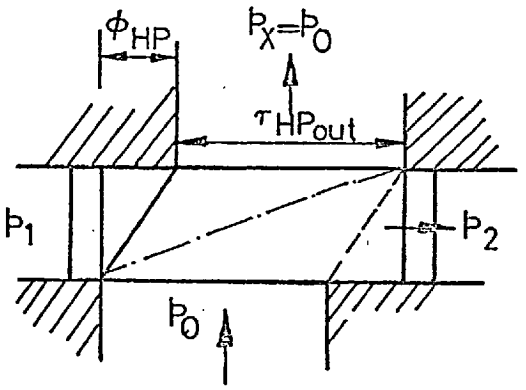


FIG. 12.5 CELL EMPTYING PERFORMANCE



$\Delta P = P_1 - P_2$

$A_{HP} = \frac{\tau_{HPout}}{\tau_{HPin}}$

SCRH = 1·0

Z_{HP} = 1·0

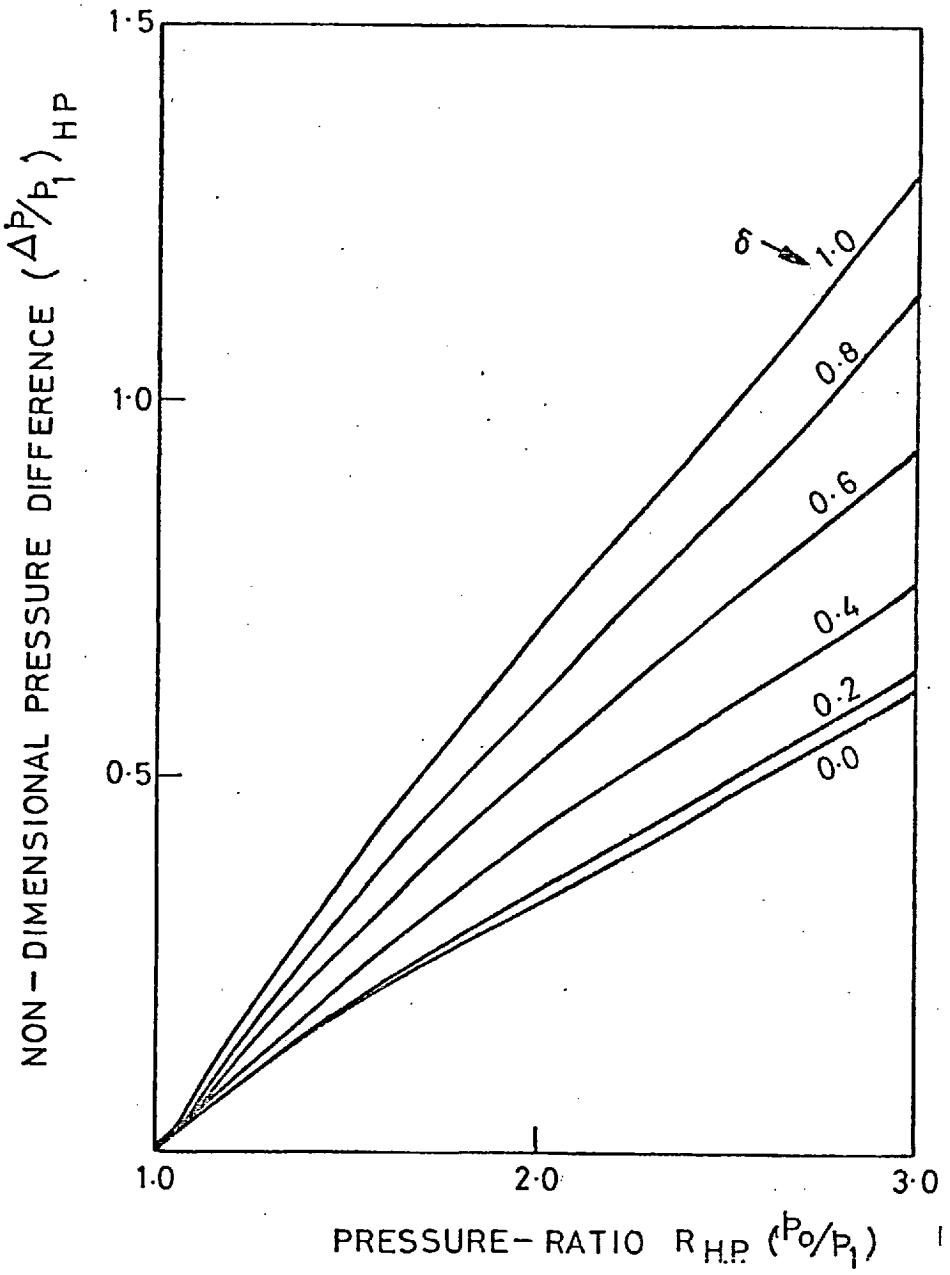
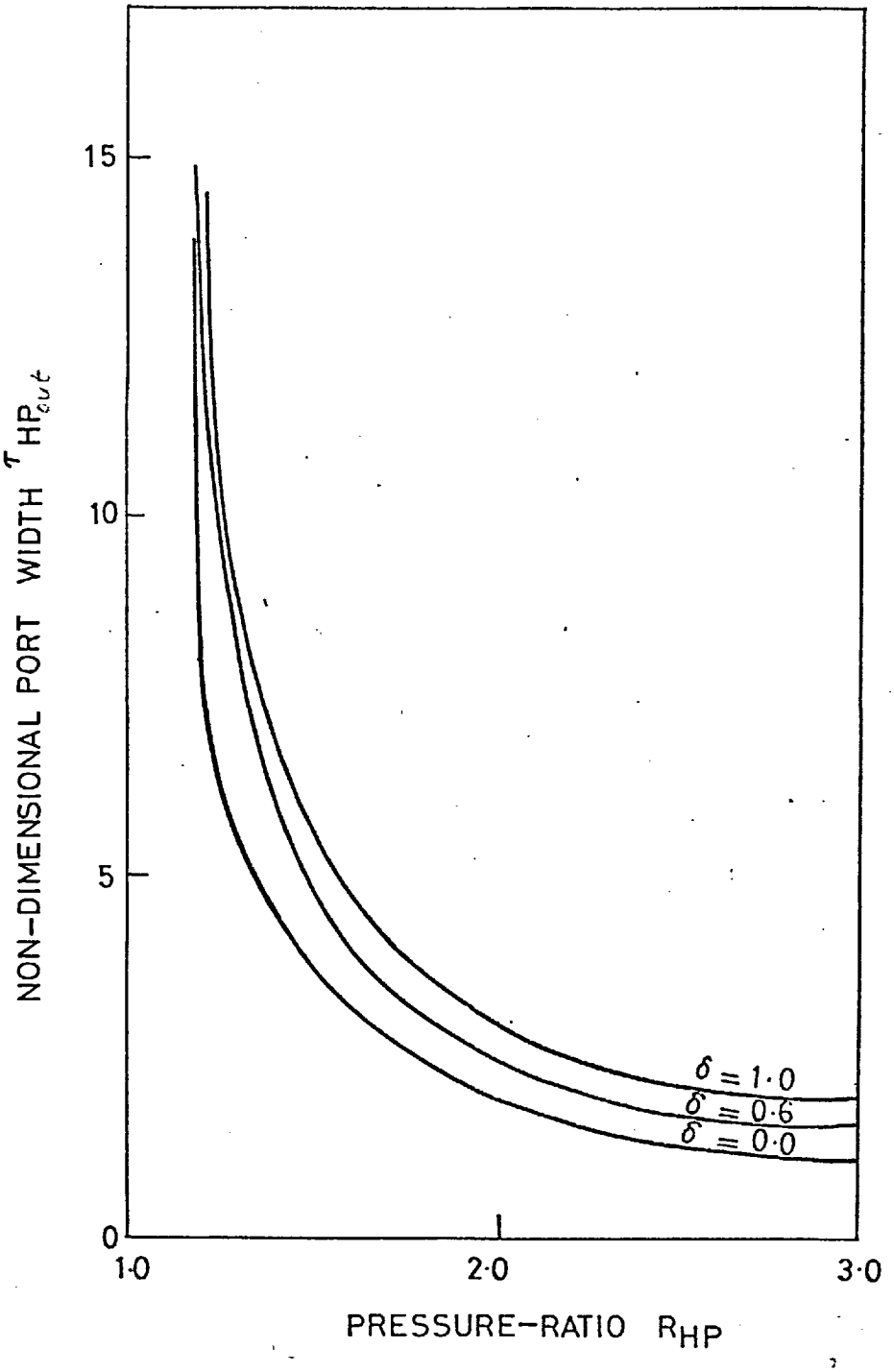


FIG. 12.6 HIGH PRESSURE SCAVENGE PERFORMANCE



HP SCAVENGE RATIO = 1·0

TEMPERATURE RATIO = 1·0

FIG. 12. HIGH-PRESSURE OUTLET PORT WIDTHS

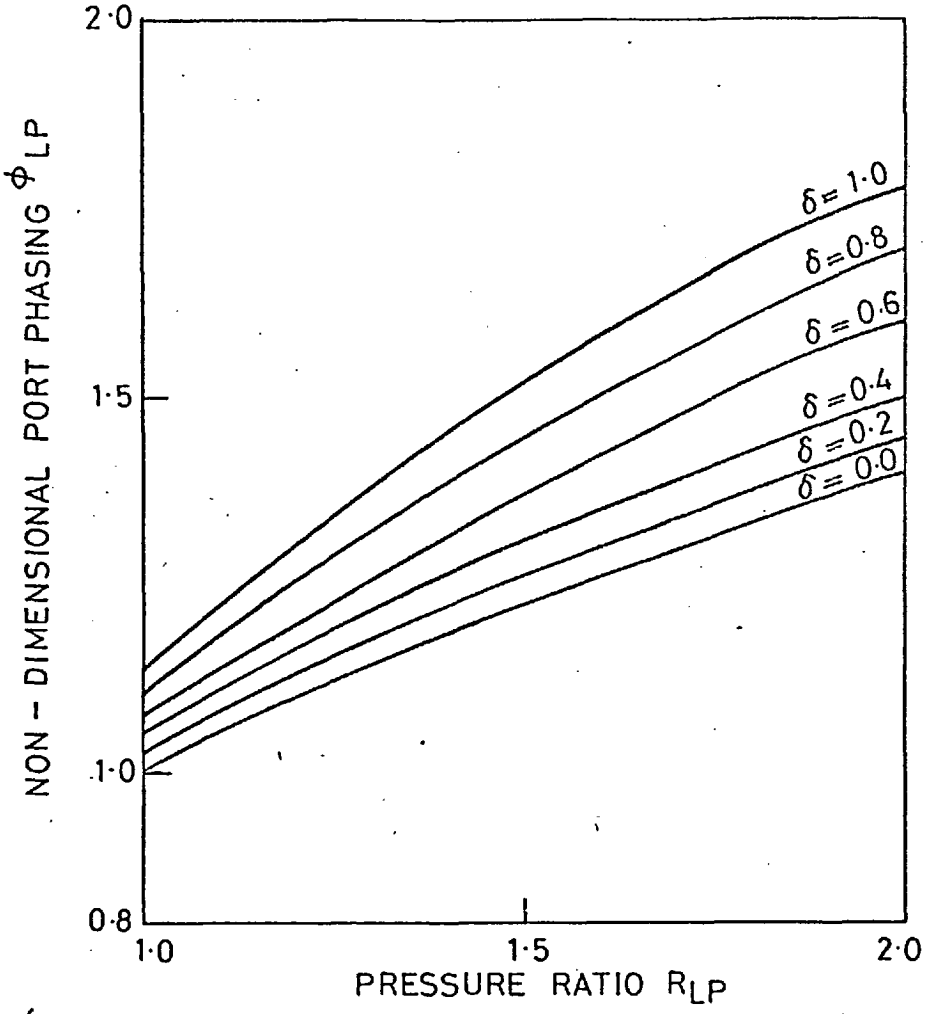


FIG. 12.9 LOW PRESSURE PORT PHASING

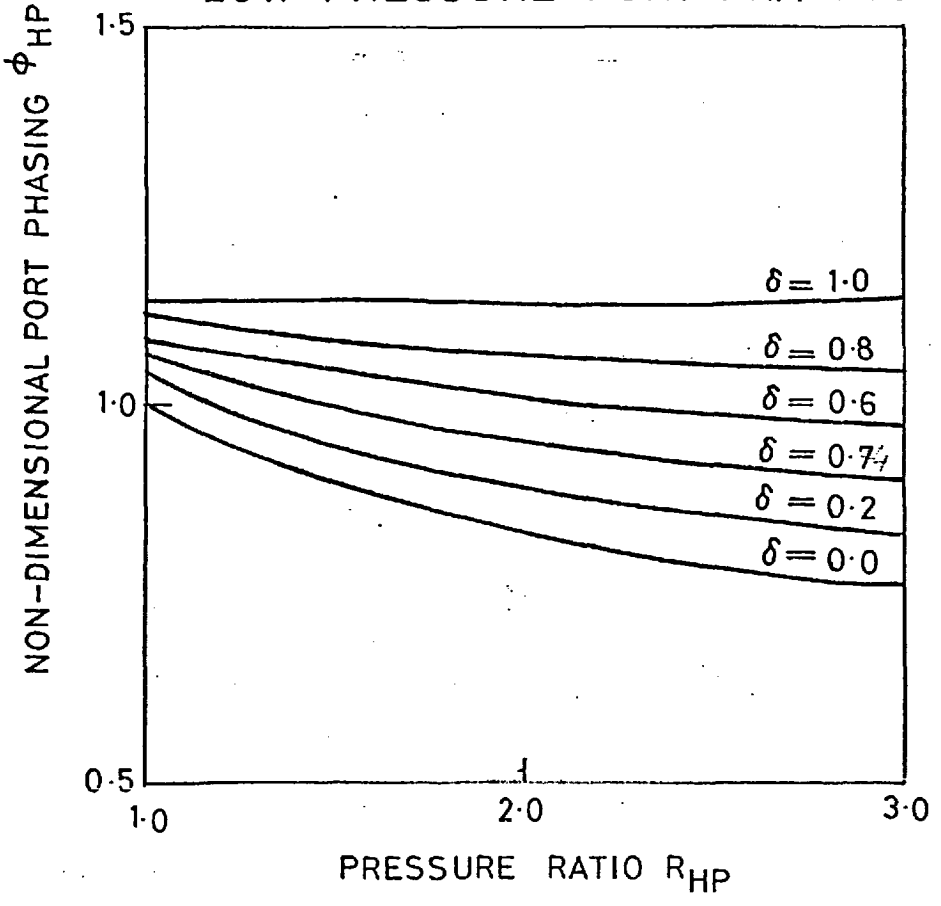


FIG. 12.8 HIGH PRESSURE PORT PHASING

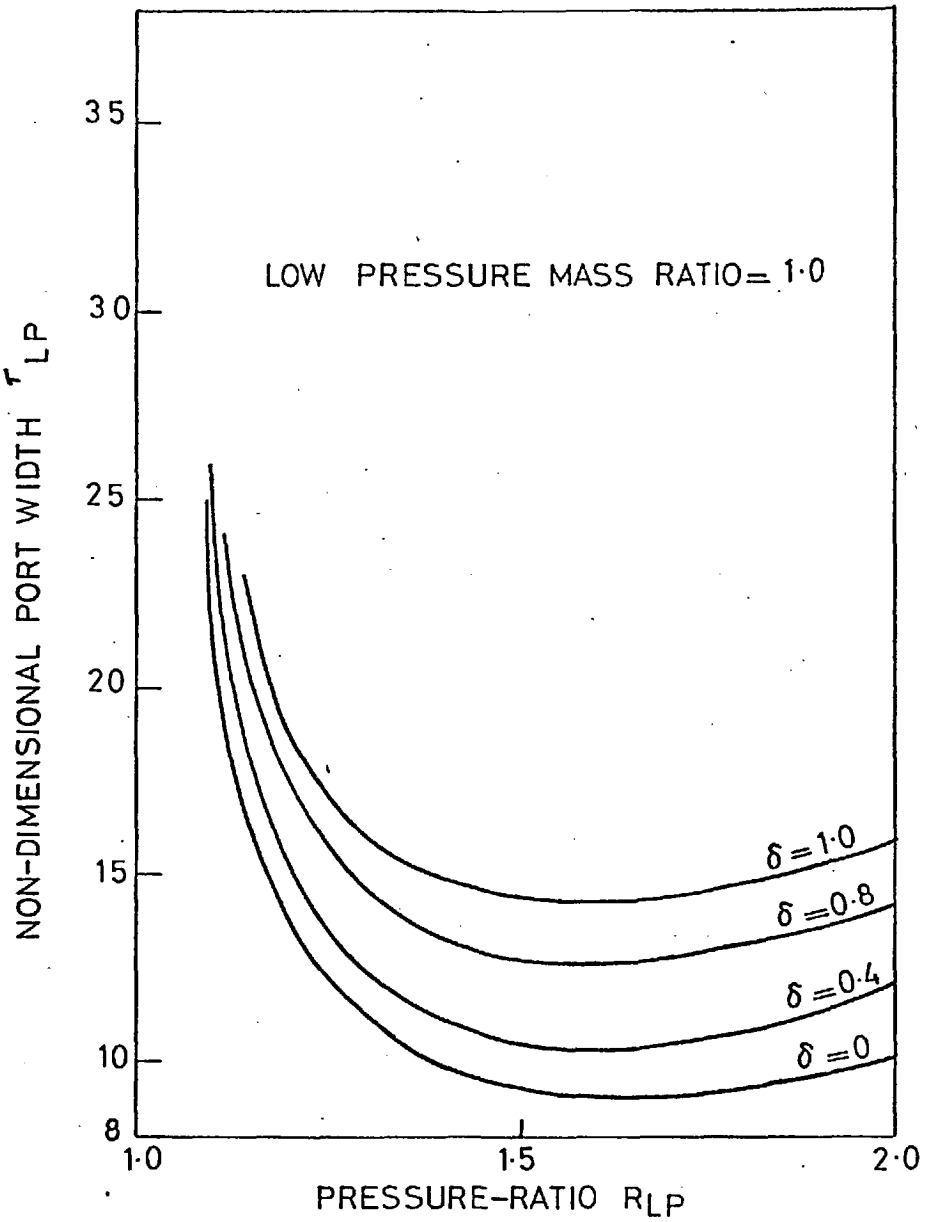


FIG. 12.11 LOW PRESSURE INLET PORT WIDTH

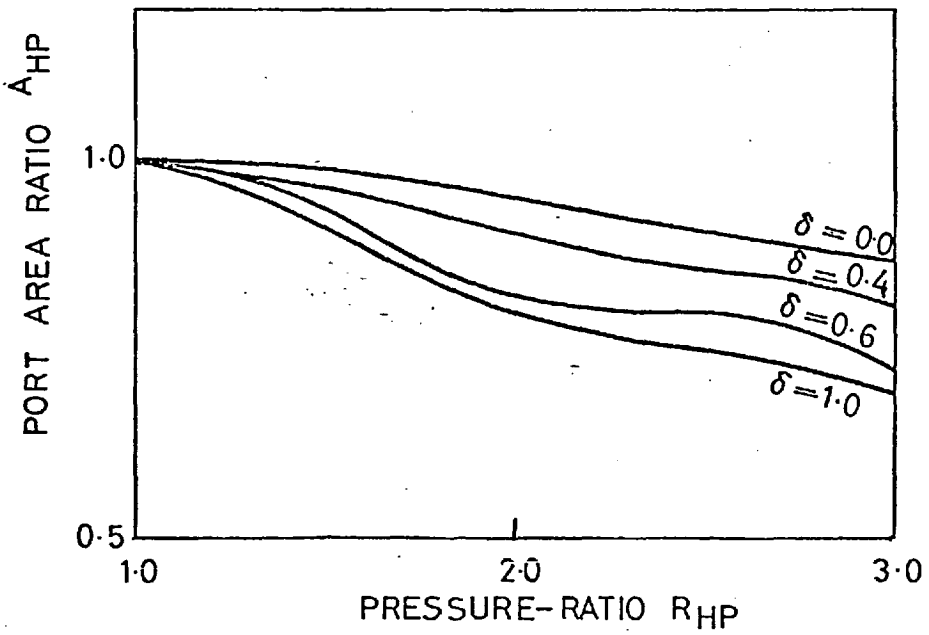
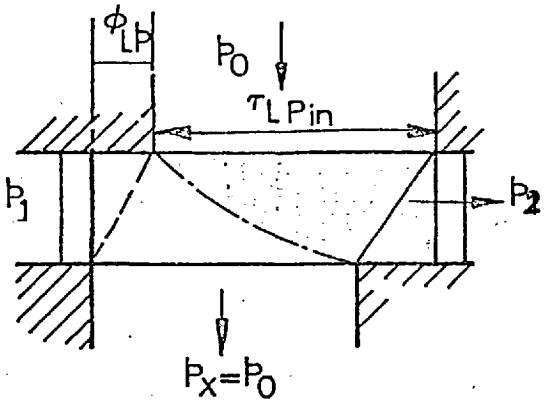


FIG. 12.10 HIGH-PRESSURE PORT AREA RATIO



$\Delta P = P_1 - P_2$

$A_{LP} = \tau_{Lout} / \tau_{Lin}$

SCRL = 1·0

z_{LP} = 1·0

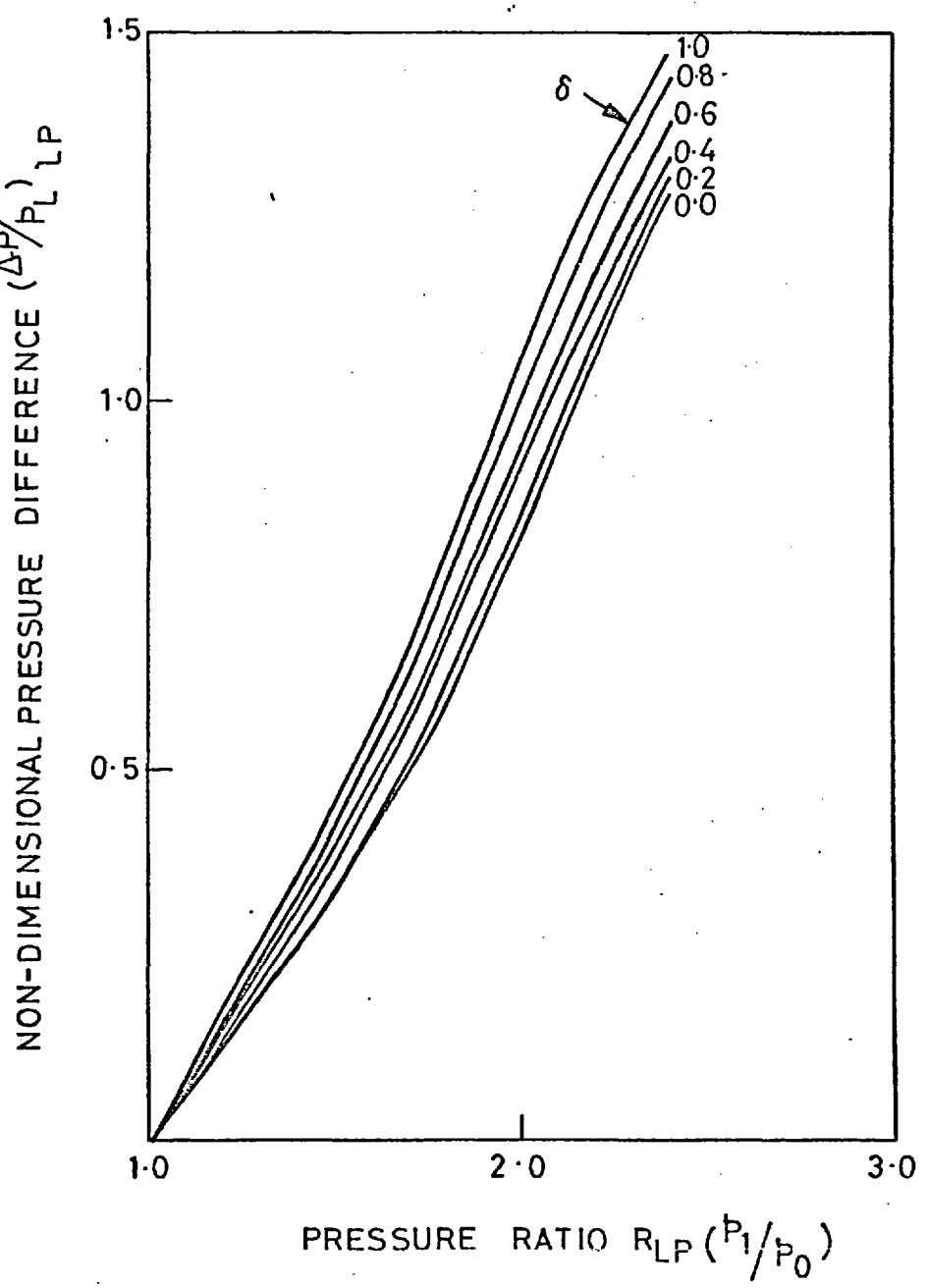
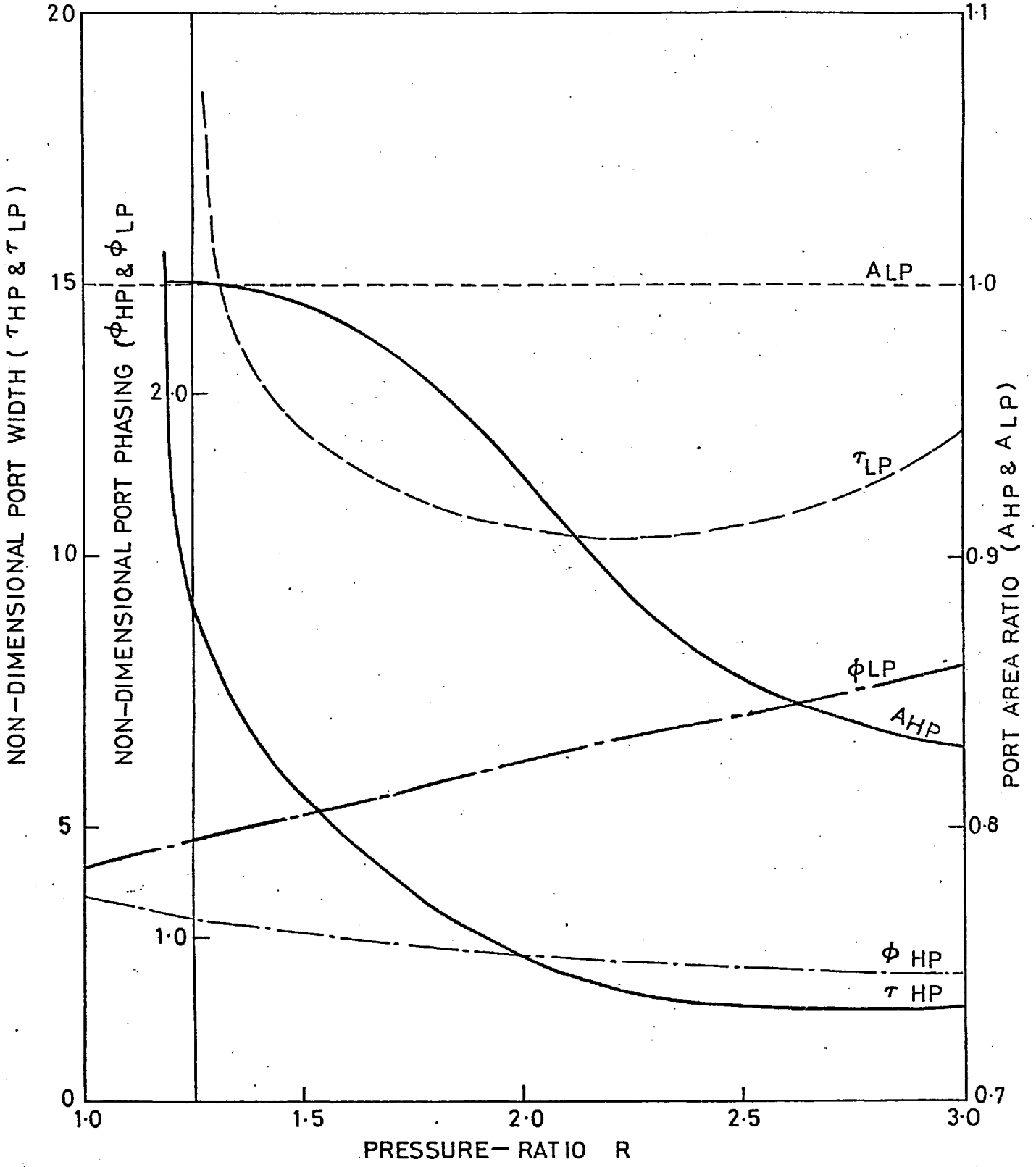


FIG. 12.12 LOW PRESSURE SCAVENGE PERFORMANCE



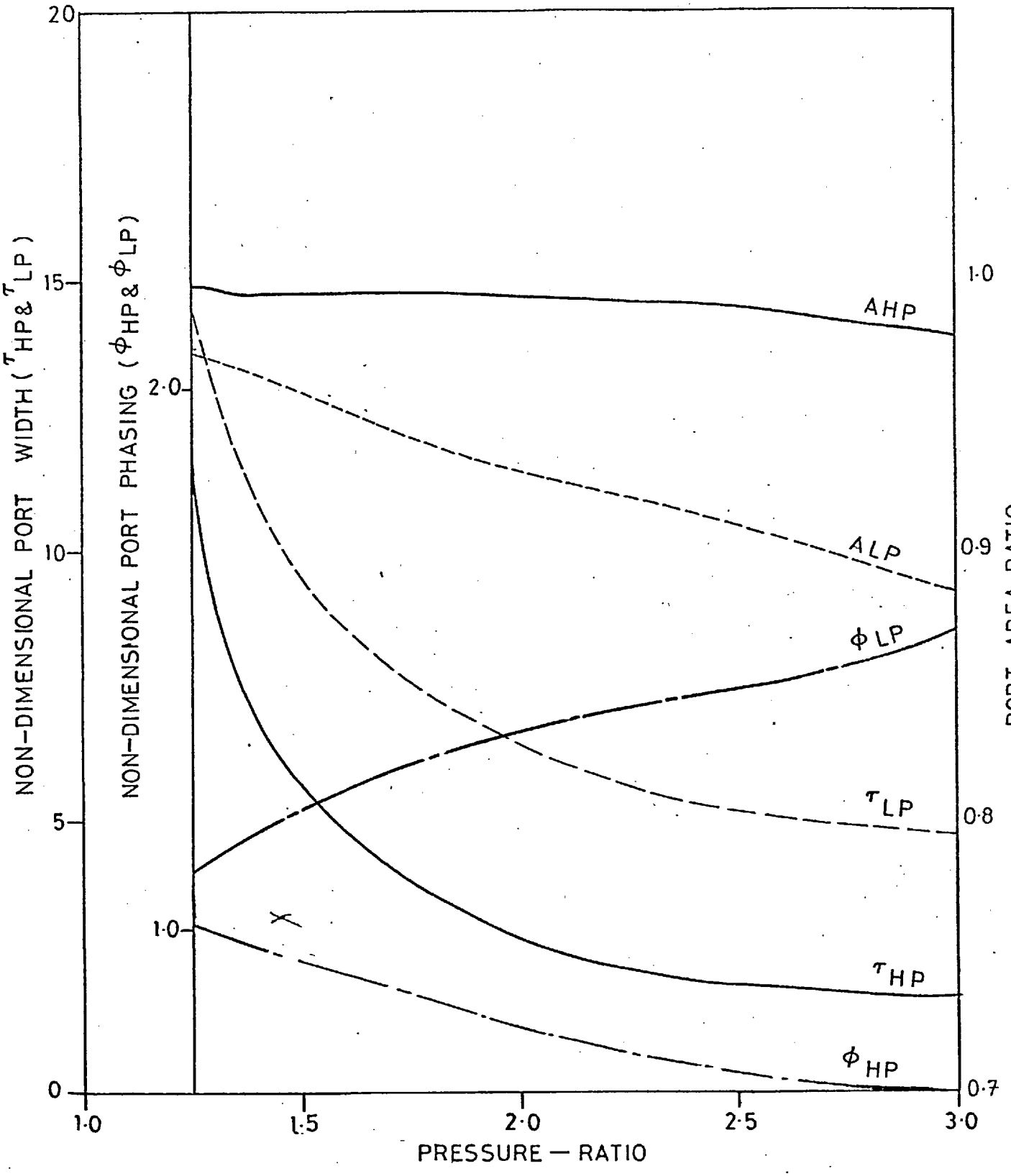
H P SCAVENGE RATIO = 1·0

L P SCAVENGE RATIO = 1·0

NON-DIMENSIONAL CELL WIDTH = 0·4

FIG. 12.13 **FOUR-PORT PRESSURE EXCHANGER GEOMETRY**

(PRESSURE DIFFERENTIAL METHOD)



H P SCAVENGE RATIO = 1·0
L P SCAVENGE RATIO = 1·0
NON-DIMENSIONAL CELL WIDTH = 0·54

FIG. 4.14 FOUR-PORT PRESSURE EXCHANGER GEOMETRY
(APPROXIMATE METHOD)

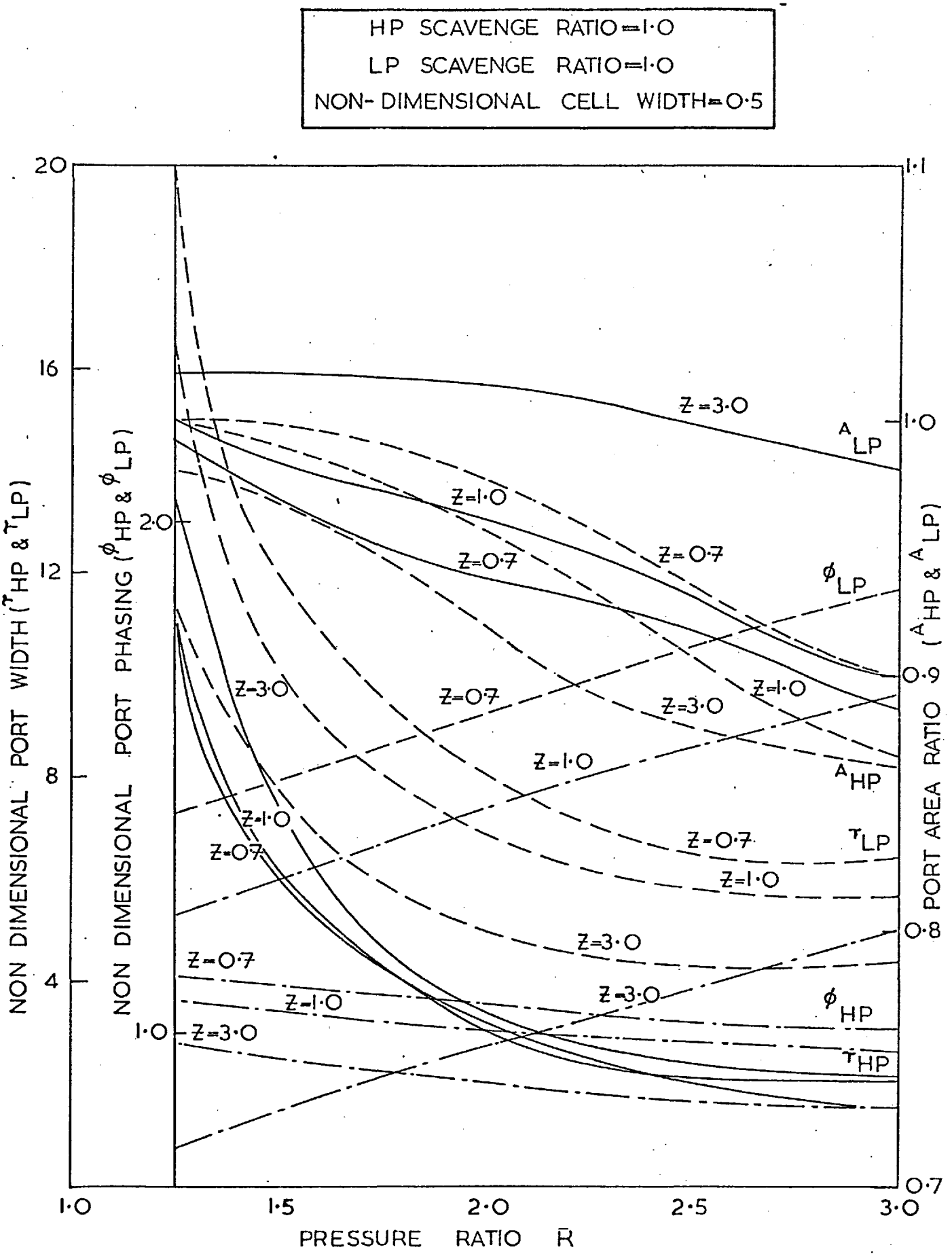
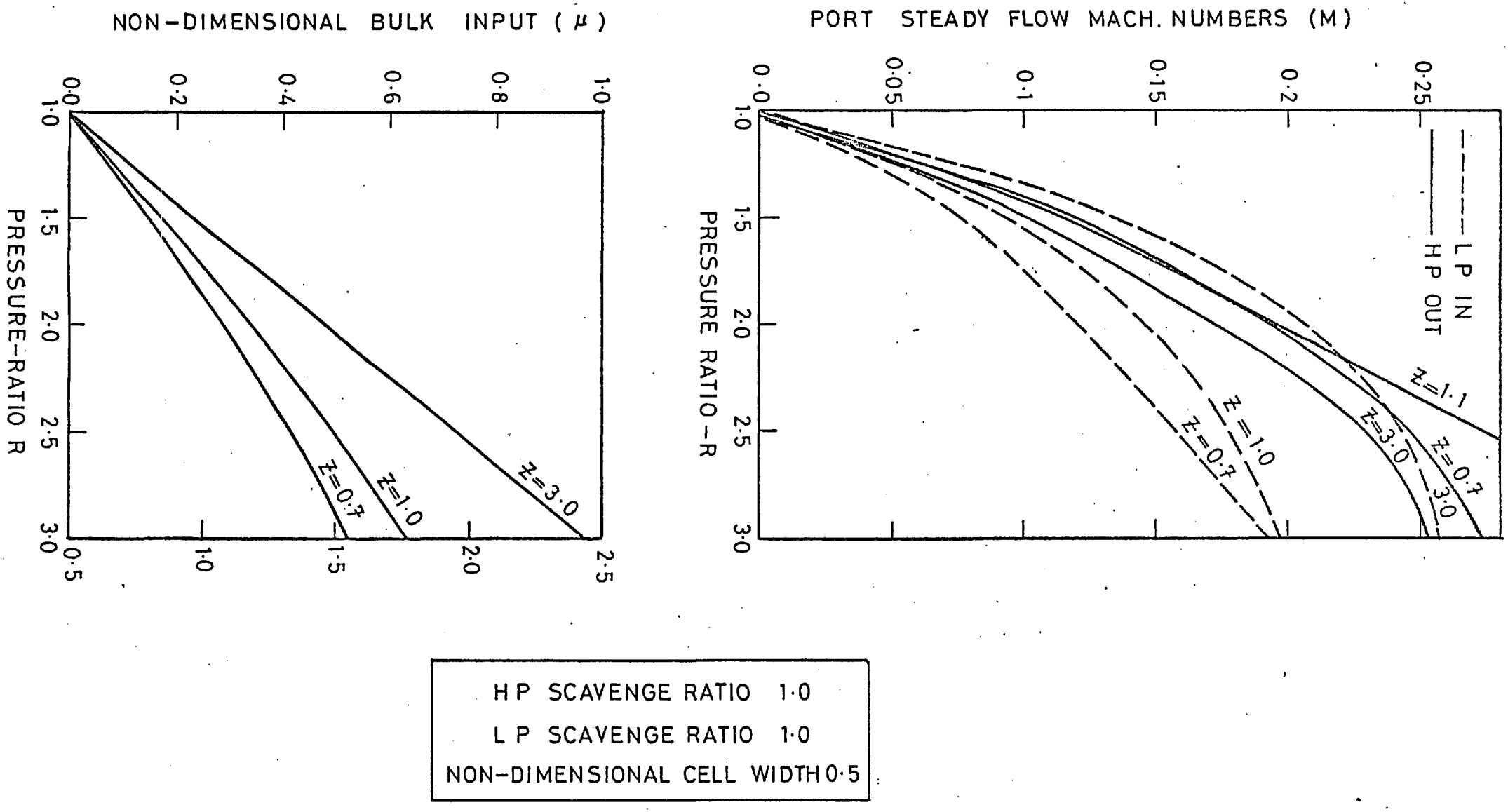


FIG. 12.15 FOUR PORT PRESSURE EXCHANGER GEOMETRY
(METHOD OF CHARACTERISTICS)



HP SCAVENGE RATIO	1·0
LP SCAVENGE RATIO	1·0
NON-DIMENSIONAL CELL WIDTH	0·5

FIG. 12.16 FOUR PORT PRESSURE EXCHANGER (VARIABLE GEOMETRY)

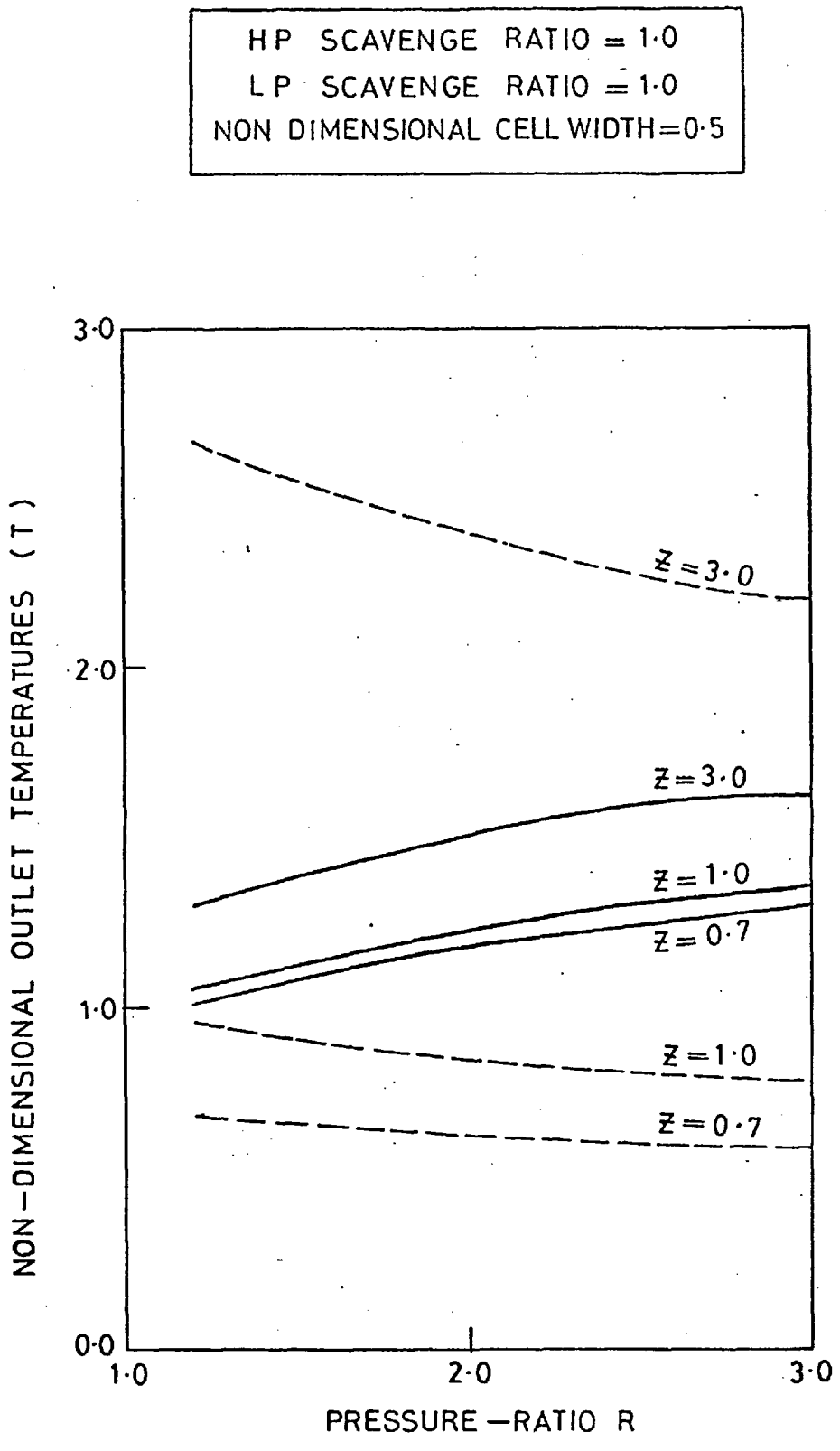


FIG. 12.17 FOUR-PORT PRESSURE EXCHANGER PERFORMANCE

(FIXED SCAVENGE RATIO)

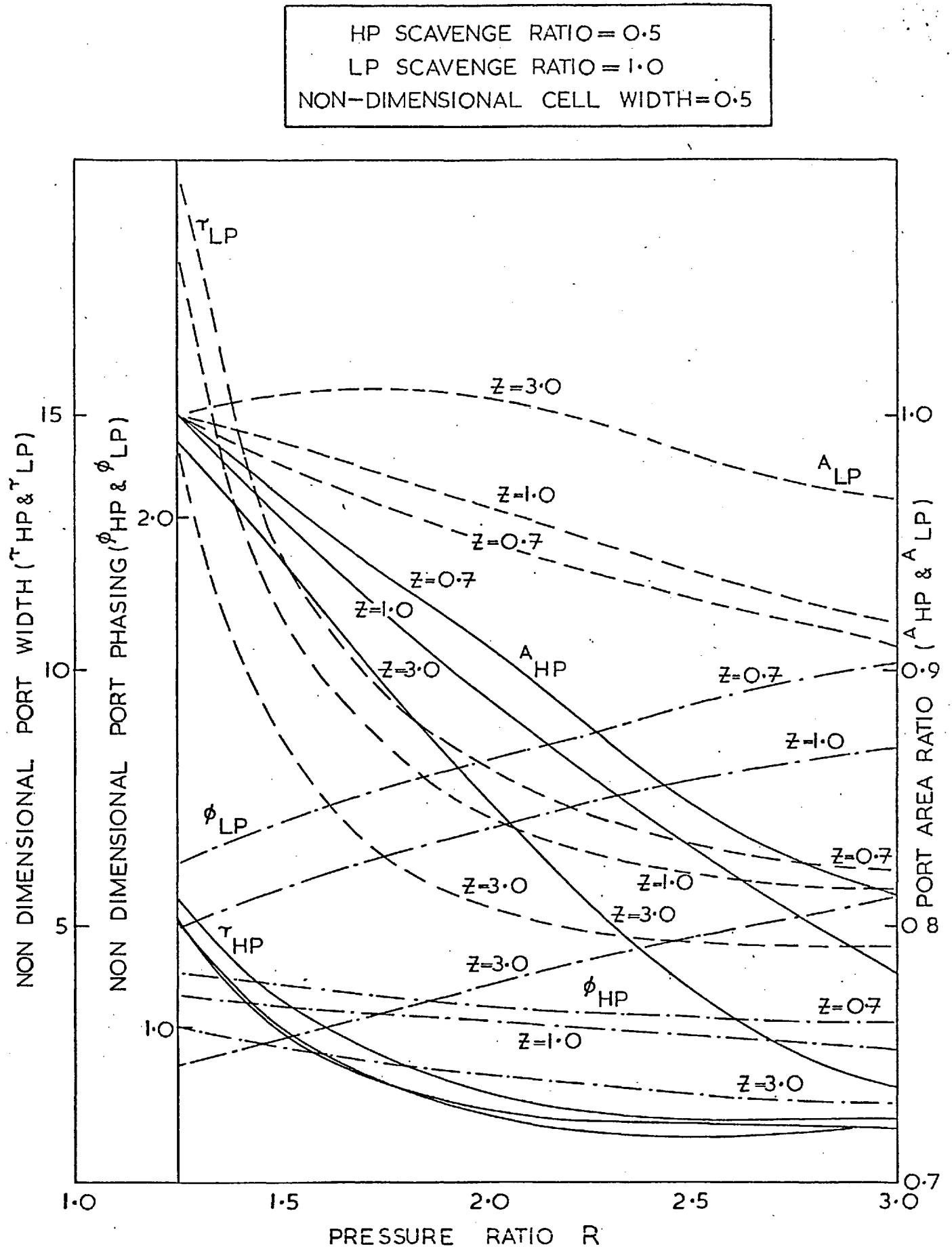


FIG. 12.18 FOUR PORT PRESSURE EXCHANGER GEOMETRY (METHOD OF CHARACTERISTICS)

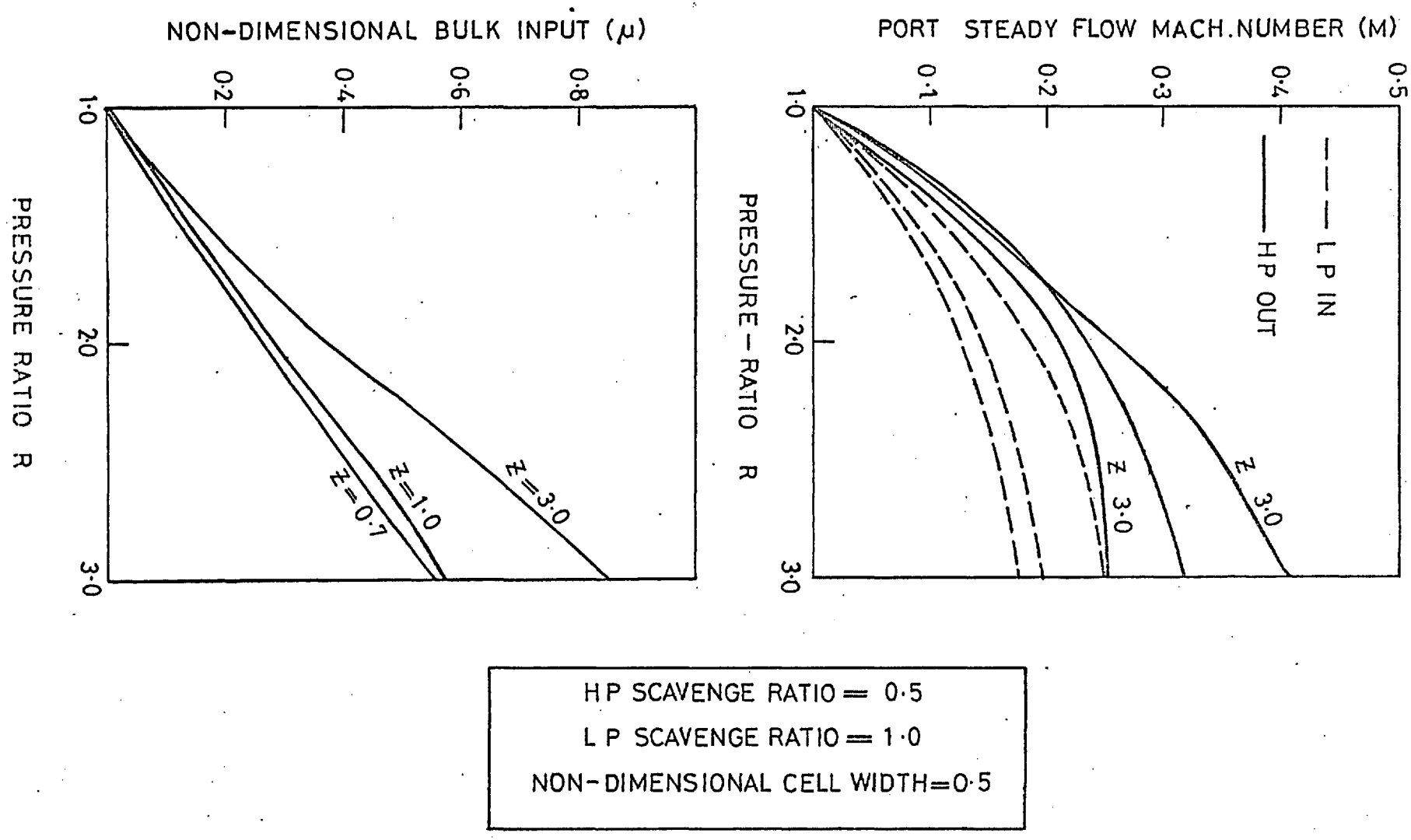


FIG. 12.19 FOUR-PORT PRESSURE EXCHANGER PERFORMANCE

(FIXED SCAVENGE RATIO)

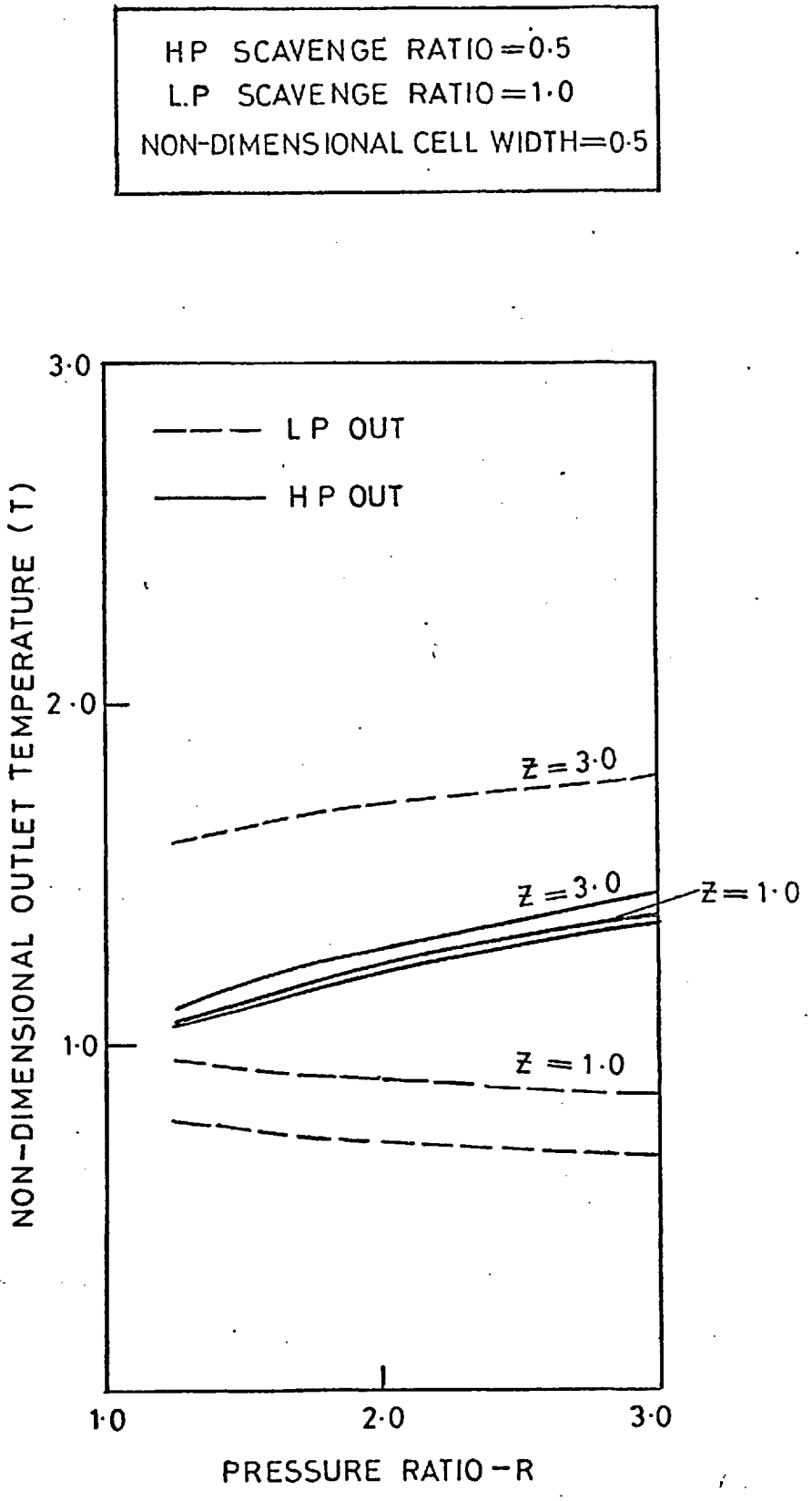


FIG.12.20 FOUR - PORT PRESSURE EXCHANGER PERFORMANCE

(FIXED SCAVENGE RATIO)

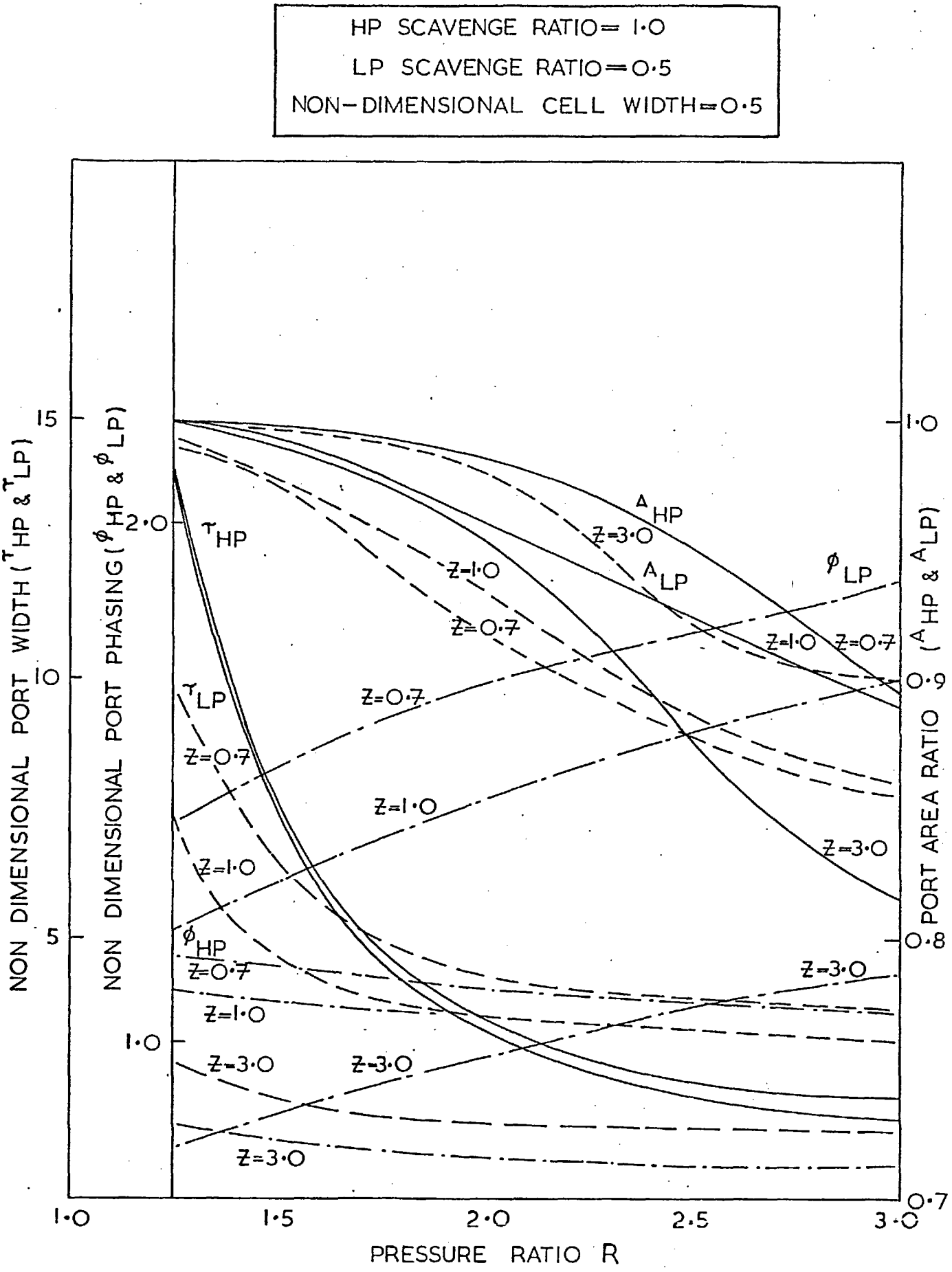


FIG. 12.21 FOUR PORT PRESSURE EXCHANGER GEOMETRY
(METHOD OF CHARACTERISTICS)

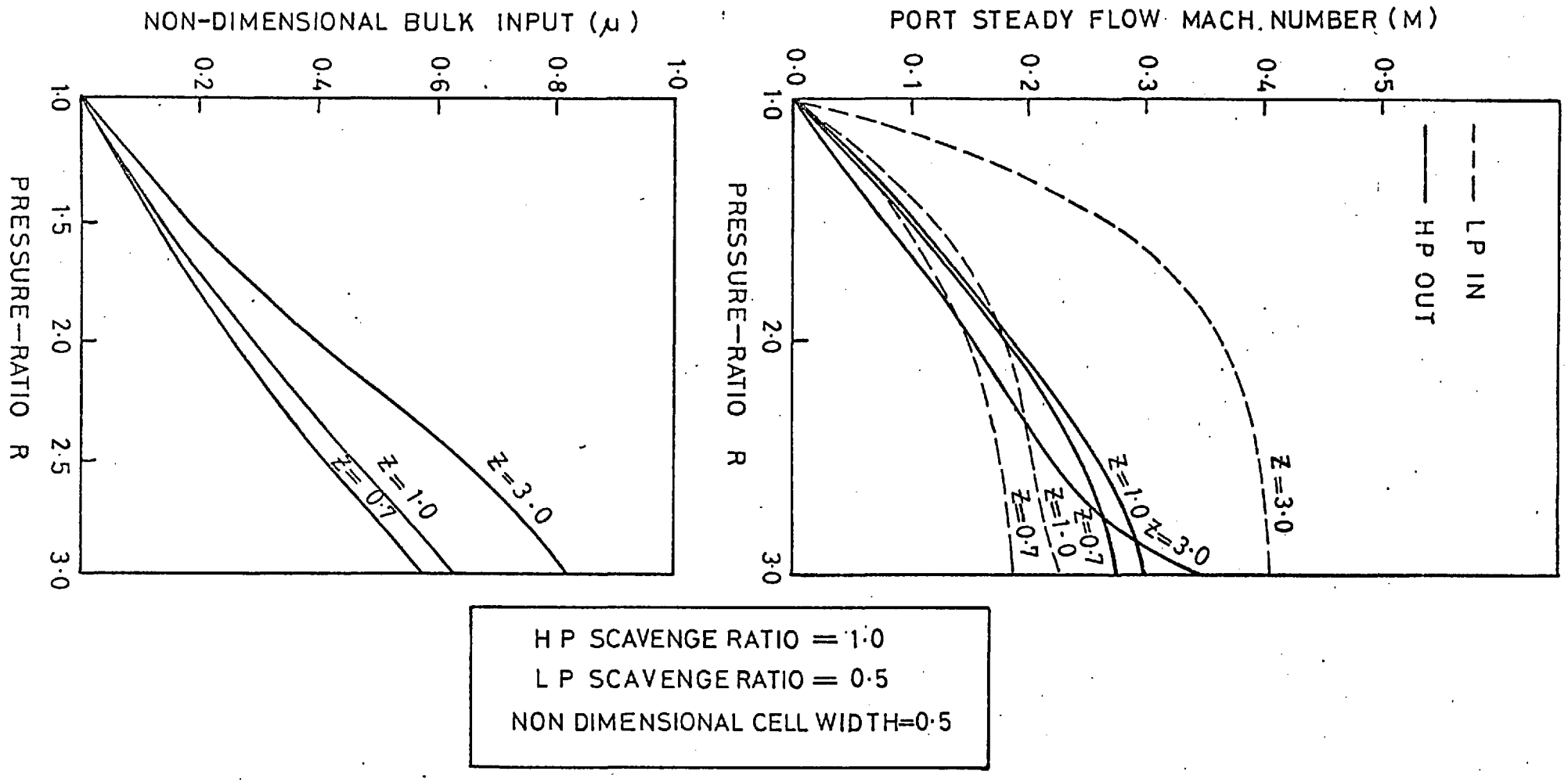


FIG. 12.22 FOUR–PORT PRESSURE EXCHANGER PERFORMANCE

(FIXED SCAVENGE RATIO)

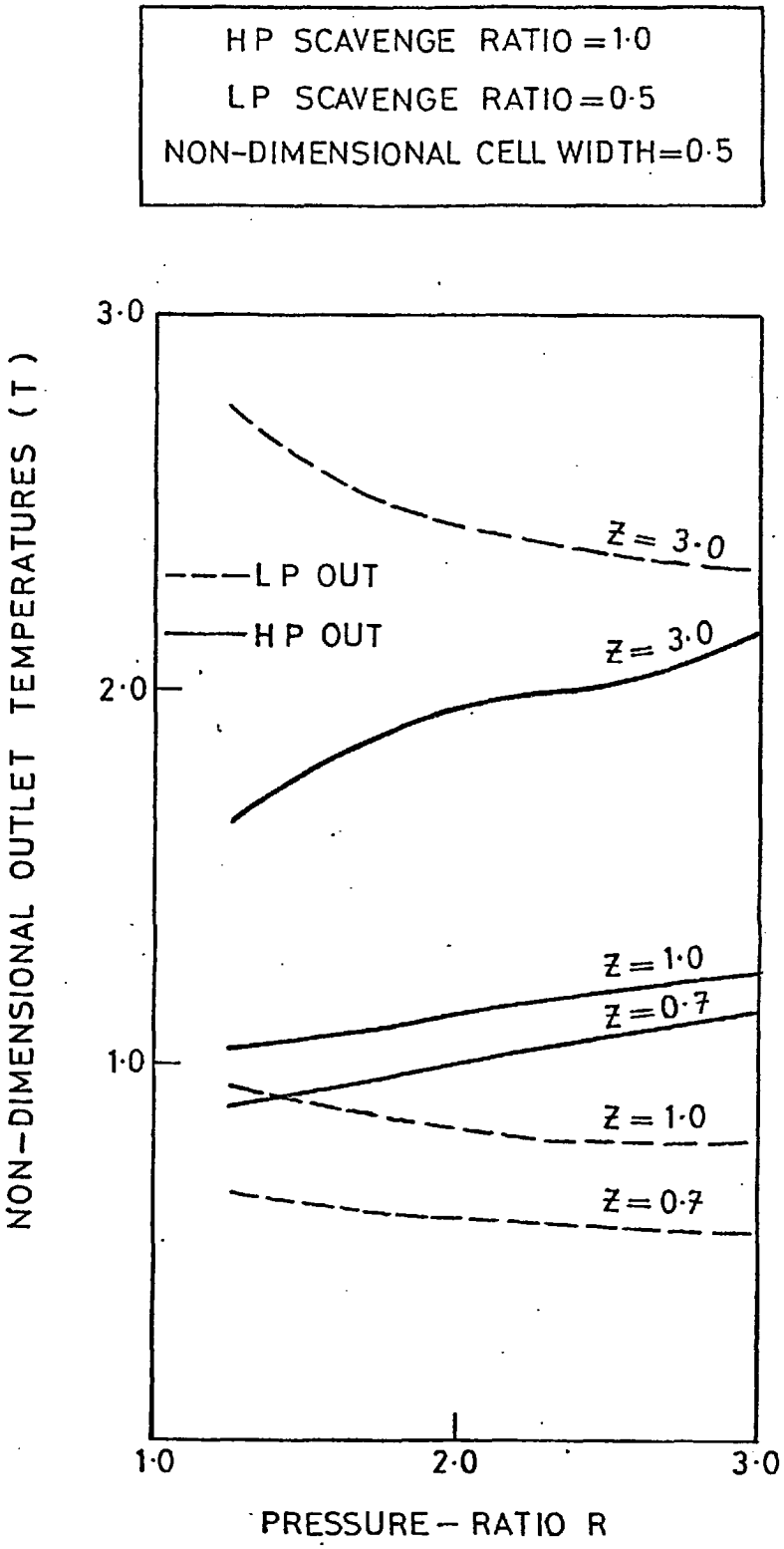


FIG. 12.23 FOUR-PORT PRESSURE EXCHANGER PERFORMANCE

(FIXED SCAVENGE RATIO)

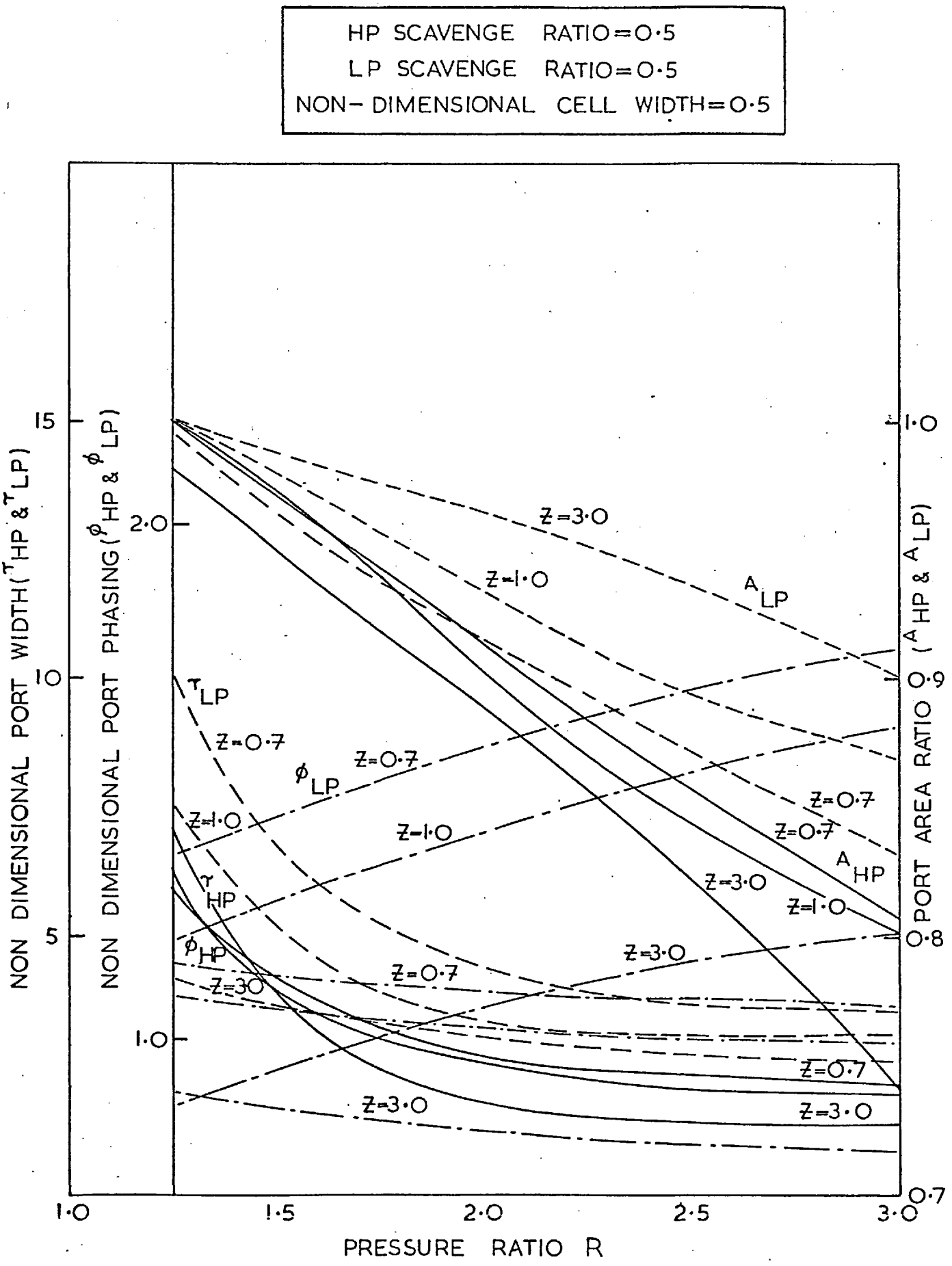
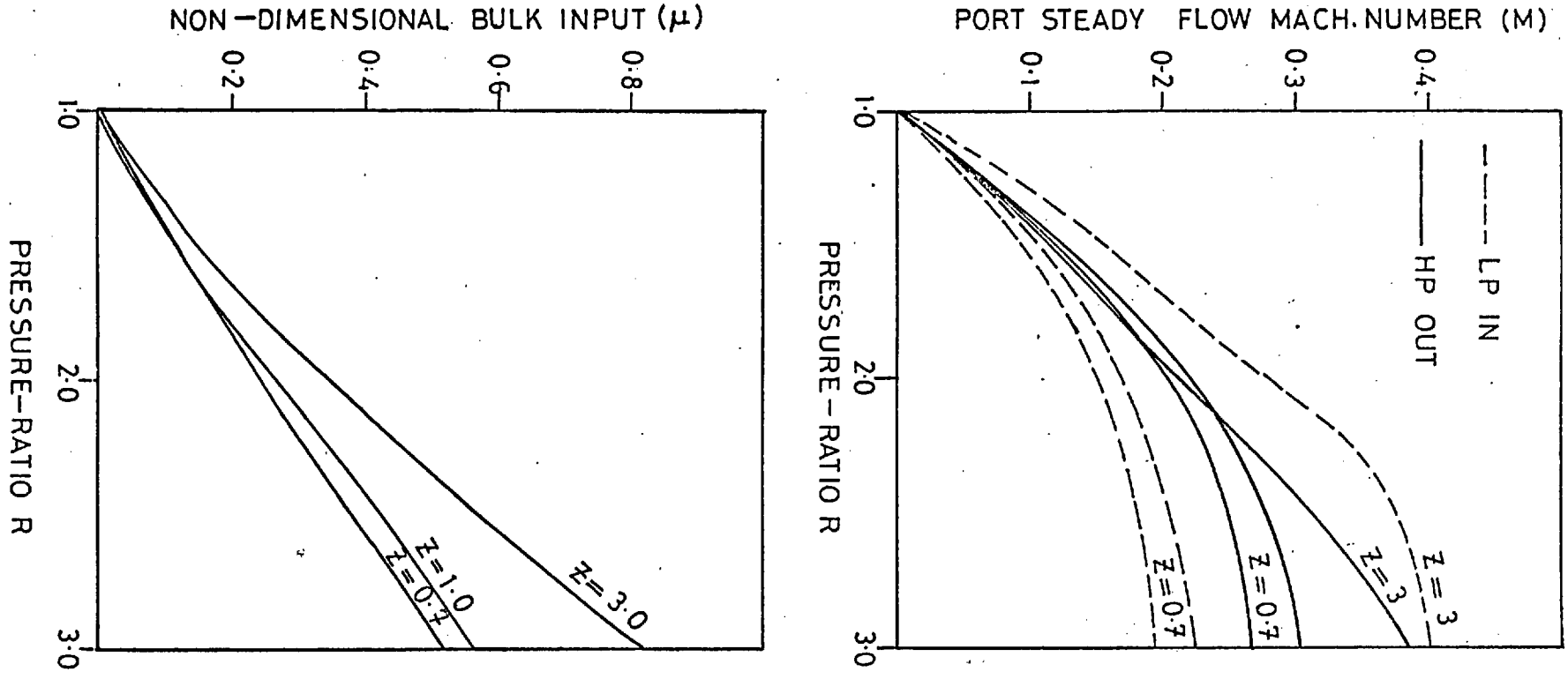


FIG. 12.24 FOUR PORT PRESSURE EXCHANGER GEOMETRY (METHOD OF CHARACTERISTICS)



H P SCAVENGE RATIO 0·5
L P SCAVENGE RATIO 0·5
NON—DIMENSIONAL CELL WIDTH 0·5

FIG. 12.25 **FOUR—PORT PRESSURE EXCHANGER PERFORMANCE**

(FIXED SCAVENGE RATIO)

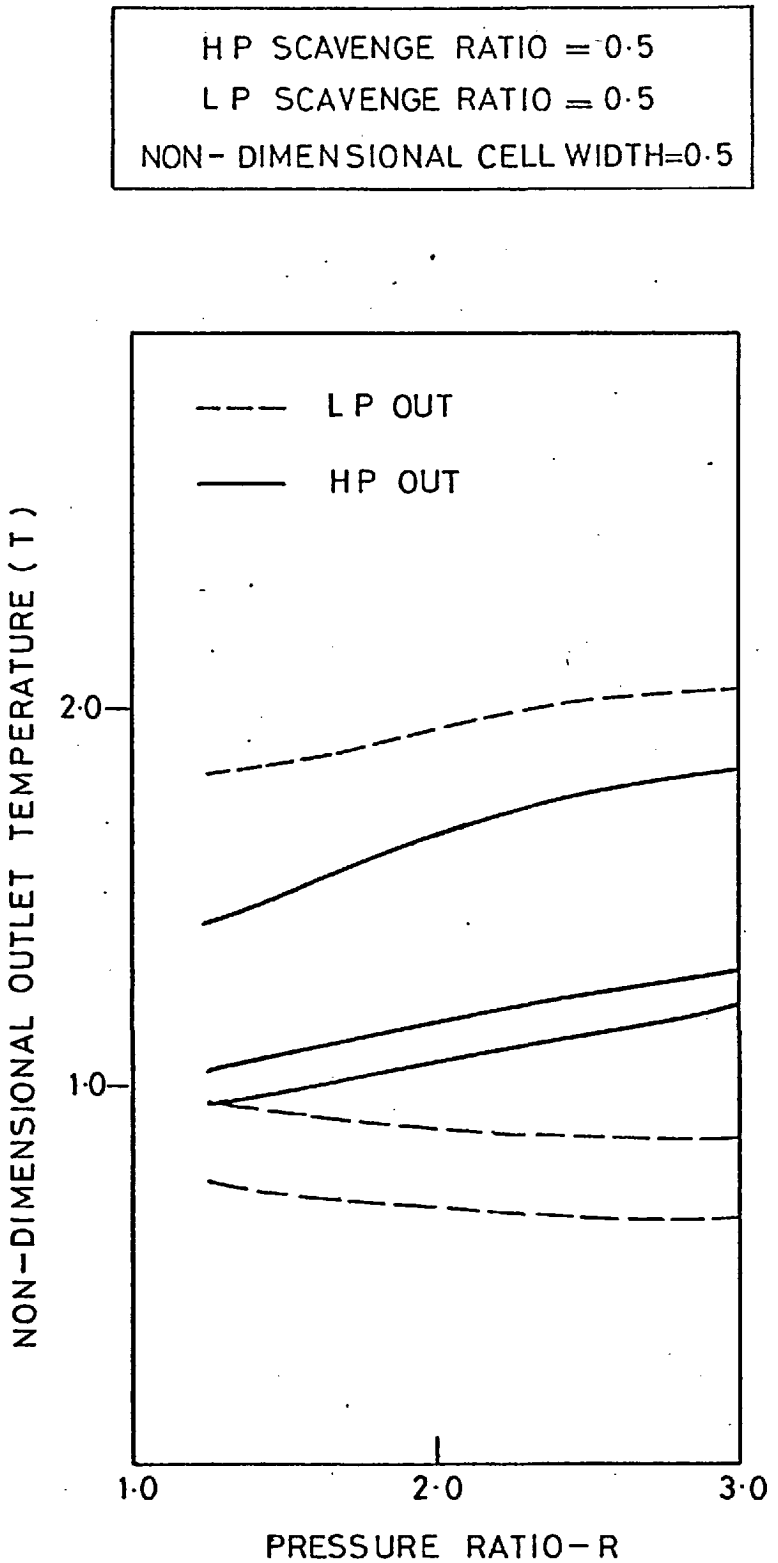


FIG. 12.26 FOUR — PORT PRESSURE EXCHANGER PERFORMANCE
(FIXED SCAVENGE RATIO)

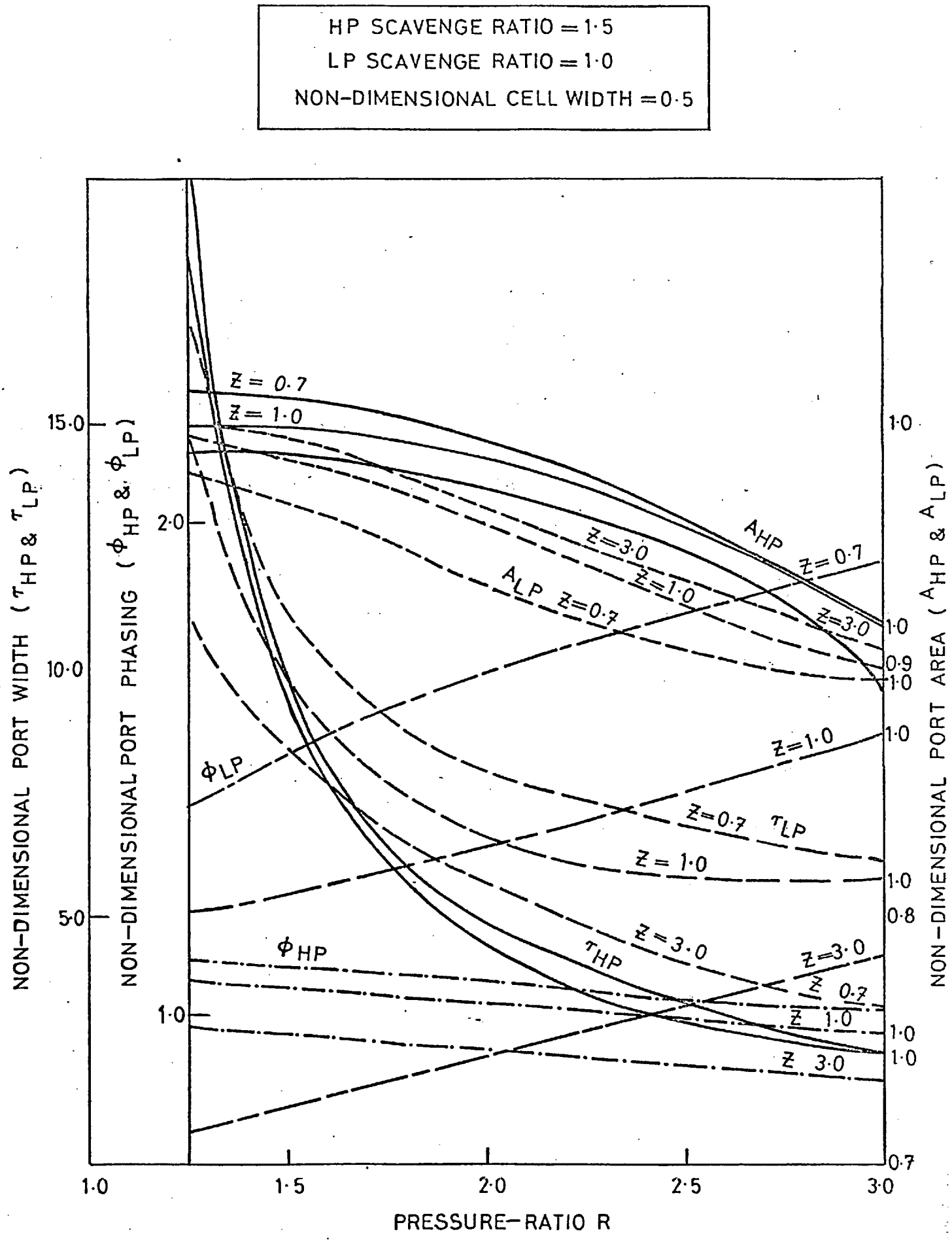
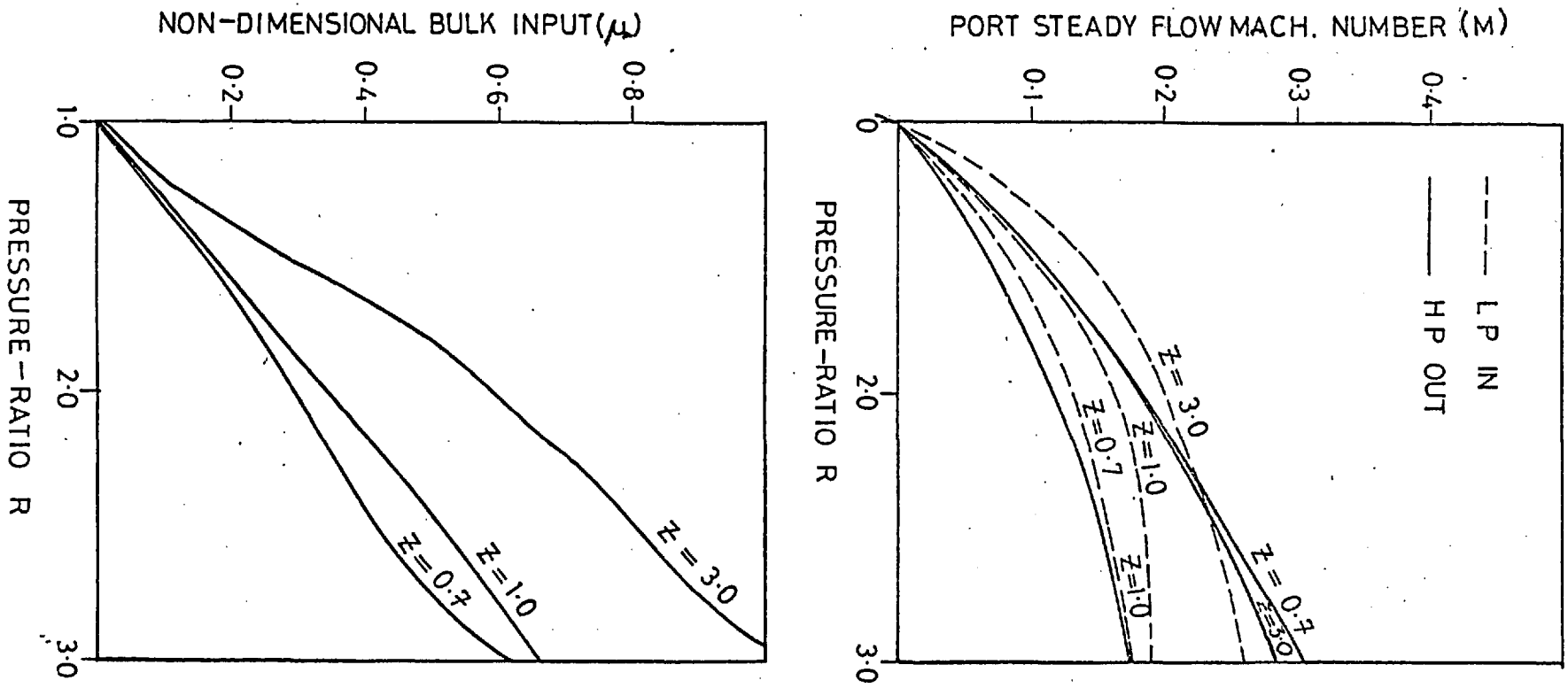


FIG. 12.27 FOUR-PORT PRESSURE EXCHANGER GEOMETRY

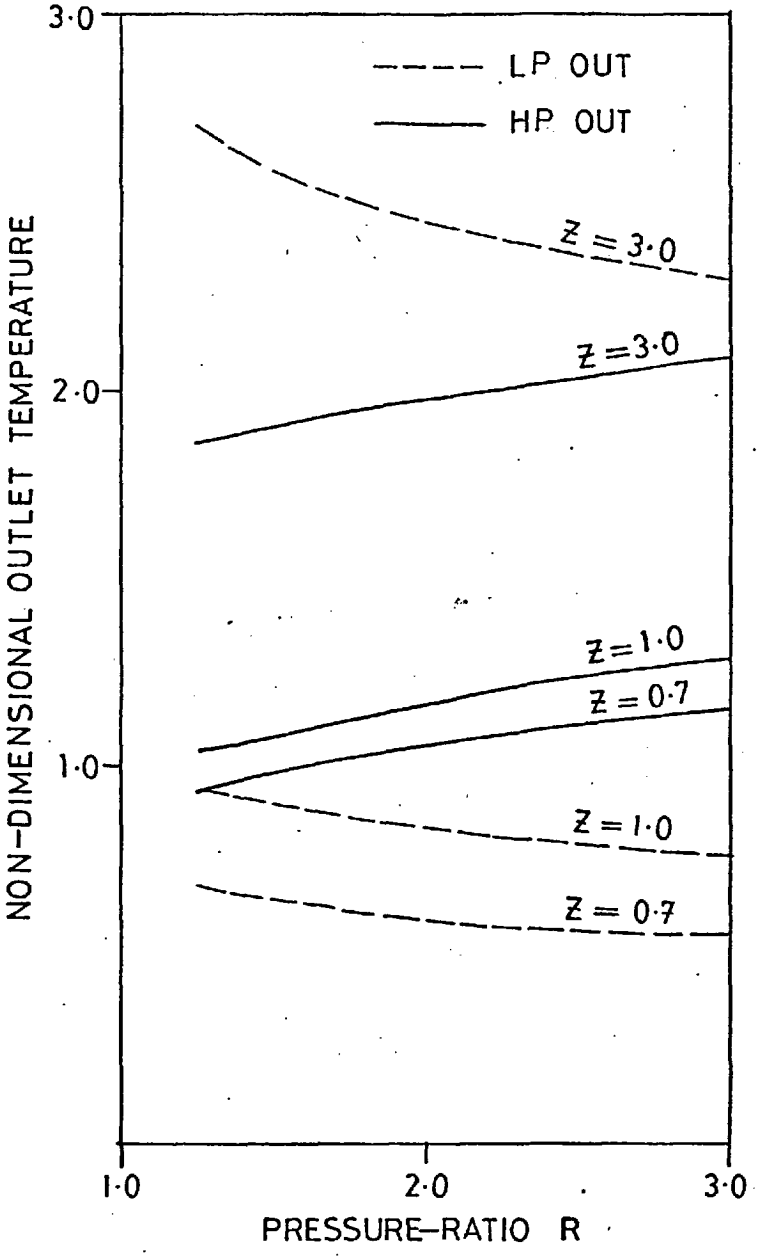
(FIXED SCAVENGE RATIO)



H P SCAVENGE RATIO 1·5
L P SCAVENGE RATIO 1·0
NON-DIMENSIONAL CELL WIDTH 0·5

FIG. 12.28 FOUR-PORT PRESSURE EXCHANGER PERFORMANCE

(FIXED SCAVENGE RATIO)



HP SCAVENGE RATIO = 1·5
LP SCAVENGE RATIO = 1·0
NON-DIMENSIONAL CELL WIDTH 0·5

FIG. 12.29 FOUR-PORT RRESSURE EXCHANGER PERFORMANCE

(FIXED SCAVENGE RATIO)

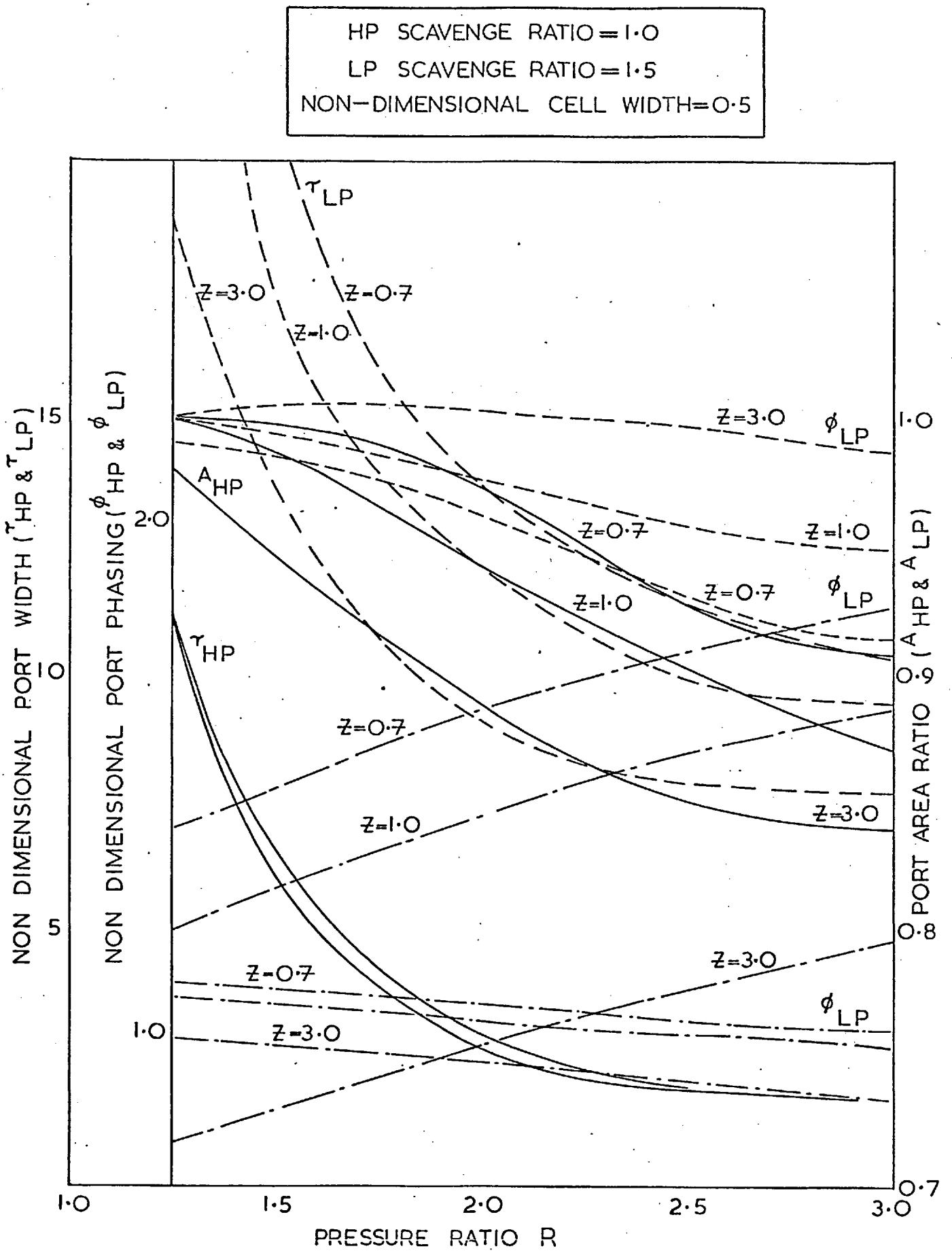


FIG. 12.30 FOUR PORT PRESSURE EXCHANGER GEOMETRY (METHOD OF CHARACTERISTICS)

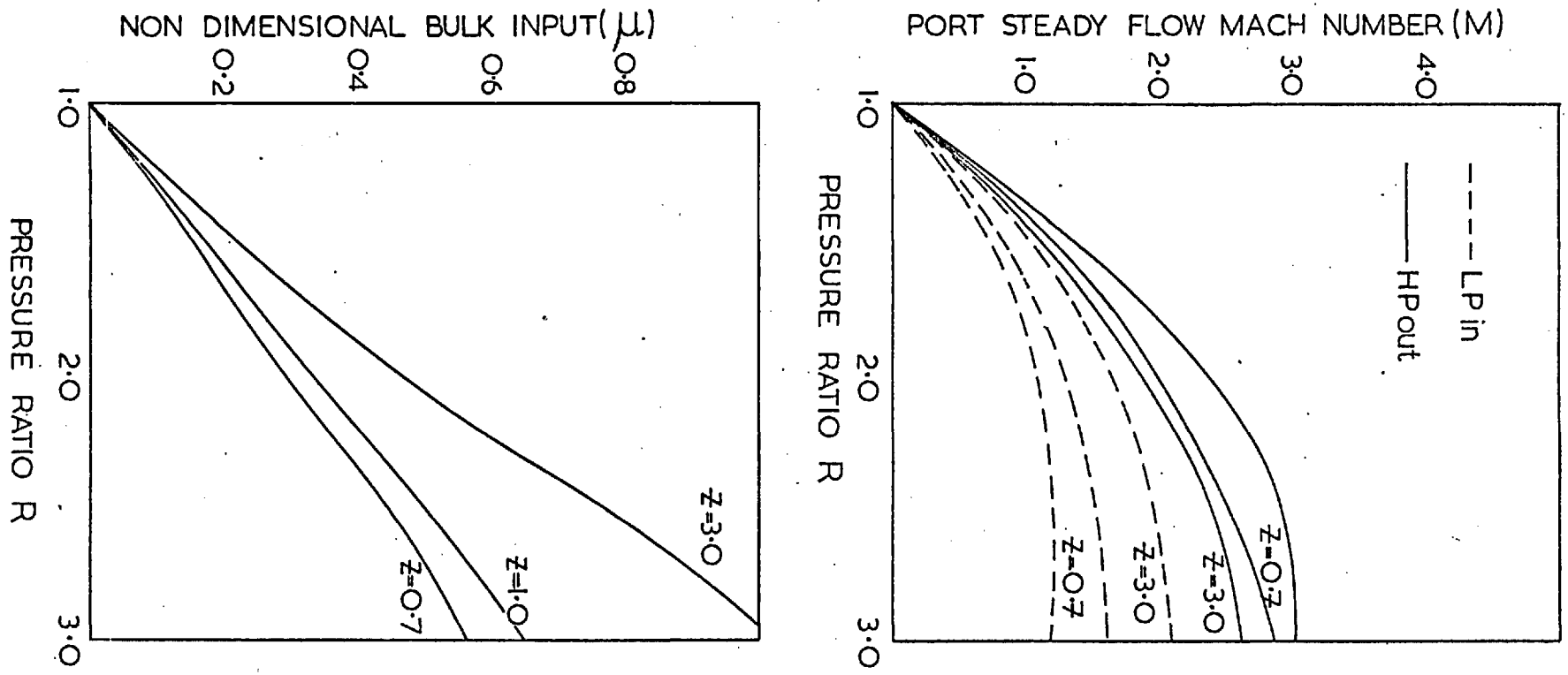
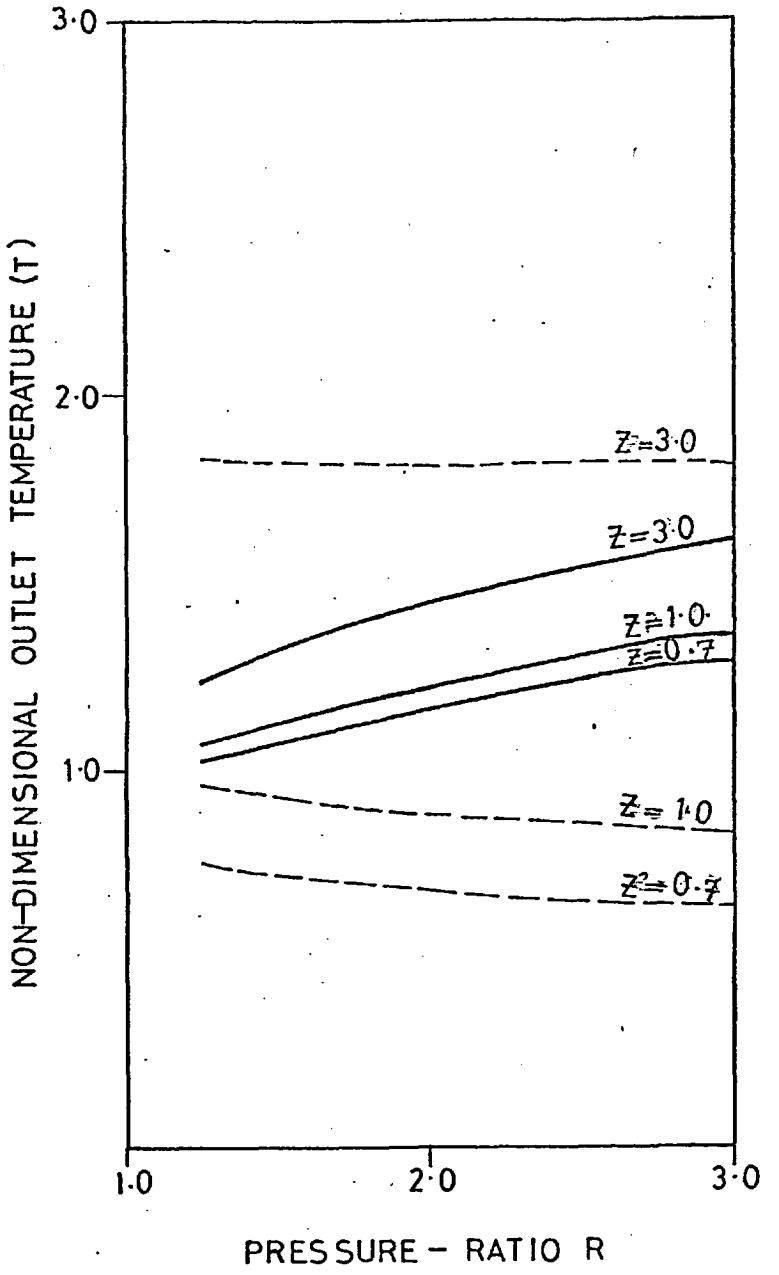


FIG. 12.31 FOUR PORT PRESSURE EXCHANGER PERFORMANCE

(FIXED SCAVENGE RATIO)



HP SCAVENGE RATIO = 1·0
LP SCAVENGE RATIO = 1·5
NON-DIMENSIONAL CELL WIDTH 0·5

FIG. 12.32 FOUR-PORT PRESSURE EXCHANGER PERFORMANCE

(FIXED SCAVENGE RATIO)

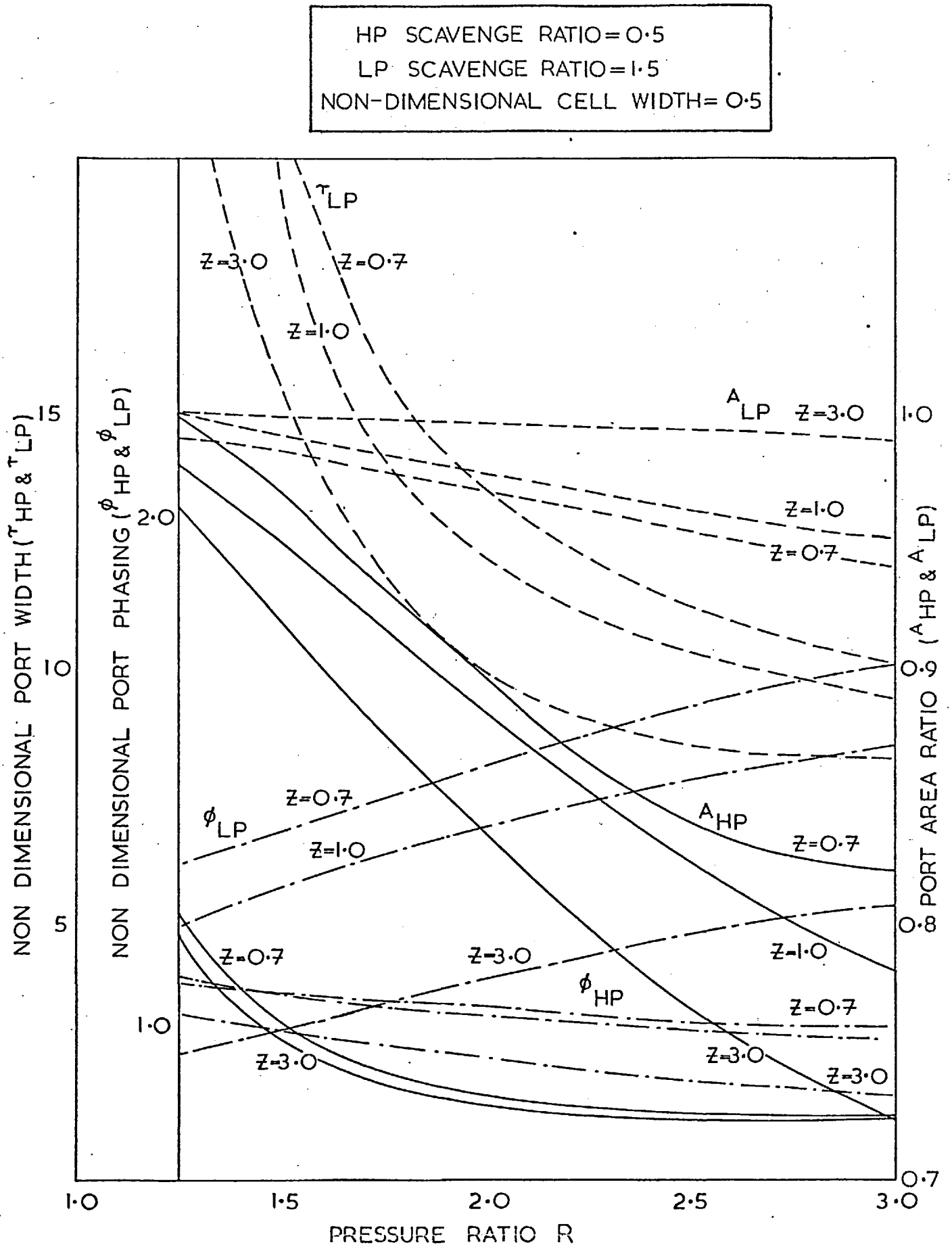


FIG. 12.23 FOUR PORT PRESSURE EXCHANGER GEOMETRY
(METHOD OF CHARACTERISTICS)

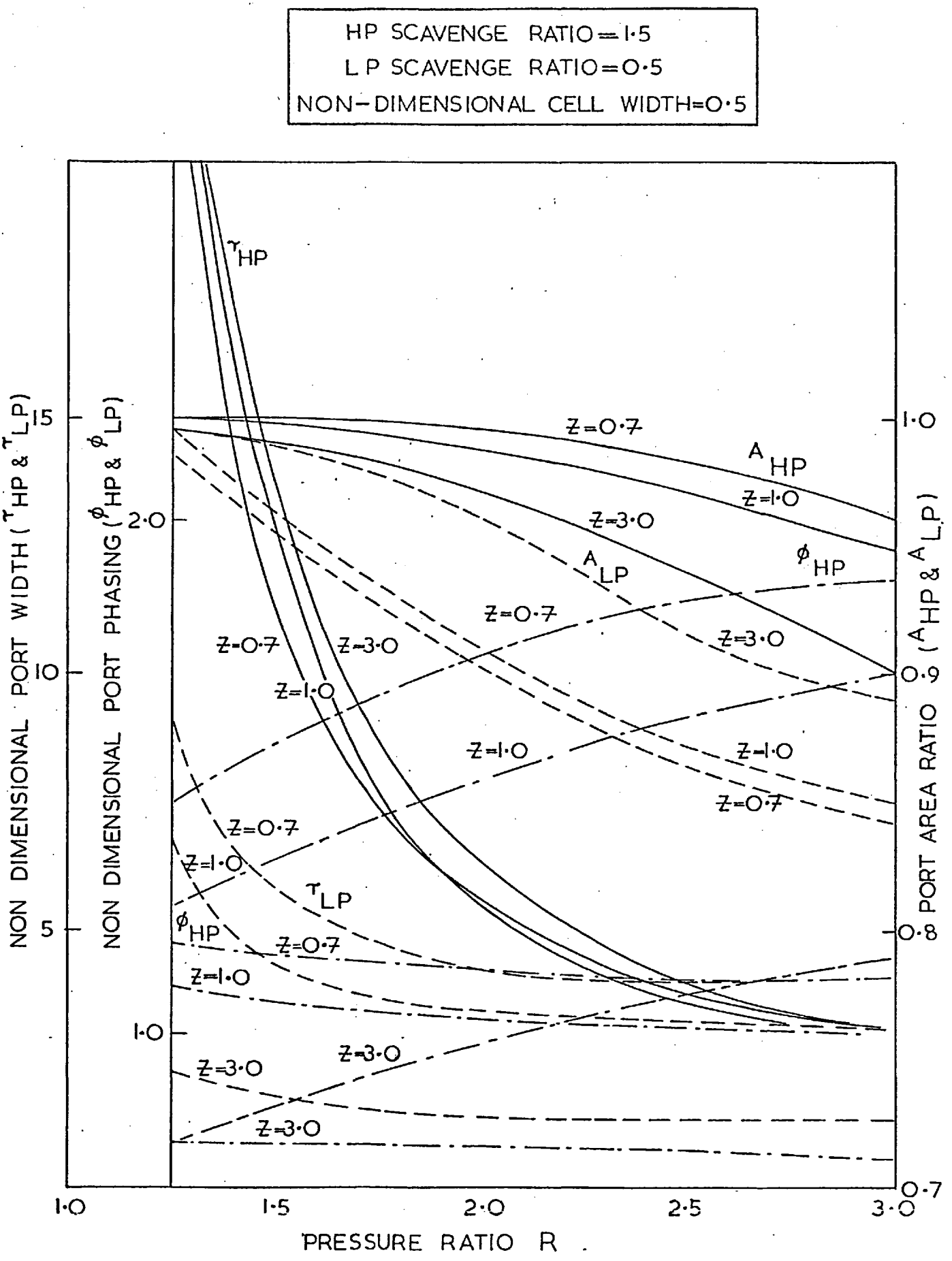


FIG. 12.34 FOUR PORT PRESSURE EXCHANGER GEOMETRY
(METHOD OF CHARACTERISTICS)

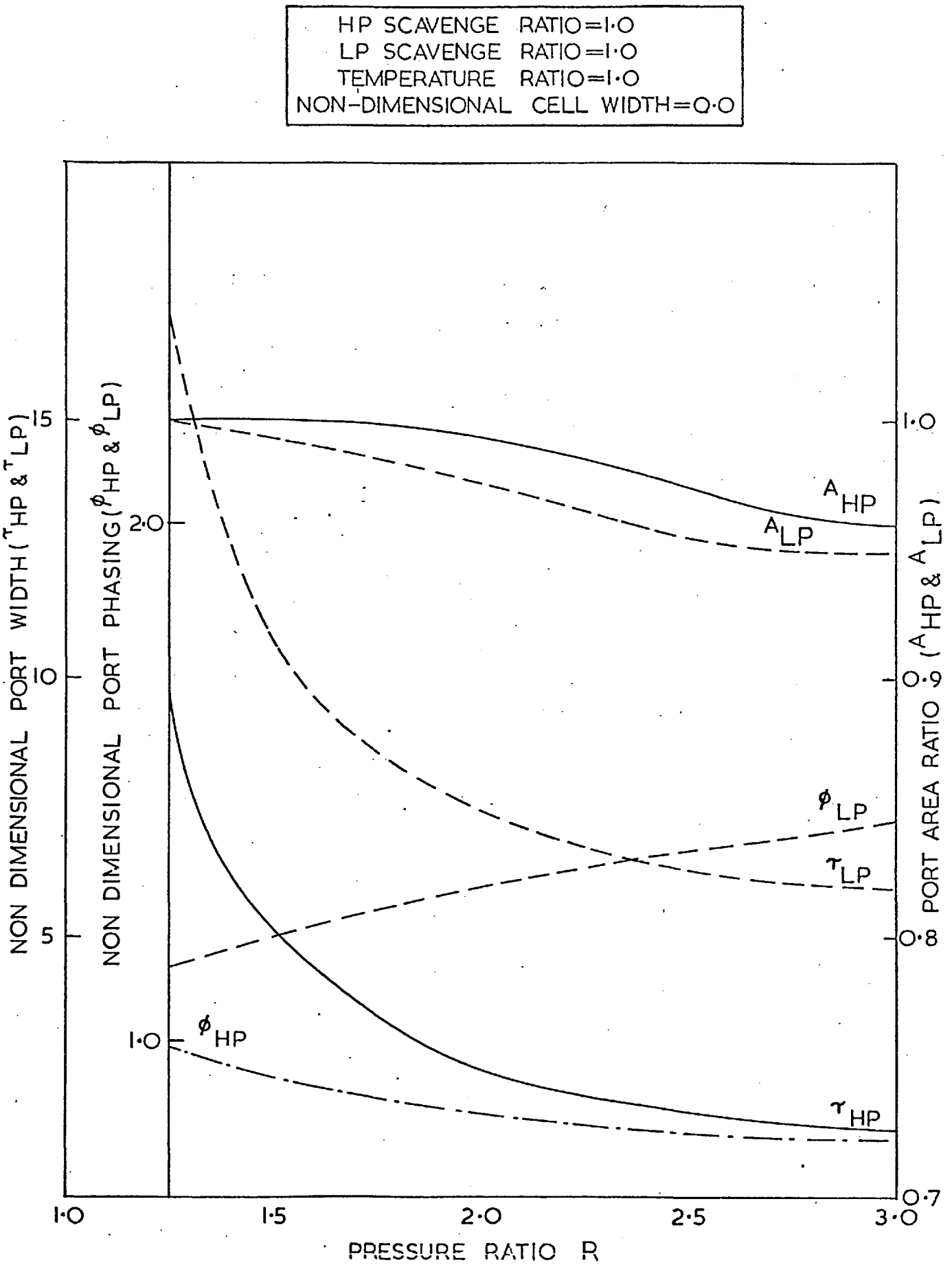
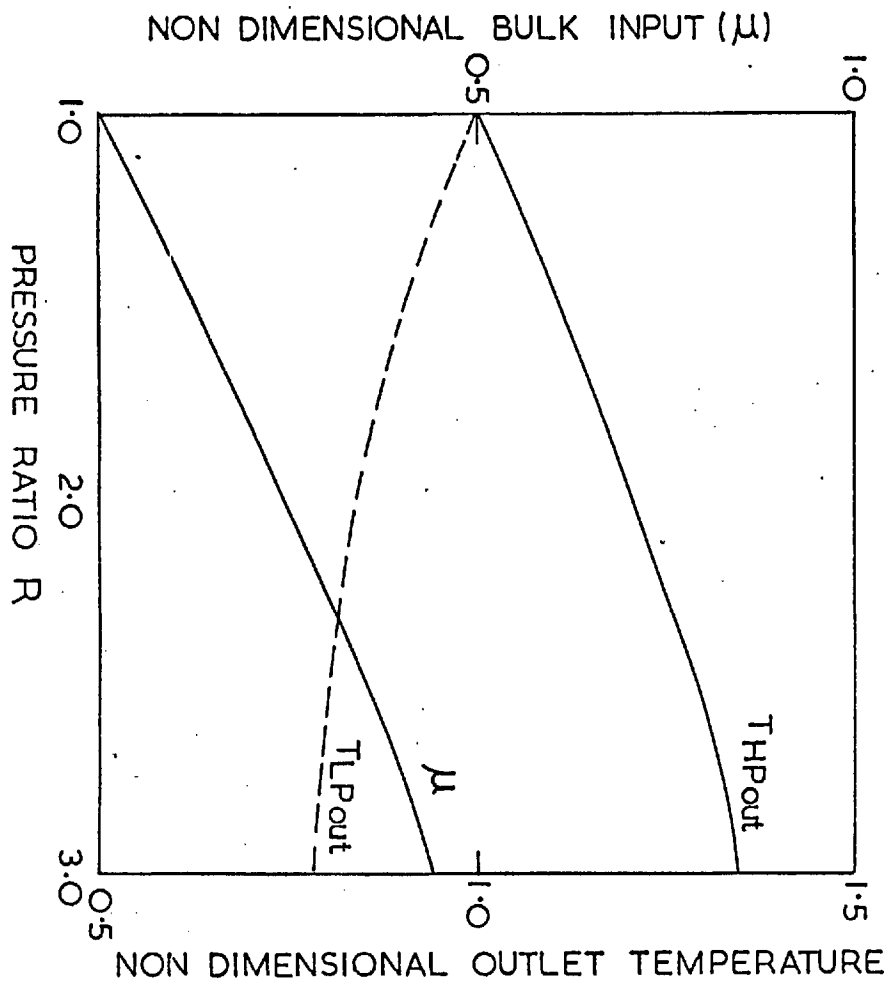


FIG. 11.35 FOUR PORT PRESSURE EXCHANGER GEOMETRY
(METHOD OF CHARACTERISTICS)



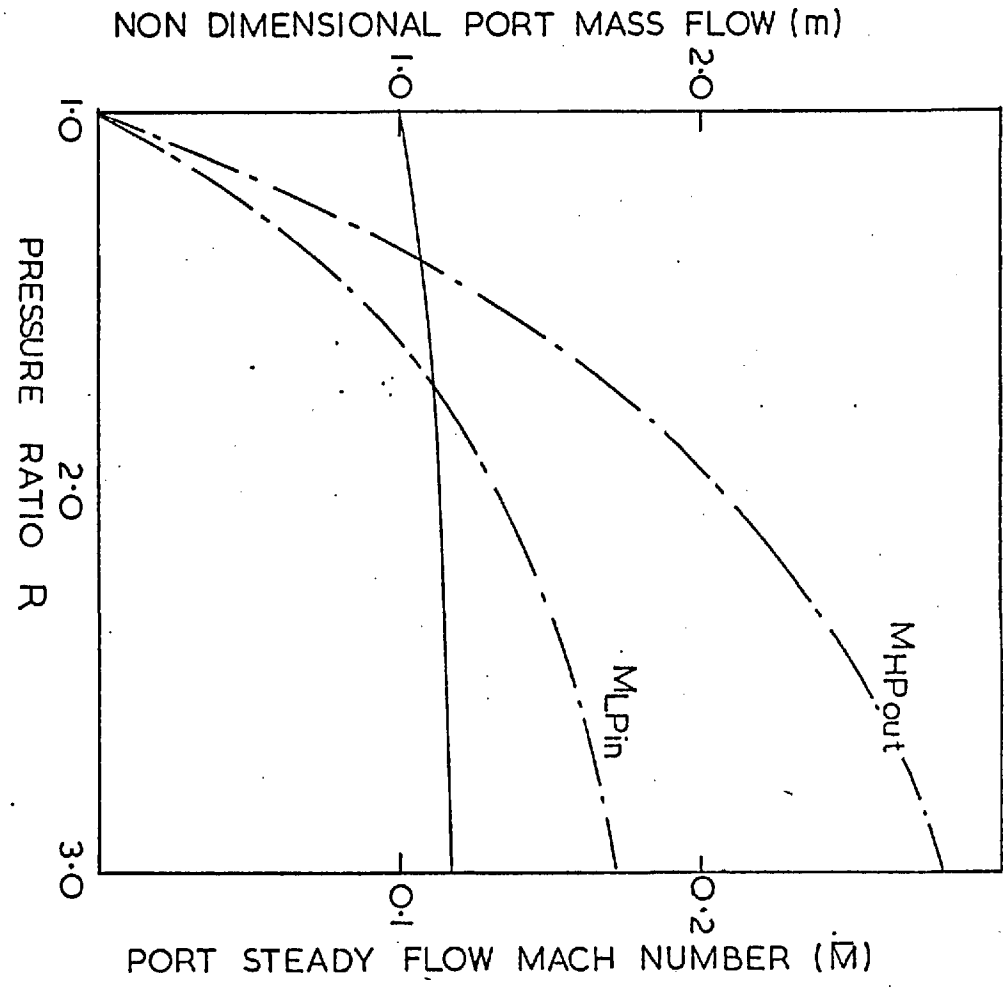


FIG.12.36 FOUR PORT PRESSURE EXCHANGER PERFORMANCE (FIXED SCAVENGE RATIO)

NO LOSSES TAKEN INTO ACCOUNT

HP SCAVENGE RATIO = 1·0
LP SCAVENGE RATIO = 1·0
TEMPERATURE RATIO = 1·0
NON DIMENSIONAL CELL WIDTH = 0·0

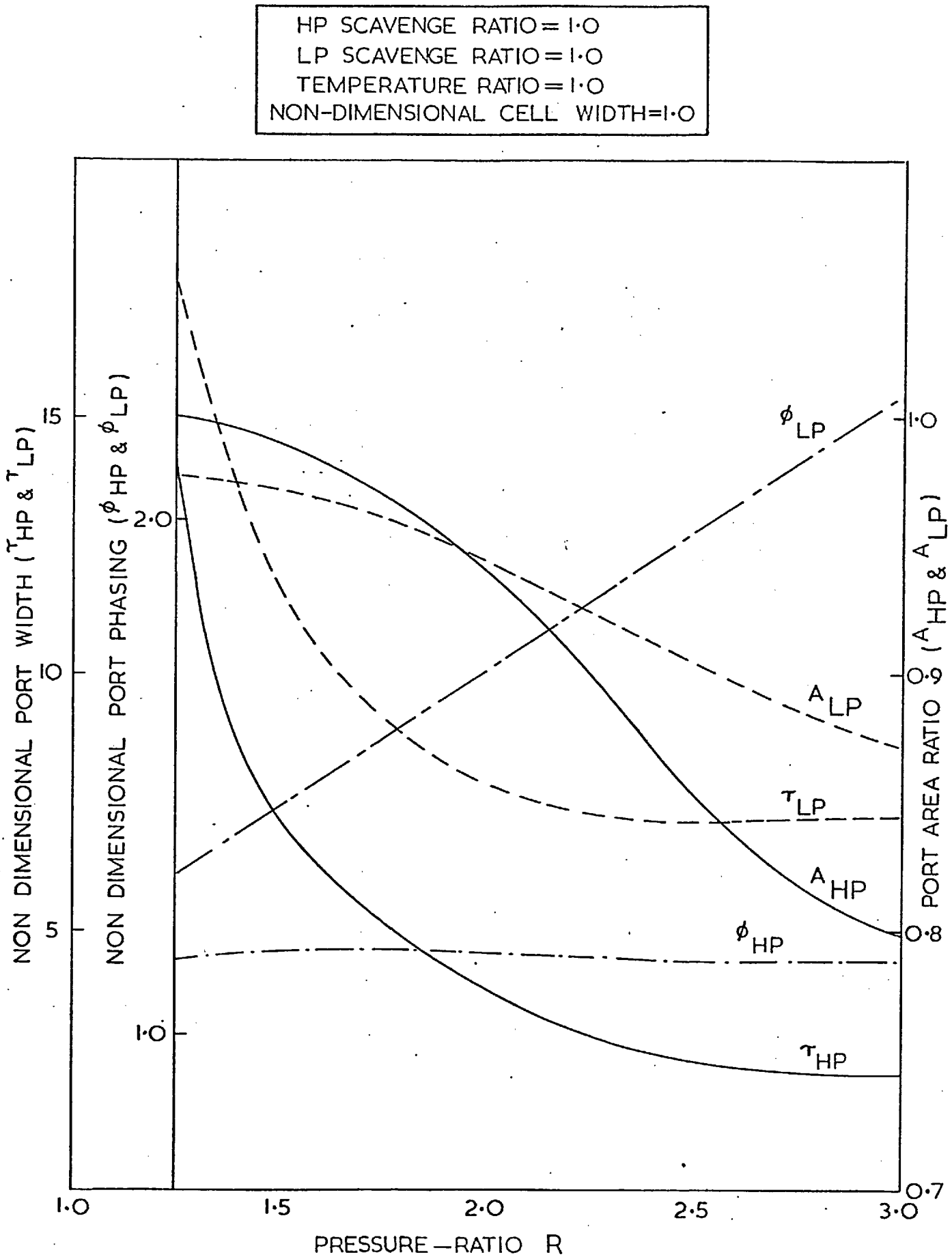
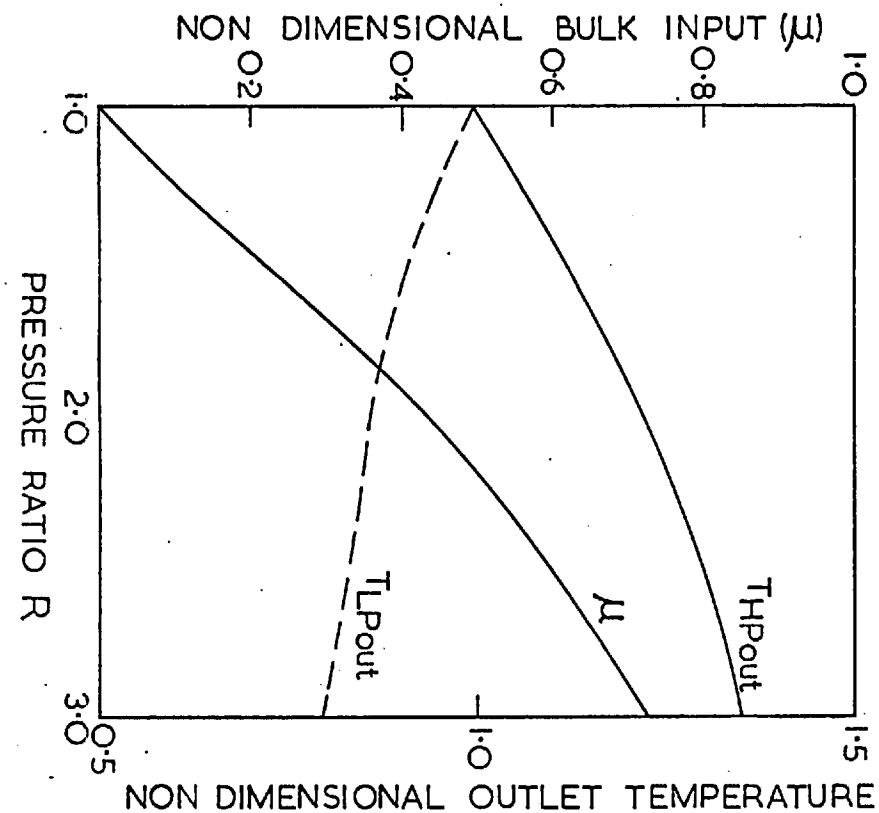


FIG. 12.37 FOUR PORT PRESSURE EXCHANGER GEOMETRY
(METHOD OF CHARACTERISTICS)



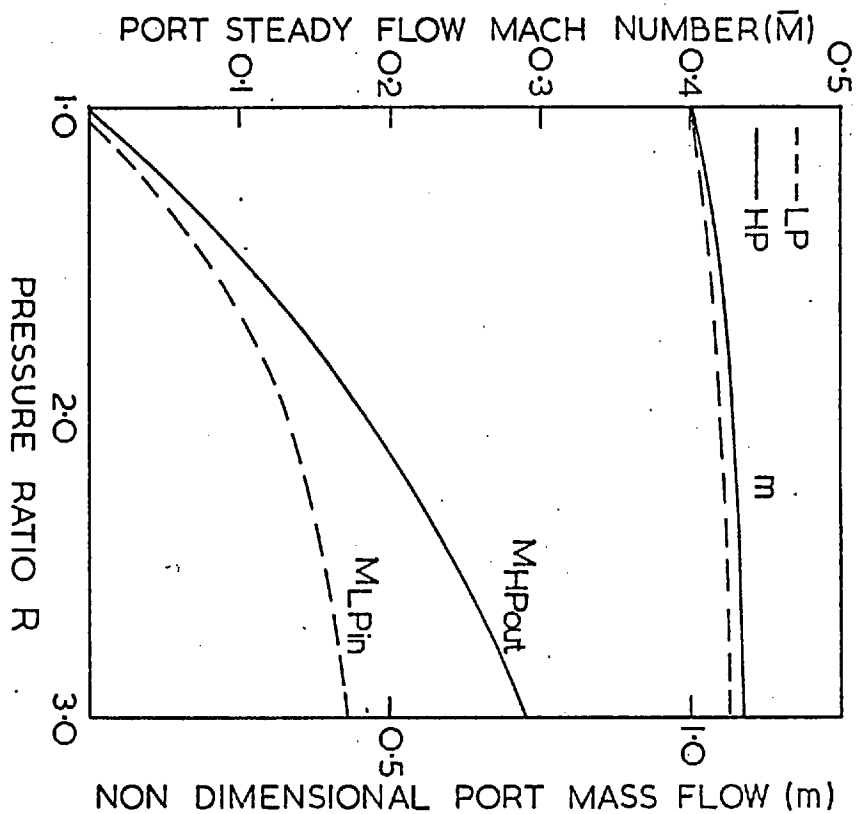


FIG. 12.38 FOUR PORT PRESSURE EXCHANGER PERFORMANCE (FIXED SCAVENGE RATIO)

HP SCAVENGE RATIO = 1·0
LP SCAVENGE RATIO = 1·0
TEMPERATURE RATIO = 1·0
NON DIMENSIONAL CELL WIDTH = 1·0

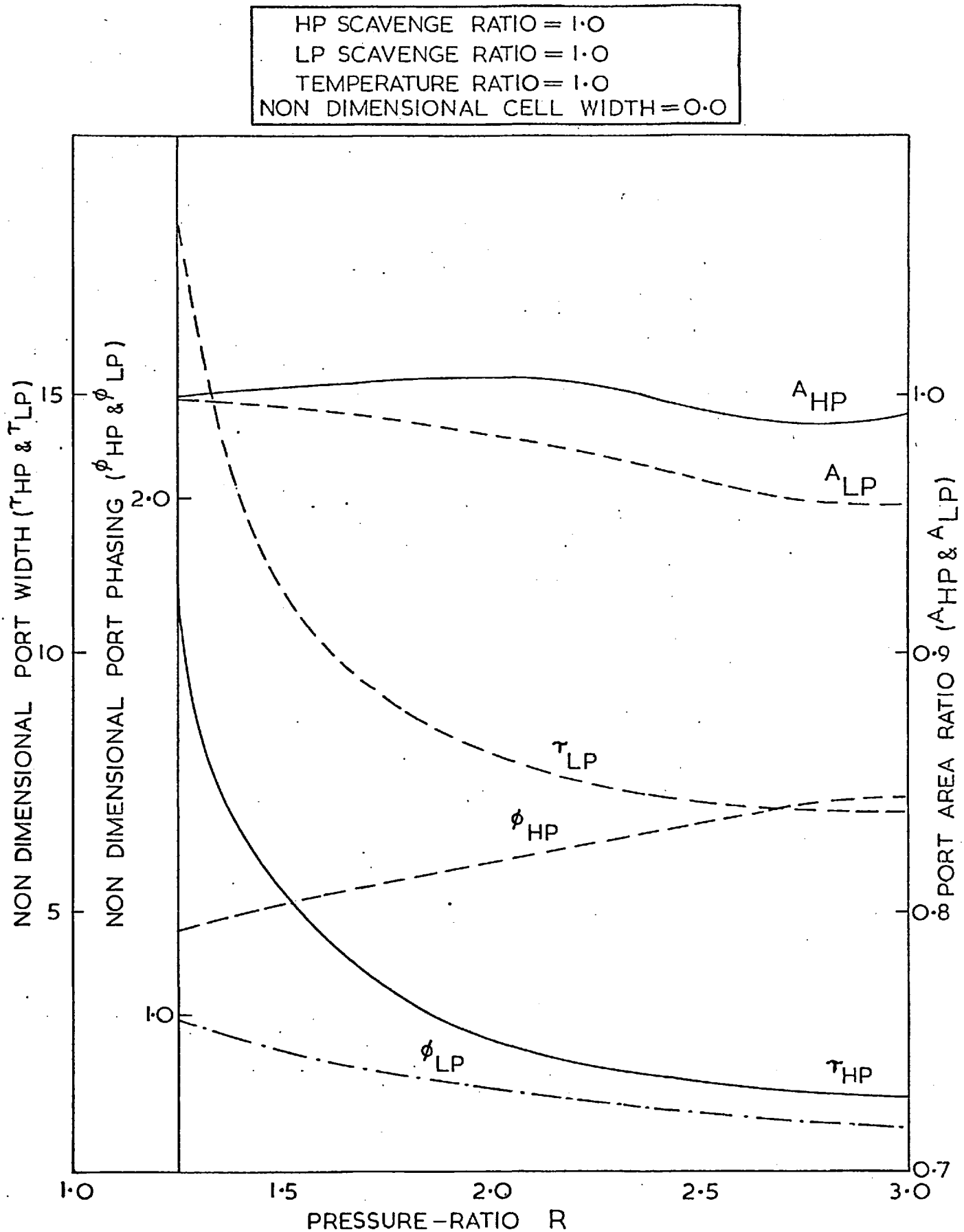
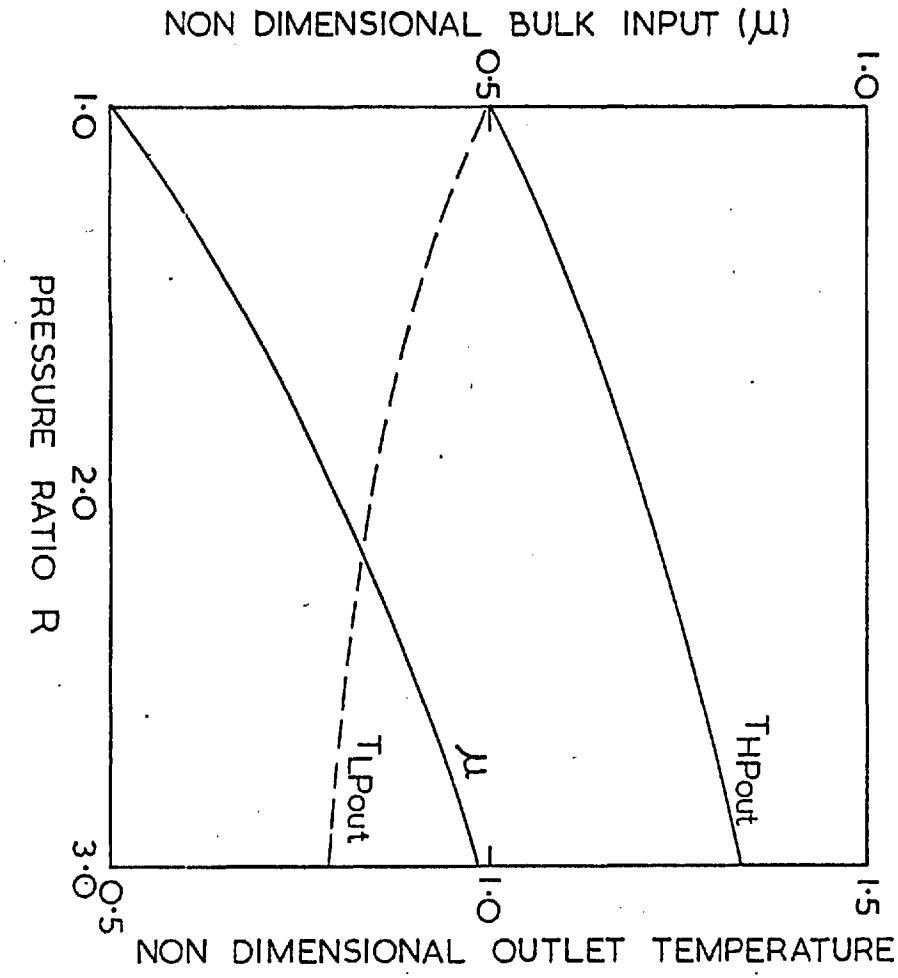
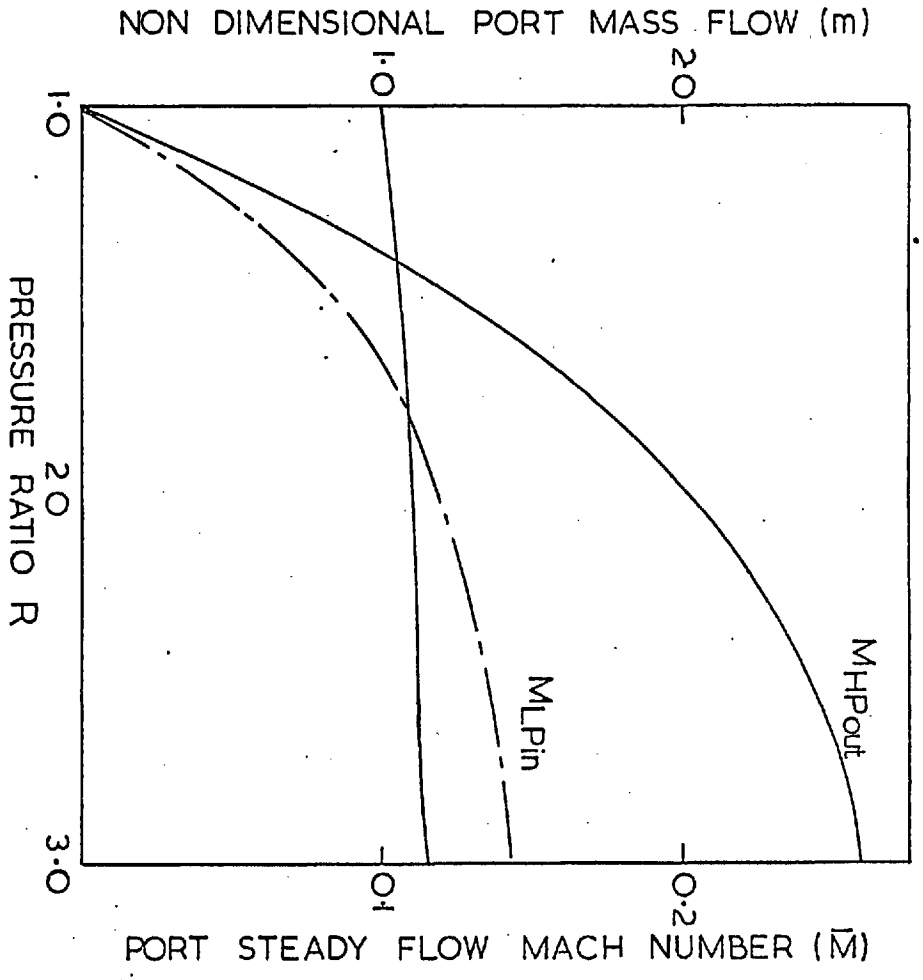


FIG 12.19 FOUR-PORT PRESSURE EXCHANGER GEOMETRY
(METHOD OF CHARACTERISTICS)
FRICTION, HEAT TRANSFER & LEAKAGE LOSSES TAKEN INTO ACCOUNT

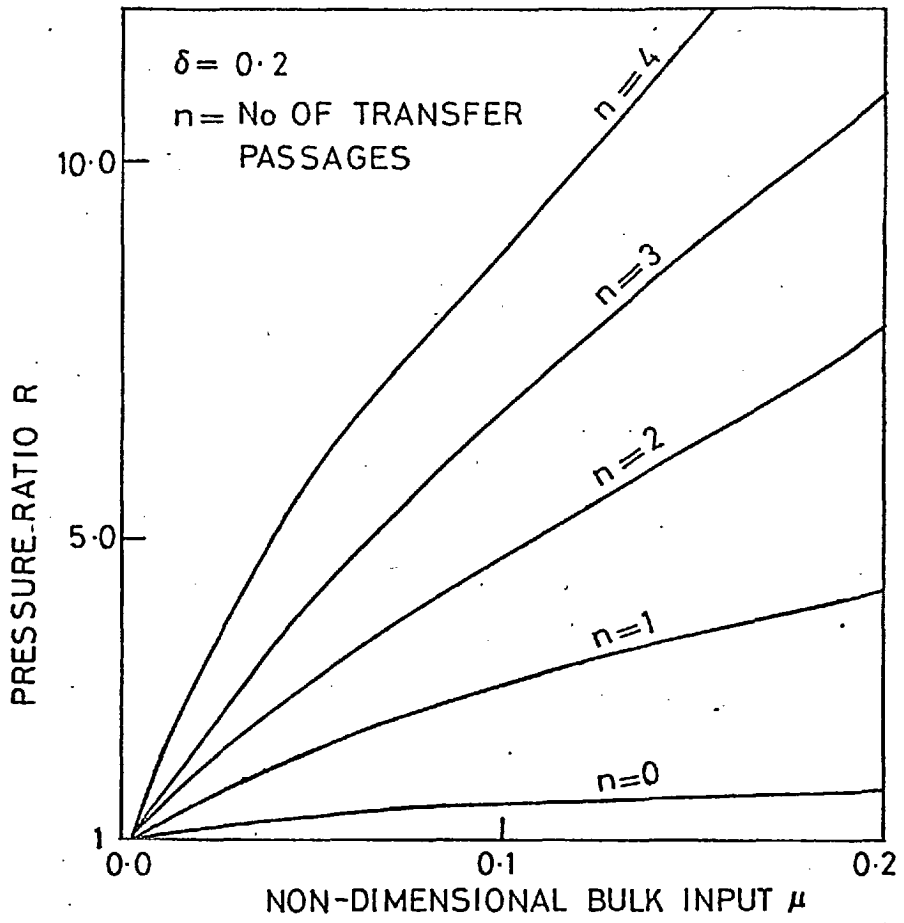




HP SCAVENGE RATIO = 1·0
LP SCAVENGE RATIO = 1·0
TEMPERATURE RATIO = 1·0
NON DIMENSIONAL CELL WIDTH = 0·0

FIG. 12.40 FOUR PORT PRESSURE EXCHANGER PERFORMANCE (FIXED SCAVENGE RATIO)

FRICTION, HEAT TRANSFER, CELL WALL THICKNESS AND LEAKAGE TAKEN INTO ACCOUNT



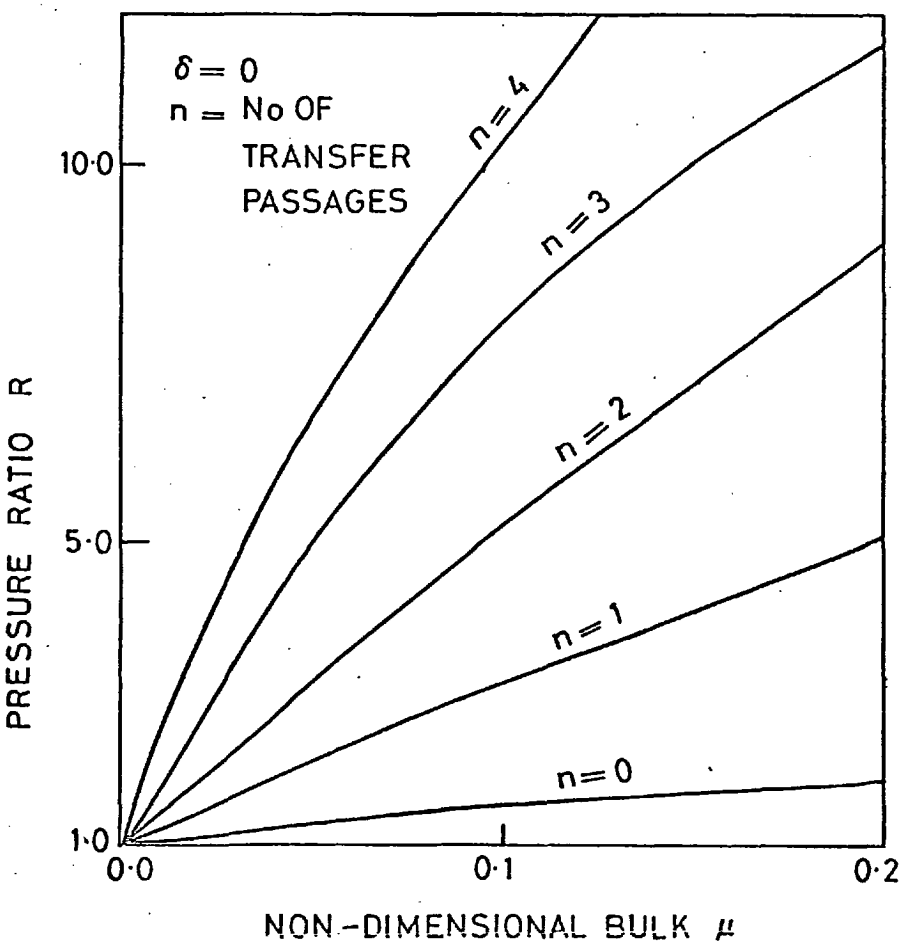


FIG. 12.41 PERFORMANCE OF FOUR-PORT PRESSURE EXCHANGER WITH TRANSFER PASSAGES

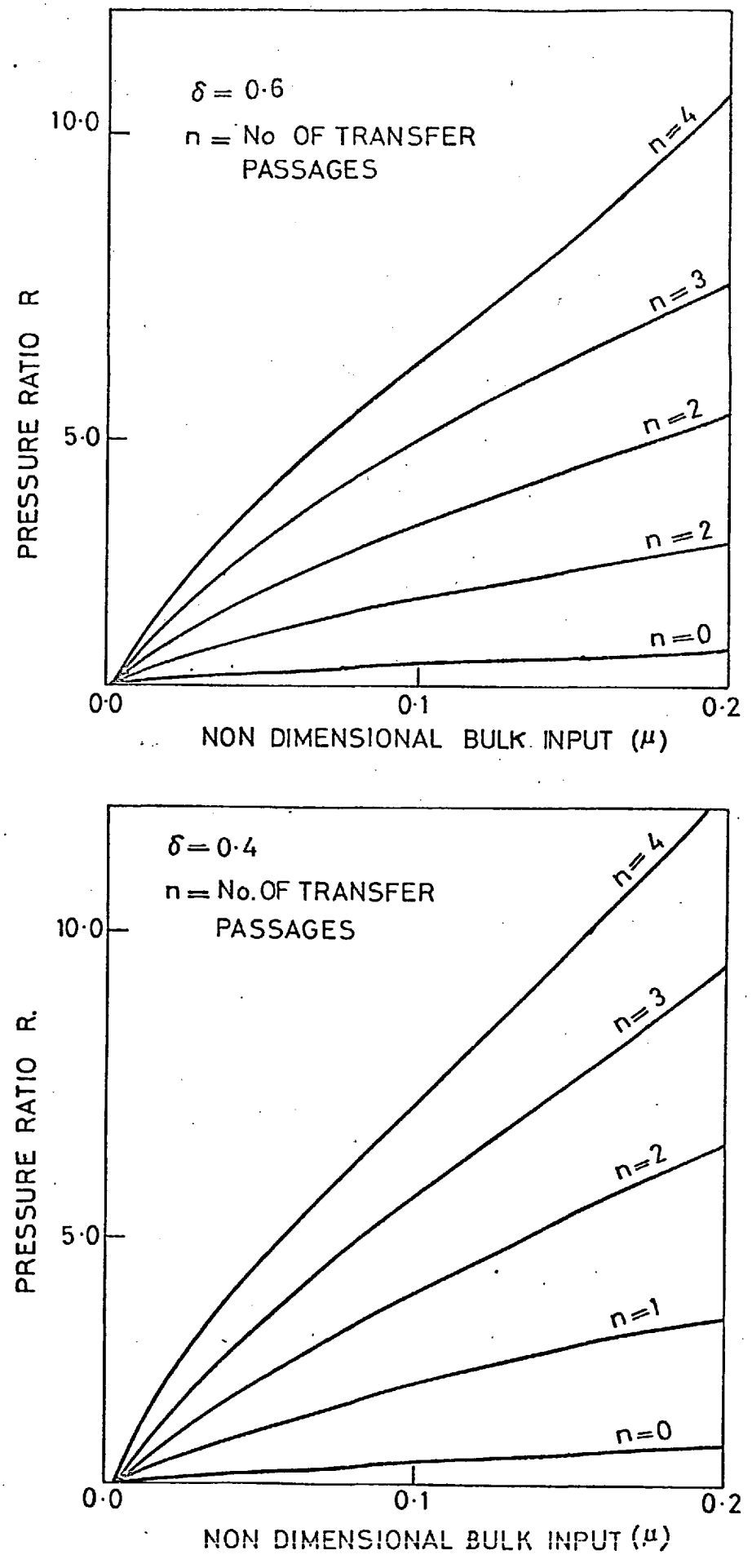
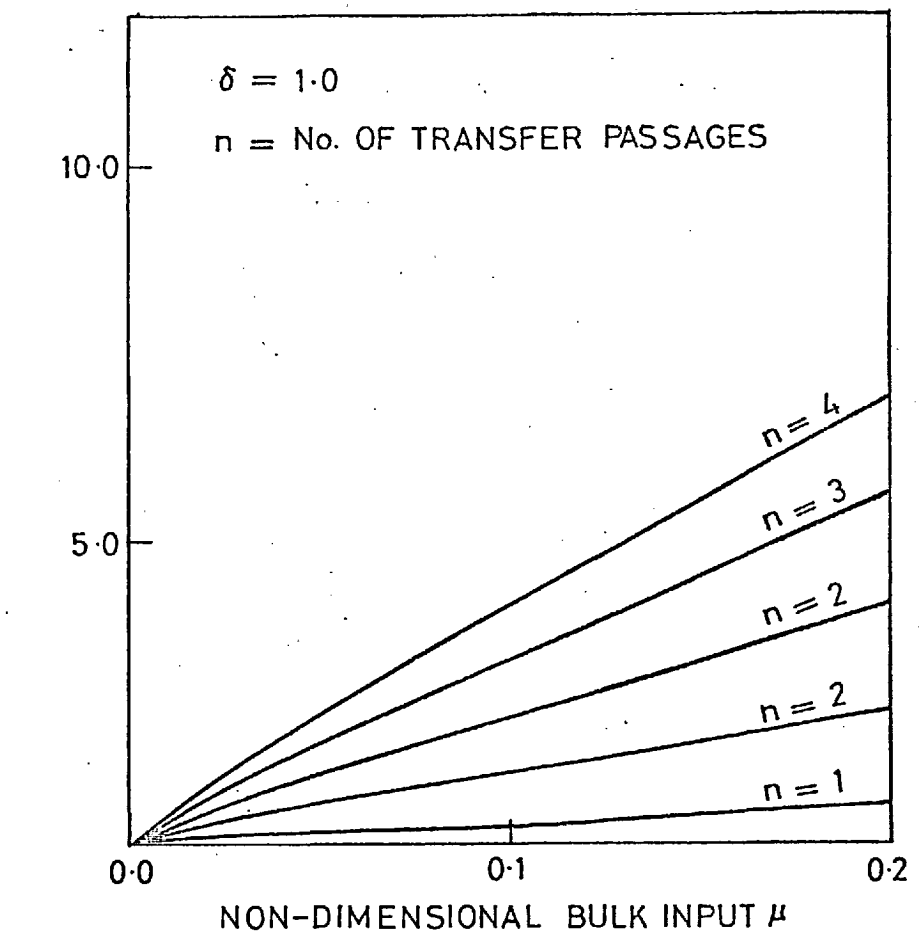


FIG. 12.42 PERFORMANCE OF FOUR-PORT PRESSURE EXCHANGER WITH TRANSFER PASSAGES



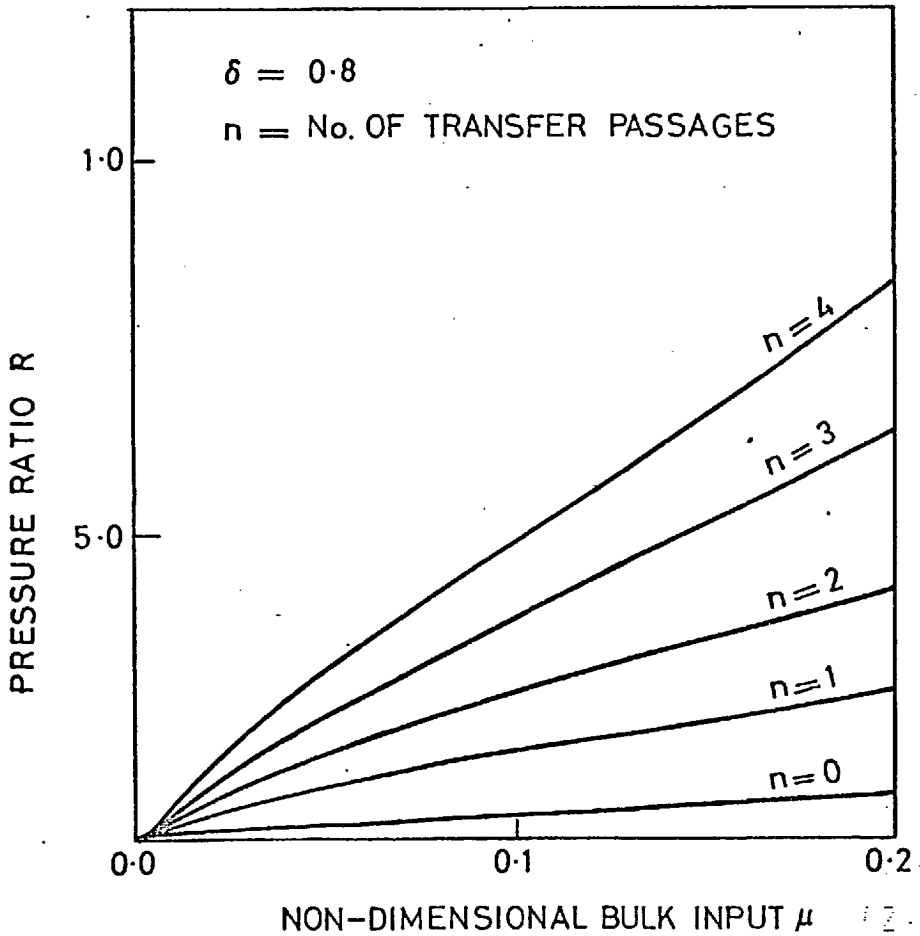


FIG. 12.43 PERFORMANCE OF FOUR PORT PRESSURE EXCHANGER WITH TRANSFER PASSAGES

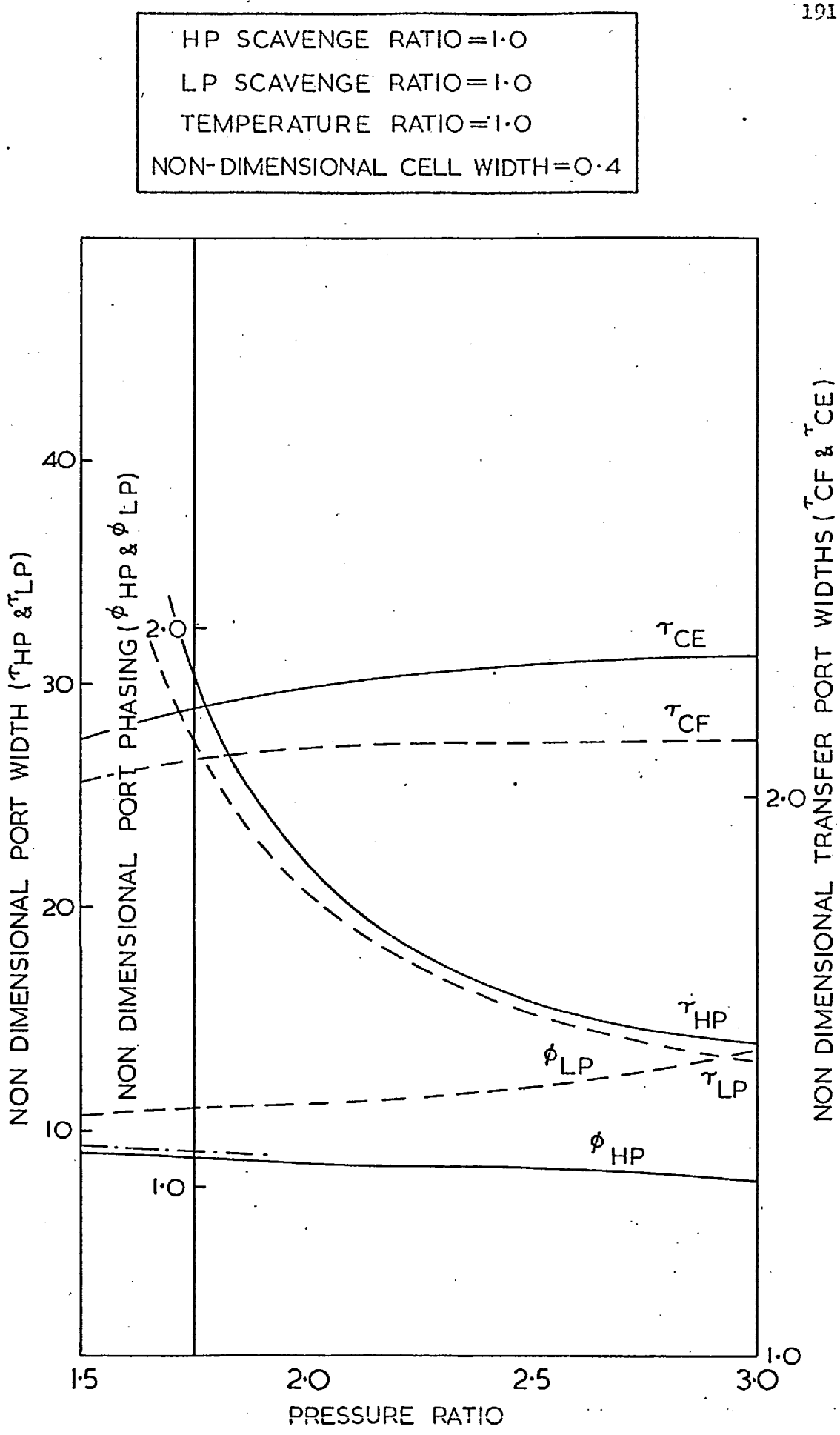


FIG. 1.44 SIX-PORT PRESSURE EXCHANGER GEOMETRY
(PRESSURE DIFFERENTIAL METHOD)

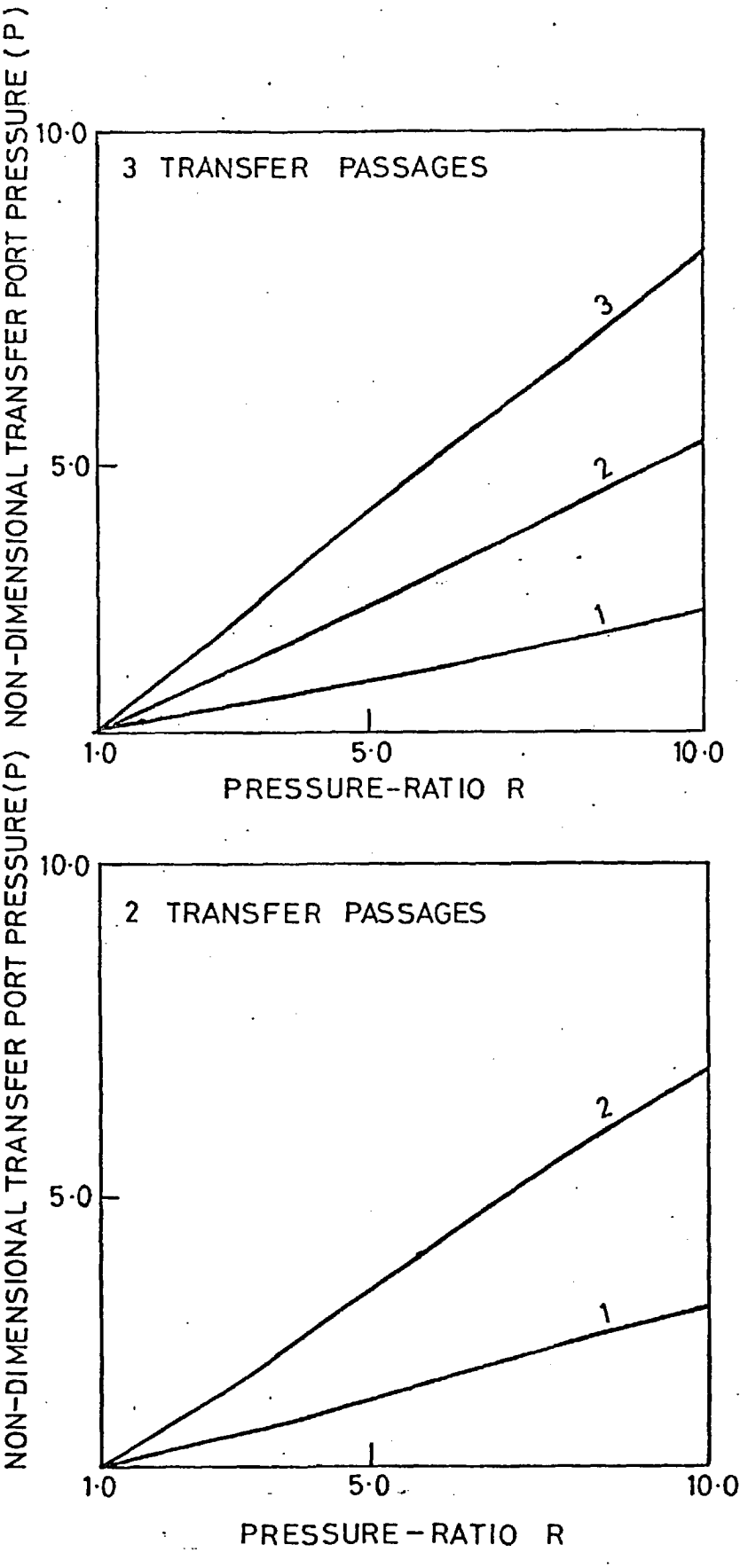
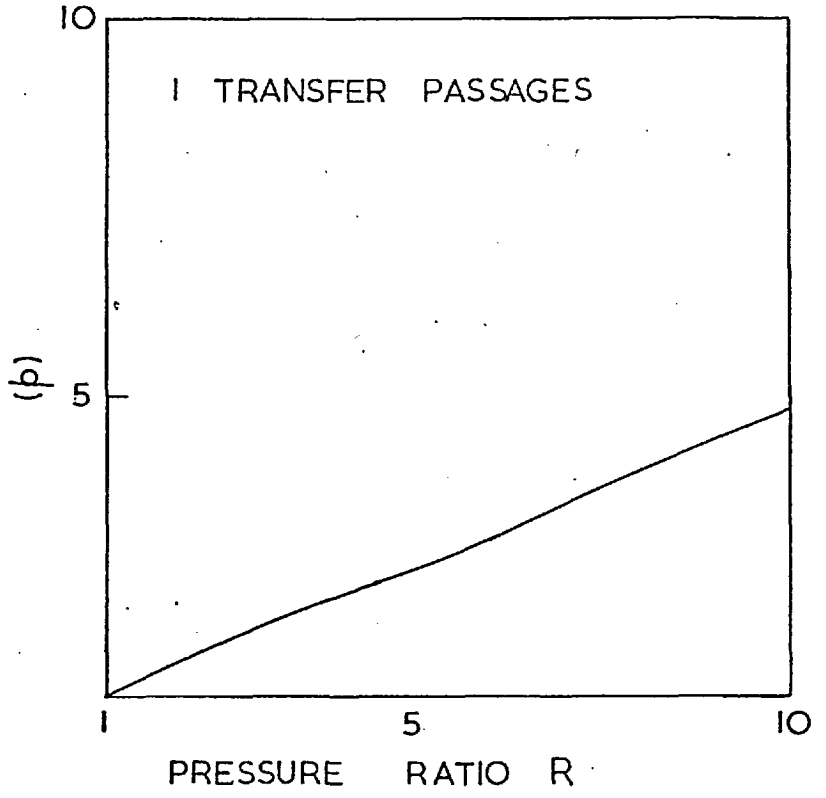


FIG. 12.45 TRANSFER PORT PRESSURES



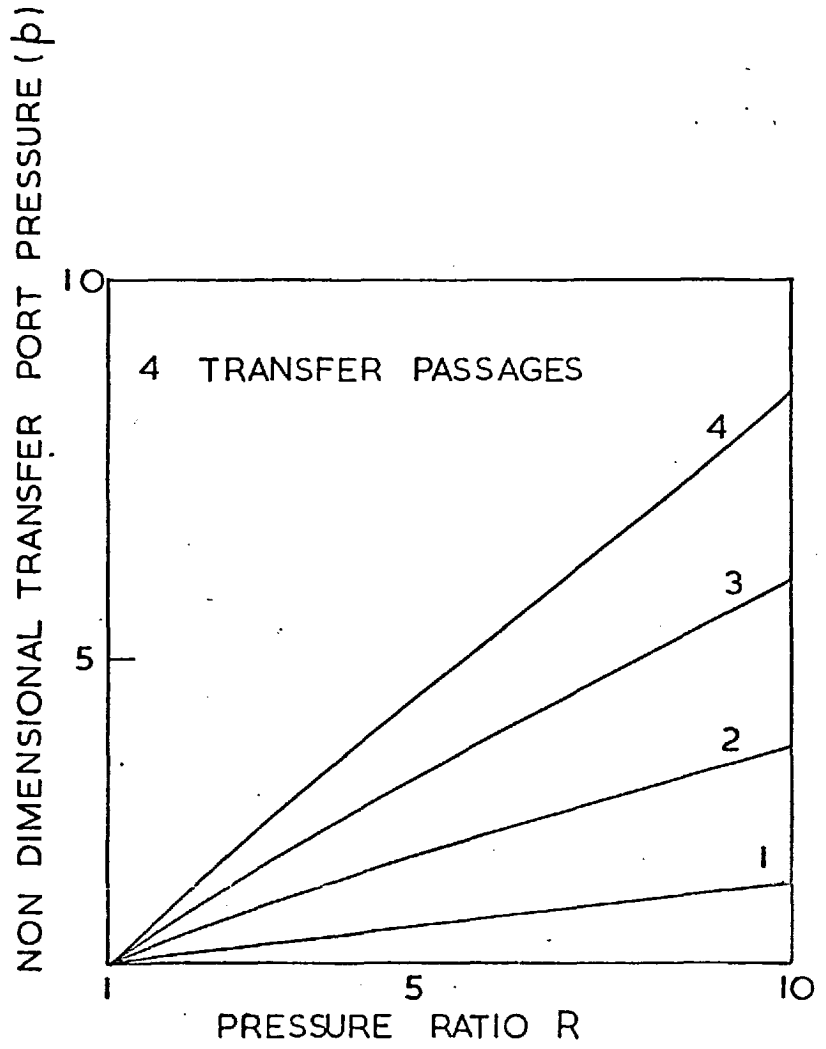


FIG. 12.46 TRANSFER PORT PRESSURES

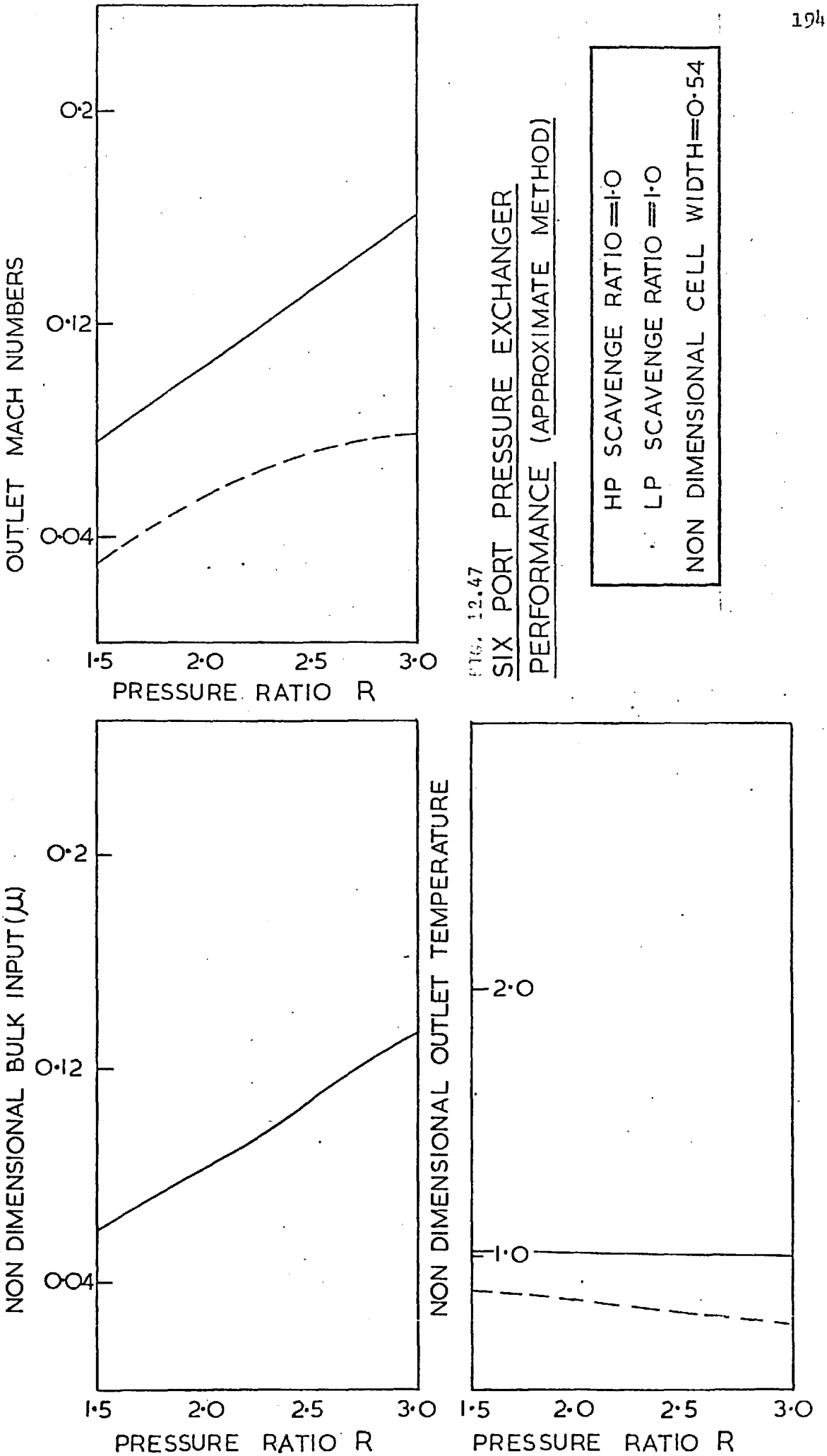


FIG. 12.47
SIX PORT PRESSURE EXCHANGER
PERFORMANCE (APPROXIMATE METHOD)

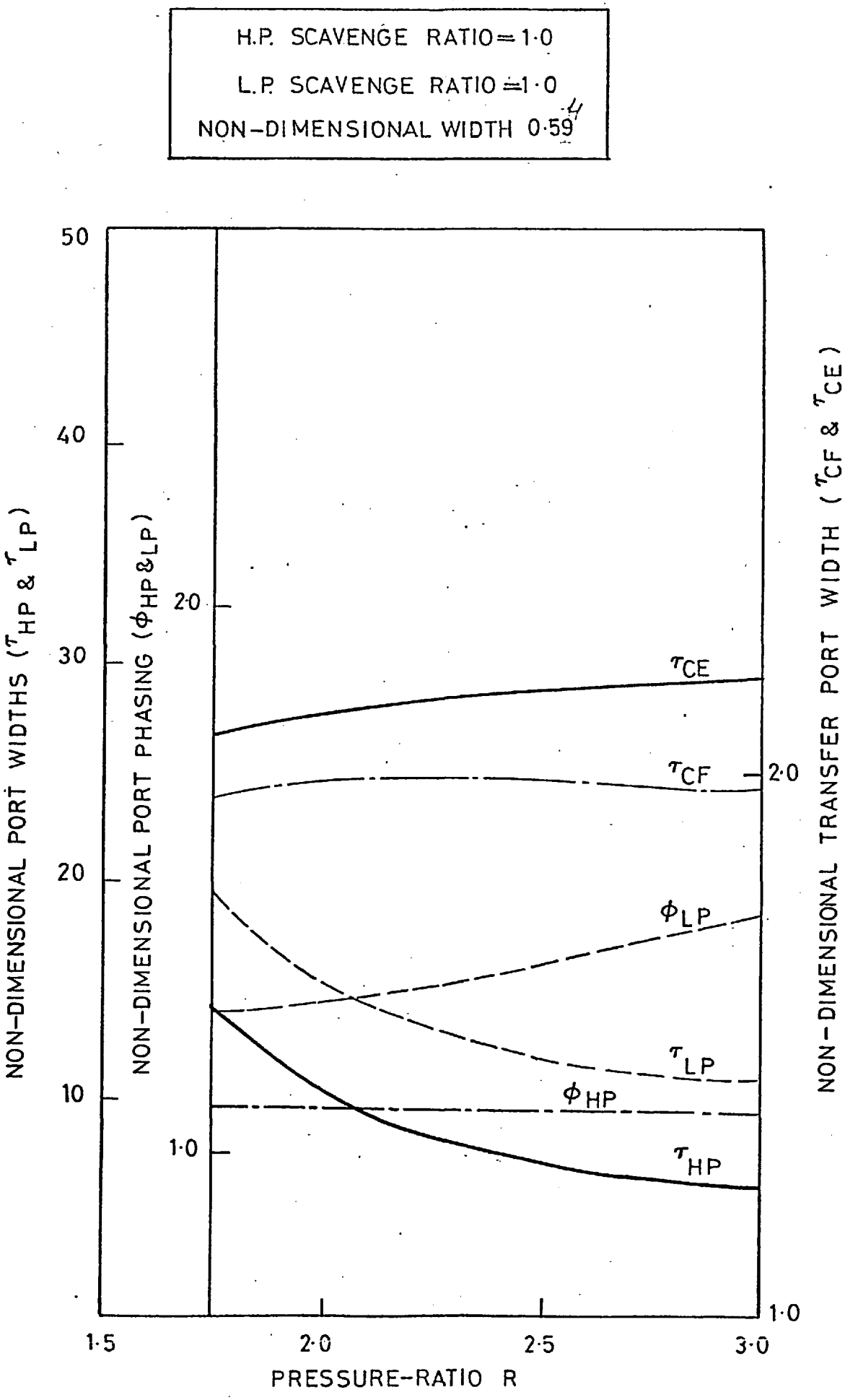


FIG. 12.43 SIX-PORT PRESSURE EXCHANGER GEOMETRY
(APPROXIMATE METHOD)

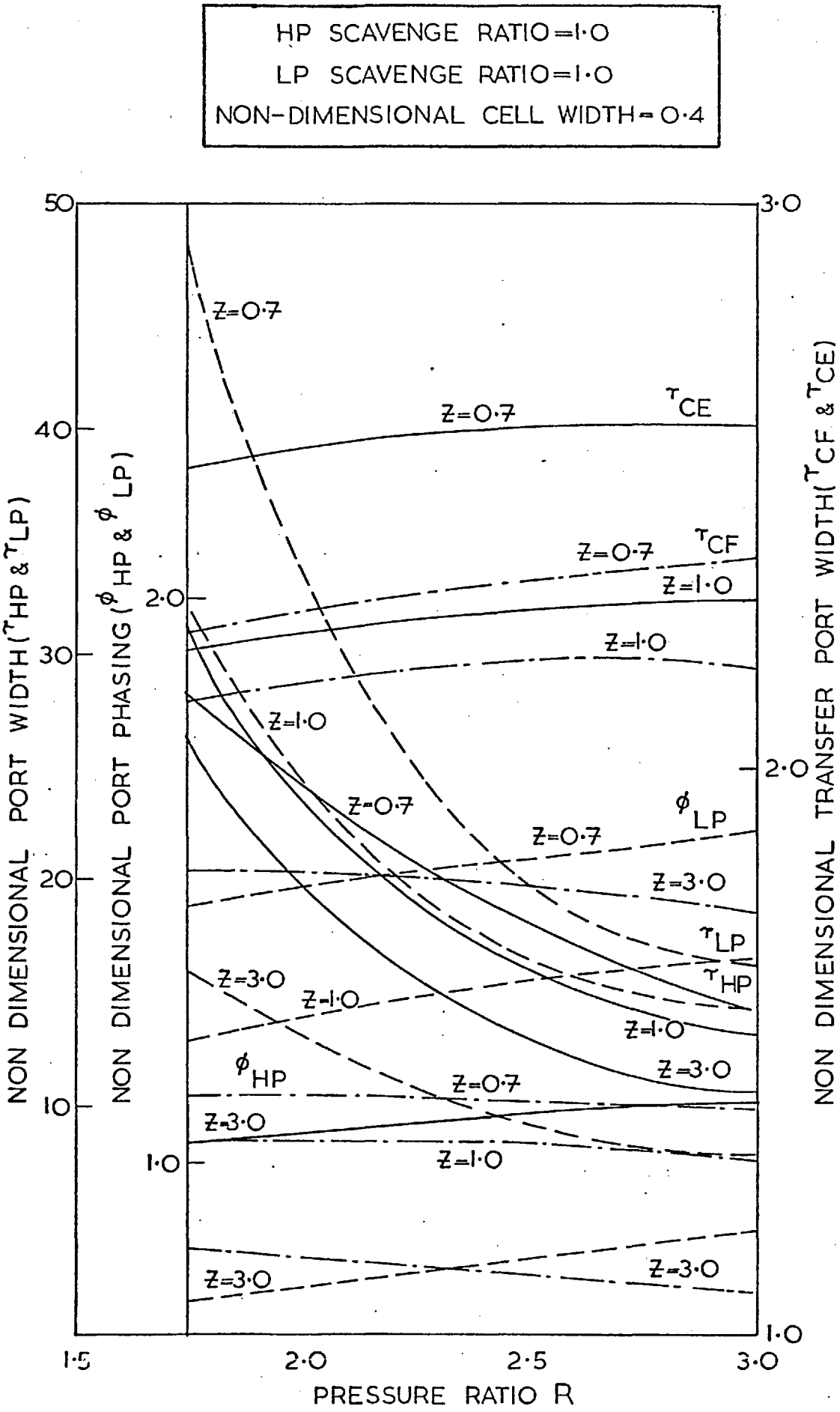
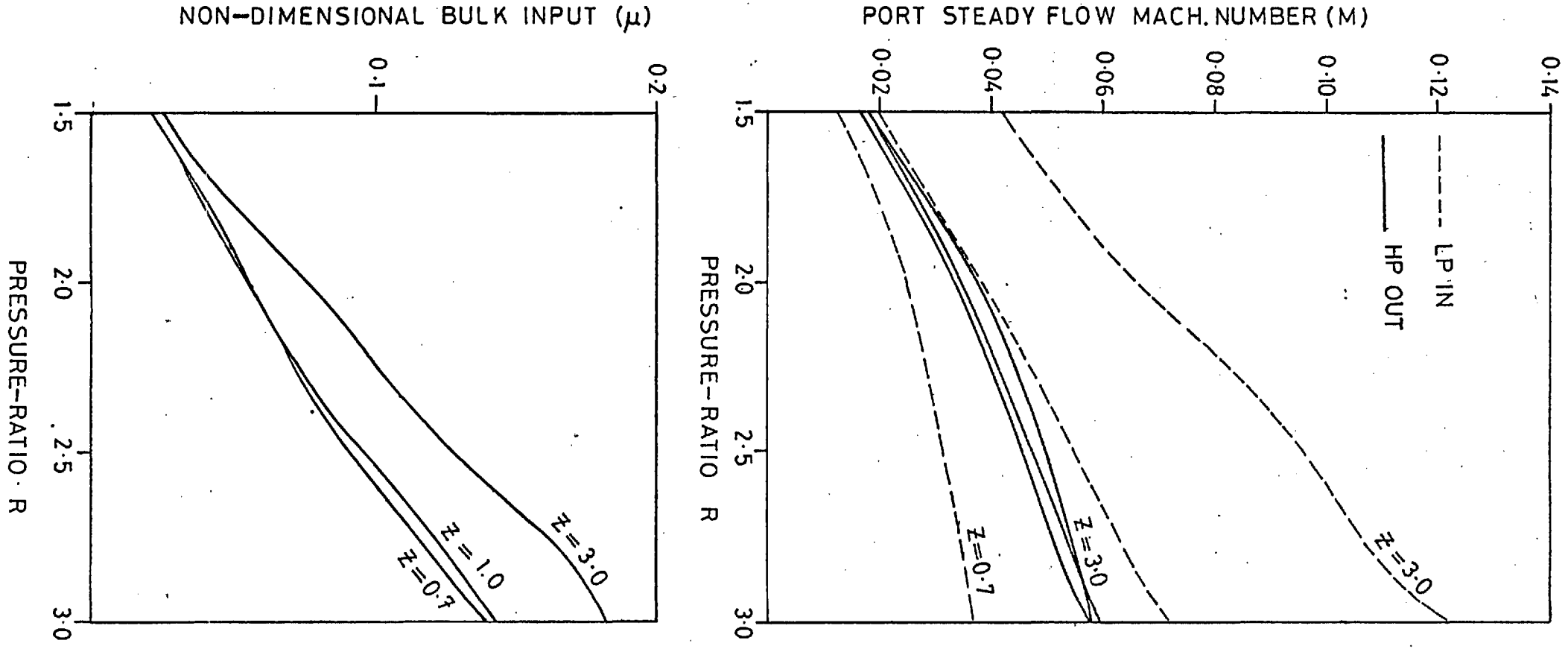


FIG. 12.49 SIX PORT PRESSURE EXCHANGER GEOMETRY (METHOD OF CHARACTERISTICS)



HP SCAVENGE RATIO = 1·0
L P SCAVENGE RATIO = 1·0
NON-DIMENSIONAL CELL WIDTH = 0·4

FIG. 12.50 **SIX-PORT PRESSURE EXCHANGER PERFORMANCE**

(FIXED SCAVENGE RATIO)

HP SCAVENGE RATIO = 1·0
LP SCAVENGE RATIO = 1·0
NON-DIMENSIONAL CELL WIDTH = 0·4

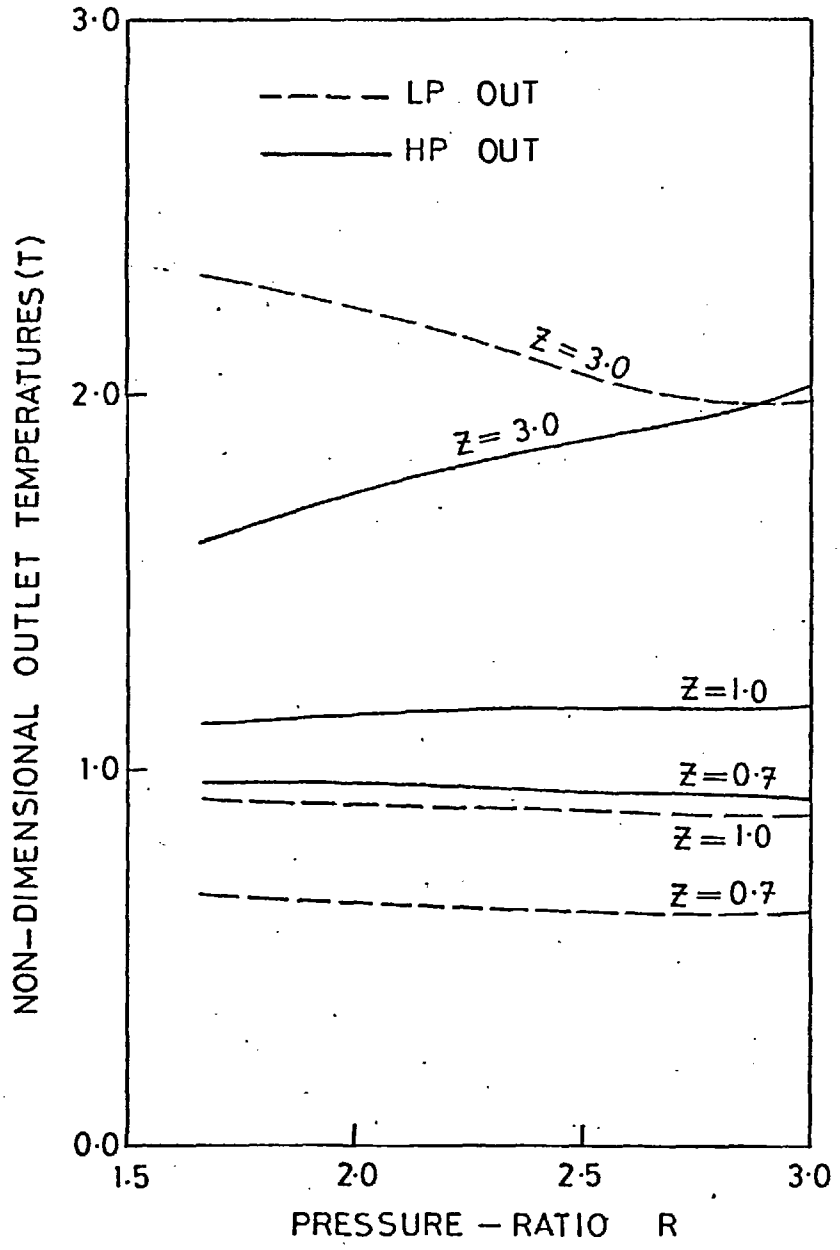


FIG. 12.51 SIX-PORT PRESSURE EXCHANGER PERFORMANCE

(FIXED SCAVENGE RATIO)

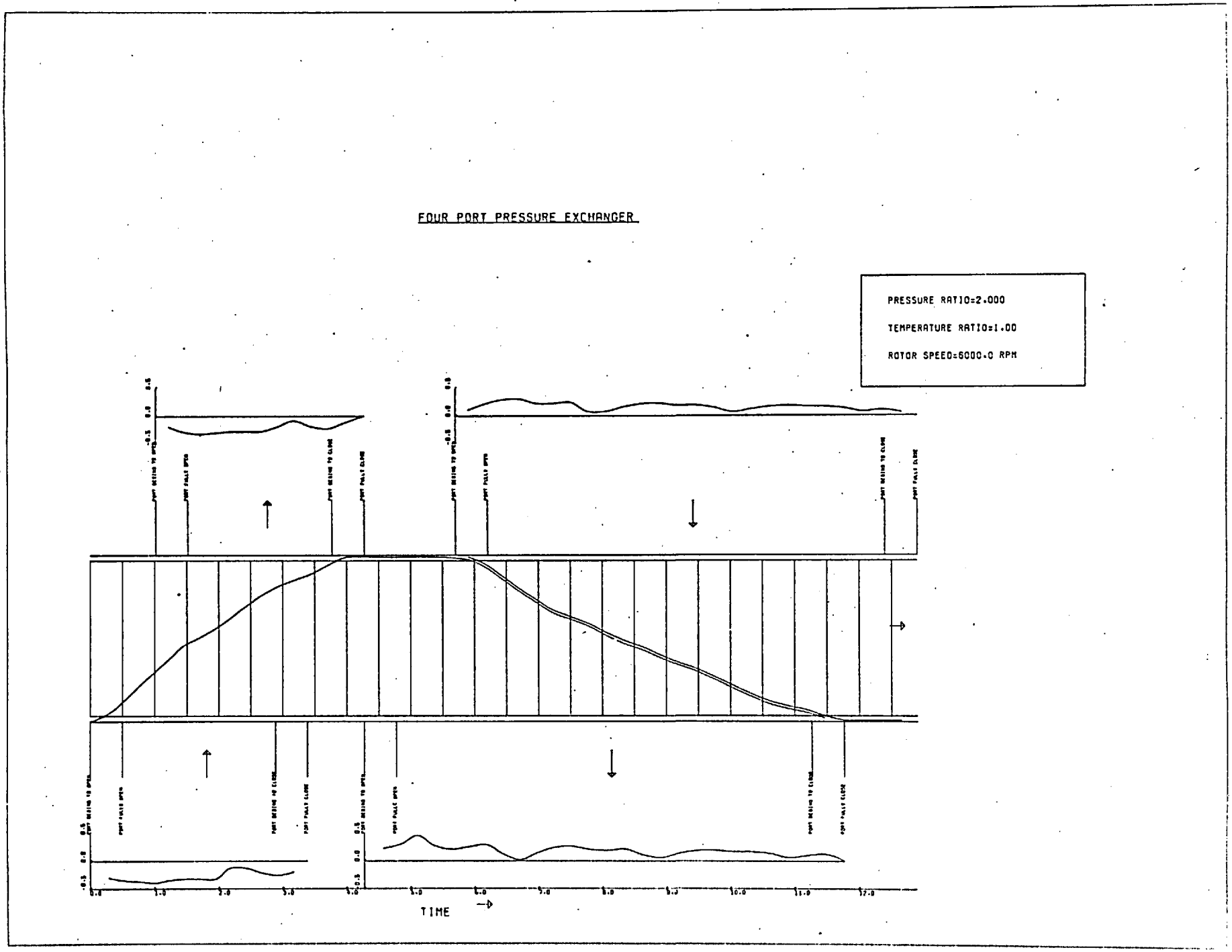

FOUR PORT PRESSURE EXCHANGER
PRESSURE RATIO=2.000
TEMPERATURE RATIO=1.00
ROTOR SPEED=6000.0 RPM
TIME

FIG. 12.52

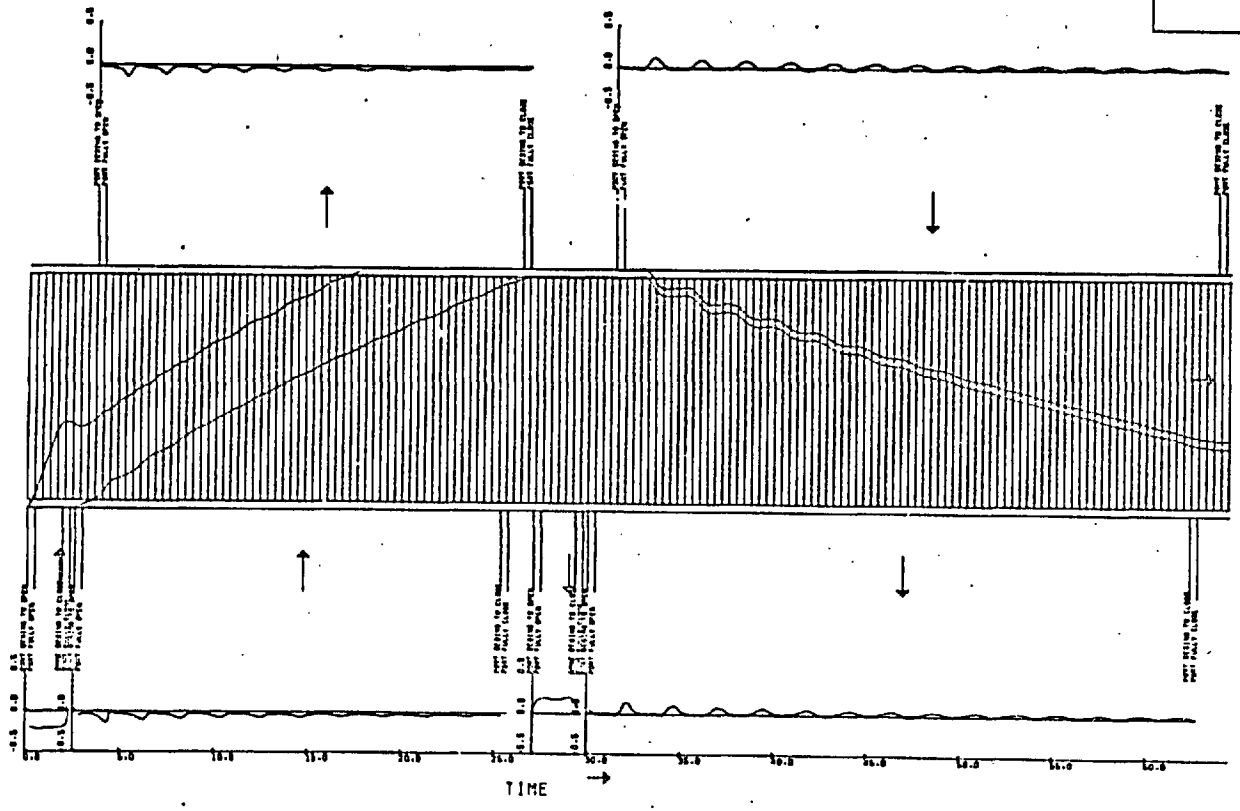

SIX PORT PRESSURE EXCHANGER
PRESSURE RATIO=2.000
TEMPERATURE RATIO=0.70
ROTOR SPEED=6000.0 RPM
TIME

FIG. 12.53

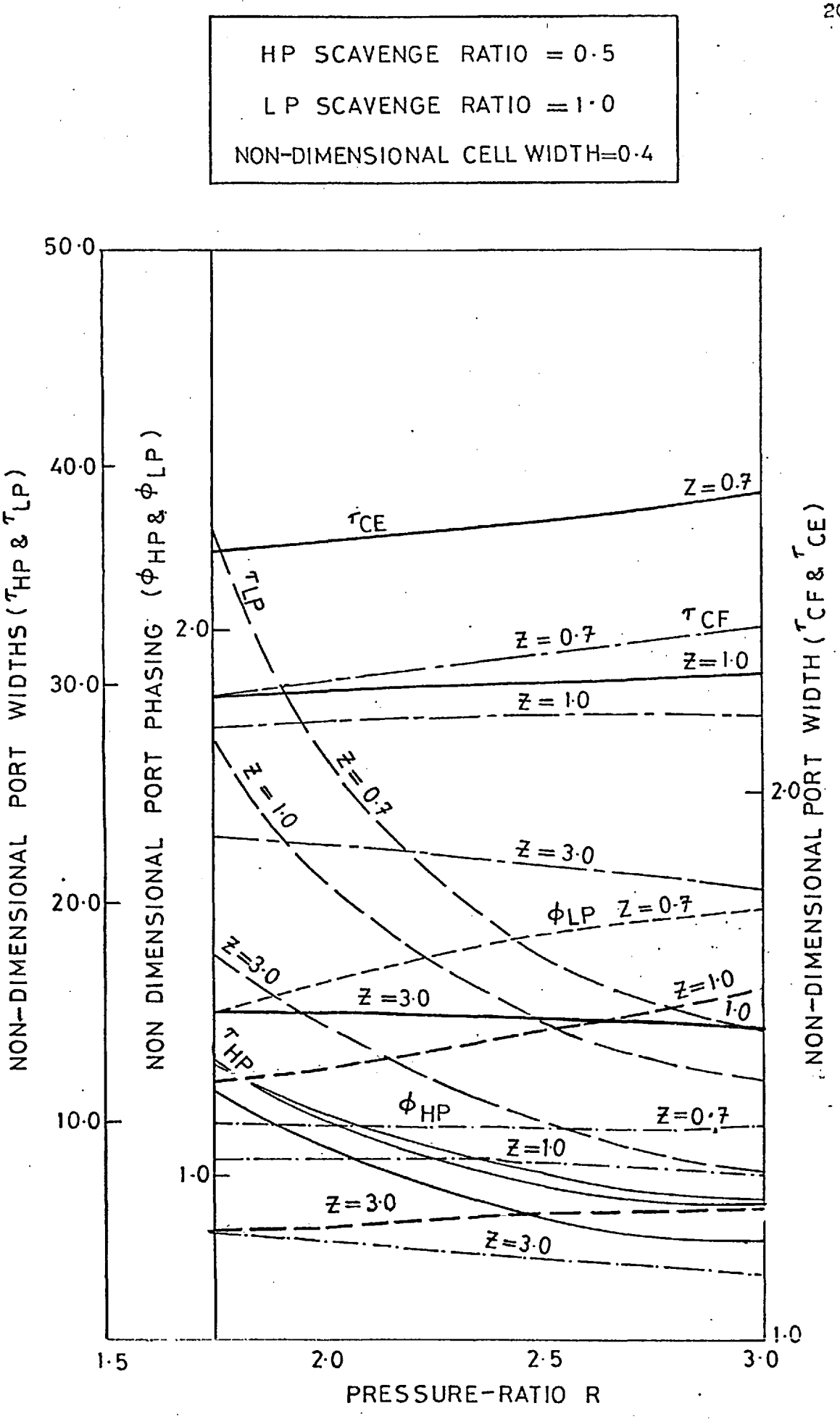
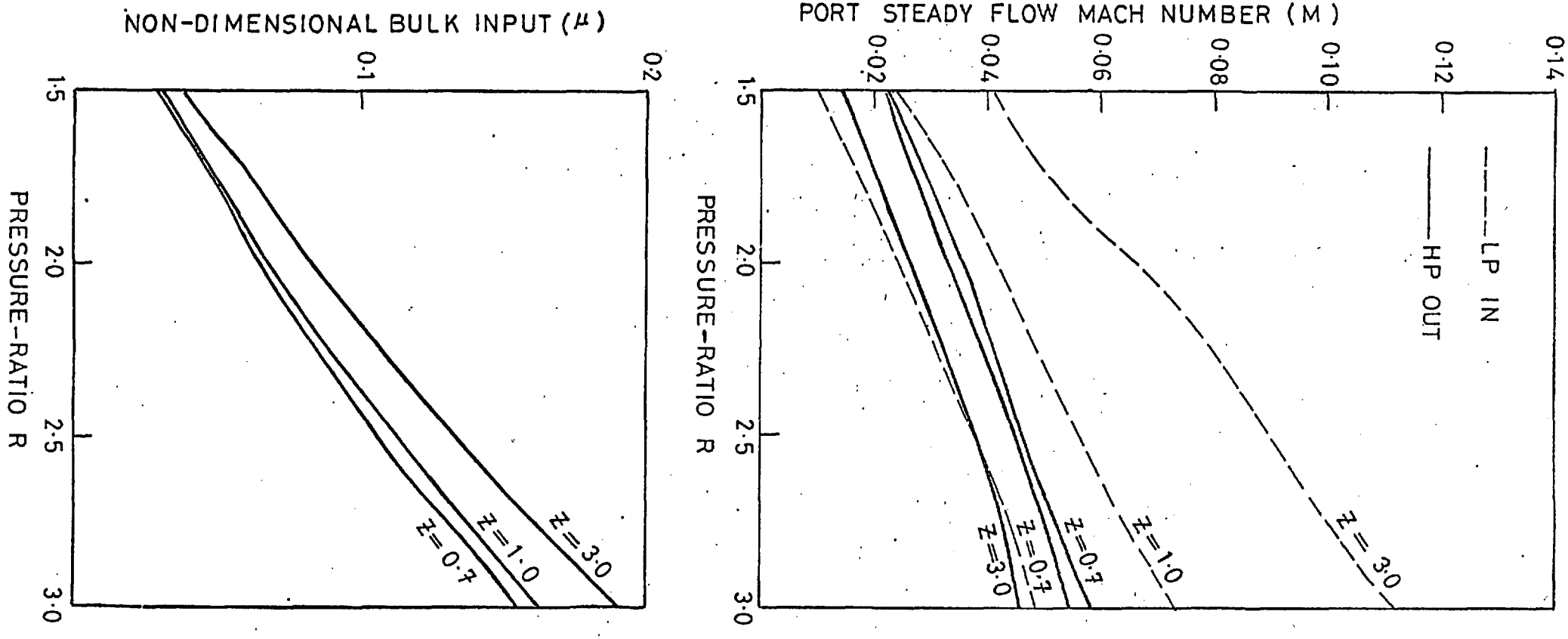


FIG. 12.54 SIX-PORT PRESSURE EXCHANGER GEOMETRY

(METHOD OF CHARACTERISTICS)



H P SCAVENGE RATIO 0·5
L P SCAVENGE RATIO 1·0
NON-DIMENSIONAL CELL WIDTH 0·4

FIG. 10.55. SIX PORT PRESSURE EXCHANGER PERFORMANCE

(FIXED SCAVENGE RATIO)

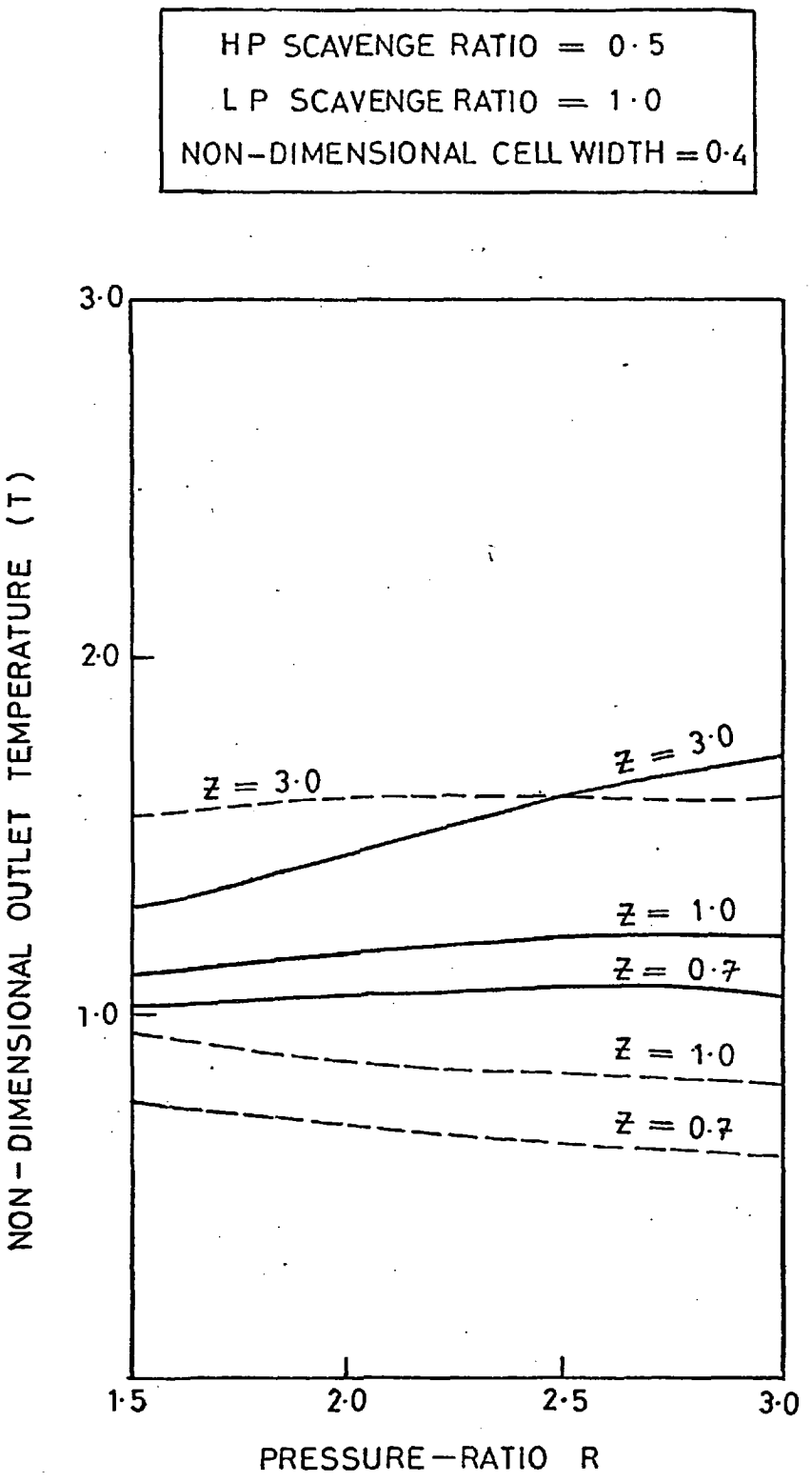


FIG. 12.56 SIX-PORT PRESSURE EXCHANGER PERFORMANCE

(FIXED SCAVENGE RATIO)

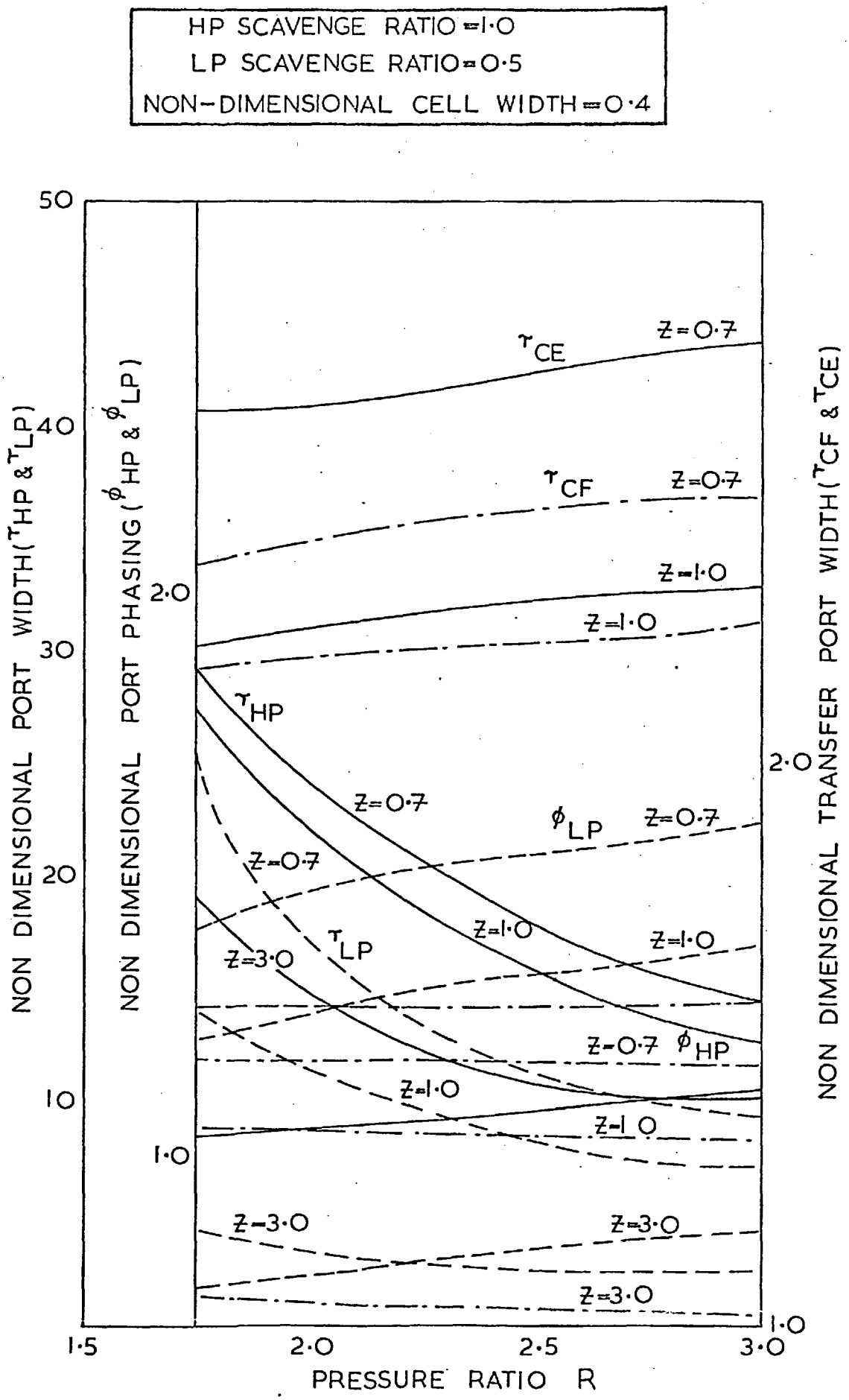
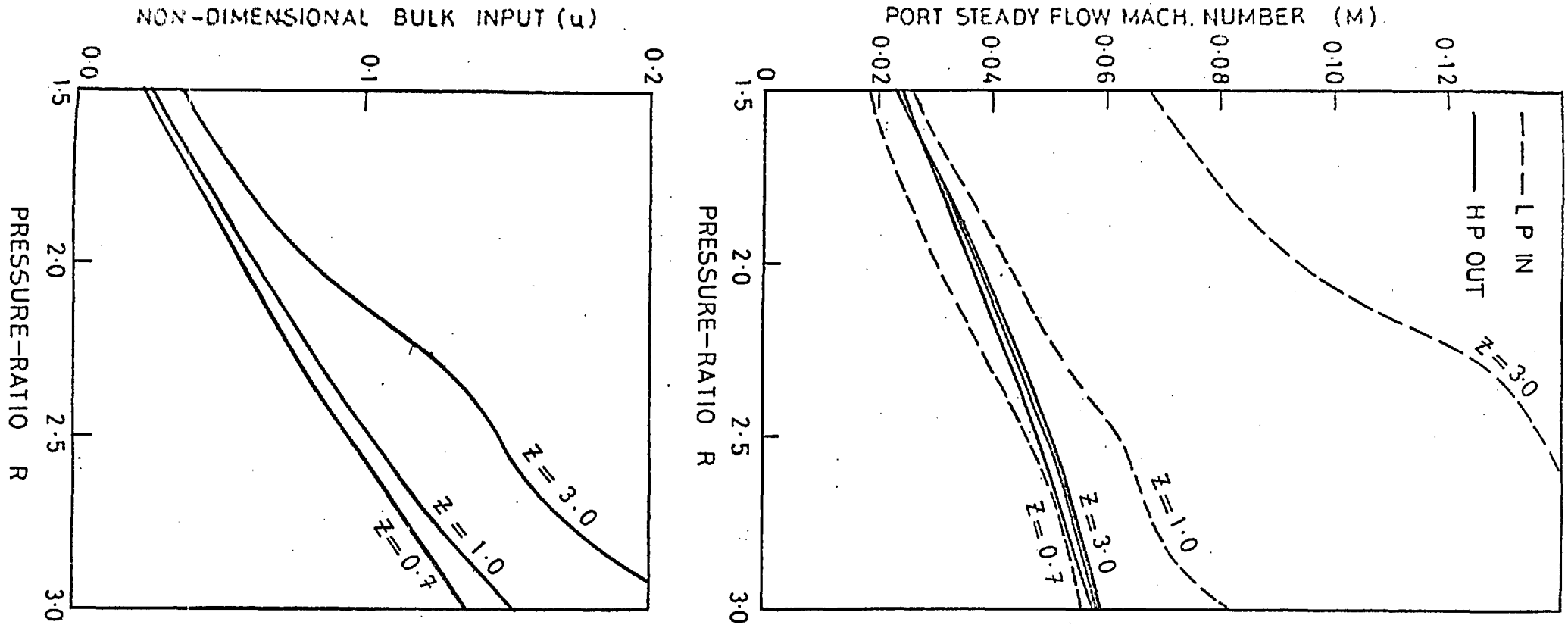


FIG. 12.7 SIX PORT PRESSURE EXCHANGER GEOMETRY (METHOD OF CHARACTERISTICS)



H.P. SCAVENGE RATIO 1·0
L.P. SCAVENGE RATIO 0·5
NON-DIMENSIONAL CELL WIDTH 0·4

FIG. 12.58 **SIX PORT PRESSURE EXCHANGER PERFORMANCE**
(FIXED SCAVENGE RATIO)

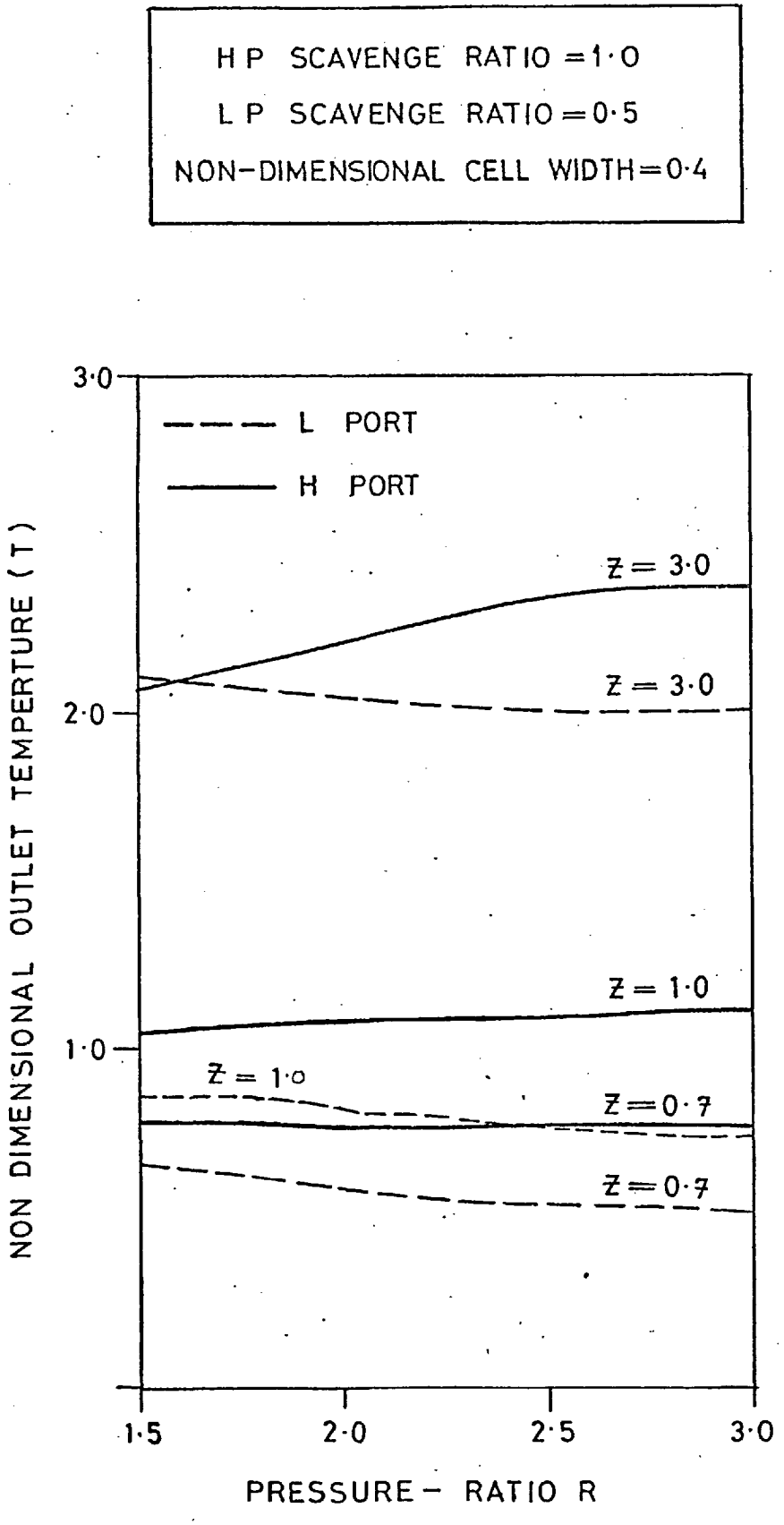


FIG. 12,59 SIX-PORT PRESSURE EXCHANGER PERFORMANCE

(FIXED SCAVENGE RATIO)

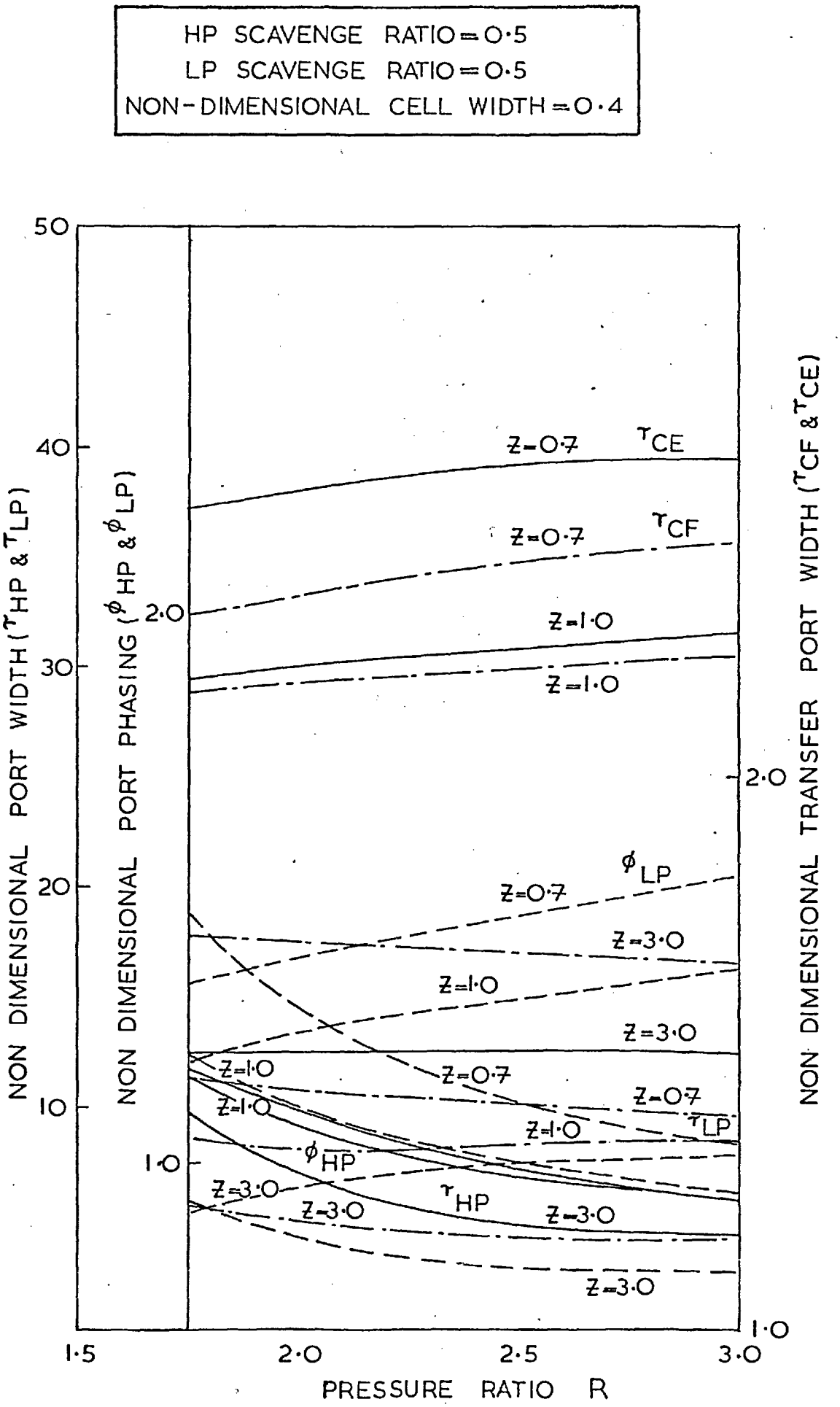


FIG. 12.60 SIX PORT PRESSURE EXCHANGER GEOMETRY

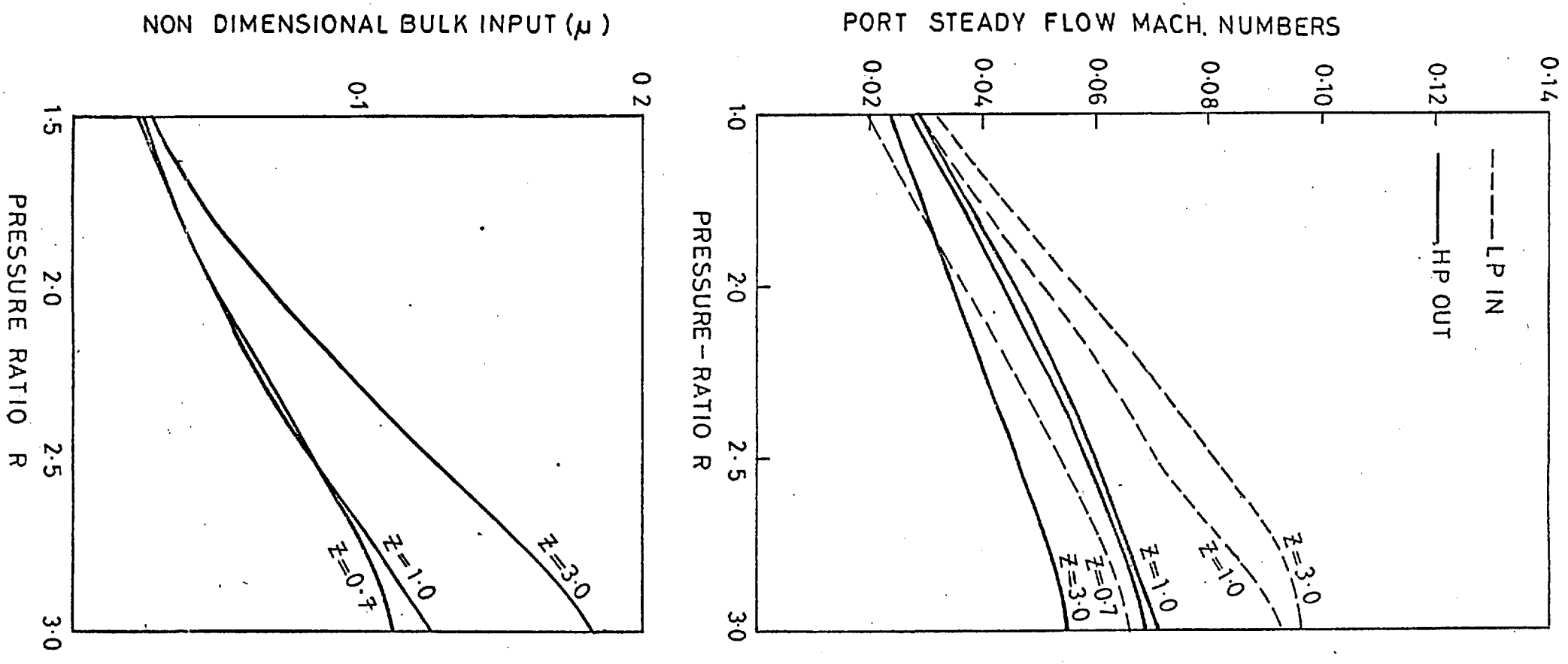


FIG. 12.61 SIX-PORT PRESSURE EXCHANGER PERFORMANCE (FIXED SCAVENGE RATIO)

H.P. SCAVENGE RATIO = 0·5
L.P. SCAVENGE RATIO = 0·5
NON-DIMENSIONAL CELL WIDTH 0·4

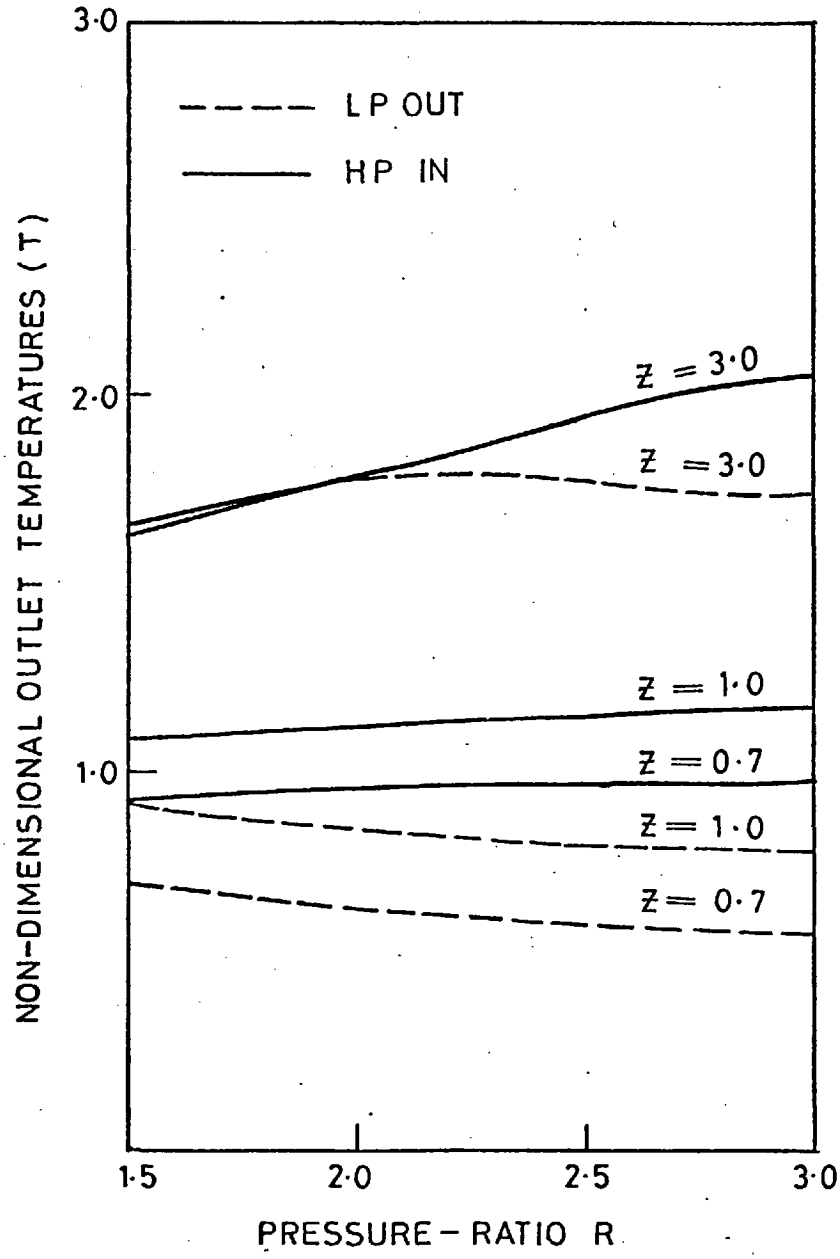


FIG. 12.62 SIX-PORT PRESSURE EXCHANGER PERFORMANCE

(FIXED SCAVENGE RATIO)

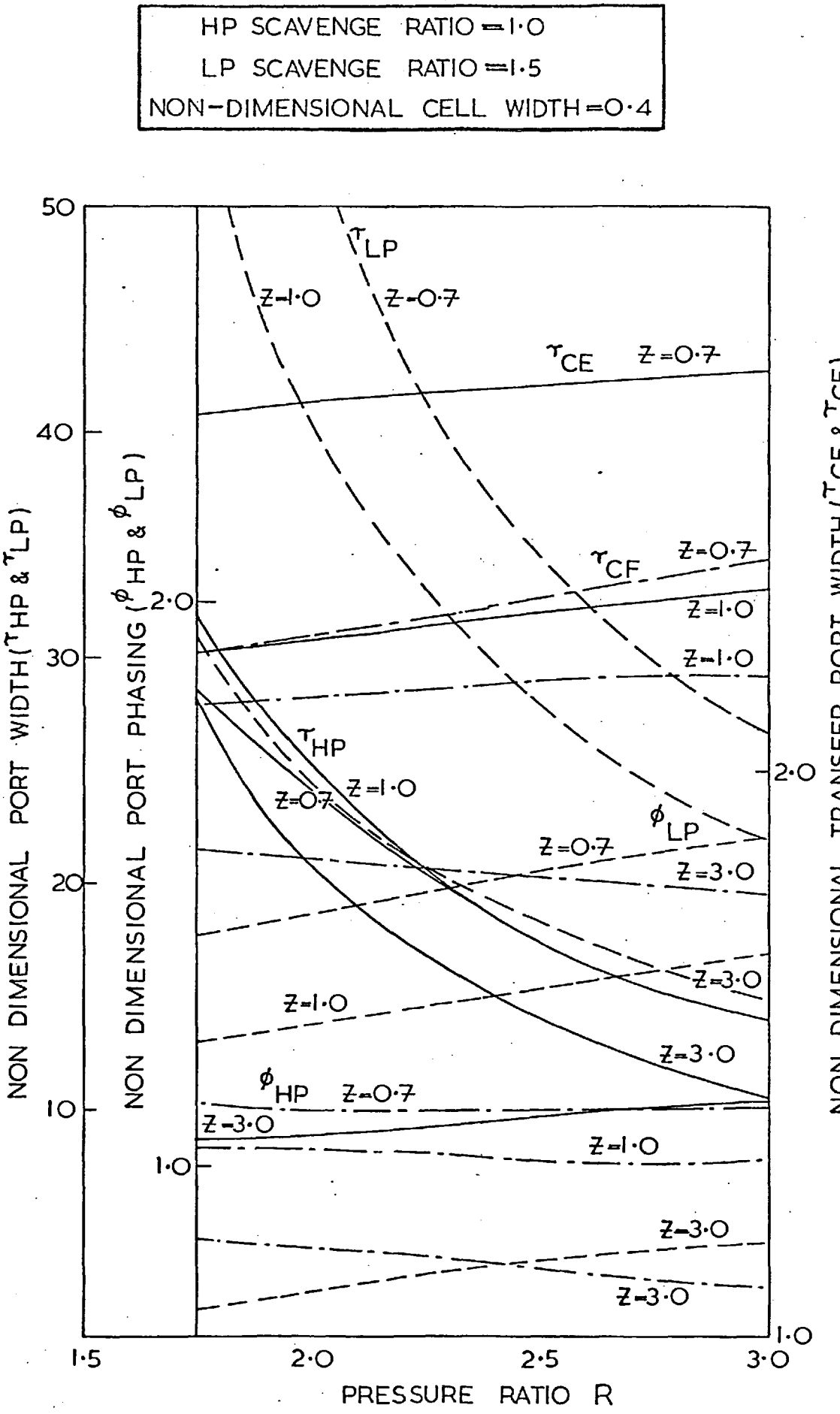


FIG. 12.63 SIX PORT PRESSURE EXCHANGER GEOMETRY (METHOD OF CHARACTERISTICS)

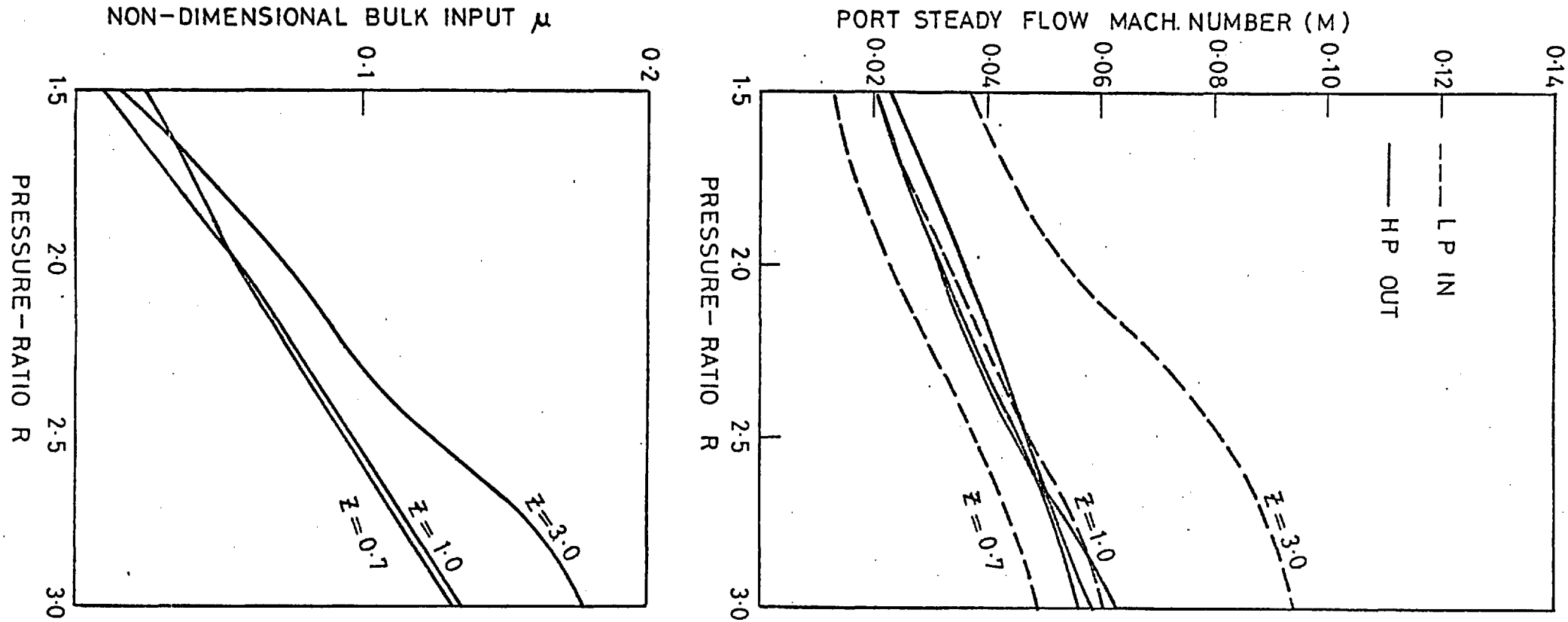
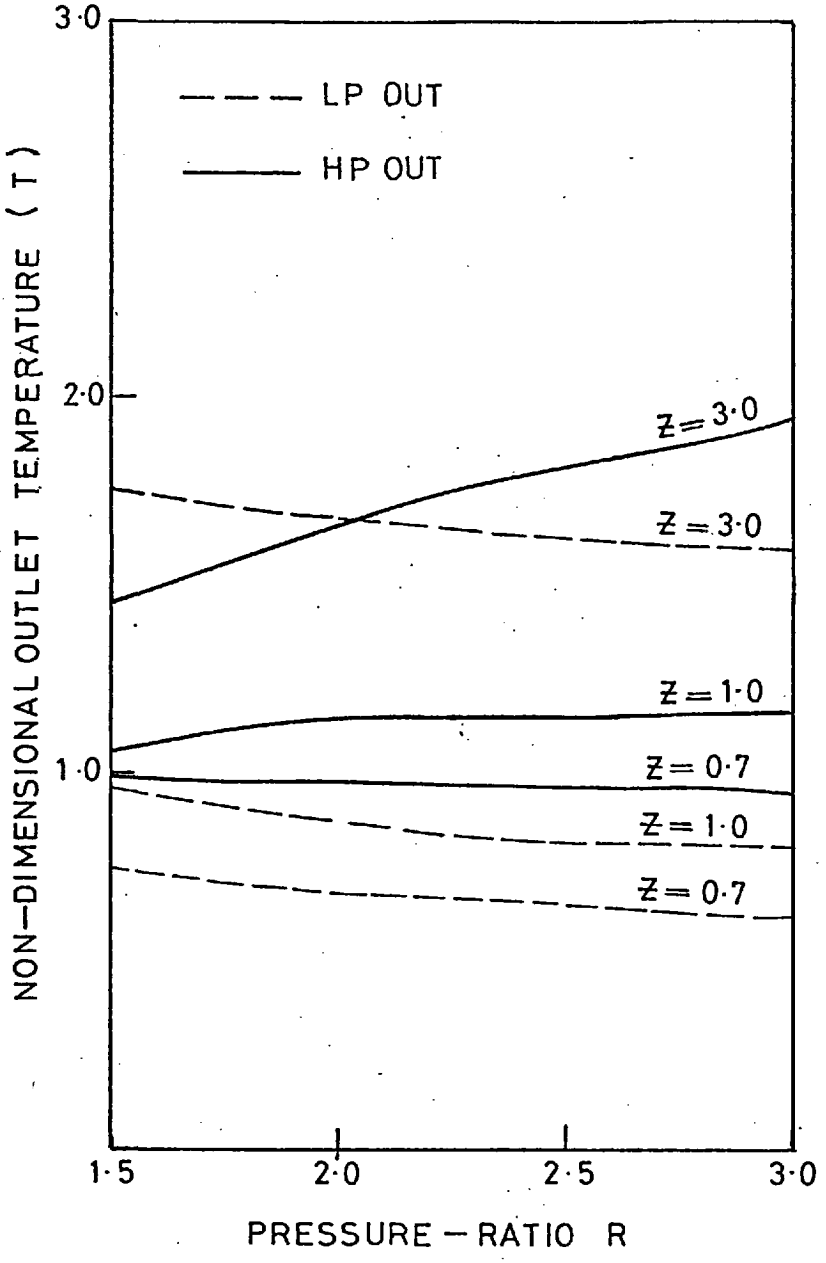


FIG. 12.64 SIX-PORT PRESSURE EXCHANGER PERFORMANCE
(FIXED SCAVENGE RATIO)



HP SCAVENGE RATIO = 1·0
LP SCAVENGE RATIO = 1·5
NON—DIMENSIONAL CELL WIDTH 0·4

FIG. 12.65 SIX — PORT PRESSURE EXCHANGER PERFORMANCE

(FIXED SCAVENGE RATIO)

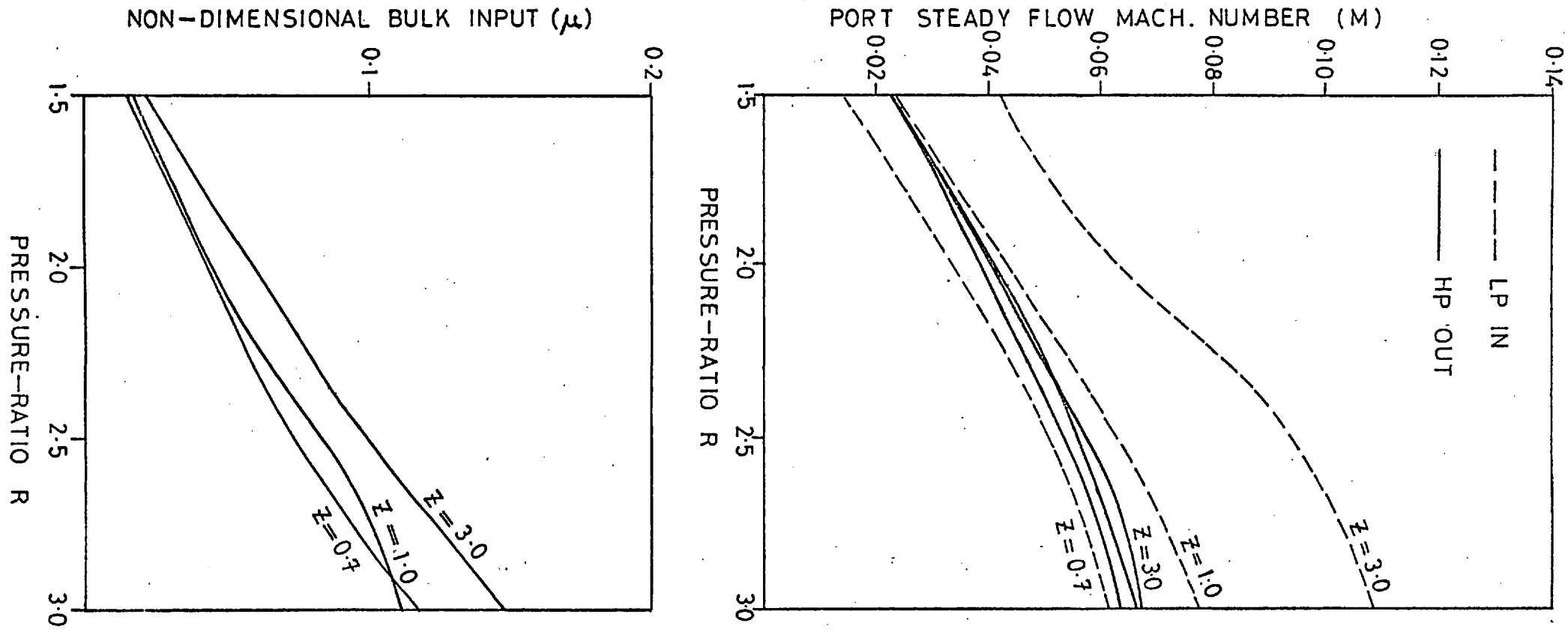
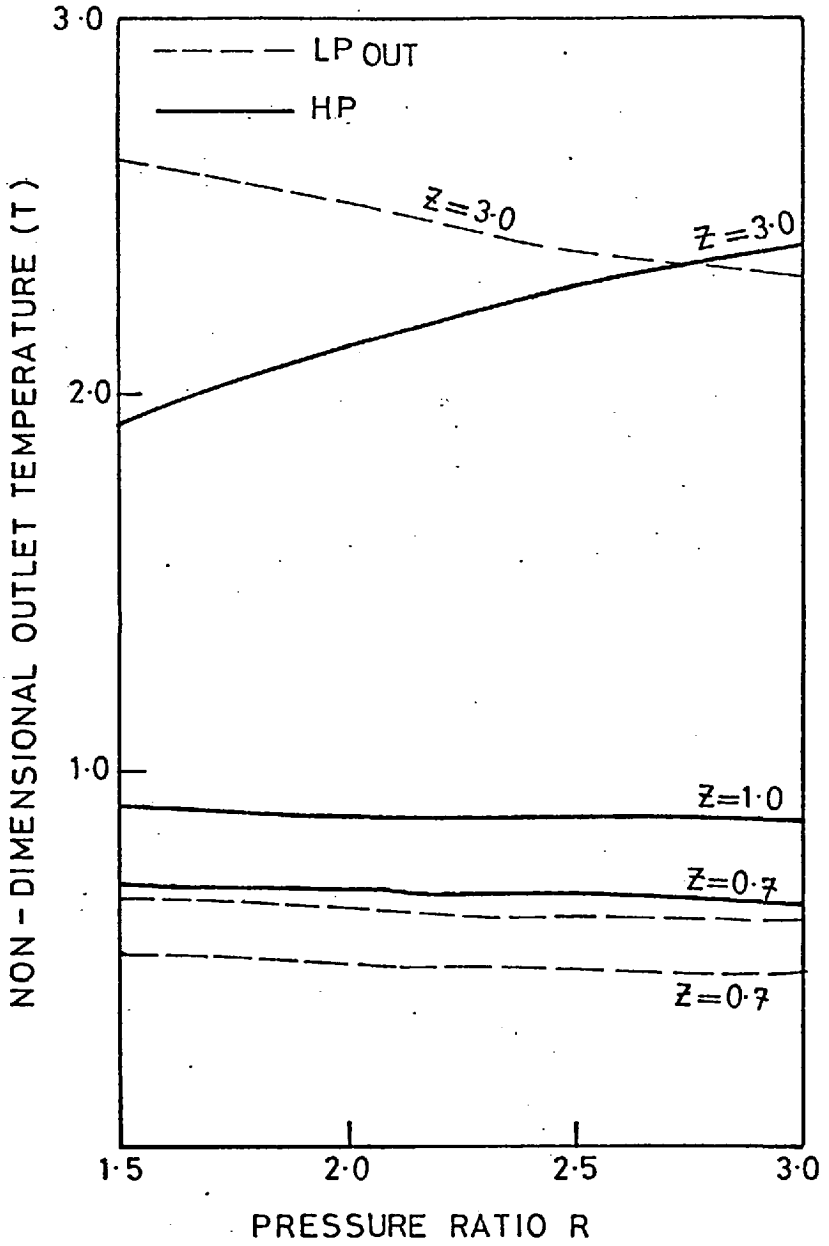


FIG. 12.66 **SIX-PORT PRESSURE EXCHANGER PERFORMANCE**

(FIXED SCAVENGE RATIO)



HP SCAVENGE RATIO = 1·5
LP SCAVENGE RATIO = 1·0
NON-DIMENSIONAL CELL WIDTH 0·4

FIG. 12.67. SIX-PORT PRESSURE EXCHANGER PERFORMANCE

(FIXED SCAVENGE RATIO)

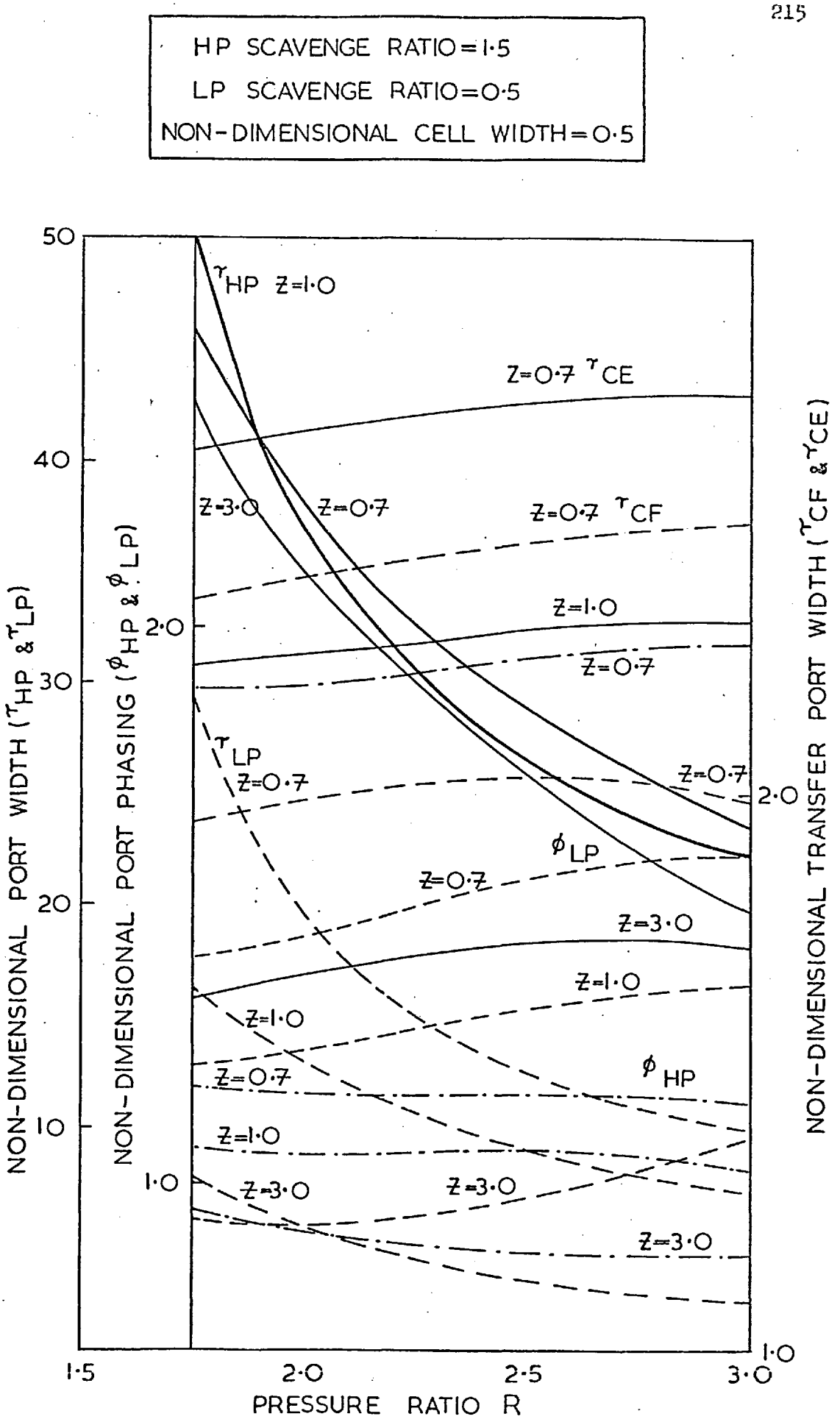


FIG. 12.68 SIX-PORT PRESSURE EXCHANGER GEOMETRY (METHOD OF CHARACTERISTICS)

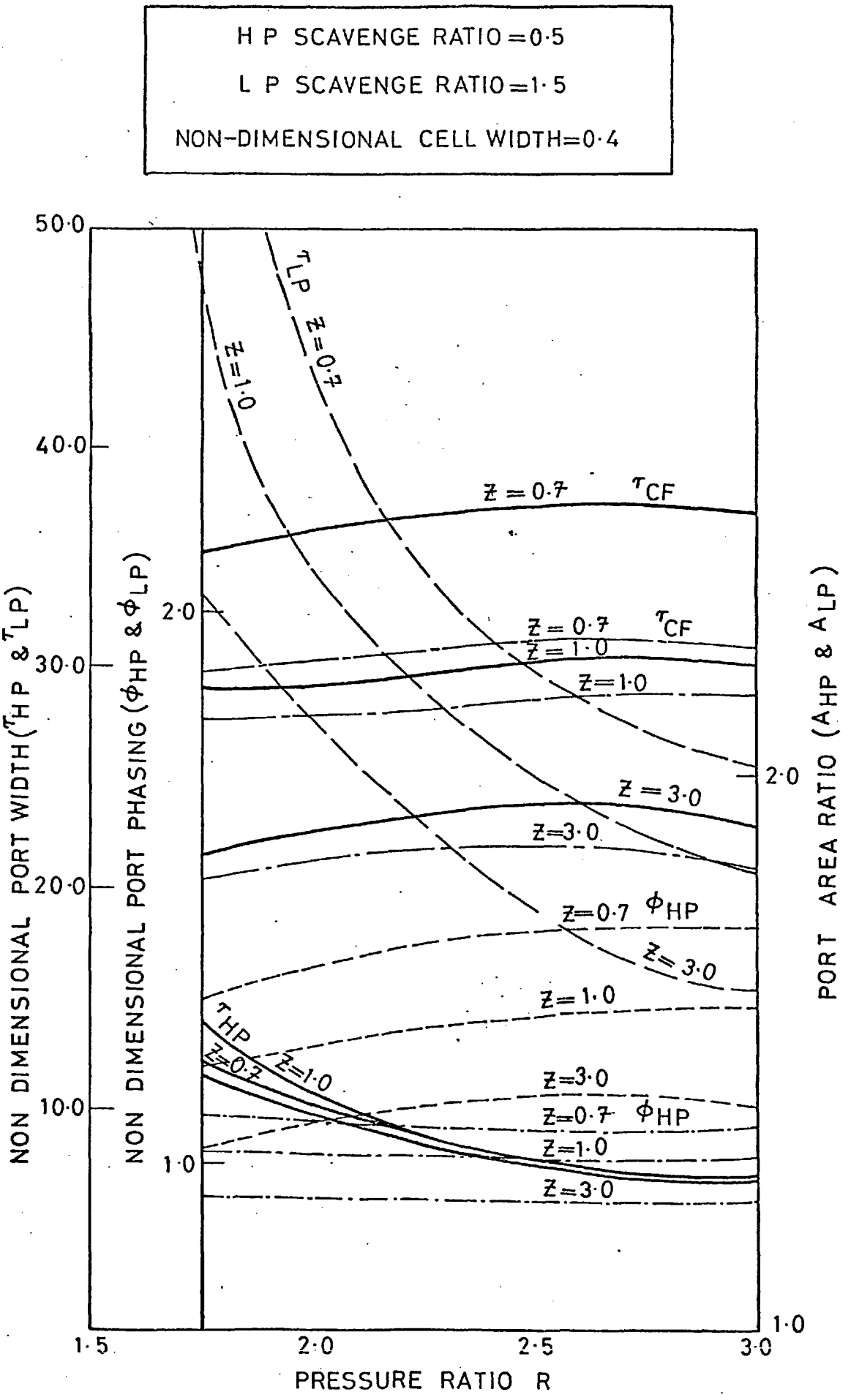


FIG. 12. SIX-PORT PRESSURE EXCHANGER GEOMETRY

(METHOD OF CHARCTERISTICS)

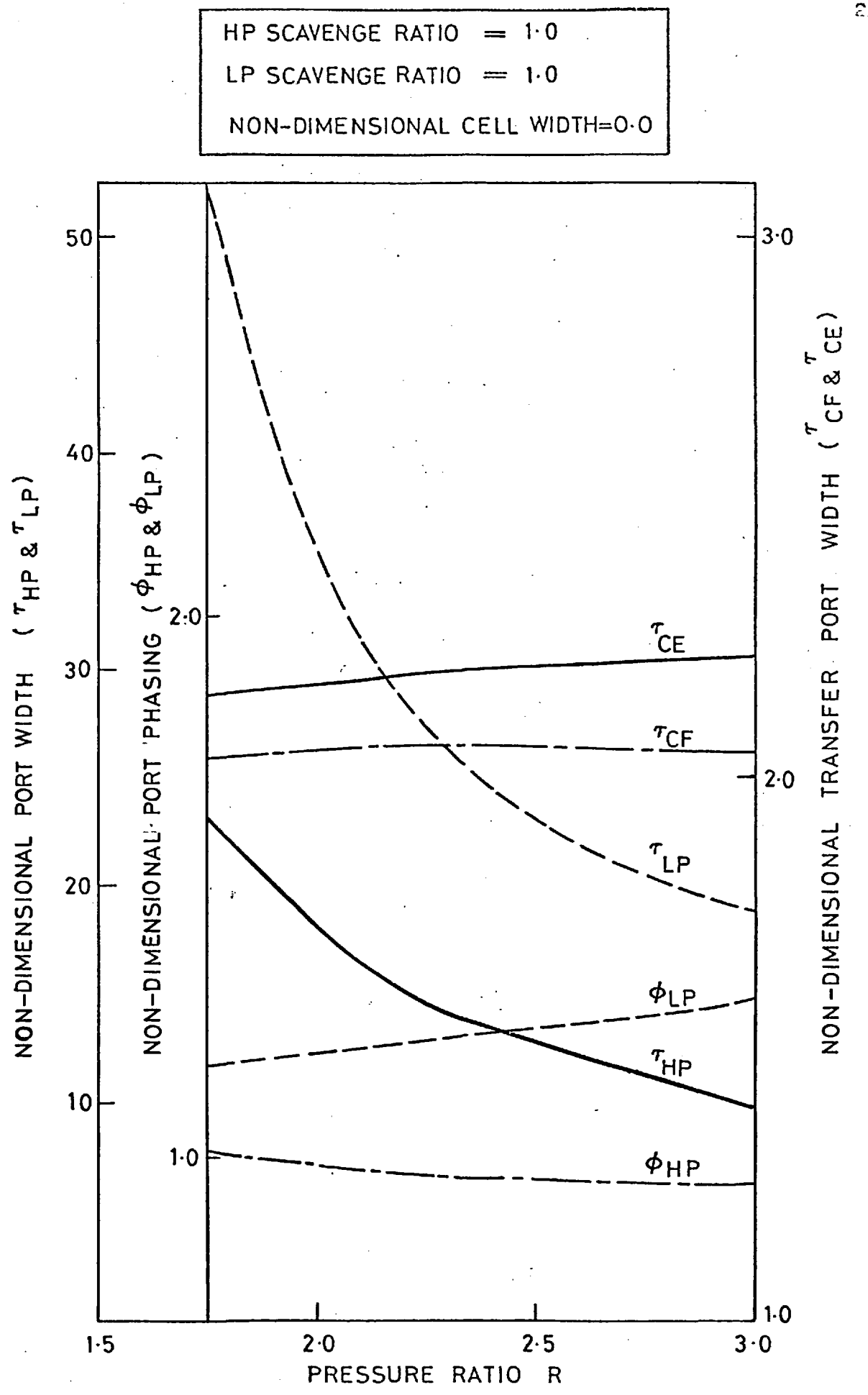


FIG. 12.70 SIX-PORT PRESSURE EXCHANGER GEOMETRY
(METHOD OF CHARACTERISTICS)

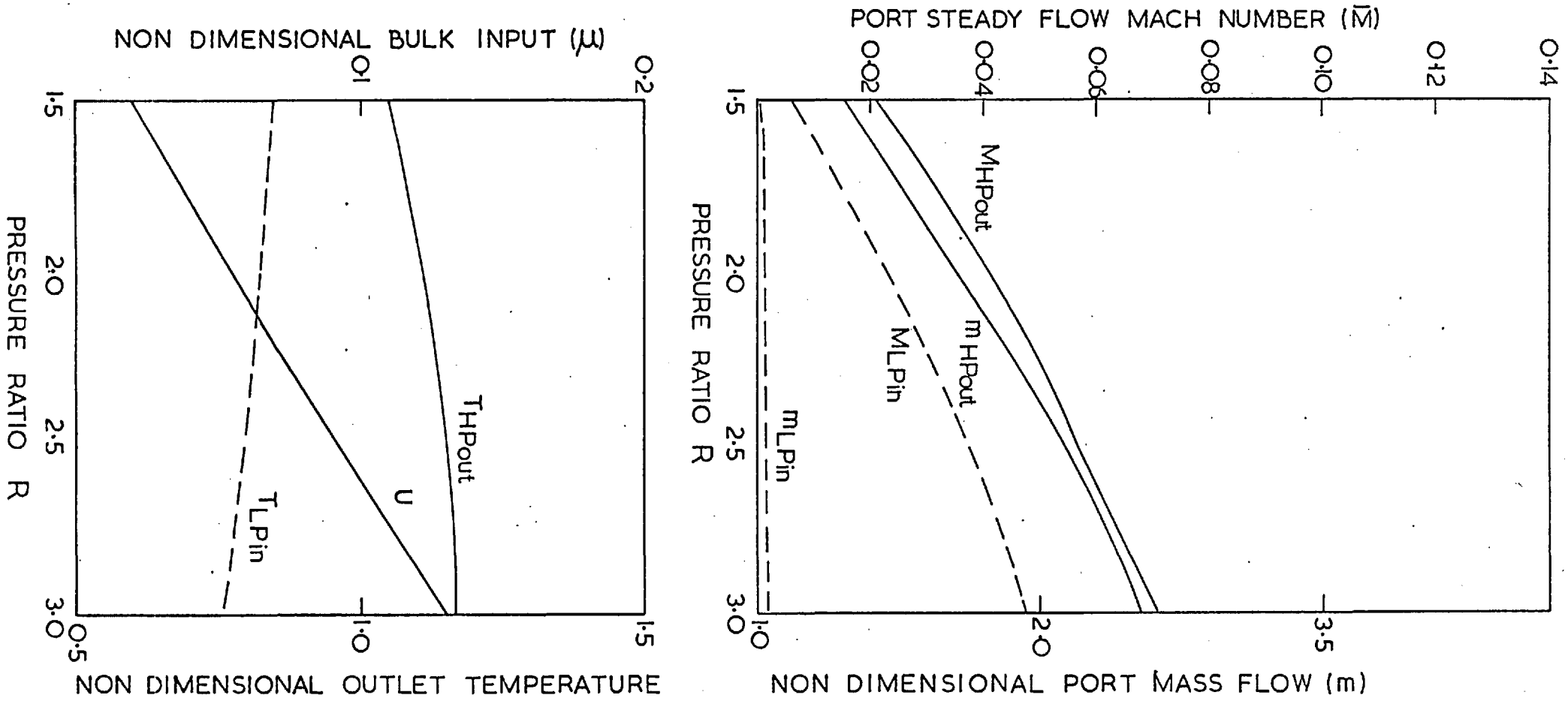


FIG. 12.71 SIX PORT PRESSURE EXCHANGER PERFORMANCE (FIXED SCAVENGE RATIO)

HP SCAVENGE RATIO=1·0
LP SCAVENGE RATIO=1·0
TEMPERATURE RATIO=1·0
NON DIMENSIONAL CELL WIDTH=0·0

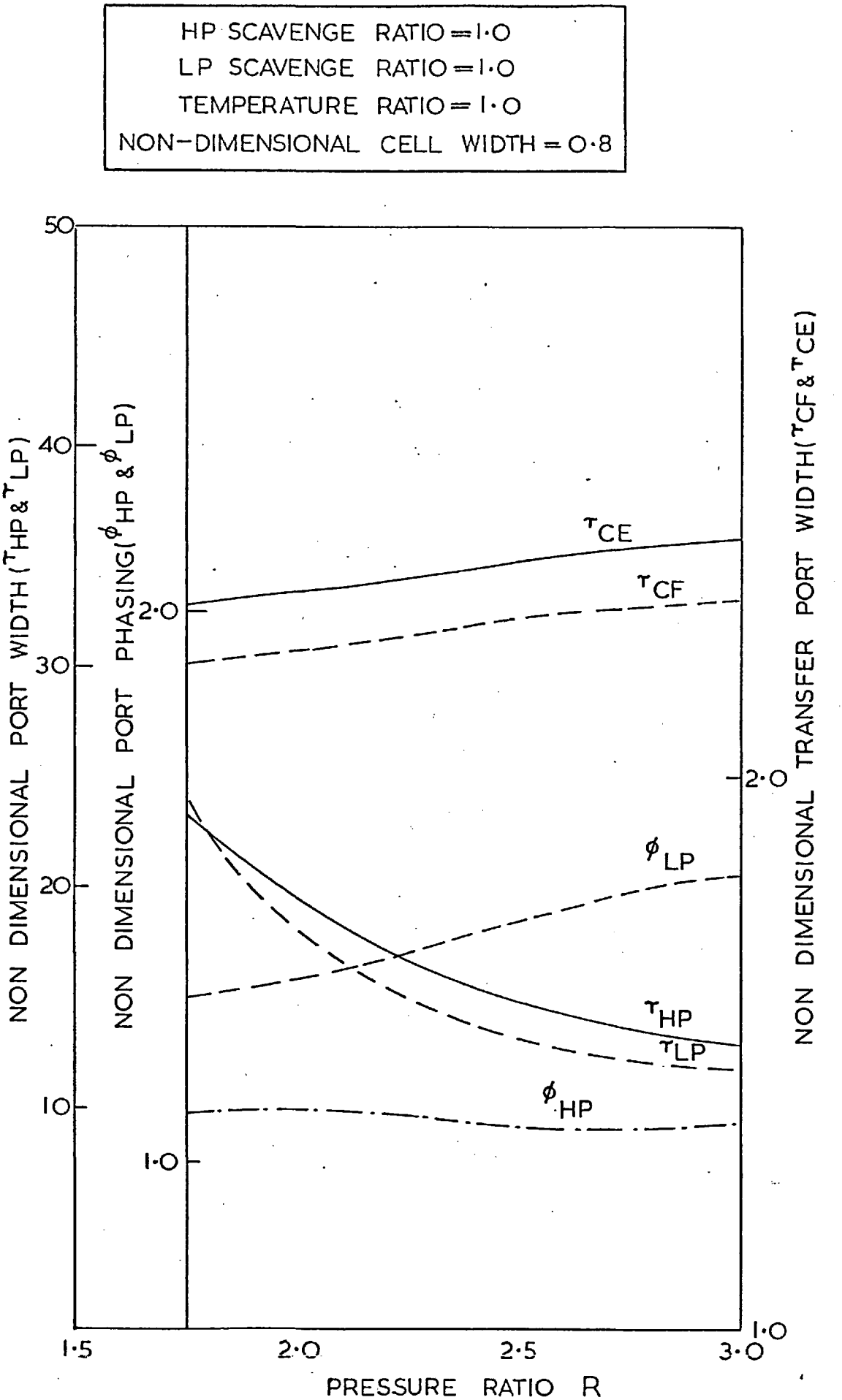
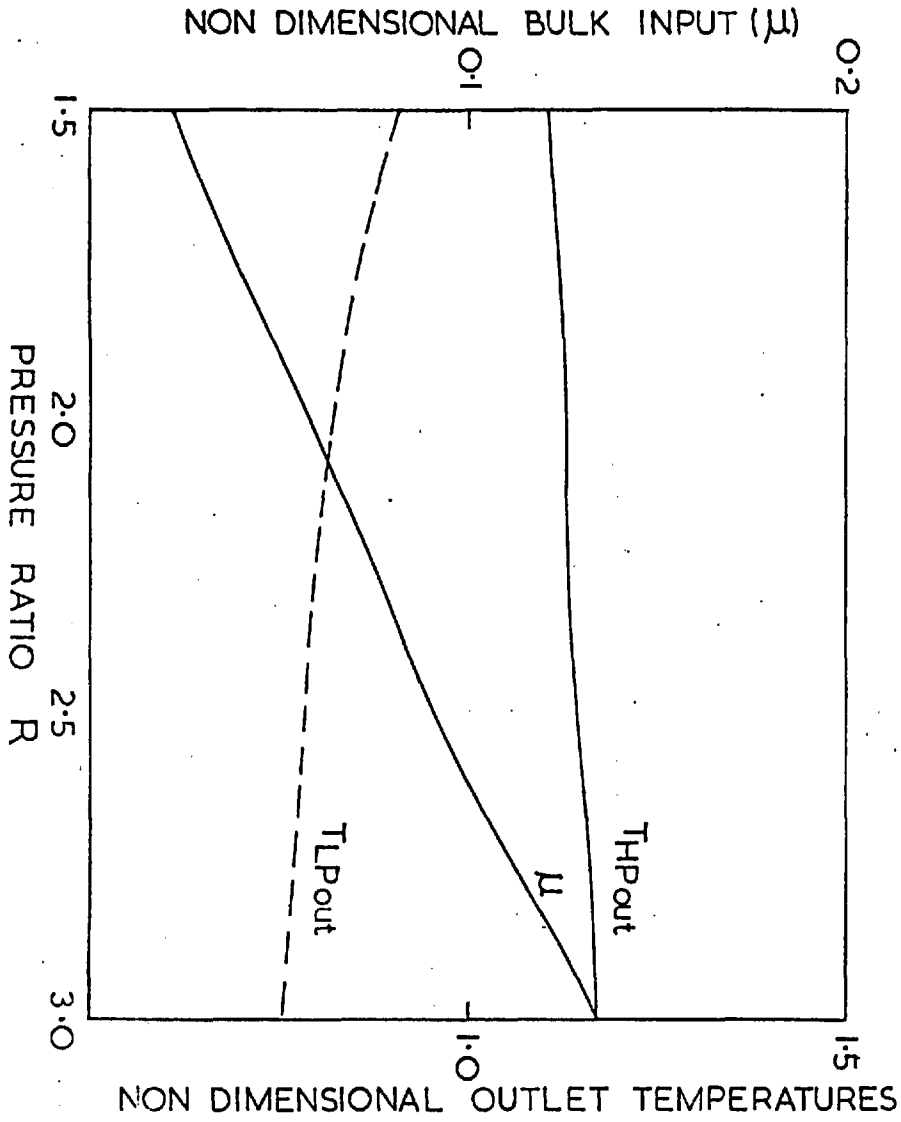


FIG. 12.72 SIX PORT PRESSURE EXCHANGER GEOMETRY (METHOD OF CHARACTERISTICS)



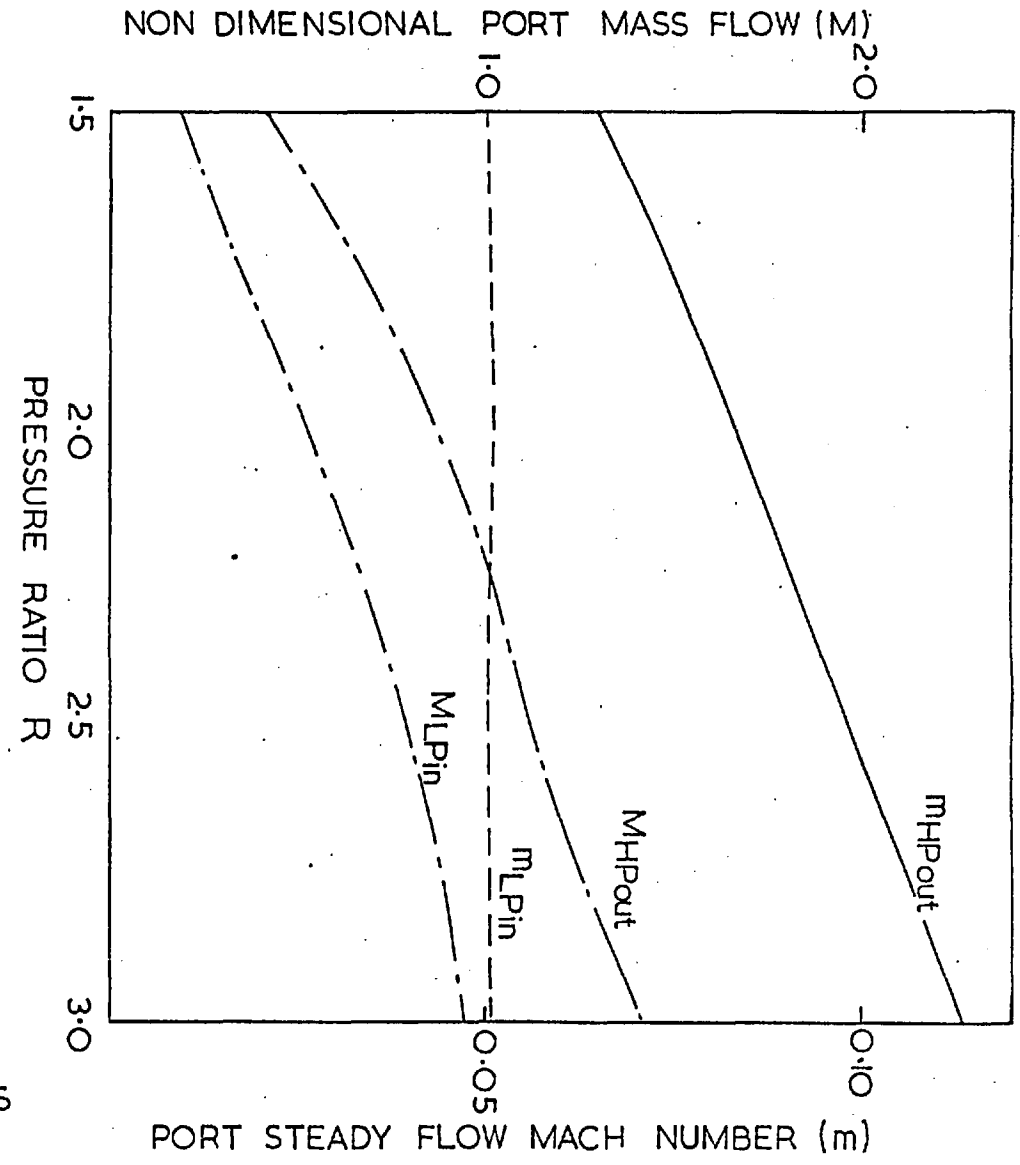


FIG. 1273 SIX PORT PRESSURE EXCHANGER PERFORMANCE (FIXED SCAVENGE RATIO)

HP SCAVENGE RATIO = 1·0	L P SCAVENGE RATIO = 1·0
TEMPERATURE RATIO = 1·0	NON DIMENSIONAL CELL WIDTH = 0·8

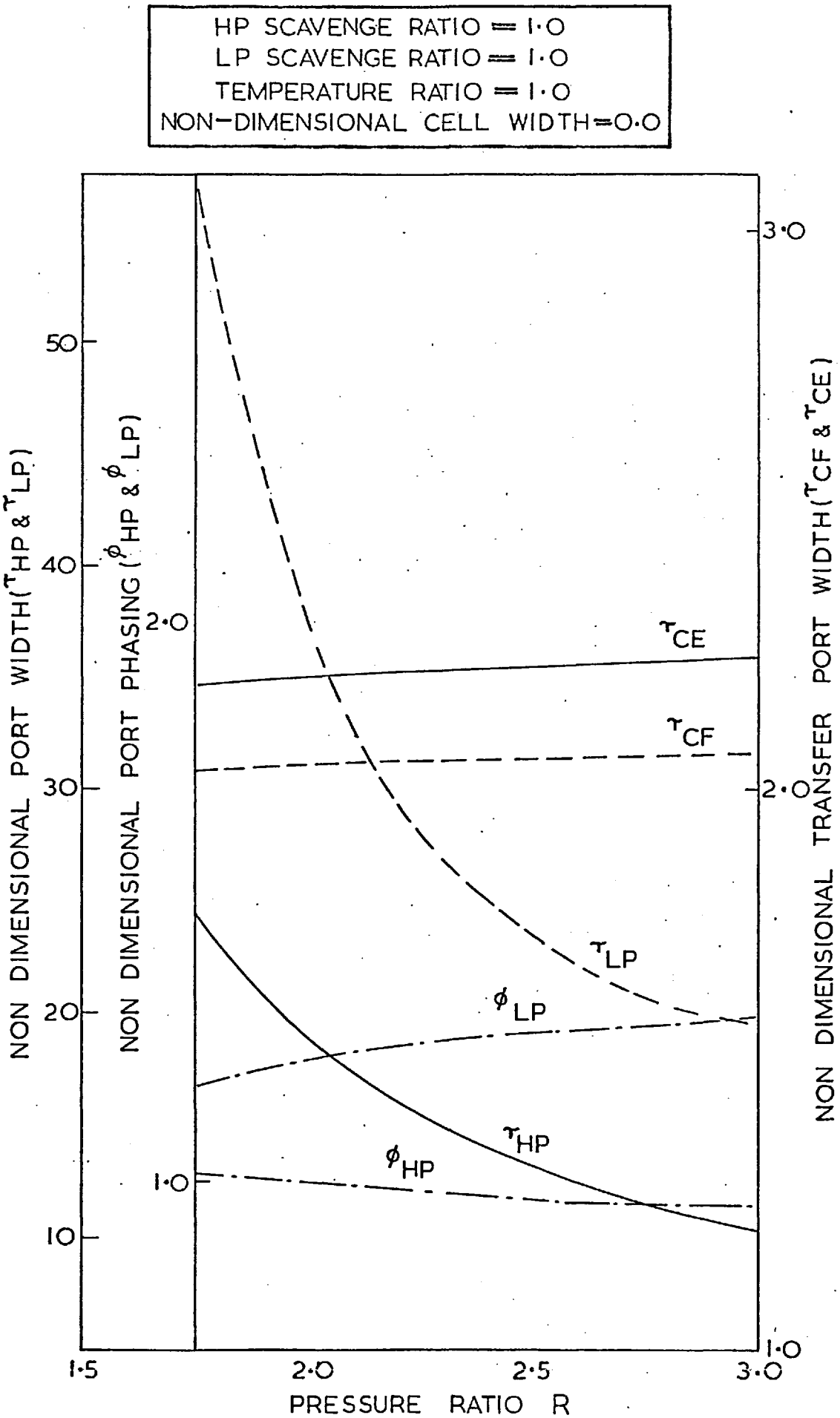
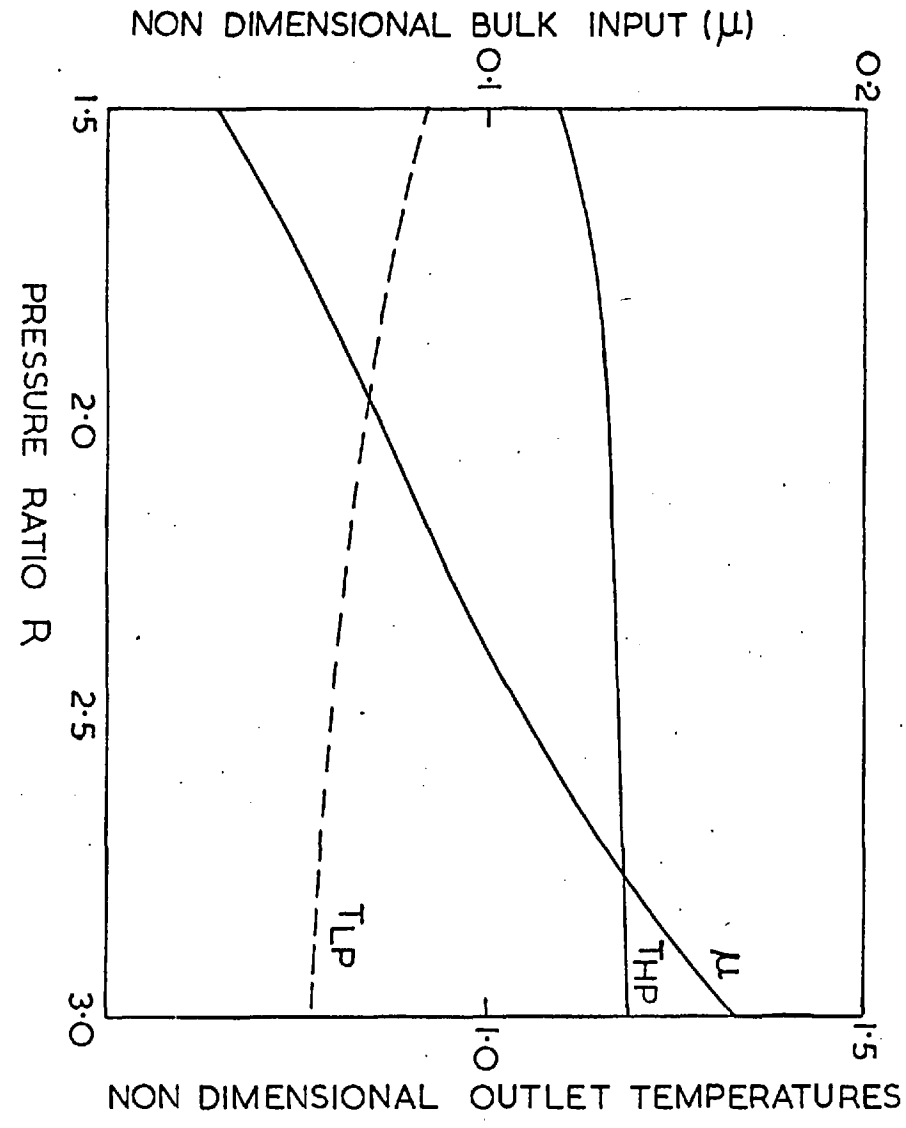


FIG. 12.74 SIX PORT PRESSURE EXCHANGER GEOMETRY
(METHOD OF CHARACTERISTICS)
FRICTION, HEAT TRANSFER & LEAKAGE TAKEN INTO ACCOUNT



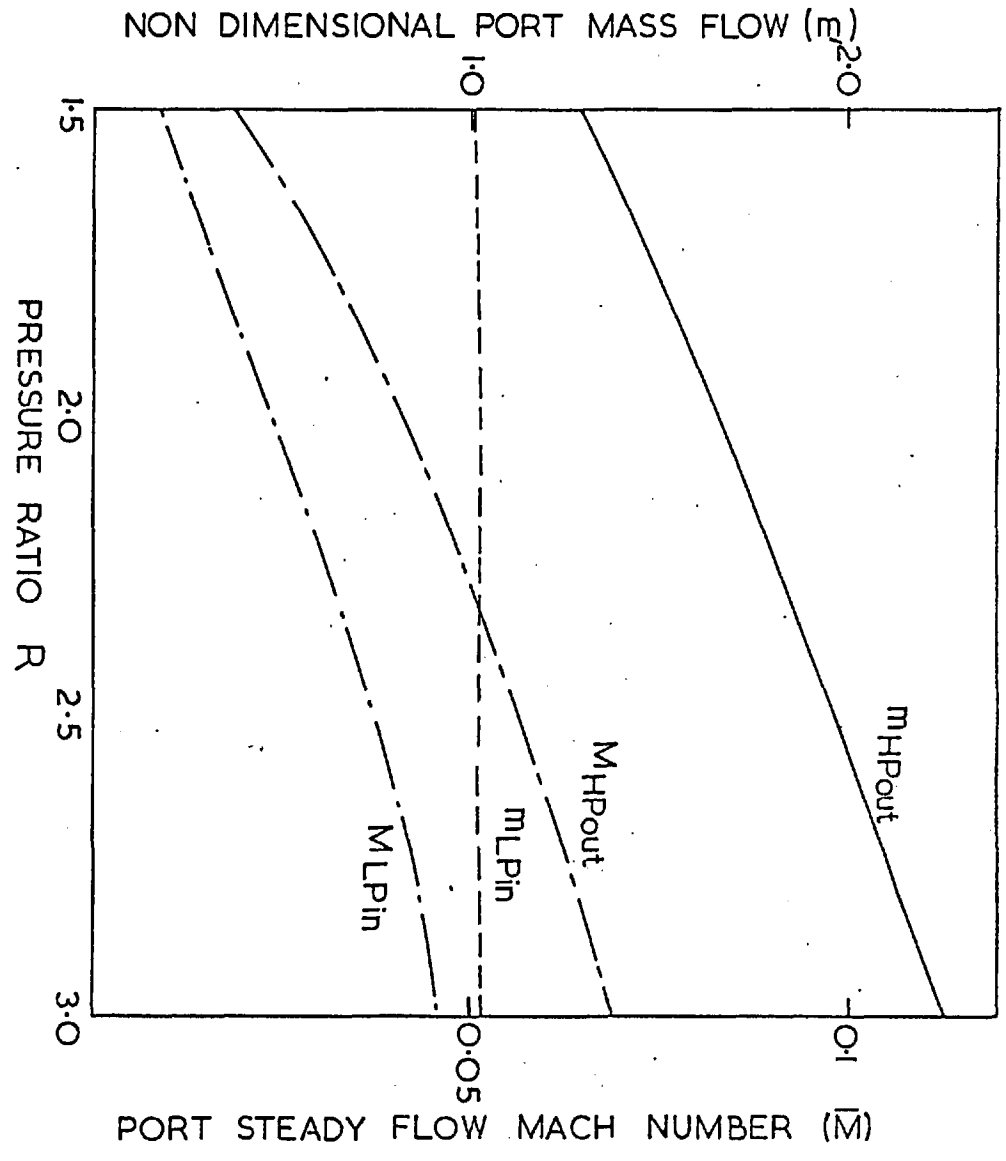


FIG. 12.75 SIX PORT PRESSURE EXCHANGER PERFORMANCE (FIXED SCAVENGE RATIO) FRICTION, HEAT TRANSFER, CELL WALL THICKNESS AND LEAKAGE TAKEN INTO ACCOUNT

HP SCAVENGE RATIO=1·0 LP SCAVENGE RATIO=1·0
TEMPERATURE RATIO=1·0 NON DIMENSIONAL CELL WIDTH=0·0

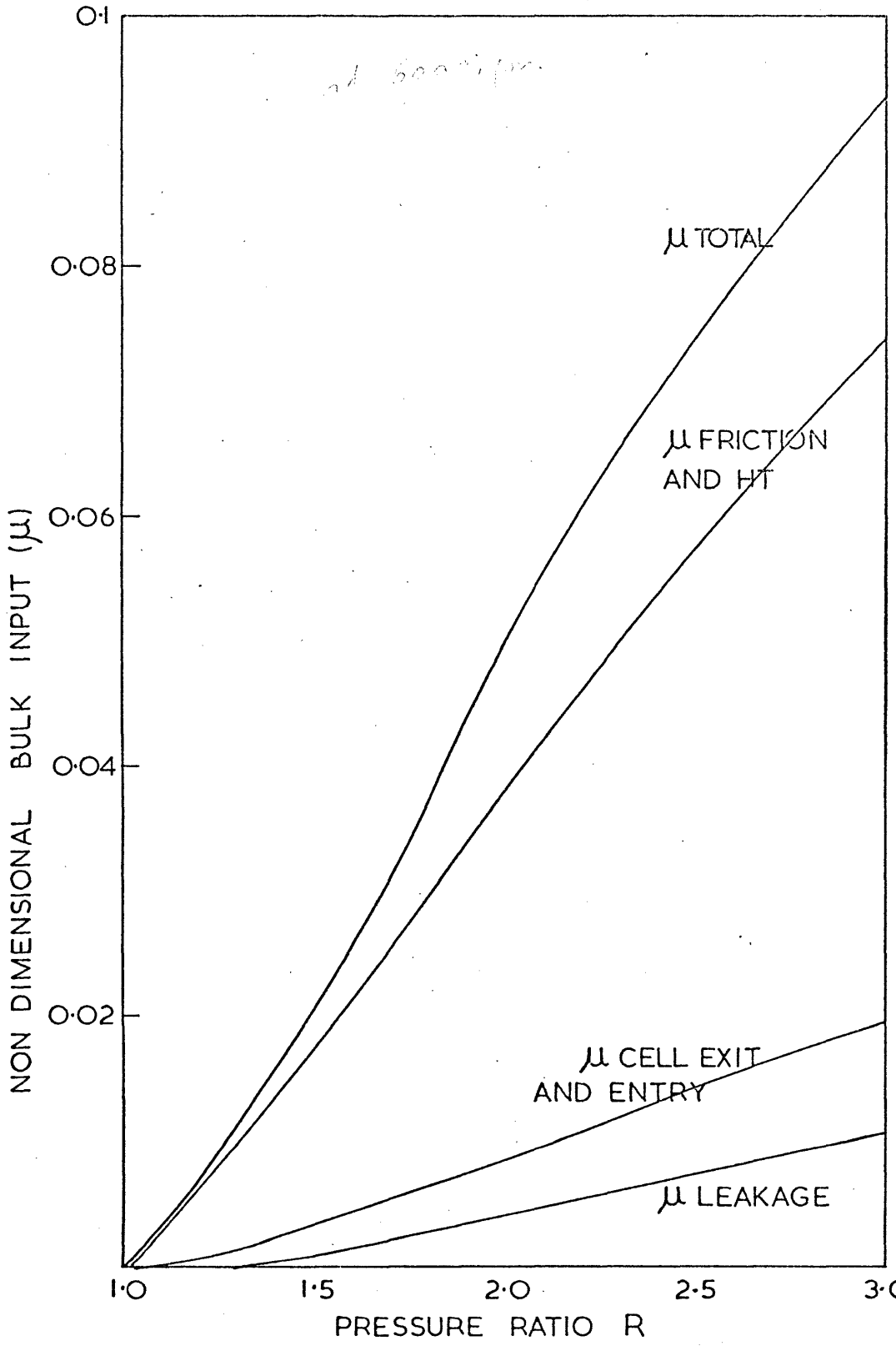


FIG. 12.76 NON DIMENSIONAL BULK INPUT FOR VARIOUS PERFORMANCE LOSSES (FIXED GEOMETRY AND CONSTANT SPEED OPERATION)

FOUR PORT PRESSURE EXCHANGER

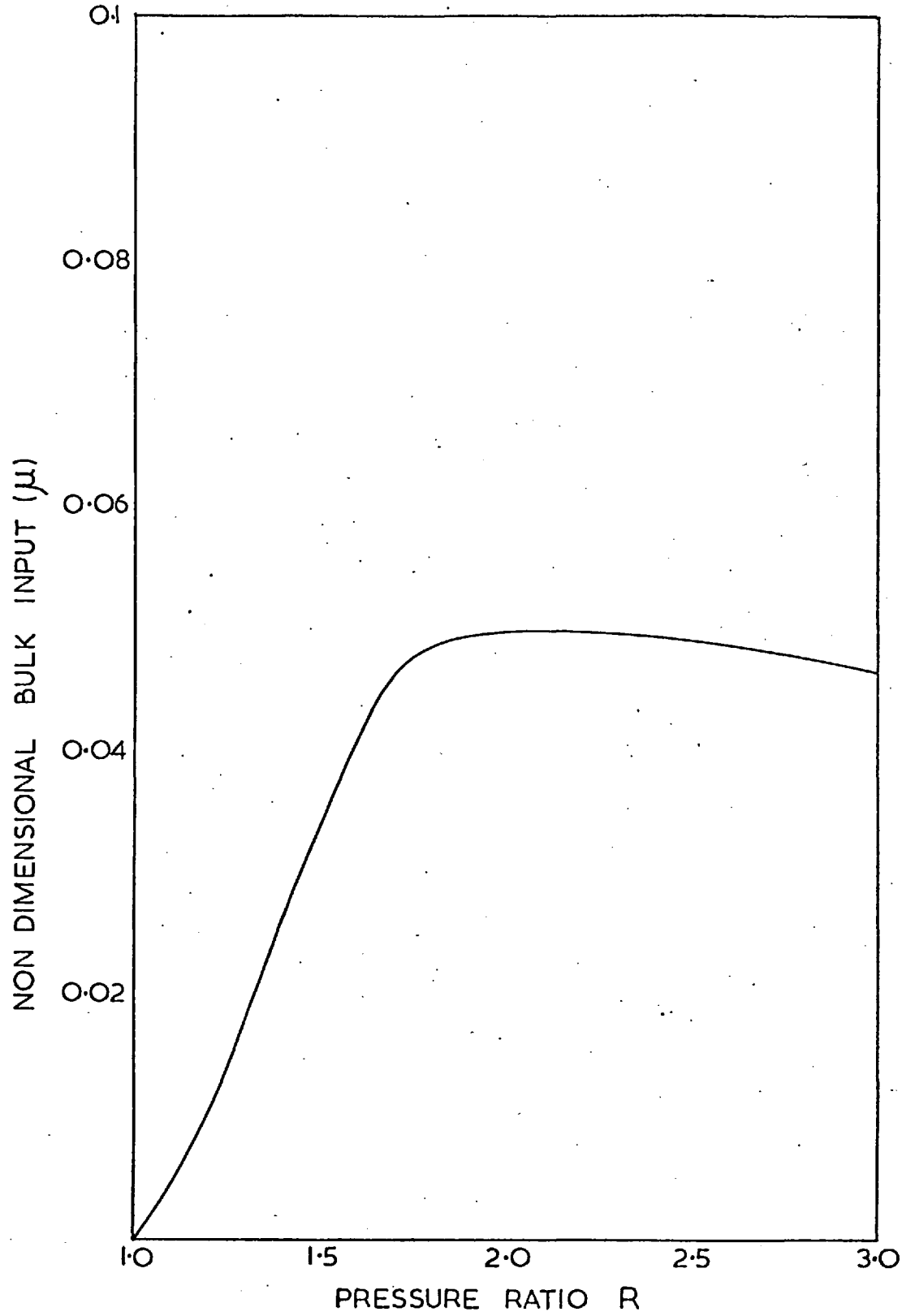


FIG. 12.77 NON DIMENSIONAL BULK INPUT FOR PERFORMANCE LOSSES (FIXED SCAVENGE RATIO OPERATION)

FOUR PORT PRESSURE EXCHANGER

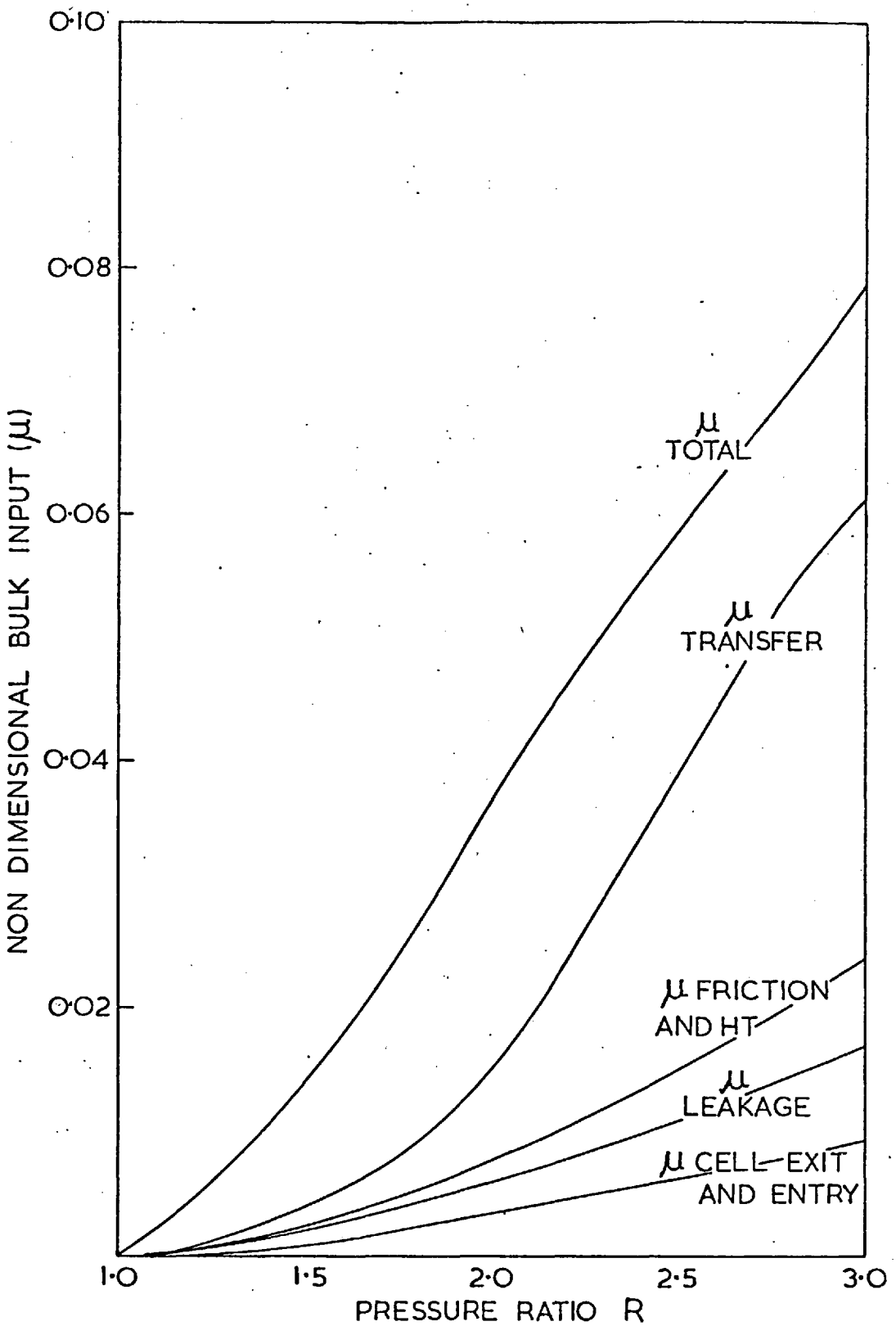


FIG. 12.78 NON DIMENSIONAL BULK INPUT FOR VARIOUS PERFORMANCE LOSSES (FIXED GEOMETRY AND CONSTANT SPEED OPERATION)

SIX PORT PRESSURE EXCHANGER

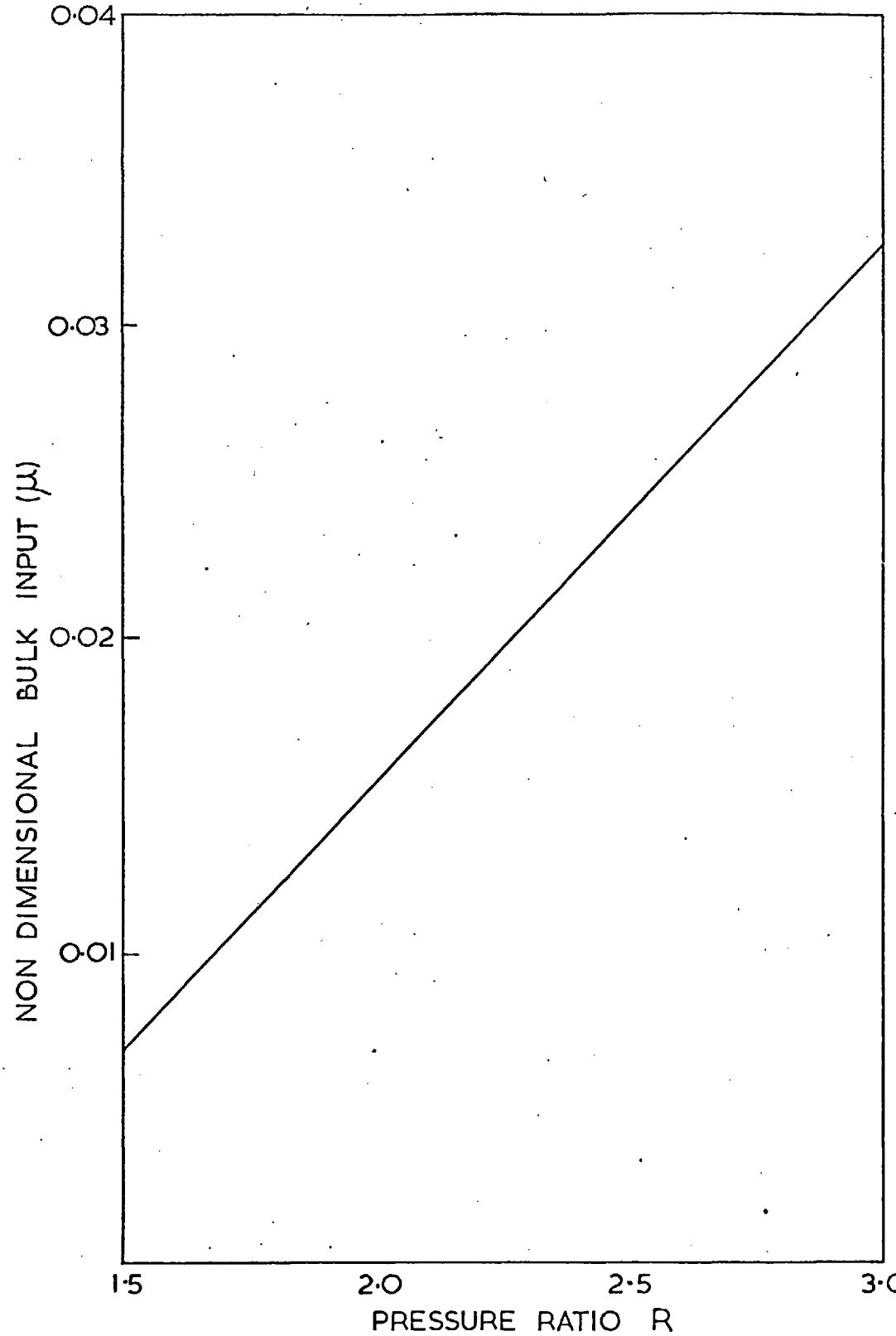


FIG. 12.79 NON DIMENSIONAL BULK INPUT FOR PERFORMANCE LOSSES (FIXED SCAVENGE RATIO)
SIX PORT PRESSURE EXCHANGER

ROTOR SPEED AND GEOMETRIC DATA		
	DIMENSIONED	DIMENSIONLESS
ROTOR SPEED	5500 REV/MIN	$M_{RO}=0.1346$
HP PORT WIDTH	47°	$\tau_H = 1.79$
LP PORT WIDTH	43°	$\tau_L = 1.63$
MP PORT WIDTH	48°	$\tau_M = 1.83$
PHASING	24°	$\tau_\phi = 0.91$
LAND WIDTH	12°	$\tau_L = 0.456$
CELL WIDTH	10.4°	$\delta = 0.393$

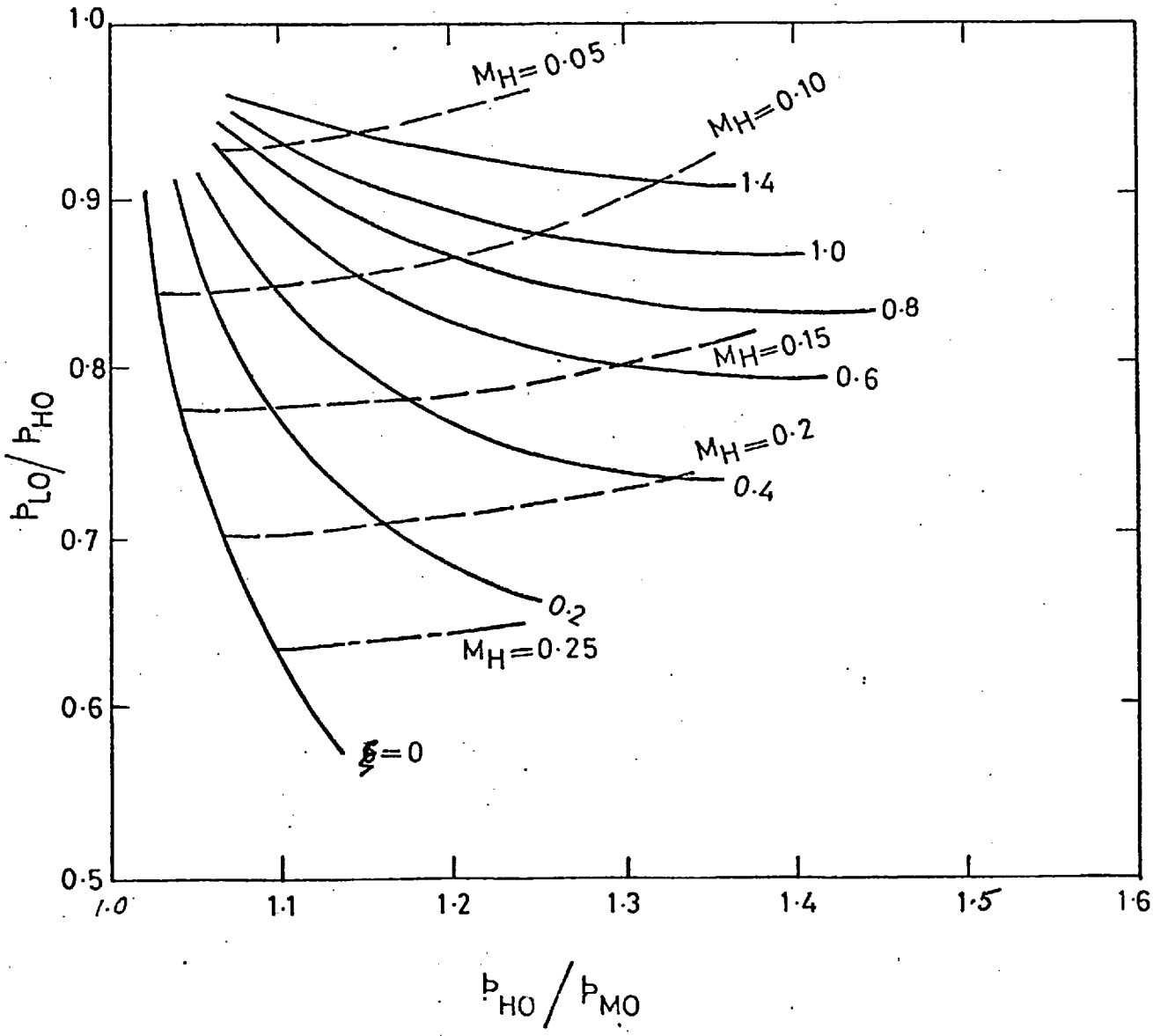


FIG. 12.80 EXPERIMENTALLY OBTAINED EQUALISER PERFORMANCE
(FIXED GEOMETRY, CONSTANT SPEED, T_{HO} 308°K, $P_{LO}=1_{ATM}$, $T_{LD}/T_{HO}=0.95$)

ROTOR SPEED AND GEOMETRIC DATA		
	DIMENSIONED	DIMENSIONLESS
ROTOR SPEED	5500 REV/MIN	M_{RO}=0·1346
HP PORT WIDTH	47°	τ_H = 1·79
L P PORT WIDTH	43°	τ_L = 1·63
MP PORT WIDTH	48°	τ_M = 1·83
PHASING	24°	τ_ϕ = 0·91
LAND WIDTH	12°	τ_L = 0·456
CELL WIDTH	10·4°	δ = 0·393

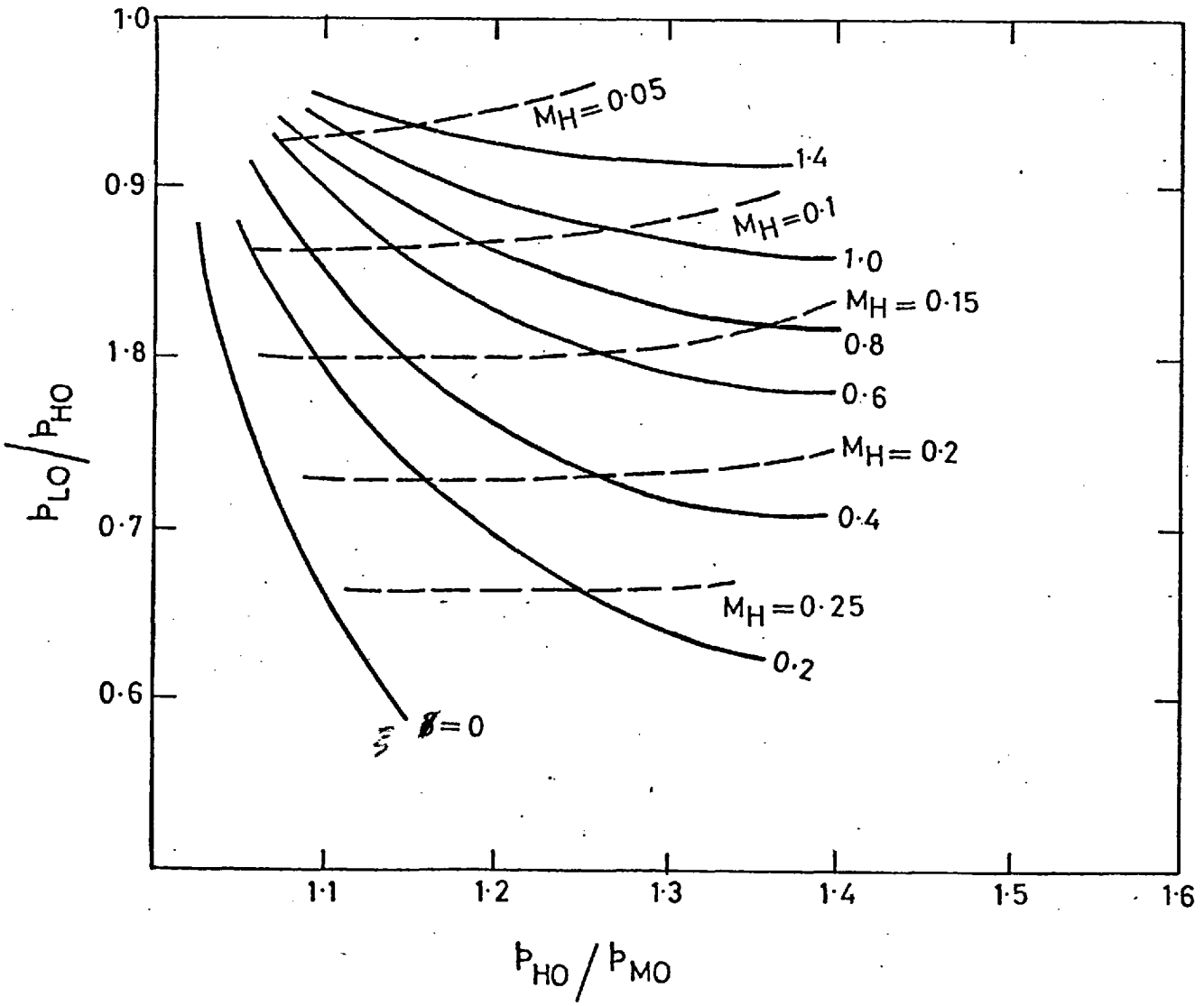


FIG. 12.81 COMPUTED EQUALISER PERFORMANCE

(FIXED GEOMETRY, CONSTANT SPEED T_{HO} 302°K P_{LO}=1 ATM T_{LO}/T_{HO}=0·95)

(LEAKAGE LOSSES TAKEN INTO ACCOUNT BY MASS & ENERGY CORRECTION METHOD)

ROTOR SPEED AND GEOMETRIC DATA		
	DIMENSIONED	DIMENSIONLESS
ROTOR SPEED	5500 REV/MIN	$M_{RO}=0\cdot1346$
HP PORT WIDTH	47°	$\tau_H = 1\cdot79$
LP PORT WIDTH	43°	$\tau_L = 1\cdot63$
MP PORT WIDTH	48°	$\tau_M = 1\cdot83$
PHASING	24°	$\tau_\delta = 0\cdot91$
LAND WIDTH	12°	$\tau_L = 0\cdot456$
CELL WIDTH	10·4°	$\delta = 0\cdot393$

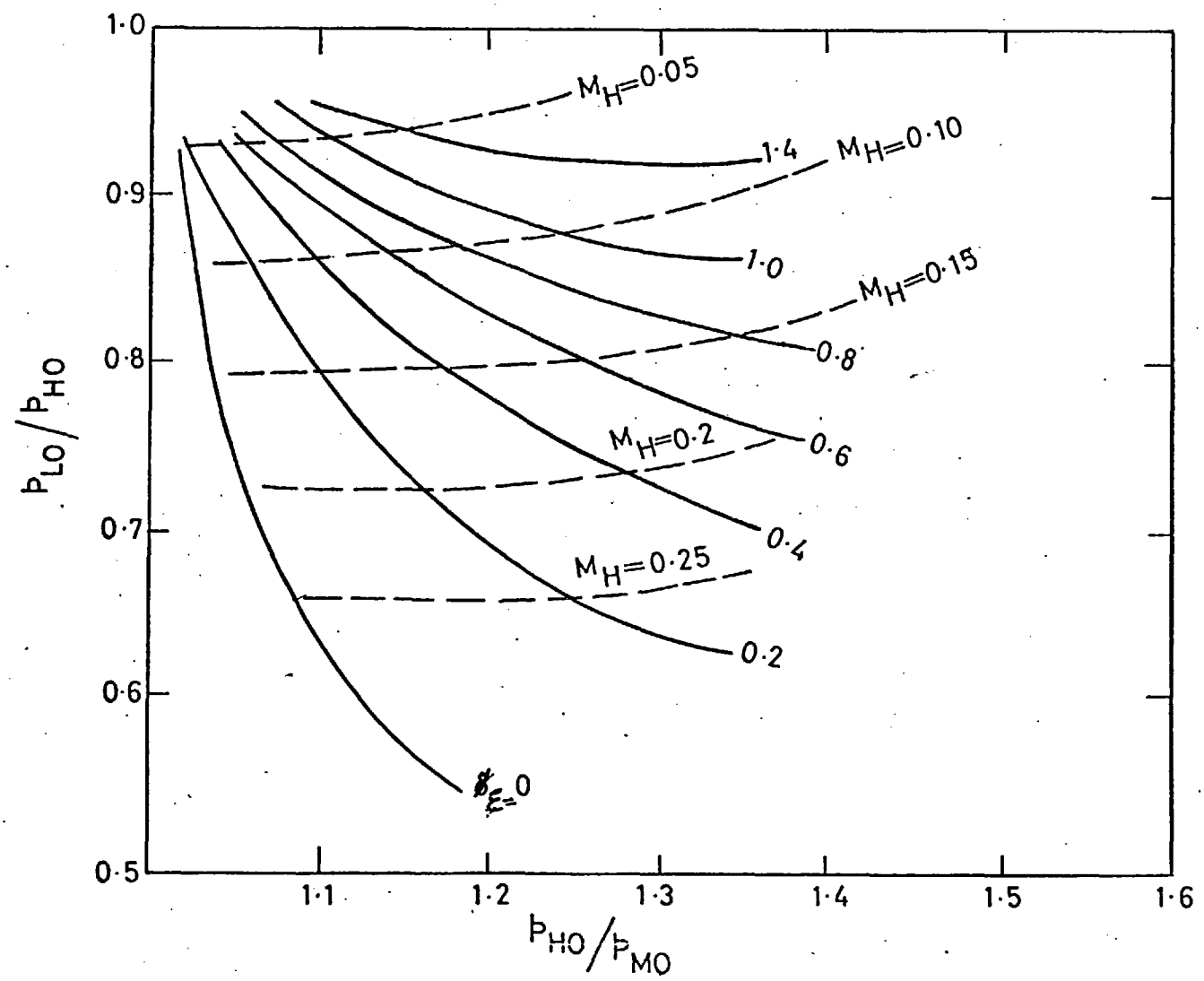


FIG. 12.82 COMPUTED EQUALISER PERFORMANCE

(FIXED GEOMETRY, CONSTANT SPEED T_{HO} 302°K $P_{LO}=1$ ATM $T_{LO}/T_{HO}=0\cdot95$)

(LEAKAGE LOSSES TAKEN INTO ACCOUNT BY POUROUS CELL WALL METHOD)

ROTOR SPEED AND GEOMETRIC DATA		
	DIMENSIONED	DIMENSIONLESS
ROTOR SPEED	5500 REV/MIN	$M_{RO}=0\cdot1346$
HP PORT WIDTH	47°	$\tau_H = 1\cdot79$
LP PORT WIDTH	43°	$\tau_L = 1\cdot63$
MP PORT WIDTH	48°	$\tau_M = 1\cdot83$
PHASING	24°	$\tau_o = 0\cdot91$
LAND WIDTH	12°	$\tau_L = 0\cdot456$
CELL WIDTH	10·4°	$\delta = 0\cdot393$

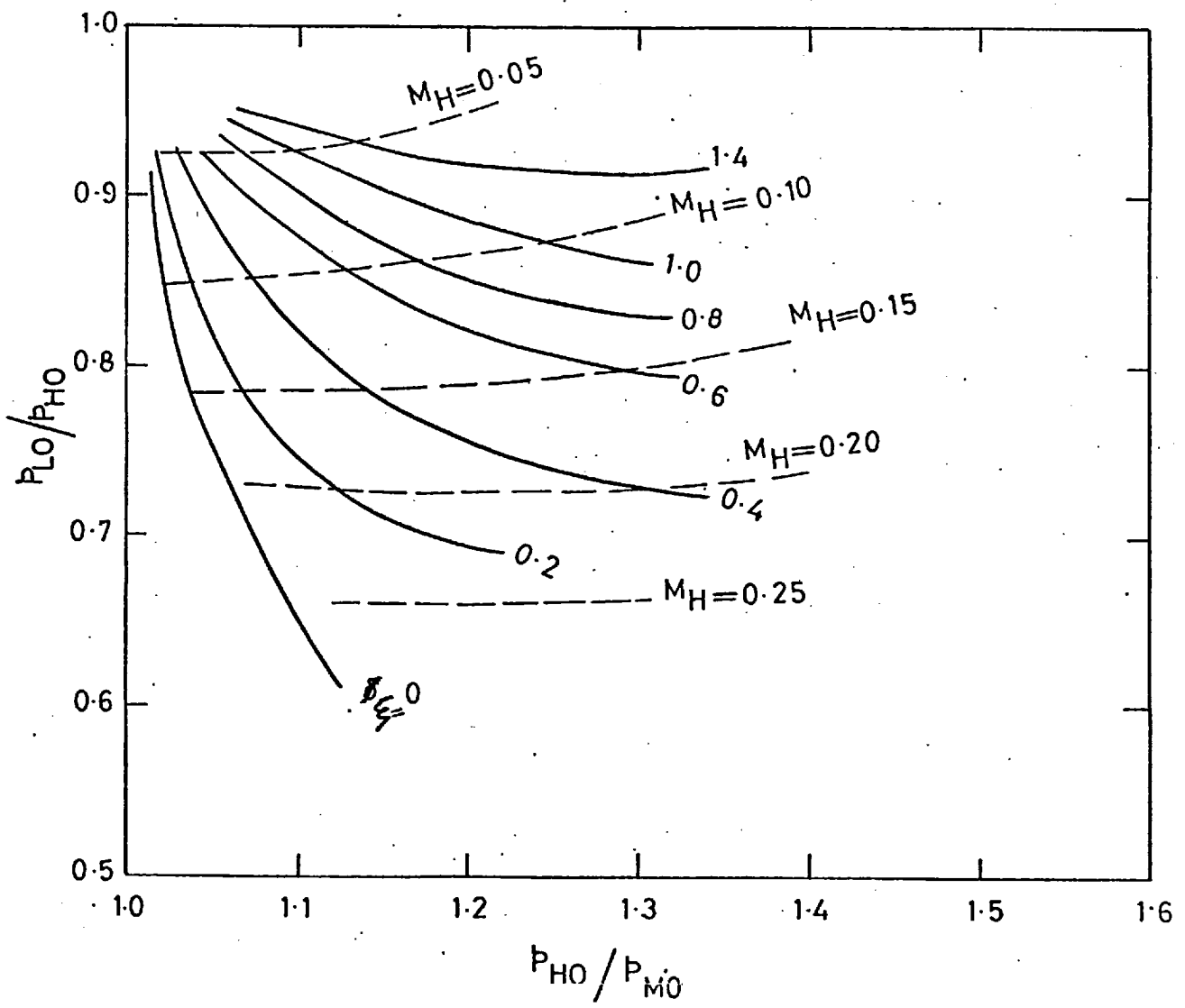
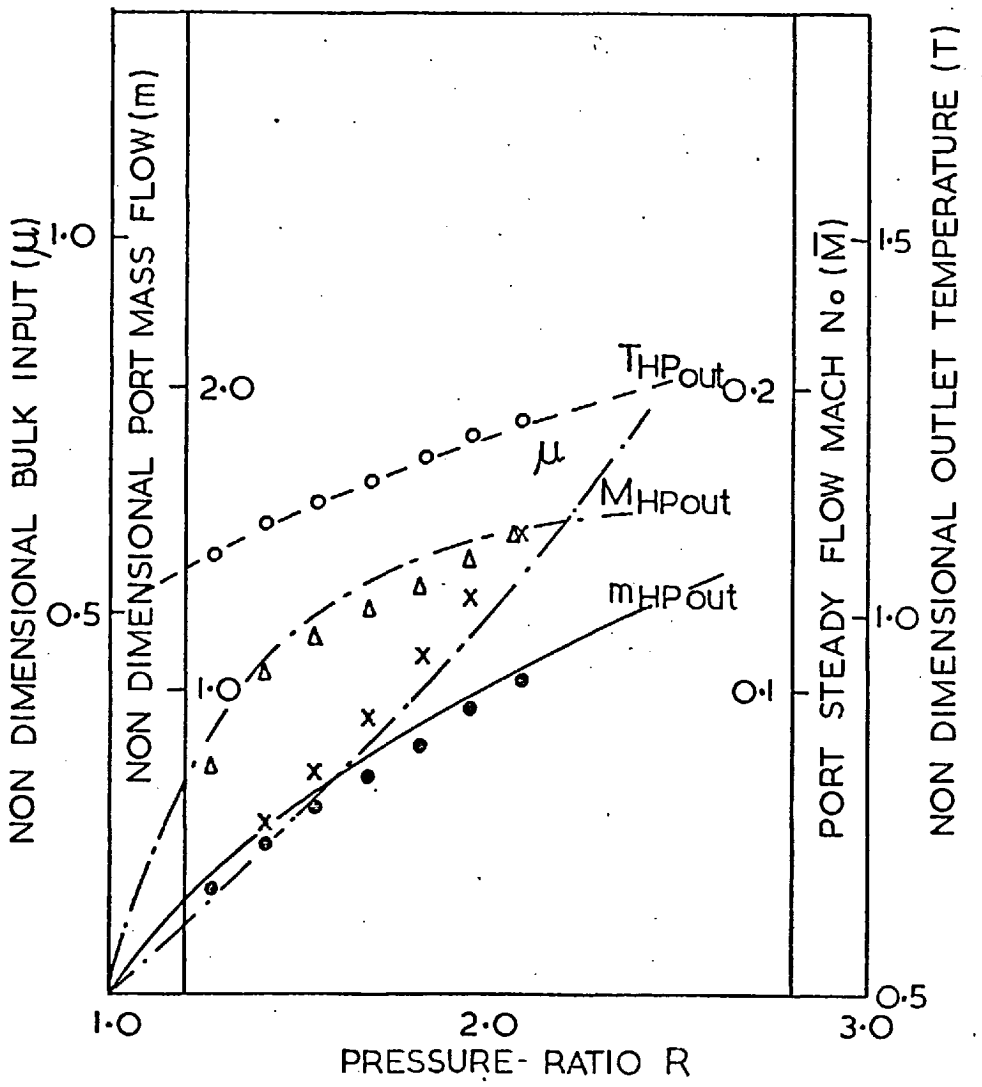


FIG. 12.83 COMPUTED EQUALISER PERFORMANCE

(FIXED GEOMETRY, CONSTANT SPEED T_{HO} 302°K P_{LO}=1 ATM T_{LO}/T_{HO}=0·95)

(LEAKAGE LOSSES TAKEN INTO ACCOUNT BY PARTLY – OPEN END METHOD)

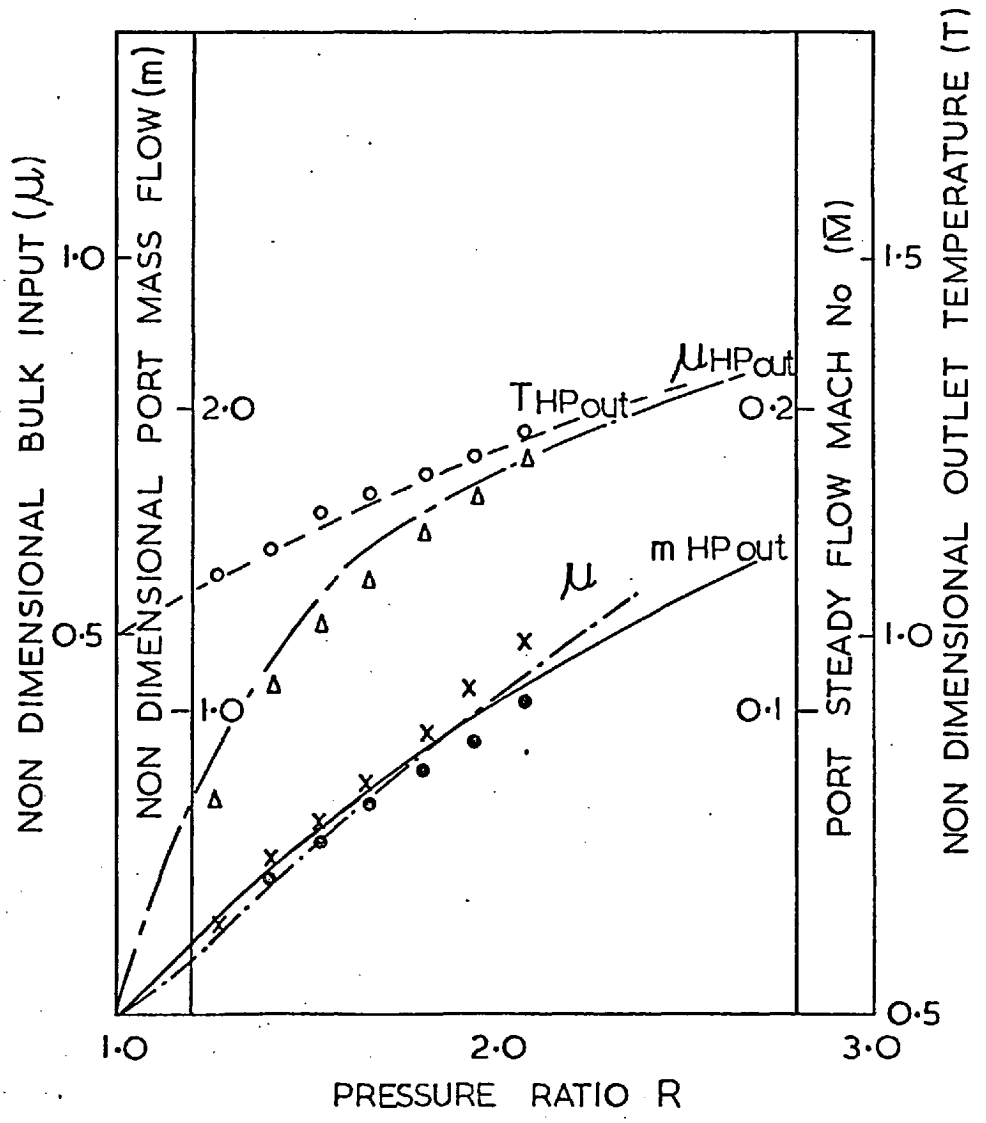
	DIMENSIONED	DIMENSIONLESS
ROTOR SPEED	5000 R P M	
τ_{HPout}	45 DEGREES	3·006
ϕ_{HP}	14·3 DEGREES	0·9572
A_{HP}	1·0	
τ_{LPin}	193 DEGREES	12·92
ϕ_{LP}	24·3 DEGREES	1·627
A_{LP}		1·03
τ_C	10 DEGREES	0·5960
τ_{L1}	50 DEGREES	3·330
τ_{L2}	65 DEGREES	4·340



EXPERIMENTALLY OBTAINED FOUR PORT PRESSURE EXCHANGER PERFORMANCE (FIXED GEOMETRY & CONSTANT SPEED)

FIG. 12.84

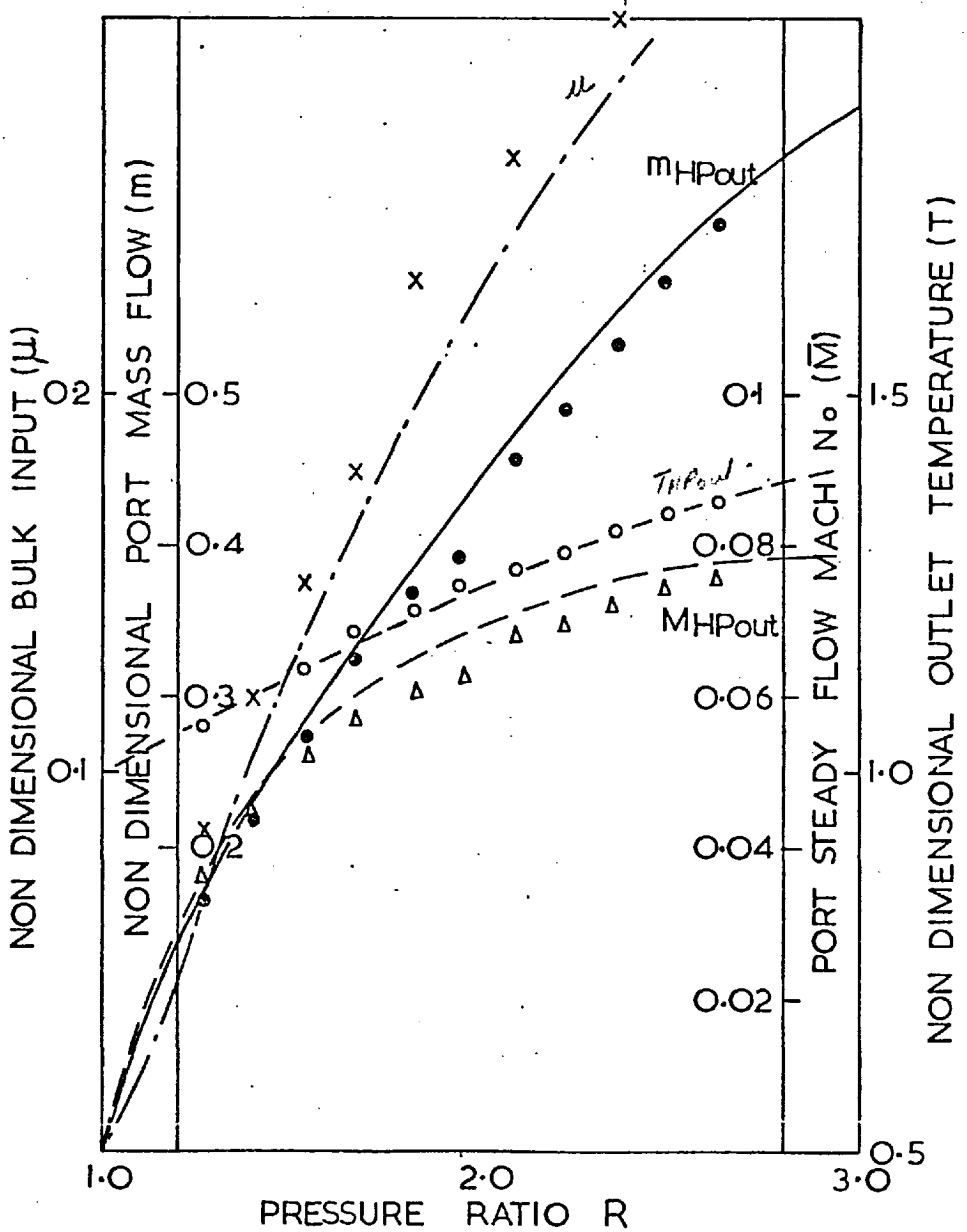
	DIMENSIONED	DIMENSIONLESS
ROTOR SPEED	6000 R P M	
$\tau_{HP\,out}$	45 DEGREES	2·507
ϕ_{HP}	14·3 DEGREES	0·7977
A_{HP}	1·0	
$\tau_{LP\,in}$	193 DEGREES	10·77
ϕ_{LP}	24·3 DEGREES	1·356
A_{LP}	1·03	
τ_C	10 DEGREES	0·4970
τ_{L1}	50 DEGREES	2·70
τ_{L2}	65 DEGREES	3·620



EXPERIMENTALLY OBTAINED FOUR PORT PRESSURE EXCHANGER PERFORMANCE (FIXED GEOMETRY & CONSTANT SPEED)

FIG. 12.83

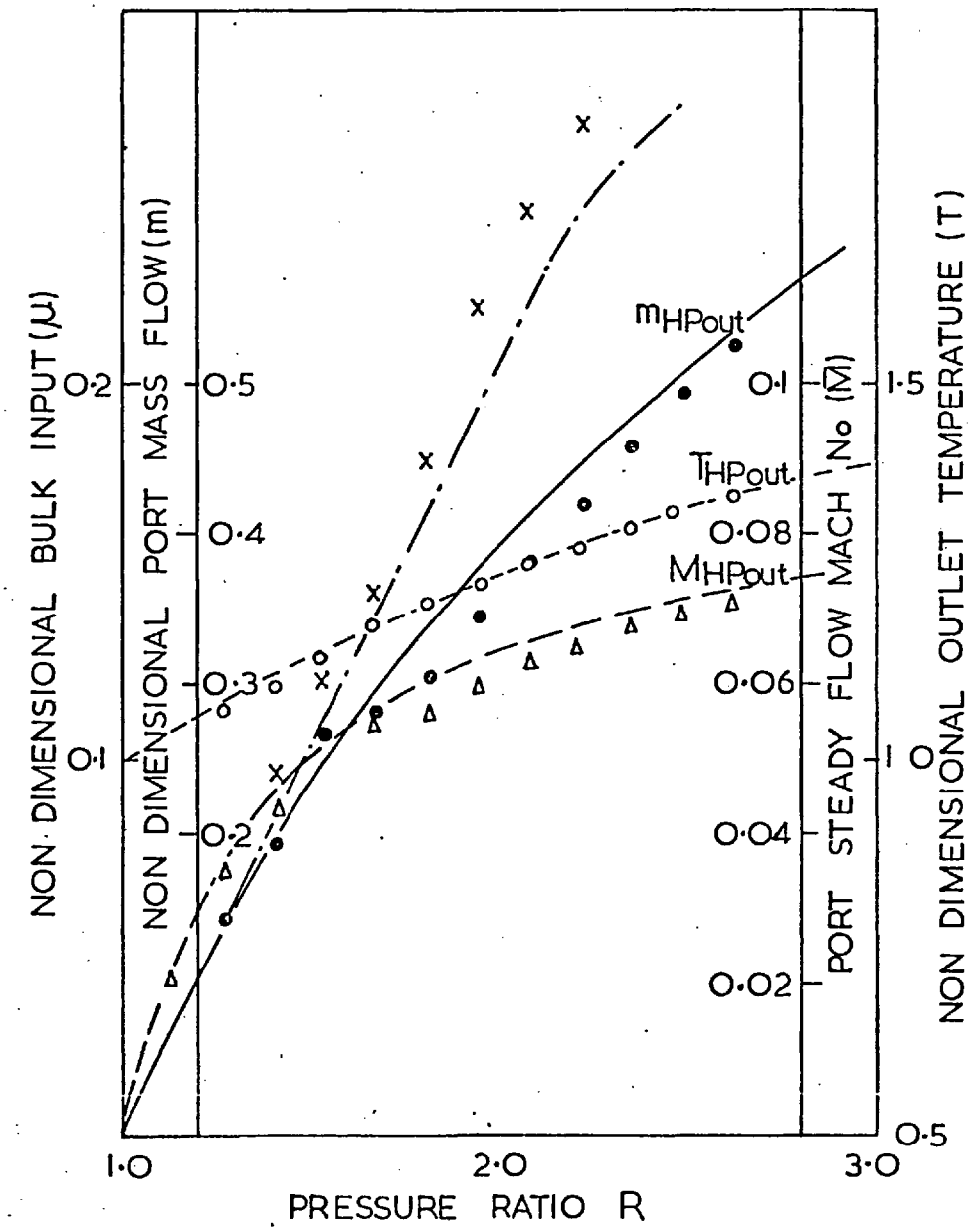
	DIMENSIONED	DIMENSIONLESS
ROTOR SPEED	5000 RPM	
τ_{HPout}	45 DEGREES	3·006
ϕ_{HP}	13·5 DEGREES	0·9036
A_{HP}	1·0	
τ_{LPin}	75 DEGREES	5·010
ϕ_{LP}	23·5 DEGREES	1·57
A_{LP}	1·0	
τ_{CF}	30 DEGREES	2·004
τ_{CE}	30 DEGREES	2·004
τ_{C}	10 DEGREES	0·5960
τ_{L1}	45 DEGREES	3·006
τ_{L2}	45 DEGREES	3·006
τ_{L3}	45 DEGREES	3·006
τ_{L4}	45 DEGREES	3·006



EXPERIMENTALLY OBTAINED SIX PORT PRESSURE EXCHANGER PERFORMANCE (FIXED GEOMETRY AND CONSTANT SPEED)

FIG. 12.86

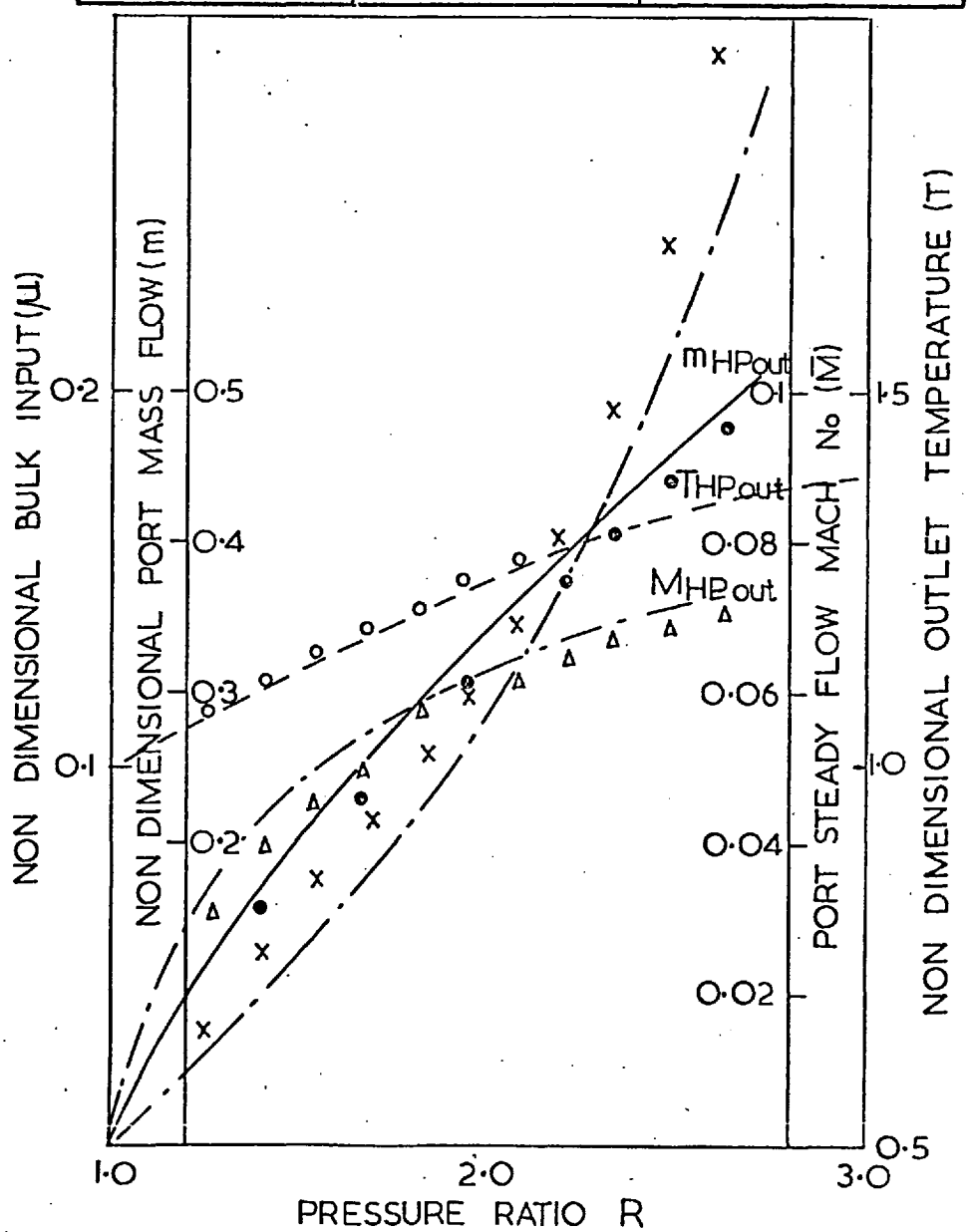
	DIMENSIONED	DIMENSIONLESS
ROTOR SPEED	5500 RPM	
τ_{HPout}	45 DEGREES	2·7333
ϕ_{HP}	13·5 DEGREES	0·820
A_{HP}	1·0	
τ_{LPin}	75 DEGREES	4·555
ϕ_{LP}	23·5 DEGREES	1·425
A_{LP}	1·0	
τ_{CF}	30 DEGREES	1·822
τ_{CE}	30 DEGREES	1·822
τ_{C}	10 DEGREES	0·5418
τ_{L1}	45 DEGREES	2·733
τ_{L2}	45 DEGREES	2·733
τ_{L3}	45 DEGREES	2·733
τ_{L4}	45 DEGREES	2·733



EXPERIMENTALLY OBTAINED SIX PORT PRESSURE EXCHANGER PERFORMANCE (FIXED GEOMETRY AND CONSTANT SPEED)

FIG. 12.87

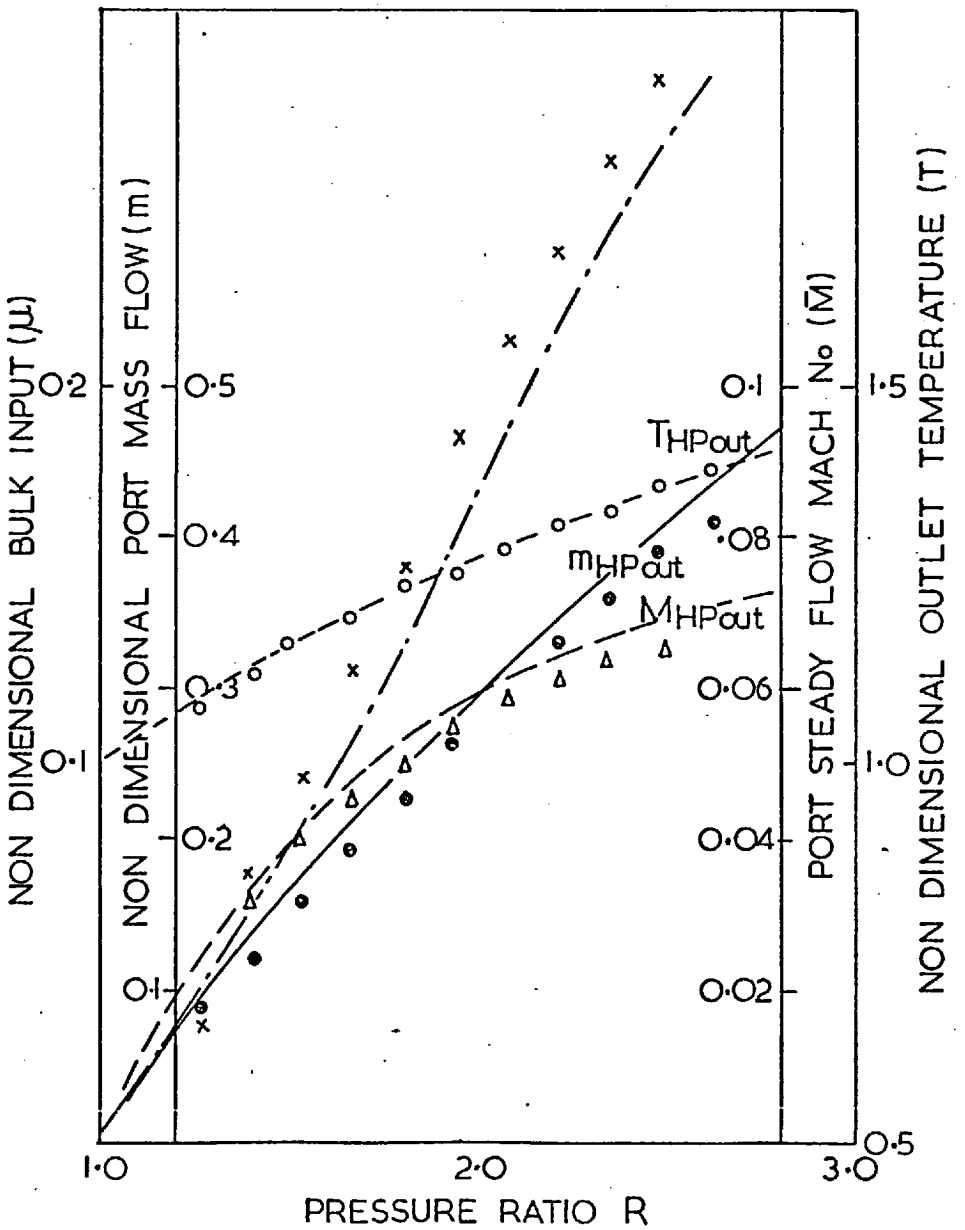
	DIMENSIONED	DIMENSIONLESS
ROTOR SPEED	6000 RPM	
τ_{HPout}	45 DEGREES	2·507
ϕ_{HP}	13·5 DEGREES	0·755
A_{HP}	1·0	
τ_{LPin}	75 DEGREES	4·1780
ϕ_{LP}	23·5 DEGREES	1·31
A_{LP}	1·0	
τ_{CF}	30 DEGREES	1·671
τ_{CE}	30 DEGREES	1·671
τ_{C}	10 DEGREES	0·4970
τ_{L1}	45 DEGREES	2·507
τ_{L2}	45 DEGREES	2·507
τ_{L3}	45 DEGREES	2·507
τ_{L4}	45 DEGREES	2·507



EXPERIMENTALLY OBTAINED SIX PORT PRESSURE EXCHANGER PERFORMANCE (FIXED GEOMETRY AND CONSTANT SPEED)

FIG. 12.88

	DIMENSIONED	DIMENSIONLESS
ROTOR SPEED	6500 R P M	
τ_{HPout}	45 DEGREES	2·327
ϕ_{HP}	13·5 DEGREES	0·7012
A_{HP}	1·0	
τ_{LPin}	75 DEGREES	3·878
ϕ_{LP}	23·5 DEGREES	1·21
A_{LP}	1·0	
τ_{CF}	30 DEGREES	1·551
τ_{CE}	30 DEGREES	1·551
τ_{C}	10 DEGREES	0·4613
τ_{L1}	45 DEGREES	2·327
τ_{L2}	45 DEGREES	2·327
τ_{L3}	45 DEGREES	2·327
τ_{L4}	45 DEGREES	2·327



EXPERIMENTALLY OBTAINED SIX PORT PRESSURE EXCHANGER PERFORMANCE (FIXED GEOMETRY AND CONSTANT SPEED)

FIG. 12.89

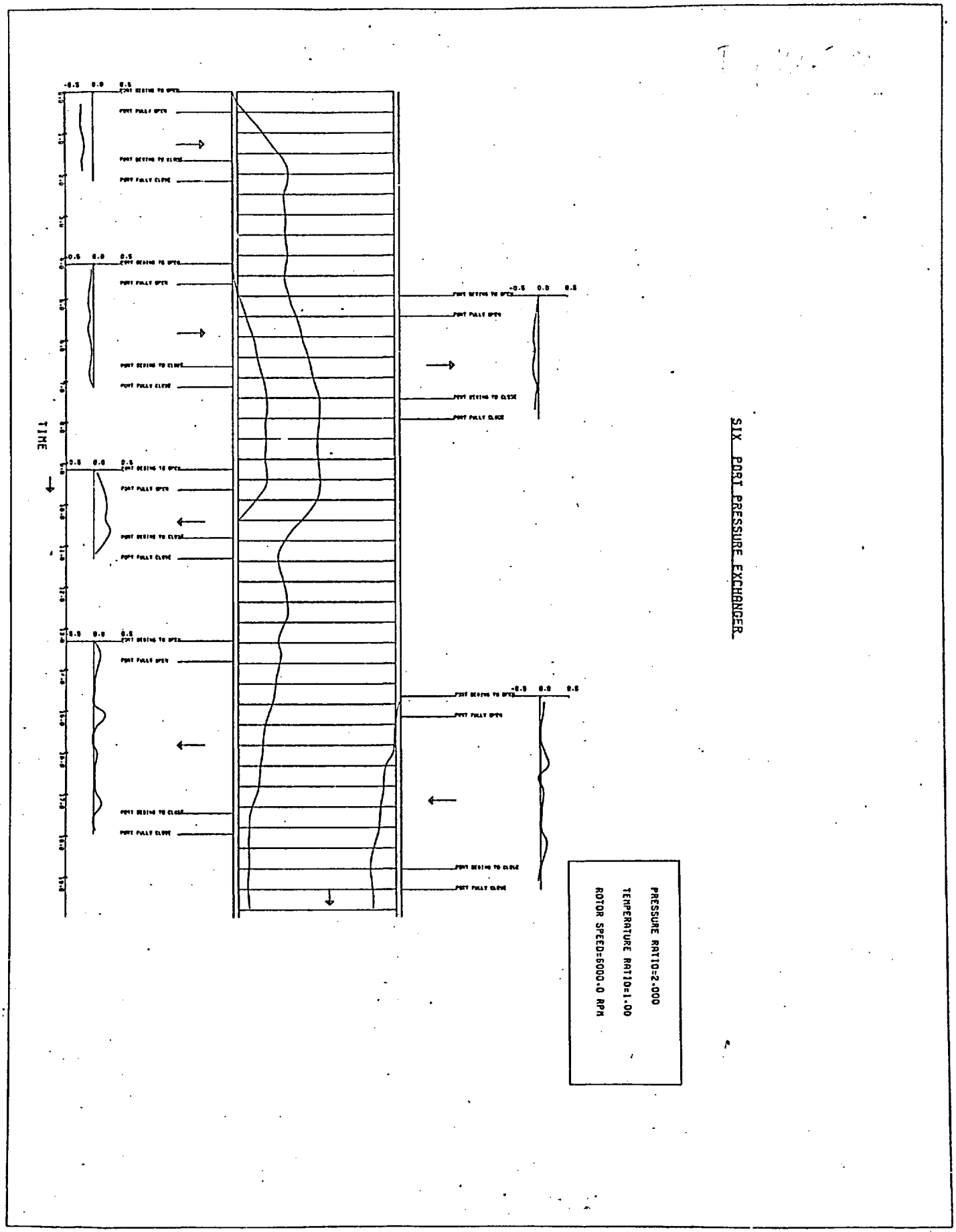

SIX PORT PRESSURE EXCHANGER
TIME
PRESSURE RATIO=2.000
TEMPERATURE RATIO=1.00
ROTOR SPEED=6000.0 RPM

FIG. 12.90

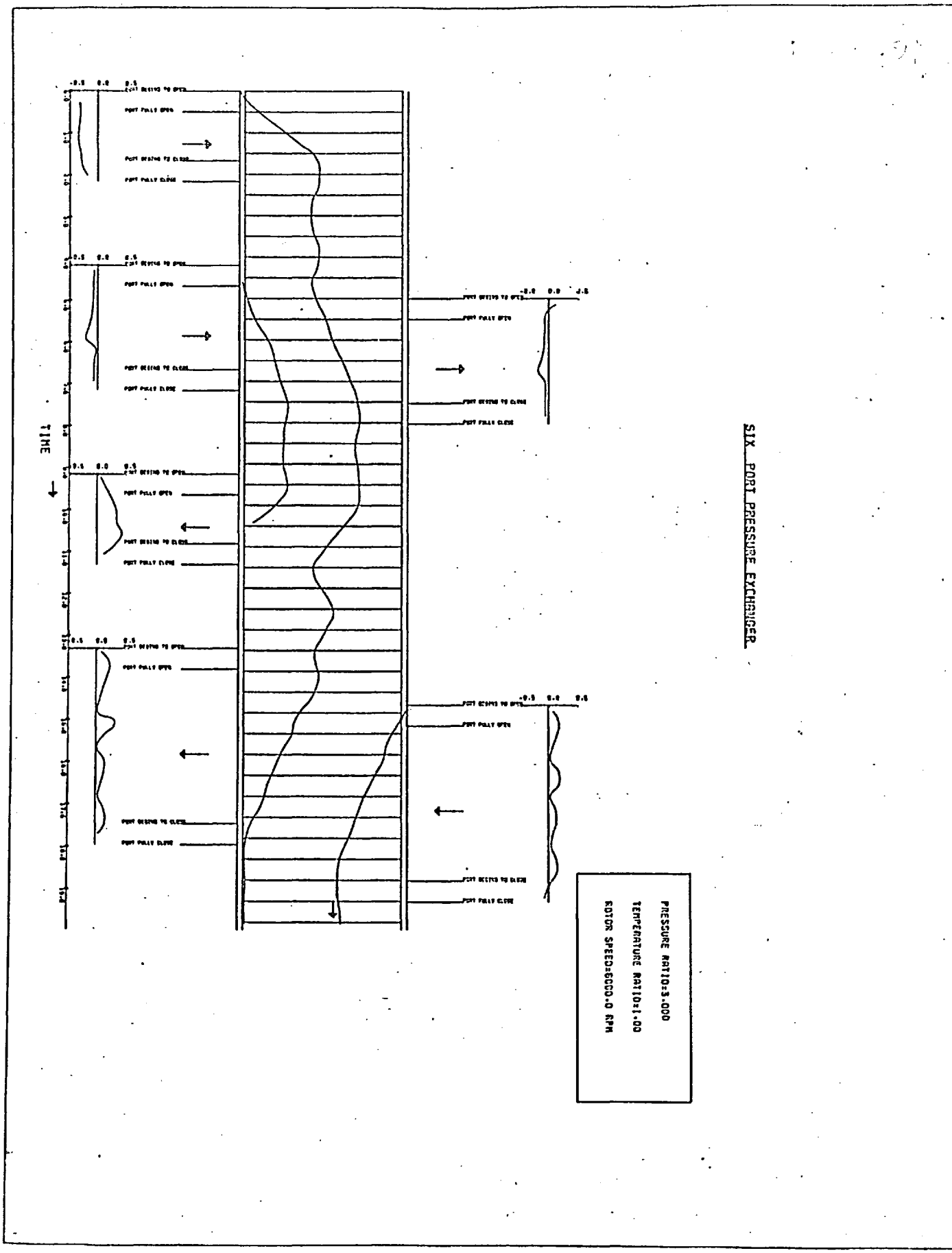
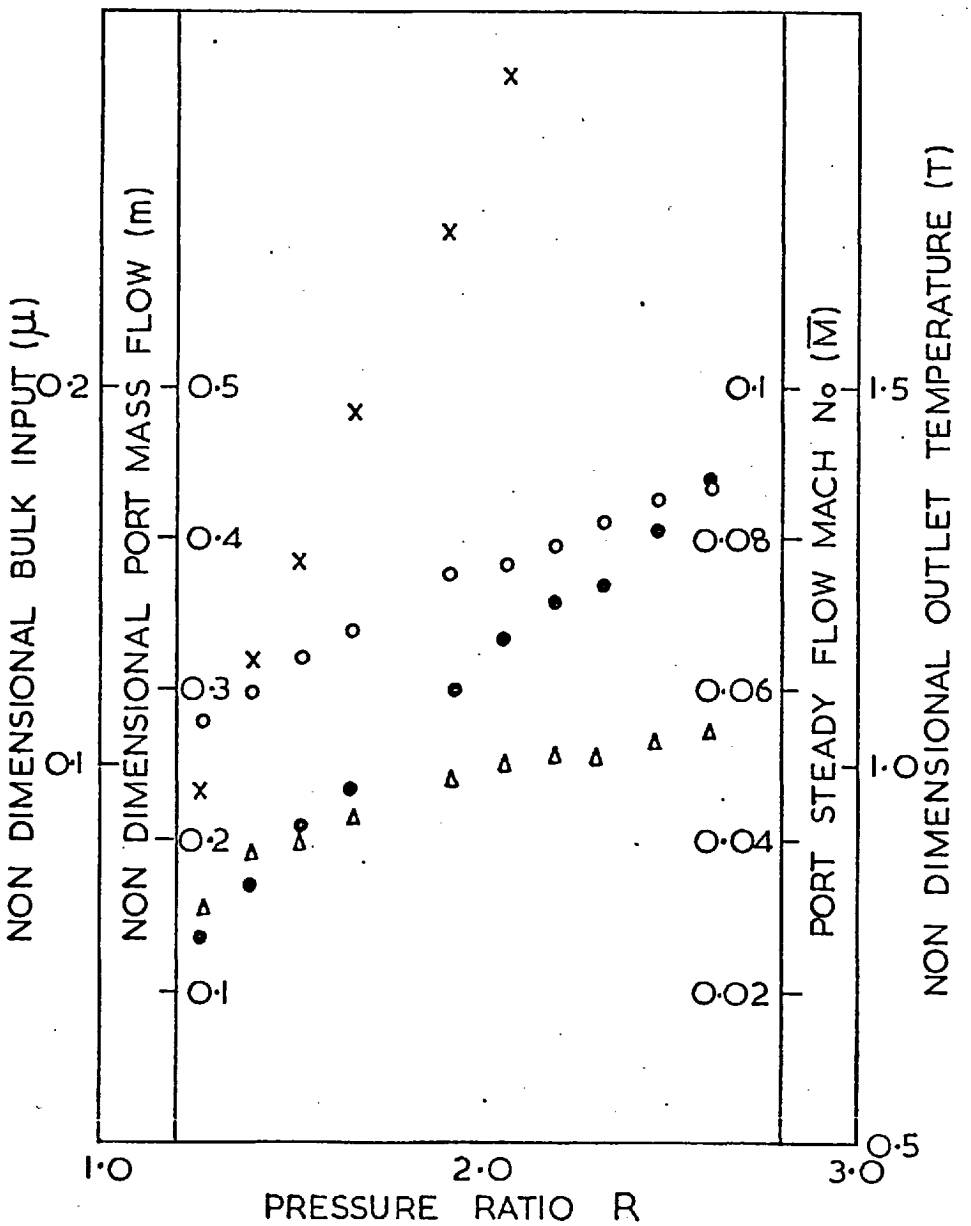

SIX PORT PRESSURE EXCHANGER
TIME
PRESSURE RATIO=3.000
TEMPERATURE RATIO=1.00
ROTOR SPEED=6000.0 RPM

FIG. 12.91

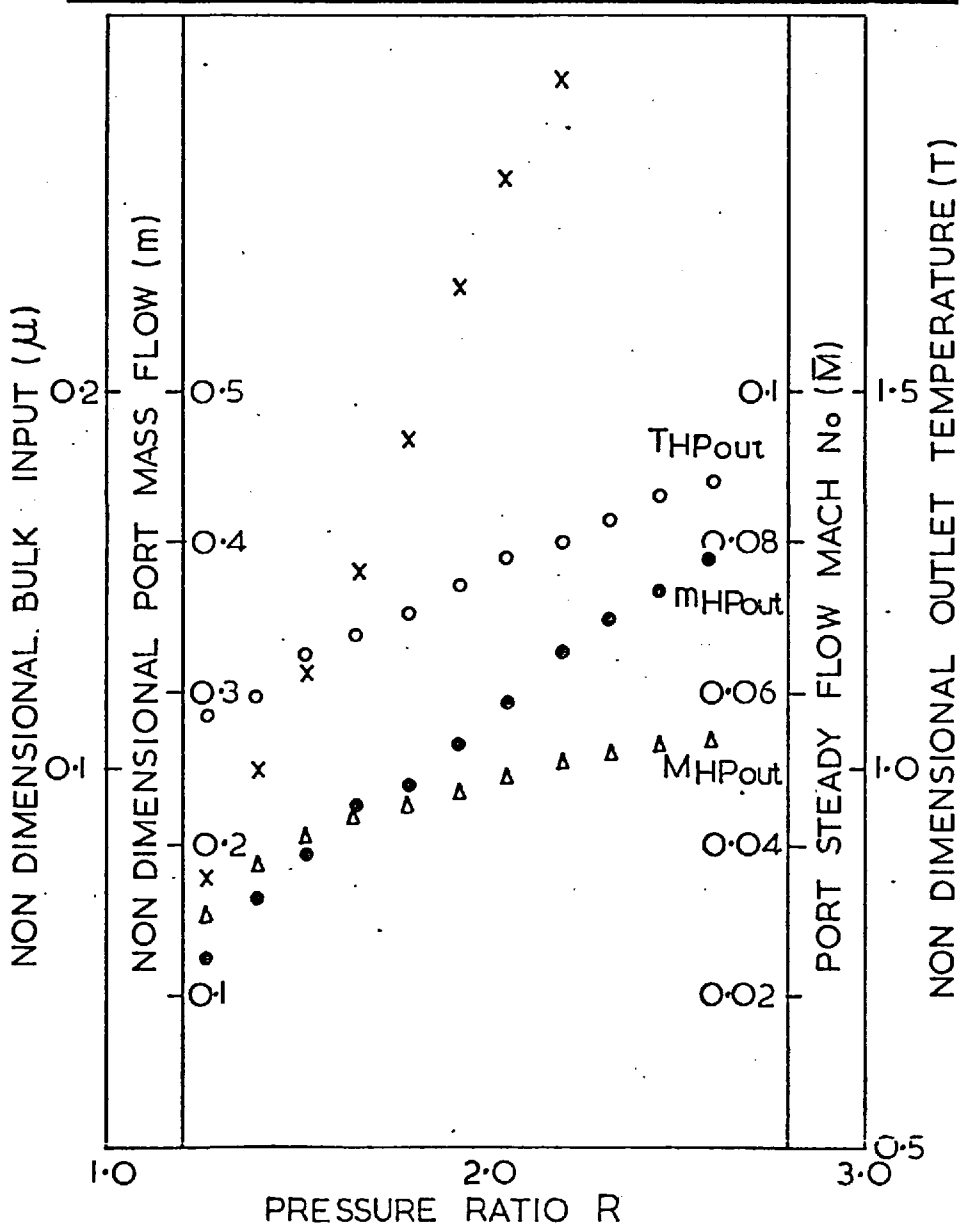
	DIMENSIONED	DIMENSIONLESS
ROTOR SPEED	5000 RPM	
τ_{HPout}	45 DEGREES	3·012
ϕ_{HP}	19·5 DEGREES	1·305
A_{HP}	1·0	
τ_{LPin}	75 DEGREES	5·021
ϕ_{LP}	29·5 DEGREES	1·975
A_{LP}	1·0	
τ_{CF}	30 DEGREES	2·008
τ_{CE}	30 DEGREES	2·008
τ_{C}	10 DEGREES	0·5972
τ_{L1}	45 DEGREES	3·012
τ_{L2}	45 DEGREES	3·012
τ_{L3}	45 DEGREES	3·012
τ_{L4}	45 DEGREES	3·012



EXPERIMENTALLY OBTAINED SIX PORT PRESSURE EXCHANGER PERFORMANCE (FIXED GEOMETRY AND CONSTANT SPEED)

FIG. 12.92

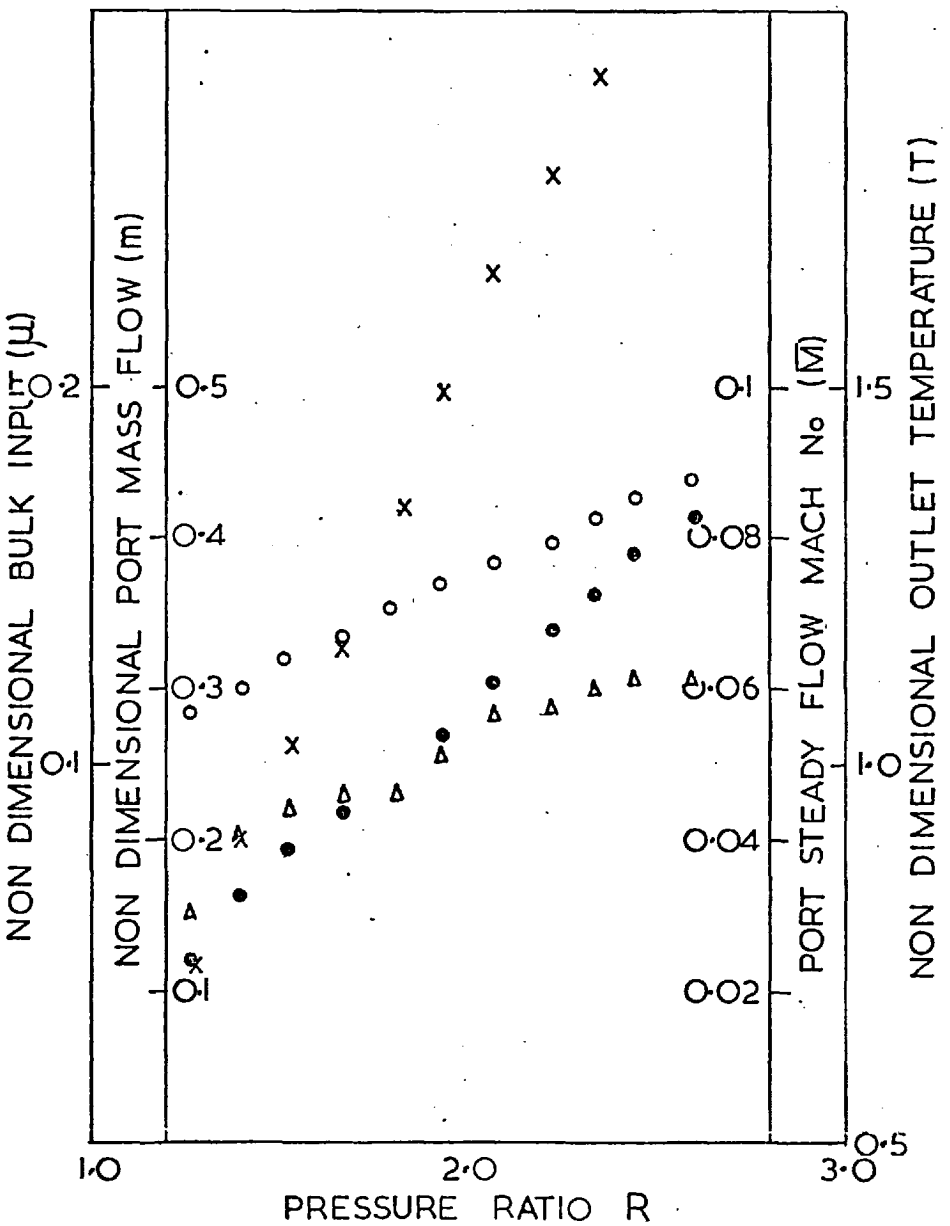
	DIMENSIONED	DIMENSIONLESS
ROTOR SPEED	5500 RPM	
τ_{HPout}	45 DEGREES	2·738
ϕ_{HP}	19·5DEGREES	1·187
A_{HP}	1·0	
τ_{LPin}	75 DEGREES	4·564
ϕ_{LP}	29·5DEGREES	1·795
A_{LP}	1·0	
τ_{CF}	30 DEGREES	1·826
τ_{CE}	30 DEGREES	1·826
τ_{C}	10 DEGREES	0·5429
τ_{L1}	45 DEGREES	2·738
τ_{L2}	45 DEGREES	2·738
τ_{L3}	45 DEGREES	2·738
τ_{L4}	45 DEGREES	2·738



EXPERIMENTALLY OBTAINED SIX PORT PRESSURE EXCHANGER PERFORMANCE (FIXED GEOMETRY AND CONSTANT SPEED)

FIG. 12.93

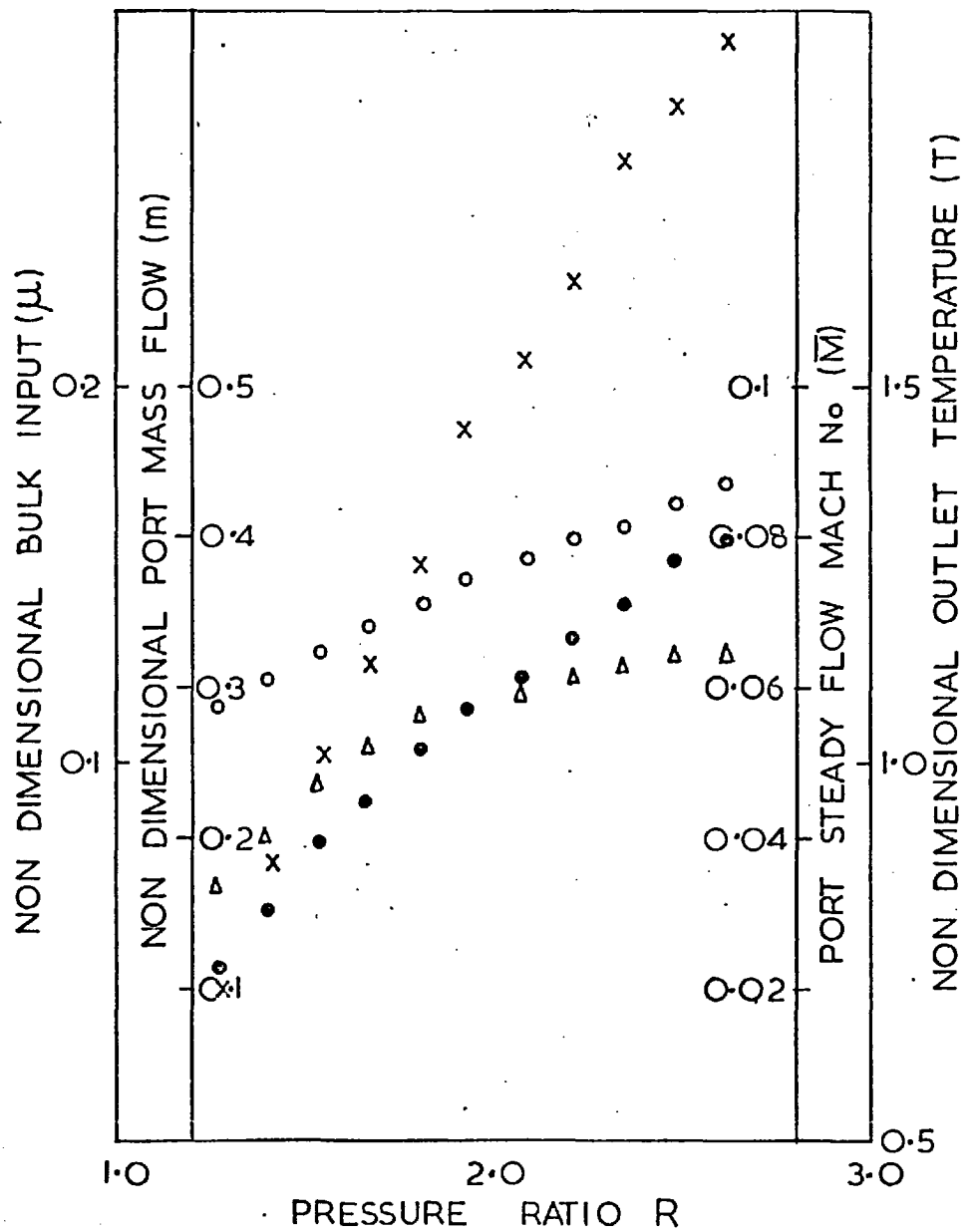
	DIMENSIONED	DIMENSIONLESS
ROTOR SPEED	6000 R P M	
τ_{HPout}	45 DEGREES	2·505
ϕ_{HP}	19·5 DEGREES	1·086
A_{HP}	1·0	
τ_{LPin}	75 DEGREES	4·175
ϕ_{LP}	29·5 DEGREES	1·642
A_{LP}	1·0	
τ_{CF}	30 DEGREES	1·670
τ_{CE}	30 DEGREES	1·670
τ_{C}	10 DEGREES	0·4967
τ_{L1}	45 DEGREES	2·505
τ_{L2}	45 DEGREES	2·505
τ_{L3}	45 DEGREES	2·505
τ_{L4}	45 DEGREES	2·505



EXPERIMENTALLY OBTAINED SIX PORT PRESSURE EXCHANGER PERFORMANCE (FIXED GEOMETRY AND CONSTANT SPEED)

FIG. 12.94

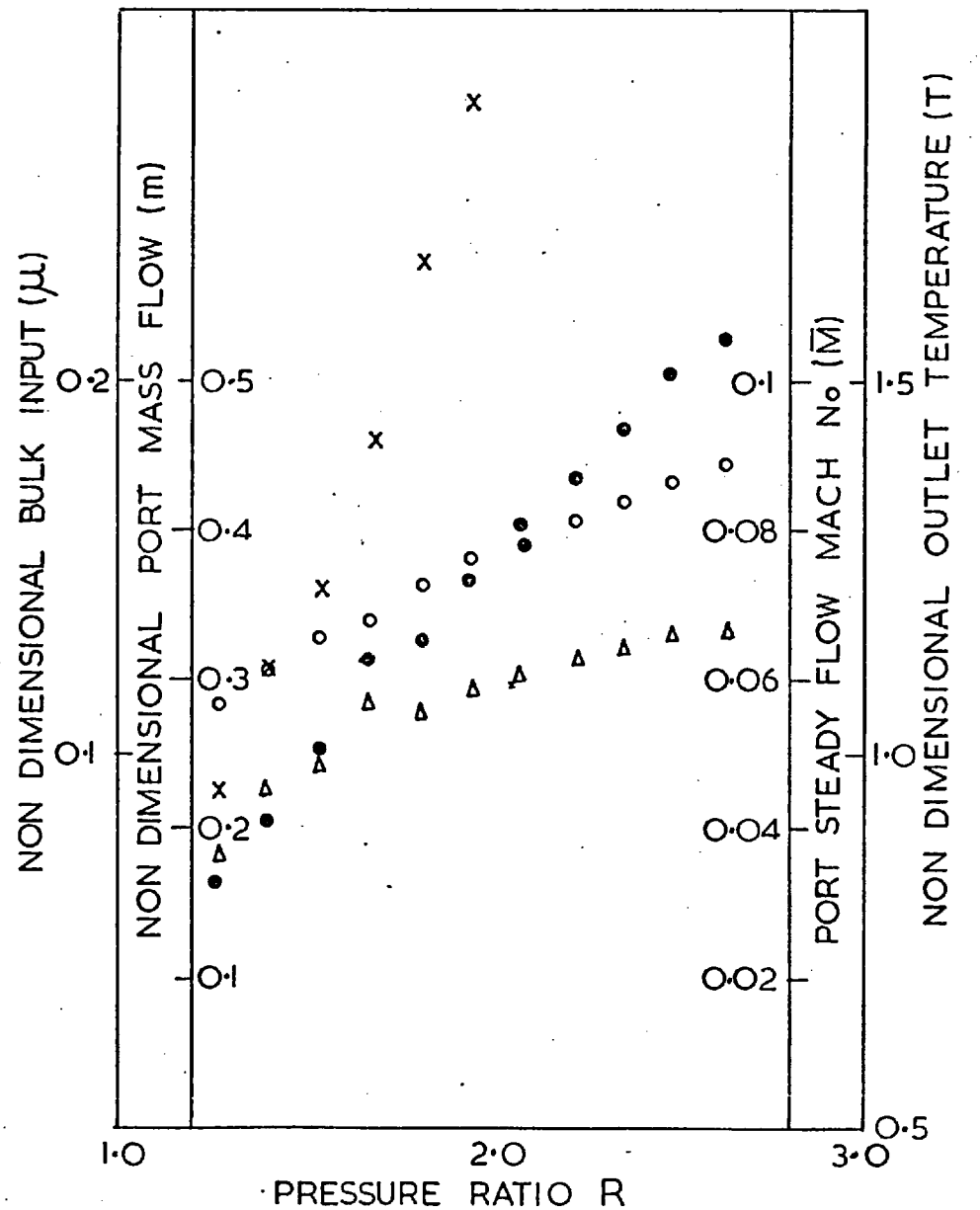
	DIMENSIONED	DIMENSIONLESS
ROTOR SPEED	6500RPM	
τ_{HPout}	45 DEGREES	2·319
ϕ_{HP}	19·5DEGREES	1·005
A_{HP}	1·0	
τ_{LPin}	75DEGREES	3·865
ϕ_{LP}	29·5DEGREES	1·520
A_{LP}	1·0	
τ_{CF}	30DEGREES	1·546
τ_{CE}	30DEGREES	1·546
τ_{C}	10DEGREES	0·4598
τ_{L1}	45DEGREES	2·319
τ_{L2}	45DEGREES	2·319
τ_{L3}	45 DEGREES	2·319
τ_{L4}	45 DEGREES	2·319



EXPERIMENTALLY OBTAINED SIX PORT PRESSURE EXCHANGER PERFORMANCE (FIXED GEOMETRY AND CONSTANT SPEED)

FIG. 12.95

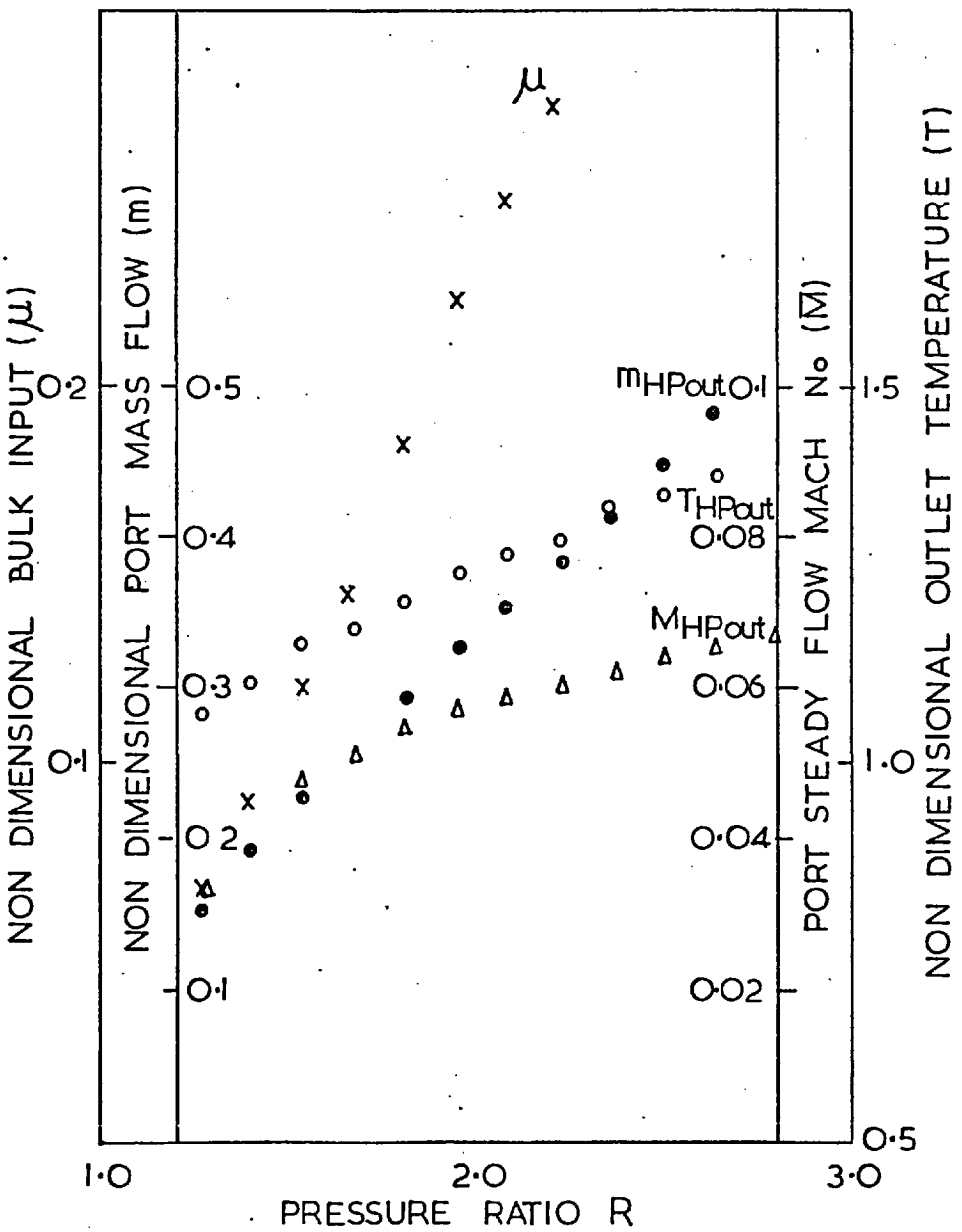
	DIMENSIONED	DIMENSIONLESS
ROTOR SPEED	5000 R P M	
τ_{HPout}	45 DEGREES	3·006
ϕ_{HP}	16·5 DEGREES	1·102
A_{HP}	1·0	
τ_{LPin}	75 DEGREES	5·010
ϕ_{LP}	26·5 DEGREES	1·770
A_{LP}	1·0	
τ_{CF}	30 DEGREES	2·004
τ_{CE}	30 DEGREES	2·004
τ_{C}	10 DEGREES.	0·5960
τ_{L1}	45 DEGREES	3·006
τ_{L2}	45 DEGREES	3·006
τ_{L3}	45 DEGREES	3·006
τ_{L4}	45 DEGREES	3·006



EXPERIMENTALLY OBTAINED SIX PORT PRESSURE EXCHANGER PERFORMANCE (FIXED GEOMETRY AND CONSTANT SPEED)

FIG. 12.96

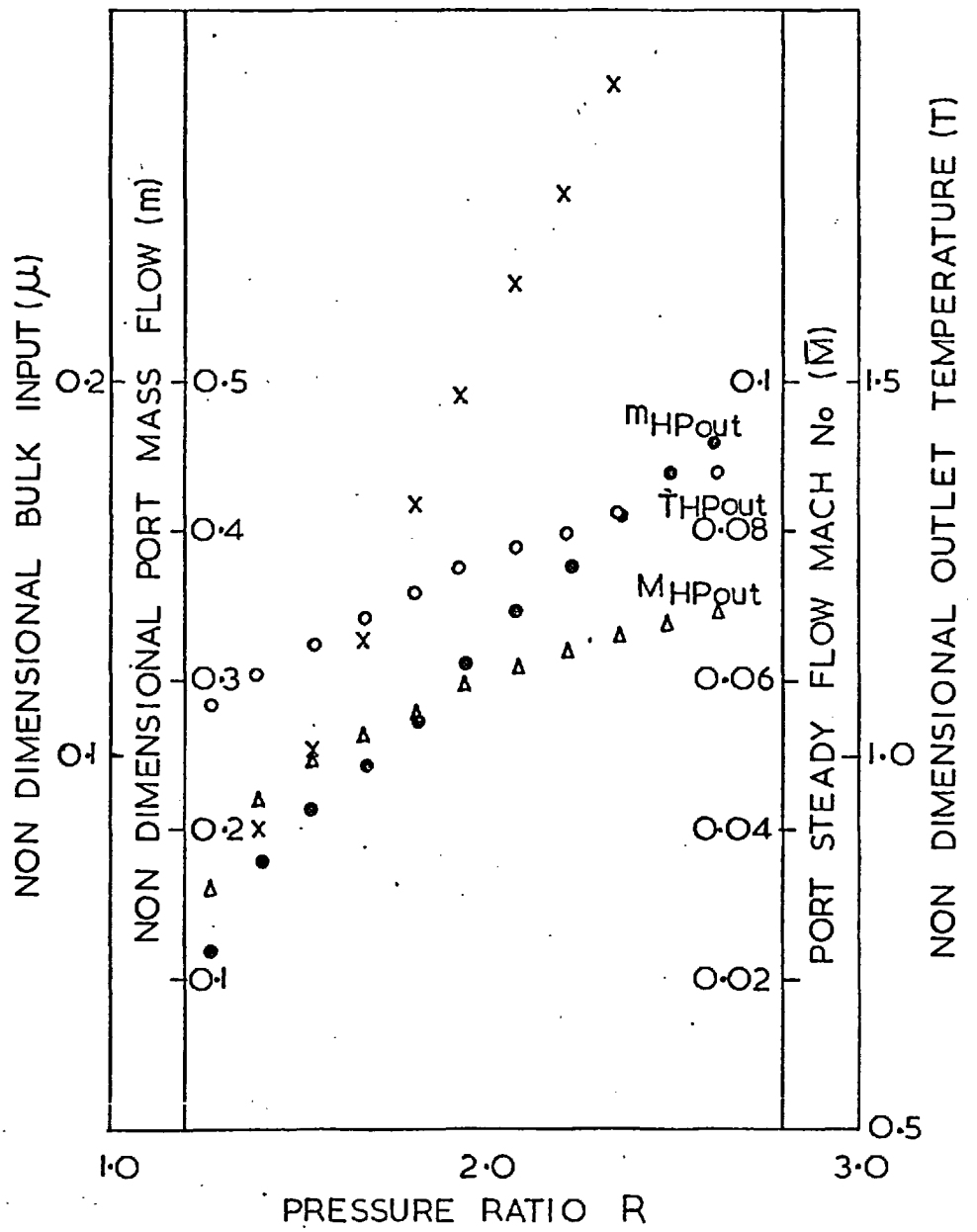
	DIMENSIONED	DIMENSIONLESS
ROTOR SPEED	5500RPM	
τ_{HPout}	45 DEGREES	2·733
ϕ_{HP}	16·5 DEGREES	1·002
A_{HP}	1·0	
τ_{LPin}	75DEGREES	4·555
ϕ_{LP}	26·5DEGREES	1·609
A_{LP}	1·0	
τ_{CF}	30DEGREES	1·822
τ_{CE}	30DEGREES	1·822
τ_{C}	10DEGREES	0·5418
τ_{L1}	45 DEGREES	2·733
τ_{L2}	45 DEGREES	2·733
τ_{L3}	45 DEGREES	2·733
τ_{L4}	45 DEGREES	2·733



EXPERIMENTALLY OBTAINED SIX PORT PRESSURE EXCHANGER PERFORMANCE (FIXED GEOMETRY AND CONSTANT SPEED)

FIG. 12.97

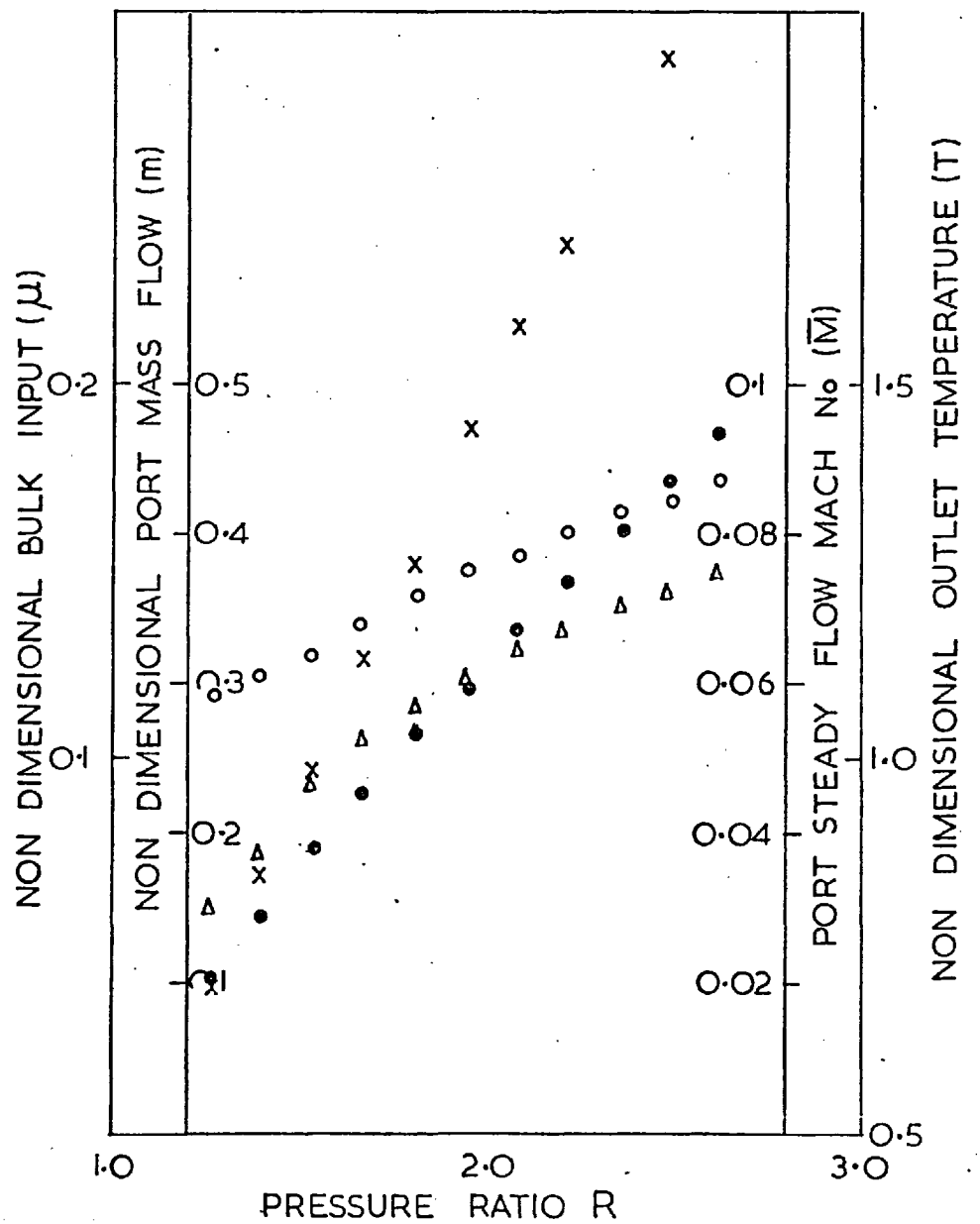
	DIMENSIONED	DIMENSIONLESS
ROTOR SPEED	6000 R P M	
τ_{HPout}	45 DEGREES	2·507
ϕ_{HP}	16·5 DEGREES	0·9192
A_{HP}	1·0	
τ_{LPin}	75 DEGREES	4·1780
ϕ_{LP}	26·5 DEGREES	1·476
A_{LP}	1·0	
τ_{CF}	30 DEGREES	1·671
τ_{CE}	30 DEGREES	1·671
τ_{C}	10 DEGREES	0·4970
τ_{L1}	45 DEGREES	2·507
τ_{L2}	45 DEGREES	2·507
τ_{L3}	45 DEGREES	2·507
τ_{L4}	45 DEGREES	2·507



EXPERIMENTALLY OBTAINED SIX PORT PRESSURE EXCHANGER PERFORMANCE (FIXED GEOMETRY AND CONSTANT SPEED)

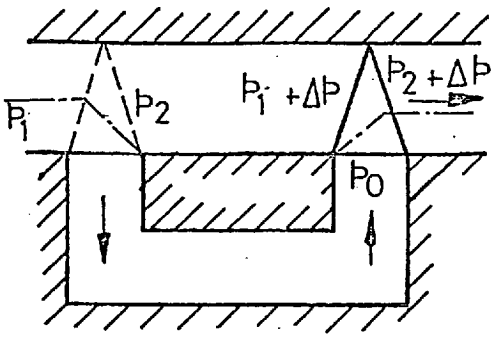
FIG. 12.98

	DIMENSIONED	DIMENSIONLESS
ROTOR SPEED	6500 RPM	
τ_{HPout}	45 DEGREES	2·327
ϕ_{HP}	16·5 DEGREES	0·8532
A_{HP}	1·0	
τ_{LPin}	75 DEGREES	3·878
ϕ_{LP}	26·5 DEGREES	1·370
A_{LP}	1·0	
τ_{CF}	30 DEGREES	1·551
τ_{CE}	30 DEGREES	1·551
τ_{C}	10 DEGREES	0·4613
τ_{L1}	45 DEGREES	2·327
τ_{L2}	45 DEGREES	2·327
τ_{L3}	45 DEGREES	2·327
τ_{L4}	45 DEGREES	2·327



EXPERIMENTALLY OBTAINED SIX PORT PRESSURE EXCHANGER PERFORMANCE (FIXED GEOMETRY AND CONSTANT SPEED)

FIG. 12.99



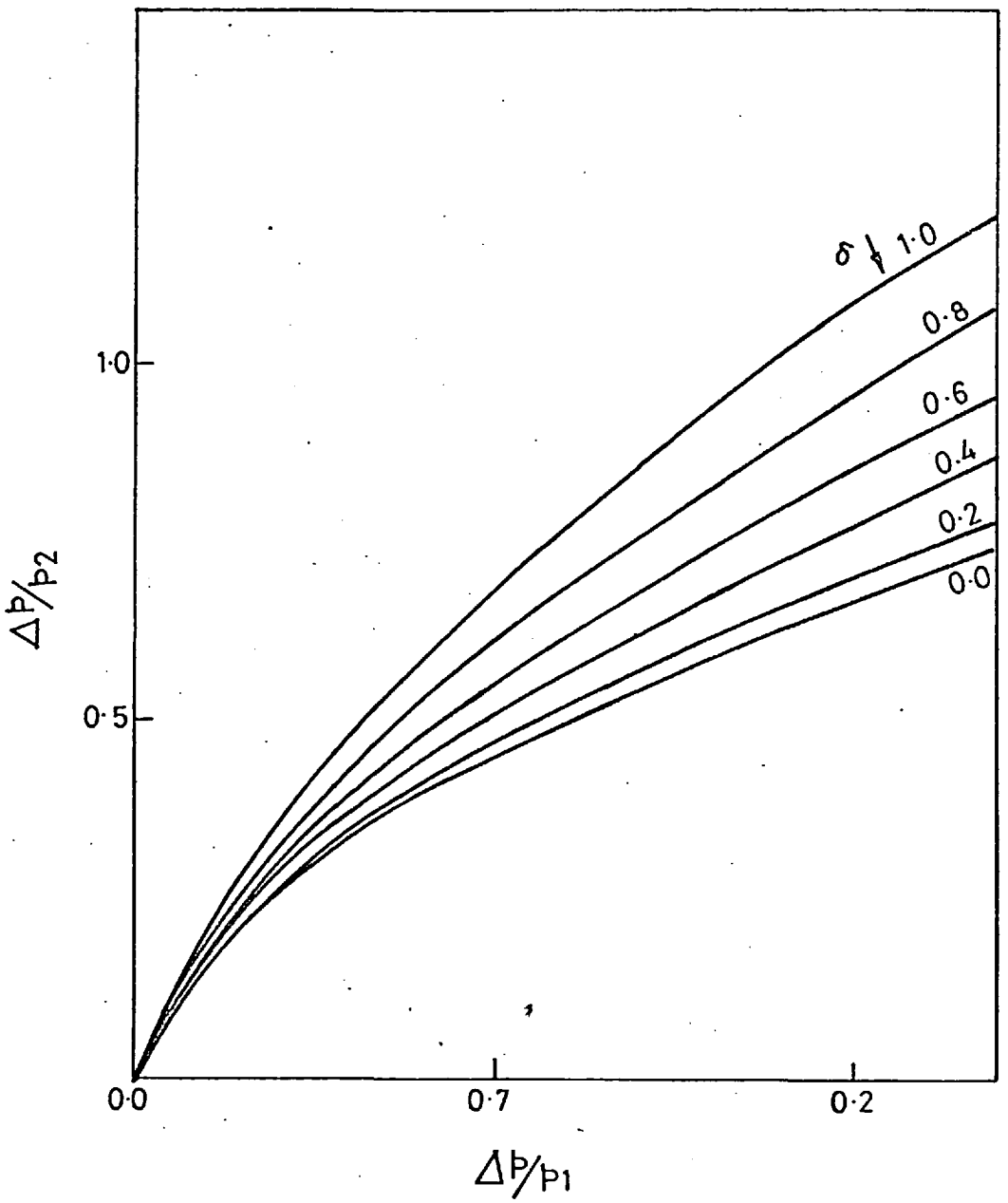


FIG. 12.100 TRANSFER CHARACTERISTICS

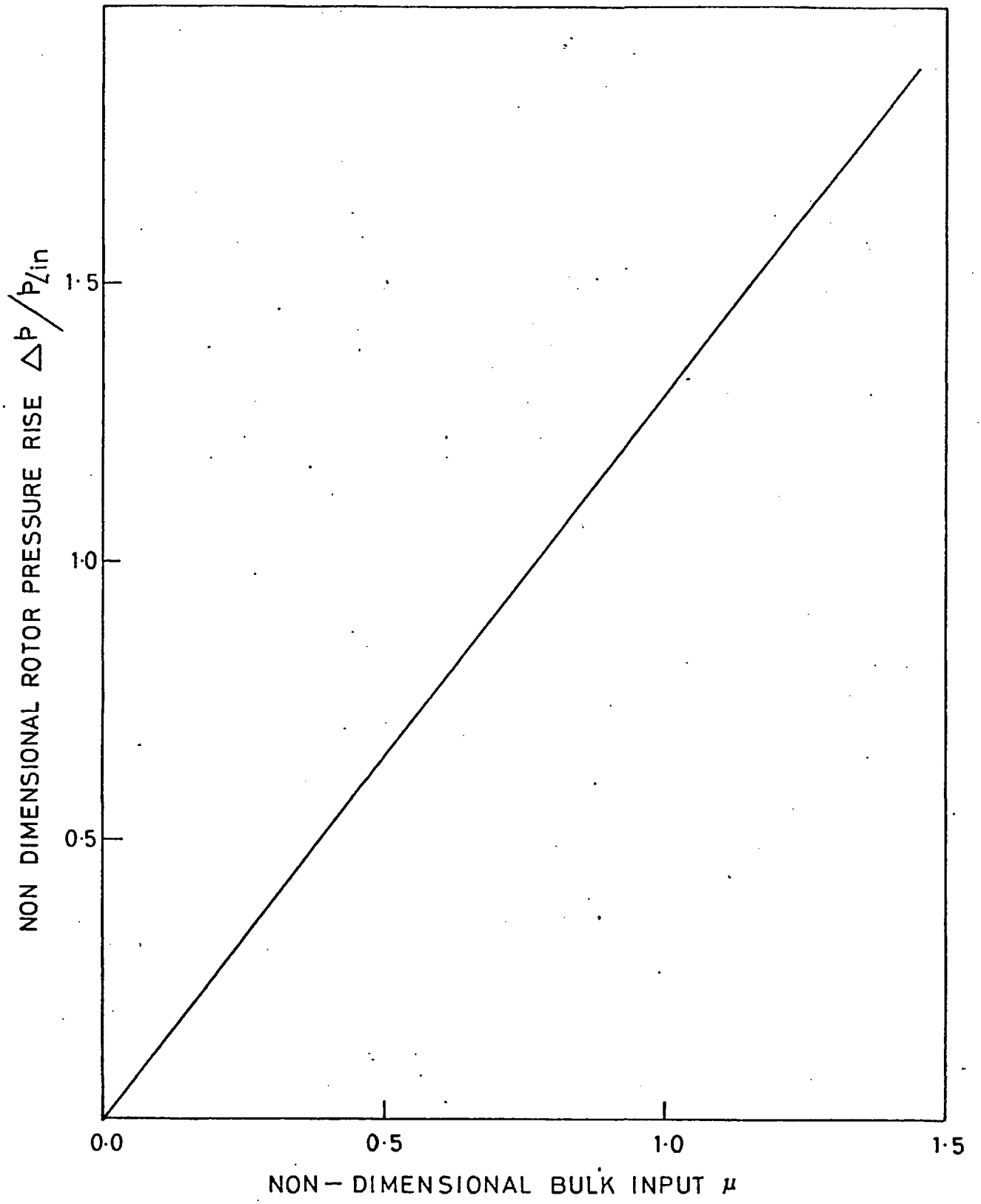


FIG. 12.101 BULK INPUT – ROTOR PRESSURE RISE RELATIONSHIP

CHAPTER 13

DIAGRAMS AND ILLUSTRATIONS

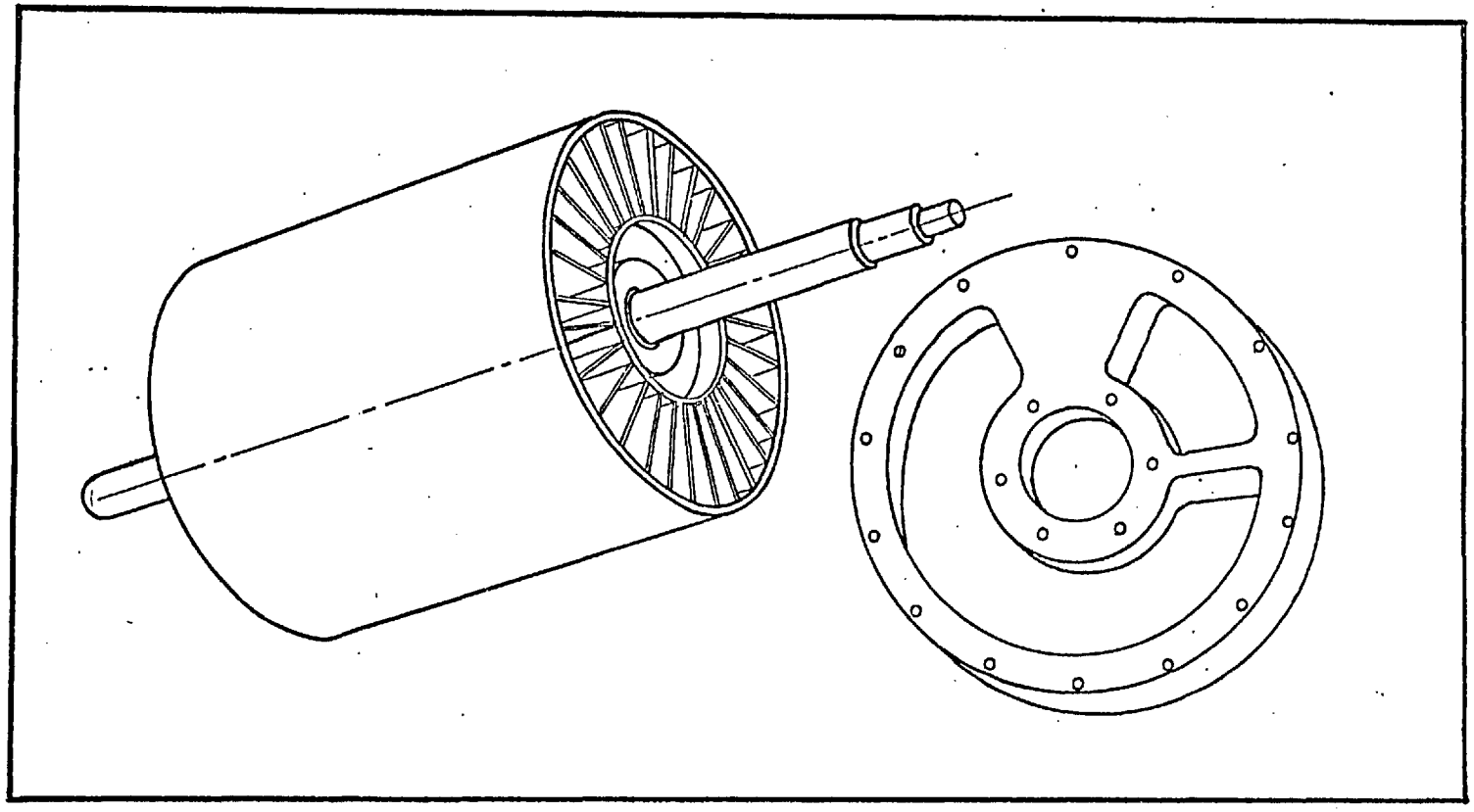


FIG. 13.1 PRESSURE EXCHANGER ROTOR AND END PLATE

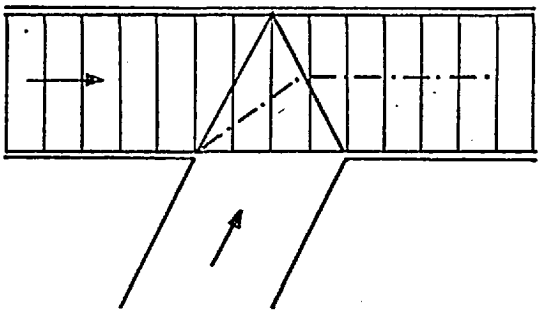


FIG. 13.2 CELL FILLING PROCESS

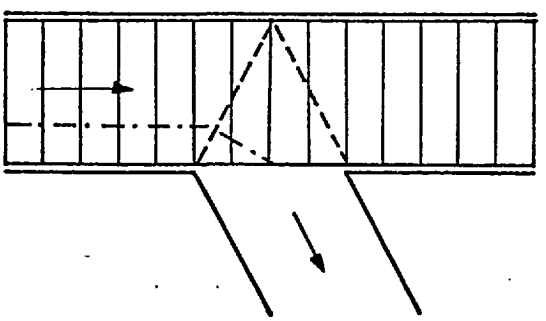


FIG. 13.3 CELL EMPTYING PROCESS

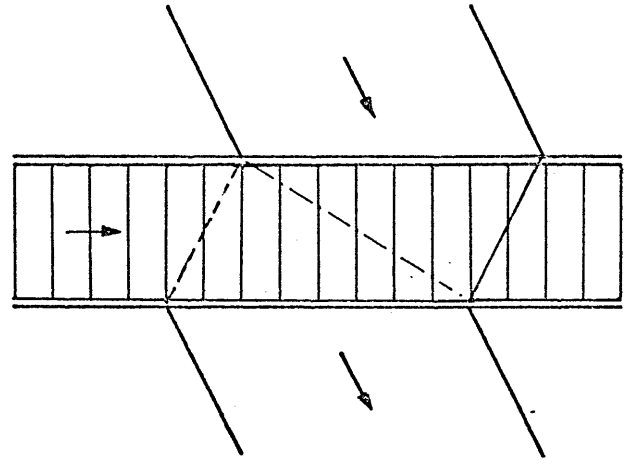


FIG.13.4 LP SCAVENGE PROCESS

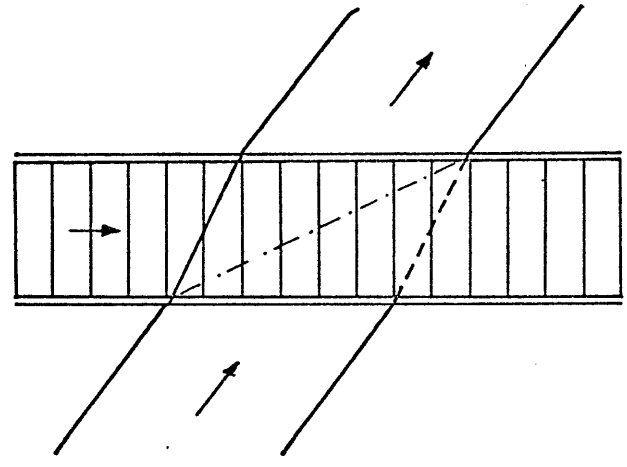


FIG. 13.5 HP SCAVENGE PROCESS

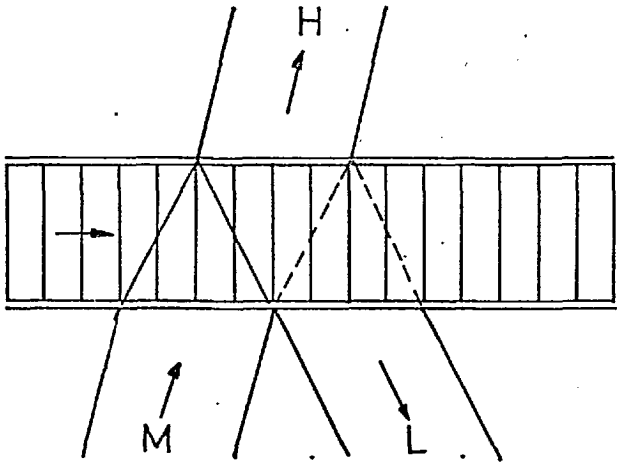


FIG. 13.6 PRESSURE DIVIDER

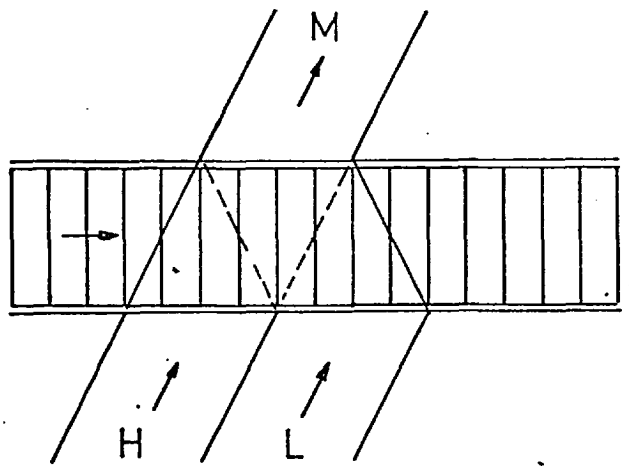


FIG. 13.7 PRESSURE EQUALISER

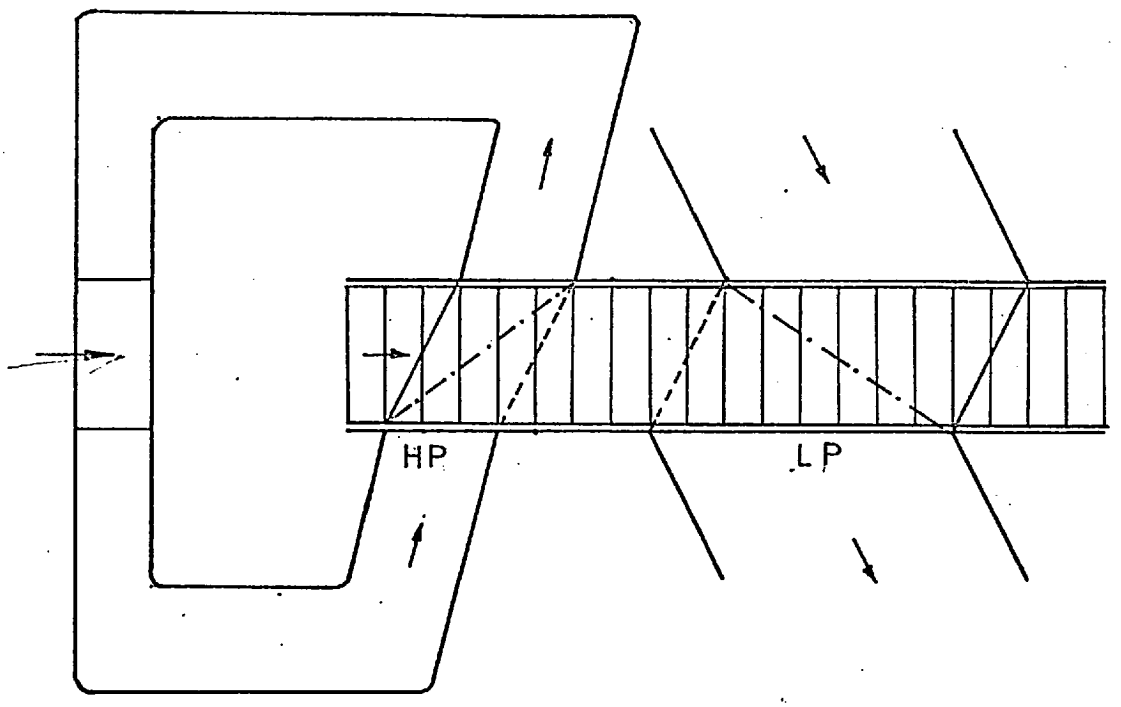


FIG. 13.8 FOUR-PORT PRESSURE EXCHANGER WITH EXTERNAL ENERGY SUPPLY

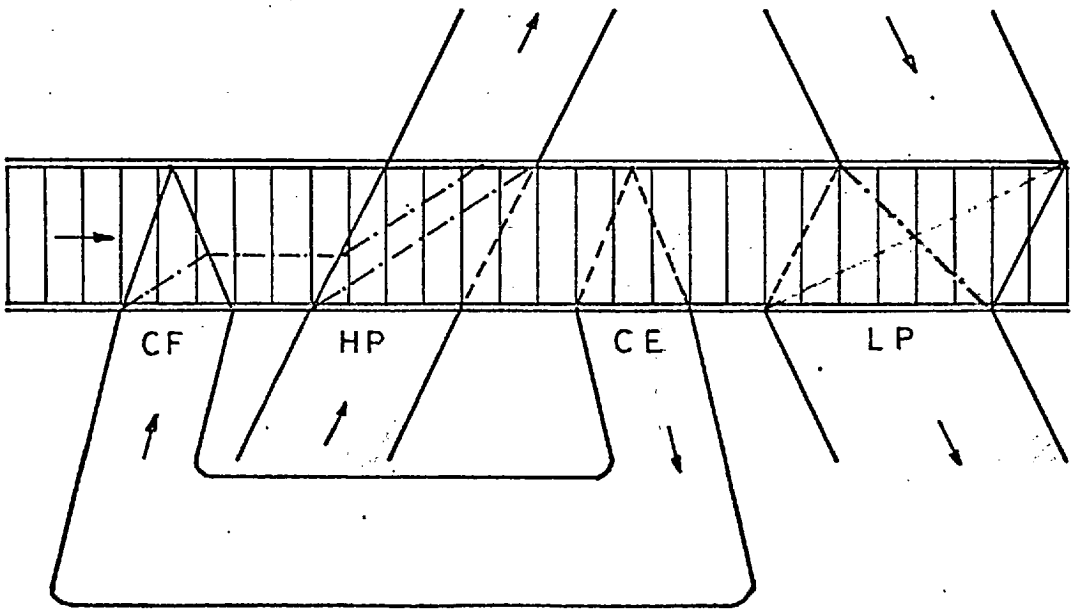
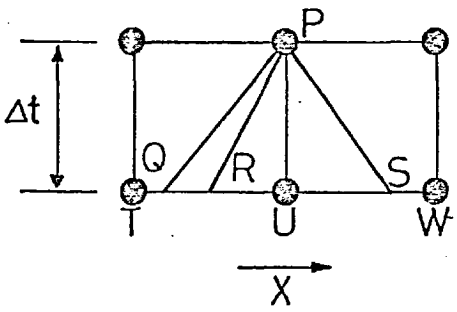


FIG. 13.9 SIX-PORT PRESSURE EXCHANGER



RP= Particle path
QP= "n" Characterstic
SP= "m" Characterstic

FIG.13.10 Central region

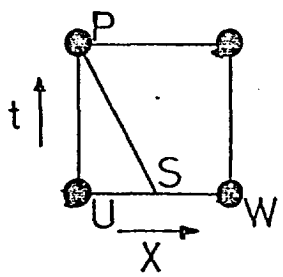


FIG.13.11 Inflow at left-hand boundary

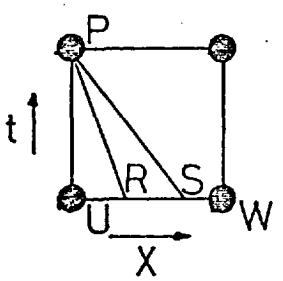


FIG. 13.12 Outflow at left-hand boundary

ILLUSTRATION OF THE POINTS WHICH MUST BE CONSIDERED DURING A FORWARD STEP

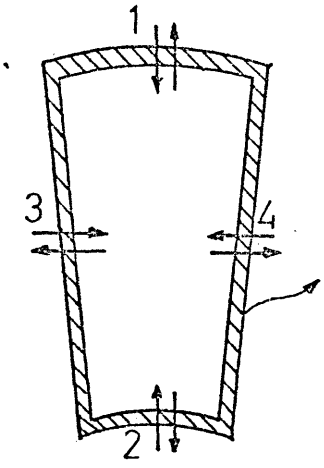
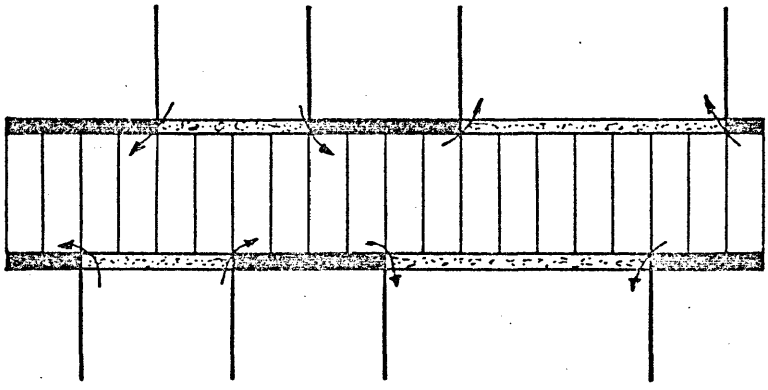


FIG. 13.13 1&2 RADIAL LEAKAGE

3&4 CIRCUMFERENTIAL LEAKAGE



Radial leakage from port to leakage sink, and vice versa.

Radial leakage from cell to leakage sink, and vice versa.

Circumferential leakage from cell to port, and vice versa.

FIG. 13.13 LEAKAGE IN PRESSURE EXCHANGERS

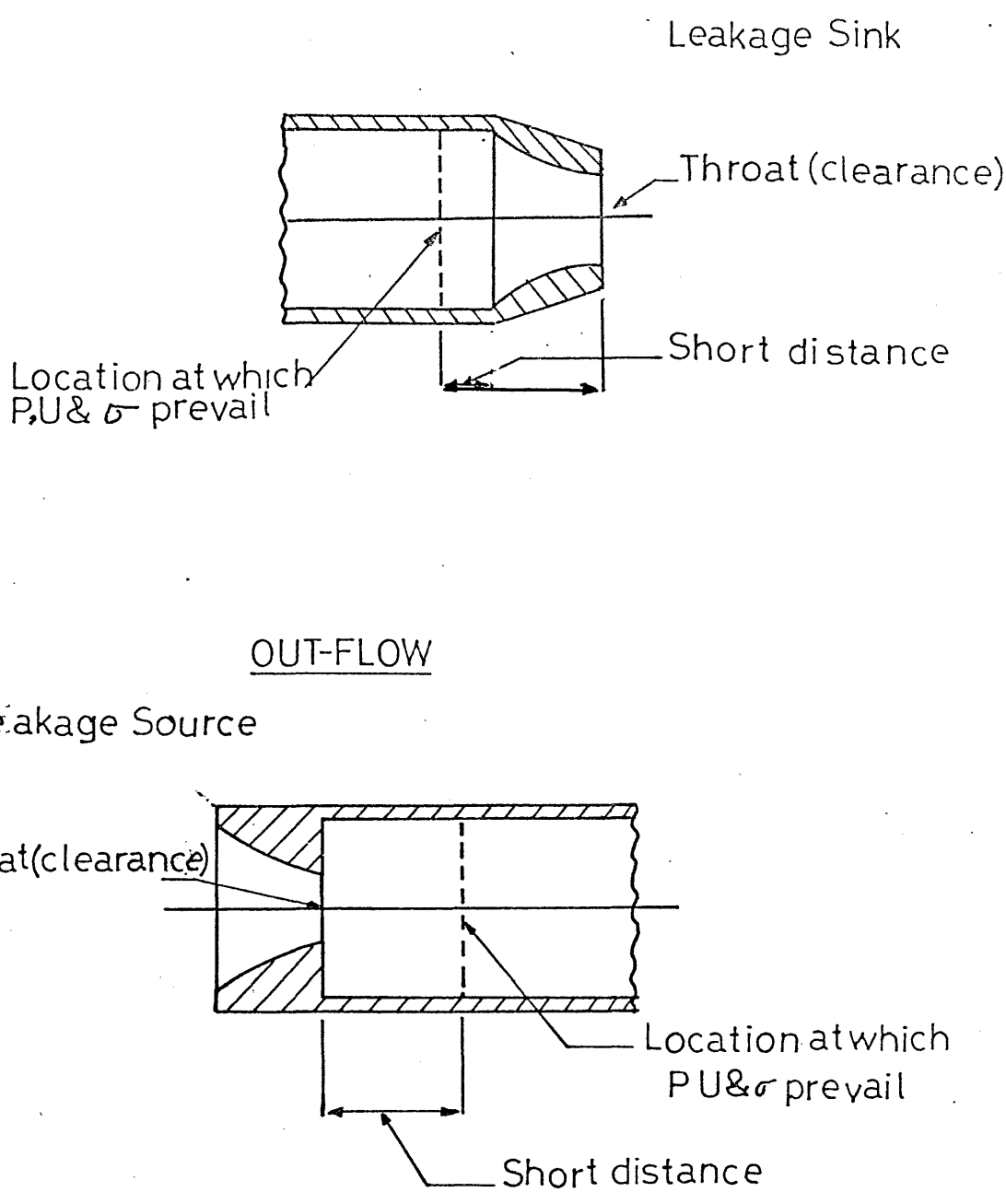


FIG. 13.14 ILLUSTRATION OF THE PARTLY OPEN END METHOD FOR LEAKAGE CALCULATIONS

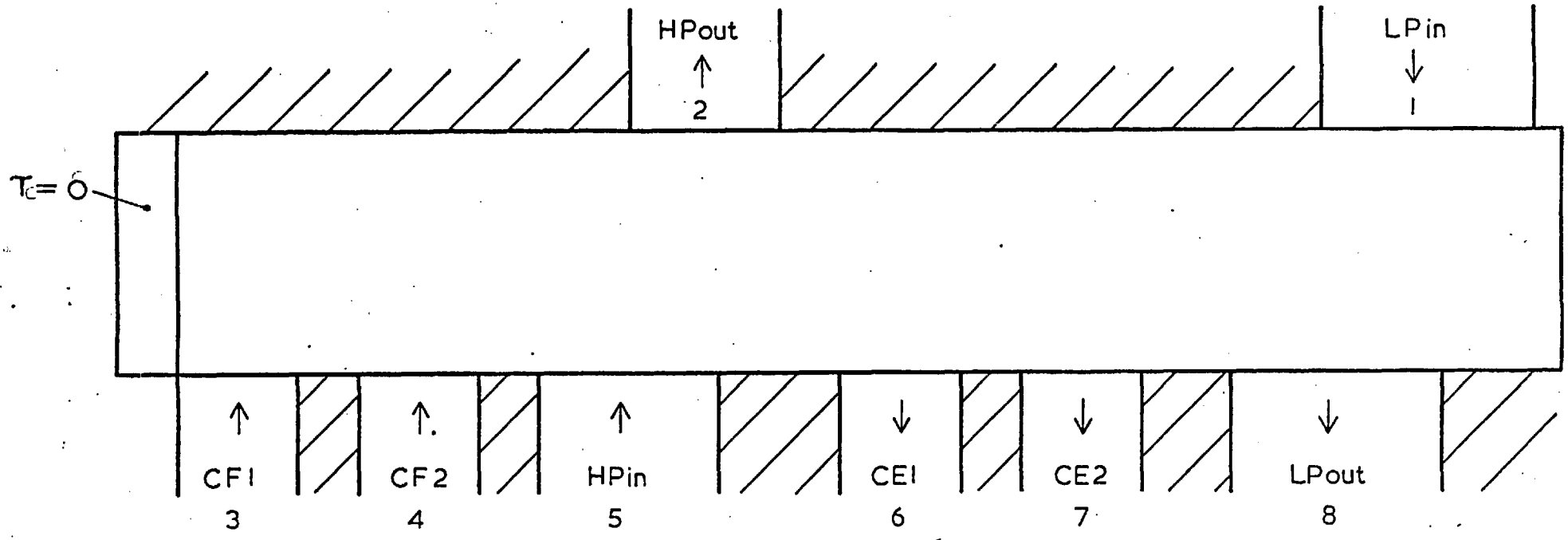


FIG. 13.15 FOUR PORT PRESSURE EXCHANGER WITH TWO TRANSFER PASSAGE DESIGN PROCEDURE

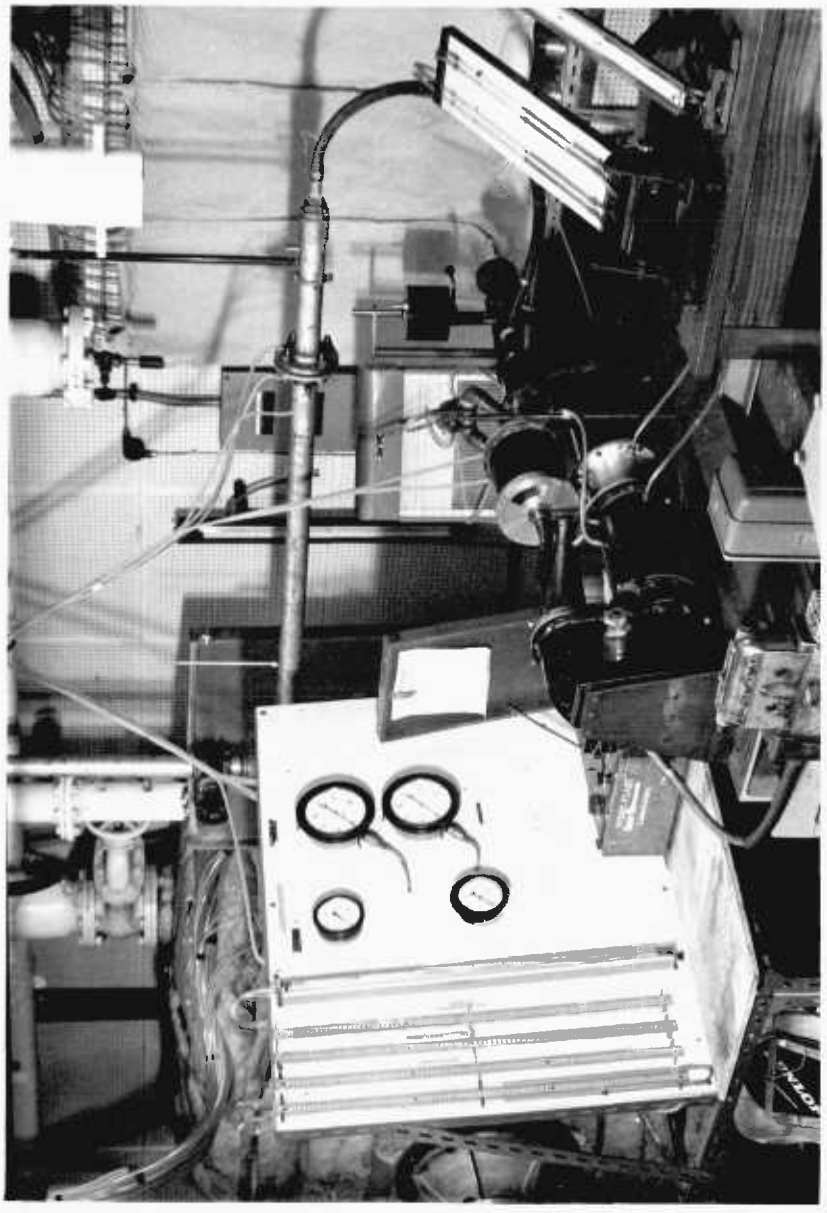


FIG. 13.16 PRESSURE EXCHANGER TEST RIG

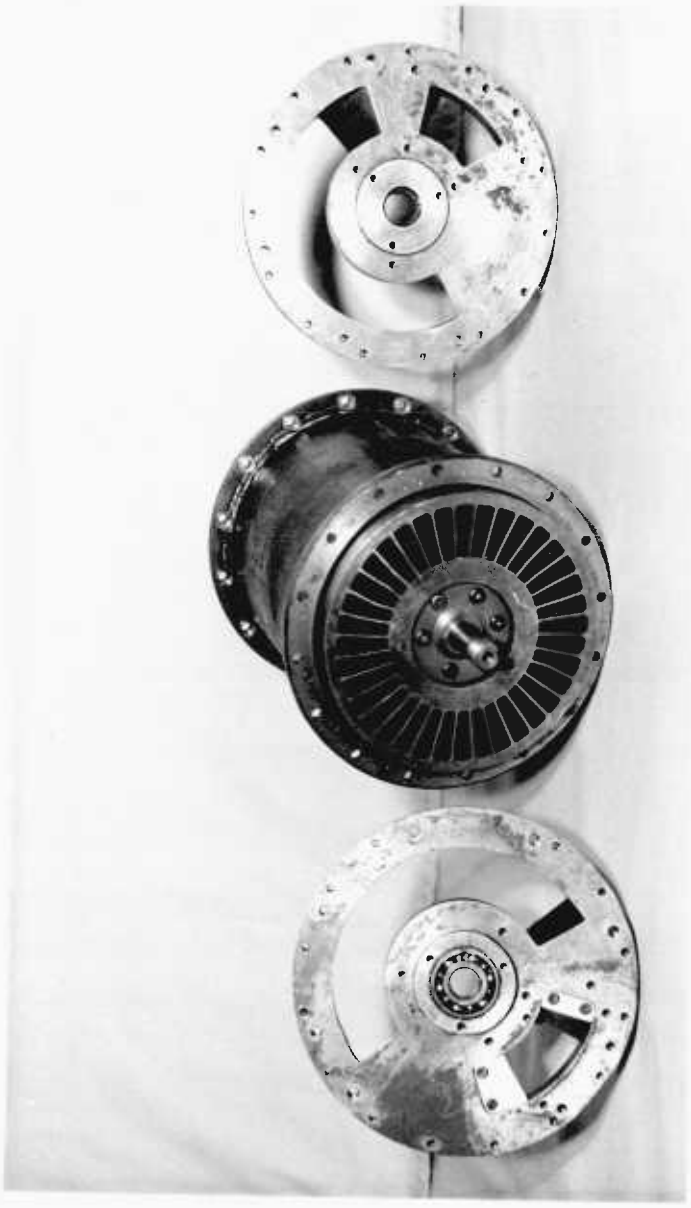


FIG. 13.17 PRESSURE EXCHANGER ROTOR & END PLATES

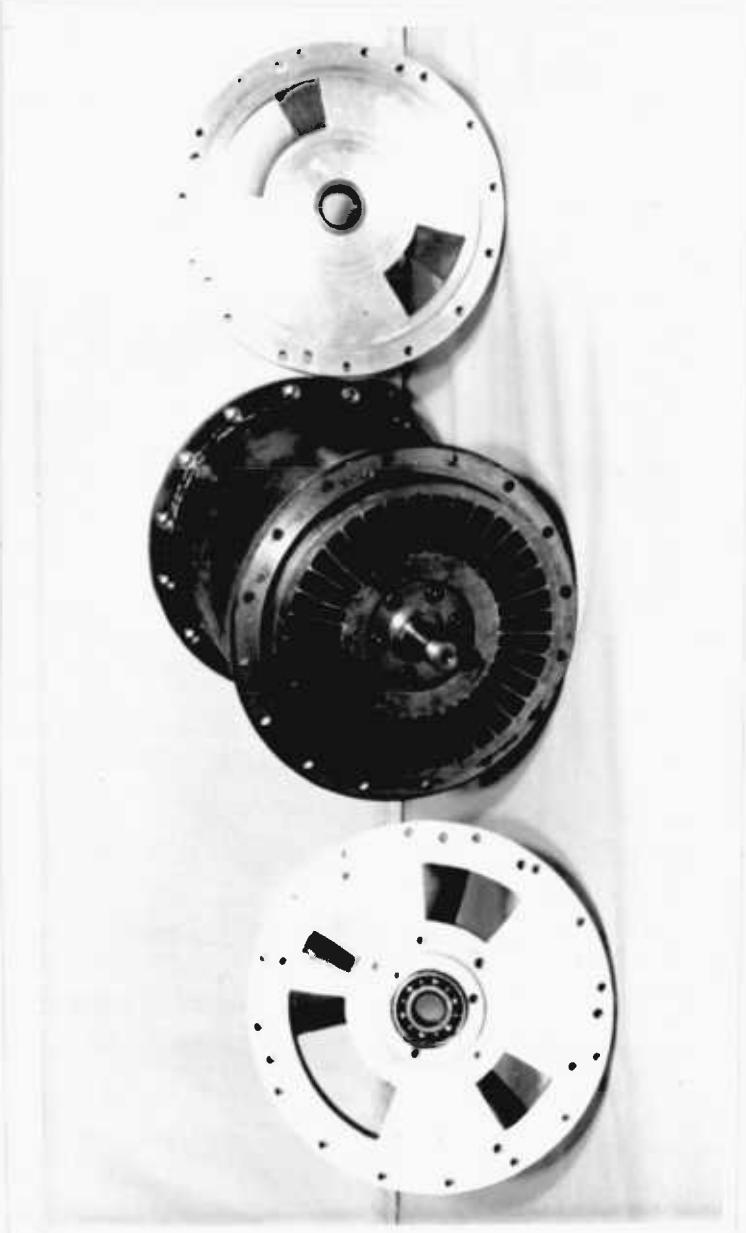


FIG. 13.18 PRESSURE EXCHANGER ROTOR & END PLATES WITH TRANSFER PORTS

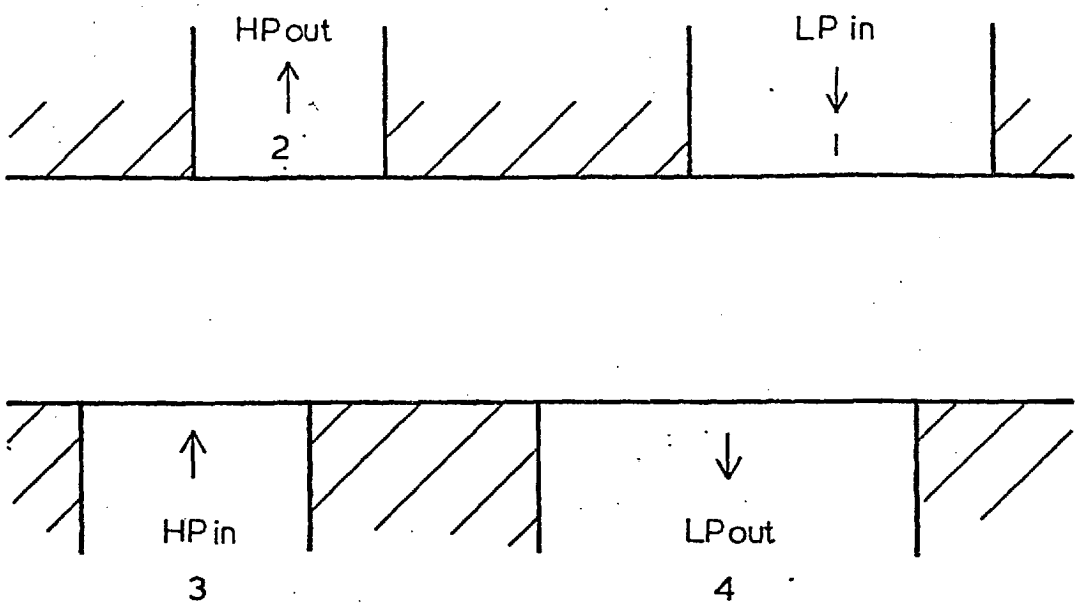


FIG. 13.19 FOUR PORT PRESSURE EXCHANGER CYCLE FOR OPTIMISATION STUDIES

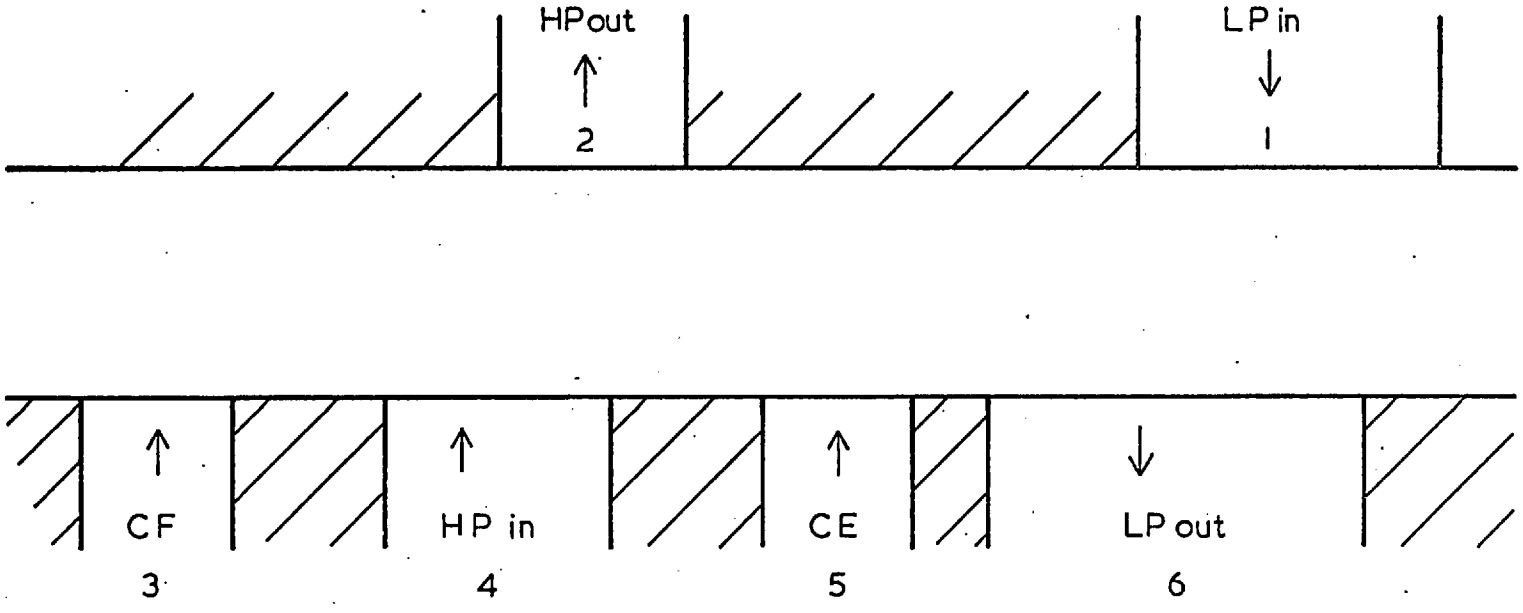
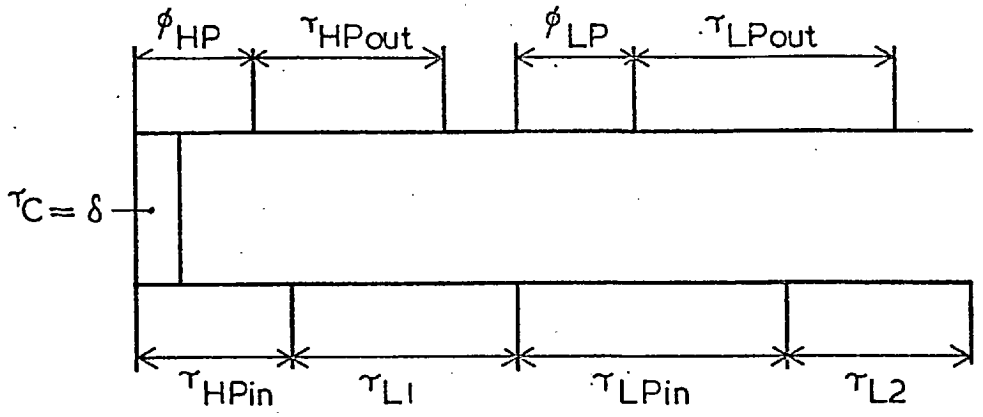
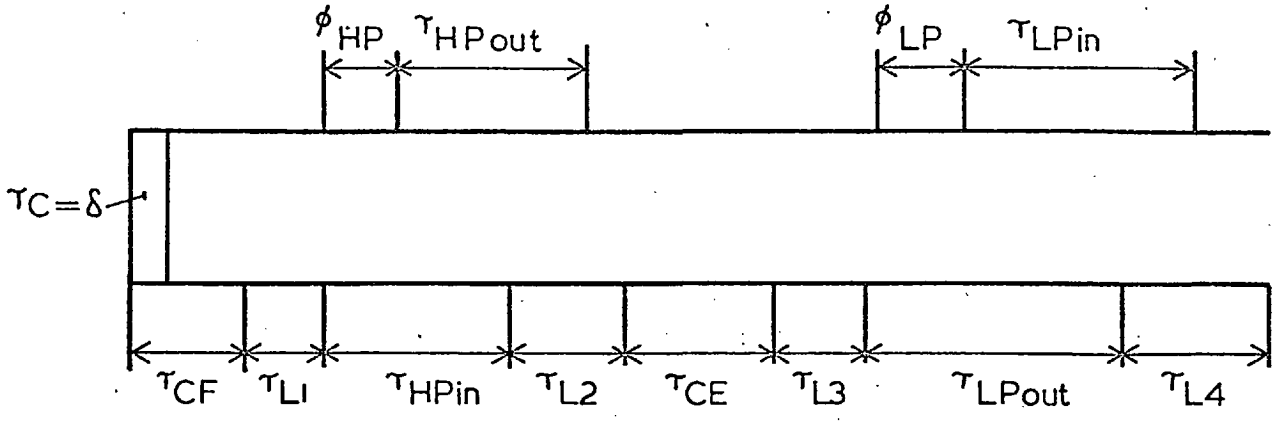


FIG. 13.20 FOUR PORT PRESSURE EXCHANGER WITH ONE TRANSFER PASSAGE. CHOSEN FOR OPTIMISATION STUDIES



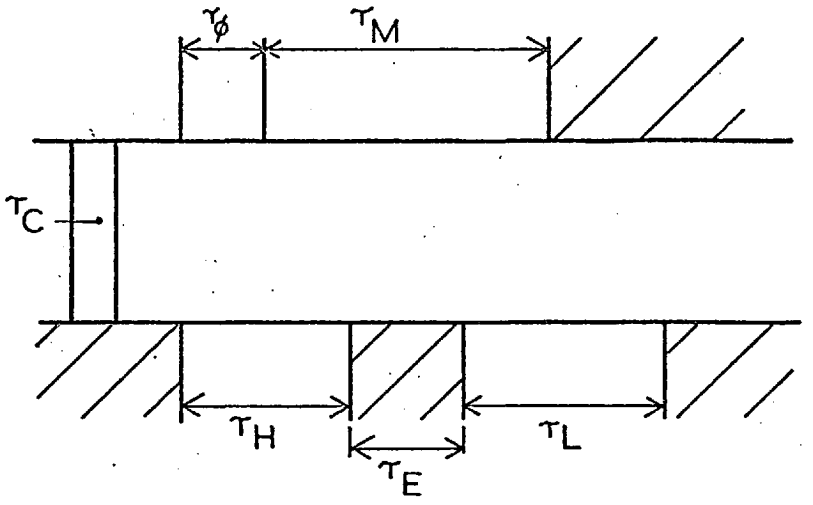
	DIMENSIONED	DIMENSIONLESS
ROTOR SPEED	6000RPM	
τ_{HPout}	45 DEGREES	2·507
ϕ_{HP}	14·3 DEGREES	0·7977
A_{HP}	1·0	
τ_{LPin}	193 DEGREES	10·77
ϕ_{LP}	24·3 DEGREES	1·356
A_{LP}	1·03	
τ_C	10 DEGREES	0·4970
τ_{L1}	50 DEGREES	2·70
τ_{L2}	65 DEGREES	3·620

FIG. 13.21 GEOMETRY AND SPEED OF THE FOUR PORT PRESSURE EXCHANGER CHOSEN FOR LOSSES STUDIES



	DIMENSIONED	DIMENSIONLESS
ROTOR SPEED	6000 R P M	
τ_{HPout}	45 DEGREES	2·507
ϕ_{HP}	13·5 DEGREES	0·755
A_{HP}	1·0	
τ_{LPin}	75 DEGREES	4·1780
ϕ_{LP}	23·5 DEGREES	1·31
A_{LP}	1·0	
τ_{CF}	30 DEGREES	1·671
τ_{CE}	30 DEGREES	1·671
τ_C	10 DEGREES	0·4970
τ_{L1}	45 DEGREES	2·507
τ_{L2}	45 DEGREES	2·507
τ_{L3}	45 DEGREES	2·507
τ_{L4}	45 DEGREES	2·507

FIG. 13.22 GEOMETRY AND SPEED OF SIX PORT PRESSURE EXCHANGER CHOSEN FOR LOSSES STUDIES



ROTOR SPEED AND GEOMETRIC DATA		
	DIMENSIONED	DIMENSIONLESS
ROTOR SPEED	5500 RPM	$M_{RO}=0\cdot1346$
HP PORT WIDTH	47°	$\tau_H = 1\cdot79$
LP PORT WIDTH	43°	$\tau_L = 1\cdot63$
MP PORT WIDTH	48°	$\tau_M = 1\cdot83$
PHASING	24°	$\tau_\phi = 0\cdot91$
LAND WIDTH	12°	$\tau_L = 0\cdot456$
CELL WIDTH	$10\cdot4^\circ$	$\delta = 0\cdot393$

FIG. 13.23 GEOMETRY AND SPEED OF EQUALISER CYCLE CHOSEN FOR COMPARISON WITH THEORETICAL PREDICTIONS

CHAPTER 14

REFERENCES

14. REFERENCES

1. Lebre, A. F.

"Process and Apparatus for Performing Conversion of Mechanical and Thermal Energy".

U.S. Patent Number 2.045.152 (1936).

2. Kentfield, J. A. C.

"An Examination of the Performance of Pressure-Exchanger Equalisers and Dividers".

Ph.D. Thesis, University of London, 1963.

3. Seippel, C.

"Pressure Exchangers".

U.S. Patent Number 2,399,394 (1946).

4. Berchtold, M.

"The Comprex Deisel Supercharger".

SAE Paper No. 63A, 1958.

5. Berchtold, M. & Gull, H. P.

"Road Performance of a Comprex Supercharged Deisel Engine".

SAE Paper No. 118 U, 1958.

Paper presented at SAE National Diesel Engine Meeting, October 1959.

6. Burri, U. H.

"Non-Steady Aerodynamics of the Comprex Supercharger".

ASME Paper presented at the Gas Turbine Power Conference & Exhibition, Washington D.C. March 2-6 1958.

7. Schultz Grunow. F.

"Nichstationare eindemensional Gasbewegung".

Forsh. Geb. Ing. Wes. 13, 1942.

8. Jenny, E.

"Unidimensional Transient Flows with Considerations of Friction,

Heat Transfer and change of Section".

Brown-Boveri Review 957 No.11 447.

9. De-Haller, P.

"The Application of a Graphic Method to Some Dynamic Problems in Gases".

Sulzer Technical Review 1945.

10. Rudinger, G.

"Wave Diagrams For Non-Steady Flow in Ducts".

D. Von Nostrand Co. Ltd., Toronto, N. York LOND. 1955.

11. Spalding, D. B.

"Wave Effects in Pressure Exchangers"

P. J. Report No. 2202/X41 1955.

12. Benson, R. S., Garg, R. D., Woollat, D.

"A Numerical Solution of Unsteady Flow Problems".

International Journal of Mechanical Sciences, Vol.6, No.1 pp.117-144.

13. Spalding, D. B.

"A Procedure for Calculating the Unsteady, One-dimensional Flow of a Compressible Fluid with Allowance for the effects of Heat transfer and Friction".

Imperial College Report No. UF/TN/D/2 1967.

14. O Shea, S.

"Integration Methods for the Unsteady Compressible One-Dimensional Fluid Flow Equations".

M.Sc. Thesis, University of London 1968.

15. Mathews, L.

"An Algorithm for Unsteady Compressible One-Dimensional Fluid Flow".

Imperial College Report No. UF/TN/E/3 1969.

16. Azouri, P. H.

"The Determination of The Optimum Number of Cells in a Pressure Exchanger Rotor".

P. J. Report No. 2261/Px. 8 1961.

17. Azouri, P. H.

"High and Low pressure scavenging processes with finite cell width".

P. J. Report No.2268/PX8. March 1961.

18. Spalding, D. B.

"Theoretical Considerations on Leakage Effects in Pressure Exchanger".

P. J. Report No. 2224/X47 1956.

19. Cotter, J. E.

"Gas Dynamics Studies of a Stationary Wave Engine Cell".

Ph.D. Thesis University of London. 1965.

20. Azouri, P. H.

"An Introduction to Dynamic Pressure Exchanger".

Procd. I. Mech. Eng. Vol.180 Part I, No.8. 1965-66.

21. Azouri, P. H.

Temperature Discontinuities in a Pressure Exchanger of Finite Cell Width".

P. J. Report No. 2262/Px.9 1961.

22. Azim, A.

"A Contribution to the Knowledge of Pressure Exchangers".

M.Sc. Thesis, University of London. 1969.

23. Kentfield, J. A. C.

"An Approximate Method for Predicting the Performance of Pressure Exchangers".

ASME Paper.

Paper presented at ASME Winter Annual Meeting New York 1968.

24. Patankar, S. V.

Private discussions.

25. Hartree, D. R.

"Numerical Analysis".

Oxford. Clarendon Press 1952.

26. Issa, R. I.

"One-Dimensional, Unsteady, Compressible Flow with Friction & Heat Transfer".

M.Sc. Thesis, University of London. 1970.

27. Emrich, I. & Wheeler, S.

"Wall effects in Shock Tube Flow".

The Physics of Fluids. Vol.1, No.1 1958.

28. Trimpi, R. L. & Cohen, N. B.

"A Theory for Predicting the Flow of Real Gases in Shock Tubes with Experimental Verifications".

NACA Technical Note 3375 1955.

29. Mirels, H.

"Attenuation in A Shock Tube due to Unsteady Boundary Layer Action".

NACA Technical Note 3278.

30. Bakhtar, F.

"Effects of Wall Friction and Heat Transfer in a Uniform Shock Tube".

Ph.D. Thesis, Birmingham University. 1956.

31. Glass, I. I.

"Theory and Performance of Simple Shock Tubes".

UTIA Review No.12, Part I. 1958.

32. Kearton, W. J. & Keh, T. H.

"Leakage of Air through Labyrinth Glands of Staggered Type".

Procds. I. Mech. E. Vol. 166, 1952.

33. Szuhowski, A. P.

"Attenuation of a Shock Wave along a Perforated Tube".

Procds. Eight International Shock Tube Symposium, Imperial College, London 1971.

34. Wu, J. H. T., & Ostrowski, P. P.

"Shock Attenuation in a Perforated Duct".

Procds. Eight International Shock Tube Symposium, Imperial College, London 1971.

35. Spiers, H. M.

"Technical Data On Fuel".

British National Committee World Power Cnnference, London 1955.

36. Snow, E. W.

Discussion of "Leakage of Air through Labyrinth Glands of Staggered Type".

Procds. I. Mech. E. Vol.166, 1952. p.191.

37. Courant, R., Friedrichs, K. and Lewy, H.

Math. Ann. 100, 32 (1928). Translation Rep. No. NYO-7689, Inst. of Math. Sci., New York Univ. (1956).

15.1 APPENDIX I

Notation

Generally, no dimensions are specified for the quantities corresponding to the symbols in the following lists. Usually the symbols are employed in such a way that equations involving them are dimensionless. Where dimensions are required they are given in the text.

English-Letter Symbols

a	sonic velocity
A	cross-sectional area
A	port area ratio
Cd	co-efficient of discharge
C_f	friction factor
C_p	specific heat at constant pressure
C_v	specific heat at constant volume
d_h	hydraulic
f	friction force per unit volume of fluid (in negative x direction)
g	acceleration due to gravity
G	integrated mass flow
h	specific enthalpy
K	Actual Cell area/Cell area (inclusive of wall thickness)
ℓ	length
M	local Mach number
m	mass flow
$\dot{m}$	mass flow rate
N	rotational speed
P	pressure variables
p	pressure
q	heat transfer to fluid per unit volume of fluid
R	pressure ratio usually PHP_{in}/PLP_{in} unless otherwise stated
Re	Reynolds

S	dynamic head
s	specific entropy
St	stanton number
T	temperature
t	time
u	velocity
U	velocity variable
v	volume
X	distance
Z	temperature ratio usually T_{HPin}/T_{LPin} unless otherwise stated

Greek alphabet

β	perforation co-efficient
γ	ratio of specific heats
δ	non-dimensional cell width
Δ	differences
ξ	equaliser stagnation enthalpy ratio $^{m}L_{p}T_{Lpo}/_{m\ HP\ THP}$
η_{pis}	isentropic product efficiency
ρ	density
σ	static pressure ratio (employed in universal ratio-temperature rates relationship)
σ	entropy variable
τ	non-dimensional time
$\dot{T}$	static temperature rate
ϕ	fraction of cross-section area of a cell communicating with a port during opening or closing
ϕ	phasing
θ	angular width
$\Delta\tau$	port widths
μ	non-dimensional bulk input

Subscripts

c	circumferential
c	cell conditions
CF	cell filling
CE	cell emptying
eff	effective
HP	high pressure
in	inlet
LP	low pressure
ℓ	leakage conditions
max	maximum
out	outlet port
r	radial
ref	reference conditions
TP	transfer passage
w	wall conditions
o	stagnation condition. When unsubscripted stagnation conditions
x	static condition

Superscripts

-	average in steady flow conditions
.	rates

15.2 APPENDIX II

The approximate method

The approximate method for the performance and design calculations of pressure exchanger cycles is based upon the generalisation of experimentally obtained cell filling and cell emptying data. The approximate method and its application to the pressure equaliser and divider cycles have been described by Kentfield (2). It involves the following main steps.

(i) The development of a generalised form of energy equation applicable to simplified models of pressure exchanger processes involving only a single wave.

(ii) Determination from experimental cell filling and cell emptying data, used in conjunction with the generalised form of the energy equation, of static pressure ratio (σ) versus static temperature ratio (γ) relations for compression and expansion waves.

(iii) Establishment, with the aid of the generalised energy equation and σ-γ relationships, of Mach number versus static pressure ratio curves for compression and expansion waves.

(iv) Pressure exchanger cycle calculations performed with the assistance of the σ-γ curves and M-σ curves.

The graphical data, for the approximate method, which includes the σ-γ relations and the families of M-σ relations are given in figs. (4, 5,6, 7 & 8) in reference (2). The calculations for four port pressure exchanger only need those M-σ relations from each family in which one of $M_{\cdot}$ is equal to zero.

The following relations are used for the scavenging processes and the geometry calculations.

(i) A relationship to estimate the decay of velocity during a scavenging process from a consideration of the viscous effects.

$$M_B = \left(\frac{aref}{a_B}\right) / \left\{\frac{aref}{a_A M_A} + \frac{\tau \ell f}{2dh}\right\} \qquad (1)$$

where τ is the dimensionless time required for a cell to move from A to B.

f is the friction factor.

ℓ is the cell length.

dh is the hydraulic diameter.

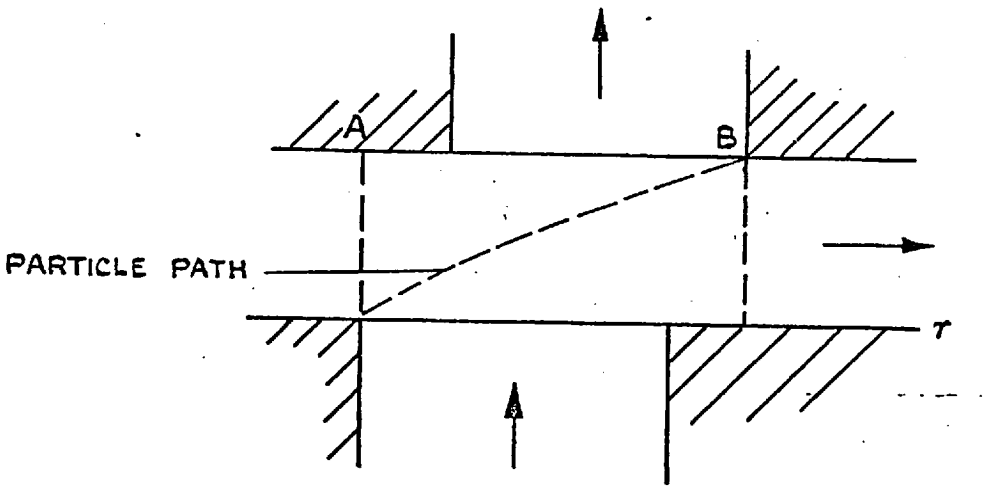


Fig. 15.II.1

The normalised time τ from A to B can also be obtained from the relationship

$$\frac{\Delta x}{\ell} = \frac{2}{f} \times \frac{dh}{\ell} \log_e \left(\frac{a_A M_A}{a_B M_B}\right) \qquad (2)$$

where $\Delta x = X_B - X_A$, which is the distance the contact surface translates along a cell during the time τ. $\frac{\Delta x}{\ell}$ therefore represents the scavenge ratio.

(ii) The approximate phasings and also the widths of transfer ports is calculated from the following relationship.

$$\tau = \pm \frac{(1 - \frac{P2}{P4} \times \frac{T4}{T2})\ (\frac{aref}{a4})}{(\frac{P2}{P4} \surd \frac{T4}{T2} \times M2 - M4)} \qquad (3)$$

The notation used is that of Kentfield (2). The positive sign applies to the first part of cell filling and the second part of cell emptying. The negative sign applies to the first part of cell emptying and the second part of cell filling.

The graphical data has been converted into the form of algebraic expressions in order to feed it to the computer. Least square method has been used to compute these expressions which are given as follows.

(i) First-part of cell filling

$$M = -0.886243 + 1.26643\sigma - 0.43387\sigma^2 + 0.054265\sigma^3 \qquad (4)$$

$$\sigma = 0.988883 + 2.5384M - 5.57146M^2 + 19.6713M^3 \qquad (5)$$

$$\gamma = 0.63169 + 0.464615\sigma - 0.11148\sigma^2 + 0.015734\sigma^3 \qquad (6)$$

$$\sigma = 2.25522 - 8.46114\gamma + 9.69241\gamma^2 - 2.48743\gamma^3 \qquad (7)$$

(ii) Second part of cell filling

$$M = -1.90554 + 3.20235\sigma - 1.61310\sigma^2 + 0.31567\sigma^3 \qquad (8)$$

$$\sigma = 1.00144 + 0.994567M + 1.55020M^2 - 0.170046M^3 \qquad (9)$$

$$\gamma = 0.631690 + 0.464615\sigma - 0.11148\sigma^2 + 0.015734\sigma^3 \qquad (10)$$

$$\sigma = 0.493738 - 2.44290\gamma + 2.94716\gamma^2 \qquad (11)$$

(iii) First part of cell emptying

$$M = -1.268212 + 2.21889\sigma - 1.32254\sigma^2 + 0.429927\sigma^3 - 0.0530722\sigma^4 \qquad (12)$$

$$\sigma = 0.99283 + 1.59237M + 1.4372M^2 + 0.961190M^3 \qquad (13)$$

$$\gamma = 0.671739 + 0.398859\sigma - 0.0745071\sigma^2 + 0.0045763\sigma^3 \qquad (14)$$

$$\sigma = 18.4058 + 51.2836\gamma - 48.2871\gamma^2 + 16.4058\gamma^3 \qquad (15)$$

(iv) Second part of cell emptying

$$M = 16.3801 - 54.78364\sigma + 66.9814\sigma^2 - 35.6081\sigma^3 + 7.0325\sigma^4 \quad (16)$$

$$\sigma = 1.00210 + 1.14363M + 2.16224M^2 - 3.373715M^3 \quad (17)$$

$$\gamma = -2.57823 + 10.8874\sigma - 12.6828\sigma^2 + 6.6994\sigma^3 - 1.3257\sigma^4 \quad (18)$$

$$\sigma = -155.123 + 445.535\gamma - 427.007\gamma^2 + 137.593\gamma^3 \quad (19)$$

Application of the approximate method to four port pressure exchangers

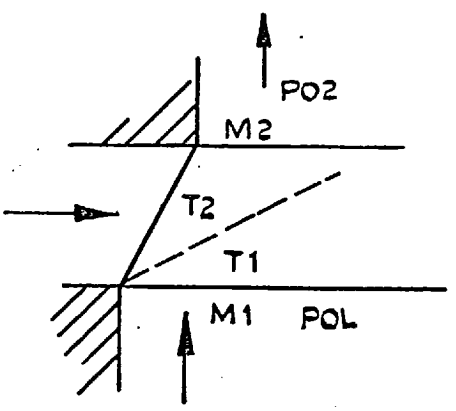
The two features, which can be neglected for the pressure equaliser and divider cycles, but which are significant for four port pressure exchanger cycles are as follows.

(i) The existence of an interface, with an appreciable temperature difference between the fluids at the two sides of the interface.

(ii) The pressure drop in the high pressure loop and the pressure difference in the low pressure ports.

These two effects are taken into account in the following manner.

(i) The Mach numbers on the two sides of an interface are assumed to be inversely proportional to the sonic velocity



$$\frac{M1}{M2} = \sqrt{\frac{T2}{T1}} \quad (20)$$

Fig. 15.2.2.

(ii) Fig.(15.II.1)shows a HP scavenging port. The pressures at the two ports are P_{o1} and P_{o2} such that $P_{o2} > P_{o1}$. Mach number M1 at port 1 is calculated from the relationships for the first part of cell filling. M2 at the port number 2 is calculated from the relation-

ship assumed in (i). Now in order to take the pressure difference $P_{o2} - P_{o1}$ into account, a small Mach number ΔM2 is calculated for first part of cell filling for a pressure ratio equal to P_{o2}/P_{o1}. The corrected value of M2 is equal to M2-ΔM2.

Similar considerations apply to the low pressure scavenge process.

The computer program

A computer program "APPROX" has been developed for the performance and design calculations of the pressure exchanger cycles by the approximate method. As compared to GENPX this program requires very small storage and time. It is also a fairly general program.

In the following sections, different subroutines and their functions have been described with reference to a four port pressure exchanger cycle with one transfer passage.

Main

The main routine initiates and controls the sequence of operations. Its first task is to read the input data which includes following informations.

(i) The boundary conditions consist of the following informations.

(a) The stagnation pressures at the scavenging inlet ports.

(b) The static pressures at the transfer and the outlet ports.

(c) The stagnation temperatures at the inlet ports.

(ii) The remaining information includes.

(a) RATIOH and RATIOL specify the requires scavenge ratios in the high and low pressure regions respectively.

(b) CP and CV are the two specific heats.

(c) CF is the friction factor, CL is the cell length, HD is the hydraulic diameter and DTP is the finite cell width.

The next task of main is to allocate values to certain variables.

NUPORT = Total number of ports.

NJPORT = The high pressure inlet port.

NIPORT = The low pressure outlet port.

KMAX = Maximum number of cycles.

The MAIN then calls subroutine CONST to calculate the γ-functions and certain geometrical constants which are frequently used in calculations.

Main then starts a DO -loop to carry out the performance and design calculations of the pressure exchanger cycle by considering each port in turn and in order of their respective location. The following procedure is adopted for a four port pressure exchanger with one transfer passage.

(i) Subroutine CFILL is called to design the cell filling port. The calculations are initiated at this point because a good guess of the conditions in the cell can be made after a long exposure to the low pressure scavenge ports.

(ii) The next call is made to the subroutine HPSC to perform design and performance calculations of the high pressure scavenge section adjacent to the cell filling port.

(iii) Subroutine CEMP is now called to operate on the next port which happens to be a cell emptying port.

(iv) Subroutine LPSC is called to perform the design and performance calculations of a low pressure scavenge section.

(v) Finally, subroutine RESULT is then called to process the information obtained from the cycle calculations and print them in an appropriate form.

CONST

The function of this subroutine is to calculate certain geometrical and γ-functions which are then frequently used in the calculation procedure.

CFILL

Subroutine CFILL operates on a cell filling port. The cell filling process is assumed to consist of two single wave processes, the first and second part of cell filling in that order. The calculation procedure,

therefore, involves two steps.

(i) The cell filling pressure ratio R_{CF} is calculated from the known values of the initial cell pressure and the port static pressure. The temperature rise TR1, the Mach number AMACA, and the normalised time τ_4 required for the single wave to travel to the opposite end, for the first port of cell filling are obtained from the relevant equations coded in this section.

(ii) AMACB is set equal to AMACA. The pressure PR2, the temperature ratio TR2, and the normalised time τ_3 required for the single wave to travel back to the open end, for the second part of cell filling are obtained from the relevant equations coded in this section.

The port width is the sum of τ_4 & τ_3, the closing time TIMC and the pressure and temperature in the cell after the process are calculated.

HPSC

Subroutine HPSC operates on the high pressure scavenge section. The high pressure scavenging process is assumed to consist of the two single wave processes only.

(i) The first part of cell filling which is initiated by the opening of the inlet port and terminates at the opening of the outlet port.

(ii) The second part of cell emptying which is initiated by the closure of the inlet port and terminates at the closure of the outlet port.

The section between the two processes if waveless and the width of this section depends upon the required scavenge ratio in the section.

The operation of HPSC is, therefore, divided in two steps

(i) The first part of cell filling is initiated at the inlet port. The boundary conditions prescribed at the inlet port are the stagnation values of pressure and temperature. Therefore, an

initial guess of the static values at the port is made. The static pressure ratio $PR1_3$ is, therefore, known from the initial values in the cell.

From the relations for the first part of cell filling, the temperature ratio TR1, the Mach number at the outlet port AMACA (not the inlet port) and hence the static temperature (for unity scavenge ratio) at the outlet port are obtained. The temperature ratio of the two ports is now known (the temperature at the inlet port is fixed) and, therefore, the value of AMACA at the inlet port is calculated being proportional to the temperature.

The stagnation values of pressure and temperatures at the inlet port are now calculated and if they are not sufficiently close to the prescribed values, the whole procedure is repeated until they are close enough.

The phase difference between the two ports is given by the time, taken by the wave to reach the opposite end and this is calculated from the relevant equation. AMACA at the outlet port is now readjusted to take into account the pressure difference at the ports.

AMACB at the inlet port, the closing time TIMC of the outlet port and AMACB at the outlet port are finally calculated from the relevant equations.

(ii) The value of AMACB at the inlet port is now used to calculate the static pressure ratio PR2, the static temperature ratio TR2, the cell pressure and temperature at the completion of the scavenging section, from the second part of cell emptying relations which are coded in this section.

The time taken by the second wave to travel across the cell length is now calculated from the appropriate equations and

hence the port width of the inlet port.

The performance and design calculations of the high pressure scavenge section is now complete.

CEMP

Subroutine CEMP operates upon a cell emptying port. The cell emptying performance is assumed to consist of the first part of cell emptying followed by second part of cell emptying. The calculation procedures are same as in CFILL except that the cell filling coding is replaced by that of the cell emptying, i.e. the equations relevant to first and second part of cell filling are substituted by the equations relevant to the first and second part of cell emptying respectively.

LPSC

Subroutine LPSC operates on the low pressure scavenging ports. The low pressure scavenging process is assumed to consist of the two single wave processes only.

(i) The first part of cell emptying which is initiated at the opening of the outlet port and terminates at the opening of the inlet port.

(ii) The second part of cell filling which is initiated at the closure of the outlet port and terminates at the closure of the inlet port.

The section between the two processes is waveless and the width of this section depends upon the scavenge ratio required at the low pressure scavenge section.

The operational procedure of the subroutine LPSC is similar to that of the subroutine HPSC. The coded equations for the first part of cell filling are replaced by the equations for the first part of cell emptying and that of the second part of cell emptying by the second part of cell filling.

RESULT

The function of subroutine RESULT is to process the information supplied by the cycle calculations and prints out the performance and geometry of the pressure exchanger cycle in an appropriate form.

15.3 APPENDIX III

The Pressure Differential Method

The pressure differential method is a graphical method for the performance and design calculations of the four port pressure exchanger cycle. It can easily be computerised.

The graphical data consists of the performance and design characteristics of the high pressure scavenging process, the low pressure scavenging process and the transfer process. The transfer characteristics are obtained from the cell filling and cell emptying characteristics.

The fundamental assumptions implied in the method are as follows.

(i) The working fluid is a perfect gas.

(ii) The heat transfer and leakage losses are negligible.

(iii) There are no losses in the transfer passages.

(iv) Mixing and diffusion losses are ignored.

(v) Effects of the residual waves between ports are ignored.

The basis of the whole procedure are the following results drawn with the help of these assumptions

(i) The rotor pressure difference ΔP has the same value for all component processes in a pressure exchanger cycle. This pressure difference bears a simple relationship with bulk input μ.

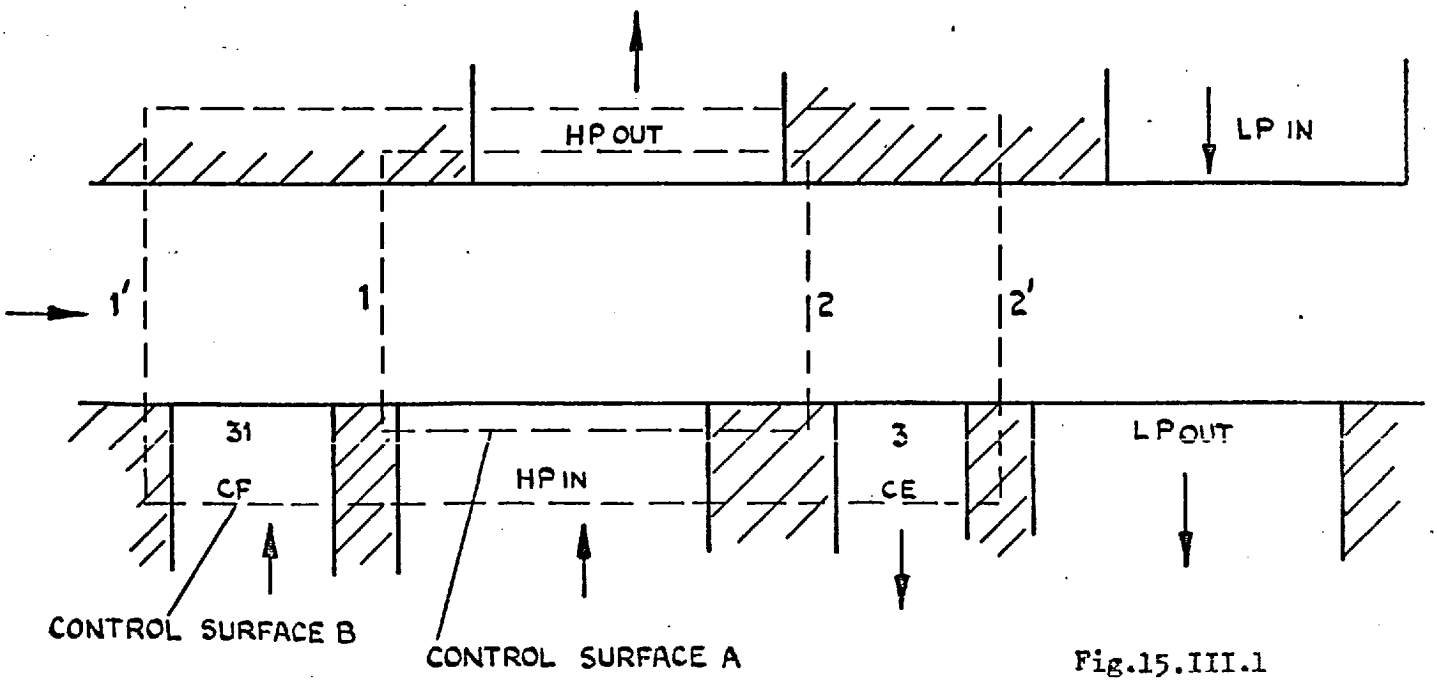


Fig.15.III.1

Fig.(15.III.1) shows a four port machine with one transfer passage.

Considering the control surface A and apply the first law of thermodynamics.

$$C_p \dot{m}_{HPout} T_{HPout} - C_p \dot{m}_{HPin} T_{HPin} \equiv (C_v \dot{m}_2 T_2 - C_v \dot{m}_1 T_1) \quad (1)$$

From the definition of the bulk input, μ

$$\mu \equiv -(\dot{m}_{HPout} T_{HPout} - \dot{m}_{HPin} T_{HPin}) / \dot{m}_{sw} T_{LPin} \quad (2)$$

From the constancy of cell volume

$$\dot{m}_1 = \frac{P_1}{RT_1} \times \dot{V}_{sw} \quad (3)$$

$$\dot{m}_2 = \frac{P_2}{RT_2} \times \dot{V}_{sw} \quad (4)$$

and $$msw = \frac{P_{LPin}}{RT_{LPin}} \times \dot{V}_{sw} \quad (5)$$

By substitution

$$\gamma \mu = \pm (p2 - p1)/p_{Lin} \quad (6)$$

$$\therefore \quad \mu = \frac{1}{\gamma} \frac{\Delta p}{P_{LPin}} \quad (7)$$

Equation (7) is the general performance equation for a four port pressure exchanger, after Azouri (20)

Considering the control surface B and applying the first law of thermodynamics

$$Cpm_{HPin} T_{HPin} - Cpm_{HPout} T_{HPout} + Cpm_3' T_3' - Cpm_3 T_3$$

$$= Cvm_2' T_2' - Cvm_1' T_1' \quad (8)$$

For an adiabatic transfer passage, there is no energy loss, hence;

$$Cp\dot{m}_3 T_3 = Cp\dot{m}_3' T_3 \qquad (9)$$

Therefore, equation is reduced to

$$Cp\dot{m}_{HPin} T_{HPin} - Cp\dot{m}_{HPout} T_{HPout} = C_v \dot{m}_2' T_2' - C_v \dot{m}_1' T_1' \qquad (10)$$

From the constancy of cell volume

$$\dot{m}_2' = \frac{p_2'}{RT_2'} \dot{V}_{sw} \qquad (11)$$

$$\dot{m}_1' = \frac{p_1'}{RT_1'} \dot{V}_{sw} \qquad (12)$$

and also considering equations (11) and (12) and substituting

$$\gamma\mu = \Delta p'/p_{LPin} \qquad (13)$$

$$\therefore \quad \mu = \frac{1}{\gamma} \frac{\Delta p'}{P_{LPin}} \qquad (14)$$

$$\therefore \quad \Delta p' = \Delta p \qquad (15)$$

(ii) In a transfer process, the pressure rise during filling is equal to pressure drop during emptying.

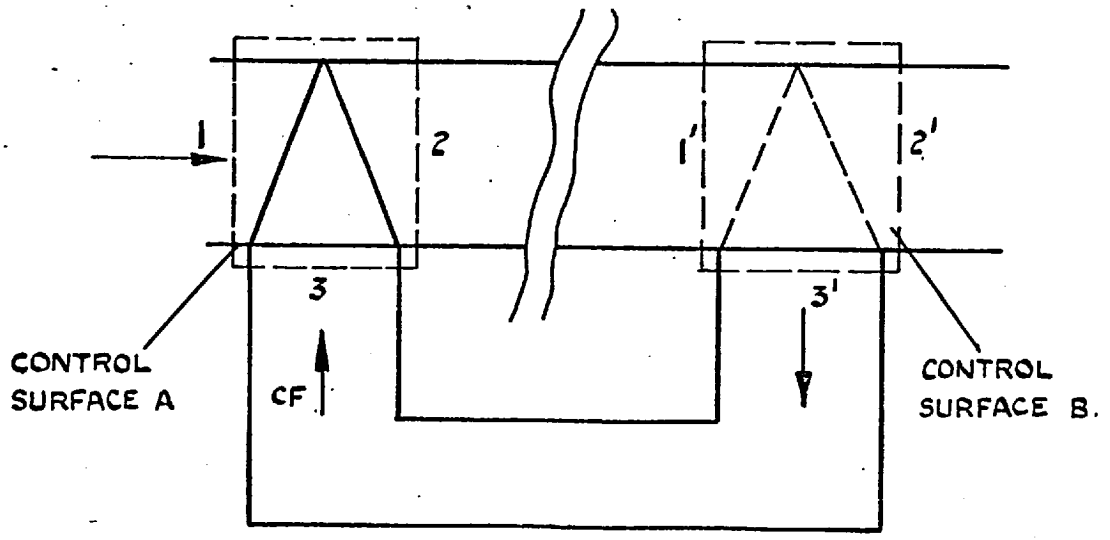


Fig. 15.III.2.

Considering control surface A and applying the first law of thermodynamic

$$C_p\dot{m}_3T_3 = C_v\dot{m}_2T_2 - C_v\dot{m}_1T_1 \tag{16}$$

Similarly for control surface B

$$C_p\dot{m}_3'T_3' = -(C_v\dot{m}_2'T_2' - C_v\dot{m}_1'T_1') \tag{17}$$

For an ideal transfer passage

$$C_p\dot{m}_3T_3 = C_p\dot{m}_3'T_3' \tag{18}$$

Therefore,

$$C_v\dot{m}_2T_2 - C_v\dot{m}_1T_1 = -(C_v\dot{m}_2'T_2' - C_v\dot{m}_1'T_1') \tag{19}$$

From the constancy of cell volume and perfect gas relations

$$p_2 - p_1 = -(p_2' - p_1') \tag{20}$$

$$\Delta p = \Delta p' \tag{21}$$

The component characteristics

The performance and design characteristics of the pressure exchanger basic processes were established with the help of the numerical procedures. These characteristics do not include the friction, heat transfer and leakage effects.

These characteristics are given in figs. (12.1 to 12.12 & 12.100) and are self-explanatory. The transfer characteristics are obtained from the cell filling and cell emptying characteristics in the following way:

Certain values of p_{1CF} and RCF are selected p_{OTP} is given by RCF/pICF. The value of $\Delta p_{CF/p_{1CF}}$ for the given RCF and hence $P2_{CF}$ is obtained from the cell filling characteristics. Δp_{CE} is equal to Δp_{CF}.

The value of R_{CE} and hence p_{1CE} is obtained from the cell emptying characteristics. ΔP is given by the difference P1CE-P1CF. $\Delta P/_{p1CF}$ can now be plotted against $\Delta P/_{P2CF}$.

The calculation procedure

In the following section, the calculation procedure for a four port pressure exchanger with two transfer passages is described and it involves the following steps.

(i) Select a value of bulk input μ. The rotor pressure difference ΔP for this value of μ is obtained from the pressure exchanger general performance equation / Fig.(12.101). We start with the low pressure scavenge port.

(ii) Assume that the atmospheric pressure prevail at the low pressure scavenge ports. This gives the value of $^{\Delta P}/_{PO_{LP}}$. The low pressure scavenge pressure ratio R_{LP} and geometry of the section ϕ_{LP} and τ_{Lin} are obtained from the low pressure scavenge characteristics. The area ratio A_{LP} is assumed to be unity. The value of P2LP can now be worked out.

(iii) The next port is a cell filling port. P1CF is equal to P_2LP (ignoring the residual wave effects). $\Delta P/_{P1CF}$ can now be calculated. $^{\Delta P}/_{P2CF}$ and hence P2CF is obtained from the transfer characteristics. ΔP_{CF} being known, R_{CF} is obtained from the cell filling characteristics and also the value of τ_{CF}. The filling port, and hence the transfer passage pressure can also be calculated.

(iv) The next port is again a cell filling port. The procedure in step (iii) is repeated to obtain the values of τ_{CF} and P_{2CF} for this port.

(v) The high pressure scavenge section has now been reached. P1HP is equal to P_{2CF}. $^{\Delta P}/_{P_{1HP}}$ being known, the values of R_{HP}, ϕ_{HP}, τ_{HPout} and A_{HP} can now be obtained from the high pressure

scavenging characteristics. The values of P_{OHP}, R and P_{2HP} can now be calculated.

(vi) The next port is a cell emptying port. P1CE is equal to P_{2HP}. ΔP_{CE} is equal to ΔP_{CF} (for the corresponding filling port) P2CE can therefore be calculated and also the value of $\Delta PCE/P1CE$. The values of R_{CE} and τ_{CE} are obtained from the cell emptying characteristics. P_{OCE} can also be calculated and it will be equal to P_{OCF}.

(vii) The last port is again a cell emptying port. The procedure in step (vi) is repeated for (vii). The final pressure is always equal to the initial step.

The performance and design calculations of a four port pressure exchanger with two transfer passages are now complete. The following information has been obtained;

(i) The overall pressure ratio for a given bulk input.

(ii) The cell pressures before and after the component processes.

(iii) The scavenging port pressures.

(iv) The transfer port pressures.

(v) The pressure exchanger geometry for unity scavenge ratios.

The temperature discontinuities have been ignored the value of Z being unity.

It may be noted that in these calculations no iterations were required to attain the equilibrium conditions and the boundary conditions at transfer ports have also been predicted during the calculations. These two special features of the pressure differential method help to make it a very quick and useful method. The approximate method and the method of characteristics both need a number of cycles before the initial conditions match the final conditions. The boundary conditions at the transfer ports, in both the methods, have to be guessed and the correct boundary conditions are obtained only by trial and error procedure until the continuity in the transfer ports is satisfied.

The usefulness of the pressure differential method therefore increases with increasing number of transfer passages in a four port pressure exchanger.

15.4 APPENDIX IV

The purpose of this Appendix is to present the derivation of the characteristic equations

The equations of conservation of mass, momentum and energy are, respectively;

$$\frac{\partial \rho}{\partial t} + \frac{\partial}{\partial x}(\rho u) = -\psi/A \qquad (1)$$

$$\frac{\partial}{\partial t}(\rho u) + \frac{\partial}{\partial x}(\rho u^2 + p) = -f \qquad (2)$$

$$\frac{\partial}{\partial t}\{\rho(h - P/\rho + u^2/2)\} + \frac{\partial}{\partial x}\{\rho u(h + u^2/2)\} = q - \psi/Ah_{o\ell} \qquad (3)$$

The symbols introduced here are as follows,

ρ = density of fluid

u = velocity of fluid in x-direction

P = pressure of fluid

h = specific enthalpy of fluid

f = friction force (in negative x-direction) per unit volume of fluid

q = heat transfer rate to fluid per unit volume

ψ = leakage mass flow rate (normal to the main flow and an outflow is positive) per unit of length of cell.

β = perforation co-efficient

A = cell cross-sectional area

Thermodynamic relationships

The properties p, ρ and u are related by the thermodynamic relationship of the fluid. Although the method of solution can be applied to fluids of arbitrary thermodynamic behaviour, attention is restricted here to perfect gases.

For all fluid, the temperature T is related to h, p, ρ and entropy s by:

$$Tds = dh - \frac{1}{\rho} dp \tag{4}$$

For an ideal gas we have

$$dh = CpdT \tag{5}$$

and

$$p = \rho RT \tag{6}$$

where Cp is the specific heat of the fluid at constant pressure. It is constant for a perfect gas. R is the gas constant.

The specific heat ratio is defined as:

$$\gamma = {}^{Cp}/_{Cv} \tag{7}$$

Where C_v is the specific heat at constant volume, γ and R are related by:

$$Cp = \frac{\gamma R}{\gamma - 1} \tag{8}$$

Finally, we introduce the velocity of sound a. It is given by:

$$a = \sqrt{\gamma RT} \tag{9}$$

or alternatively

$$a = \sqrt{\frac{\gamma p}{\rho}} \tag{10}$$

The transformed equations

In order to bring out the three characteristic directions into prominence in the conservation equations, some transformation to the equations must be affected.

By differentiating all terms in equation (1), (2) and (3), then

manipulating and combining equations (2) and (3) we get: $(\psi' = \beta\psi)$

$$\frac{\partial \rho}{\partial t} + u \frac{\partial \rho}{\partial x} + \rho \frac{\partial u}{\partial x} = -\psi'/A \tag{11}$$

$$\frac{\partial u}{\partial t} + u \frac{\partial u}{\partial x} + \frac{1}{\rho} \frac{\partial p}{\partial x} = -f/\rho + \frac{u\psi'}{\rho}/A \tag{12}$$

$$\frac{\partial h}{\partial t} + u \frac{\partial h}{\partial x} - \frac{1}{\rho} \left(\frac{\partial p}{\partial t} + u \frac{\partial p}{\partial x}\right) = q/\rho + uf/\rho$$

$$- \psi'(h_\ell + \frac{u^2\ell}{2})/\rho A + (h + u^2/2)\psi'/\rho A - u^2\psi'/\rho A \tag{13}$$

The variables a, u and s are of special interest, thus the thermodynamics relations are invoked in order to obtain these quantities as dependent variables in the equations. To do this we obtain from equations (4), (5), (6), (8) and (9) after performing the necessary differentiation and substitution, the following results:

$$\frac{d\rho}{\rho} = \frac{2}{\gamma-1}\frac{da}{a} - \frac{1}{R}\,ds \tag{14}$$

$$\frac{dp}{p} = \frac{2\gamma}{\gamma-1}\frac{da}{a} - \frac{1}{R}\,ds \tag{15}$$

$$dh = \frac{1}{\gamma-1}\,da^2 \tag{16}$$

From equations (12) and (15)

$$\frac{\gamma-1}{2}\left(\frac{\partial u}{\partial t} + u \frac{\partial u}{\partial x}\right) + a \frac{\partial a}{\partial x} = \frac{a^2}{2c_p}\left(\frac{\partial s}{\partial x} - \frac{Rf}{P}\right) + \frac{a^2}{2c_p}\frac{Ru\psi'/A}{p} \tag{17}$$

From equations (13), (14) and (15) we find:

$$\frac{\partial s}{\partial t} + u \frac{\partial s}{\partial x} = \frac{R(q+Uf)}{P} - \frac{R(h_\ell + u_\ell^2/2)\psi'/A}{P} + \frac{R(h+u^2/2)\psi'/A}{P}$$

$$- R\,\frac{u^2}{P}\,\psi'/A \tag{18}$$

Similarly, equations (11), (14) and (18) will combine giving:

$$\frac{\partial a}{\partial t} + u\frac{\partial a}{\partial x} + a\frac{\partial}{\partial x}\left(\frac{\gamma-1}{2}u\right) = \frac{\gamma-1}{2}\frac{a(q+Uf)}{P} - \frac{\gamma-1}{2}a$$

$$\frac{(h_\ell+u^2\ell/2)\psi'/A}{P} + \frac{\gamma-1}{2}\frac{a(h+u^2/2)\psi'/A}{P} - \frac{\gamma-1}{2}\frac{a}{\rho}\psi'/A - \frac{\gamma-1}{2}\frac{a}{\rho}u^2\psi'/A \quad (19)$$

Addition of equation (17) to equation (19) produces:

$$\frac{\partial}{\partial t}\left(a + \frac{\gamma-1}{2}u\right) + (u + a)\frac{\partial}{\partial x}\left(a + \frac{\gamma-1}{2}u\right) = \frac{a^2}{2c_p}\left(\frac{\partial s}{\partial x} - \frac{Rf}{P}\right)$$

$$+ \frac{\gamma-1}{2}a\left(\frac{q + uf}{P}\right) + \frac{a^2}{2c_p}\frac{Ru\psi'/A}{\rho} - \frac{\gamma-1}{2}a\left(\frac{h_\ell+u^2\ell/2}{P}\right)\psi'/A +$$

$$\frac{\gamma-1}{2}a\left(\frac{h+u^2/2}{P}\right)\psi'/A - \frac{\gamma-1}{2}\frac{a}{\rho}\psi'/A - \frac{\gamma-1}{2}\frac{a}{\rho}u^2\psi'/A \quad (20)$$

Subtracting equation (17) from (19) gives:

$$\frac{\partial}{\partial t}\left(a - \frac{\gamma-1}{2}u\right) + (u-a)\frac{\partial}{\partial x}\left(a - \frac{\gamma-1}{2}u\right) = \frac{\gamma-1}{2}a\left(\frac{q+uf}{P}\right)$$

$$- \frac{a^2}{2c_p}\left(\frac{\partial s}{\partial x} - \frac{Rf}{P}\right) - \frac{a^2}{2c_p}\frac{Ru\psi'/A}{\rho} - \frac{\gamma-1}{2}a\left(\frac{h_\ell+u^2\ell/2}{P}\right)\psi'/A$$

$$+ \frac{\gamma-1}{2}a\left(\frac{h + u^2/2}{P}\right)\psi'/A - \frac{\gamma-1}{2}\frac{a}{\rho}\psi'/A - \frac{\gamma-1}{2}\frac{a}{\rho}u^2\psi'/A \quad (21)$$

New dependent variables

The dependent variables in equation (20) and (21) are called the Riemann variables; an earlier version of the method solves for these variables. However, when applied to non-homentropic flows, the method produced unrealistic results. A new set of dependent variables was introduced to cure this problem. They are:

$$U = \frac{\gamma-1}{2}u \quad (22)$$

$$P = p^{\frac{\gamma-1}{2\gamma}} \tag{23}$$

$$\sigma = \exp\left(\frac{\gamma-1}{2\gamma}\, s\right) \tag{24}$$

From the thermodynamic relations mentioned earlier, it can be shown that:

$$a = P\sigma$$

$$\rho = \frac{2}{\frac{P^{\gamma-1}}{\sigma}} \tag{26}$$

$$T = P^2\sigma^2$$

The final form of equations can now be obtained by the substitution of these new variables from the old ones.

$$\frac{\partial}{\partial t}(P\sigma + U) + (u+a)\frac{\partial}{\partial x}(P\sigma + U) = D + E\frac{\partial s}{\partial x} - G + L1 \tag{28}$$

$$\frac{\partial}{\partial t}(P\sigma - U) + (u-a)\frac{\partial}{\partial x}(P\sigma - U) = D - E\frac{\partial s}{\partial x} + G + L2 \tag{29}$$

$$\frac{\partial \sigma}{\partial t} + u\frac{\partial \sigma}{\partial x} = \sigma(F + L3) \tag{30}$$

where in terms of the normalised form:

$$D = \frac{\gamma-1}{2}\frac{a}{\rho}\left(\frac{q+uf}{P}\right) \tag{31}$$

$$E = \frac{\gamma-1}{2\gamma}a^2 \tag{32}$$

$$F = \frac{\gamma-1}{2\gamma}\left(\frac{q+uf}{P}\right) \tag{33}$$

$$G = \frac{\gamma-1}{2\gamma}\frac{a^2 f}{P} \tag{34}$$

$$B1 = \frac{\gamma-1}{2}\frac{a}{\rho}\psi' \tag{35}$$

$$B2 = \frac{\gamma-1}{2}\frac{a^2}{P}(h_\ell + u^2_\ell/2)\psi' \tag{36}$$

$$B3 = \frac{\gamma-1}{2}\frac{a^2}{P}(h + u^2/2)\psi' \tag{37}$$

$$B4 = \gamma\frac{\gamma-1}{2}\frac{a}{P}u^2\psi' \tag{38}$$

$$B5 = \frac{\gamma-1}{2}\frac{a^2}{P}u\psi' \tag{39}$$

$$B6 = \frac{u^2}{P}\psi' \times \frac{\gamma-1}{2}' \tag{40}$$

$$L1 = -B1 - B2 + B3 - B4 + B5 \tag{41}$$

$$L2 = -B1 - B2 + B3 - B4 - B5 \tag{42}$$

$$L3 = -B2 + B3 - B6 \tag{43}$$

If $B2 \simeq B3$

$$L1 = -B1 - B4 + B5 \tag{44}$$

$$L2 = -B1 - B4 - B5 \tag{45}$$

$$L3 = -B6 \tag{46}$$

15.5 APPENDIX V

Calculation of the performance losses in pressure exchangers

The purpose of this Appendix is to provide details of the different methods used to calculate the performance losses in pressure exchangers. These losses include the friction, heat transfer, leakage and transfer passage losses. The calculations are then incorporated in the numerical procedure based on the hybrid method.

Friction

The frictional losses are calculated in two steps;

(i) The cell wall friction

A friction factor C_f may be defined as:

$$C_f = \frac{\tau_w}{\rho u^2} \tag{1}$$

where τ_w is the shear stress at the wall. It is equal to the frictional force at the wall per unit surface area of the cell. Thus, τ_w is related to f by:

$$\tau_w = f \frac{A}{b} \tag{2}$$

where A and b are the cross-sectional area and parameter of the cell respectively.

A hydraulic diameter may be defined as:

$$d = \frac{4A}{b} \tag{3}$$

Shear stress can be written in terms of the hydraulic diameter as:

$$\tau_w = \frac{d}{4} f \tag{4}$$

Thus, by combination of equations (2) and (4), f can now be written as:

$$f = \frac{4}{d} C_f \rho u|u| \tag{5}$$

The $|u|$ is used here so that the direction of the frictional force f is dictated by the direction of flow. Normalisation of the quantities give

$$f = \frac{4}{d} \gamma C_f \rho u|u| \qquad (6)$$

The friction factor C_f is assumed to vary with the Reynolds number based on hydraulic diameter according to the turbulent pipe flow formula which has been used by Bakhtar (30) in his work on frictional flow in shock tubes

$$C_f = \text{const}/R_e^{0.214} \qquad (7)$$

The best value of the constant term has been found by Issa (26) based on comparison with the experimental results by Glass (31) to be equal to 0.035, hence:

$$C_f = 0.035/R_e^{0.214} \qquad (8)$$

The calculations of the local Reynolds number is based on the hydraulic diameter of the cell and the local flow variables.

(ii) The cell entry and exit losses

Because the edges of the cell walls of the pressure exchangers are unstreamlined, the appropriate data is that applying to sudden contraction and sudden enlargement. According to Spiers (35)

For a sudden contraction:

$$S = 0.5\ (1 - K) \qquad (9)$$

For a sudden enlargement

$$S = (1 - K)^2 \qquad (10)$$

where S is the number of dynamic heads loss due to unstreamlined entry and exit and K is equal to a/A: where a is the cell area excluding the cell wall thickness and A is the total cell area.

The total head loss at any step is the sum of the two head losses at the cell ends. Thus,

$$S_{TOT} = S_{left} + S_{right} \tag{11}$$

An apparent friction factor C_{f1} based on S_{TOT} is calculated using the well-known equation:

$$C_{f1} = \frac{S}{\ell / d_h} \tag{12}$$

The apparent friction factor is added to the cell wall friction factor calculated from equation (7). The total friction factor is now used to calculate the value of f from equation (6). The terms D, F and G are now given by

$$D = \frac{\gamma-1}{2}\frac{a}{P}q + \frac{4}{d}\gamma\left(\frac{\gamma-1}{2}\right)C_f \, a\frac{Pu^2|u|}{P} \tag{13}$$

$$F = \frac{\gamma-1}{2}\frac{q}{P} + \frac{4}{d}\left(\frac{\gamma-1}{2}\right)C_f\frac{Pu^2|u|}{P} \tag{14}$$

$$G = \frac{4}{d}\left(\frac{\gamma-1}{2}\right)C_f\frac{a^2Pu|u|}{P} \tag{15}$$

Heat transfer

A Stanton number is defined as:

$$S_t = \frac{Q}{\rho \, C_p \, u(T_w - T_o)} \tag{16}$$

T_w is the temperature of wall of the cell through which the fluid is flowing. T_o is the stagnation temperature of the fluid and Q is the rate of heat transfer to the fluid per unit surface area of the cell.

With the hydraulic diameter d as defined before, Q can be related to q by:

$$Q = \frac{d}{4}q \tag{17}$$

Thus, q can be written as:

$$q = \frac{4}{d} S_t \rho C_p |u| (T_w - T_o) \tag{18}$$

The $|u|$ is used so that the heat transfer rate is independent of the direction of flow.

The above equation in a normalised form gives:

$$q = \frac{4}{d} \cdot \left(\frac{\gamma}{\gamma-1}\right) S_t \rho |u| (T_w - T_o) \tag{19}$$

The local Stanton number is assumed to be a function of the local Reynolds and Prandt number according to the turbulent pipe flow formula used by Bakhtar (30).

$$S_t = \text{const}/(R_e^{0.2} \times Pr^{0.6}) \tag{20}$$

or for constant P_r

$$S_t = \text{const}/R_e^{0.2}$$

The best value of the constant term has again been found by Issa (26) equal to 0.02 constant hence:

$$S_t = 0.02/R_e^{0.2} \tag{21}$$

With the expression for q given in equation (19) terms D, G and F now become:

$$D = \frac{4}{d} \frac{\gamma}{2} S_t \frac{\rho a |u|}{P} (T_w - T_o) + \frac{4}{d} \gamma \left(\frac{\gamma-1}{2}\right) C_f \, a \frac{\rho u^2 |u|}{P} \tag{22}$$

$$F = \frac{4}{d} \frac{S_t}{2} \frac{\rho |u|}{P} (T_w - T_o) + \frac{4}{d} \left(\frac{\gamma-1}{2}\right) C_f \frac{\rho u^2 |u|}{P} \tag{23}$$

$$G = \frac{4}{d} \left(\frac{\gamma-1}{2}\right) C_f \frac{a^2 \rho u |u|}{P} \tag{24}$$

These terms expressed in terms of the dependent variables P, σ and U are given by the following equations:

$$D = \frac{4}{d}\gamma\left(\frac{2}{\gamma-1}\right)^2 C_f \frac{U^2|U|}{P\sigma} + \frac{4}{d}\left(\frac{\gamma}{\gamma-1}\right) S_t \frac{|U|}{P\sigma}\left[T_w - P^2\sigma^2 - \left(\frac{2}{\gamma-1}\right) U^2\right] \quad (25)$$

$$F = \frac{4}{d}\left(\frac{2}{\gamma-1}\right)^2 C_f \frac{U^2|U|}{P2\sigma 2} + \frac{4}{d}\left(\frac{1}{\gamma-1}\right) S_t \frac{|U|}{P2\sigma 2}\{T_w - P^2\sigma^2 - \left(\frac{2}{\gamma-1}\right)U^2\} \quad (26)$$

$$G = \frac{4}{d}\left(\frac{2}{\gamma-1}\right) C_f U|U| \quad (27)$$

Leakage

In chapter 5 different methods to account for the leakage losses in pressure exchangers have been described. In this Appendix, the three methods and various calculations associated with these methods have been explained.

The energy and mass flow correction method

The energy and mass flow correction method has been explained for a four port pressure exchanger without transfer passages but similar consideration will apply to four port pressure exchanger with transfer passages, pressure equalisers and pressure dividers.

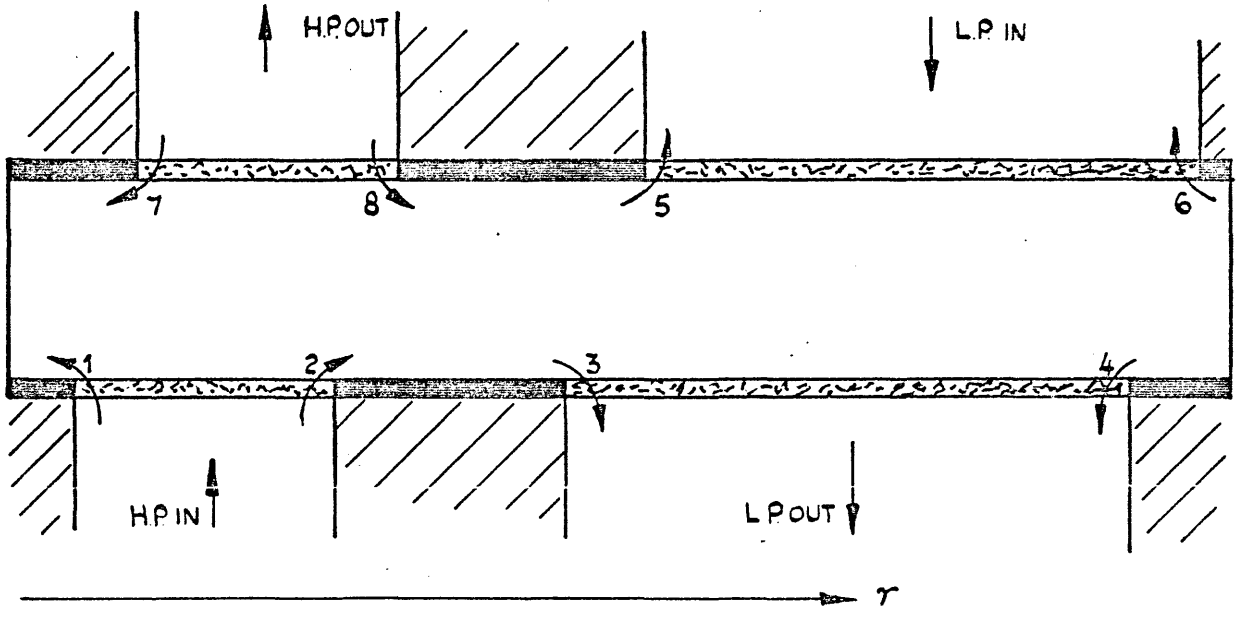


Fig. 15.V.1.

Fig.(15.V.1) shows leakage flows in a four port pressure exchanger. As explained in fig.(15.V.1) the black spaces represent regions of radial leakage from cells to leakage sink (close end), the dotted regions are regions of radial leakage from ports to leakage sink and arrows show regions of the circumferential leakage from port to cell.

Circumferential leakage from cell to cell are ignored.

The non-dimensional bulk input for a leakage free operation is defined as:

$$\mu = \int_{\tau_1}^{\tau_2} E d\tau - \int_{\tau_7}^{\tau_8} E d\tau \qquad (28)$$

and the mass flow per cycle through each port is given by:

$$G = \int_{\tau_b}^{\tau_a} m d\tau \qquad (29)$$

where $\tau_b - \tau_a$ is the respective port width. The leakage losses modify the situation as:

$$\mu = \int_{\tau_1}^{\tau_2} E d\tau - \int_{\tau_7}^{\tau_8} E d\tau + \left(\int_{o}^{\tau_{max}} E_\ell d\tau\right)_L + \left(\int_{o}^{\tau_{max}} E_\ell d\tau\right)_R \qquad (30)$$

where the third and fourth additional terms on the right hand side of equation (30) represent the leakage energy loss per cycle on the left hand and the right hand end of the cells, respectively; and,

$$G = \int_{\tau_a}^{\tau_b} m d\tau \pm \int_{\tau_a}^{\tau_b} m_\ell d\tau \qquad (31)$$

where the second additional term represent the leakage mass flow through the respective ports. The sign convention has been explained in chapter 5. Similar corrections are applied to the port energy flows.

Therefore, in order to take into account the leakage effects using the energy and mass correction method, the main task is to calculate different types of leakage mass and energy flows at each time step at the two cell ends.

As it has been described in chapter 5, the leakage flows are calculated by a formula due to Kearton & Keh (32):

$$m_\ell = A_\ell C_d \sqrt{\frac{2g\gamma}{\gamma-1}\frac{p_\ell^2}{RT_\ell}\left\{\left(\frac{p_x}{p_\ell}\right)^{2/\gamma} - \left(\frac{p_x}{p_\ell}\right)^{\frac{\gamma+1}{\gamma}}\right\}} \qquad (32)$$

where

p_x = static pressure at the discharge of the leak.

p_ℓ = effective stagnation pressure at entry to the leak.

A_ℓ = cross-sectional area of the leak.

C_d = co-efficient of discharge of the leak.

In normalised quantities the formula becomes:

$$m_\ell' = A_\ell' C_d \sqrt{\frac{2}{\gamma-1}\frac{p_\ell^{2'}}{T_\ell'}\left\{\left(\frac{p_x}{p_\ell}\right)^{2/\gamma} - \left(\frac{p_x}{p_\ell}\right)^{\frac{\gamma+1}{\gamma}}\right\}} \qquad (33)$$

(i) The radial leakage

For radial leakage calculations the leakage sink conditions are assumed to be atmospheric. The leak area is equal to the sum of the clearance area at the inner and outer rim of the rotor.

For an outflow, the formula becomes:

$$m_{\ell r} = \phi_r C_d \sqrt{\frac{2}{\gamma-1}\frac{p_{ocell}^2}{T_{ocell}}\left\{\left(\frac{p_{sink}}{p_{ocell}}\right)^{2/\gamma} - \left(\frac{p_{sink}}{p_{ocell}}\right)^{\frac{\gamma+1}{\gamma}}\right\}} \qquad (34)$$

For sonic outflow

$$m_{\ell r}' = \phi_r C_d \sqrt{\frac{2}{\gamma-1}\frac{p_{ocell}^2}{T_{ocell}}\left\{\left(\frac{1}{R_c}\right)^{2/\gamma} - \left(\frac{1}{R_c}\right)^{\frac{\gamma+1}{\gamma}}\right\}} \qquad (35)$$

For an inflow the cell and sink conditions shall interchange.

(ii) The circumferential leakage

The cell to cell circumferential leakage is ignored. Only port to cell (and vice versa) leakages are calculated.

For an outflow, i.e. circumferential leakage from cell to port, the formula becomes:

$$m_{\ell c} = \phi_c \, Cd \sqrt{\frac{2\gamma}{\gamma-1} \frac{P_{ocell}^2}{T_{ocell}} \left\{ \left(\frac{P_{port}}{P_{ocell}}\right)^{2/\gamma} - \left(\frac{P_{port}}{P_{ocell}}\right)^{\frac{\gamma+1}{\gamma}} \right\}} \quad (36)$$

and for sonic outflow:

$$m_{\ell c} = \phi_c \, Cd \sqrt{\frac{2\gamma}{\gamma-1} \frac{P_{ocell}^2}{T_{ocell}} \left\{ \left(\frac{1}{R_c}\right)^{2/\gamma} - \left(\frac{1}{R_c}\right)^{\frac{\gamma+1}{\gamma}} \right\}} \quad (37)$$

For an inflow cell and port conditions interchange their places.

The porous cell wall method

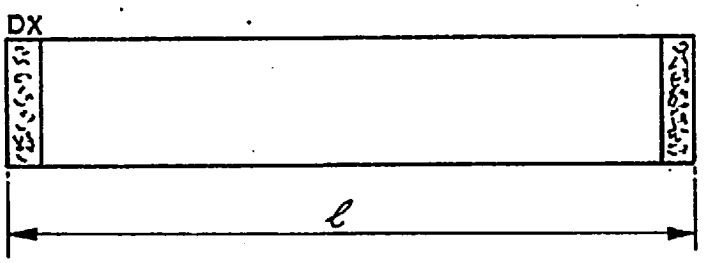


Fig. 15.V.2.

Fig. (15.V.2) shows a pressure exchanger cell with porous cell walls at the cell ends. Each perforated portion occupies a length equal to the spatial interval DX. The leakage flow is simulated by an equivalent mass flow in or out through the perforated portion of the cell in a direction normal to the main flow. The equivalent mass flow is the sum of the instantaneous value of the radial and circumferential leakage flow rates of the cell end which are calculated according to the different formulae described in the previous sections. Thus,

$$m_\ell = m_{\ell r} + m_{\ell c} \tag{38}$$

The perforation co-efficient β is given by:

$$\beta = \text{clearance area/surface area of a spatial interval} \tag{39}$$

$$= Ar/DX \times Acell \times 4/dh \tag{40}$$

$$= \phi_r/DX \times 4/dh \tag{41}$$

and

β $\frac{\phi_r + \phi_c}{DX} \times \frac{dh}{4}$ when circumferential leakage is also taken into account.

$$\psi = \text{leakage mass flow/unit length} \tag{42}$$

$$= m_\ell/DX \tag{43}$$

$$\therefore \quad \beta\psi = \phi_r m_\ell \times \frac{dh}{4DX^2} \tag{44}$$

Therefore, the B terms can now be calculated. $\phi_r' = \phi_r \times \frac{dh}{4DX^2}$

$$B1 = \frac{\gamma-1}{2}\frac{a}{\rho} \times \phi_r' m_\ell \tag{45}$$

$$B2 = \frac{\gamma-1}{2}\frac{a^2}{P}(h_\ell + u^2{}_\ell/2) \times \phi_r' \times m_\ell \tag{46}$$

$$B3 = \frac{\gamma-1}{2}\frac{a^2}{P}(h + u^2/2)\phi_r' m_\ell \tag{47}$$

$$B4 = \gamma\frac{\gamma-1}{2}\frac{a}{P}u^2 \phi_r' m_\ell \tag{48}$$

$$B5 = \frac{\gamma-1}{2}\frac{a^2}{P} u \phi_r' m_\ell \tag{49}$$

$$B6 = \frac{u^2}{P} \phi_r' m_\ell \times \frac{\gamma-1}{2} \tag{50}$$

If B2 is assumed equal to B3 then the calculation procedure is much simplified.

The partly open end method

The partly open end method, as discussed in chapter 5, is based on the calculation of a residual velocity of the fluid leaking through the gap between the rotor and its end plates. This residual velocity is then added algebraically to the main flow velocity to determine the value of the velocity variable corrected for leakage losses. The pressure variable is adjusted to the corrected value of the velocity variable. Entropy is assumed to remain unaltered, although this method can easily be further developed to take entropy variations into account.

In order to calculate the residual velocity and the corrected values of the pressure and velocity variables, the existing solution procedure for the boundary calculations has been utilised. The flow through the gap between the rotor and its end plates is simulated by a flow through the partly open cell end. The supposed geometry at the cell end has been illustrated in fig. (13.15). An examination of the supposed geometry shows that it is similar to the assumed cell end configuration for the derivation of the boundary relations by Spalding (13) based on Jenny's approach.

From fig. (13.15), the following features should be noted.

(i) The fraction of cell opening ϕ varies from 0 to 1 linearly with time, in case of the boundary conditions for the main flow, depending on the non-dimensional cell width. Whereas the fraction of cell opening for leakage flow calculations is calculated from the clearance geometry and remains constant for the whole cycle.

The fraction of cell opening for the radial leakage calculations ϕ_r is calculated from a knowledge of the sum of the clearance area at the inner and outer rims of the cell.

The fraction of cell opening for the circumferential leakage calculations ϕ_c is calculated from a knowledge of clearance area along the cell height.

(ii) The external conditions, which happen to be the prescribed conditions at the ports for the main flow calculations at the boundaries, are replaced by the leakage sink conditions.

The conditions at the leakage sink for the radial leakage flow calculations are assumed to be the atmospheric conditions and for the circumferential leakage flow calculations, the leakage sink conditions are assumed to be the conditions in the port participating in the leakage flow. Intercell leakage has been ignored. The method can easily be developed to take intercell leakage into account.

The following relations, originally derived for the main flow calculations at the boundaries for partly open ends, are applicable to the leakage flow calculations.

(i) Subsonic Inflow

$$\frac{\frac{u}{a_o}}{1 - (\frac{\gamma-1}{2})(\frac{u}{a_o})^2} = \phi \left(\frac{P_o}{P}\right)^{\frac{\gamma-1}{2\gamma}} \sqrt{(\frac{2}{\gamma-1})\{(\frac{P_o}{P})^{\frac{\gamma-1}{\gamma}} - 1\}} \qquad (51)$$

(ii) Sonic Inflow

$$\frac{\frac{u}{a_o}}{1 - (\frac{\gamma-1}{2})(\frac{u}{a_o})^2} = \phi \left(\frac{2}{\gamma+1}\right)^{\frac{1}{2}(\frac{\gamma+1}{\gamma-1})} \frac{P_o}{a \frac{2\gamma}{\gamma-1} e^{-S}} \qquad (52)$$

(iii) Subsonic Outflow

$$(\frac{u}{a})^2 = (\frac{2}{\gamma-1})\{1 - (\frac{P}{P_x})^{\frac{1-\gamma}{\gamma}}\} / \{\frac{1}{\phi_2} (\frac{P}{P_x})^{2/\gamma} - 1\} \qquad (53)$$

(iv) Sonic Outflow

$$\frac{u}{a} = \phi \{\frac{2}{\gamma+1} + (\frac{\gamma-1}{\gamma+1})(\frac{u}{a})^2\}^{\frac{\gamma+1}{2(\gamma-1)}} \qquad (54)$$

These calculations are based on the previous values of p and a. The corrected value of the velocity variable u given by $u + u_\ell$

$$U = 2/_{\gamma-1}\, u \tag{55}$$

The new value of P is now obtained by application of the appropriate cell equation:

$$P_P\, \sigma_P + U_P = P_Q\, \sigma_Q + U_Q + \tfrac{1}{2}(P_P + P_Q)(\sigma_P - \sigma_Q) \tag{56}$$

$$P_P\, \sigma_P + U_P = P_s\, \sigma_s - U_s + \tfrac{1}{2}(P_P + P_s)(\sigma_P - \sigma_s) \tag{57}$$

where σ_P is again the previous value of σ.

Transfer passage losses

The transfer passage flow is assumed to be the steady flow. The losses associated with a transfer passage are therefore obtained from the steady flow loss data. These losses include the friction, heat transfer and minor losses. In the present method transfer passages are assumed to be perfectly insulated and therefore the heat transfer losses are negligible. The head loss due to the friction and bends depends mainly on the length and cross-section of the transfer passage and the radius of curvature of the bends for given conditions and can be obtained from the technical data on fuel (34).

The procedure to calculate the transfer passage losses and their effects on the performance of pressure exchangers is explained for a four port pressure exchanger with one transfer passage. Similar considerations will apply to pressure exchangers with higher number of transfer passages.

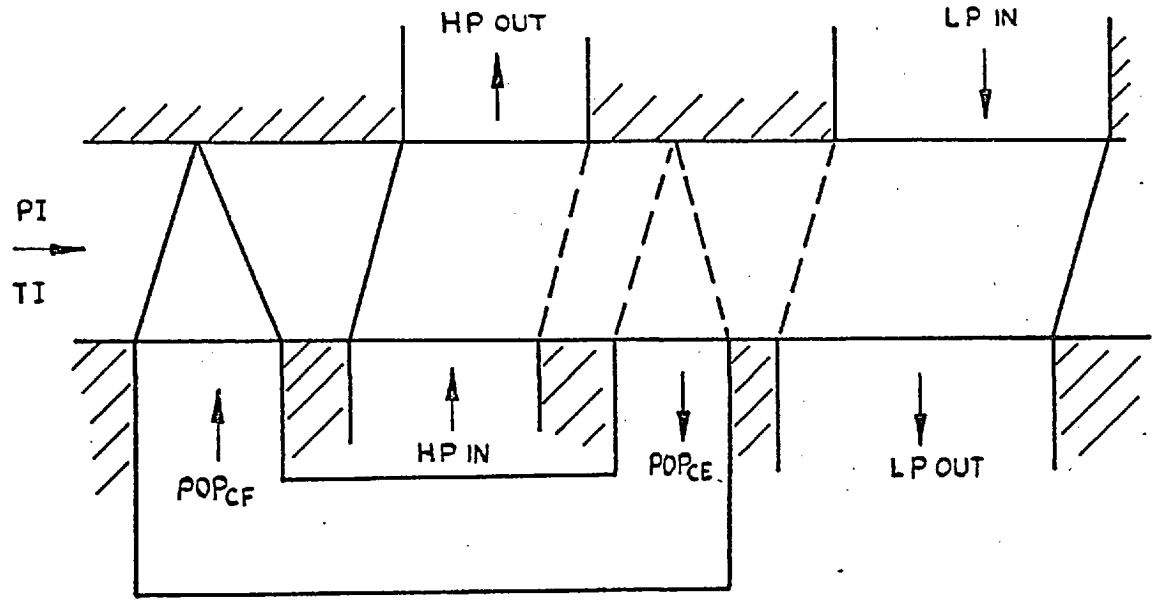


Fig. 15.V.3.

(i) As an initial step, the transfer passage is assumed to be an ideal transfer passage which means that the stagnation pressures and temperatures at the two ends of a transfer passage are the same.
Even in an ideal transfer passage, the boundary conditions at the transfer ports are unknown. An initial guess is obtained by application of the pressure differential method. These conditions are further refined by recycling the calculation procedure until the mass continuity in the transfer ports is satisfied and also the initial conditions in the cell match the final conditions.

(ii) The steady flow values in the transfer passage are now calculated. The ~~head~~ pressure loss at the transfer passage is obtained as follows:

$$\Delta p_{TP} = \text{const} \times \frac{\gamma}{2} \rho u^2 \qquad (58)$$

where the value of the constant depends upon the geometry of the transfer passage. From the head loss is obtained the pressure drop in the transfer passage.

The cycle calculations are now performed again with the boundary conditions at the transfer ports adjusted to accommodate the pressure drop in the transfer passage and are repeated until the equilibrium conditions are attained.

15.6 APPENDIX VI

STEADY STATE CONDITIONS IN THE PORTS OF A PRESSURE EXCHANGER

Object:

To form a relation between flow conditions in the cell ends and assumed steady state conditions in the ports of a pressure exchanger such that the mass and energy flows are conserved in an area equal to the port area taking account of the cell wall thickness. Three different cases, covering the three likely situatinns in pressure exchanger ports have been analysed.

(i) Inlet port; the stagnation values of pressure and temperature P_o and T_o respectively are prescribed at the port

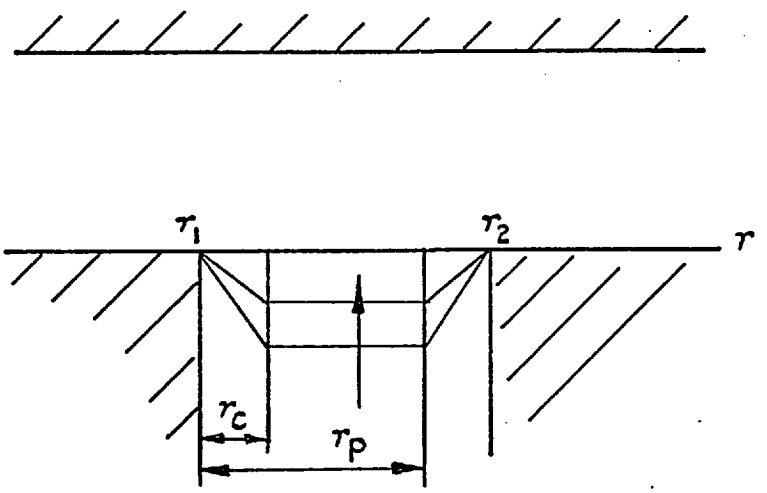


Fig. 15.VI.1

The computerised procedure provides mass and energy flow rate profile through the port for each cycle.

Let us say

$$m'_{port} = \int_{\tau_1}^{\tau_2} \dot{m}' d\tau \qquad (1)$$

where prime denotes non-dimensional quantities.

The port area taking into account the cell wall thickness

$$A'_p = \frac{1}{K} \cdot \frac{\tau_p}{\tau_c} \qquad (2)$$

where K is equal to actual cell area divided by the cell area inclusive of the wall thickness.

If $\dot{N}(1/\tau_c)$ cells pass through a fixed point in unit time, then the port mass flow rate is given by

$$\dot{m}'_{port} = \int_{\tau_1}^{\tau_2} m' d\tau/\tau_c \tag{3}$$

From the continuity equation

$$\bar{\rho}' \bar{u}' A'p = \dot{m}'_{port} \tag{4}$$

where the quantities with a bar denote the steady state conditions in the port. Invoking equation (3)

$$\bar{\rho}' \bar{u}' A'_p = \int_{\tau_1}^{\tau_2} m' d\tau \tag{5}$$

From equation (2)

$$\bar{\rho}' \bar{u}' = \frac{K}{\tau_p} \cdot \int_{\tau_1}^{\tau_2} m' d\tau \tag{6}$$

From the definition of a Mach number

$$\bar{M} = \frac{\bar{u}'}{\bar{a}'} \tag{7}$$

Substituting from equation (7) and rearranging

$$\bar{M} = \frac{1}{\bar{\rho}' \bar{a}'} \cdot \frac{K}{\tau_p} \cdot \int_{\tau_1}^{\tau_2} \dot{m}' d\tau \tag{8}$$

From the definition of the stagnation quantities

$$\frac{T_o'}{T'} = (1 + \frac{\gamma-1}{2} \bar{M}^2) \tag{9}$$

$$\frac{a_o'}{a'} = (1 + \frac{\gamma-1}{2} \bar{M}^2)^{\frac{1}{2}} \tag{10}$$

$$\frac{\rho_o'}{\rho} = \left(1 + \frac{\gamma-1}{2}\overline{M}^2\right)^{1/\gamma-1} \tag{11}$$

From equation (10) and (11)

$$\frac{1}{\overline{\rho a}} = \frac{1}{\rho_o a_o}\left(1 + \frac{\gamma-1}{2}\overline{M}^2\right)^{\frac{\gamma+1}{2(\gamma-1)}} \tag{12}$$

Substituting from equation (12) into equation (8)

$$\overline{M} = \frac{K}{\tau_p} \times \frac{1}{\rho_o a_o}\left(1 + \frac{\gamma-1}{2}\overline{M}^2\right)^{\frac{\gamma+1}{2(\gamma-1)}} \int_{\tau_1}^{\tau_2} \dot{m}' d\tau \tag{13}$$

From the gas relation and the sonic speed definition in non-dimensional form;

$$\overline{\rho_o'} = \frac{\overline{P}_o'}{\overline{T}_o'} \tag{14}$$

$$\overline{a_o'} = \sqrt{T_o'} \tag{15}$$

Substituting from equation (14) and (15) into equation (13)

$$\overline{M} = \frac{K}{\tau_p} \times \frac{\sqrt{T_o'}}{P_o'} \times \left(1 + \frac{\gamma-1}{2}\overline{M}^2\right)^{\frac{\gamma+1}{2(\gamma-1)}} \times \int_{\tau_1}^{\tau_2} \dot{m}' d\tau \tag{16}$$

(ii) Outlet port; stagnation pressure P_o prescribed at the port.

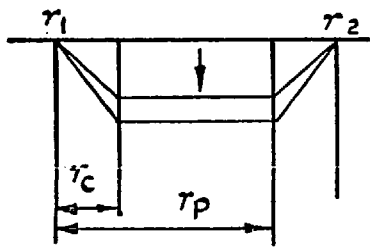


Fig. 15.VI.2.

From the energy equation and assuming a constant specific heat

$$\dot{m}'_{port}\,\overline{T_o}' = \int_{\tau_1}^{\tau_2} E\,d\tau/\tau_c \qquad (17)$$

Therefore,

$$\overline{T_o}' = \int_{\tau_1}^{\tau_2} E'\,d\tau/(\tau_c \times \dot{m}'port) \qquad (18)$$

Substituting from equation (3)

$$\overline{T_o}' = \int_{\tau_1}^{\tau_2} E'\,d\tau/\int_{\tau_1}^{\tau_2} \dot{m}'\,d\tau \qquad (19)$$

Substituting from equation (19) into (16)

$$\overline{M} = \frac{K}{\tau_p} \times \frac{1}{P_o} \times \sqrt{\left(\int_{\tau_1}^{\tau_2} \dot{m}\,d\tau \times \int_{\tau_1}^{\tau_2} E\,d\tau\right)} \times \left(1 + \frac{\gamma-1}{2}\overline{M}^2\right)^{\frac{\gamma+1}{2(\gamma-1)}} \qquad (20)$$

(iii) Outlet port; static pressure P_X prescribed at the port.

From the definition of stagnation pressure

$$\frac{\overline{P_o}'}{\overline{P_X}'} = \left(1 + \frac{\gamma-1}{2}\overline{M}^2\right)^{\gamma/\gamma-1} \qquad (21)$$

Substituting from equation (21) into (20)

$$\overline{M} = \frac{K}{\tau_p} \times \frac{1}{P_X'} \times \sqrt{\int_{\tau_1}^{\tau_2} E\,d\tau \times \int_{\tau_1}^{\tau_2} m\,d\tau} \times \left(1 + \frac{\gamma-1}{2}\overline{M}^2\right)^{-\frac{1}{2}} \qquad (22)$$

15.8 APPENDIX VII

	Subroutine Names	Function
1)	AUX	Calculates auxiliary values.
2)	BLEAK	Calculates leakage functions for porous wall method.
3)	CEMF	Designs cell filling and cell emptying ports.
4)	CEXEN	Calculates cell exit and entry losses.
5)	CFST	Calculates friction and heat transfer terms.
6)	CSCR	Designs scavenging ports.
7)	CYCLE	Sets up boundary conditions.
8)	DESIGN	Velocity-profiles and contact surface calculations.
9)	DIVIDE	Calculates divider performance.
10)	DUCT1	Calculates steady state conditions in ports.
11)	DUCT2	Calculates steady state conditions in ports.
12)	EQUAL	Calculates equaliser performance.
13)	FINI	Calculates mean pressure and flow in the cell.
14)	INIT	Calculates the initial values.
15)	INITIA	Initialises the different quantities.
16)	INTEG	Integrates the different quantities.
17)	IRESID	Recalls the stores quantities.
18)	KING	Plotting and microfilm package.
19)	LEK	Controls leakage flow calculation.
20)	LEK1	Calculates the leakage flows.
21)	LININT	Performs linear interpolation.
22)	MAIN	Controls the whole operation.
23)	OPTIM	Controls the design calculations.
24)	PHASE	Designs the phasing between scavenging ports.
25)	PORTS	Operates on the boundaries.
26)	PORTX	Controls the boundary calculation.
27)	RESID	Stores different quantities.

	Subroutine Names	Function
28)	RESULT	Calculates the performance of a four port machine.
29)	SLOPE	Calculates the slopes of the characteristics.
30)	STEP	Calculates the dependent variables at all central grid points for a forward time step.
31)	TPLOSS	Calculates transfer passage losses.

Labelled common blocks

1)	Bar	15)	LEAK
2)	C	16)	LFLOW
3)	C1	17)	PORT
4)	C2	18)	PROP
5)	C3	19)	PLOT
6)	CC1	20)	REC
7)	CELL	21)	REC1
8)	COMP	22)	RECOVR
9)	CONST	23)	SCR
10)	CYC	24)	SCR1
11)	DIST	25)	SPACE
12)	ENERGY	26)	STAG
13)	FLOW	27)	TRIGER
14)	GAMMA	28)	TWALL

LISTING OF THE VARIABLE NAMES USED IN COMPUTER PROGRAM

Fortran	Algebraic	
A(I)	a	Sonic velocity
A4(I,NPORT)		Two dimensional array to store AM(I)
AA		Coefficient of $(U/A)^2$ in quadratic
ABAR(NPORT)	$\bar{a}$	Port steady flow sonic velocity
AK		Fraction of maximum allowable time

Fortran	Algebraic	
AM(I)	U	Velocity variable
AM1(I)		AM interpolated along "n" characteristics
AM2(I)		" " " "m" "
AM3(I)		" " " "s" "
AMAC(I)	M	Local Mach number
AMB		Mass flow in the cell
AMBAR(NPORT)	$\overline{M}$	Port steady flow Mach number
AMEW	u	Fluid kinematic velocity
AN(I)	P	Pressure variable
AN1(I)		AN interpolated along "n" characteristics
AN2(I)		" " " "m" "
AM3(I)		" " " "s" "
AO	a_o	Stagnation sonic velocity
B1,B2,B3,B4,B5,B6		Leakage terms
B4(I,NPORT)		Two dimensional array to store AN(I)
BE(I)	β	Characteristic slope
BEM(I)	βm	Slope of m characteristics
BEN(I)	βn	" " n "
BES(I)	βs	" " s "
BMAX	βmax	Maximum of BES, BEM, BEN
BLEK		Total leakage mass flow rate
BLEK1, BLEK2, BLEK3,) BLEK4, BLEK5, BLEK6)		Individual leakage flow rate
BLEFT		Total leakage mass flow rate at the left-hand side
BRITE		Total leakage mass flow rate at the right-hand side
C4(I,NPORT)		Two dimensional array to store SIG(1)
CDIS	C_d	Co-efficient of discharge

Fortran	Algebraic	
CF,CF1,CF2,CF3	c_f	Co-efficient of friction
CP	C_p	Specific heat at constant pressure
CV	C_V	Specific heat at constant volume
D	d_h	Cell hydraulic diameter
D1,D2		Friction & heat transfer terms
D4(NPORT)		One dimensional array to store TIM
DELPH	ΔP_{HP}	Pressure drop in HP loop
DELPOP	ΔH_{TP}	Head loss in transfer passage
DELPL	ΔP_{LP}	Pressure difference between LP ports
DELPT1,DELPT2	ΔP_{TP}	Pressure drop in transfer passage
DELEAK (NPORT)	ΔE_{leak}	Increment in port leakage energy flow
DENTH (NPORT)	ΔE	Increment in port energy flow
DELT (NPORT)	τ_{port}	Port width
DFMBAR	$d(f(\bar{M}))$	Derivative of $f(\bar{M})$
DG (NPORT)	Δm	Increment in port mass flow
DGLEAK(NPORT)	Δm_{leak}	Increment in port leakage mass flow
DIFF,DIFF1,DIFF2		Differences
DISTX(NPORT)		Distance travelled by a contact surface
ELCC		Leakage energy flow through a closed end
ELEAK(NPORT)		Leakage energy flow through a port
ENTH(NPORT)		Energy flow through a port
FACTH		Initial guess of HP area ratio
FACTOR		Dummy argument
FACTL		Initial guess of LP area ratio
FMBAR	$F(\bar{M})$	$f(\bar{M})$
FRA		Fraction in linear interpolation
FUA		$f(U/A)$
FUA1		Function of UA1
FUAP		Derivative of FUA

Fortran	Algebraic	
G(NPORT)		Mass flow through a port
G1,G2,G3,G4,G5,G6		Cell mass flows
G1,G2		Friction & heat transfer terms
GX		Dummy argument
GAM	γ	Ratio of $^{CP}/_{CV}$
GAM1	$\frac{\gamma-1}{2}$	
GAM2	$-4/(\gamma-1)$	
GAM3	$2(\gamma-1)/(\gamma+1)$	
GAM4	$\{2/(\gamma+1)\}^{\frac{\gamma+1}{2(\gamma-1)}}$	
GAM5	$2\gamma/(\gamma-1)$	
GAM6	$(\gamma-1)/2\gamma$	
GAM8	$2/\gamma$	
GAM9	$(\gamma+1)/\gamma$	
GAM10	$\gamma-1$	
GAM11	$\gamma+1$	
GAM12	$\gamma-2$	
GAM13	$\gamma-3$	
GAM14	$2/(\gamma-1)$	
GAMX1	$(\gamma+1)/2(\gamma-1)$	
GAMX2	$(3-\ )/(2(\gamma-1))$	
GLEAK(NPORT)		Leakage mass flow through ports
GLEK		Leakage mass flow rate
GLCC		Leakage mass flow through close ends
GUA1		Function of UAI and PHI
I		Subscript variables
IDATA(NPORT)		INDEX, = 1 If port static pressure prescribed
		= 2 If port stagnation pressure prescribed

Fortran	Algebraic	
IFLIP		Indicator of flow reversal = 2 if reversal occurs = 1 if no reversal occurs
IHAND		Index identifying ports = 1 for left-hand port = 2 for right-hand port
IDESIN		Index for design calculations = 1, no design calculations required = 2, design calculation required
IFRIC		Index for friction & heat transfer losses = 1, friction and heat transfer losses ignored = 2, friction and heat transfer losses included with cell entry and exit losses = 3, only friction and heat transfer losses included
IL		Alphameric symbol for left port
ILEAK		Index for leakage losses = 1, leakage losses are neglected = 2, partly open end method is used for leakage losses = 3, energy and mass correction method to be used for leakage losses = 4, porous cell wall method to be used for leakage losses
IND		Indicator to route boundaries computation = 1 for no flow = 2 for sub-critical inflow through partly open end = 3 for super-critical inflow through partly open end

Fortran	Algebraic	
		= 4 for sub-critical inflow through fully open port
		= 5 for super-critical inflow through fully open port
		= 6 for sub-critical outflow through partly open port
		= 7 for super-critical outflow through partly open port
		= 8 for super-critical outflow through fully open port
		= 9 for sub-critical outflow through fully open port
INDEX1		Index to control calling sequence in OPTIM
INDL		IND at left hand port
INDR		IND at right hand port
INPORT		PORT indicator in PHASE & CSCR
IOPEN		Index
		= 2 if port closed
		= 1 if port open
IP		Alphameric symbol identifying port
IPR		INDEX for pressure recovery
		= 2 if recovery is taken into account
		= 1 if recovery is not taken into account
IR		Alphameric symbol for right hand port
IT1, IT2		Indices identifying transfer port numbers
ITER		Iteration counter
ITP		Index for transfer passage losses
		= 1, if losses are taken into account
		= 2, if losses are not taken into account

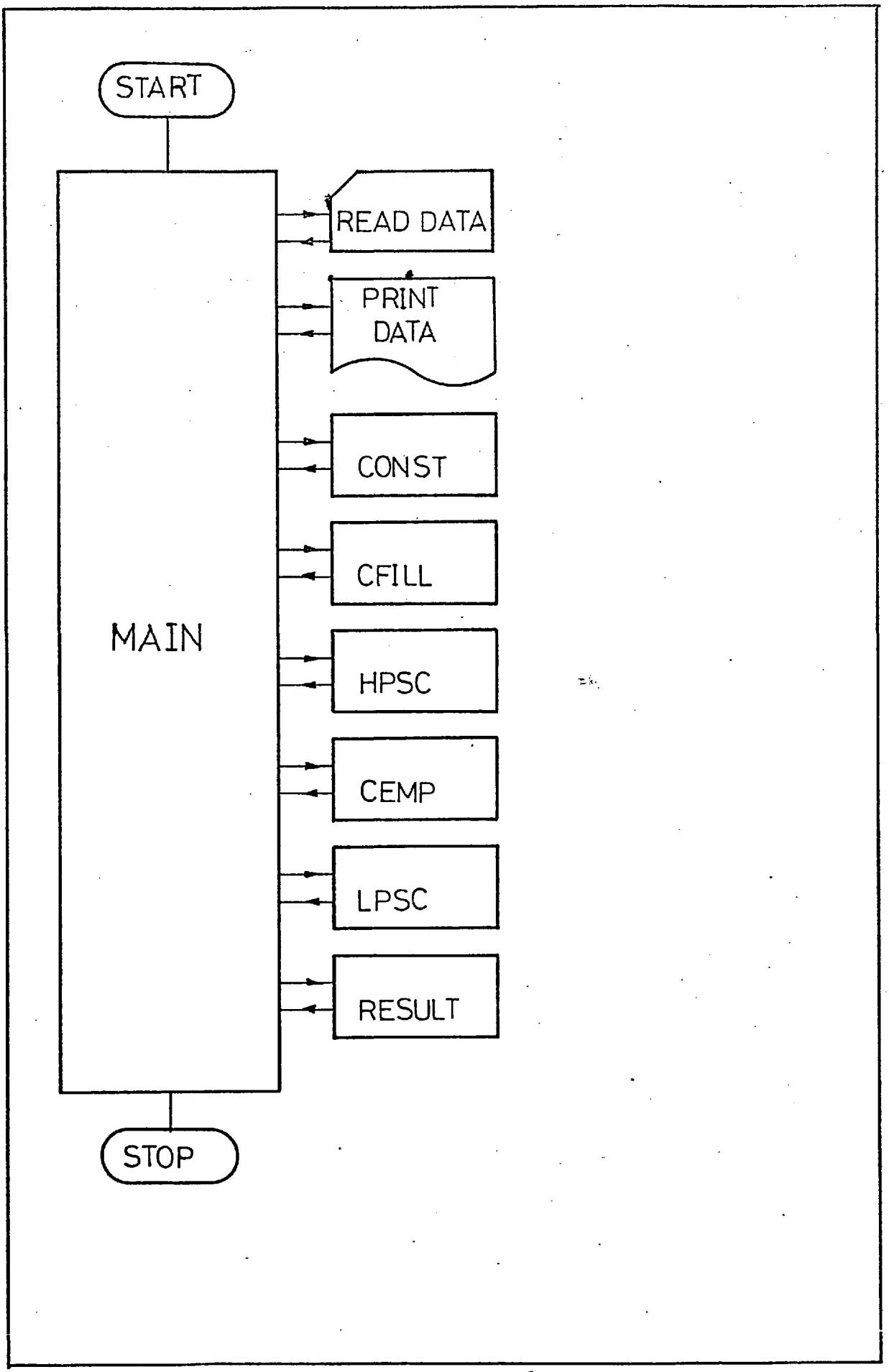
Fortran	Algebraic	
IREC(NPORT)		Index for storing different values = 0, if values have not been recorded = 1 if values have been recorded
ISCR		Index for scavenging calculations = 1, for high pressure scavenging process = 2, for low pressure scavenging process
J		Counter & subscript variables
JPR		Counter in pressure recovery section
JNPORT		Index to identify port in PHASE & CSCR
K		Counter
KCYCLE		Cycle counter
KMAX		Maximum number of cycles
LOOP		Iteration counter
N		Number of grid intervals in spatial direction
N1		Number of grid points in spatial direction
NFLOW		Index for phasing = 1, if outflow is the criterion = 2, if inflow is the criterion
NINIT		Indicator identifying the first port in a DO-loop
NMAX		Indicator to identify the last port
NOPENL		Number of port open on the right hand side
NOPENR		Number of port open on the left hand side
NP		Subscript
NPORT		Subscript and counter for ports
NSCR		Index to guide the scavenge port design calculations
NSTEP		Number of step

Fortran	Algebraic	
P(I)	P	Pressure
PB		Mean pressure in cell
PBAR(NPORT)	$\overline{P}$	Port steady flow static pressure
PHASH	ϕ_{HP}	High pressure phasing
PHASL	ϕ_{LP}	Low pressure phasing
PHI	ϕ	Fraction of cell opening
PHIEFF	ϕ_{eff}	Cell effective area
PHIL		Fraction of cell opening on left hand end
PHIMIC	ϕ_c	Circumferential clearance area
PHIMIR	ϕ_r	Radial clearance area
PHIR		Fraction of cell opening on right hand end
PI		Cell initial pressure
PLK	P_{sink}	Leakage sink pressure
TLK	T_{sink}	Leakage sink temperature
PM		AM2(I)
PN		AN1(I)
PO		Stagnation pressure
POBAR(NPORT)	$\overline{P}_o$	Port steady flow stagnation pressure
POCL		Stagnation pressure in cell, left boundary
POCR		Stagnation pressure in cell, right boundary
POL		Stagnation pressure in the left hand port
POP(NPORT)		Stagnation pressure in ports
POR		Stagnation pressure in the right hand port
POS		Dummy argument for POL, POR
PP		AM at cell boundary
PP1)) PP2)) PP3)		PP during Newton-Raphson method
PR		Ratio of stagnation to static pressure

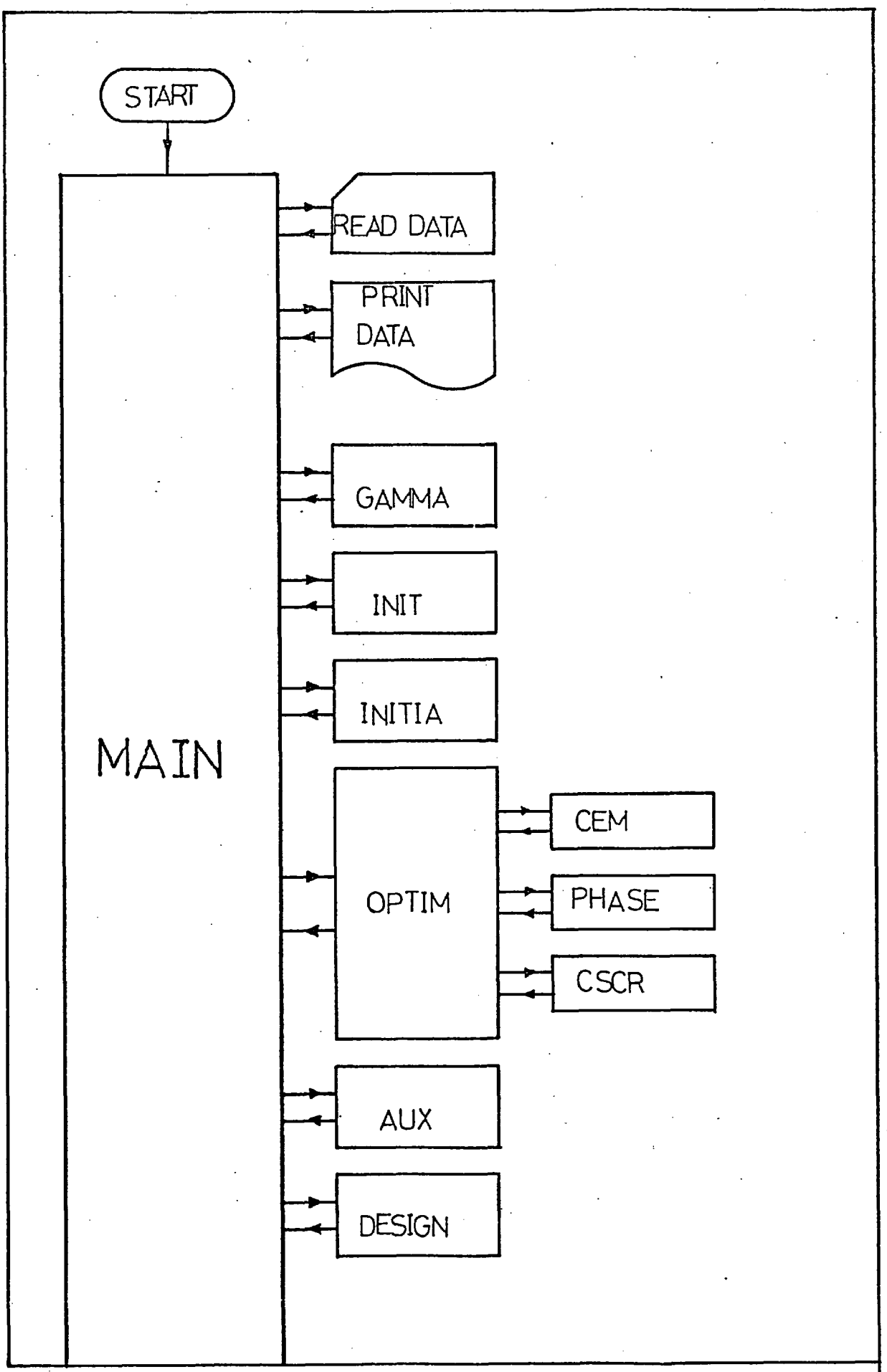
Fortran	Algebraic	
PRL		PR at left port
PRR		PR at right port
PX		Static pressure in ports
PXL		PX in left hand port
PXP(NPORT)		Static pressure in ports
PXR		PX in right hand port
PXS		Dummy argument for PX
R		Overall pressure ratio
RATIOH		High pressure scavenge ratio
RATIOL		Low pressure scavenge ratio
RC		Critical pressure ratio
RE1,RE2,RE3	R_e	Local Reynolds numbers
RO(I)	ρ	Specific density
ROBAR(NPORT)	$\bar{\rho}$	Port steady flow density
S(I)	S	Specific entropy
S(I), S1(I)		Dummy variables
SCRH		Calculated high pressure scavenge ratio
SCRL		Calculated low pressure scavenge ratio
S1G(I)	σ	Entropy variable
S1G1(I)		S1G interpolated along "n" characteristic
S1G2(I)		" " " "m" "
S1G3(I)		" " " "s" "
S1GI		Initial value of S1G
S1GM		S1G2(I)
S1GN		S1G1(I)
S1GO		Stagnation value of S1G
S1N		Head loss at cell entry
SL		Slope
SOL		Stagnation entropy at left hand port
SOR		" " " right " "

Fortran	Algebraic	
SOUT		Head loss at cell exit
ST	S_t	Stanton number
STOT		Total head loss due to cell exit and entry
T(I)	T	Temperature
TBAR(NPORT)	$\overline{T}$	Port steady flow static temperature
TEMPU(I)		AN(I)
TEMPX		Temporary value
TIM	τ	Normalised time
TIMO(NPORT)		Port opening time
TIMC(NPORT)		Port closing time
TIMU(I,NPORT)		Two dimensional to store time
TIMX(I,NPORT)		"
TIN(I)		Local internal energy
TLK		Leakage sink temperature
TMAX	τ_{MAX}	Cycle maximum time
TO		Stagnation timperature
TOBAR(NPORT)	$\overline{T}_o$	Port steady flow stagnation temperature
TOCL		TO at cell left hand boundary
TOCR		TO at right hand boundary
TOL		TO in left hand port
TOP(I)		Stagnation temperature in port
TOR		Stagnation temperature in right hand port
TPS		Head loss in transfer passages
TR	Z	Temperature ratio
TW(I)	T_w	Cell wall temperature
U(I)	u	Velocity
UA		(UU/A) for outflow, (UU/A_o) for inflow
UAI		Local Mach number in throat
UEX		Velocity at a previous instant
UM		AM2(I)

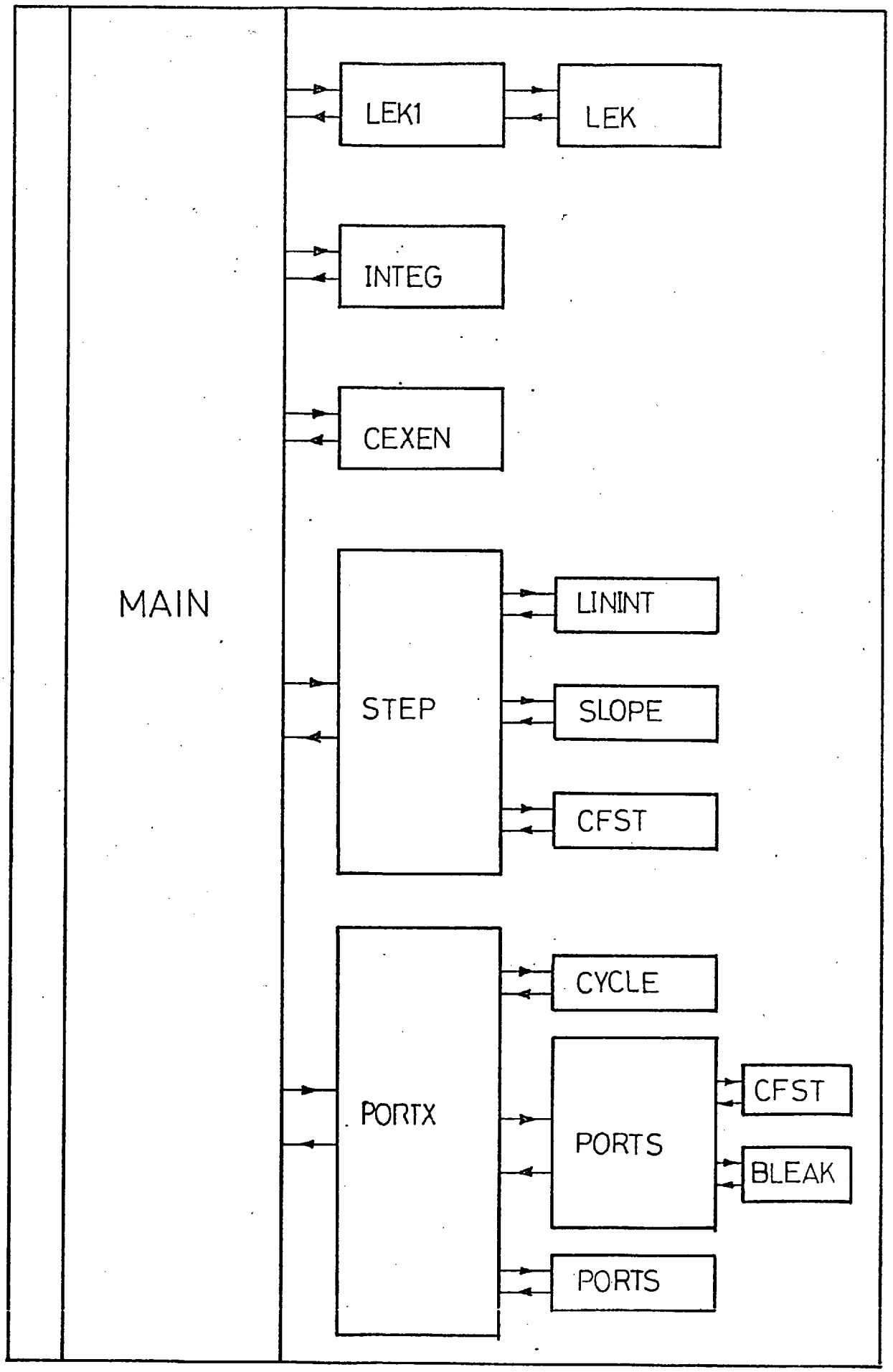
Fortran	Algebraic	
UN		AM1(I)
UU		AM(I) at cell boundary
X		Dummy variable
X(I)	x	Distance
X1(I)		x-interpolated along BEN
X2(I)		" " BEM
X3(I)		" " BES
XADD		Energy loss due to leakage
XMEW	μ	Bulk input
AMEWT		Total bulk input
XMEWT1, XMEWT2		Energy deficit in transfer passage
ZC		Critical pressure ratio in outflow
ZE		" " " " inflow

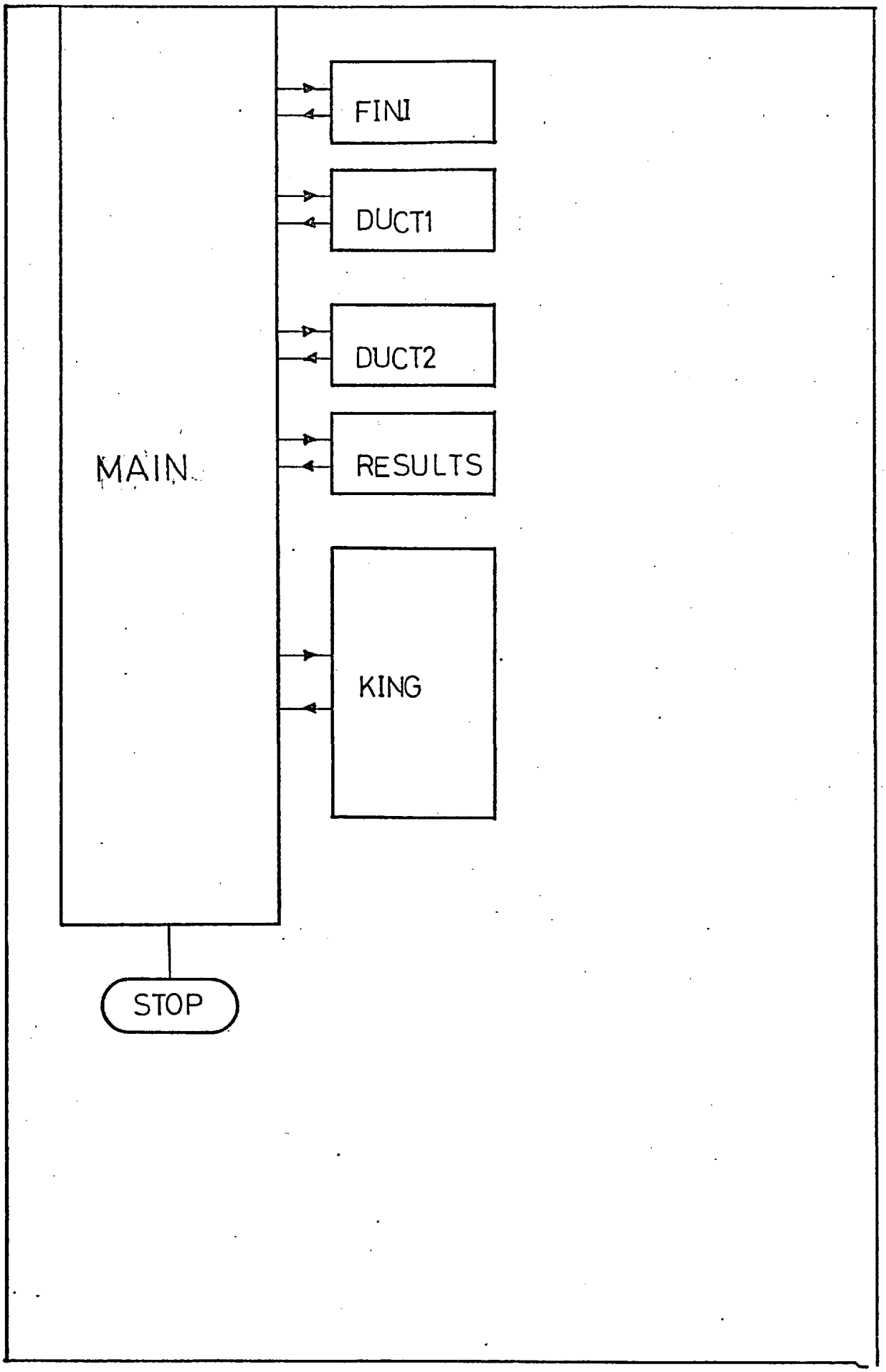


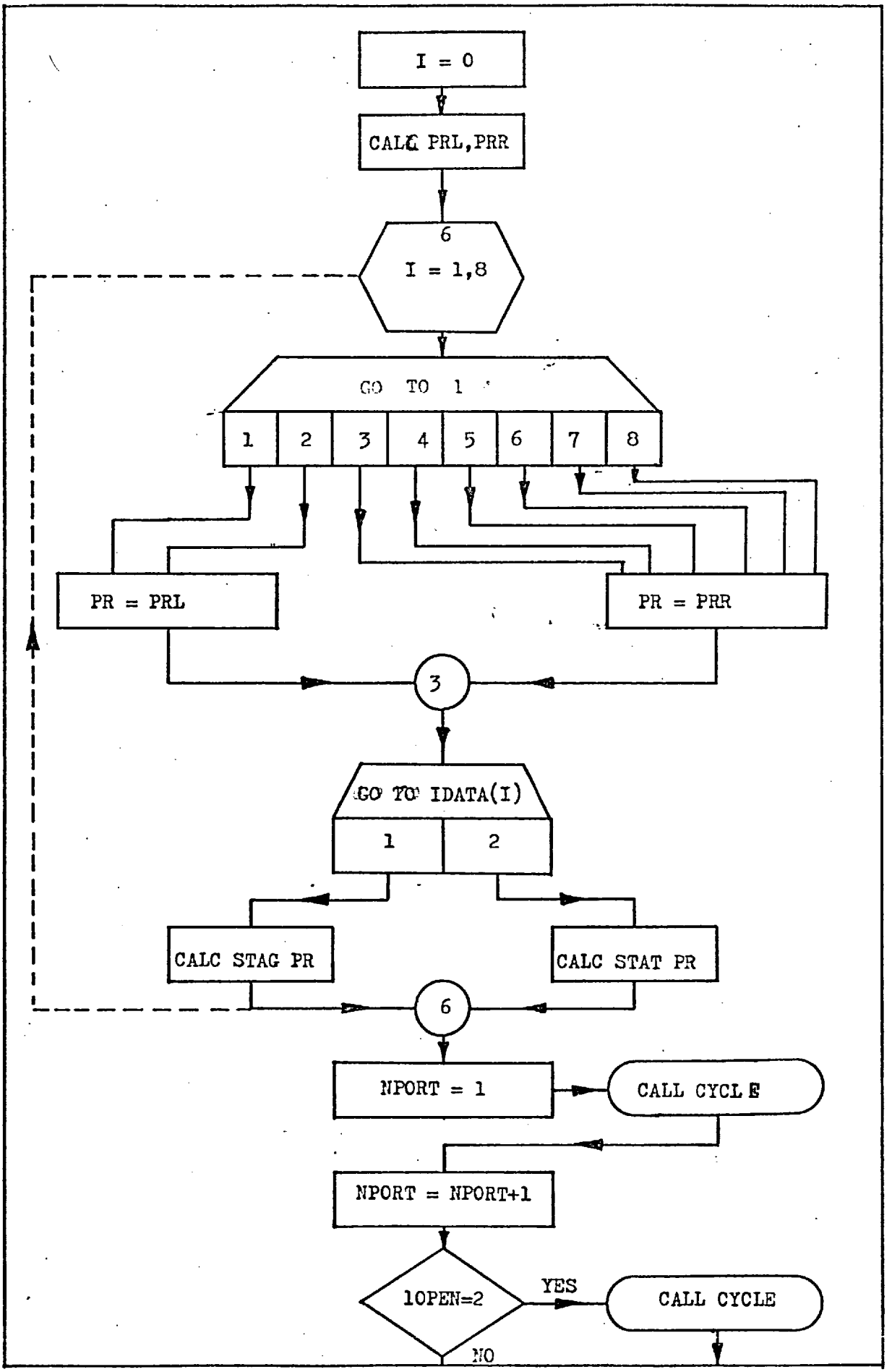
FLOW DIAGRAM FOR APPROX



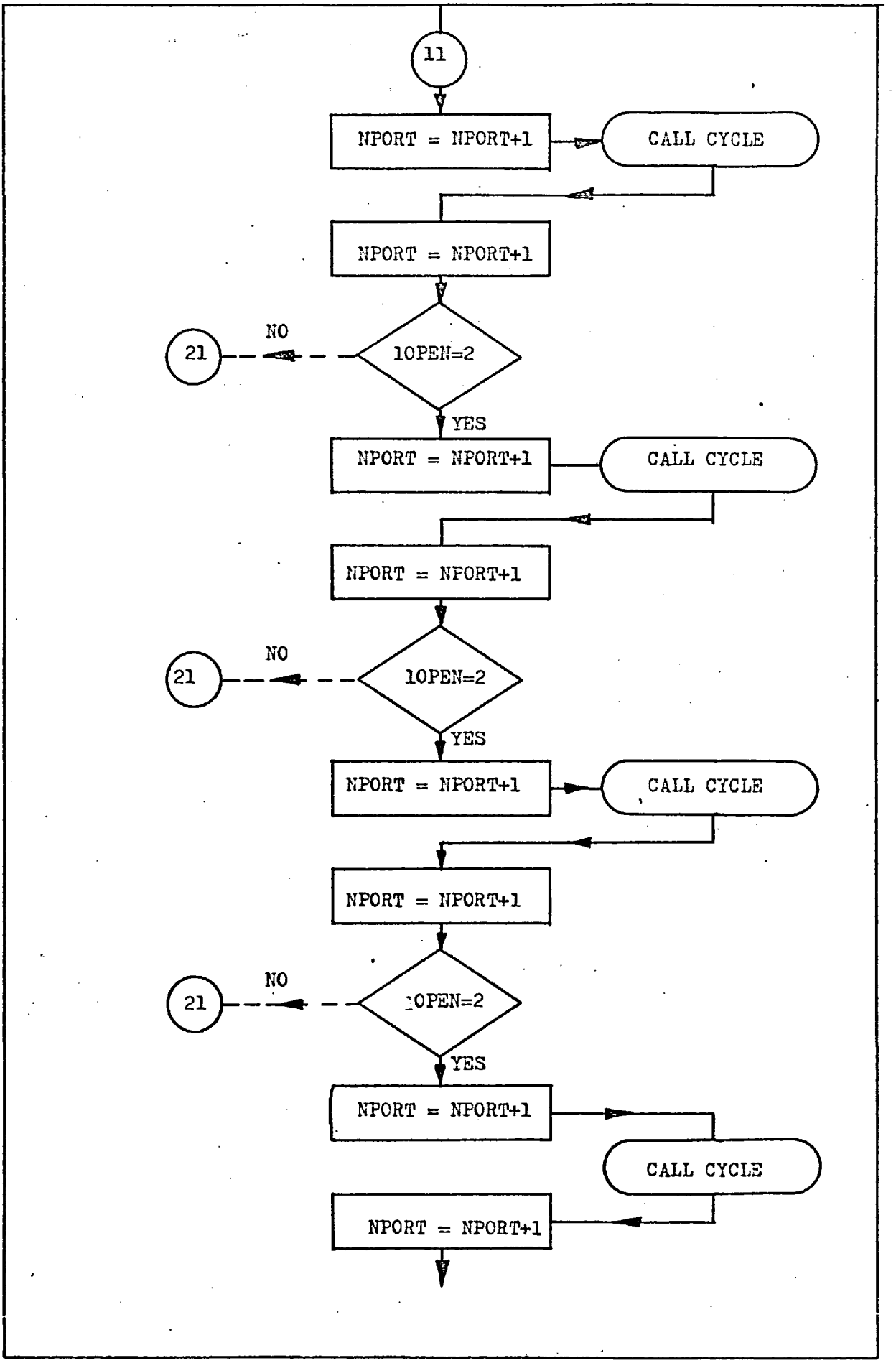
FLOW DIAGRAM FOR GENPX

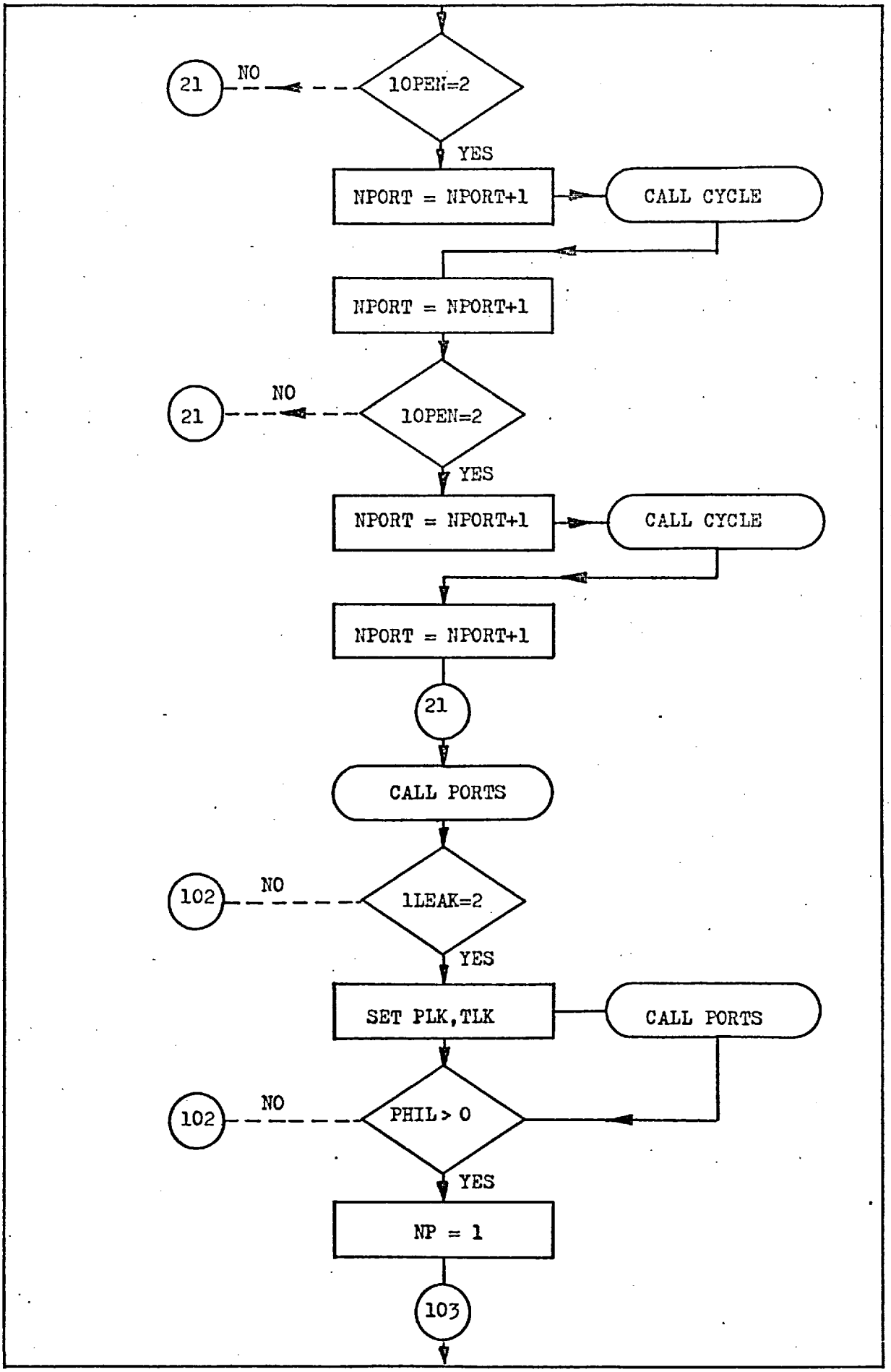

MAIN
LEK1
LEK
INTEG
CEXEN
STEP
LININT
SLOPE
CFST
PORTX
CYCLE
PORTS
CFST
BLEAK
PORTS

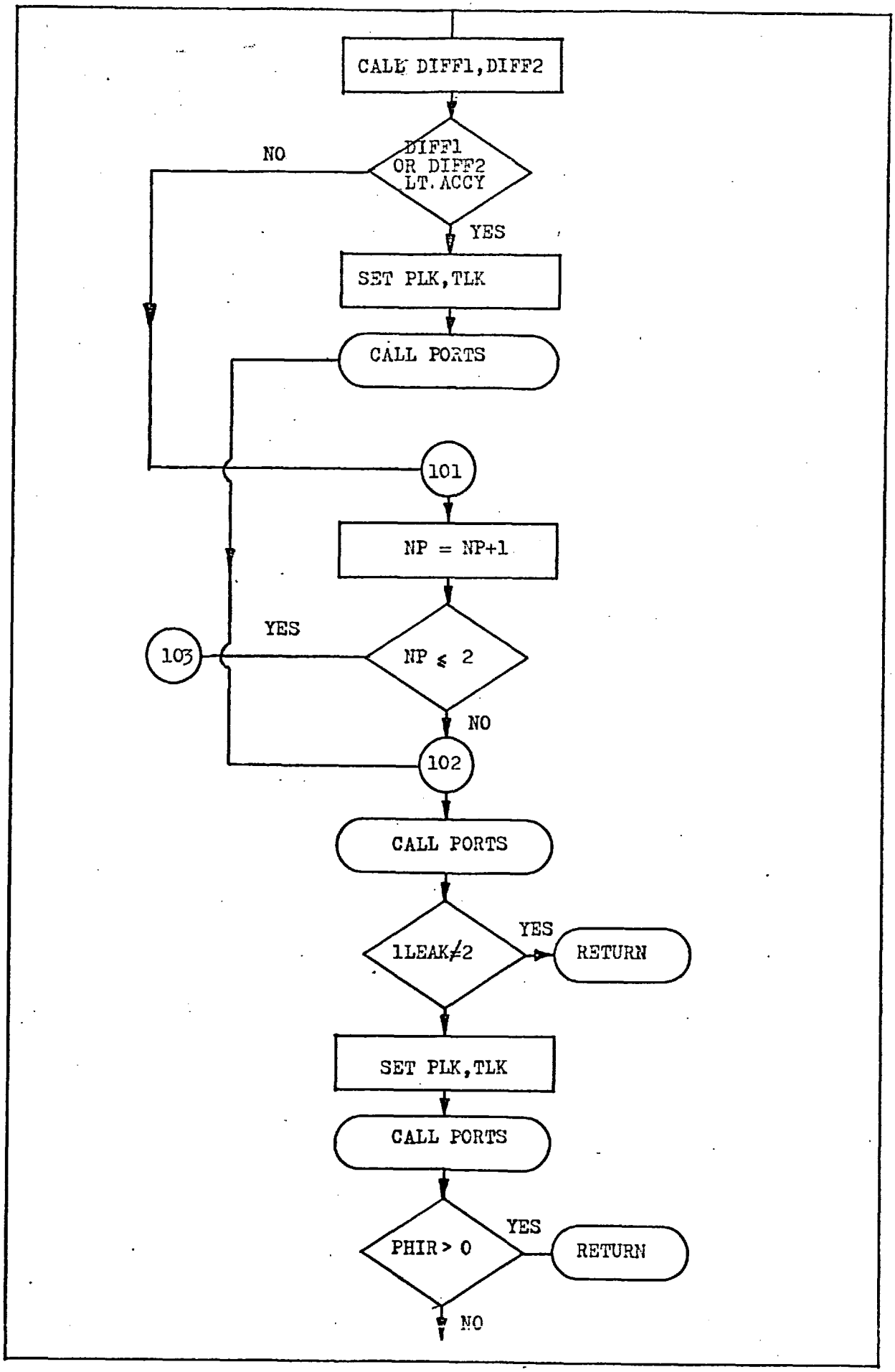

MAIN
FINI
DUCT1
DUCT2
RESULTS
KING
STOP

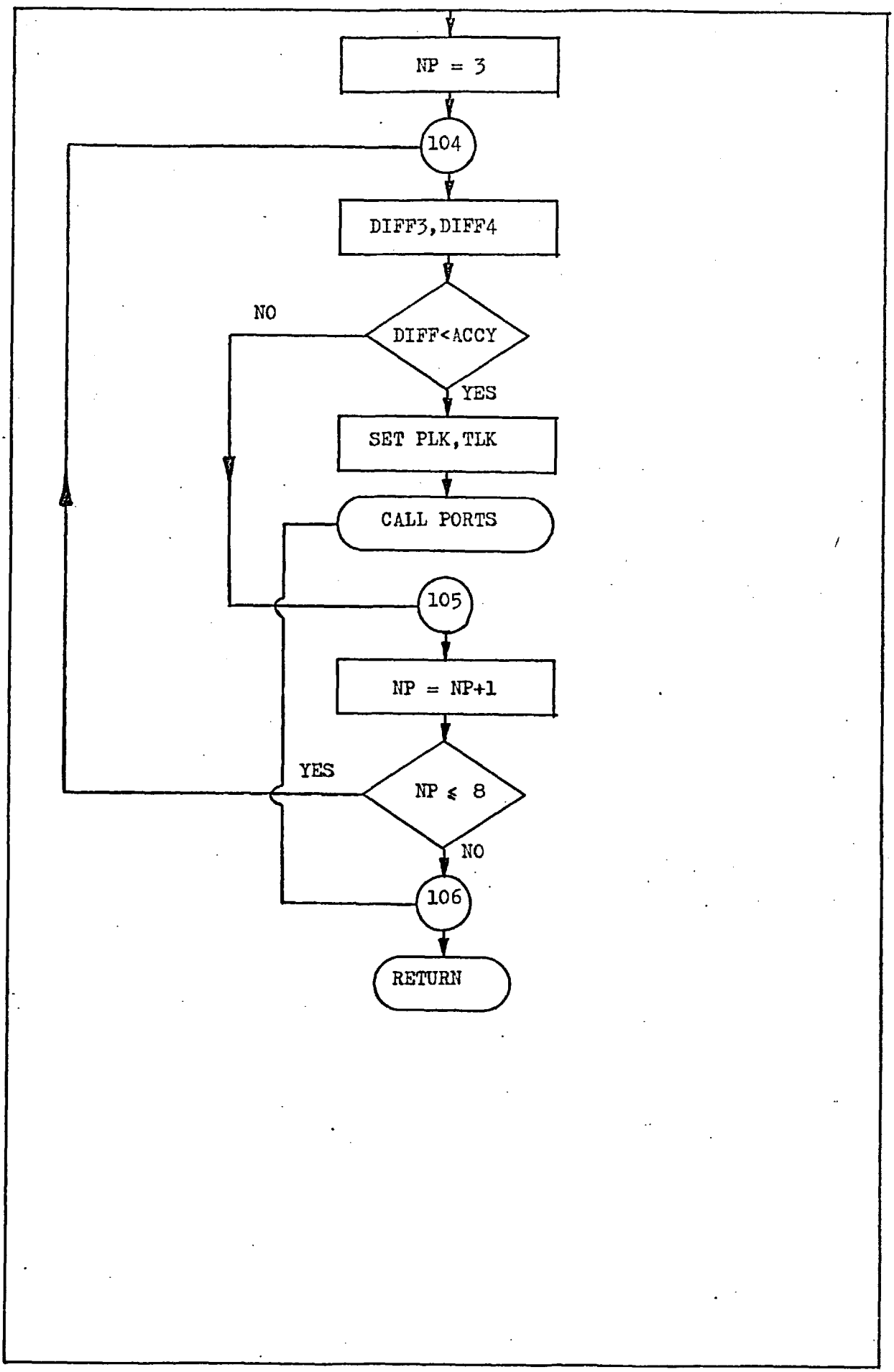


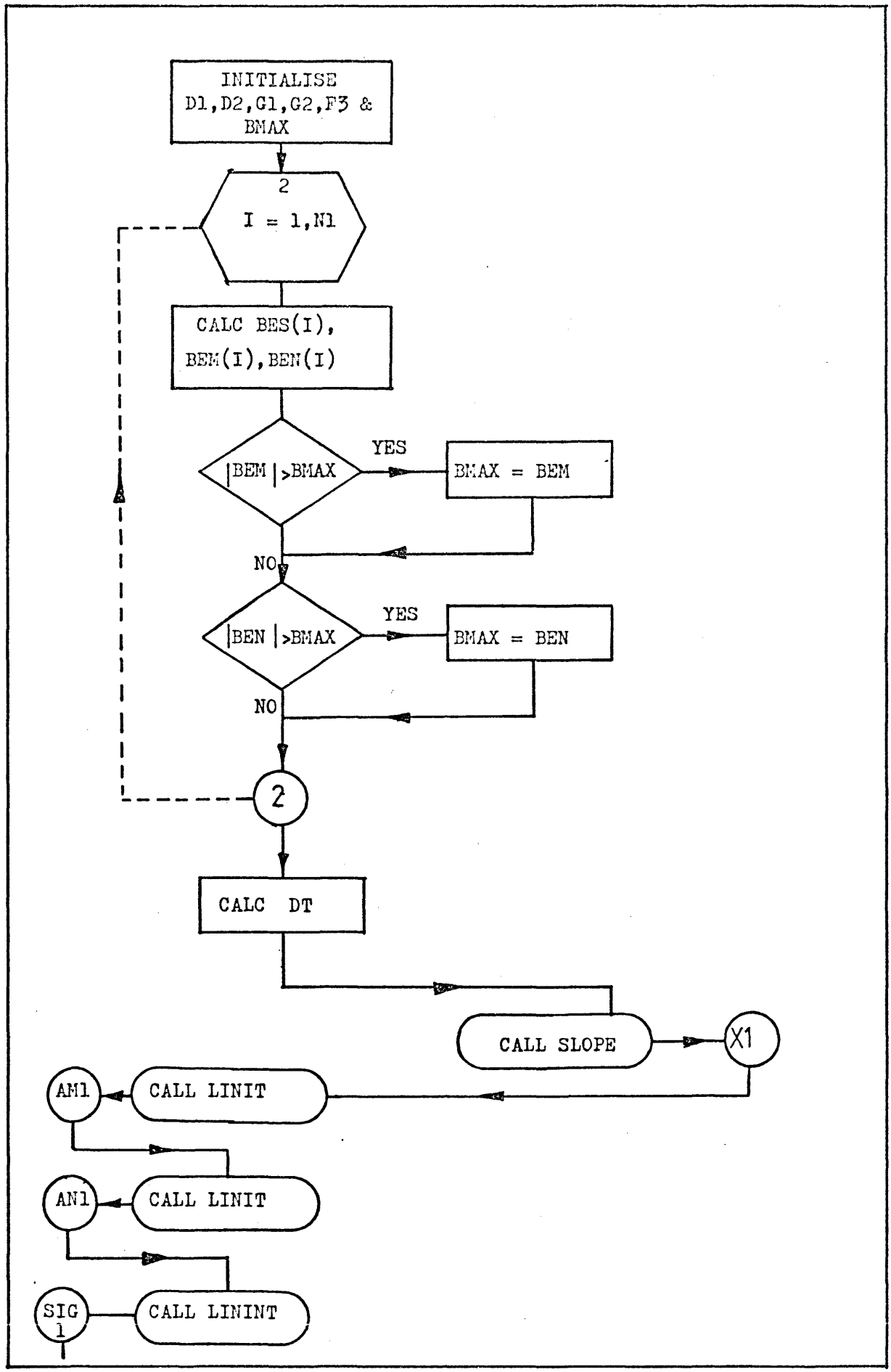
FLOW DIAGRAM OF SUBROUTINE PORTX


11
NPORT = NPORT+1
CALL CYCLE
NPORT = NPORT+1
NO
21
IOPEN=2
YES
NPORT = NPORT+1
CALL CYCLE
NPORT = NPORT+1
NO
21
IOPEN=2
YES
NPORT = NPORT+1
CALL CYCLE
NPORT = NPORT+1
NO
21
IOPEN=2
YES
NPORT = NPORT+1
CALL CYCLE
NPORT = NPORT+1

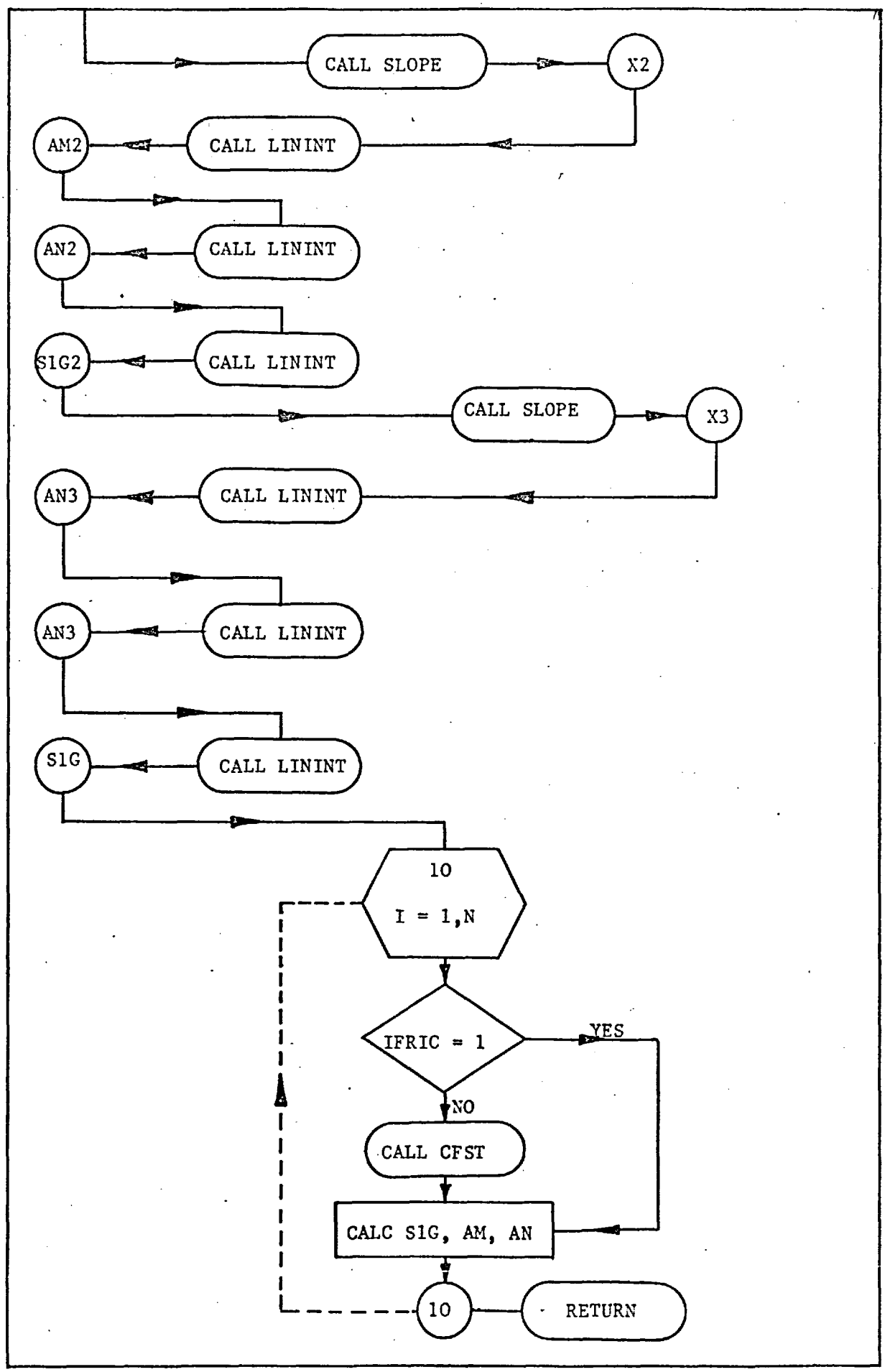

21
NO
10PEN=2
YES
NPORT = NPORT+1
CALL CYCLE
NPORT = NPORT+1
21
NO
10PEN=2
YES
NPORT = NPORT+1
CALL CYCLE
NPORT = NPORT+1
21
CALL PORTS
102
NO
1LEAK=2
YES
SET PLK,TLK
CALL PORTS
102
NO
PHIL > 0
YES
NP = 1
103

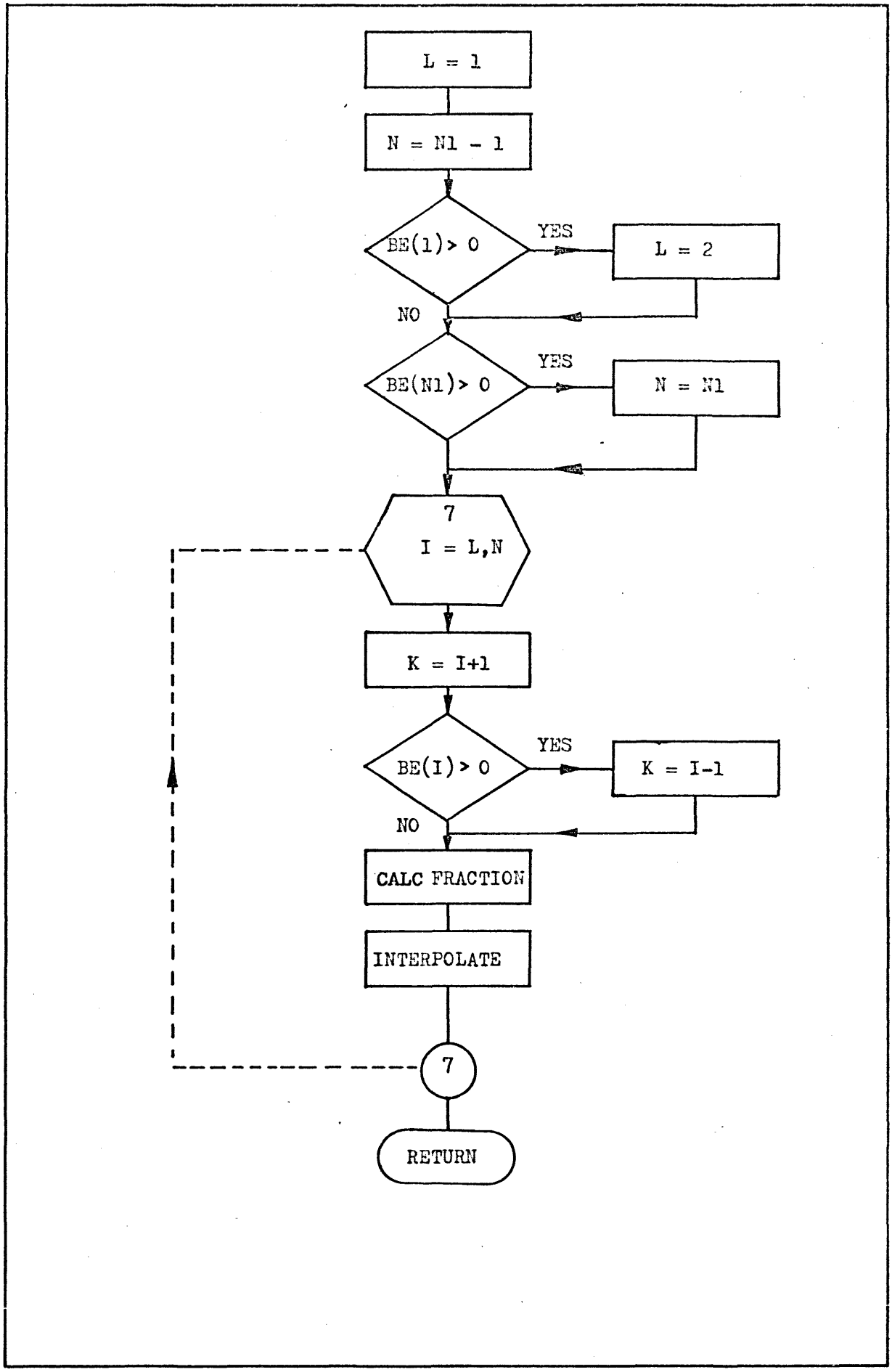

CALL DIFF1,DIFF2
DIFF1 OR DIFF2 LT. ACCY
NO
YES
SET PLK,TLK
CALL PORTS
101
NP = NP+1
YES
103
NP ≤ 2
NO
102
CALL PORTS
YES
1LEAK≠2
RETURN
SET PLK,TLK
CALL PORTS
YES
PHIR > 0
RETURN
NO


NP = 3
104
DIFF3,DIFF4
NO
DIFF<ACCY
YES
SET PLK,TLK
CALL PORTS
105
NP = NP+1
YES
NP ≤ 8
NO
106
RETURN

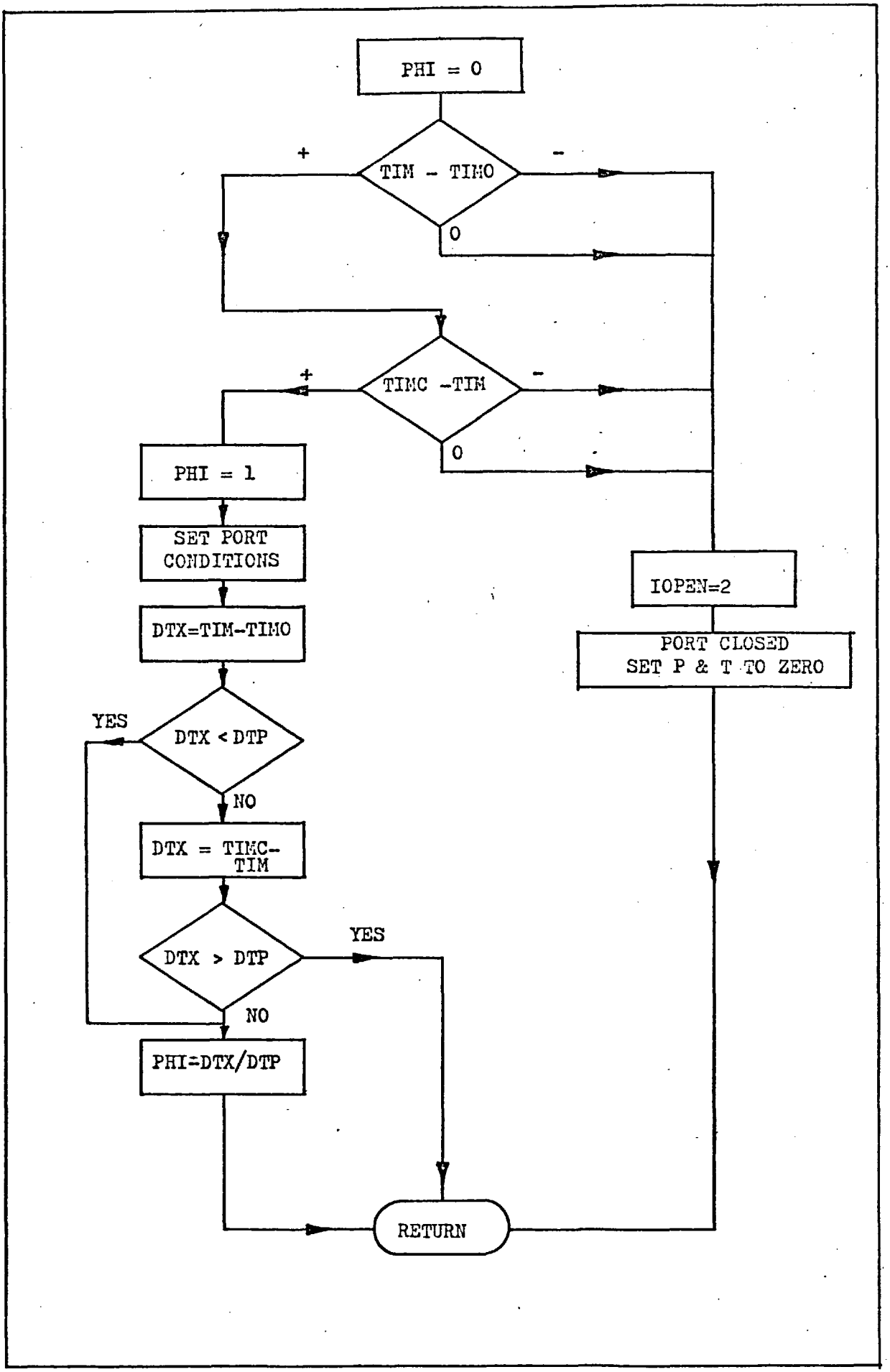


FLOW DIAGRAM OF SUBROUTINE STEP

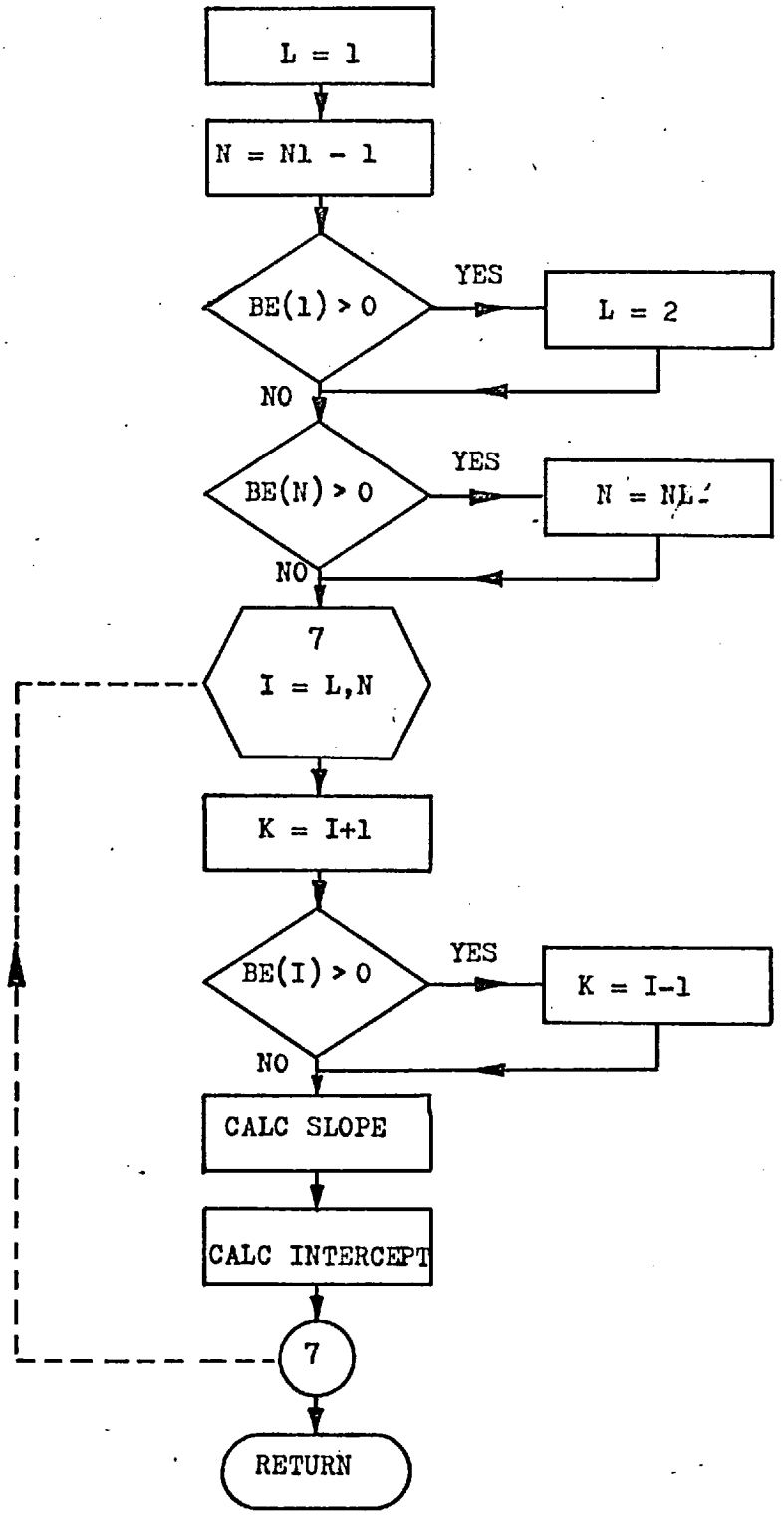

CALL SLOPE
X2
AM2
CALL LININT
AN2
CALL LININT
S1G2
CALL LININT
CALL SLOPE
X3
AN3
CALL LININT
AN3
CALL LININT
S1G
CALL LININT
10
I = 1,N
IFRIC = 1
YES
NO
CALL CFST
CALC S1G, AM, AN
10
RETURN



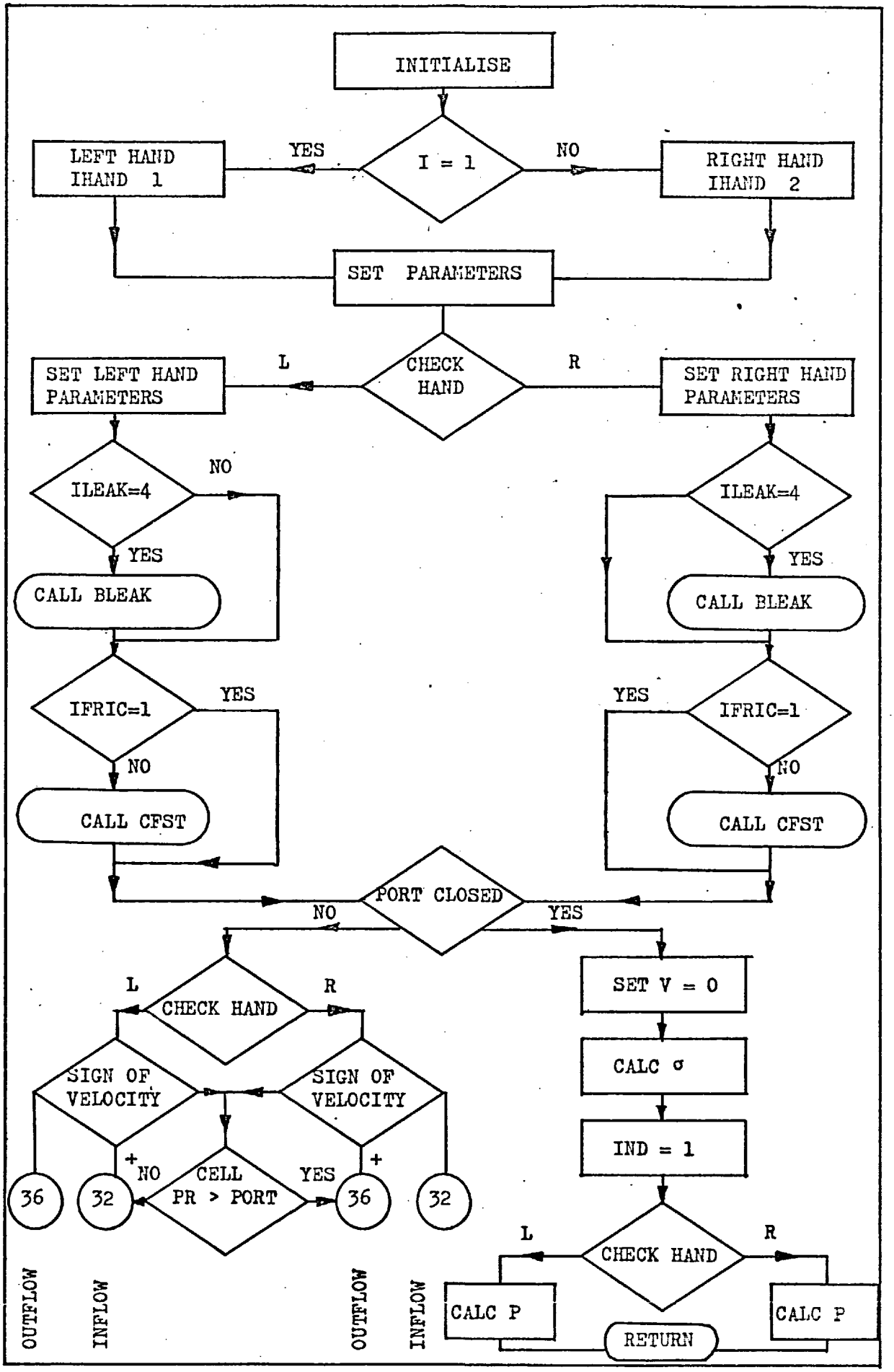
FLOW DIAGRAM OF SUBROUTINE LININT



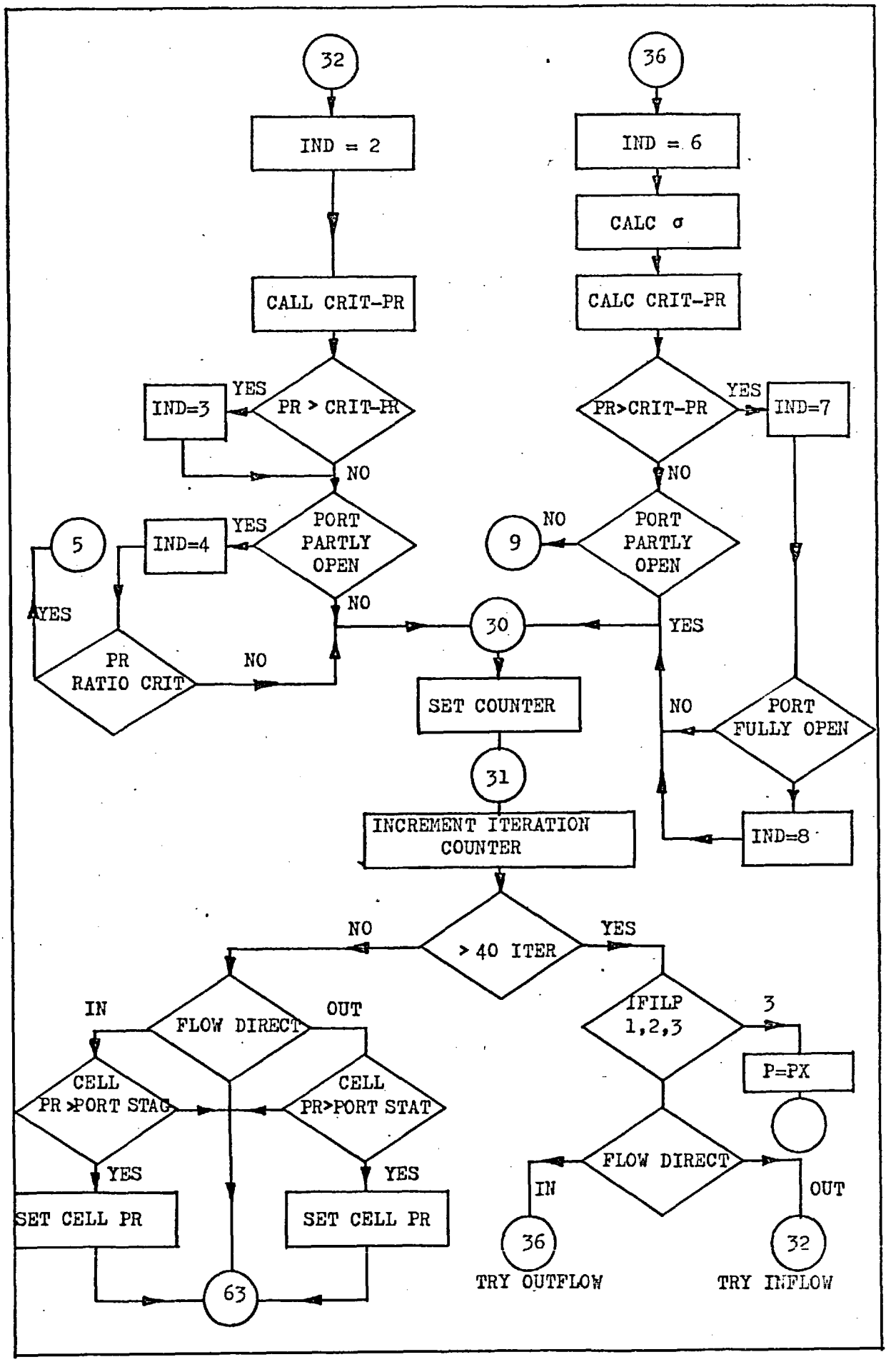
FLOW DIAGRAM OF SUBROUTINE CYCLE

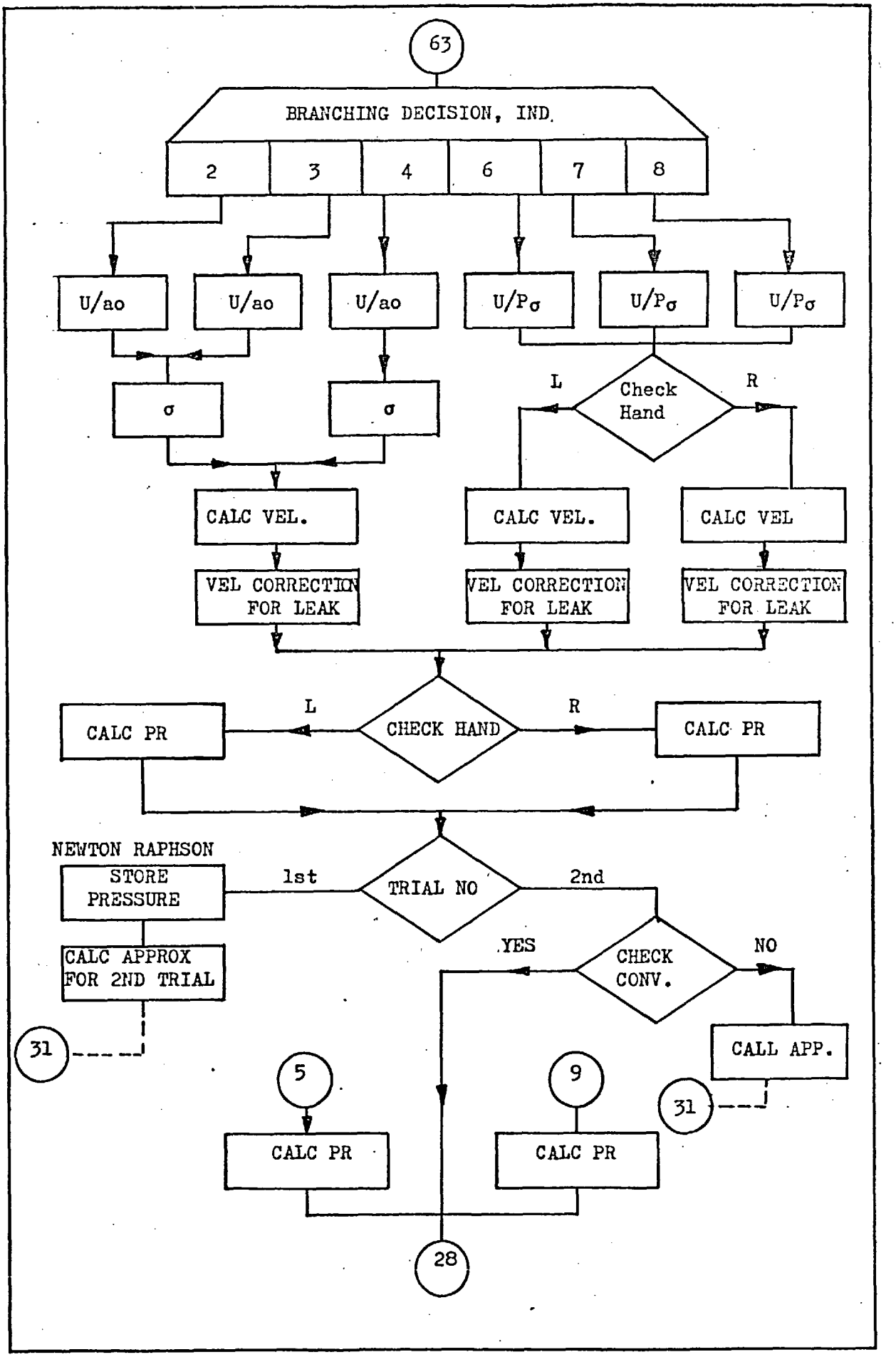


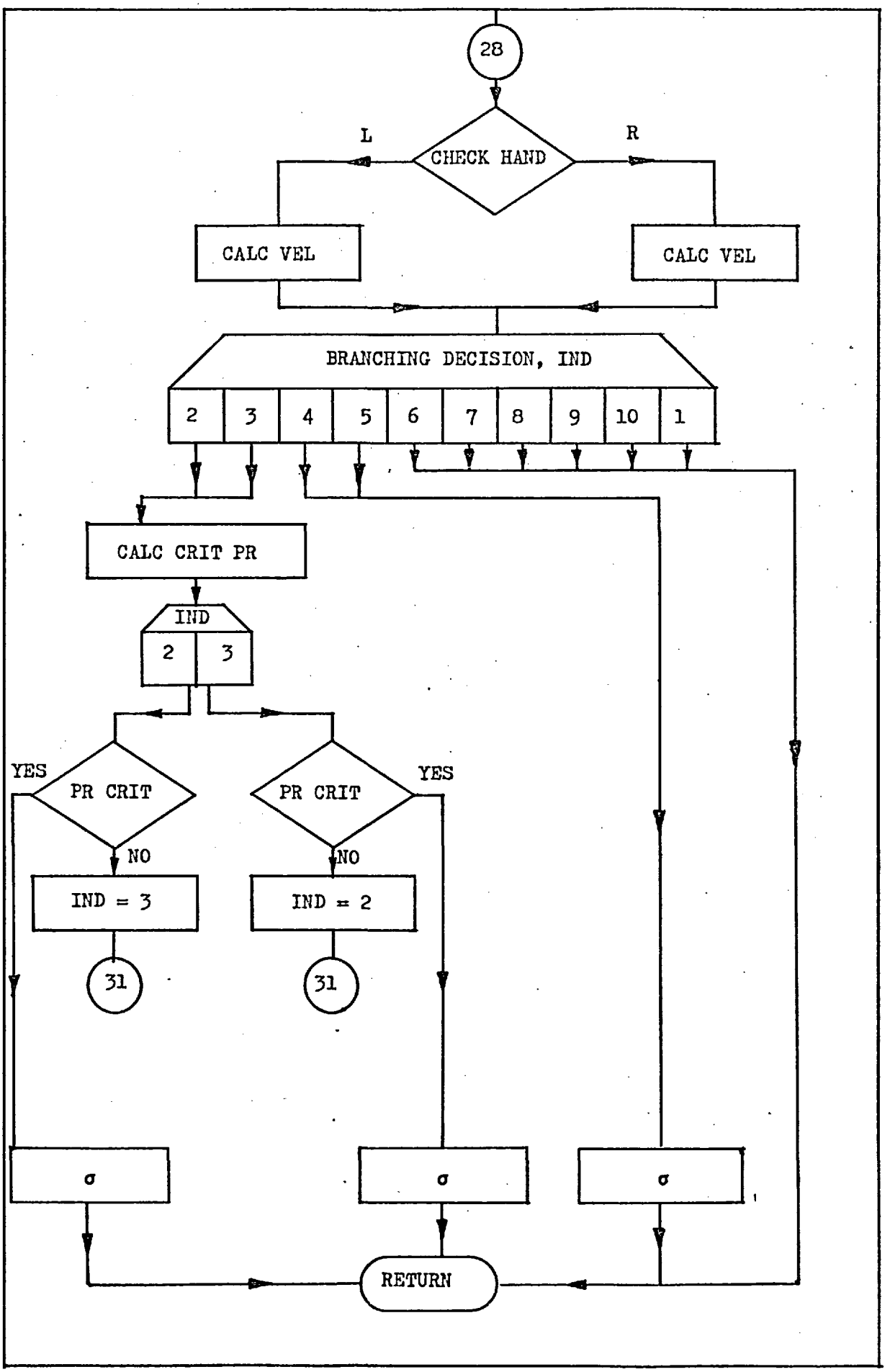
FLOW DIAGRAM OF SUBROUTINE SLOPE

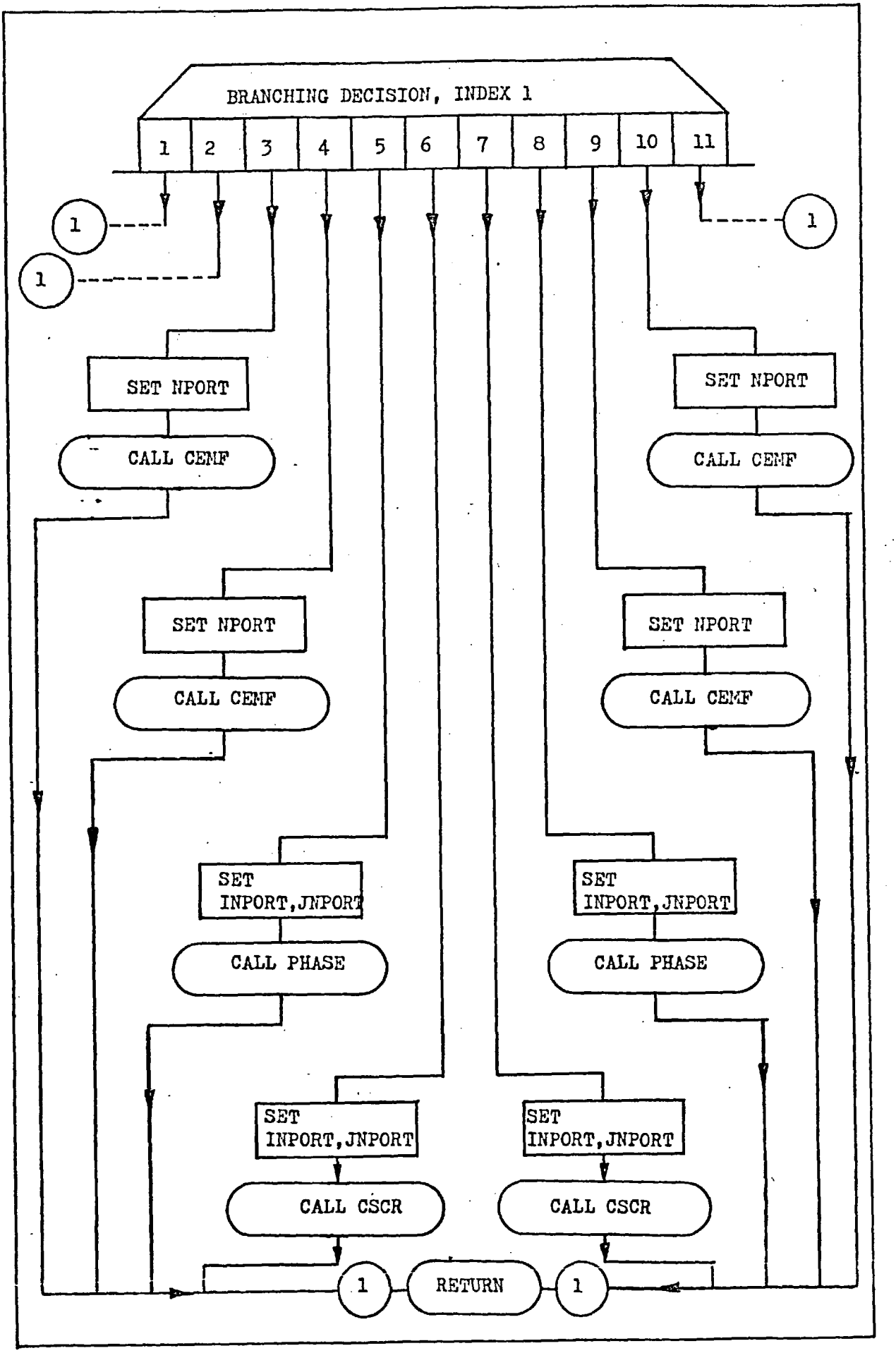


FLOW DIAGRAM OF SUBROUTINE PORTS

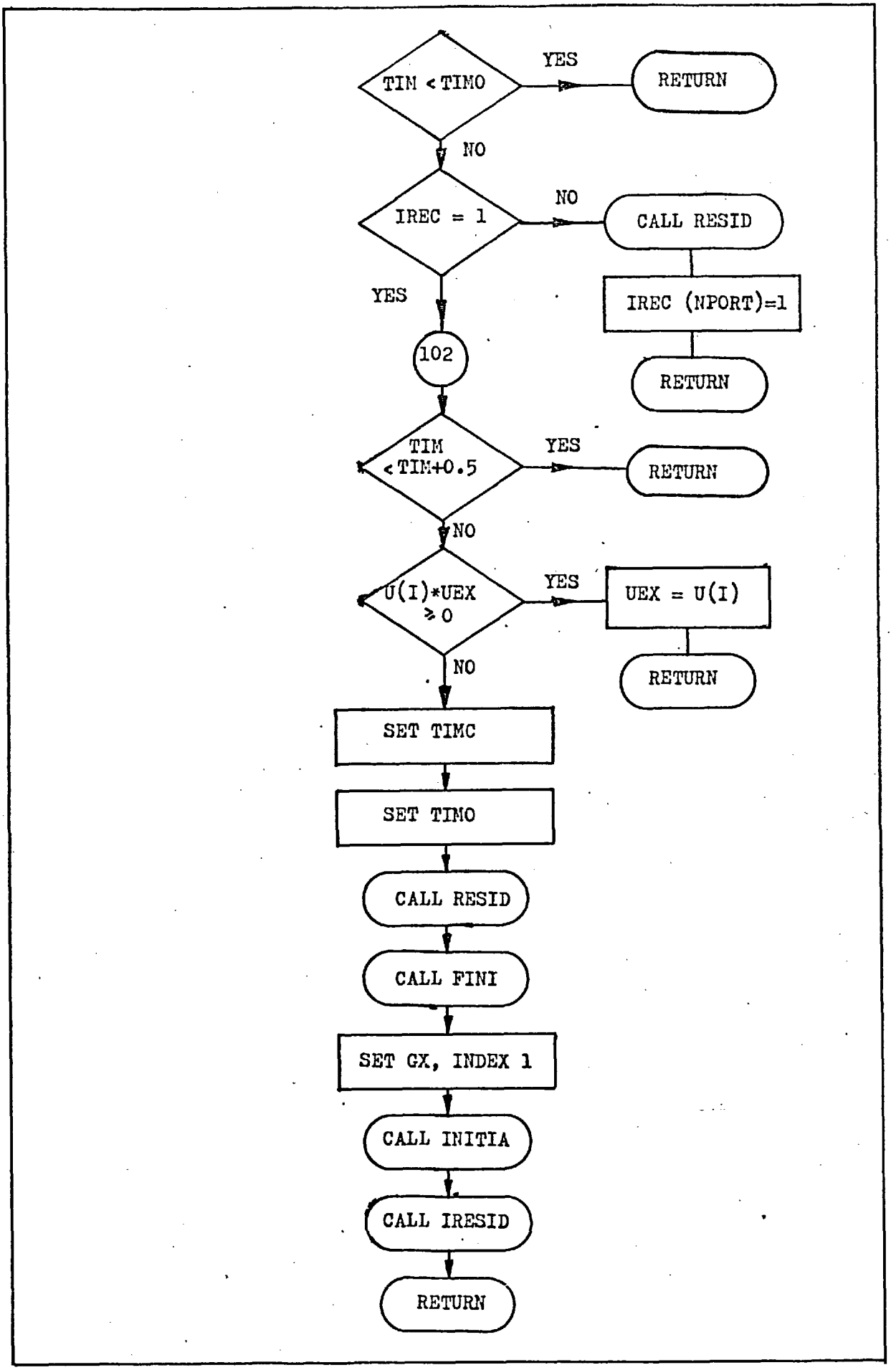

32
IND = 2
CALL CRIT-PR
PR > CRIT-PR
YES
IND=3
NO
PORT PARTLY OPEN
YES
IND=4
5
YES
PR RATIO CRIT
NO
NO
30
SET COUNTER
31
INCREMENT ITERATION COUNTER
> 40 ITER
NO
YES
IN
FLOW DIRECT
OUT
CELL PR >PORT STAT
YES
SET CELL PR
CELL PR>PORT STAT
YES
SET CELL PR
63
36
IND = 6
CALC σ
CALC CRIT-PR
PR>CRIT-PR
YES
IND=7
NO
PORT PARTLY OPEN
NO
9
YES
NO
PORT FULLY OPEN
IND=8
IFILP 1,2,3
3
P=PX
FLOW DIRECT
IN
OUT
36
TRY OUTFLOW
32
TRY INFLOW


63
BRANCHING DECISION, IND.
2
3
4
6
7
8
U/ao
U/ao
U/ao
U/Pσ
U/Pσ
U/Pσ
σ
σ
L
Check Hand
R
CALC VEL.
CALC VEL.
CALC VEL
VEL CORRECTION FOR LEAK
VEL CORRECTION FOR LEAK
VEL CORRECTION FOR LEAK
CALC PR
L
CHECK HAND
R
CALC PR
NEWTON RAPHSON
STORE PRESSURE
1st
TRIAL NO
2nd
CALC APPROX FOR 2ND TRIAL
YES
CHECK CONV.
NO
CALL APP.
31
31
5
9
CALC PR
CALC PR
28

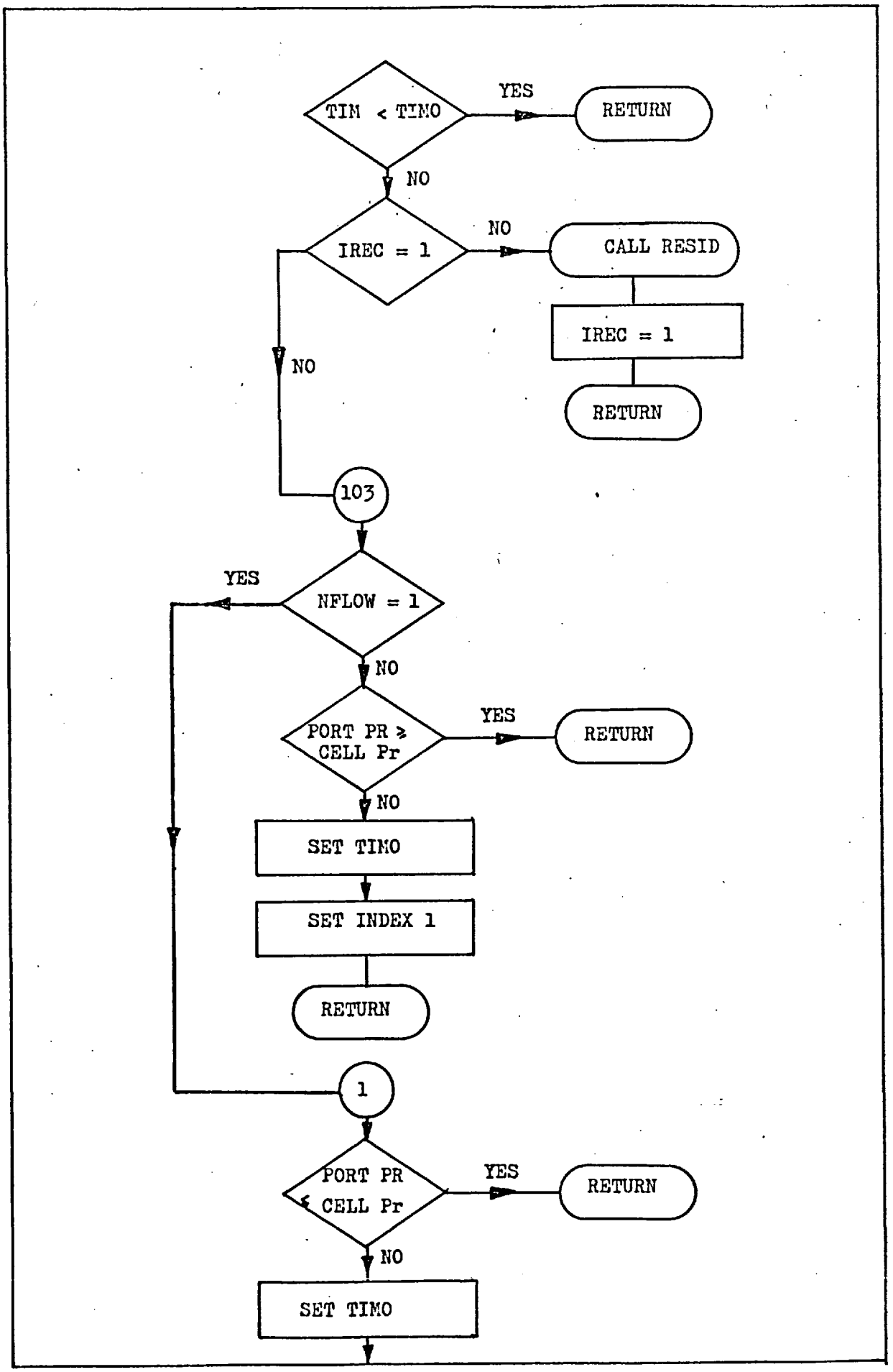

28
CHECK HAND
L
R
CALC VEL
CALC VEL
BRANCHING DECISION, IND
2
3
4
5
6
7
8
9
10
1
CALC CRIT PR
IND
2
3
YES
PR CRIT
NO
IND = 3
31
PR CRIT
YES
NO
IND = 2
31
σ
σ
σ
RETURN



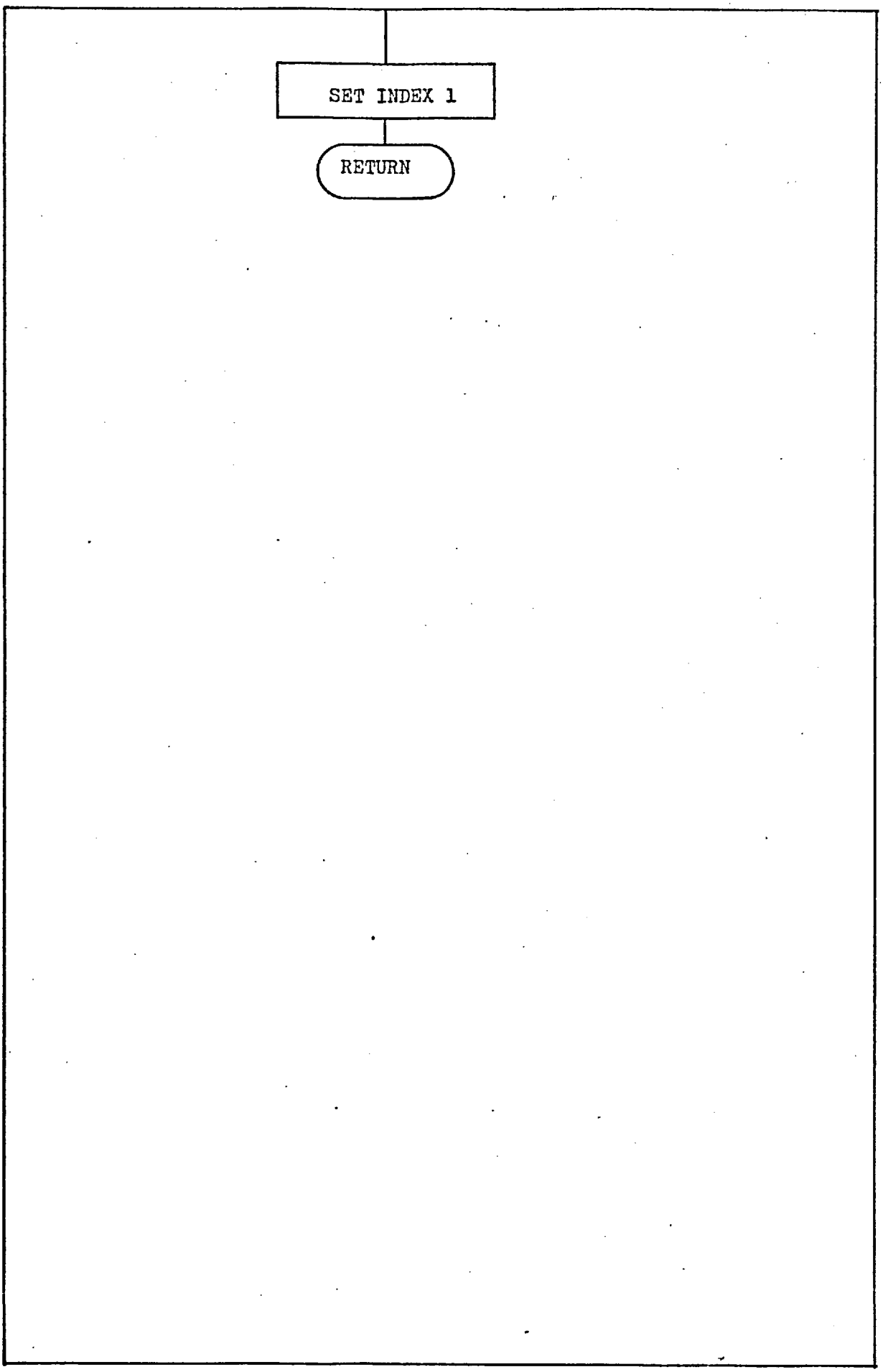
FLOW DIAGRAM OF SUBROUTINE OPTIM

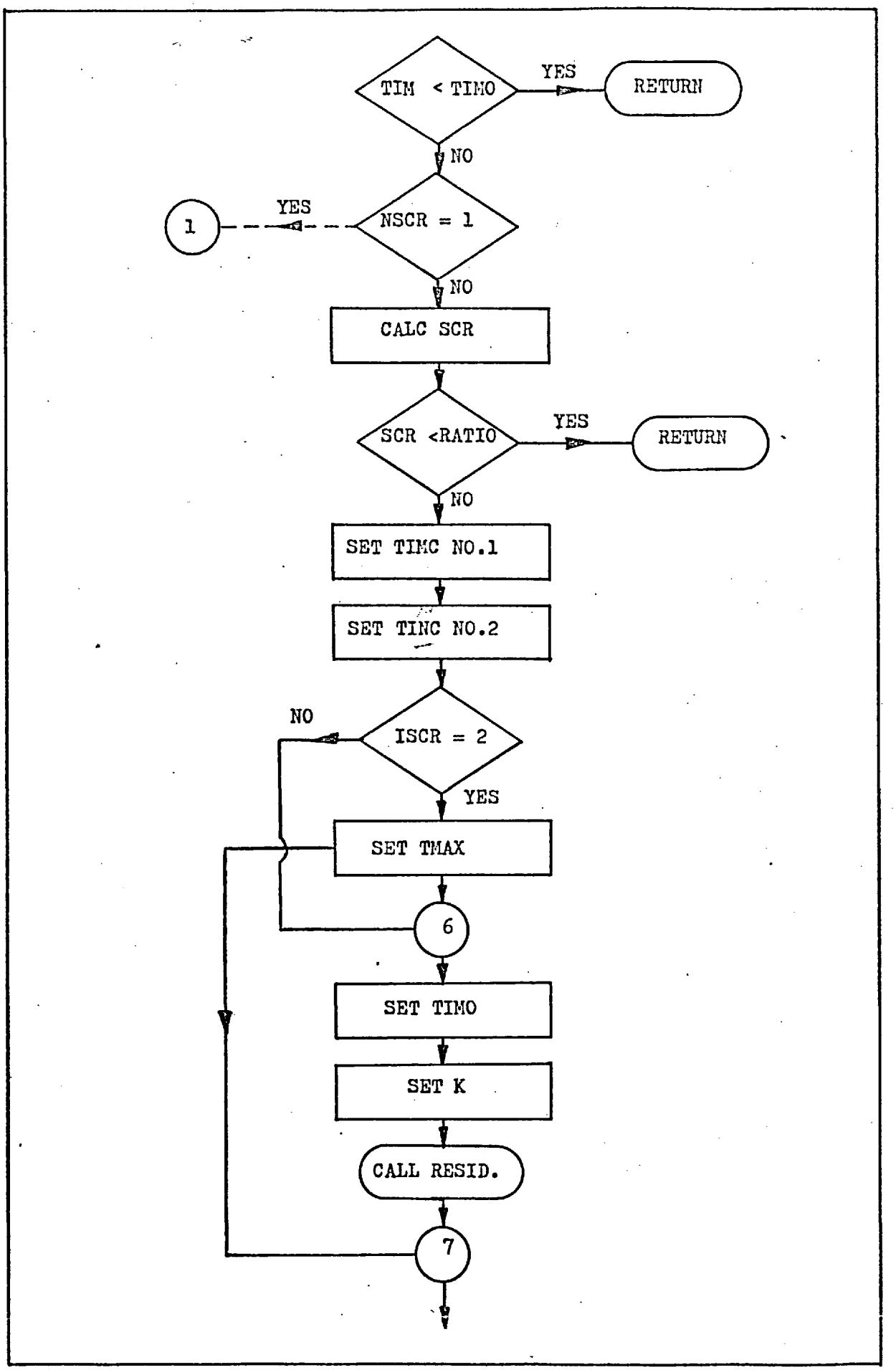


FLOW DIAGRAM OF SUBROUTINE CEMF

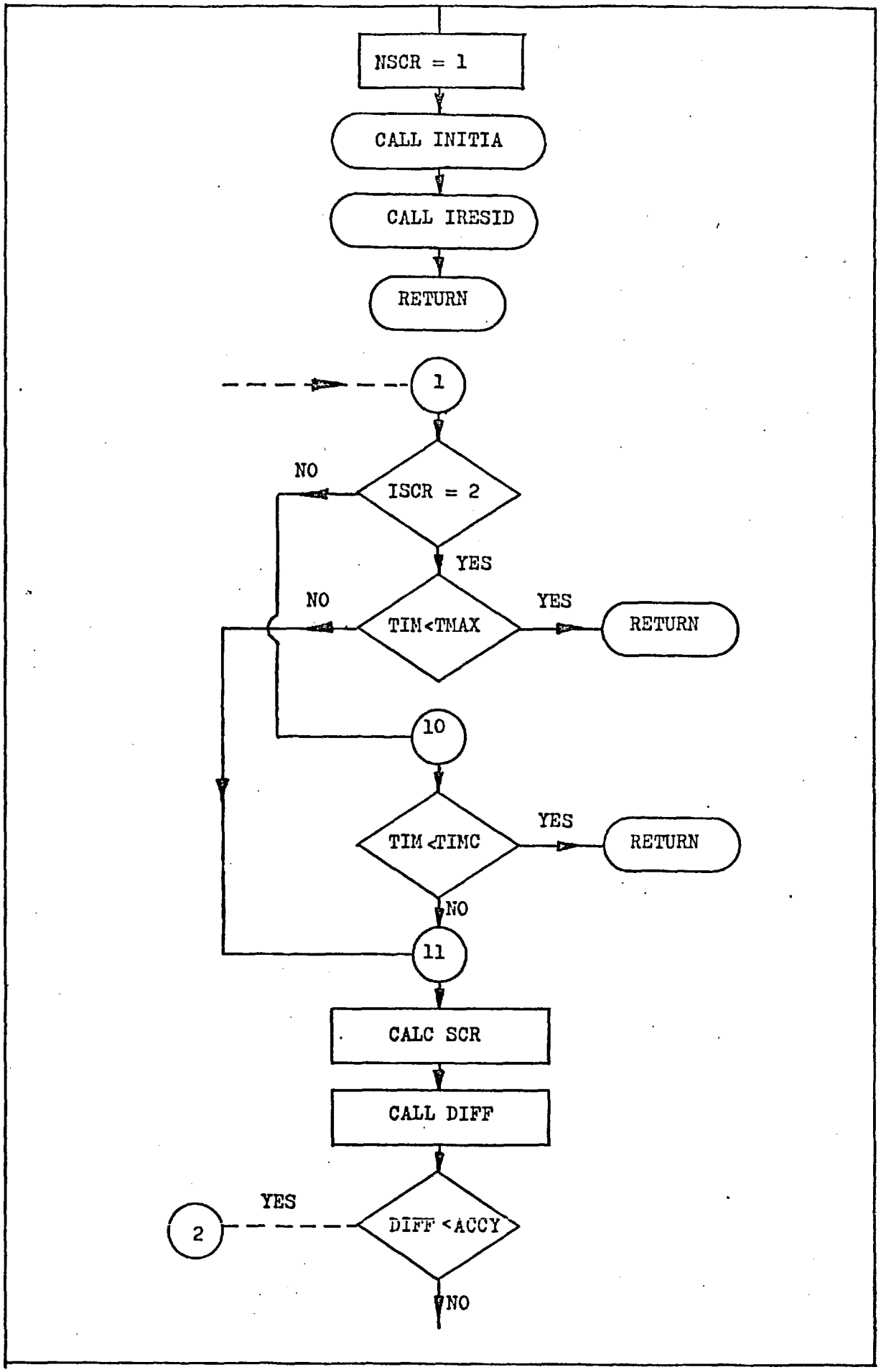


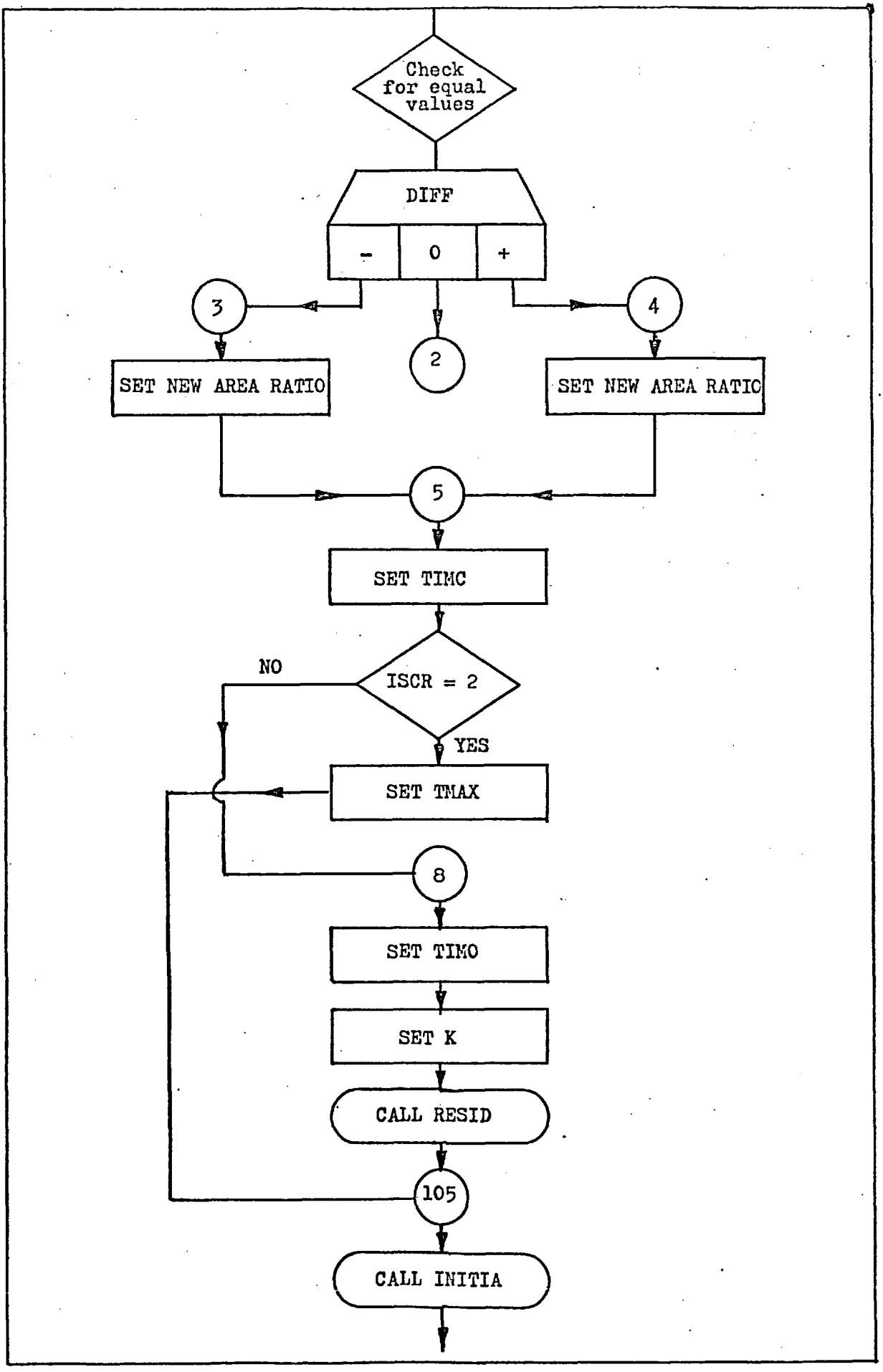
FLOW DIAGRAM OF SUBROUTINE PHASE

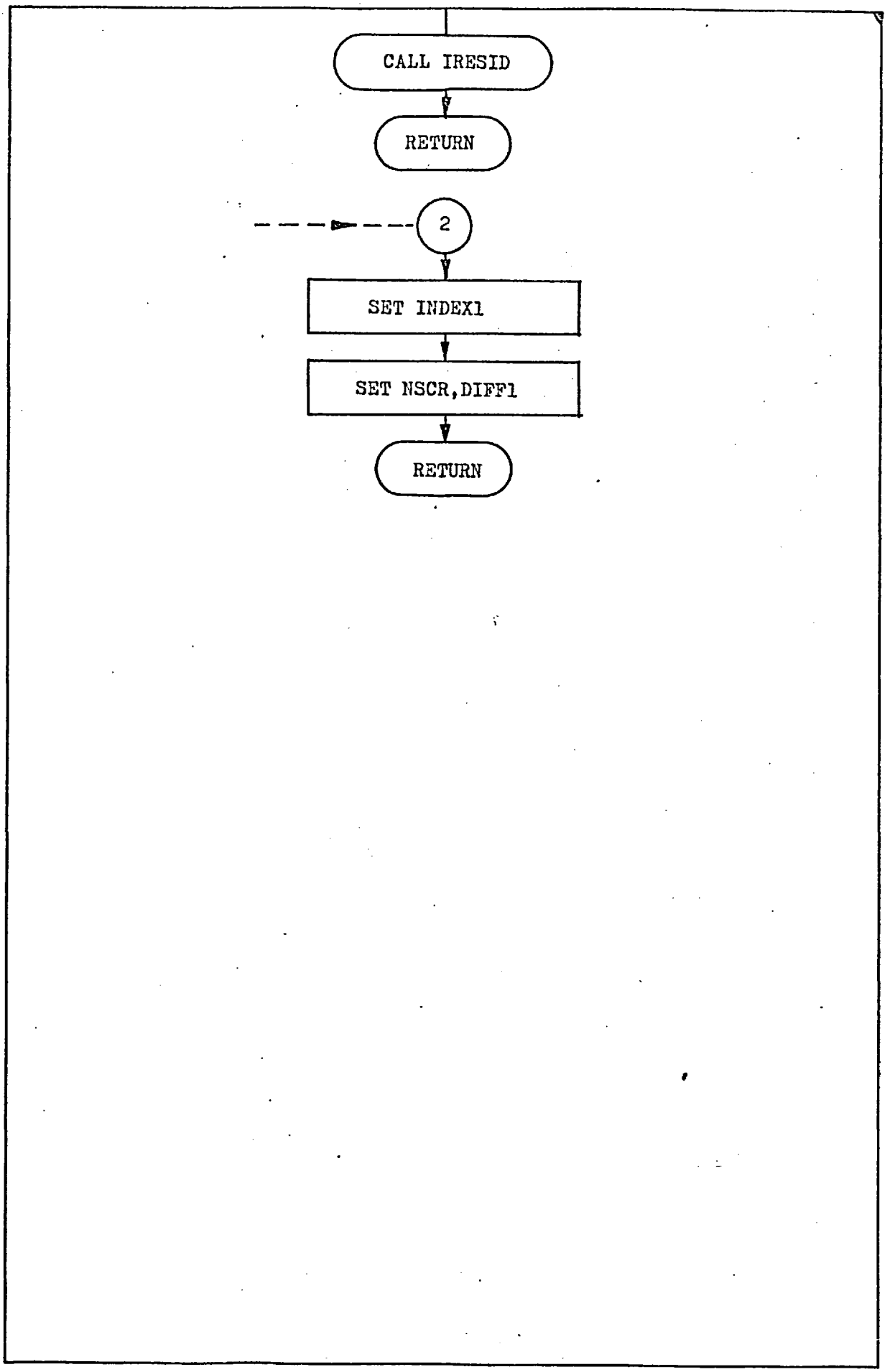

SET INDEX 1
RETURN

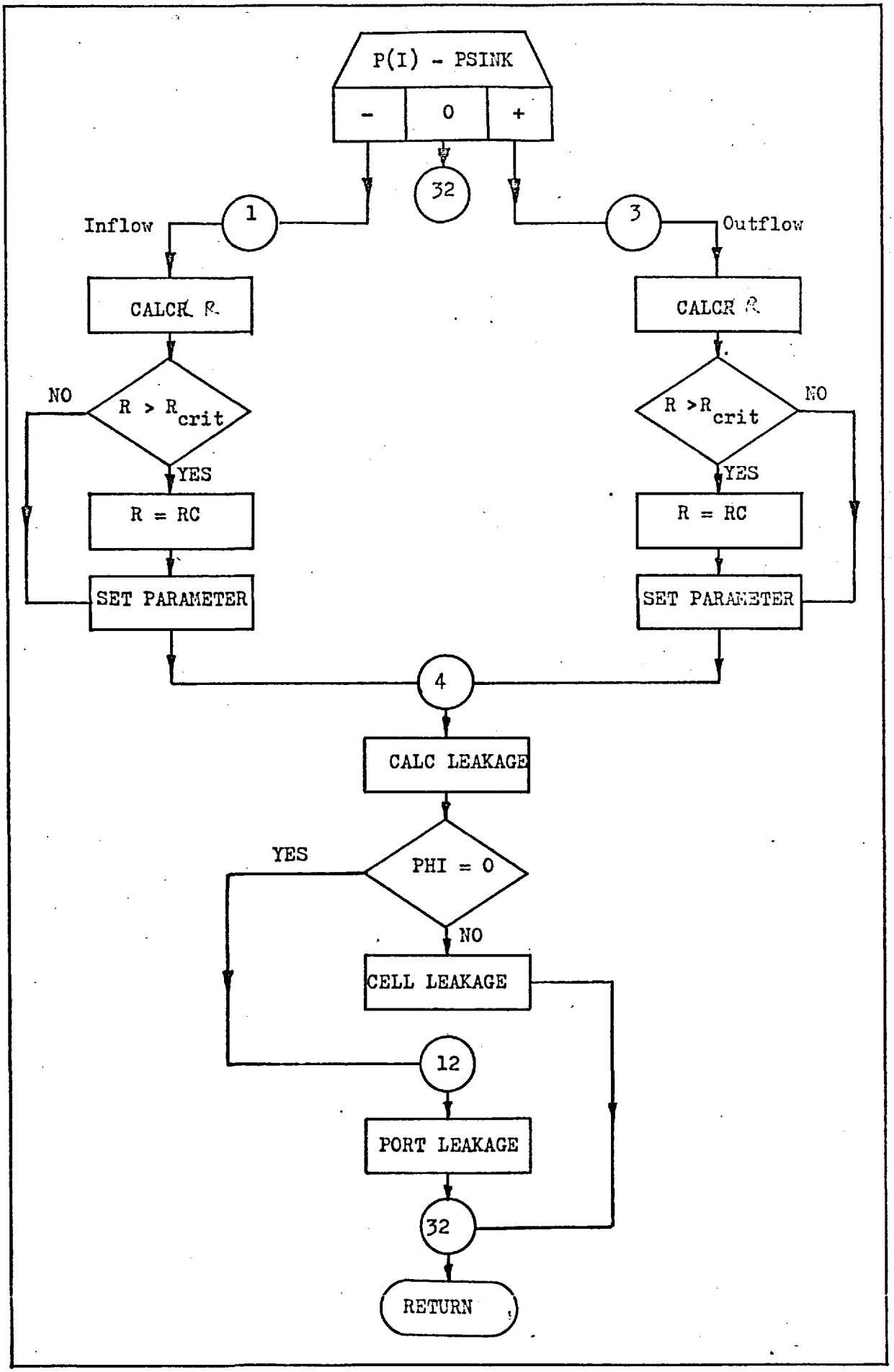


FLOW DIAGRAM OF SUBROUTINE CSCR

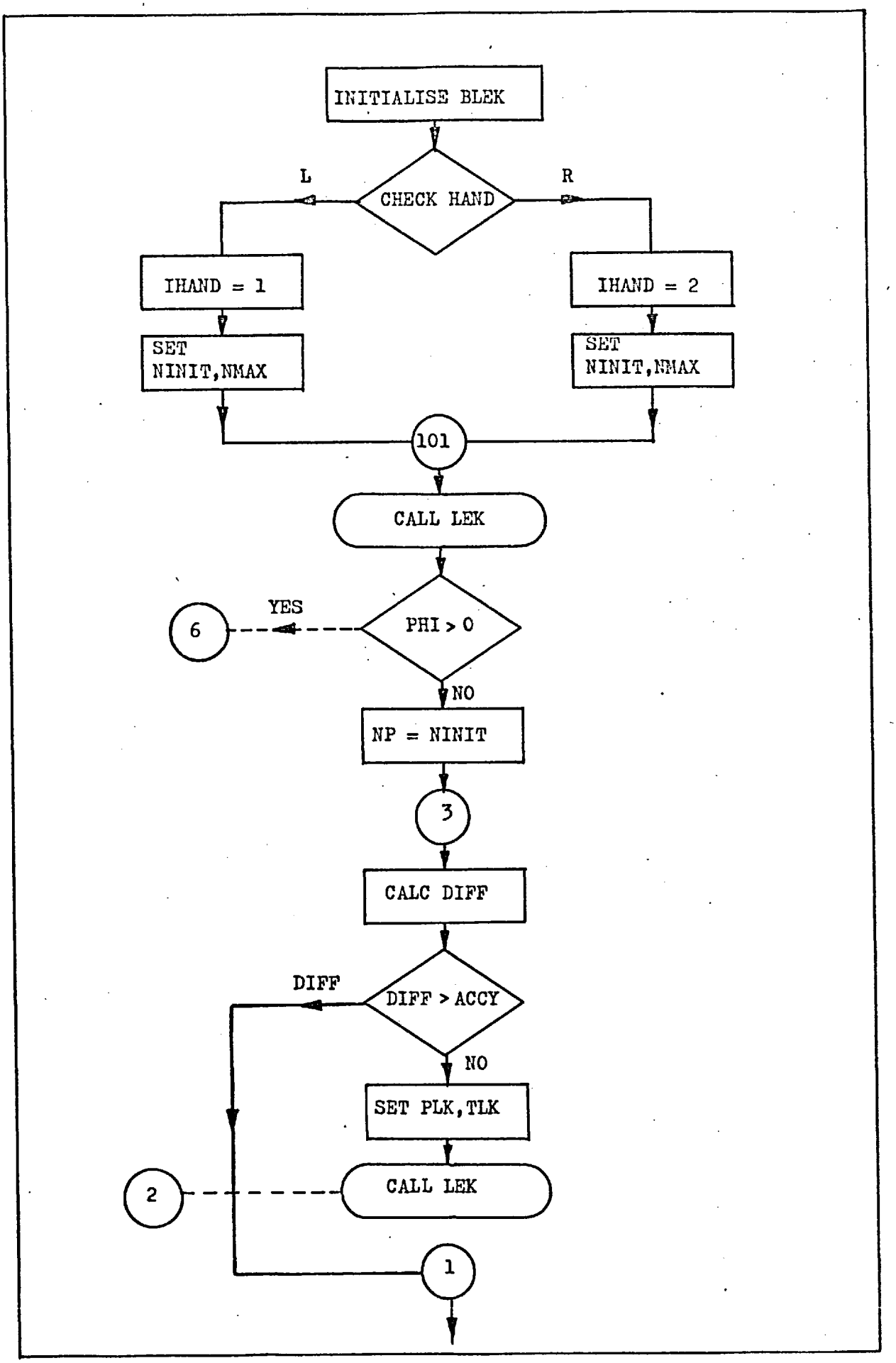

NSCR = 1
CALL INITIA
CALL IRESID
RETURN
1
NO
ISCR = 2
YES
NO
TIM<TMAX
YES
RETURN
10
TIM <TIMC
YES
RETURN
NO
11
CALC SCR
CALL DIFF
YES
2
DIFF <ACCY
NO


Check for equal values
DIFF
-
0
+
3
2
4
SET NEW AREA RATIO
SET NEW AREA RATIO
5
SET TIMC
NO
ISCR = 2
YES
SET TMAX
8
SET TIMO
SET K
CALL RESID
105
CALL INITIA

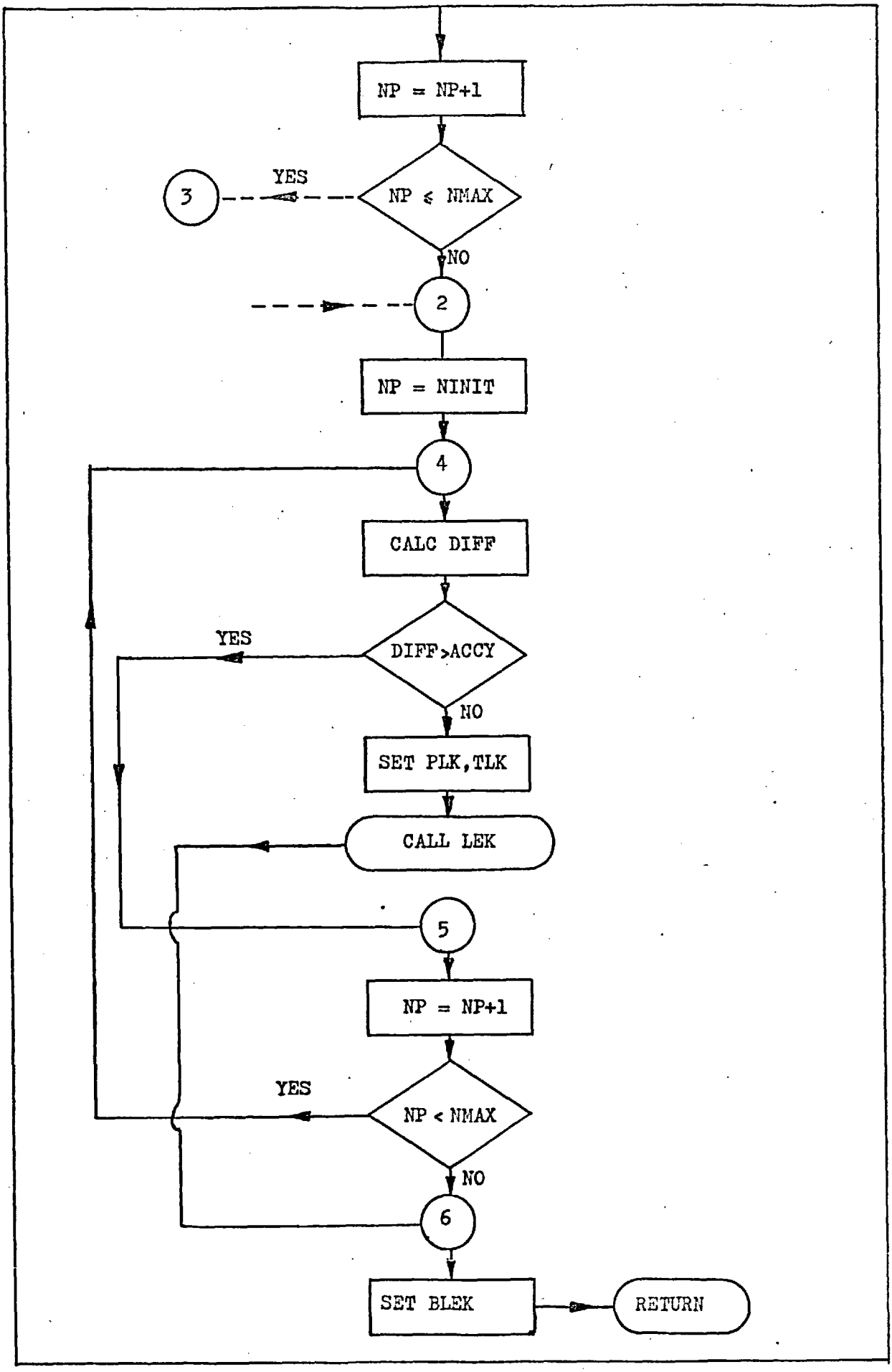

CALL IRESID
RETURN
2
SET INDEX1
SET NSCR,DIFF1
RETURN

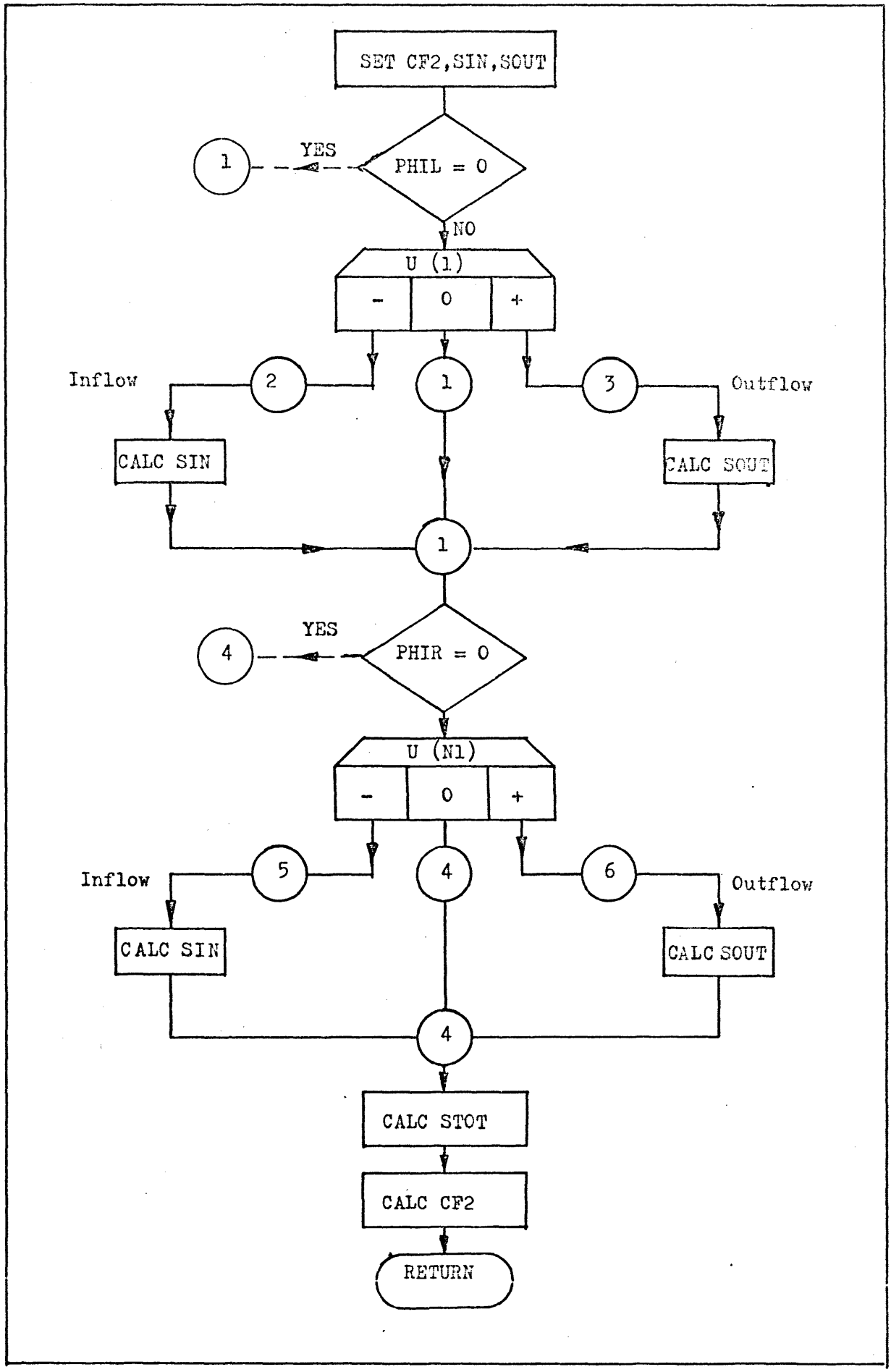


FLOW DIAGRAM OF SUBROUTINE LEK



FLOW DIAGRAM OF SUBROUTINE LEK1


NP = NP+1
YES
3
NP ≤ NMAX
NO
2
NP = NINIT
4
CALC DIFF
YES
DIFF>ACCY
NO
SET PLK,TLK
CALL LEK
5
NP = NP+1
YES
NP < NMAX
NO
6
SET BLEK
RETURN



FLOW DIAGRAM OF SUBROUTINE CEXEN